Models for the Active Site of the

[FeFe]-Hydrogenase

Dissertation

zur Erlangung des akademischen Grades doctor rerum naturalium

(Dr. rer. nat.)

seit 1558

vorgelegt dem Rat der Chemisch-Geowissenschaftlichen Fakultät

der Friedrich-Schiller-Universität Jena

von Dipl.-Chem. Ulf-Peter Apfel

geboren am 14.03.1984 in Jena

Gutachter:

1. Professor Dr. Wolfgang Weigand (Universität Jena)

2. Professor Dr. Dr. h. c. Dieter Seebach (Eidgenössische Technische Hochschule Zürich)

3. Professor Dr. Nils Metzler-Nolte (Ruhruniversität Bochum)

Tag der öffentlichen Verteidigung: 29.09.2010

"Water will be the coal of the future."

Jules Verne

1874, in *"The Mysterious Island"*

Table of contents

Abbreviations

Ac	acetyl	DMF	Dimethylformamide
Ac$_2$O	acetic anhydride	DPMK	diphenylmethyl potassium
Acm	acetamidomethyl	dppe-suc	cholesterin-hemisuccinat
AdoH	5'-deoxyadenosine	Dppv	*cis*-1,2-bis(diphenylphosphino)-
AdoMet	*S*-adenosylmethionine		ethylene
ADT	4-amino-1,2-dithiolane-4-	*DvHase*	[FeFe]-hydrogenase from
	carboxylic acid		*Desulfovibrio vulgaris*
adt	azadithiolato	*E.coli*	*Escherichia coli*
Boc	*tert*-butoxylcarbonyl	E/C	electrochemical reaction /
Boc$_2$O	di-*tert*-butyldicarbonate		chemical reaction (cyclic
CD	circular dichroism		voltammetry)
CDI	carbonyl diimidazole	EDC	1-(3-dimethylaminopropyl)-3-
CORM	CO releasing molecule		ethylcarbodiimide hydrochloride
CpI	[FeFe]-hydrogenase from	ENDOR	electron nuclear double
	Clostridium pasteurianum		resonance
CV	cyclic voltammetry	E$_{pa}$	electrochemical potential
Cys	cysteine		(oxidation)
DBU	1,8-diazabicyclo[5.4.9]undec-7-	E$_{pc}$	electrochemical potential
	ene		(reduction)
DCC	dicyclohexyl carbodiimide	EPR	electron paramagentic
DdHase	[FeFe]-hydrogenase from		resonance
	Desulfovibrio desulfuricans	eq.	equivalents
DEI	direct electron ionization	ESEEM	electron spin-echo envelope
DFT	density functional theory		modulation
dides-NTX	didesmethyl-nereistoxin	ESI	electron spray ionization
DIPEA	diisopropylethylamine	FAB	fast atom bombardment
DMAP	4-*N*,*N*-dimethylaminopyridine	FcPF$_6$	ferrocenium hexafluoro-

	phosphate	HydG	[FeFe]-hydrogenase maturation protein G
Fe_d	distal iron		
FHE	film-hydration-extrusion	IR	infrared
Fmoc	[(9H-fluoren-9-yl)-methoxy]-carbonyl	LC-MS	liquid chromatography with MS detection
FTIR	Fourier transformation infrared	LDA	lithium diisopropylamide
GFP	green fluorescent protein	Lys	lysine
Gly	glycine	MALDI	matrix assisted laser desorption ionization
GPC	gel permeation chromatography		
H_2ase	hydrogenase	MCD	magnetic circular dichroism
hAla	homo alanine	Mes	mesityl
HATU	O-(7-azabenzotriazol-1-yl)-1,1,3,3-tetramethyluronium hexafluorophosphat	Met	methionine
		MS	mass spectrometry
		MSNT	1-(2-mesitylensulfonyl)-3-nitro-1H-1,2,4-triazol
hCys	homo cysteine		
hLeu	homo leucine	NADH/H$^+$	nicotinamide adenine dinucleotide (reduced form)
HMD	methylenetetrahydro-methanopterin		
		NBS	N-bromosuccinimide
HOBt	1-hydroxy-1H-benzotriazol	NMR	nuclear magnetic resonance
HOTs	toluoylsulfonic acid	odt	oxadithiolato
hPhe	homo phenylalanine	PB-PEO2	polybutadien-polyethyleneoxide based polymer
HPLC	high performance liquid chromatography		
		PCS	photon correlation spectroscopy
hTyr	homo tyrosine	pdt	propanedithiolato
hVal	homo valine	Phe	phenylalanine
HydE	[FeFe]-hydrogenase maturation protein E	pK_a	negative decadic logarithm of the acid dissociation constant
HydF	[FeFe]-hydrogenase maturation protein F	POPC	palmityloleylphosphatidylcholine
		ppm	parts per million

PrNH$_2$	propylamine	TFA	trifluoroacetic acid
RT	room temperature	THF	tetrahydrofurane
SCE	saturated calomel electrode	TIS	triisopropylsilane
sdt	sulphurdithiolato	TLC	thin layer chromatography
SPPS	solid phase peptide synthesis	TNBS	2,4,6-trinitrobenzene sulphonic acid
TEM	transmission electron microscopy		

1 Introduction

Since the limitations of fossil energy sources and their polluting impact have become obvious, the search for alternative energy sources is promoted by scientists and politicians. Besides the common renewable energy sources (wind, sun, geothermal and water energy), dihydrogen can act as energy storage and for the transportation of energy in very efficient ways.[1] It has a high energy density[2] and produces a clean combustion product, namely water.[3] Many different ways to form dihydrogen are known (*e.g.* steam methane reforming,[4] electrolysis of water,[5] coal gasification,[6] and biomass processing techniques[7]). However, a considerable amount of energy is needed to produce one mole of dihydrogen. Especially the electrolysis of water is accompanied by a high overpotential and therefore by an unfavourable need of energy for standard industrial applications.[8]

Not only the industry dissipates and generates dihydrogen, but also nature uses an enormous amount of dihydrogen in different forms (*e.g.* $NADH/H^+$) as energy source and transporter.[9] The generation and depletion is regulated by enzymes, the hydrogenase enzymes, either to avoid a surplus of reducing power or to provide an energy source.[10] Hydrogenases are very efficient enzymes, catalyzing the one-electron reduction equilibrium of a proton (see Scheme 1).

Three different kinds of hydrogenase enzymes are currently discussed in literature. They are differentiated according to the shape of their active site, occurrence, localization and function (Table 1). (i) The cluster-free hydrogenase methylenetetrahydro-methanopterin (HMD) is found to possess a co-factor with a low-spin Fe(II).[11,12,13,14] (ii) The [FeNi]-hydrogenase exhibits a [FeNiS$_2$] active site and catalyzes the depletion of dihydrogen. A subgroup of [FeNi]-hydrogenase provides a [FeNiSe] centre, whereby one cysteine is replaced by a selenocysteine.[15] (iii) The third type of hydrogenase is called [FeFe]-hydrogenase and will be in the focus of this work.[16,17]

$$2H^+ + 2e^- \rightleftharpoons H_2$$

Scheme 1. Two-electron reduction equilibrium of protons/dihydrogen.

Table 1. Classification of the different hydrogenases.[18]

Classification	Occurrence	Structure	Localization	Function
[FeFe]-H$_2$ase	photosynthetic bacteria, anaerobic fermentative bacteria cyanobacteria, green algae, protozoan	monomeric, heteromeric	cytoplasmic, membrane bound, periplasmic, chloroplasts, hydrogenosomes	formation of dihydrogen
[FeNi]-H$_2$ase	anaerobic, photosynthetic bacteria, cyanobacteria	heterodimeric, multimeric	cytoplasmic, membrane bound, periplasmic	uptake of dihydrogen
[FeNiSe]-H$_2$ase	sulphate-reducing bacteria, methanogenes	oligomeric	cytoplasmic, membrane-bound	oxidation of dihydrogen
[Fe]-H$_2$ase	methanogenes	monomeric	cytoplasmic	formation of dihydrogen

1.1 [FeFe]-Hydrogenase

The [FeFe]-hydrogenase (previously known as [Fe-only]-hydrogenase) was found to efficiently catalyze the generation of dihydrogen (6000-9000 molecules H$_2$/s per site).[19,20] It is therefore an interesting target for biomimetic modelling, as it offers the possibility for the electrolysis of water at moderate potential (-0.4 V vs. SCE at pH = 7) and neutral pH value. [21,22]

1.1.1 Enzymatic Topology

Attributable to the sensitivity to air, the [FeFe]-hydrogenase is found in strictly anaerobic organisms.[19] It is suggested that this enzyme originates from ancestral monomeric cytoplasmic enzymes as a result of gene splitting and insertion of new sequences.[23] Nicolet *et al.* and Peters *et al.* unveiled the topology of the [FeFe]-hydrogenase from *Desulfovibrio desulfuricans* (DdHase)[24] and *Clostridium pasteurianum* (CpI).[25] They found that the enzyme consists of a small and a large subunit with molecular weights of 11 and 42 kDa, respectively, which are very similar to

the ones in the well-investigated [FeFe]-hydrogenase from *Desulfovibrio vulgaris* (DvHase) (Figure 1).[26]

An unprecedented [2Fe2S] cluster is deeply imbedded in the peptide matrix and is jointly connected to a [4Fe4S] cluster by a cysteine. Additionally, two more [4Fe4S] clusters are involved and form a ferredoxin-like domain which can serve as electron transport unit.[27] The [2Fe2S] cluster was proclaimed to be the reactive centre for dihydrogen formation.

Further on, it bears five nonprotein triple bonded diatomic molecules.[28] The sixth coordination site at the distal iron centre (Fe_d) (Figure 1) was assigned to be either a free coordination site as in DdH or a water ligand as found in CpI.[29] In agreement with IR studies,[26,30] magnetic circular dichroism spectra (MCD),[19] electron spin-echo envelope modulation (ESEEM)[31] and electron double resonance (ENDOR) measurements[33,31a,32] it was inferred that CN^- and CO ligands are bound to the [2Fe2S] cluster.
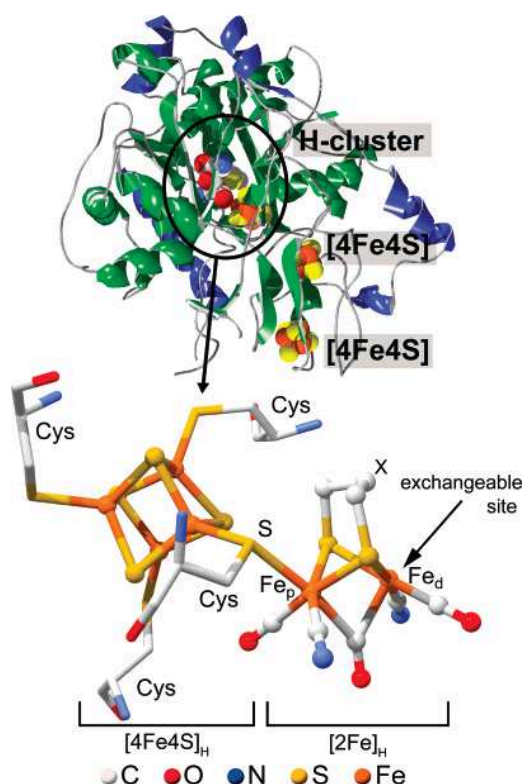
Figure 1. Active site and overall fold of DdHase representing the different [FeS] assemblies imbedded into the small (blue) and large subunit (green).[33]

Two hydrogen bonds can be seen, established by alanine (A109) and isoleucine (I204) to the nonprotein CN^- ligands (Figure 2). Furthermore, the cluster is closely positioned to a lysine (K237), which is only 440 pm away from the distal iron centre (Fe_d or Fe2) (Figure 1 and Figure 2) and can act as a possible proton distributor during the dihydrogen generation.
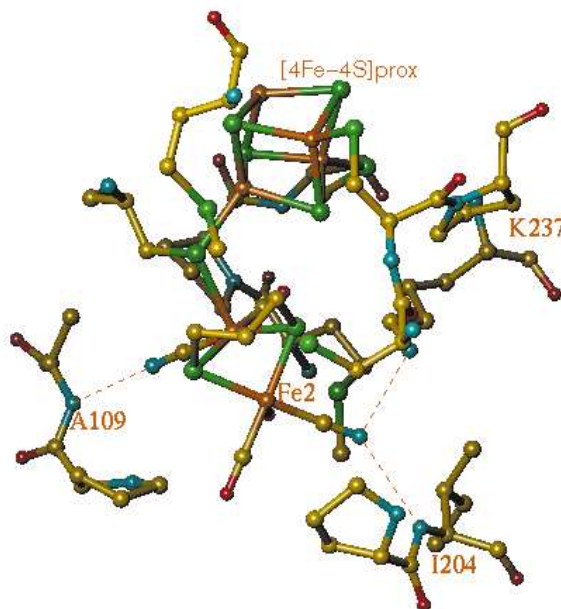
Figure 2. Enzymatic environment of the [2Fe2S] cluster of DdHase {green... sulphur; gold...carbon; brown... iron; red...oxygen; blue...nitrogen}.[24]
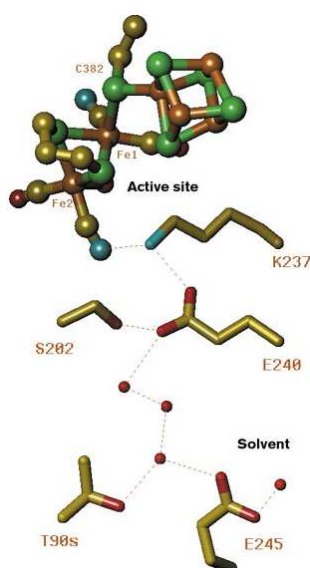
Figure 3. Possible proton channel of the [FeFe]-hydrogenase.[24]

In analogy to the [FeNi]-hydrogenase,[34] the diatomic ligands are proposed to be CN^- ligands, whereas the CO ligands are positioned in a hydrophobic environment.[24] The two iron centres are bridged by a dithiolato ligand of the general form $(SCH_2)_2X$, where the atom X could be assigned to be either O, NH or CH_2, and is alleged to play a key role during dihydrogen formation.[24] Another interesting property is displayed in Figure 1. The distal iron (Fe_d) exhibits a free coordination site and a bridging or semi-bridging CO molecule.[24,25]

The conformation of this iron is called the "rotated" form and should allow the formation of a terminal hydride. In nature the approximation of a proton may occur through a proton channel formed by lysine (K237), serine (S202), water molecules as well as glutamine (E240 and E245) (Figure 3).[24]

1.1.2 Biosynthesis of CO, CN^- and (-S-CH_2-NH-CH_2-S-)

Hitherto, the origin of the three different non-proteinogenic ligands is not fully clarified and only assumptions can be made about the biological access to these molecules. These assumptions will be provided in the following chapter.

The (-S-CH_2-X-CH_2-S-) Linker

As mentioned in chapter 1.1.1, the nature of the S-to-S linker has not yet been verified. Assuming that the active site possesses an azadithiolato linker, Fontecave *et al.* suggested a plausible mechanism for the formation of the azadithiolato ligand (Scheme 2).[35]

They found that HydG is responsible for the formation of the dithiomethylamine bridge and supposed that the initial step is cleavage of tyrosine, induced by a degradation of *S*-adenosylmethionine (AdoMet) to 5'-deoxyadenosine (AdoH) and methionine. As a result of the tyrosine cleavage a reactive species, 2-iminioacetate (**1**), is formed and attacks a peptide bound {FeS} cluster to form the intermediate **2**. Subsequent elimination of CO_2 and NH_3 affords the iron-bound dithiomethylamine assembly **3**. By all means, no plausible mechanism for the formation of a propanedithiolato (pdt) or an oxadithiolato (odt) bridge is known so far.
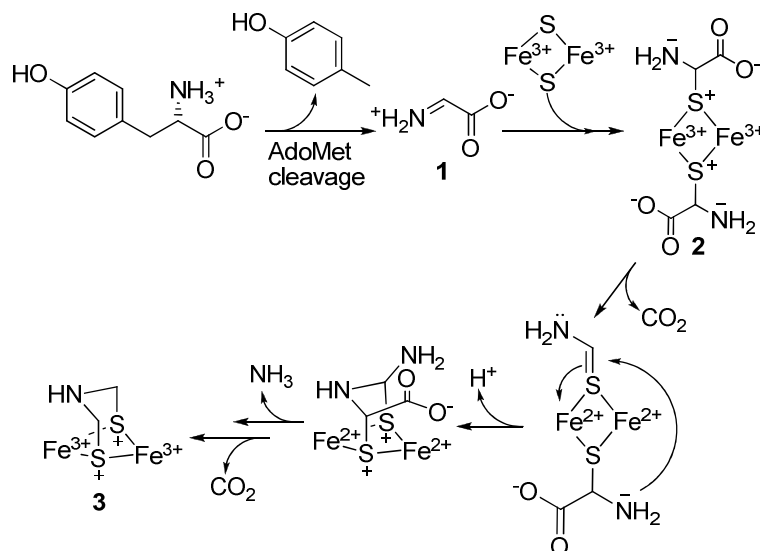
Scheme 2. Proposed mechanism for the formation of diiron(azadithiolato) clusters.[35]

CO and CN Ligands

In contrast to the vague assumptions on the nature and the formation of the S-to-S linker, the bioavailability of the very toxic diatomic molecules CN^- and CO is considerably better investigated.[36] First investigations proposed glycine[37] or carbamoylphosphate,[38] generated from HCO_3^- in nature,[39] to be the precursor of both the CN^- and CO ligand (Scheme 3). However, it was later shown that they have a dissimilar origin[40] and only CN^- arises from carbamoylphosphate.[40,41,42]

Using ^{13}C-labeled *L*-[ureido-^{13}C]-citrulline, that is enzymatically degradable to carbamoylphosphate and ornithine,[43] as well as $NaH^{13}CO_3$, Friedrich *et al.* investigated the role of carbamoylphosphate as source for CN^- and CO.**[40]** During investigation of *Ralstonia eutropha H16*, overproduced in *E. coli*, they noticed that in the presence of *L*-[ureido-^{13}C]-citrulline or $NaH^{13}CO_3$, exclusively the CN^- vibrations of the [FeNi]-hydrogenase reveal an isotope shift to lower frequencies. Only when offering free [13]CO, an isotope shift of the CO-band to lower frequencies is observable.

This implies that solely CN^- originates from carbamoylphosphate and that CO_2 is not a source for CO, as was proposed by Roseboom and co-workers.[44]
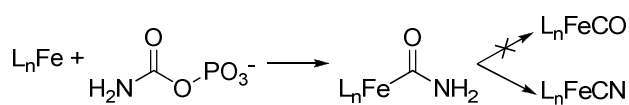
Scheme 3. Role of carbamoylphosphate for the bioavailability of CN^- and CO.
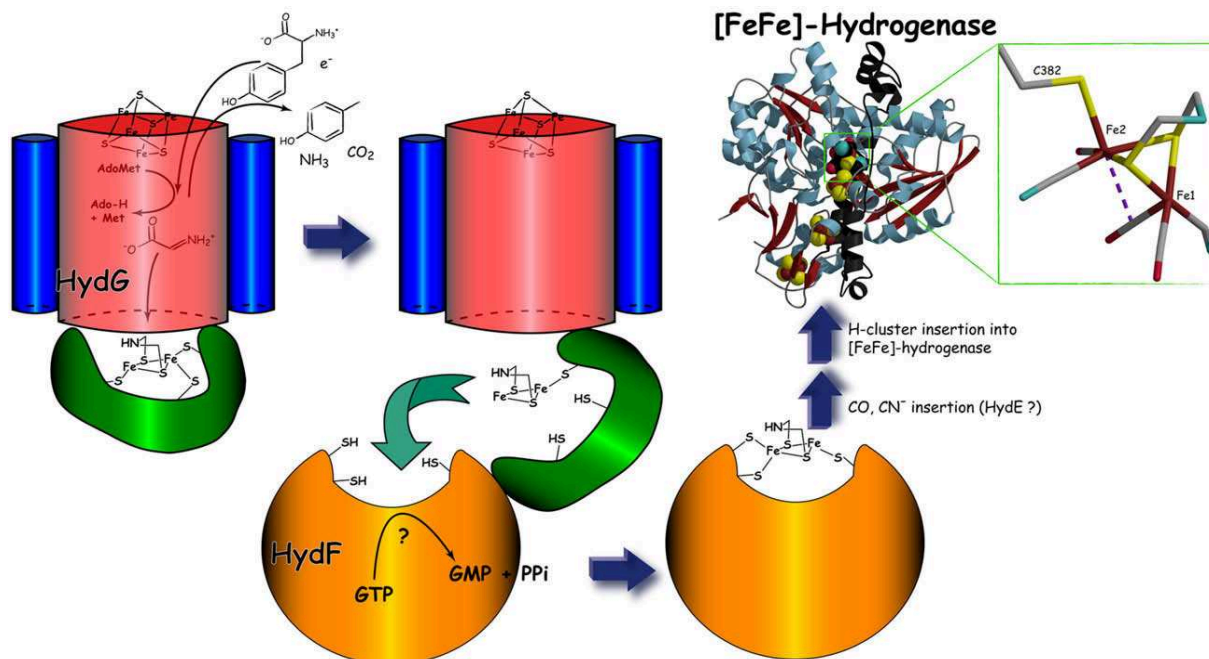
Figure 4. Enzymatic pathway towards the formation of the active site of [FeFe]-hydrogenase.[35]

The source of the "free" CO as potential ligand is still unclear. However, a recent investigation by Roach *et al.* suggested CN^- and CO formation from tyrosine degradation.[45] Besides all ambiguities the overall process for the formation of the [FeFe]-hydrogenase can be described as depicted in Figure 4: Formation of the dithiomethylamine *via* HypG and HypF bearing an [Fe2S] cluster and transfer of CN^- and CO *via* HypE.[44,46]

1.1.3 States of the Active Site

Based on the structural properties of the active site the question evokes on the different catalytic states of the [FeFe]-hydrogenase. Therefore, EPR measurements[19,47] and Mössbauer experiments[48] were carried out to uncover the different electronic states of the active centre. Based on the EPR data, five different electronic states could be established (Scheme 4).[49] In the presence

$$H_{ox}^{air}$$
$$[4Fe4S]^{2+}\text{-}[2Fe](CO)_b(OH) \xrightleftharpoons{e^-} [4Fe4S]^+\text{-}[2Fe](CO)_b(OH)$$
$$S = 0 \qquad\qquad\qquad\qquad\qquad H_{trans} \quad S = 1/2$$

$$\downarrow\; OH^-$$

$$H_{ox}^{CO} \qquad\qquad\qquad\qquad\qquad H_{ox}$$
$$[4Fe4S]^{2+}\text{-}[2Fe](CO)_b(CO) \xrightleftharpoons[CO]{} [4Fe4S]^{2+}\text{-}[2Fe](CO)_b(\;)$$
$$S = 1/2 \qquad\qquad\qquad\qquad\qquad\qquad S = 1/2$$

$$\updownarrow\; H_2$$

$$H_{red}$$
$$[4Fe4S]^{2+}\text{-}[2Fe](\;)_b(CO)$$
$$S = 0$$
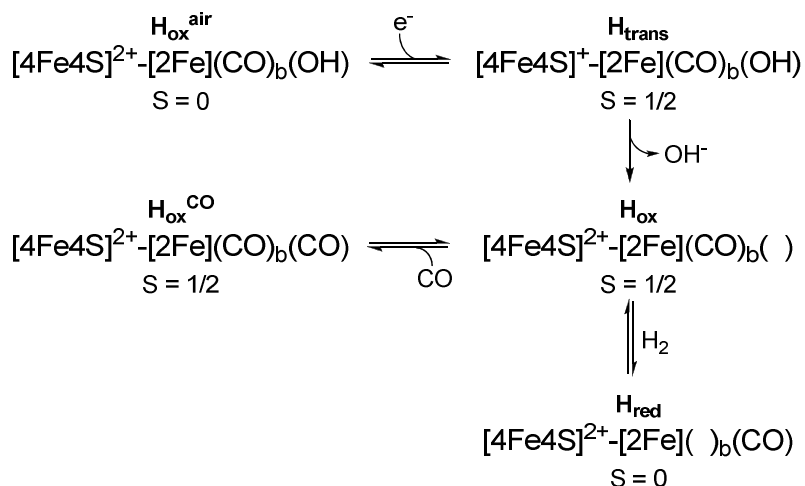
Scheme 4. EPR states of the active site (b…bridging ligand).[49]

of air, the active site is EPR silent (S = 0) and called H_{ox}^{air}. Reduction at E = -110 mV leads to rhombic EPR signals (g = 2.06, 1.96 and 1.89) with a total electron spin of S = ½ and a change of the charge in the [4Fe4S] cluster. Later on, this was found to be the only state with changed electronic properties of the [4Fe4S] cluster within the potential area of the [2Fe2S] cluster.[48b] This species has a vacant (exchangeable) site at the distal iron atom and a bridging CO ligand. It can be characterized by an axial EPR spectrum with $g_\parallel = 2.065$ and $g_\perp = 2.01$. As it is known from literature the [FeFe]-hydrogenase is sensitive to CO.[29] Inhibition of the active site due to a coordination of CO to the distal iron atom is a direct consequence and leads to H_{ox}^{CO}. However, the coordination is reversible and the CO ligand can be cleaved by light irradiation.[26,30b,47,50] Further treatment of the H_{ox} state with dihydrogen results in another EPR silent state. It is called H_{red} and bears no bridging CO ligand.

Inspired by the different EPR states the question evokes about the oxidation states of the iron centres in the [2Fe2S] cluster. Initial assumptions were based on a [$Fe^{II}Fe^{III}$] state for the H_{ox} and [$Fe^{II}Fe^{II}$] state for H_{red}.[48b,51] But in contrast to these assumptions DFT calculations suggest different oxidation states.[52] These DFT investigations assume that H_{ox}^{air} is an [$Fe^{II}Fe^{II}$] assembly. For H_{ox} and H_{red} an [$Fe^{II}Fe^{I}$] and [$Fe^{I}Fe^{I}$] assembly, respectively, was proclaimed. To establish these assumptions, Mössbauer experiments on *Desulfovibrio vulgaris*[51] and ENDOR measurements on *Desulfovibrio desulfuricans*[49] were carried out and showed a paramagnetic behaviour of the proximal
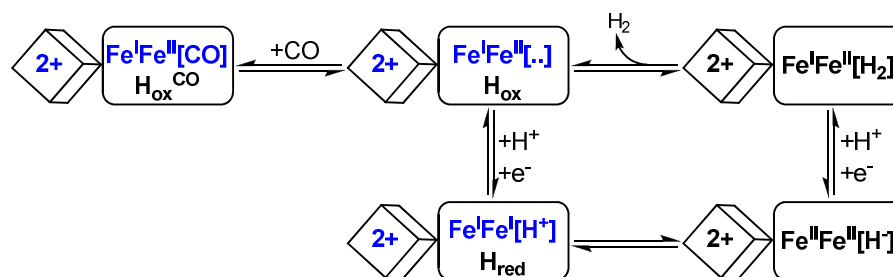
Scheme 5. Possible oxidation states of the active site (box) as well as the [4Fe4S] cluster (cube) and catalytic mechanism for the H_2 development in nature.[54]

iron in the H_{ox} and the H_{ox}^{CO} state. Since both iron centres exhibit a low-spin state caused by the strong field CN^- and CO ligands,[48b] an oxidation state of +1 or +3 for the proximal iron atom can be assumed.[51] Based on ENDOR measurements the oxidation state +3 could be excluded.[49,53] As a result of these investigations the oxidation state +1 was assumed and the different catalytic states were assigned. This led to a simple catalytic mechanism as shown in Scheme 5.[54]

1.2 Active Site Models

1.2.1 Early Research

Since the structure of the active site of the [FeFe]-hydrogenase was unveiled, numerous [2Fe2S] compounds were synthesized and investigated regarding their electrochemical features. Nevertheless, first model complexes were already known and well-investigated since the early 20th century, but without a structural relationship to the [FeFe]-hydrogenase. Already in 1928, Reihlen *et al.* described the formation of a [2Fe2S] cluster and alluded to a low-valent iron species.[55] In 1937, Hieber *et al.* synthesized the first complex of the type $[Fe_2(SR)_2(CO)_6]$ by the reaction of $Fe_2(CO)_9$ and propanethiol.[56] In the following years, especially Hieber,[56,57] Huttner,[58] and Seyferth[59] promoted the systematic research on low valent [2Fe2S] species. This unit was found to arise selectively from the reaction of a thiol and $Fe_2(CO)_9$ or $Fe_3(CO)_{12}$.[60] Magnetic susceptibility measurements and infrared spectroscopy studies were performed to unveil the properties of the diamagnetic [2Fe2S] units.[61] Scheme 6 displays a simplified depiction of the historical development of the synthetic and natural approaches towards [FeFe]-hydrogenase models.[62] The ancestor of the today-known hydrogenase might be FeS_x, as discussed by Wächtershäuser[63] and Weigand.[64] Structural evidence for a [2Fe2S] cluster compounds was first
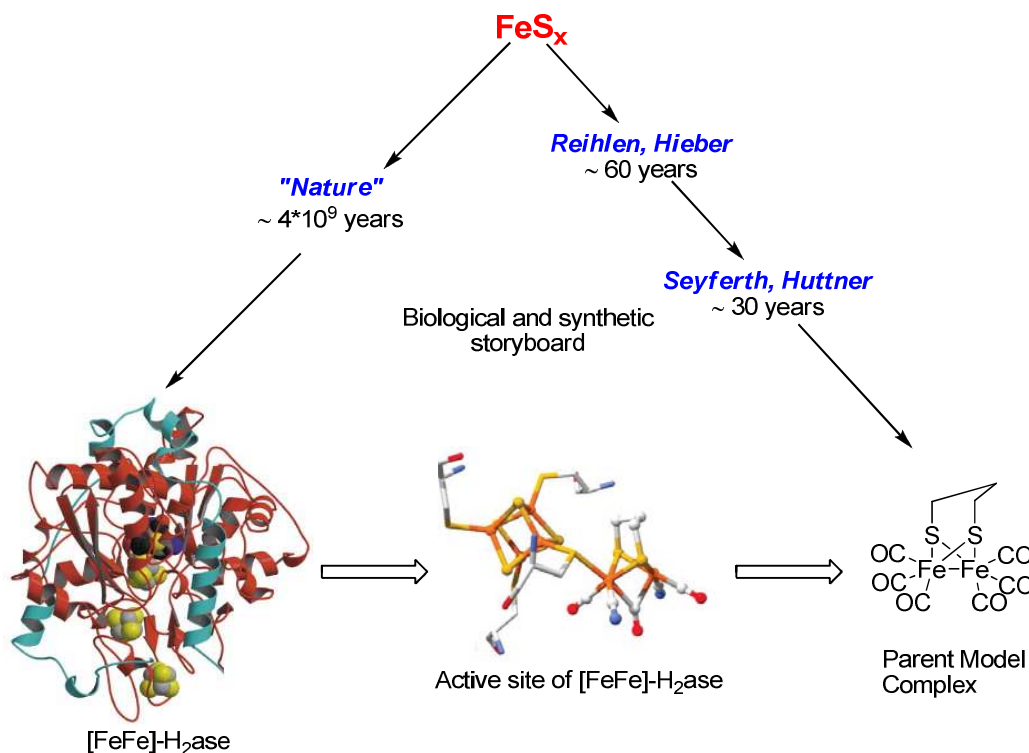
Scheme 6. Schematic depiction of the history of [2Fe2S] model complexes in contrast to the natural enzyme (in analogy to Ref. 62, structures depicted are from Ref. 33).

provided by Dahl *et al.* for [C$_2$H$_5$SFe(CO)$_3$]$_2$.[65] In agreement to the proposed structure of King *et al.*,[66] they disclosed the two isomers of [Fe$_2$(SC$_2$H$_5$)$_2$(CO)$_6$]. At the end of the 20th century, numerous publications dealing with [2Fe2S] complexes were known and the topic was found to be emaciated.[59,61,67,68] However, with the enlightenment of the structure of the active site of the [FeFe]-hydrogenase the chemistry of [2Fe2S] clusters revived and lead to a considerable number of publications.

Scheme 7 displays key areas and ideas for the synthetic approach towards the active site, namely electrocatalysis, solid state devices, terminal and bridging hydride species, mixed-valent systems, as well as H-cluster systems.[69]
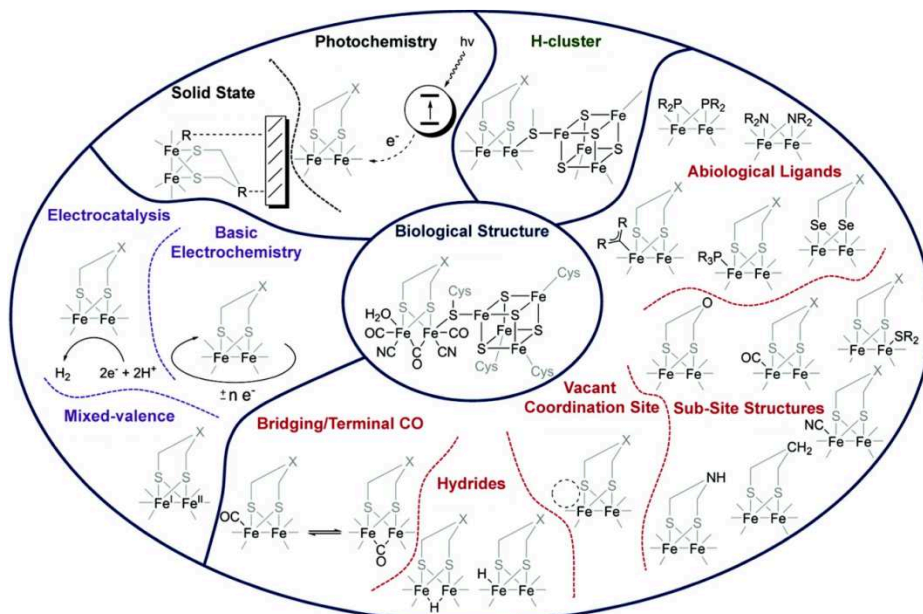
Scheme 7. Recent key areas of [FeFe]-hydrogenase research.[69]

1.2.2 Sub-Site Structures

With the reconnaissance of the active site structure, the [2Fe2S] complexes were seen from a different angle. First experiments with propane dithiolato diiron hexacarbonyl **4** (Scheme 8) demonstrated that an exchange of two CO by CN$^-$ is possible and gives water soluble dianions **8**, representing the structural key aspects of the active site.[70] In 2002 Rauchfuss *et al.* described the synthesis of the nitrogen containing analogue **5**, pointing out a possible influence of a pendant base towards the catalytic mechanism (which will be discussed in chapter 1.2.3) and leading to a parallel development of azadithiolato complexes.[70c]

In the following time, much effort was made to prepare disubstituted CN$^-$ complexes (**8**, **9**).[70,71] Access to the oxygen analogue **6** was described by Rauchfuss,[72] followed by Song and co-workers.[73] The structural features of the three different complexes **4**-**6** are similar and no eminent shift of the CO vibrations is visible in IR studies. In contrast to the hexacarbonyl complexes **4** and **6**, the azadithiolato (adt) hexacarbonyl complexes **5** can easily be protonated at the sp^2-NH function causing a significant change of the peak potential during cyclic voltammetry.[74] Still it has to be mentioned that the hexacarbonyl system **6** can be protonated with strong acids (*e.g.* HBF$_4$).[75] Recently, the sulphur homologue **7** was described by Weigand *et al.*[76] as well as Song *et al.*,[77]
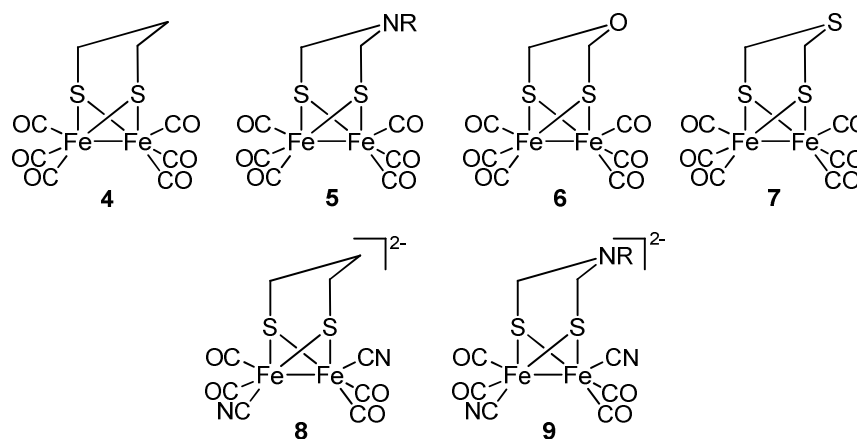
Scheme 8. Sub-site structures of the [FeFe]-hydrogenase.[70-73,76,77]

leading to a shift of the peak potential (electrochemical properties will be discussed in detail in chapter 1.3.3).

Modifications were carried out and afforded numerous model complexes for the [FeFe]-hydrogenase.

Especially the modification of the S-to-S linker and substitution reactions, such as exchange of CO by phosphine,[73b,78] nitrosyl,[79] *N*-heterocyclic carbene[80] and cyanide[70] ligands are the most common possibilities to modify the [2Fe2S] clusters. This leads to a wide range of possible derivatizations – *e.g.* erection of photoactive systems[81] or anchoring of the compounds to electrode surfaces or (electro-)polymers.[82]

1.2.3 Proton Relay Models/ Models of the Enzymatic Environment

As stated in chapter 1.2.2, the azadithiolato compound **5** entrenched a new and parallel development of the chemistry of [FeFe]-hydrogenase research, since it offers the possibility to establish a proton relay between the amino function and the distal iron atom (Scheme 9).[75,78g,83]

Initially, protonation occurs at the amino function and the proton is subsequently transferred to the distal iron centre. It has to be noted that the acidity of the distal iron and the amino function is almost identical (pK_a ~ 8 in acetonitrile for both moieties).[78g] However, the apposition of a proton to the amine function is kinetically favoured, even if the basicity of the Fe centres is increased *e.g.* by derivatization with trimethylphosphine.[84] There are also indices that instead of the amine function, the bridgehead sulphur atoms can be protonated.[76a,85]

Since the first synthesis of the azadithiolato complex **5**, numerous analogous complexes have been synthesized. Especially in the last years, the investigation of pendant base effects became more and more attractive and lead to a manageable amount of new compounds.[75,78g,86,89-92] Some intriguing examples are depicted in Scheme 10.

Two interesting and outstanding complexes (**10a** and **10b**) were obtained by derivatization of the amino function, whereby thiophene and furane was bound to the basic $Fe_2(CO)_6(adt)$ unit **5**.[86]
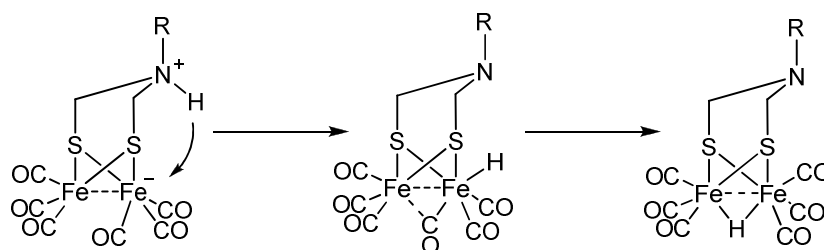
Scheme 9. Hypothetic tautomerisation of the reduced and rotated [2Fe2S] cluster.[83]

10a: X = O
10b: X = S

11

12

13a: X = NR
13b: X = O
13c: X = CH$_2$

14
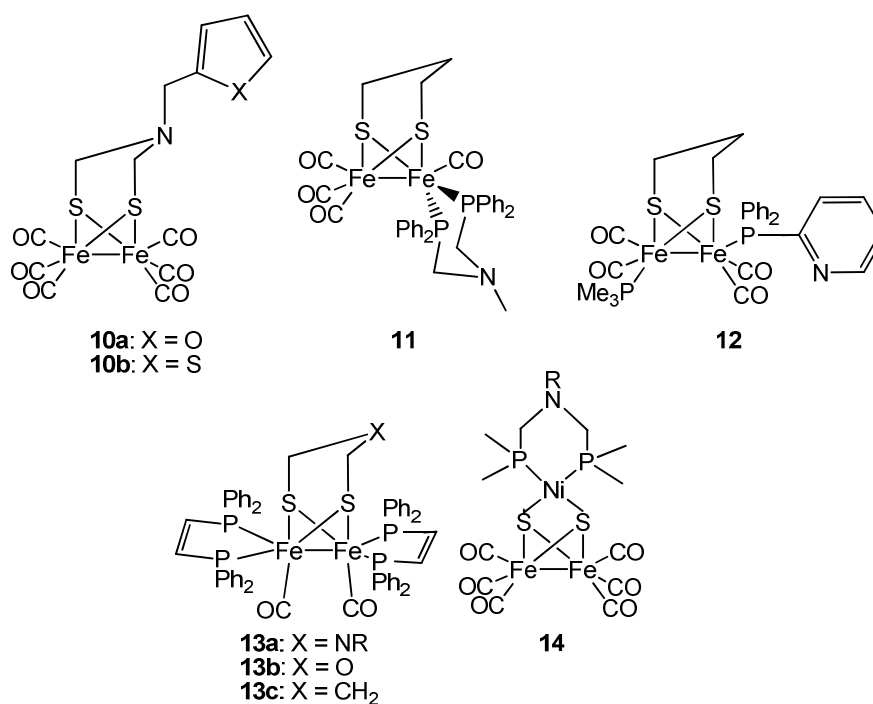
Scheme 10. Representative models for the structural proton relay models.[75,78g,86,89-92]

It was found that the formation of H_2 occurs at moderate potential (**10a**: -1.13 V, **10b**: -1.2 V) when using the strong acid $HClO_4$. Sun *et al.* assumed that a hyperconjugation of both the thiophene and furane ring has influence not only on the amine function, but also on the [2Fe2S] assembly.[86] Thus, the Fe-Fe bond has a higher electron density and can be easily protonated. The formation of the ammonium species is favoured as the proton is stabilized by the heteroatom of the furane and thiophene substituents *via* a hydrogen bond. However, a double protonated species could not be isolated and only the ammonium species were detected and isolated.

The twofold exchange of CO *via* phosphines in a mixed valent state leads to a "rotated state" and to a stabilization of terminal hydrides.[78g,87] These investigations led to a new class of compounds, implementing a chelating bisphosphine **11** or a monophosphine **12** with an internal base into the [2Fe2S] cluster. An efficient way to introduce a pendant base into the second coordination sphere of a metal was developed by DuBois *et al.* by using $(R_2PCH_2)_2NCH_3$.[88] It combines the chelating effect of a bisphosphine and a pendant base as described for the azadithiolato bridge in compound **5**. This concept was also used by Talarmin *et al.* to develop a new [FeFe]-hydrogenase model complex **11**.[89] They showed that the bisphosphine ligand occupies a chair conformation. Protonation with HBF_4 in acetone yields the ammonium species and results in a fluxional exchange of the basal and apical coordination site. No protonation of the iron site was observed. Nevertheless, complex **11** exhibits a differing behaviour in dichloromethane, since the chair configuration is alterable. In this solvent, a proton relay between the bisphosphine ligand and the iron centre could be established, whereby a bridging hydride was formed.[89] Similar properties were observed for complex **12**, where a trimethylphosphine and a pyridylphosphine are attached.[90] The latter can serve as a pendant base. The N(pyridine)···Fe distance is variable due to rotation around the Fe-P and P-C bonds. Using $HClO_4$, the Fe-Fe bond is protonated, forming a bridging hydride. In case of the absence of trimethylphosphine no protonation of the Fe-Fe bond is observed. It is noteworthy that compound **12** is one of the rare examples, where the Fe-Fe bond is protonated instead of the pendant base. In contrast to compound **12**, compound **13a** is able to form terminal hydrides:[75,78g] Initially the amine is protonated and due to the spatial vicinity to the distal iron atom and the steric demand of the *cis*-1,2-bis(diphenylphosphino)-ethylene (dppv) ligands, a terminal hydride is favoured. However, this terminal hydride is instable above -78 °C and rearranges, forming a bridging hydride. The same features were observed for compound **13b**. The heteroatom

in the S-to-S linker has a strong influence on the protonation of the iron centres, whereby the acidity of the iron centres of **13a-c** is almost the same. Unlike **13a**, the mere fact that **13c** and **13b** form no hydrides with weaker acids is an indication that an initial protonation of the amine has to be taken into account.[78g] In a second step, this proton is transferred to the iron centres. Interestingly, it was found that the ammonium tautomer is stabilized in methanol, whereas the hydride is stabilized in dichloromethane.[75] Using strong acids both the amine and the iron centre are protonated.[91] It is notable that under these conditions even the ether derivative **13b** is able to establish a proton relay between iron and the oxygen atom ($pK_a(R_2OH^+)$ ~ 4.7 to 1.6 in dichloromethane).[78g] In contrast to the previously described complexes, complex **14** bears a pendant base attached to a nickel ion. However, it was not verifiable that the amine function is able to establish a proton relay as was described before by taking up one proton.[92]

As already described in chapter 1.1.1, pendant base effects can also be caused by adjacent amino acids. It is therefore surprising that only a handful of amino acid containing [2Fe2S] complexes (**15-17**, Scheme 11) are described in literature[93,94,95] and even less is reported on their electrocatalytic properties.[95]
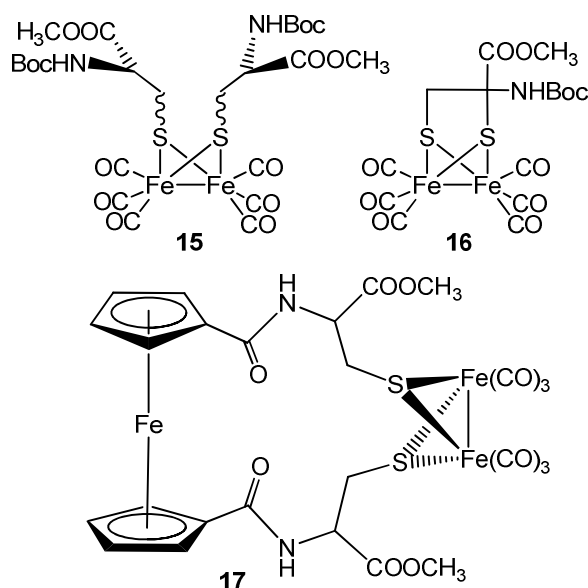
Scheme 11. Amino acid containing [2Fe2S] cluster.[93-95]

1.2.4 Bridging Carbonyls, [2Fe3S] Cluster Compounds and Mixed Valence Species

Besides the variation of the S to S linker, much effort was done to establish models with a bridging carbonyl ligand and a mixed valent $Fe^I Fe^{II}$ cluster to reflect the key features of the H_{ox} and H_{ox}^{CO} states (see also Chapter 1.1.2 and literature cited therein). Razavet *et al.* synthesized the first $Fe^I Fe^{II}$ assembly containing a bridging carbonyl ligand.[96] Thereby chemical and electrochemical oxidation affords an instable mixed valent [2Fe3S] dicyanide. Comparison of the infrared data with the natural system reveals good conformity. It was noticed that by increasing the electron density on the iron centres by coordination of nitriles or a combination of phosphines and cyanides, the stability of these complexes could be increased (compounds **18**-**29**, Scheme 12).[78i,78s,97] It is noteworthy that only one moderately stable dicyanide is known, containing a bridging carbonyl ligand (**30**, Scheme 13).[98] Up to now, this remains the only sub-site structure which possesses both a bridging carbonyl and two cyanides and is not supported by "non-biological ligands" (*e.g.* phosphines).
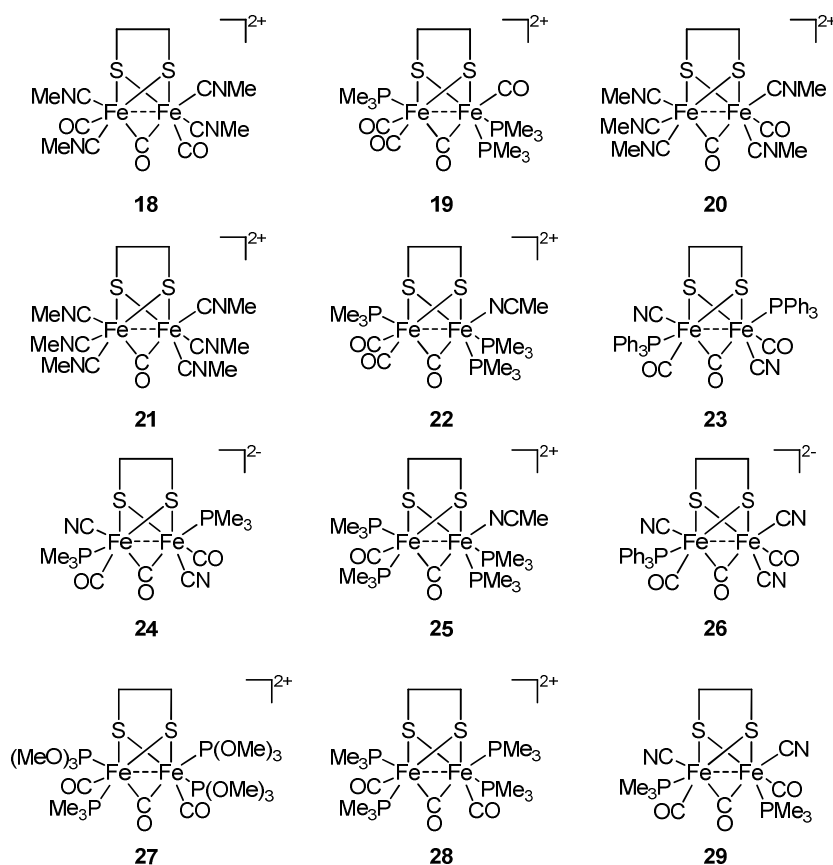
Scheme 12. Model complexes **18**-**29** with bridging or semibridging carbonyl ligands.
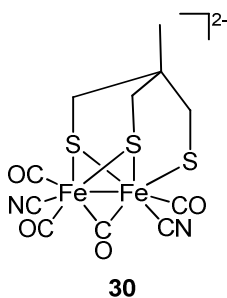
Scheme 13. Stable dicyanide complex **30** with a bridging CO and a [Fe2S3] cluster.[96]
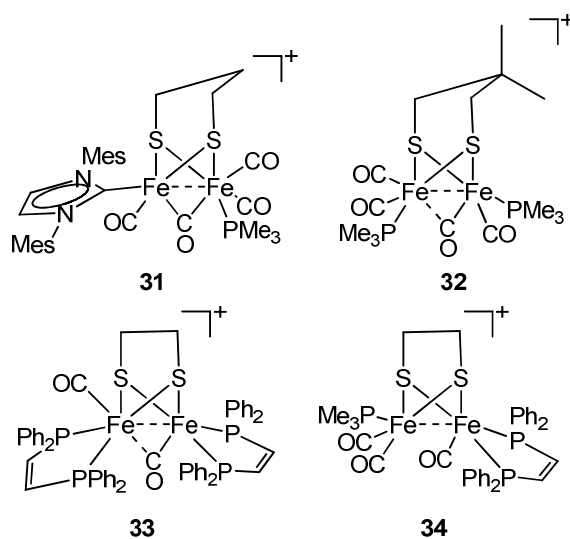
Scheme 14. Mixed valent [FeFe]-hydrogenase model complexes exhibiting the "rotated state".
78e,78h,80h,99

Recently, new syntheses and calculations showed that Fe^IFe^{II} complexes can be stabilized by combination of monophosphines and/or diphosphines and carbenes (**31-34**, Scheme 14) in non-coordinating solvents (*e.g.* dichloromethane).[78e,78f,78h,80e,80h,99]

It is fascinating that all these complexes exhibit a "rotated state" and are therefore in compliance with the natural H_{ox} state. This means that a bridging or semibridging carbonyl and a vacant coordination site on one iron atom with square pyramidal coordination geometry is present in the molecule.

Especially Darensbourg *et al.* emphasized the role of sterically bulky S-to-S linkers as a necessity for the stabilization of the "rotated state" since the vacant site is shielded by the enzymatic environment.[99] Furthermore, the increased electron density caused by the introduction of
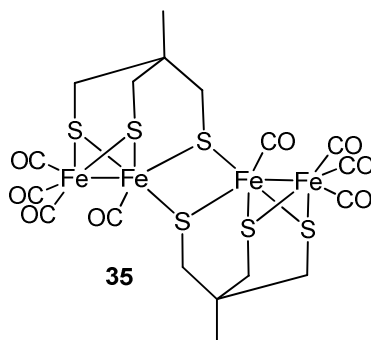
Scheme 15. Mixed-valent complex **35**.[101]
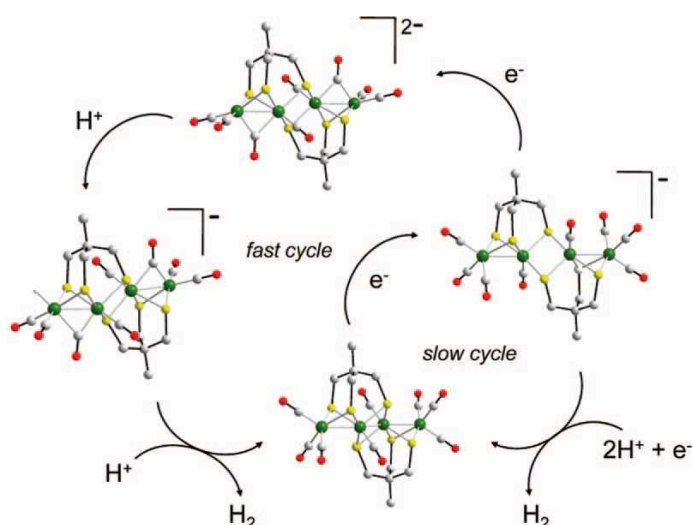
Scheme 16. Supposed mechanism for the formation of dihydrogen for compound **35**.[69]

carbenes (**31**) or phosphines (**32**-**34**) (Scheme 14) additionally engender stabilization, which is in accordance with DFT calculations by Hall *et al..*[100] In contrast to the previously discussed complexes, compound **35** (Scheme 15) exhibits a mixed-valent state without bridging carbonyls or a "rotated state".[101]

This compound was rather discussed as a Fe^{I}Fe^{II}···Fe^{II}Fe^I assembly. However, complex **35** is a very efficient catalyst for the formation of dihydrogen. During the proposed catalytic cycle (Scheme 16), a switching between terminal and bridging carbonyls and the formation of a "rotated state" is assumed. These assumptions are supported by DFT calculations and spectro-electrochemistry.[102] Remarkably, the rate constant of the rate-determining step is estimated to be higher than 2000 s^{-1} in comparison to 5 s^{-1}, described for [Fe$_2$(CO)$_6$(μ-pdt)] (**4**)[103] and 6000 s^{-1} for the natural enzyme.[19]

1.2.5 Protonation at the [2Fe2S] Sub-site

The [FeFe]-hydrogenase chemistry is closely related to the formation of hydrides, since terminal hydrides are present in the rotated state during the catalytic cycle.[103,104] However, in the model systems terminal hydrides are thermodynamically unstable and further functional groups are available for protonation.[75,78g] Beside the protonation of pendant bases (see chapter 1.2.3) or the protonation of cyanide ligands, the formation of bridging hydrides is most common. The formation of bridging hydrides is well investigated and reveals bridging hydrides in "non-rotated states".[105]

While treatment of the pdt-complex **4** with strong acids affords no protonation, substitution of a carbonyl by cyanide leads to the protonation of the cyanide.[78k] In contrast to these results the introduction of a neutral thioether selectively gives bridging hydrides.[106] Experiments with symmetrically disubstituted phosphine complexes revealed an increased basicity of the Fe-Fe bond and solely bridging hydrides.[67i,67j]

Using asymmetrical bisphosphine complexes, Talarmin *et al.* pointed out that at low temperatures a kinetically favoured hydride complex **36** is formed (Scheme 17).[87] At higher temperatures, a rearrangement to the thermodynamically stable bridging hydride is observable. Later on, investigations by Rauchfuss *et al.* showed that the kinetically favoured product is a terminal hydride (complex **37**, Scheme 18).[78g] Interestingly, it was possible to stabilize the terminal hydride by using two bis(diphenylphosphino)ethane ligands. The isomerisation reaction which generated the bridging hydride was very slow.
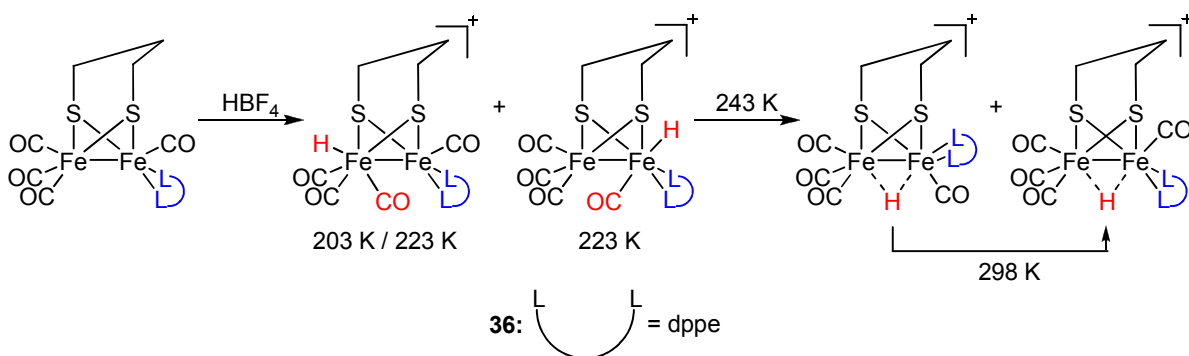
Scheme 17. Protonation behaviour of compound **36** at various temperatures.[87] The temperatures at which the different hydridic species were found are given below the ascertained hydride.
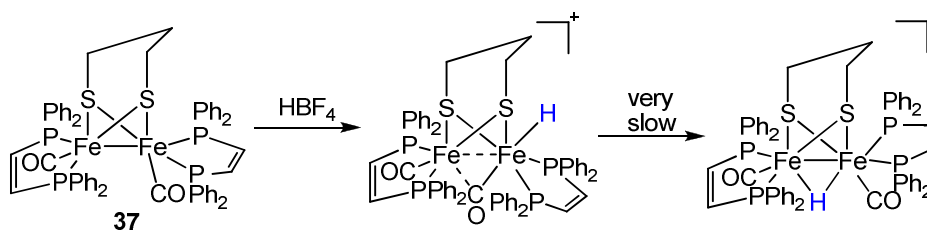
Scheme 18. Bis(diphenylphosphino)ethane complex **37** and protonation pathway.[78g]
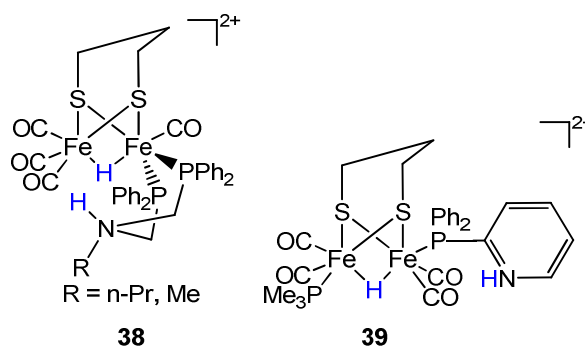
Scheme 19. Doubly protonated model complexes **38** and **39**.[89,90,107a]

Several systems exist, revealing both a protonation on a pendant base and a bridging hydride (complex **38**-**39**, Scheme 19).[78c,89,90,107]

As already described in chapter 1.2.3, it is assumed that these complexes are able to form dihydrogen *via* an internal proton relay. However, the role of bridging hydrides is peripheral for the formation of dihydrogen, since the release of dihydrogen is very slow and the reduction potential is more negative than for the corresponding terminal hydrides.[78g]

1.2.6 Resin Bound Complexes

Up to date, minor attention was directed towards the immobilization of [FeFe]-hydrogenase model complexes. However, this would be an attractive field of research if the model complexes could be attached to the electrode material, providing a fast electron transfer between the complex and the conducting regime.[69] This would provide the opportunity for the preparation of inexpensive electrodes for the development of dihydrogen, compared to the expensive and resource-limited platinum electrodes currently used.[108] These chemically modified electrodes would also enable the
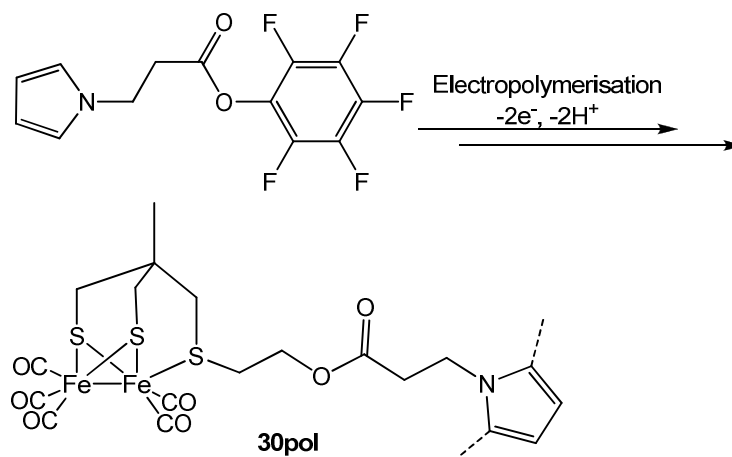
Scheme 20. Polypyrrole anchored [FeFe]-hydrogenase models derived from compound **30**.[82c]

catalytic reduction of protons to dihydrogen in water, which is normally not possible due to the insolubility of the model complexes in polar solvents (*e.g.* water).[82a]

Besides these plausible requirements, anchoring of the compounds to a resin is said to mimic the enzymatic surrounding.[82b] An increased specifity towards the substrate, a hindered aggregation and a specific H-bonding should be the result even though it has not been observed yet.

Anchoring on glassy carbon electrodes,[82a] TentalGel® resin beads[82b] and polypyrroles[82c] afforded electrochemically stable substances. However, only the latter one is stable in acidic conditions but allows hydrogen development only at unsatisfactory low potentials (**30pol**, Scheme 20). Nevertheless, due to a fast electron transfer through the electrode-bound polymer film and the stability under acidic conditions this is a promising attempt to replace platinum electrodes by anchored [FeFe]-hydrogenase models.

1.3 Electrocatalytic Mechanisms for the Dihydrogen Formation on Model Complexes

Since the structure of the active site is known, enhanced progress is observable on investigating the electrocatalytic properties of the enzyme and model complexes. However, up to now, model complexes exhibit different electrochemical features than reported for the natural system. Where the enzyme reduces protons at -0.4 V vs. SCE at pH = 7,[21] the artificial systems require lower pH values and strong acids (*e.g.* HBF$_4$, HOTs, TFA) to initiate development of dihydrogen at more

negative potentials.[109] Additionally, it is noteworthy that the natural systems are mainly based on water as solvent and the enzyme is anchored within a peptide matrix. In contrast, the electrocatalytic properties of model complexes are determined in less polar solvents (*e.g.* acetonitrile, dichloromethane) and these molecules are not surrounded by a peptide matrix.

Another crucial point of the mechanistic properties has to be stated. As discussed in literature, the enzyme is initially oxidized to form a [Fe^{II}Fe^{I}] state (Scheme 5, Chapter 1.1.4),[54] whereas model complexes exhibit irreversible oxidations and dihydrogen development is closely connected to the [Fe^{I}Fe^{0}] or [Fe^{0}Fe^{0}] state.[109]

Detailed electrochemical investigations of the [FeFe]-hydrogenase model complexes by Pickett *et al.*,[103,110] Talarmin *et al.*[104,111] and Weigand *et al.*[76a] disclose important key features of [FeFe]-hydrogenase model compounds. Therefore, the electrochemical properties of compounds **4**, **5** and **7** (Scheme 8, chapter 1.2.2) will be explained in detail. These compounds unveil important aspects of the electrochemistry of [FeFe]-hydrogenase model complexes and are therefore important for the understanding of modifications presented in this thesis.

For the following part, electrochemical reactions will be assigned with E and chemical reactions with C, in agreement with *IUPAC* notation.[112]

1.3.1 Electrochemistry of Fe$_2$(μ-pdt)(CO)$_6$

One fundamental complex to describe the electrocatalytical processes of model complexes is Fe$_2$(μ-pdt)(CO)$_6$ (**4**) (Scheme 8). Electrochemical investigations in acetonitrile using cyclic voltammetry reveal two irreversible processes at -1.3 V and -1.9 V.[78p] Both processes can be addicted to two irreversible one-electron reduction processes, since controlled potential coulometry exhibits 0.95 electrons per reduction step. Further confirmation was given by bulk electrolysis. The first potential step can be assigned to the [Fe^{I}Fe^{I}] → [Fe^{I}Fe^{0}] reduction process. The latter one was ascribed to the [Fe^{I}Fe^{0}] → [Fe^{0}Fe^{0}] process. Using acetic acid (pK$_a$ = 22.6 in acetonitrile[113]), the catalytic properties concerning the development of dihydrogen were investigated and afford the EECC mechanism (meaning that two electrochemical processes are followed by two chemical conversions), as displayed in Scheme 21. Following the two one-electron reductions, one proton is

$$Fe^I\text{-}Fe^I \xrightarrow{e^-} [Fe^0\text{-}Fe^I]^-$$
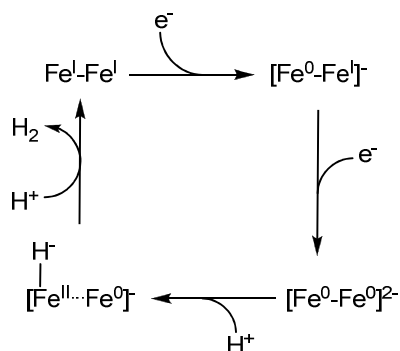
Scheme 21. Proposed EECC mechanism for dihydrogen development of Fe$_2$(μ-pdt)(CO)$_6$ (**4**).[78p]

added to the iron centre, forming a [Fe^{0}Fe^{II}-H$^-$] intermediate. Further addition of protons leads to the cleavage of dihydrogen and regeneration of the initial [Fe^{I}Fe^I] species

Slow decomposition was notable during the electrochemical investigations. Further studies showed that by using Fe$_2$(μ-pdt)(CO)$_5$L (L = acetonitrile or PrNH$_2$) a dimerization could be observed upon reduction in the absence of acid (Scheme 22).[110,114]

In contrast to the electrochemical properties in acetonitrile, investigations performed in THF revealed a different voltammogram. This study facilitated the detection of the decomposition products and an alternative process for the development of dihydrogen was observed in the presence of toluoylsulfonic acid (HOTs) (Scheme 23).[103] It was noticed that the one-electron reduction product reacted very fast with additional protons. The accrued compound **4H** was reduced at equal or more positive potential than **4** and forms **4H⁻**. Typically, such potential inversion is accompanied by structural rearrangement, making the transfer of a second electron thermodynamically easier.[115] Ongoing protonation can either result in direct cleavage of dihydrogen (Process II, Scheme 23) or in further protonation at higher concentrations of acid.
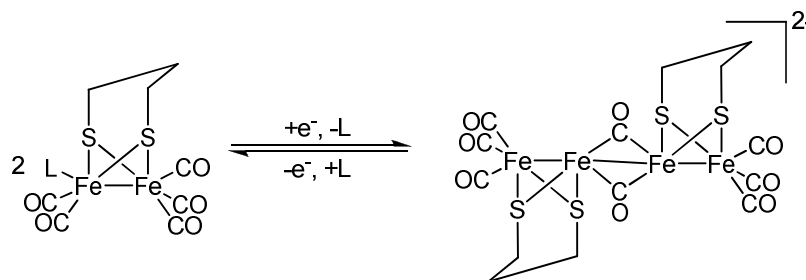
Scheme 22. Reductive dimerization of Fe$_2$(μ-pdt)(CO)$_5$L (L = acetonitrile or PrNH$_2$).[110]

The latter is leading to **4H$_2^-$** as reported for similar complexes.[78m] Tentatively, dihydrogen development can occur from the **4H$_2$** or the **4H$^-$** state. However, the latter one was excluded due to theoretical considerations. The following reduction of **4H$_2$** to **4H$_2^-$** was arbitrarily defined as one-electron reduction. The elimination of dihydrogen from the **4H$_2^-$** state finally leads to the regeneration of the **4$^-$** state (process II).

However, as already noticed by Darensbourg *et al.*,[78p] compound **4** decomposes during electrochemical investigations. This process was further investigated and lead to an additional mechanism, in which the decomposition of **4** can be best described by the formation of a dimer **4C^{2-}** and the monomer **4B**. The dimerization of **4H$_2^-$** would be an easy route towards this dimer. However digital simulations reveal no such process. The key intermediates are displayed in Scheme 24. In contrast, electrochemical reduction of **4** in the presence of CO exclusively gives rise to **4B** *via* **4$^-$**. In this process, two electrons are acquired, which could be confirmed by conventional and thin-layer coulometric techniques. *Via* one-electron reduction, **4** is conversed to **4$^-$** and **4C^{2-}**. Finally, **4CH$^-$** is converted to **4B** by a subsequent one-electron step, accompanied by a significant change of the molecule geometry which is detectable with IR spectroscopy.
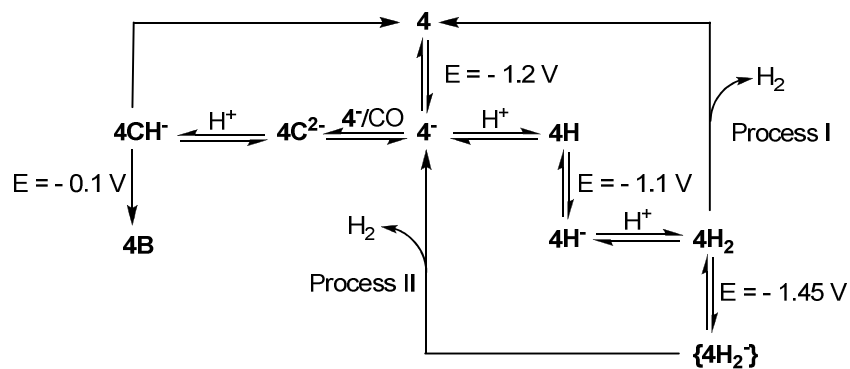
Scheme 23. Processes of Fe$_2$(μ-pdt)(CO)$_6$ (**4**) for the electrocatalytic proton reduction in THF/HOTs.[103]
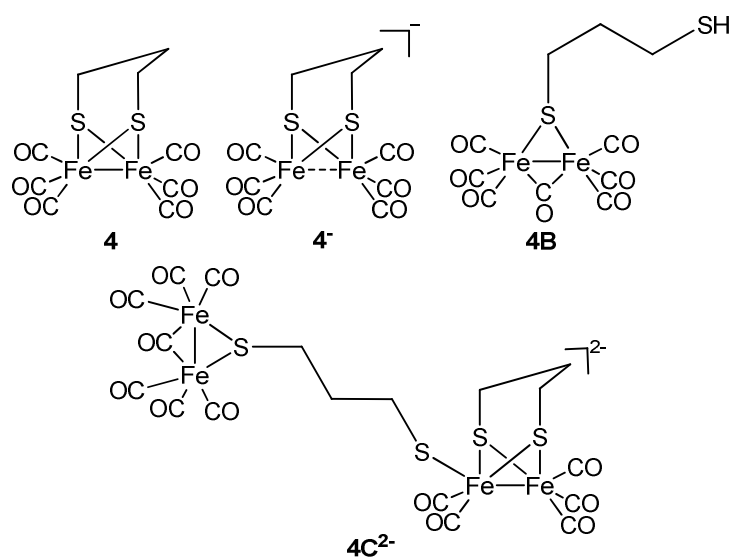
Scheme 24. Key intermediates of the electrocatalytic proton reduction of Fe$_2$(μ-pdt)(CO)$_6$ (**4**).

1.3.2 Electrochemistry of Fe$_2$(μ-adt)(CO)$_6$

In contrast to the previously discussed compound **4**, compound **5** reveals different electrocatalytic behaviour, since the pendant amino function can be protonated (Scheme 8 and Scheme 25). However, this capability is influenced by the strength of the acid.[78q] In weak acids (*e.g.* TFA, pK$_a$ = 12.65 in acetonitrile[113]) no protonation occurs. In this case the amine has no influence and the catalytic mechanism is an EECC mechanism as described in chapter 1.3.1 for compound **4**.

In the case of stronger acids, such as HBF$_4$/Et$_2$O (pK$_a$ = 0.1 in acetonitrile[113,116]) or HOTs (pK$_a$ = 8 in acetonitrile[113]), protonation of the pendant base was observed (Scheme 25).[104] Thereby a cation **5H⁺** is formed first and reduced at a more positive potential (ΔE ≈ 0.4 V) than the starting material **5**. In acetonitrile/Bu$_4$NPF$_6$ a reduction peak was found at -1.19 V for HBF$_4$ and -1.24 V for HOTs, respectively.[104] It was found that reduction of **5H⁺** to **5H$_2$** follows an ECE mechanism. In the first step **5H⁺** is reduced to **5H**, which affords a similar structure as **5**.[78t] This reduction is the starting point of two competing reactions. These chemical reactions can either be the release of hydrogen or a fast protonation, forming **5H$_2$⁺**. Alternatively, a bimolecular reaction of two molecules **5H** is conceivable and accompanied by the release of dihydrogen. The following reduction of **5H$_2$⁺** to **5H$_2$** is characterized by potential inversion. In the presence of low concentrations of acid, gradual release of dihydrogen was observed (Scheme 25, part A).

Thereby a bridging hydride is formed, which is slowly released from the [2Fe2S] cluster. The amino function is assumed to have a spectator's role.[111] However, in the presence of higher acid concentrations the release of dihydrogen is diminished and different consecutive reactions dependent on the acid strength appears. At even higher concentrations the current of this first reduction is independent of the amount of acid. A new acid-dependent reduction signal is visible at -1.4 V for HBF$_4$ and -1.6 V for HOTs. This indicates that at higher acid concentrations the reaction of **5H$_2$** to **5H$_3$** becomes preferred (Scheme 26). When using the strong acid HBF$_4$/Et$_2$O a further CE mechanism is visible, whereupon protonation of **5H$_2$** to **5H$_3$⁺** and subsequent reduction to **5H$_3$** is supposed. Opposed to the strong acid HBF$_4$/Et$_2$O, the weaker acid HOTs provokes an EC mechanism leading to **5H$_3$**. At this level, dihydrogen development can be observed and was also described for similar derivatives of **5**.[86,117,118] Gas chromatographic analyses of the components confirmed the formation
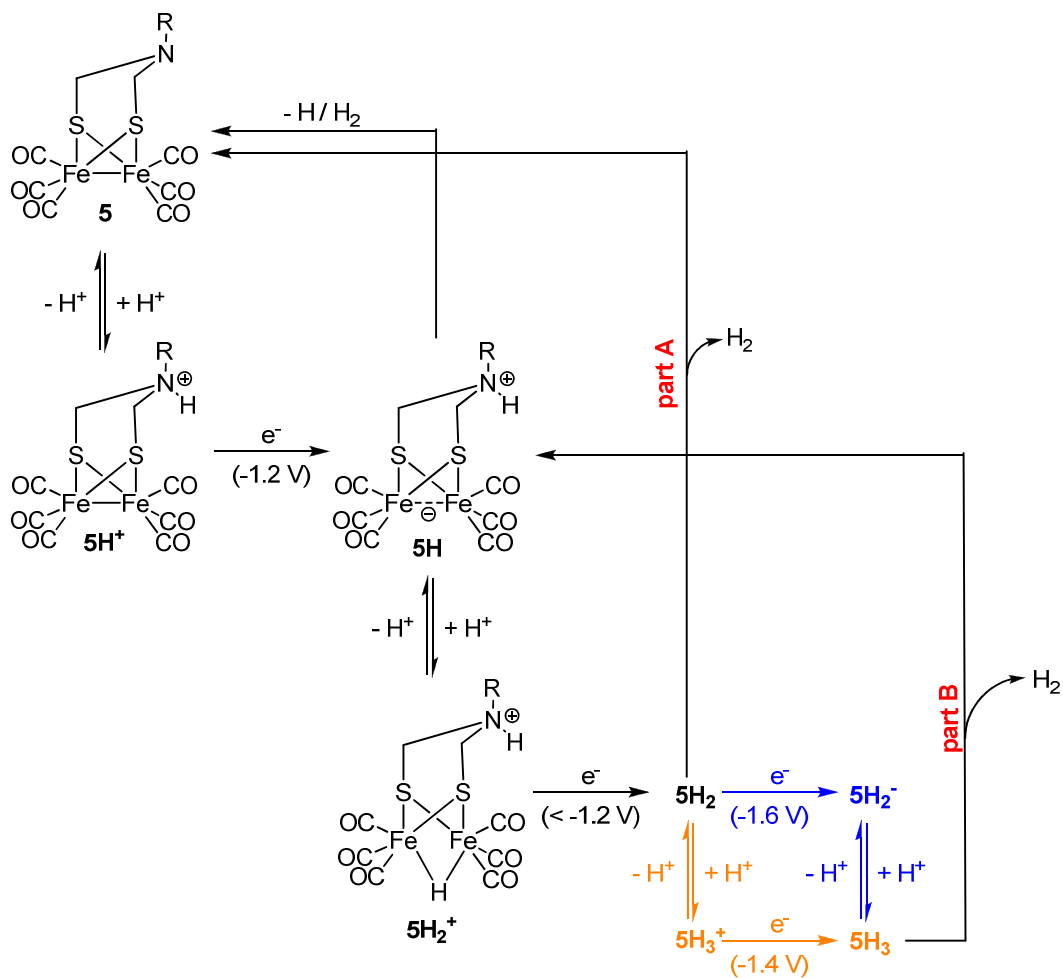
Scheme 25. Mechanistic details of the electrochemistry of compound **5** in the presence of HBF$_4$ (orange) and HOTs (blue).[104]
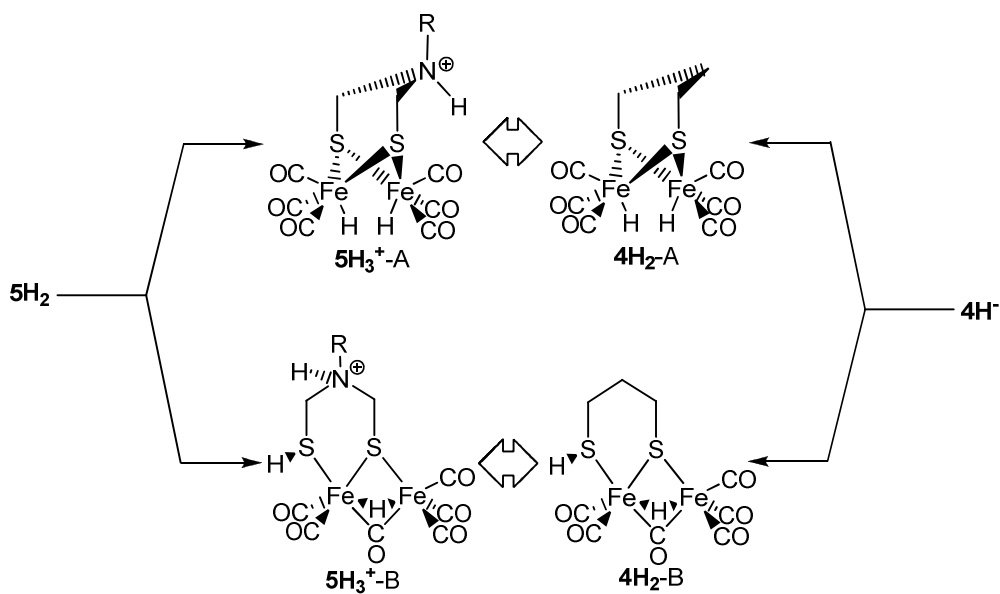
Scheme 26. Supposed electrochemical intermediates of compounds **4** and **5** in comparison.[111]

formation of dihydrogen under electrochemical conditions.[119,120]

Due to the supposed spectators' role of the amine function in the presence of HBF$_4$ it was assumed that both compounds **4** and **5** reveal comparable structural intermediates.[111] On the basis of DFT calculations these possible intermediates were assigned as depicted in Scheme 26.[121]

1.3.3 Electrochemistry of Fe$_2$(μ-sdt)(CO)$_6$

In contrast to the previously discussed electrochemical features, Weigand *et al.* used a weak acid, namely pivalic acid, to investigate the electrochemistry of compound **7** in acetonitrile (Scheme 8 and Scheme 27).[76a] Thereby, well-separated initial reduction signals, without beginning dihydrogen development was observed. In the absence of an acid an initial two-electron reduction process at -1.51 V was observed (Scheme 27, blue part). A potential inversion for the second transferred electron gives hint for structural reorganisation, which may occur due to a Fe-Fe bond cleavage. Further reduction affords the hitherto unknown decomposition product **Q**. In the presence of pivalic acid, the reduction process at -1.505 V reveals no influence of the acid towards the reduction potential (Scheme 27). However, reoxidation takes place in four different steps, depending on the concentration of pivalic acid. These oxidation signals appear due to a charge transfer reaction caused by the dissociation of pivalic acid. Thereby, different FeFe(HP)$_n$ complexes according to Scheme 27 are formed. As no dependency of the peak current on an increasing scan rate was observed, an irreversible reaction was assigned to these processes. This means that the effect of dissociation is negligible. The nature of the chemical interaction between the iron complexes and the acid is not yet clarified. Both, a strong hydrogen bond or a direct protonation can be considered. However, the latter one was excluded since pivalic acid is a rather weak acid in acetonitrile. It is also unlikely that more protons than required are coordinated to compensate negative charges. In contrast to these strongly bound dissociation complexes, a disparate coordination of additional pivalic acid was observed and $^-$FeFe$^-$(HP)$_2$[HP]$_n$ was formed. *Via* digital simulation the labile coordination of three pivalic acid molecules was found to be a suitable explanation. It was assumed that these interactions are caused by the sulphur atoms. As a dominating species $^-$FeFe$^-$(HP)$_2$ was assigned.

An additional reduction peak was observed at -2.2 V attributed to the formation of dihydrogen. But no reoxidation was visible in the potential area using different scan rates. Therefore, one reaction step for the release of dihydrogen is necessarily slow and irreversible.

A possible explanation for this behaviour is a concerted proton-electron-transfer of ⁻H-FeFe-H⁻ to ⁻H-FeFe (Scheme 27, violet part). At this stage dihydrogen is cleaved and the remaining iron species either decomposes or traces back to the catalytic dihydrogen development.

Compound **7** is one of the very rare examples which reveal an interaction of an acid with an iron-bound sulphur atom in [FeFe]-hydrogenase models. In contrast to literature reports,[103,104,111] the coordination of protons either *via* hydrogen bonds or as a direct bond was observed within cyclic voltammetry.
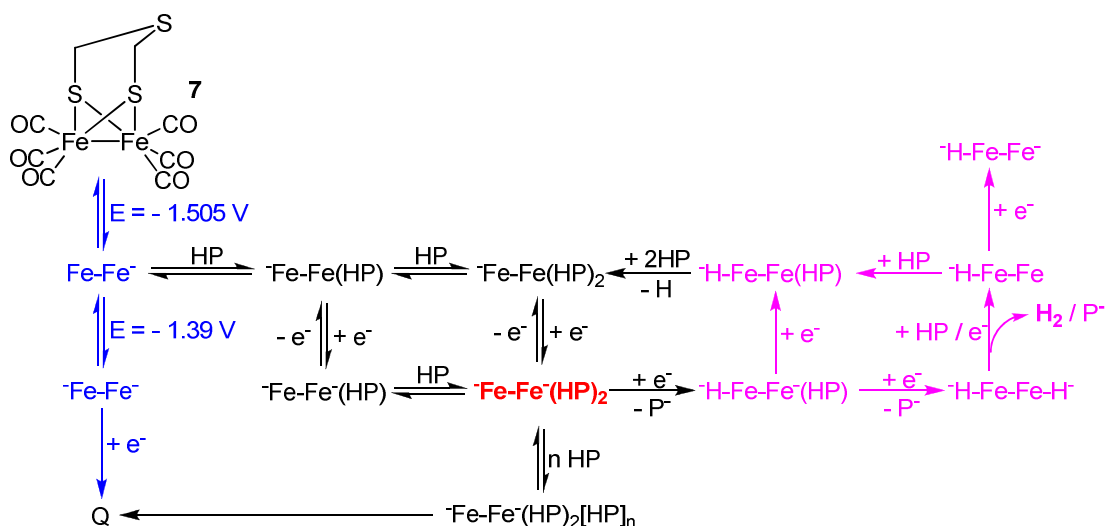
Scheme 27. Electrochemical reactions of compound **7**. The blue path exhibits the basic reactions without acid added. The complexation reactions with pivalic acid are shown in the black path as well as in the pink path, reflecting the formation of dihydrogen. The red species is set to be a pivotal compound of the reaction mechanism.[76a]

1.4 Analytical Methods

The bioinorganic relevance of these systems and the electrochemical behaviour of the [2Fe2S] cluster need some additional comments about the analytical methods used to reveal the structural and catalytical properties of the compounds as active site models.

1.4.1 General Analytical Methods

The [2Fe2S] centres exhibit a d^7-configuration with anti-ferromagnetic coupling and therefore allow the acquirement of NMR spectra. However, line broadening is observed in most cases due to small paramagnetic impurities resulting from slow degradation of the complexes in solution. This led to a difficult assignment of the signals.

In addition, mass spectrometry gives further proof of the complexes as the stepwise cleavage of C≡O groups is visible in the most cases. The basic investigations are completed by single crystal X-ray diffractometry and infrared (IR) spectroscopy. IR spectroscopy provides the unique C≡O vibrations between 1900 and 2150 cm^{-1}. These vibrations are very sensitive to changes of the electronic environment and are therefore applicable to evaluate the basicity of the iron atoms.[122] The smaller the basicity of the iron atoms, the higher the wavenumbers and *vice versa*. This behaviour allows an initial superficial estimation of the electrochemical behaviour.

1.4.2 Cyclic Voltammetry[123]

To evaluate the properties of the complexes concerning the electrocatalytical development of dihydrogen, cyclic voltammetry can be applied. The different electronic states as well as possible chemical reactions can be assumed using digital simulations. However, no full catalytic cycle can be established without further experiments (IR, spectro electrochemistry, isolation of the intermediates).

Cyclic voltammetry is a potentiostatic method, *i.e. I* = f(U) (I = current, U = voltage). The common experimental setup uses three electrodes, namely the working electrode, the counter or auxiliary electrode and the reference electrode, all connected to a potentiostat (Figure 5). The potentiostat induces a potential difference between the reference and the working electrode according to the

ohmic law ($U_0 \neq U_1$; $U = I \cdot R$).[124] This $I \cdot R$ drop is corrected by the counter electrode. The current (I) is displayed as a function of the potential (U_0).

The reference electrode is commonly an Ag/AgCl or a calomel half cell.[125] If a conventional reference electrode is not available (*e.g.* in the case of some organic solvents, salt leakage, junction potentials) "pseudo" reference electrodes such as platinum or silver wires with an internal standard (normally ferrocene) can be used.[126] The counter electrode is an inert electrode with a high surface area (platinum or titanium wire), whereas the working electrode is a disc electrode (*e.g.* glassy carbon, dropping or hanging mercury hemisphere) with a well-defined area.
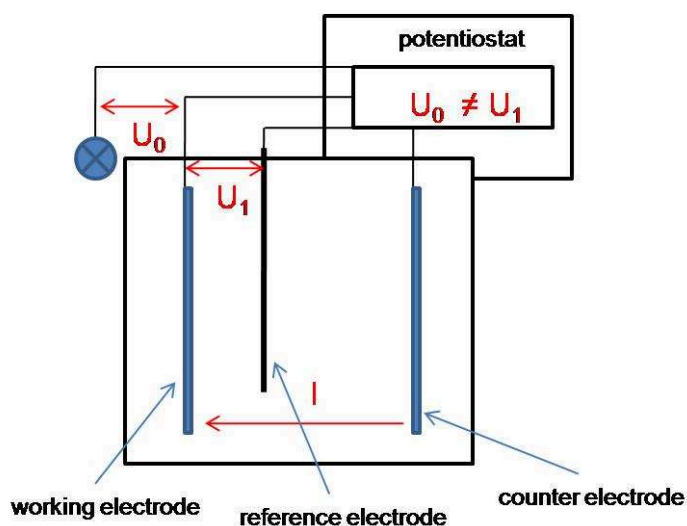
Figure 5. Simplified experimental setup for cyclic voltammetry.

1.5 Motivation

In the preceding sections the most important results of several years of research from different working groups were illustrated. These investigations lacked of the improvement in efficiency of hydrogenase model systems. Hitherto, electrocatalytic systems operate at potentials considerably more negative compared to that of the reversible proton/dihydrogen pair in nature and exhibit no or poor water solubility.

In this thesis, the improvement of the solubility of model complexes in water and the applicability of water as proton source will be investigated. Since the negative potential of dihydrogen development is dependent on various factors (solvent, acid strength, model complex), a relationship of different conditions and compounds will be shown to gain a little insight into the improvement of efficiency, which is partially an alchemistic proposition. Furthermore, especially the investigations of Windhager *et al.*[76] put forth new questions about the possibility of sulphur protonation and therefore about mechanistic details of dihydrogen formation. The question of sulphur protonation and protonation of pendant bases will therefore be in the focus of the presented work. A third selected issue will be the synthesis of [FeFe] model complexes which can be used for the anchoring of [FeFe] model complexes into membranes or vesicles. As a last topic of this thesis, the enthralling question about the importance of sulphur as bridgehead atom will be discussed.

To sum up, three main properties of the [2Fe2S] cluster will be altered (see Scheme 28):

i) the substitution pattern and the atom X in the S-to-S linker (green arrow)

ii) selenium and tellurium will be used as bridgehead atom instead of sulphur (yellow arrow)

iii) the CO ligands will be exchanged by cyanide and phosphine ligands (blue arrow).
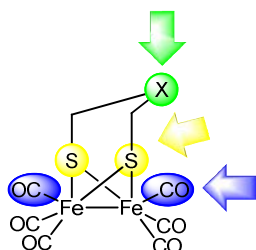
Scheme 28. Derivatizations planned in this thesis. The various coloured arrows display the different ways to alter the [2Fe2S] cluster.

2 Results and Discussions

2.1 Hydroxy Functionalized Model Compounds and Derivatives

2.1.1 Hydroxy and Ether Functionalized Complexes (*publication number 1*)

As shown in the introduction of this thesis, the electrochemistry of [2Fe2S] complexes is dependent on the nature of the S-to-S linker. Since those ligands were easily accessible and alterable, 1,3-dimercaptopropan-2-ol and *D,L*-1,4-dithiobutane-2,3-diol were reacted with $Fe_3(CO)_{12}$ to the respective iron complexes **40** and **41** (Figure 6), providing a modifiable group (*e.g.* esterification).[78w,127,128] This group should also be protonateable or reveal intermolecular interactions with protons through hydrogen bonds. Therefore it should be able to establish proton relays between the hydroxyl group and the iron centres.

Whereas in case of 1,3-dimercaptopropan-2-ol a [2Fe2S] cluster was formed (Figure 6),[127,128] complexation with *D,L*-1,4-dithiobutane-2,3-diol did not lead to the typical butterfly arrangement. Instead, two molecules of *D,L*-1,4-dithiobutane-2,3-diol connected two [2Fe2S] clusters, which is sparsely known in literature.[129] In contrast to the electrochemical features of **40**, compound **41** revealed two distinct redox potentials for the reduction $[Fe^IFe^I] \rightarrow [Fe^0Fe^I]$ at -1.51 and -1.63 V (Figure 7, Table 3). This splitting shows up the dissimilar electrochemical behaviour of both [2Fe2S] sub-sites, either caused by the different geometry or interactions of both sites.
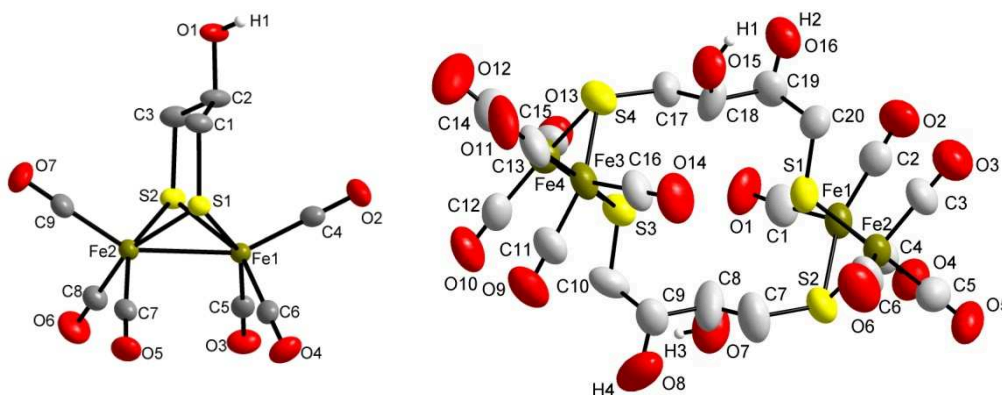
Figure 6. Hydroxy functionalized iron complexes **40** (left) and **41** (right) as models for the [FeFe]-hydrogenase.
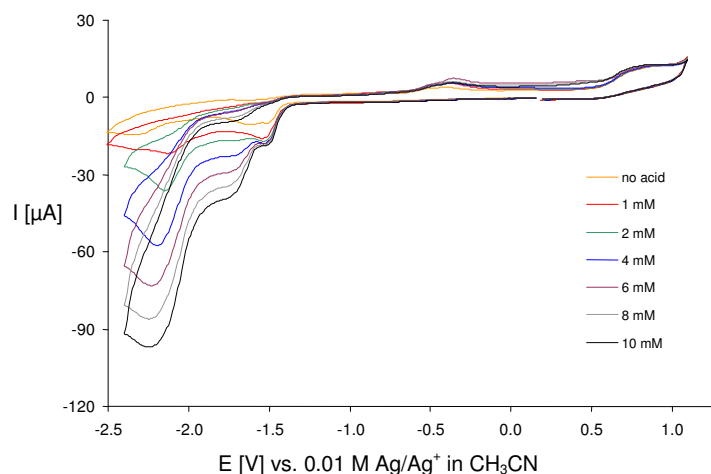
Figure 7. Cyclic voltammogram of compound **41** in the presence of 0,1-10 molar equivalents of acetic acid.

A further reduction to the all-Fe^0 level was found at -2.33 V. Upon addition of acid two new reduction processes were observed around -1.7 V and -2.2 V. These signals increased with each equivalent of acid added and can therefore be assigned to the electrocatalytic formation of dihydrogen. It is reasonable that the signal at -1.7 V insists dihydrogen development from the $[Fe^IFe^0]$ state and not from the $[Fe^0Fe^0]$ state (-2.2 V), which is scantily known for the formation of dihydrogen from acetic acid. Furthermore, large bond $S\text{-}CH_2\text{-}CH(OH)$ angles were noticed for compound **40**. DFT calculations revealed that these angles are a result of an increased p-character of the C-OH bond and a decreased p-character of the C-C bond in the S-to-S linker. As a result of this influence the C-C bonds are slightly shortened and the bonding angles are enlarged. Thus this structural property of compound **40** can be assigned to the rule of Bent.[130] However, it was assumed that the hydroxyl function has no influence on the electrocatalytic mechanism – this means that no protonation of the hydroxyl group and no subsequent shift of these protons to the iron centre occurs. Since hydrogen bonds are present in the solid state it is arguable that the apical arrangement of the hydroxyl group is only found in the crystal structure. A "flipping" of the S-to-S linker (exchange of basal and apical conformation of the hydroxyl group) cannot be excluded during the catalytic mechanism even though no change of the conformation was observed in NMR studies. To avoid these hydrogen bonds and to gain further

insight into the chemistry and electrochemistry of oxygen functionalized complexes, the methyl ether **44** (Scheme 29) was synthesized.

Initial attempts to react complex **40** with standard methylation reagents (*e.g.* methyliodide,[131] dimethylsulphate[132]) failed or were not applicable due to interfering reactions with the hexacarbonyl diiron unit. The desired complex was readily accessible *via* the reaction of $Fe_3(CO)_{12}$ and 1,3-dimercapto-2-methoxy-propan, which was synthesized according to Scheme 29. Initial oxymercuration of allylbromide with mercury(II)-acetate, followed by treatment with bromine and potassium bromide afforded 1,3-dibromo-2-methoxy-propane (**42**).[133] Reaction of compound **42** with potassium thioacetate yielded 1,3-dithioacetyl-2-methoxy-propane (**43**), which was deprotected with sodium hydroxide to give 1,3-dimercapto-2-methoxy-propane (**44**). Finally, compound **44** was reacted with $Fe_3(CO)_{12}$ whereby the hexacarbonyl diiron complex **45** was obtained in 76% yield.

Slow crystallization at 4 °C from pentane afforded crystals suitable for structure determination (Scheme 29). Compound **45** exhibits similar features as reported for **40** (*e.g.* coordination sphere, bonding angles and distances). Bond angles and distances are given in Table 2.

The electrocatalytic behaviour was investigated using cyclic voltammetry (Figure 8) and it was shown that the electrochemical properties are in good agreement to those found for compound **40** (Table 3).
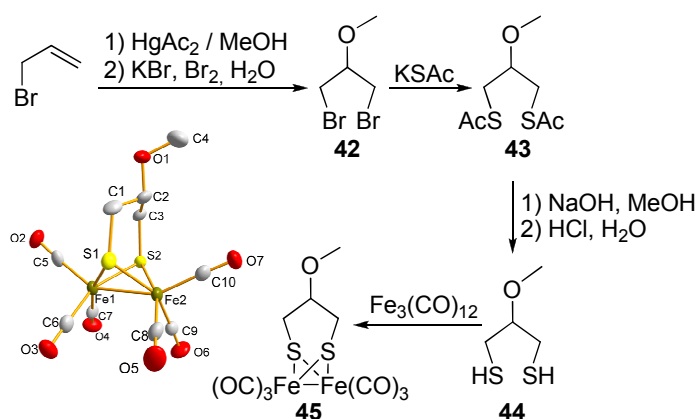
Scheme 29. Reaction pathway towards 1,3-dimercapto-2-methoxy-propane **44** and reaction with $Fe_3(CO)_{12}$. The crystal structure of compound **45** is depicted at 50% probability level (Hydrogen atoms are omitted for clarity).

Table 2. Selected bond angles [°] and distances [pm] of compound **45**.

Fe(1)-Fe(2)	251.78(14)	C(1)-C(2)	150.9(12)
Fe(1)-S(1)	225.0(2)	C(2)-C(3)	151.3(11)
Fe(2)-S(2)	225.90(19)	C(2)-O(1)	142.5(9)
S(1)-C(1)	182.4(8)	O(1)-C(4)	139.3(10)
S(2)-C(3)	181.7(7)		
S(1)-Fe(1)-S(2)	85.67(8)	C(1)-C(2)-C(3)	114.4(7)
S(1)-Fe(2)-S(2)	85.14(7)	C(1)-C(2)-O(1)	105.9(7)
S(1)-C(1)-C(2)	115.8(6)	C(2)-O(1)-C(4)	113.8(7)
S(2)-C(3)-C(2)	117.6(5)		
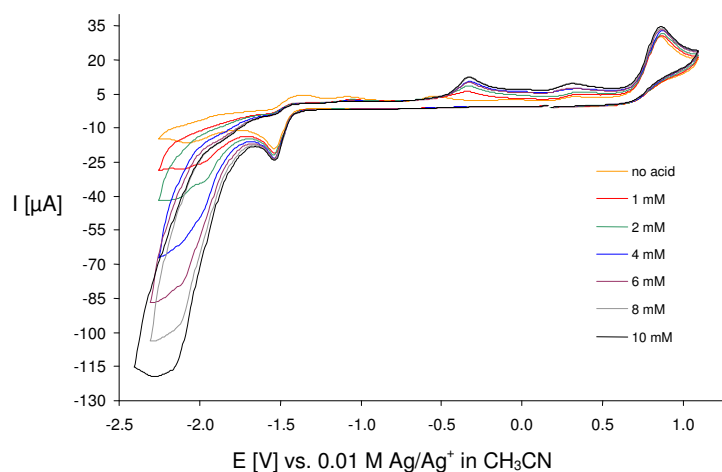
Figure 8. Cyclic voltammogram of compound **45** in the presence of 0,1-10 molar equivalents of acetic acid.

Table 3. Electrochemical data of compound **40** related complexes.

Compound[a]	E_{ox} [V] $Fe^IFe^I/Fe^{II}Fe^I$	E_{red} [V] Fe^IFe^I/Fe^0Fe^I	E_{red} [V] Fe^0Fe^I/Fe^0Fe^0
40[127]	+0.85[b]	−1.53 (E_{pc}), −1.42 (E_{pa})	-2.15[b]
41	+0.83[b]	−1.51[b] and −1.62[b]	−2.33[b]
45	+0.87[b]	−1.54[b]	−2.09[b]
49	+0.78[b]	−1.54[b]	−2.18[b]

[a] Potentials in V ± 0.01 *vs.* 0.01 M Ag/Ag$^+$ in CH$_3$CN in 0.10 M [*n*-Bu$_4$N][BF$_4$]/CH$_3$CN; [b] irreversible wave

Again an oxidation signal at +0.87 V and an one-electron reduction at -1.54 V was observed for $Fe^IFe^I \rightarrow Fe^0Fe^I$. A second reduction appeared at -2.09 V ($Fe^IFe^0 \rightarrow Fe^0Fe^0$), which was assigned to form the catalytically active species and became obvious by an increase of the current with each equivalent of added acid.

Since the etherification of the hydroxy group causes no significant change of the electrochemistry, the participation of the hydroxyl function of compound **40** in the catalytic cycle can be entirely excluded. Further modification was done, establishing compound **48**. According to the investigations of Darensbourg *et al.*, the implementation of an additional methyl group should constrain the "flipping" of the S-to-S linker.[99] Therefore, the synthesis of compound **49** was established (Scheme 30).

Via Finkelstein reaction, 2-methylallylchloride was conversed to 2-methylallylbromide (**46**).[134] The reaction of compound **46** with *N*-bromosuccinimide (NBS) and water gave compound **47** in moderate yield (47%).[135] Further reaction with sodium hydrogensulphide afforded the dimercapto compound **48**, which after reaction with $Fe_3(CO)_{12}$ yields the hexacarbonyl diiron complex **49**. However, electrochemical investigations on this system revealed no significant differences compared to **40** and **45** (Table 3, Figure 9). Since no change of the electrochemical properties was visible in the course of cyclic voltammetry, no proton relay between the hydroxyl group and the iron centre can be assumed under these conditions. This "inactivity" can be best explained by the low pK_a of acetic acid, which is not strong enough to protonate the hydroxyl group. But the use of stronger acids (*e.g.* HBF_4) would mislead this study since nature successfully uses weak acids and the aim is to model complexes with natural behaviour.
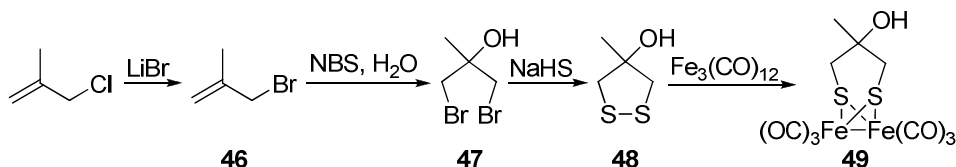
Scheme 30. Synthesis of 4-methyl-4-hydroxy-dithiolane **48**. Reaction of **48** with $Fe_3(CO)_{12}$ affords complex **49**.
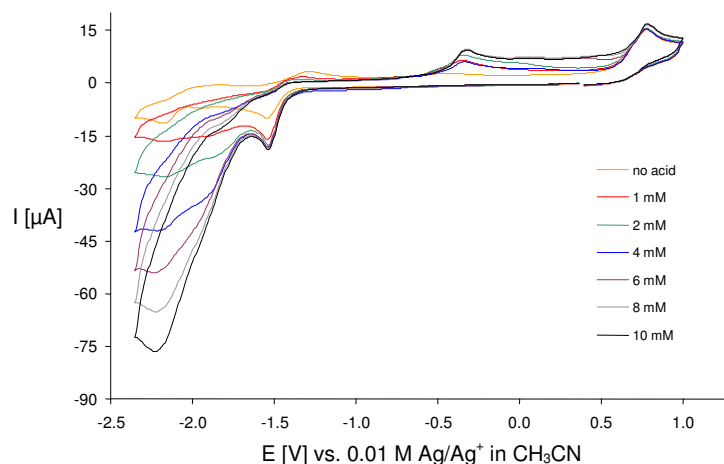
Figure 9. Cyclic voltammetry of compound **49** in the presence of 0,1-10 molar equivalents of acetic acid.

2.1.2 Aromatic Esters

Since all three complexes (**40**, **45** and **49**) reveal similar properties, reactions on hydroxyl functionalized complexes were exclusively studied on compound **40** due to its straight forward accessibility. In course of this study, three different methods were used for the esterification of the hydroxyl group in complex **40** (Scheme 31).

In continuation of the investigation of hydroxyl functionalized complexes, complex **40** was reacted with 1,3,5-benzenetricarbonyl trichloride and terephtalic acid (Scheme 32).
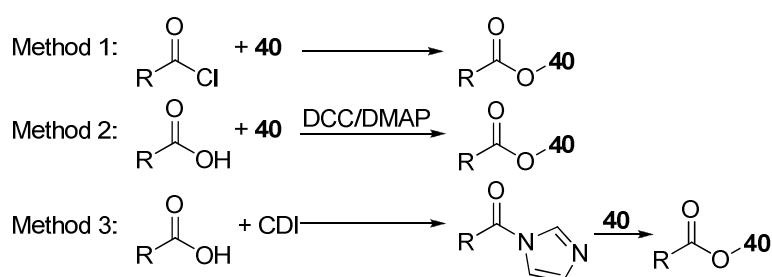
Scheme 31. Methods for esterification of complex **40** with *i*) a carbonyl chloride (Method 1);[136] *ii*) a carboxylic acid using the coupling reagents dicyclohexyl carbodiimide (DCC) or 1-(3-dimethylaminopropyl)-3-ethylcarbodiimide hydrochloride (EDC) and 4-dimethylaminopyridine (DMAP) or 1-hydroxybenzotriazol (HOBt)[137] (Method 2); *iii*) an activated carboxylic acid using carbonyl diimidazole (CDI) (Method 3).[138]

The ability to shuffle electrons *via* the S-to-S linker was thereby in the focus. It was calculated that the s-character of the C-C bond lengths would be increased.[127] This would suggest that an electron transfer along the C-C single bond should be feasible. The reaction of 1,3,5-benzenetricarbonyl trichloride with complex **40** according to method 1 exclusively affords complex **50** (Scheme 32). In contrast to this reaction, terephtalic acid was reacted according to method 2 and afforded complex **51** as well as **52**. It is notable that even with excess of compound **40**, complex **52** was isolated as major product.

Complex **50** was investigated *via* cyclic voltammetry (Table 4). An interaction between the three metal fragments should result in three different reduction potentials, since every metal core is subject to the influence of the others: The reduction of one metal core leads to a change in the reduction potential of the others.

However, this behaviour was not observed and electron transfer along the S-to-S linker has to be excluded. On the contrary, two irreversible reduction processes and an irreversible oxidation process were observed in the course of CV measurements. The addition of acetic acid once again led to the formation of dihydrogen. This means that the electrochemical properties are solely a result of the metal fragment and substitutes on the S-to-S linker have no influences on the electrochemical properties.
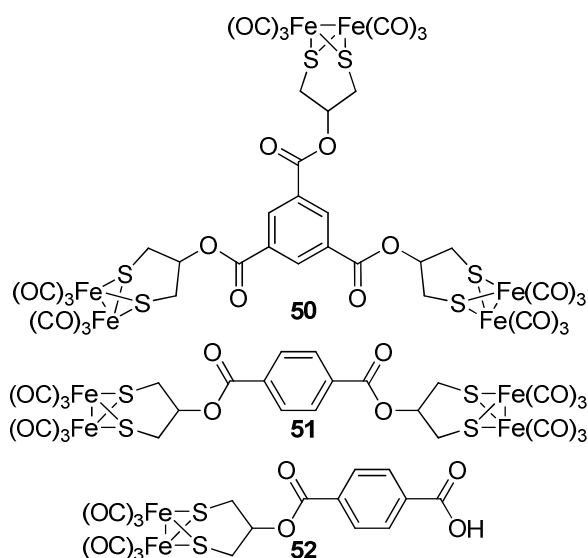
Scheme 32. Polynuclear complexes **50** and **51** as well as the mono-substituted "side product" **52**.

Table 4. Electrochemical data of compound **50**.

Compound[a]	E_{ox} [V] $Fe^IFe^I/Fe^{II}Fe^I$	E_{red} [V] Fe^IFe^I/Fe^0Fe^I	E_{red} [V] Fe^0Fe^I/Fe^0Fe^0
40[127]	$+0.85^b$	-1.53 (E_{pc}), -1.42 (E_{pa})	-2.15^b
50	$+0.92^b$	-1.47^b	-2.18^b

[a] Potentials in V ± 0.01 *vs.* 0.01 M Ag/Ag$^+$ in CH_3CN in 0.10 M [*n*-Bu$_4$N][BF$_4$]/CH$_3$CN; [b] irreversible wave

2.1.3 Sugar Derived Complexes (*publication number 2*)

Due to the isolatedness of the different metal cores, complex **40** is an ideal molecule to investigate properties evoked by substitutes attached to the hydroxyl functionalized S-to-S linker.

This enables the investigation of the [2Fe2E] core (E = S, Se) in an aqueous solution. Therefore, the ligand systems **54** and **57** were established and reaction of Fe$_3$(CO)$_{12}$ with **54** and **57**, respectively, afforded the acetyl-protected complexes **55** and **58** (Scheme 33).[139] As shown in Table 5, modification of the S-to-S linker with acetyl-protected glucose did not lead to significant changes of the electrochemical features. However, deprotection of **55** with sodium methanolate lead to the water soluble complex **56**. Since the purification of **55** was aggravated, in further experiments **55** and **58** were deprotected *in situ* during cyclic voltammetry. Both experiments exhibited similar changes of the electrochemical behaviour (*e.g.* shape of the CV). It was assumed that the deprotection of the sugar also takes place in the case of complex **58**. Upon addition of acid or water an increase of the catalytic current was observed in both cases. This shows that water can serve as both, solvent and proton distributor. Unexpectedly, the deprotected selenium compound reveals higher stability in water, compared to its respective sulphur compound **56**. This effect can be explained by the more electropositive selenium which increases the electron density on the iron atoms. This leads to a stronger π-back bonding of the iron centres to the CO ligands and to a stabilization of both the CO ligands (minimized electrophilic character of the CO ligands) and the iron atoms. This was further confirmed by a bathochromic shift of the CO ligand signals in the IR spectrum of **58**.[139]
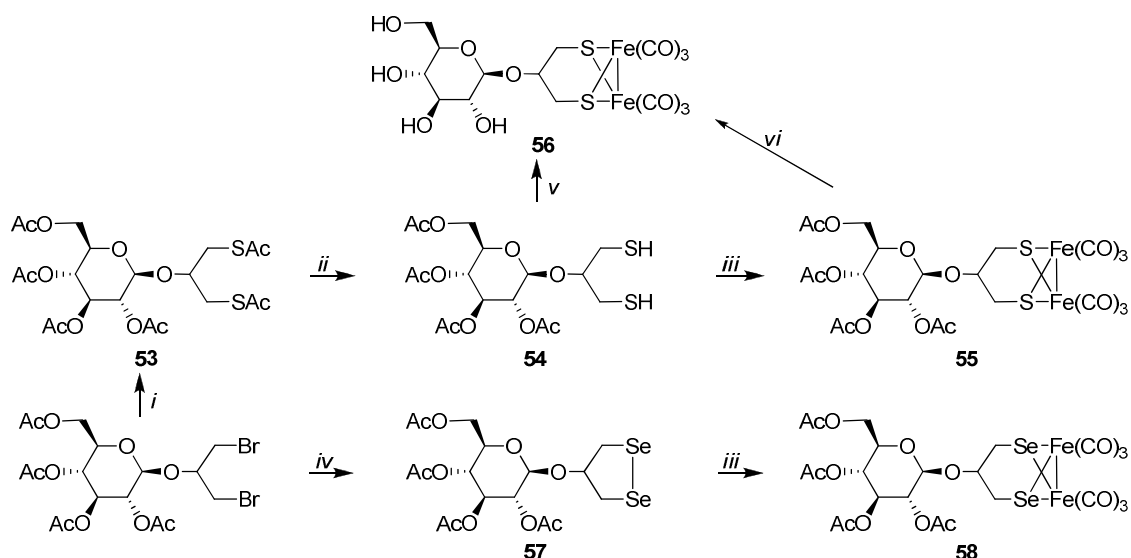
Scheme 33. Synthesis of the sugar substituted iron carbonyl complexes; *i*) KSAc, acetone; *ii*) $N_2H_4 \cdot 2H_2O$/ HOAc; *iii*) $Fe_3(CO)_{12}$, toluene; *iv*) Na_2Se_2, ethanol/ THF, *v*) 1. NaOMe, 2. $Fe_3(CO)_{12}$, *vi*) NaOMe.

Table 5. Electrochemical data of the glucose derivatives **55** and **58** as well as the related hydroxyl functionalized [2Fe2E] (E = S, Se) complexes.

Compound	E_{ox} [V] $Fe^IFe^I/Fe^{II}Fe^I$	E_{red} [V] Fe^IFe^I/Fe^0Fe^I	E_{red} [V] Fe^0Fe^I/Fe^0Fe^0
40[127,a]	+0.85[b]	-1.53 (E_{pc}); -1.42 (E_{pa})	-2.15[b]
$Fe_2[Se_2C_3H_5OH)](CO)_6$[140]	+0.7[b]	-1.63 (E_{pc}); -1.53 (E_{pa})	-2.30[b]
55[a]	+1.09	- 1.50 (E_{pc}); -1.39 (E_{pa})	-1.89 (E_{pc})
58[a]	+0.97	- 1.46 (E_{pc}); - 1.36 (E_{pa})	- 2.02 (E_{pc})

[a] Potentials in V ± 0.01 *vs.* 0.01 M Ag/Ag$^+$ in CH_3CN in 0.10 M [n-Bu$_4$N][BF$_4$]/CH_3CN;

[b] irreversible wave

Due to the promising solubility properties of the complexes **55** and **58**, the synthetic route should be simplified. Thereby, the direct reaction of complex **40** and a reactive sugar derivative was intended. However, attempts to generate the desired complexes *via* the trichloracetimidate method[141] or the Königs-Knorr method[142] (reaction of 2,3,4,6-tetra-*O*-acetyl-*α*-D-glucopyranosylbromide, silver carbonate and compound **40**) failed. No conversion of the starting complex **40** was observed.

2.1.4 Membrane Bound Complexes

Since it was shown that complex **56** and its selenium analogue **58** reveal solubility in water with moderate stability towards water during the electrochemical reduction, the implementation of the basic complex **40** into vesicles or membranes appears to be a new challenge. In contrast to the sugar based derivatives of **55** and **58**, this approach should offer a [2Fe2S] cluster which is protected against environmental influences, as discussed in chapter 1.2.6. Furthermore, the permeability of membranes can be modified by implementation of different membrane proteins, peptides or polymers. Thereby, the exchange of reactants throughout the membrane should be improved, affording a controllable conversion rate in the inner sphere of membranes or vesicles.[143]

Suitable membrane models would be accessible by dispersion of liposomes (derived from phospholipids) in aqueous solutions. Uniform vesicles in defined sizes can be obtained by extrusion.[144] These vesicles afford semi-permeable membranes and can be best described as synthetic models for natural occurring cell membranes. The combination of a membrane with a [FeFe]-hydrogenase model would be a suitable system for a micro-reactor which allows the formation of dihydrogen.

For this purpose, the [FeFe]-hydrogenase models have to be derivatized in such a way that the resulting molecules are able to either form liposomes by themselves or to allow an insertion of the model system into vesicles. In a further going step the outer hull of the vesicle has to be modified to reveal a solely membrane standing hydrogenase situated inside the vesicle (Figure 10, right).

This approach is closely related to natural systems and similar "artificial" systems are already known in literature (*e.g.* the formation of GFP - green fluorescent protein - in liposomes).[145] Furthermore, a primary metabolism was proceeded on the assumptions of Madigan *et al.* throughout a primitive cell membrane (Figure 10, left)[146] and exhibits good coincidence with the desired liposomal system (Figure 10, right). The liposomal bound [FeFe]-hydrogenase models should be a suitable approach to display the properties of a primitive membrane standing and dihydrogen developing enzyme.
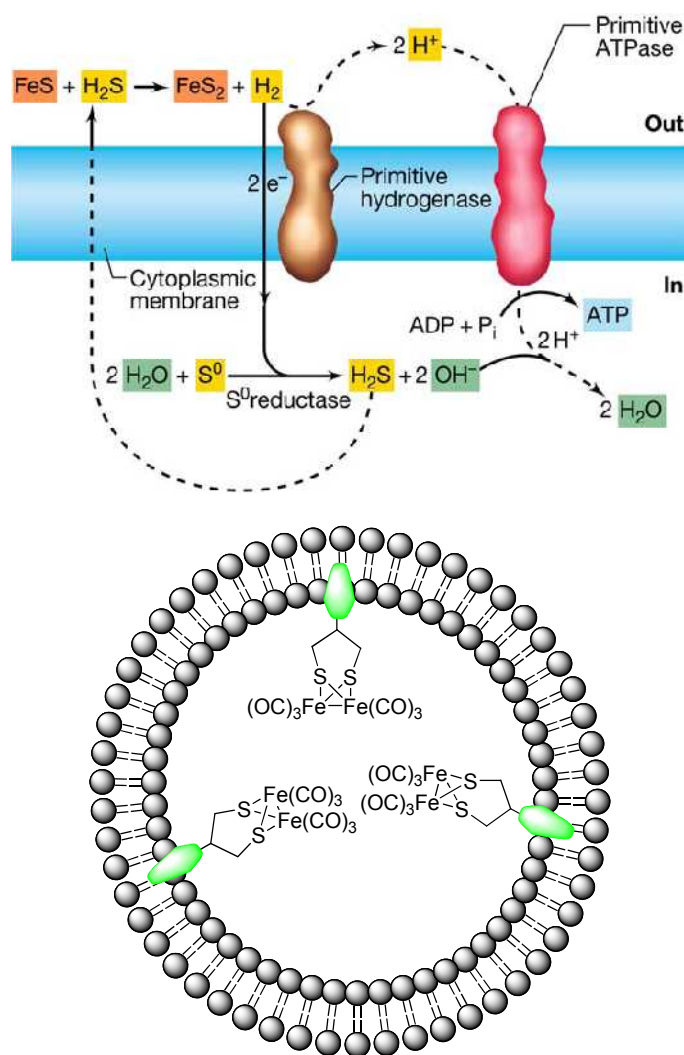
Figure 10. Primitive cell membrane metabolism according to Madigan *et al.* (top)[146] and illustration of a desired membrane-standing [FeFe]-hydrogenase model within the core of a vesicle (bottom).

Also the behaviour of these molecules towards biological systems is interesting, since researchers commenced the investigation of CO containing molecules as medicinal agents.[147] CO is known as cytotoxin and messenger substance.[148] If it would be possible to detach CO ligands from the metal core within the diseased cell this would cause cell death. However, the lack of solubility and stability of $2Fe2S(CO)_6$ fragments in aqueous systems make them unamenable for the use as a medicinal agent. The encapsulation in liposomes should offer
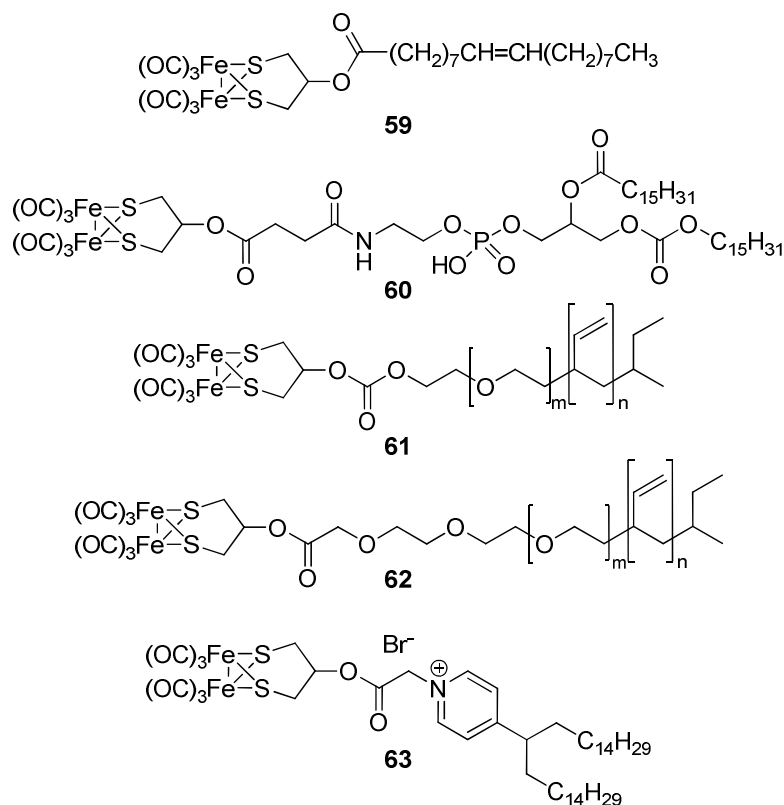
Scheme 34. Synthesized lipophilic systems (**59**, **61**, **62** and **63**) as well as the desired complex **60**.

both, an increased solubility in physiological solutions and a notably improved stabilization with coinstantaneous reduced toxicity. This concept is proven, encapsulated drugs are already in daily use and reveal a prolonged bloodstream circulation, higher efficacy and lowered toxicity (*e.g.* Caelyx®,[149] AmBisome®,[150] Depocyte®[151]).

For these reasons, complex **40** was modified and linked to lipophilic molecules in collaboration with the working groups of Prof. S. Förster (Hamburg) and Prof. D. Gabel (Bremen) (Scheme 34).

Four different chemical systems were chosen for this approach, all of them offering long lipophilic chains.

i) Since oleic acid is known to form vesicles by itself,[152] it was linked to complex **40** *via* the chloride method 1 (Scheme 31). Reaction of complex **40** with excess of oleic acid chloride (2.5 eq.) in dichloromethane afforded complex **59** in 75 % yield. The obtained compound was verified *via* NMR spectroscopy and mass spectrometry. Incorporation of complex **59** into palmityloleylphosphatidylcholine (POPC) liposomes was performed *via* film hydration method[153]

in the group of Prof. A. Fahr. Extrusion of these particles afforded vesicles with an average diameter of 100 nm. The amount of incorporated complex varied between 15 and 31% and was found to be dependent on the concentration of complex **59** and POPC in the stock solutions. The maximum loading was obtained when an 8 mM POPC (80 mol%) stock solution was combined with a 2 mM solution of complex **59** (20 mol%), dissolved in chloroform. In contrast to oleic acid, complex **59** is not able to form micellar aggregations. However, the behaviour of this complex in lipidic bilayers was comparable to pure oleic acid. These results concluded a heavily diminished amphiphilic character of compound **59** and give an explanation for the small loading. These initial results are far from satisfaction since the low "loading" would complicate further investigations on this system.

ii) To increase the amphiphilic character of the complexes, cholesterin-hemisuccinat (dppe-suc) was reacted with complex **40** to afford complex **60**. However, reaction of these two species according to method 2 did not result in the desired product. Neither the use of DCC/DMAP nor the use of EDC/HOBt afforded complex **60**. Only a DCC-dppe-suc or an EDC-dppe-suc adduct was found *via* mass spectrometry and suggested therefore a reaction on the phosphorous part and not on the carboxylic acid part. The starting complex could be re-isolated in almost quantitative amount. Unfortunately, dppe-suc-chloride is not accessible. A suitable way for the functionalization of dppe-suc would be method 3, where the carboxylic acid initially reacts with an excess of CDI. The formed imidazole-compound affords similar reactivity as described for acid chlorides and should react with complex **40** to give **60**. However, during the preparation, Fahr *et al.* noticed that the POPC liposomes are not stable in the presence of iron(II) and iron(III) compounds. Further reactions with this expensive system were therefore aborted, since an *in situ* formed Fe^IFe^{II} or $Fe^{II}Fe^{II}$ species is present during cyclic voltammetry.

iii) An alternative to liposomes are polymersomes. In contrast to liposomes, the formed polymersomes provide increased stability towards temperature, pressure and different pH values. A suitable system (PB-PEO2, Scheme 35) was provided by the group of Prof. Förster (Hamburg) and co-workers.

R = -H, -(CH$_2$)$_2$OCH$_2$COOH
n = 33 ; m = 27
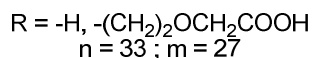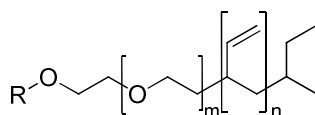
Scheme 35. PB-PEO2 (R = H) and the carboxylic acid (R = CH$_2$COOH) derivative used for synthesis of the polymer attached complexes **61** and **62**.

Formation of Carbonate **61**:
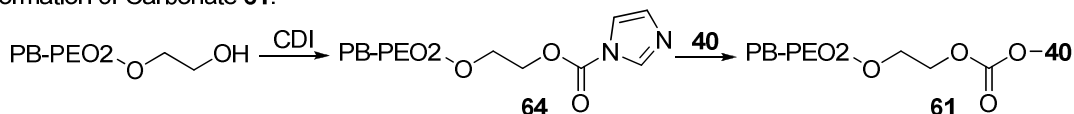
Formation of Ester **62**:
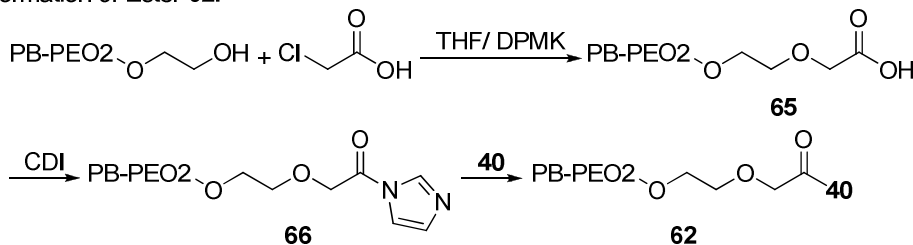
Scheme 36. Synthesis of polymer attached complex **40** as a carbonate **61** and ester **62**.

These systems are known to form polymersomes by themselves.[154] In collaboration with N. Wolter (group of Prof. Förster), the complexes **61** and **62** were synthesized according to method 3 (Scheme 36).

Initially, PB-PEO2 was reacted with CDI at room temperature and afforded compound **64** in quantitative yield. The purity of **64** was analyzed by gel permeation chromatography (GPC) and ^{1}H NMR spectroscopy. The consecutive reaction of **64** with complex **40** and following workup resulted in a mixture of PB-PEO2 and complex **61**. Since the polymersome matrix consists of pure PB-PEO2, this mixture can be used for the incorporation into polymersomes. The generation of polymersomes was realized by two different techniques: Injection of the modified polymers, dissolved in THF or ethanol into Tris-HCl buffer at pH = 7.4 and film-hydration-extrusion (FHE), whereby the polymers were dissolved in chloroform and a thin film was prepared by slow evaporation. Subsequent, Tris-HCl buffer was added to enable the formation

of polymersomes. The obtained vesicles were extruded to 200 nm and then investigated with photon correlation spectroscopy (PCS) as well as Cryo-transmission electron microscopy (Cryo-TEM) to reveal the average size, stability and morphology of the obtained vesicles.

It is notable that the polymersomes obtained from the ethanol injection were unstable and show significant size changes during an interval of seven days. In contrast, the polymersomes obtained *via* THF injection or FHE remained stable and PCS show a monomodal particle size distribution with an average vesicle diameter of 180 nm (THF injection) and 210 nm (FHE). Unilamellar and multilamellar vesicles were found in the course of Cryo-TEM investigations (Figure 11). Dark areas (red arrow) were noticed. In contrast to the polymeric elements, this darkening gives hint towards the atoms with higher atom numbers - here iron. Furthermore, half cells (blue arrow), which can be best described by a structural diversity of the polymer (*e.g.* different chain length, different shape of the head group) and polymeric agglomerations (yellow arrow) were found. The amount of iron within the samples was determined spectro-photometrically with 1,10-phenantroline.[155] Different values were obtained for the methods. Whilst the THF injection afforded 24.9 mg/L iron, the vesicles generated *via* FHE contained 47.2 mg/L iron. The maximum amount of iron could be 165 mg/L for both methods. These values are not fully comparable with the maximum amount since the modified polymers contained non-modified polymer. Vesicles generated by the film method (FHE) revealed the highest iron
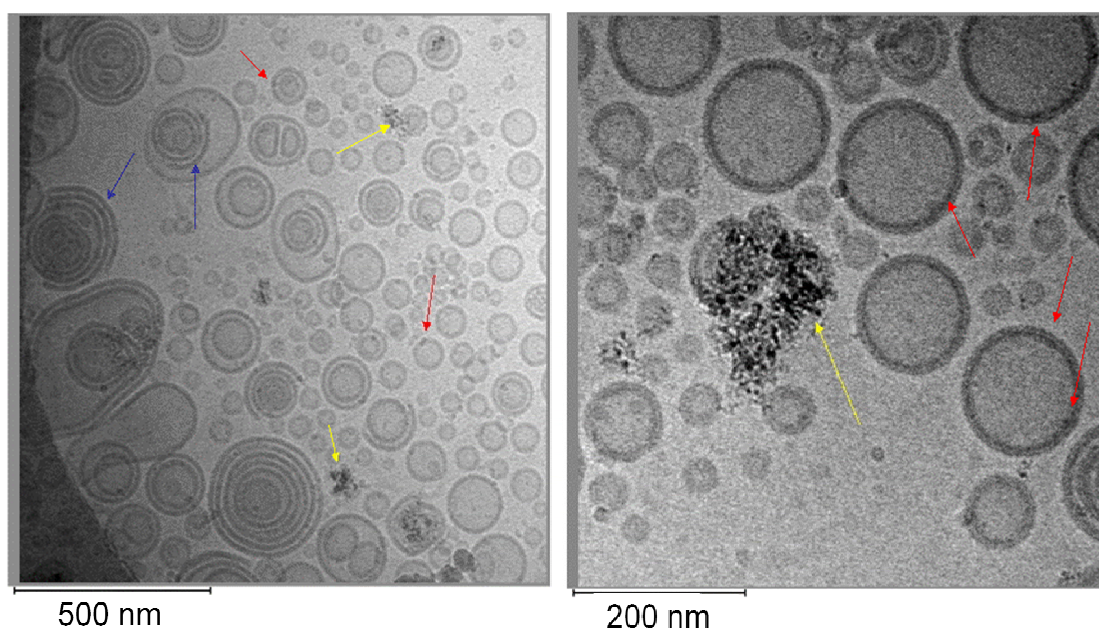
Figure 11. Modified polymersomes, generated *via* THF injection.

content and therefore the highest implemented amount of [2Fe2S] cluster. It has to be mentioned that within the vesicles formed by FHE and injection techniques, the [2Fe2S] clusters are randomly allocated on the inner and outer hull of the vesicles. To get an analytical pure and chemically more stable polymer-bound complex **40**, chloroacetic acid was reacted with PB-PEO2 and afforded the -COOH functionalized polymer **65**. Activation of **65** with CDI and consecutive treatment of the obtained polymer **66** with complex **40** yielded complex **62**. Complex **62** is currently under investigation in the group of Prof. Fahr to reveal its properties according to the incorporation into vesicles.

iv) A different approach was commenced with the preparation of the pyridinium species **63**. Therefore, 4-picoline was reacted with lithium diisopropylamide and 1-bromo-tetradecane to afford **67** within 12 hours stirring at room temperature in moderate yield (37 %).[156] The obtained amine was reacted with bromoacetic acid and afforded compound **68**.[157]

Subsequent activation with CDI (compound **69**) and reaction with complex **40** to afford complex **63**, as displayed in Scheme 37, failed. The activation of **68** with CDI led to cleavage of the -CH$_2$COOH linker and only partially to **69**. Attempts to separate compound **69** from **68** were unsuccessful and direct reaction of the crude material with complex **40** failed as well. The reaction of an activated complex, obtained by reaction of complex **40** with bromoacetyl chloride, and compound **67** to afford **63** are currently under investigation.

The advantage of this complex towards the incorporation into vesicles is obvious. An increased amphiphilic character due to the positive charge on the amine should concede the unaffiliated formation of vesicles. It was recently shown for similar compounds that this increased amphiphilic character lead to further stabilization of the formed vesicles.[158]
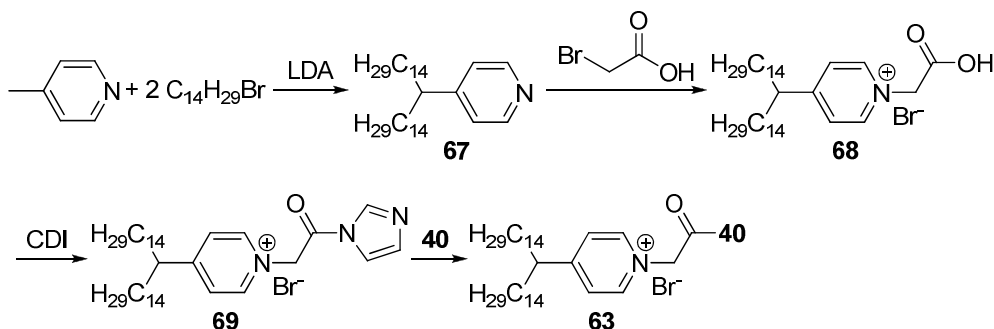
Scheme 37. Synthesis of the amphiphilic pyridinium complex **63**

2.2 Peptidic-, Amino- and Amino Acid Containing [2Fe2S] Cluster Compounds

Since the hydroxyl functionalized [2Fe2S] complexes reveal no proton relay between the iron atoms and the pendant base, a new class of complexes was established (Scheme 38). These compounds should provide both, the possibility to establish a proton relay between an adjacent amino- or amide-function and the iron cluster, as well as a possibility for further derivatizations. As suitable precursors for the complexes amines, amino acids and peptides were chosen. These molecules are known to allow protonation of the amine function under physiological conditions (*e.g.* pH value, weak acids). They should therefore be able to act as a proton distributor after initial protonation. Furthermore, especially for amino acid or peptide containing complexes, the carboxylic acid function should either allow the incorporation into larger peptides or the attachment on surfaces.[159] Additionally, these complexes would display in an extraordinary way a possible miniature for a second coordination sphere of an enzyme.

R = H, CH_3, amino acids ...
R' = H, Boc, amino acids
R'' = $\alpha-$ and β-peptides
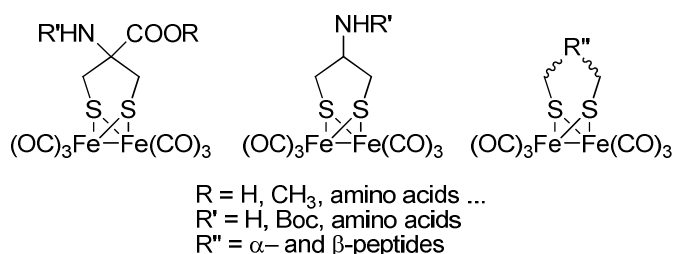
Scheme 38. Desired amino- and amino acid containing [2Fe2S] cluster complexes.

2.2.1 Amino Functionalized and Amino Acid [FeS] Complexes

(*publication number 4 and manuscript number 1*)

Initial attempts were conducted with 4-amino-dithiolane **74** (Scheme 39). This compound is known as didesmethyl-nereistoxin (dides-NTX) and is a biological active substance. It can be used as an insecticide, blocking the nicotinic acetylcholine receptor.[160] Beside these biological properties, compound **74** offers a primary amine which can be easily protonated with weak acids. It allows further derivatizations, whilst preserving the basic character. Compound **74** can be obtained within a five step synthesis (Scheme 39). The reaction of 1,3-dichloroacteone and two molar equivalents of benzylmercaptane afforded the thioether **70** in 93 % yield.[161] Further treatment of **70** with hydroxylamine in refluxing ethanol gave 1,3-dithiobenzylacetoneoxime **71** (72 % yield), which could be reduced to the free amine **72** with lithium aluminium hydride (53 % yield).[162] The cleavage of the benzyl protection groups was realized under Birch conditions (sodium/ammonia).[163] The *in situ* generated dithiol was directly reacted with iodine to afford the ring-closed disulphide and to avoid uncontrolled oxidation, eventually leading to polymeric compounds.[163] Compound **74** was isolated as a pale yellow solid (54 %) in form of the hydrochloride.
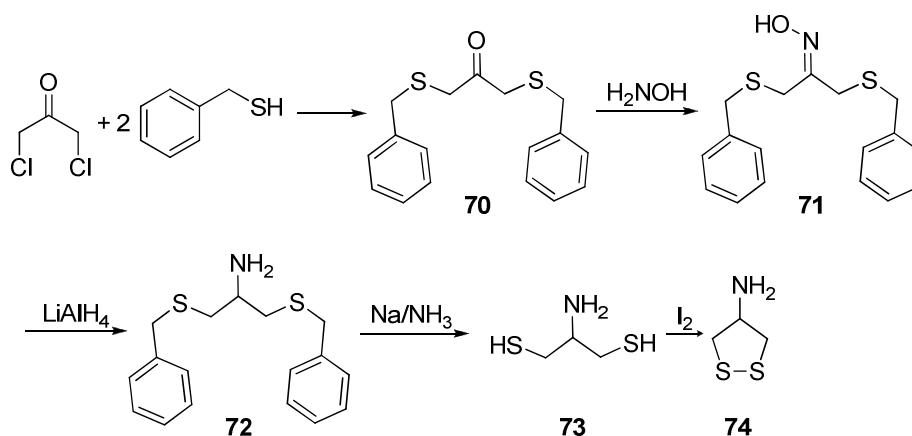
Scheme 39. Synthesis of 4-aminodithiolane **74**.

Compound **74** was reacted with $Fe_3(CO)_{12}$ in boiling toluene. However, no desired product could be isolated. Consequently, the reaction was tuned changing solvents (toluene, THF, dichloromethane, acetonitrile, diethyl ether), reaction temperature as well as the iron precursors ($Fe_2(CO)_9$ and $Fe_3(CO)_{12}$). In all cases only degradation products, like iron sulphides and oxides, could be isolated. It was assumed that the degradation relies on the presence of the free amine, which can also coordinate to the iron centre under these conditions.[164] Due to these synthetical problems the amine **74** was reacted with di-*tert*-butyldicarbonat (Boc$_2$O) to give the *tert*-butoxylcarbonyl protected compound **75** in 42 % (Scheme 40).[165] This protection group is especially known in peptide chemistry and offers an easy detachment using trifluoro acetic acid, p-toluene sulphonic acid,[166] or hydrogen chloride[167]. These conditions are feasible for the deprotection of the corresponding complex, since the [FeFe] complexes are stable under these conditions.[168] Other protection groups require basic (e.g. Fmoc-group) or non-controllable oxidative or reductive methods[169] and are therefore an unsuitable access towards the free amine complexes.

The reaction of *tert*-butyl-1,2-dithiolan-4-ylcarbamate (**75**) and $Fe_3(CO)_{12}$ in refluxing toluene afforded the diiron complex **76** in moderate yield (55 %) (Scheme 40).[170] Various attempts to deprotect complex **76** in dichloromethane or THF under argon atmosphere failed. During the experiments no conversion of compound **76** was observed, which was visible by TLC. Even stirring of complex **76** for four weeks with TFA under argon atmosphere in dichloromethane or THF revealed no conversion. By a fortunate coincidence, the reaction solutions were kept without the exclusion of air and afforded red crystals. NMR experiments reveal no resonances. In contrast, EPR experiments were conducted and revealed an axial signal set with two g-values of 2.217 and 2.0063 indicating an iron(III) low spin configuration. Single crystal X-ray analysis revealed the molecular structure as depicted in Scheme 41 (**77**). It was obvious that this complex was only formed in the presence of an oxidative atmosphere. However, the question remains, if any low-valent iron species is able to generate compound **77**. To answer this question, $Fe_3(CO)_{12}$ was reacted with TFA in THF.
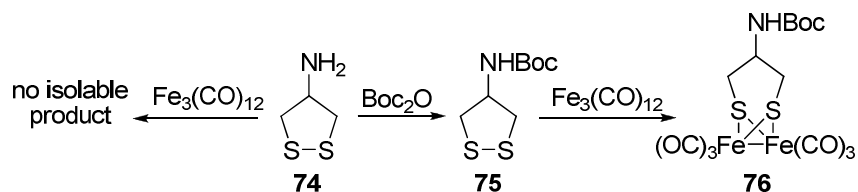
Scheme 40. Conversion of compound **74** with $Fe_3(CO)_{12}$ and derivatization with Boc_2O to afford compound **75** and finally the complex **76** after reaction with $Fe_3(CO)_{12}$.
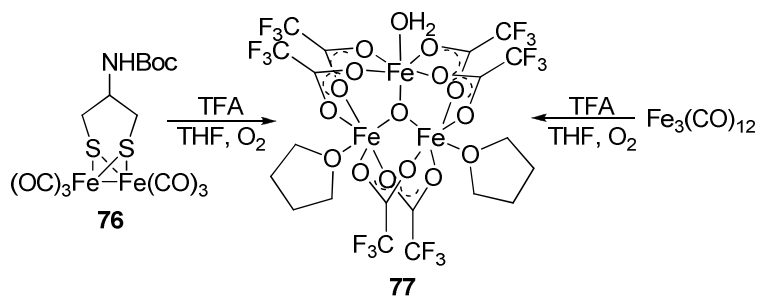
Scheme 41. Reaction pathways to compound **77**.

Reaction under the exclusion of air resulted in no visible conversion of $Fe_3(CO)_{12}$. However, treatment of the same mixture in the presence of air lead to a red crystalline product, which by X-ray analysis was determined as compound **77**. This means that the μ^3-oxygen atom must originate from the scission of molecular oxygen and oxidation of a low-valent iron species (Scheme 41).

A possible influence of the amine function towards the catalytic mechanism of the H_2 development was investigated by cyclic voltammetry. Neither in the presence of weak acids like acetic acid nor stronger acids like TFA, an influence of the amide group as a pendant base was observed. The electrochemical data of compound **76** are displayed in Table 7.

In continuation of this study and to get further insight into biological active dithiolanes, 4-amino-1,2-dithiolane-4-carboxylic acid (ADT) and derivatives were selected as target species (Scheme 42, compound **78**).

ADT (**78**) can be regarded as the oxidized form of the proteinogen amino acid cysteine with two side chains. It was known as pure synthetic building block for a long time.[171] In 2003 it was found that this conformational restricted dithiolane is a natural occurring molecule and
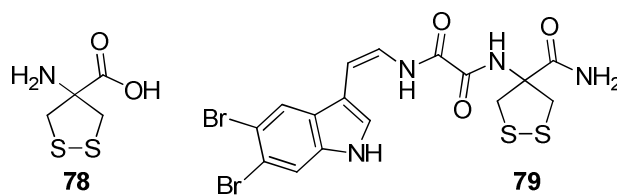
Scheme 42. 4-Amino-1,2-dithiolane-4-carboxylic acid (**78**) and Kottamide E (**79**), containing the ADT unit.

was found in the dibrominated indole enamide derivative Kottamide E (compound **79**, Scheme 42) isolated from *Pycnoclavella kottae*.[172]

Since reaction of iron carbonyls and dithiolanes afford stable double chair conformation, ADT is an ideal precursor molecule for hydrogenase models, offering an internal base and further capability for derivatizations. If compound **84** (Scheme 43) allows the establishment of a proton relay it could be regarded as a miniature of the enzyme.

The reaction procedure followed the route displayed in Scheme 43. Starting from compound **70**, reaction of potassium cyanide and ammonium carbonate in a sealed tube afforded the hydantoine **80** in 23 % yield within 24 hours at 120 °C.[171] Suspension of **80** in an aqueous sodium hydroxide solution and reaction in a pressure bottle at 170 °C for 20 hours gave 2,2-bis(benzylthiomethyl)glycine **81** in good yield (65 %).[173] To avoid polymerization of the desired compound **78** (Scheme 42) during the course of deprotection *via* Birch reduction, the amine and the carboxylic function was protected. Attempts to protect the amino- and the carboxylic acid group with common protection methods failed due to the sterical hindrance at the *α*-carbon atom. Lucente *et al.* described an elegant way to solve this problem. Thereby, compound **81** was reacted with phosgene to give *N*-carboxy-2,2-bis(benzylthiomethyl)glycine anhydride **82** in 88 % yield.[173] This easily accessible compound was transformed into compound **83** *via* reaction with Boc_2O and methanol/*N*-methylmorpholine.[174] Thereby, compound **82** *in situ* reacts with Boc_2O to give the *N*-Boc protected urethane. By further treatment with methanol and *N*-methylmorpholine, this highly reactive species was converted to compound **83** in 83 % yield. The cleavage of the benzyl protection groups were committed under Birch reduction conditions
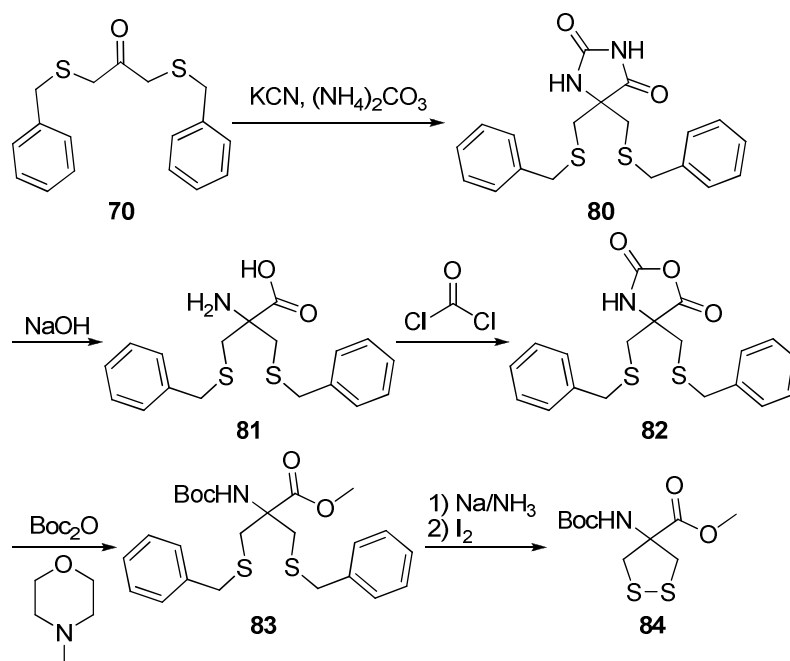
Scheme 43. Synthesis of the cysteine analogue **84**.

and the cleavage was followed by treatment with iodine to give 4-(*N-tert*-butyloxycarbonyl)-amino-1,2-dithiolane-4-carboxylic acid methyl ester (**84**) in 84 % yield. The complexation of compound **84** was carried out with $Fe_3(CO)_{12}$ in boiling toluene and afforded complex **85** in 93 % yield as a red solid (Scheme 44).[170] Compared to compound **84**, complex **85** shows a heavily decreased torsion angle for C-S···S-C of 3.2° (**85**) related to 31.5° (**84**). This behaviour can be explained by the "double" chair conformation of the six membered rings formed by the former dithiolane unit and one iron atom. However, also in the case of compound **85** the cleavage of the Boc protection group could not be realized.

Compound **84** was deprotected according to the same procedures used for the deprotection of the complexes (TFA, thionyl chloride).[175] Unfortunately, also the reaction of the deprotected species with $Fe_3(CO)_{12}$ did not result in the free amine complex.

Further efforts were committed with compound **86**. The idea behind this molecule is the formation of a [2Fe3S] cluster and would provide the first synthetic model complex with a pure amino acidic backbone. Reaction of compound **84** and thionyl chloride generated the free amine, which was *in situ* reacted with 1-(3-dimethylaminopropyl)-3-ethylcarbodiimide hydrochloride (EDC), 1-hydroxy-1H-benzotriazol (HOBt) and *N*-Boc-Met-OH to give the

dipeptide **86**. Further reaction with $Fe_3(CO)_{12}$ under reflux conditions brought forth complex **87** in moderate yield (52 %). NMR spectroscopy, mass spectrometry as well as elemental analysis revealed the molecular structure of compound **87**. No complexation of the thioether of methionine could be verified under thermal conditions. In following attempts, compound **87** was treated with trimethylamine-*N*-oxide. This reaction should force a detachment of one CO ligand *via* the formation of CO_2.[176] Even under these conditions no [2Fe3S] cluster could be substantiated and the electrochemical properties remain closely the same as described for compound **85** (Table 7). Thus the interesting properties of the disulphides could not be converted to the complex molecules. Incited by these initial results, compound **86** was conversed to compound **88**. This kind of compound is known to enable the formation of hydrogen bonds between the amide function and one sulphur atom of the disulphide.[177] This interaction should probably endeavour a fast protonation of the sulphur atoms in compound **89**. Compound **88** was accessible by the reaction of **86** with sodium hydroxide and the *in situ* generated carboxylic acid was used without further purification. It was converted into **88** *via* standard esterification procedure using EDC, HOBt and H_2N-Phe-OMe. Reaction of **88** with $Fe_3(CO)_{12}$ afforded the respective complex **89**. However, any N-H···S interaction is not retained in the complex or is very weak in the complex, since no proton exchange could be established and proofed with cyclic voltammetry and within IR experiments. Furthermore, compound **90** and complex **91** were synthesized according the above described procedures, but revealed no altered electrochemical data compared to **85**, **87** and **89**.

For all these complexes a deprotection with TFA was attempted but did not reveal the free amine complexes.

As a result of the inert peptide backbone, another amino acid was implemented. The incorporation of proline as side chain should allow a stabilization of the free amine, since stable secondary and tertiary amine complexes are known in hydrogenase model complexes (see chapter 1.2.2). Unfortunately, attempts to generate the free amine of **92** merely resulted in a number of different oligopeptides, which were not isolable in a sufficient amount.
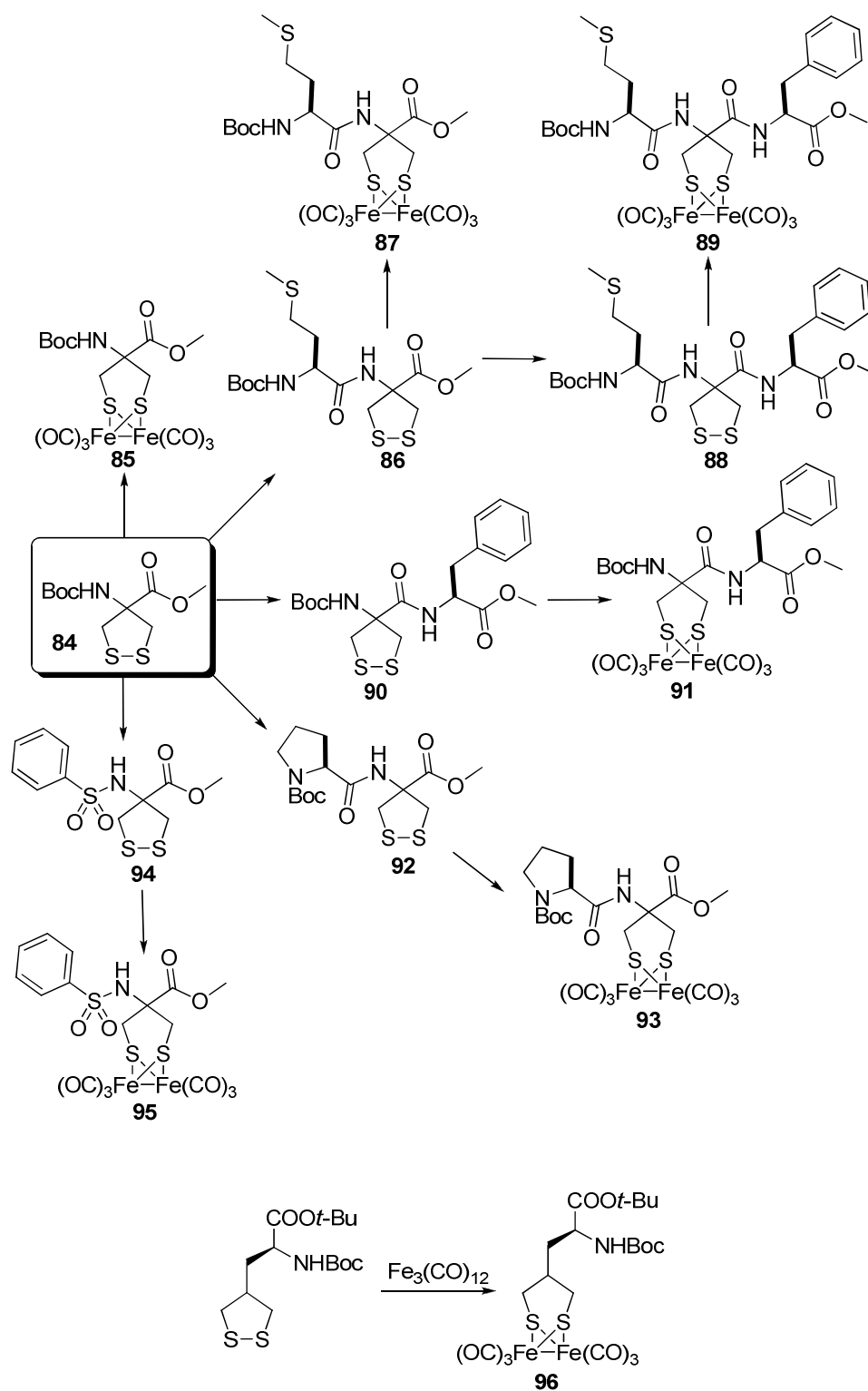
Scheme 44. Amino acidic and peptidic [2Fe2S] compounds.
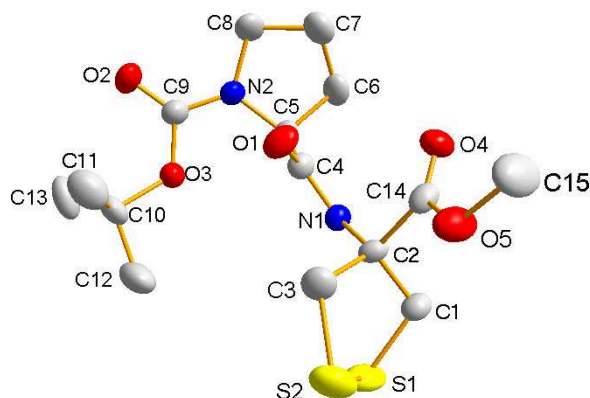
Figure 12. Molecular structure of compound **92** (thermal ellipsoids at 50 % probability level). Hydrogen atoms are omitted for clarity.

Therefore proline was protected with Boc$_2$O and reacted with compound **84** to give **92** in moderate yield. Single crystals for structure determination were obtained by slow evaporation of a solution of chloroform (Figure 12).

Compound **92** was co-crystallized with chloroform and confirms the expected molecular structure. Studying the bond lengths and angles in the ADT-part, some interesting features were obtained. The dithiolane ring shows up two different bonding distances (S-C) of 178.8(5) and 182.3(6) pm and bonding angles (S-S-C) of 92.66(19) and 90.20(19) ° (Table 6). In comparison to Boc-ADT-OMe, the torsion angle C-S-S-C is increased from 31.5 to 44.97° and the sulphur-sulphur distance is slightly reduced from 205.6(3) to 204.6(3) pm.[175]

Table 6. Selected bond angles [°] and distances [pm] of compound **92**.

S(1)-S(2)	204.6(3)	C(2)-C(14)	154.0(7)
S(1)-C(1)	178.8(5)	C(2)-N(1)	147.0(5)
S(2)-C(3)	182.3(6)	C(4)-N(1)	132.2(7)
C(1)-C(2)	1.54.5(7)	C(4)-O(1)	123.7(6)
C(2)-C(3)	155.6(7)	C(4)-C(5)	154.4(6)
N(2)-C(9)	132.1(6)	C(5)-N(2)	145.2(6)
S(1)-S(2)-C(3)	92.66(19)	C(1)-C(2)-N(1)	108.3(4)
S(2)-S(1)-C(1)	90.20(19)	C(1)-C(2)-C(14)	107.7(4)
S(1)-C(1)-C(2)	107.8(3)	N(1)-C(2)-C(14)	108.8(4)

S(2)-C(3)-C(2)	109.7(4)	C(2)-N(1)-C(4)	121.0(4)
C(1)-C(2)-C(3)	110.3(4)	N(1)-C(4)-C(5)	115.0(4)
C(4)-C(5)-N(2)	111.2(4)		

These results are similar to Boc-ADT-ADT-NHMe, where the torsion angle (C-S-S-C) is increased up to 42.6° and sterical reasons have been suggested for the distortion of the dithiolane ring.[177] Subsequently, compound **92** was reacted with $Fe_3(CO)_{12}$ and resulted in complex **93** in good yield (65 %). Once more, trials to deprotect the complex with standard deprotection reagents (TFA, thionylchloride, HCl) failed and the peptide moiety revealed no catalytic relevant influence. The same behaviour was found for compound **96**, which was obtained in 63% from the corresponding Boc-(S)-2-amino-3-(1,2-dithiolan-4-yl)propionic acid *tert*-butyl ester.[178] All these complexes were thought to display the adjacent amino acid lysine (K237) of the enzyme, providing different Fe···N distances and a proton relay between the amine and the iron centre. However, this concept failed since no deprotection of the amide could be achieved and acetic acid was too weak for protonation of the amide.

Since the complexes **76** - **93** and **96** exhibit no influence to the catalytic mechanism of the H_2 generation and it was not possible to generate the free amine complexes within this work, the compound class was changed from basic amides to acidic sulphonamides with preservation of the ADT structure.

This class of compounds bears interesting properties. Sulphonamides have been known as the largest class of antimicrobial agents for a long period and have shown to be irreversible inhibitors of the cysteine proteases.[179] Beside the importance for medicinal chemistry,[180] the special properties of the S-N bond provide an incredible feature. Sulphonamides reveal a non-neglegible acidity and can be deprotonated under mild conditions, forming a basic anion.[181] This was confirmed by kinetic studies on the hydrolysis of *p*-nitrophenyl-*o*-methansulfonamidobenzoate[182] (pK$_a$ = 8.41 in acetonitrile) and *p*-nitrophenyl-*p*-methansulfonamidobenzoate[183] (pK$_a$ = 7.34 in acetonitrile). In contrast to amides, the high acidity can be explained by the interaction of the sulphur d-orbitals with the lone pair electrons of the surrounding oxygen atoms. Furthermore, a second p(π)-d(π) interaction can be described between the d-orbitals of the sulphur atom and the lone pair of nitrogen.[184]

Inspired by these properties, compound **94**[*] was reacted with $Fe_3(CO)_{12}$ and afforded compound **95** in very good yield (83%) as an air and moisture stable red solid.

A comparison of the electrochemical data of complexes **76** - **96** is shown in Table 7. The complexes **76**, **85** and **96** exhibit similar electrochemical properties which appear natural since their structures are related. Furthermore, the di- and tripeptidic complexes **87**, **89**, **91** and **93** give comparable data for the reduction potentials of the one-electron reduction $\{Fe^IFe^I \rightarrow Fe^0Fe^I + e^-\}$. A possible explanation for the appearance of the two oxidation signals in the CV's of compound **91** and **93** is a slightly different geometry of the Fe^IFe^I state. It is already known that distortions can lead to significant shifts of the reduction potentials.[76a] But since the oxidized states appear irreversible and are not integrated in the catalytic cycle, these processes were not further investigated.

Since the electrochemical features of the dithiolanes are very similar, the electrochemistry and the catalytic behaviour of these compounds will be described in detail for compound **93** and compared to the sulphonamide **95**.

The cyclic voltammogram of compound **93** is displayed in Figure 13. In the absence of acid, a reduction signal can be seen at -1.48 V. This process seems to be rather irreversible, since the signal proportion between the oxidation current and the reduction current is smaller than 1.

This further suggests an EC mechanism (means the initial reduction step is followed by a fast chemical reaction).[185] In this special case, the Fe^IFe^I state is transferred into Fe^0Fe^I by an one-electron reduction and is followed by a fast change of the bonding properties within the molecule. This change of bonding properties can be best described by the break of the Fe-Fe bond and/or the appearance of a bridging carbonyl and a rotated state (see also chapter 1.2.4).

---

[*] This compound was provided by Professor G. Lucente ("Sapienza" Università di Roma). It was derived from compound **84** and benzenesulfonyl chloride.

Table 7. Electrochemical data of the amine complex **76** as well as the amino acidic complexes **85**-**96**.

Compound[a]	E_{ox} [V]	$E_{red,1}$ [V]	$E_{red,2}$ [V]
76[170]	+0.92[b]	-1.51[b]	-2.04[b]
85[170]	+0.81[b]	-1.47[b]	-2.09[b]
87	+0.98[b]	-1.52[b]	-1.76[b]
89	+0.95[b]	-1.57[b]	-
91	+0.71[b] and +0.94[b,c]	-1.51[b]	-1.89[b]
93	+0.8[b] and +0.97[b,c]	-1.48[b]	-
95	+0.8[b] and +1.0[b,c]	-1.48[b]	-1.77[b]
96[170]	+0.91[b]	-1.52[b]	-2.15[b]

[a] Potentials in V ± 0.01 *vs.* 0.01 M Ag/Ag$^+$ in CH_3CN in 0.10 M [*n*-Bu$_4$N][BF$_4$]/CH_3CN; [b] irreversible wave; [c] the latter value reflects a further oxidation to the Fe^{II}Fe^{II} state.

In the presence of acetic acid the initial reduction potential remains constant and only little increase of the current is noticed. This raise, however, is caused by the increased basic current due to the addition of acid. Since the process is a one-electron reduction and no shift appears in positive direction, no pre-equilibrium is assumable.

This means, that preliminary to the reduction no protonation of compound **93** takes place, which would be important for displaying the natural role of an adjacent base. In contrast to the first reduction peak, the second, new reduction peak at ~2.2 V increases with increasing concentration of acid, indicating the electrocatalytic formation of dihydrogen. Thereby, the acid is not strong enough to protonate the iron centre, which is in good agreement to literature (see chapter 1.2.5). The second reduction is followed by a doubly protonation of the [Fe^{0}Fe^0]$^{2-}$ state and the generation of dihydrogen whilst simultaneous regeneration of the initial [Fe^{I}Fe^I] state takes place (Scheme 45, see also Scheme 21, chapter 1.3.1). In contrast to Scheme 21 a rearrangement of the complex due to the formation of a bridging CO ligand has to be supposed.
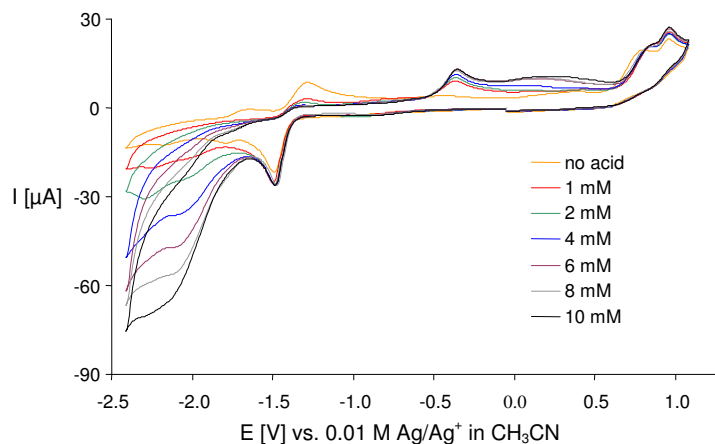
Figure 13. Cyclic voltammogram of compound **93** in the presence of acetic acid (0, 1 - 10 mM).
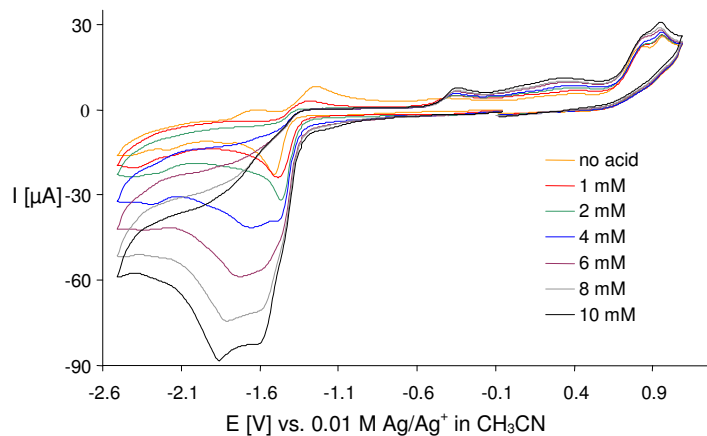
Figure 14. Cyclic voltammogram of compound **93** in the presence of trifluoroacetic acid (0, 1 - 10 mM).

In contrast to the electrochemical properties in acetonitrile and acetic acid, investigations performed with trifluoroacetic acid in acetonitrile revealed a different voltammogram (Figure 14). This facilitated an alternative process for the development of dihydrogen, which is in good coincidence to literature reports (Scheme 45).[103] It is known that the one-electron reduction product reacts very fast with additional protons from strong acids to give a Fe-Fe-H (**93H**) assembly.[103] This state is reduced at -1.61 V and ongoing protonation either resulted in a direct cleavage of dihydrogen or in further protonation at higher concentrations of acid, followed by
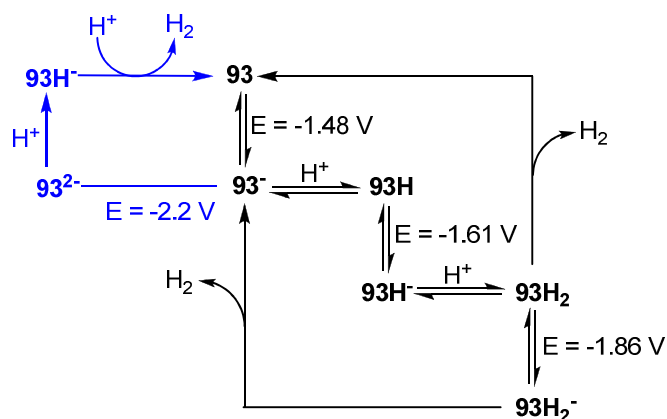
Scheme 45. Catalytic mechanism of compound **93** in the presence of acetic acid (blue) and trifluoro acetic acid (black).

dihydrogen development at -1.86 V. This ECEC mechanism (Scheme 45) is in good accordance to the results found by Pickett *et al.*[103]

The cyclic voltammogram of **95** reveals two oxidation steps at 0.8 and 1.0 V (Figure 15). An irreversible one-electron reduction is visible at -1.48 V. To confirm the features to act as a [FeFe]-hydrogenase model, acetic acid was subsequently added to compound **95** during CV investigations (Figure 15). Inspired by the remarkable acidity of sulphonamides, IR and NMR spectroscopic investigations were commenced to show the influence of the sulphonamide group as a proton distributor. However, neither NMR spectroscopic studies in the presence of CD_3COOD nor IR spectroscopic studies in the presence of acetic acid could confirm any protonation or a proton transfer according to a S_E2 mechanism as discussed by Mandell *et al* (Scheme 46).[186]

In contrast to this initial reduction signal, the second reduction signal at *ca.* -2.2 V increases with each increment of acid added. This signal is not a reduction of pure acetic acid on the electrode, since acetic acid was shown to be reduced at more negative potential.[170] In comparison to the electrochemistry of **93**, this part might be an EC part and is assigned to the catalytic formation of dihydrogen.

To get more information about complexes with a peptidic moiety, the literature-known compound **99** as well as complex **101** was synthesized.
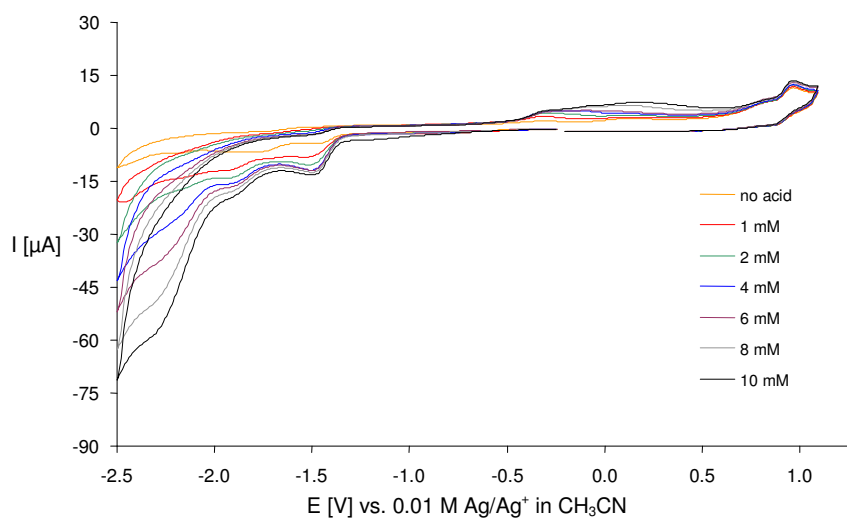
Figure 15. Cyclic voltammogram compound **95** in the presence of 0,1 - 10 mM acetic acid.
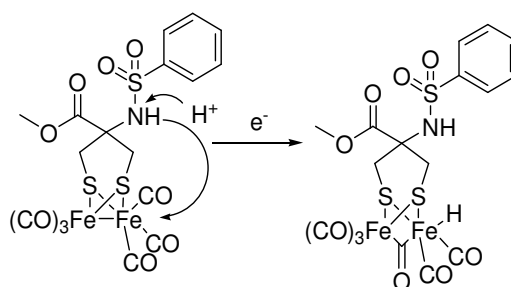
Scheme 46. Assumed mechanistic pathway for the first protonation reaction of the [FeFe] core of compound **95**.

Especially, complex **99** allows more insight into the electrochemistry of these complexes. It is thereby interesting if the open chain form reveals different properties than described for the closed ring systems. Initially, cystine was reacted with two equivalents thionylchloride in methanol to give compound **97** in 98 % yield. To avoid side reactions during the complexation, the amine **97** was protected with Boc_2O in dioxane/water and afforded **98** in 59 % yield. Complex **99** was obtained in 74 % yield *via* the reaction of compound **98** with $Fe_3(CO)_{12}$. In contrast to the literature-known procedure, the use of the disulphide resulted in considerably higher yield.[93] NMR spectroscopic investigations confirmed a similar composition. It is reasonable to mention that the electrochemical properties of the "open" system **99** are the same as reported for related amino acidic "closed" ring systems (Table 8).

Table 8. Electrochemical data of the open chain complex **99** and the tripeptidic complex **101** in comparison to complex **76**.

Compound[a]	E_{ox} [V]	$E_{red,1}$ [V]	$E_{red,2}$ [V]
76[170] (CH$_3$CN)	+0.92[b]	-1.51[b]	-2.04[b]
99 (CH$_3$CN)	+0.91[b]	-1.53[b]	-
101 (DMF)	-	-1.54[b]	-2.42[b]

[a] Potentials in V ± 0.01 *vs.* 0.01 M Ag/Ag$^+$ in CH$_3$CN in 0.10 M [n-Bu$_4$N][BF$_4$]/CH$_3$CN or DMF, [b] irreversible wave.
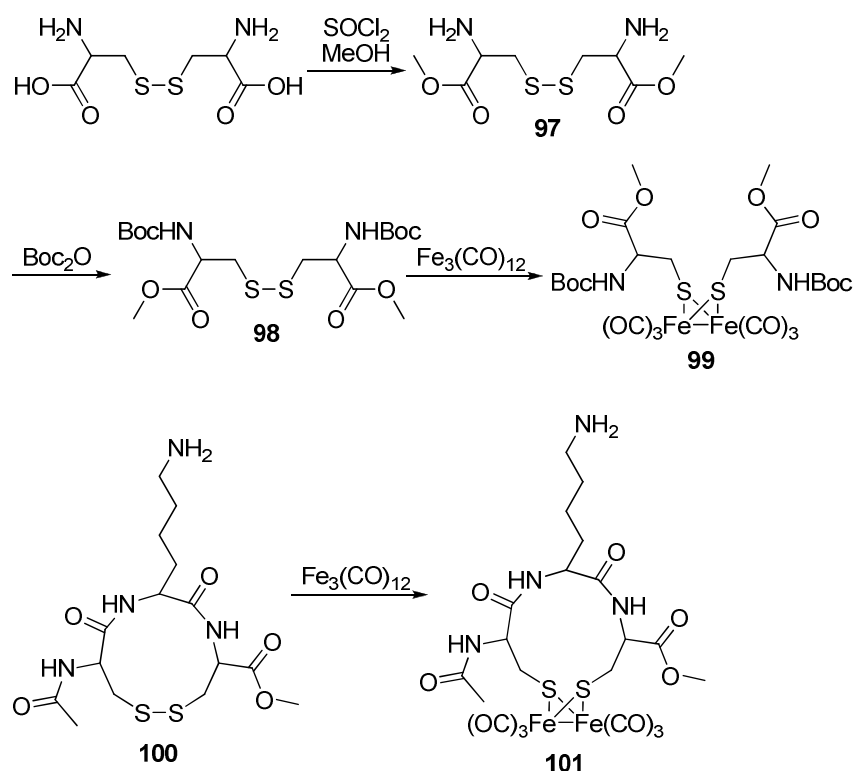
Scheme 47. Synthesis of the open chain compound **99** as well as the tripeptidic complex **101**.

To increase the number of amino acids incorporated into a [2Fe2S] cluster, the tripeptide **100** was synthesized.[†] The sequence, Cys-Lys-Cys, was carefully selected for two reasons: *i*) the two cysteines allow the connection to the Fe$_2$(CO)$_6$ subunit and therefore the establishment of a hydrogenase-like molecule. *ii*) Since a lysine (K237) in the enzyme is said to have eminent influence concerning pendant base effects,[24,25] one molecule lysine was implemented to offer a flexible chain containing an amine, which should reveal similar features as discussed for

[†] This compound was provided by PD Dr. D. Imhof (Friedrich-Schiller-University Jena).

Lys(K237). But neither IR investigations nor electrochemical measurements in the presence of TFA revealed any influence of protons towards the catalytic mechanism *via* establishment of an initial proton relay. It was rather noticed that the activity of **101** towards the catalytic dihydrogen generation was distinctly diminished in dimethylformamide.

2.2.2 Macrocyclic Peptidic Complexes (*publication number 6*)

Following the continued interest to use biologically active substances for mimicking the enzymatic environment of the [FeFe]-hydrogenase, the macrocyclic, peptidic disulphide Sandostatin® (octreotide **102**, Scheme 48) was reacted with three equivalents $Fe_3(CO)_{12}$ and afforded complex **103** as an amorphous orange solid in 39% yield (Scheme 48).[187]

The structure of complex **103** was confirmed *via* NMR-, IR spectroscopy, mass spectrometry as well as elemental analysis. Furthermore, differential scanning calorimetry and thermogravimetric investigations were carried out and further confirmed compound **103**.

Albeit **103** is not very stable in solution, it could be used for catalysis of electrochemical hydrogen formation in dimethylformamide (DMF) and for affinity assays for the somatostatin receptors $hsst_{1-5}$.[187,‡(188)] It is notable that the affinities were surprisingly high in spite of the fact that complexation must lead to major distortion of the macrocyclic backbone, which is important for the affinities towards the hsst receptors.[187] In contrast to these interesting affinity tests, cyclic voltammetry provided insufficient low reduction potentials for the electrochemical dihydrogen formation.

Since the low stability of compound **103** was thought to be a result of awkward coordination geometry around the sulphur atoms, another approach towards the incorporation of a peptidic moiety had to be found.

To increase the stability of the desired complex, the *β*-peptides **104** - **106** (Scheme 49) were synthesized.

---

‡ Octreotide **102** is known as a somatostatin ($SRIF_{14}$, somatotropin-releasing inhibiting factor) analogue; it binds to the five human somatostatin receptors $hsst_{1-5}$ (affinities ranging from 0.8 nM ($hsst_2$) to 1.7 μM ($hsst_4$)). It inhibits the release of the growth hormone somatotropin, with an activity that is 70 times higher than that of the natural hormone somatostatin. Octreotide derivatives are used in diagnosis and therapy of endocrine and gastro entero pancreatic tumours, breast and prostate cancers.
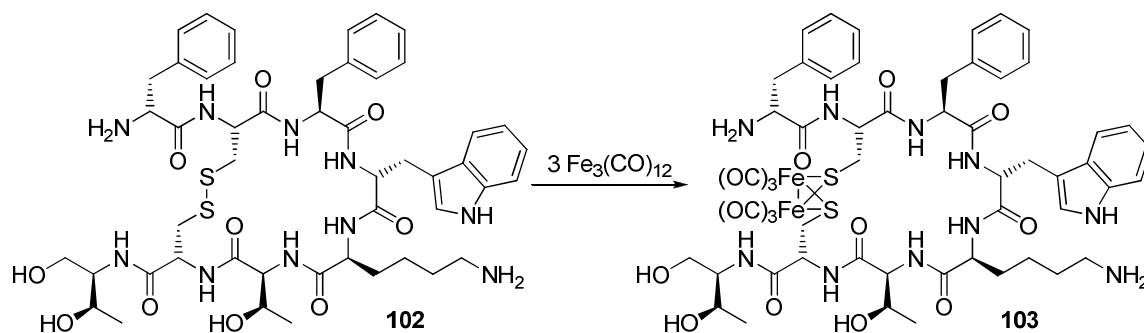
Scheme 48. Reaction of octreotide **102** with excess $Fe_3(CO)_{12}$ to form the product **103** of insertion into the (S,S)-bond.

This class of compounds is well-known to reveal increased stability of the secondary structure with respect to α-peptides.[189] The secondary structure of β-peptides is easily predictable, since peptides formed by at least six amino acids of the same configuration prefer the erection of a 3_{14}-helix.[189] This means that the amino acids in *i* and *i+3* position are on top of each other with a 14-membered ring of hydrogen bonds. The prospect of further stabilization of the helix was shown by Seebach *et al.*.[190] Using β-cysteine in *i* and *i+3* positions they were able to establish additional disulphide bridges, which further stabilised the backbone.

The peptides were prepared with solid phase peptide synthesis (SPPS) *via* the Fmoc-strategy.[191] The reaction of the octapeptide **104** and $Fe_3(CO)_{12}$ in acetonitrile resulted in the desired [2Fe2S] complex, which precipitated from solution immediately after formation. However, it has to be mentioned that the formation of the complex could exclusively be confirmed *via* mass spectrometry. Unfortunately, the complex revealed less stability as the α-peptidic complex **103** and worse solubility in any solvents.

These two problems (mindered stability, worse solubility) should be solved stepwise. Initially, the nonapeptide **105** were synthesized and should provide a more rigid 3_{14}-helix backbone, since the additional amino acid is able to further stabilize the helix by additional hydrogen bonds. Additionally, the free functional groups were protected by generating an amide (*C*-terminal) and acetyl-protection (*N*-terminal) to avoid unsolicited side reactions. However, no reaction with $Fe_3(CO)_{12}$ was possible, since **105** was not soluble in neither polar nor unpolar solvents.

A suitable alternative was found in compound **106**, where phenylalanine was surrogated by tyrosine and the acetyl protection group was abandoned. These little changes led to a considerable improvement of the solubility properties. Reaction of the nonapeptide **106** with $Fe_3(CO)_{12}$ following the same procedure as described for **104** afforded no detectable iron complex.
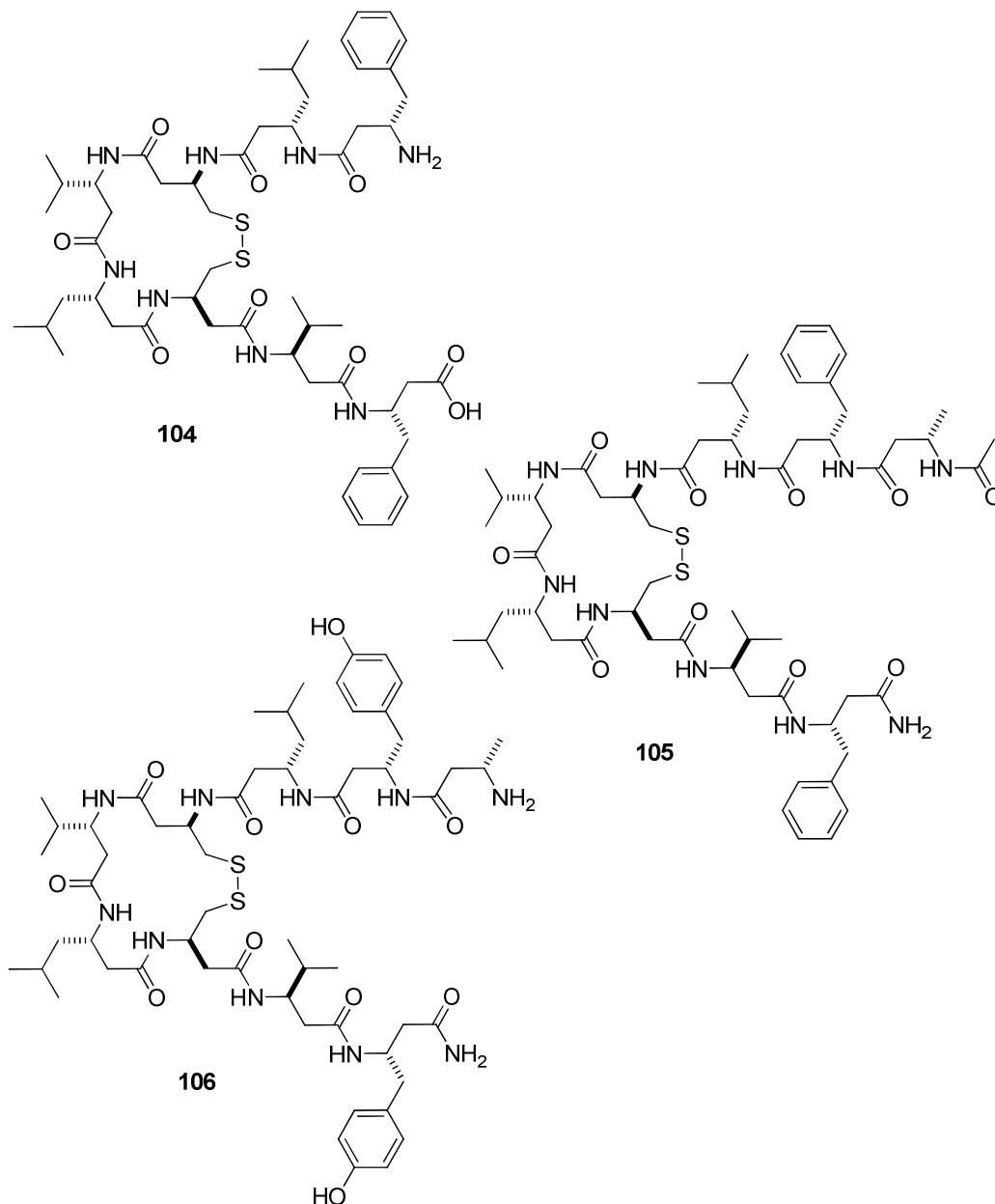
Scheme 49. Synthesized *β*-peptides **104 - 106** used for the conversion with $Fe_3(CO)_{12}$.
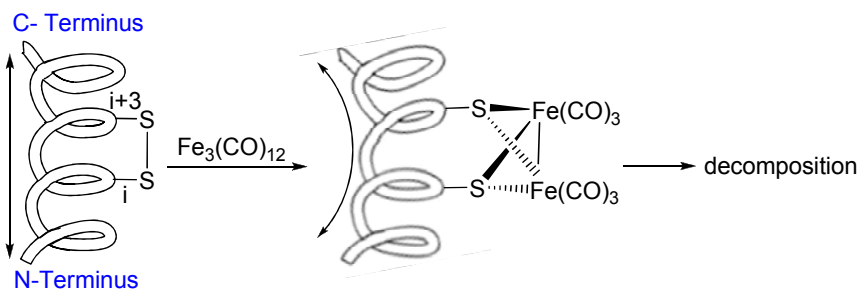
Scheme 50. Reaction of β-peptide and $Fe_3(CO)_{12}$ presumably lead to a distortion of the backbone and finally to the decomposition of the complex.

A possible explanation can be found by the increase of the S···S distance and the C-S···S-C torsion angle which is accompanied by the complexation[§] and in agreement to literature deliberations.[187] In contrast to compound **103**, a significant distortion of the peptide backbone seems to be the case in β-peptidic iron bound compounds (Scheme 50). Thereby, the rigid backbone of the β-peptide antagonises this trend and destabilizes the complex. Presumably, this structural change leads to decomposition of the *in situ* formed complex, which was confirmed by mass spectrometry.

[§] By analogy to compound **94**: the S···S distance is increased from 205.6(3) to 302.5 pm and the torsion angle C-S···S-C decreases from 31.5 to 3.2°.

2.3 Complexes Containing Platinum and Iron

In continuation of the efforts to investigate the coordination chemistry of dithiolanes and thiols, the tetrathiol **107** (Scheme 51) was reacted with bis(triphenyl-phosphine)-platinum(II)-dichloride and $Fe_3(CO)_{12}$. Only little is known about the metal uptake of **107**.[192] It is therefore interesting to reveal conditions for a targeted synthesis for complexes with either two free thiol groups or two different metal centres. Within this investigation the desired complex **109** affords two different active sites (Scheme 51). One site reveals the Pt-site, where the other reflects a [FeFe]-hydrogenase sub-site.

In initial attempts compound **107** was reacted with different amounts of $Fe_3(CO)_{12}$ (0.3; 0.5; 1 and 2 equivalents). Nonetheless, exclusively compound **108** was obtained in varying yields, which is in good agreement to a publication by Song *et al.*,[193] published shortly after the synthesis of compound **108**. Single crystals were obtained by slow evaporation of a solution of **108** in chloroform at 4 °C. The molecular structure of **108** is depicted in Figure 16 and shows the typical butterfly arrangement of the [2Fe2S] clusters. Except of the S-C-C bonding angles, the distances and angles are in good accordance to the previously described complexes and to literature.[193] The high values of 123.12(15)° for S(1)-C(1)-C(2) and 119.97(13)° for S(2)-C(3)-C(2) are somewhat surprising, since sp^3 hybridization would anticipate an angle of 109.5°. A possible explanation for this widening can be seen in sterical reasons, since otherwise both iron sites would come close together. Instead of $Fe_3(CO)_{12}$, bis(triphenyl-phosphine)
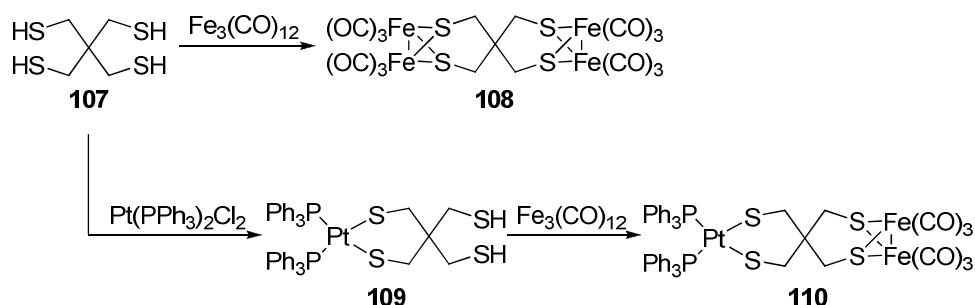
Scheme 51. Reaction of the tetrathiol **107** with $Pt(PPh_3)_2Cl_2$ and $Fe_3(CO)_{12}$ afforded different substitution patterns. The reaction of **109** and $Fe_3(CO)_{12}$ afforded the heterotrimetallic complex **110**.

platinum(II)-dichloride was reacted in a 1:1 molar ratio with **107** and potassium carbonate. Unexpectedly, this reaction afforded exclusively **109** (Scheme 51) in 94% yield and the nature of the complex was confirmed *via* elemental analysis, NMR (^{1}H, ^{13}C), IR spectroscopy as well as mass spectrometry. Subsequently, complex **109** was reacted with one equivalent of $Fe_3(CO)_{12}$ for 4.5 hours at room temperature in dichloromethane and afforded compound **110** in 21 % yield. Similar procedures with THF or diethyl ether under refluxing conditions lead to decomposition of the complexes and only marginal amounts of **110**.
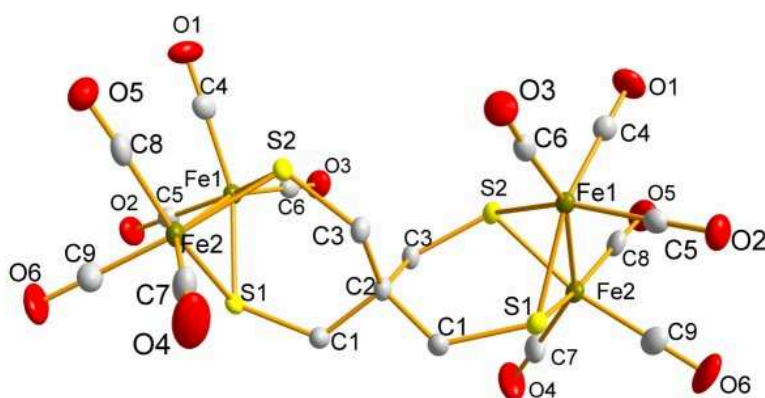
Figure 16. Molecular structure of **108** at 50% probability level. Hydrogen atoms are omitted for clarity.

Table 9. Selected bond angles [°] and distances [pm] of compound **108**.

Fe(1)-Fe(2)	250.17(4)	S(1)-C(1)	182.5(2)
Fe(1)-S(1)	224.01(5)	S(2)-C(3)	184.2(2)
Fe(1)-S(2)	228.59(6)	C(1)-C(2)	155.3(3)
Fe(2)-S(1)	225.37(6)	C(2)-C(3)	152.5(3)
Fe(1)-Fe(2)-S(1)	55.913(15)	S(1)-C(1)-C(2)	123.12(15)
Fe(1)-Fe(2)-S(2)	57.125(16)	S(2)-C(3)-C(2)	119.97(13)
Fe(1)-S(1)-Fe(2)	67.655(18)	C(1)-C(2)-C(3)	110.64(12)
Fe(1)-S(2)-Fe(2)	66.802(17)		

The ^1H NMR spectrum of **110** showed the expected doublet at 2.85 ppm for the methylene group neighboured to the Pt centre with Pt-H coupling constants ($^3J_{Pt,H}$ = 66.4 Hz). The methylene groups at the iron subside did not reveal this splitting and were visible as a singlet at 2.33 ppm. Additional confirmation was obtained by the ^{31}P NMR spectrum, revealing a singlet at 27.5 ppm with platinum satellites ($^1J_{Pt,P}$ = 2852 Hz). The structure of **110** was reaffirmed by ^{13}C NMR experiments, IR spectroscopy, as well as mass spectrometry and elemental analysis. Single crystals suitable for structure determination were obtained by slow diffusion of hexane into a concentrated solution of **110** dissolved in chloroform. The molecular structure is depicted in Figure 16 and further confirms the structure of **110**. It shows the two different active sites within the molecule.

One side of the tetradentate ligand is square planar coordinated by the bis(triphenyl-phosphine)-platinum(II) moiety. The other active site bears a $Fe_2(CO)_6$ fragment with a typical butterfly arrangement. The bonding distances and angles at both metal centres are within the expected range (Table 10). However, it is again notable that the bonding angles S(2)-C(4)-C(1) (121.3(4)°) and S(4)-C(5)-C(1) (118.7(4)°) are quite large and significantly wider than the corresponding angles at the platinum(II) coordination site. The carbon atom C(1) reveals a slightly distorted tetrahedral geometry.
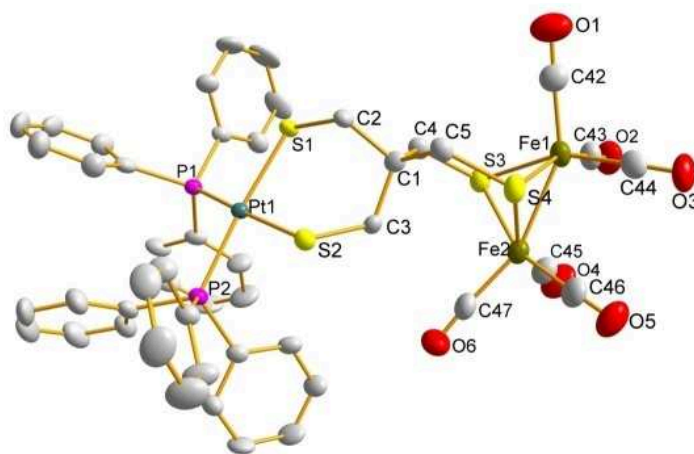
Figure 17. Molecular structure of compound **110** at 50% probability level. Hydrogen atoms are omitted for simplicity reasons.

Table 10. Selected bond angles [°] and distances [pm] of compound **110**.

Fe(1)-Fe(2)	249.58(12)	Pt(1)-P(1)	229.49(15)
Fe(1)-S(3)	225.82(18)	Pt(1)-P(2)	229.49(13)
Fe(1)-S(4)	226.08(18)	Pt(1)-S(1)	233.75(13)
Fe(2)-S(3)	225.57(18)	Pt(1)-S(2)	235.21(15)
Fe(2)-S(4)	229.11(18)	S(1)-C(2)	182.5(6)
S(3)-C(4)	181.9(6)	S(2)-C(3)	182.8(6)
S(4)-C(5)	182.7(6)	C(2)-C(1)	156.2(8)
C(4)-C(1)	152.7(8)	C(3)-C(1)	154.7(7)
C(5)-C(1)	152.1(8)		
Fe(1)-Fe(2)-S(3)	56.48(5)	P(1)-Pt(1)-P(2)	99.66(5)
Fe(1)-Fe(2)-S(4)	56.17(5)	P(1)-Pt(1)-S(1)	87.39(5)
Fe(1)-S(3)-Fe(2)	67.13(5)	P(1)-Pt(1)-S(2)	172.97(5)
Fe(1)-S(4)-Fe(2)	66.50(5)	P(2)-Pt(1)-S(1)	172.92(5)
S(3)-C(4)-C(1)	121.3(4)	P(2)-Pt(1)-S(2)	83.03(5)
S(4)-C(5)-C(1)	118.7(4)	S(1)-Pt(1)-S(2)	89.89(5)
C(4)-C(1)-C(5)	110.6(5)	S(1)-C(2)-C(1)	114.4(4)
C(2)-C(1)-C(3)	109.7(4)	S(2)-C(3)-C(1)	117.2(4)

2.4 Silicon Containing Model Complexes

It is well known that the presence of one or more silicon atoms influences the chemical, physical as well as biological properties of drugs.[194] This exchange of carbon by silicon (sila-substitution) affects the pharmacodynamics and kinetics in an extraordinary way. It was shown that these properties can be exploited for drug design in medicinal chemistry and have already been used for the development of new silicon-based pharmaceuticals. Likewise, sila-substitution of odorants has also been demonstrated to affect their olfactory properties.[195] However, not only silicon containing biological active compounds reveal these interesting properties. A recent study showed that the impact and friction sensitivity of explosives can be altered by sila substitution.[196] Beside the polymeric silicones, especially polysilol polymers and oligomers are known and reveal strong light emission and absorption in the longer wavelength region or electroluminescent properties and electron or hole transport.[197] These properties are in principle a result of a different covalent radius and electronegativity compared to carbon. A comparison of the electronegativities, covalence radii, average bonding distances and energies can be seen in Table 11.

In contradistinction to the C-C bond, the polarity of the $C^{\delta-}$-$Si^{\delta+}$ bond is changed due to the smaller electronegativity of Si. Moreover, the covalent radius and bonding distance C-Si are eminent larger than those for C-C bonds. Nevertheless, it is notable that the stability of the E-C bonds are comparable, supporting the high stability of the Si-C bond.

Inspired by these unique features, silicon containing dithiols were used as ligands for [FeFe]-hydrogenase models. The [2Fe2S(Si)] model complexes were investigated according to their structural and electrochemical properties.

Table 11. Carbon/Silicon Comparison.[198]

E	electronegativity of E	covalent radius of E [pm]	bonding distance E-C [pm]	bond energy E-C [kJ/mol]
C	2.5	77	154	358
Si	1.9	117	188	311

2.4.1 Synthesis and Characterization of Silicon-Containing Thiolato Complexes with $R_2Si(CH_2SH)_2$ and $Si(CH_2SH)_4$ Type Ligands (*manuscript number 2 and 3*)

To reveal the principle features of [2Fe2S(Si)] complexes the alkylic silanes **111** - **113** were reacted with $Fe_3(CO)_{12}$ in boiling toluene to give the [2Fe2S] complexes **114** - **116** in good yields (Scheme 52). Compounds **114** - **116** were confirmed *via* spectroscopic techniques (^{1}H, ^{13}C, ^{29}Si NMR, IR) as well as mass spectrometry and elemental analyses.[199]

It was possible to obtain single crystals suitable for structure determinations for compounds **114** - **116**. It is important to say that the S-C-Si bond angle was found to be unexpectedly high. In contrast to the expected angle of 109.5° for sp^3 hybridized methylene groups, a value of around 120° was obtained. It is notable that these wide bonding angles are ubiquitous for all silane complexes.[199]

To reveal the electrocatalytic features of these complexes, cyclic voltammetry was commenced to figure out their potential as [FeFe]-hydrogenase model complexes. The redox potentials are pictured in Table 12. When compared to related carbon-based complexes, these complexes are both, easier to oxidize and to reduce by about 100 mV. This property is somewhat surprising, since a less positive oxidation potential would suggest an increased electron density at the iron centres; but if this would be the case, the reduction would be more difficult leading to reduced redox potential.
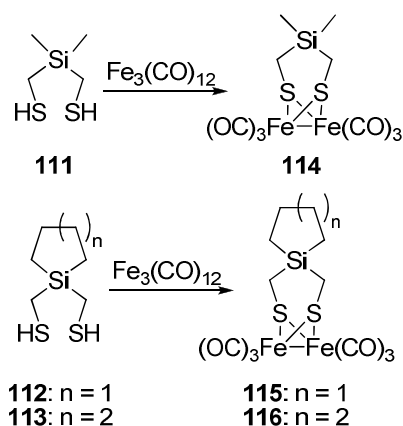
Scheme 52. Reaction of $Fe_3(CO)_{12}$ and $R_2Si(CH_2SH)_2$ type ligands.

Table 12. Electrochemical data of **114 - 116** and **118**.[199]

Compound[a]	E_{ox} [V]	$E_{red,1}$ [V]	$E_{red,2}$ [V]
40[127]	+0.85[b]	−1.53 (E_{pc}); −1.42 (E_{pa})	-2.15[b]
114	+0.79[b]	−1.48 (E_{pc}), −1.40 (E_{pa})	-
115	+0.81[b]	−1.49 (E_{pc}), −1.40 (E_{pa})	-
116	+0.81[b]	−1.49 (E_{pc}), −1.39 (E_{pa})	-
118	+0.99[b]	-1.05[b]	-2.15 (E_{pc}), -1.89(E_{pa})

[a] Potentials in V ± 0.01 *vs.* 0.01 M Ag/Ag⁺ in CH₃CN in 0.10 M [*n*-Bu₄N][BF₄]/CH₃CN; [b] irreversible wave.

The fact that this is not observed may suggest that the two redox processes involve different orbitals. In contrast to literature known complexes, another difference observed during this study is that, these complexes undergo a two-electron reduction, whereby the second reduction step reveals a more positive reduction potential. This behaviour can be explained by a reduction accompanied by structural change as described in earlier sections (chapter 1.3).

However, in the presence of acid a difficult behaviour was found. On the basis of digital simulations, reaction equations (1) - (21) were assumed to play an important role during the electrocatalytic formation of dihydrogen and were in good agreement with the experimental data (Figure 18). An additional catalytic reduction signal at -2.2 V (Figure 19) could only be simulated in a qualitative way for reactions on a mercury drop electrode.
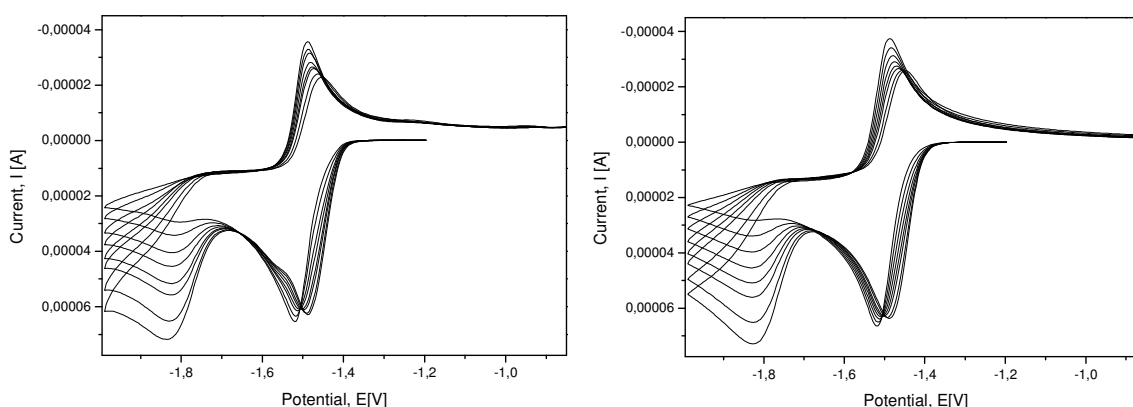
Figure 18. Cyclic voltammetric reduction of a 1.4 mM solution of **115** in acetonitrile on a mercury drop electrode in the presence of varying concentrations of pivalic acid (left) and simulated CVs (right). The scan rate is 1 V/s. The HP concentration was varied as follows: [HP]/[**115**] = 1/3, 2/3, 1, 4/3, 5/3, 2, 8/3, 10/3. The mechanism and simulation parameters are given by reaction (1) to (11), *vide infra*.
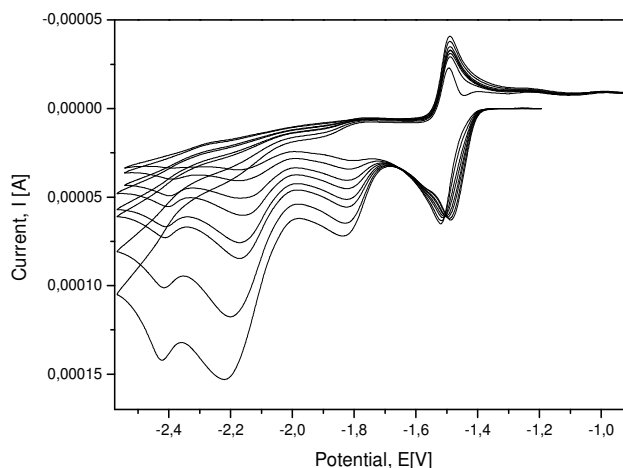
Figure 19. Cyclic voltammetric reduction of compound **115** on a mercury drop electrode in the presence of varying concentrations of pivalic acid. The scan rate is 1V/s. The HP concentration was varied as follows: [HP]/[**115**] = 1/3, 2/3, 1, 4/3, 5/3, 2, 8/3, 10/3.

$$Fe\text{-}Fe + e^- = Fe\text{-}Fe^- \qquad (E°_1 = -1.538V, \; k°_1 = 0.4 \pm 0.1 \; cm/s) \qquad (1)$$

$$Fe\text{-}Fe^- + e^- = {}^-Fe\text{-}Fe^- \qquad (E°_2 = -1.475V, \; k°_2 \geq 1 \; cm/s) \qquad (2)$$

$${}^-Fe\text{-}Fe^- + Fe\text{-}Fe = Fe\text{-}Fe^- + Fe\text{-}Fe^- \qquad (k_{f3} \approx 650 \; l/mol/s) \qquad (3)$$

$$Fe\text{-}Fe^- \rightarrow Q \; (decomposition) \qquad (k_{f4} \approx 50 \; s^{-1}) \qquad (4)$$

$$Fe\text{-}Fe + HP = Fe\text{-}Fe\text{-}HP \qquad (K_5 \approx 350\pm200, \; k_{f5} < 10^3 \; l/mol/s) \qquad (5)$$

$${}^-Fe\text{-}Fe^- + HP = {}^-Fe\text{-}Fe\text{-}HP^- \qquad (K_6/K_5 \approx 4, \; k_{f6} \approx 5\times10^8 \; l/mol/s \,) \qquad (6)$$

$${}^-Fe\text{-}Fe\text{-}HP^- + HP = H\text{-}Fe\text{-}Fe\text{-}HP^- + P^- \qquad (K_7 \leq 1, \; diffusion \; controlled) \qquad (7)$$

$$P^- + HP = HP\text{-}P^- \qquad (K_8 \geq 5000,, \; k_{f8} > 2\times10^6 \; l/mol/s \,) \qquad (8)$$

$$Fe\text{-}Fe\text{-}HP + e^- = Fe\text{-}Fe\text{-}HP^- \qquad (E°_3 = -1.48V, \; k°_3 \approx 0.4 \; cm/s) \qquad (9)$$

$$Fe\text{-}Fe\text{-}HP^- + e^- \rightarrow \text{-}Fe\text{-}Fe\text{-}H + P^- \qquad (E°_4 = -1.168 \; V, \; k°_4 = 1.75\times10^{-5} \; cm/s) \qquad (10)$$

$$Fe\text{-}Fe^- + HP + e^- \xleftarrow{\;P-\;} {}^-Fe\text{-}Fe\text{-}H \qquad (E°_5 = -1.168 \; V, \; k°_5 = 0.1 \; cm/s) \qquad (11)$$

$$H\text{-}Fe\text{-}Fe\text{-}HP^- + e^- = {}^-H\text{-}Fe\text{-}Fe\text{-}HP^- \qquad (E°_6 = -1.77V, \; k°_6 \approx 0.2 \; cm/s) \qquad (12)$$

$${}^-H\text{-}Fe\text{-}Fe\text{-}HP^- \rightarrow Fe\text{-}Fe^- + P^- + H_2 \qquad (k_{f13} = 7 \; s^{-1}) \qquad (13)$$

$${}^-H\text{-}Fe\text{-}Fe\text{-}HP^- + HP \rightarrow Fe\text{-}Fe\text{-}HP^- + P^- + H_2 \qquad (k_{f14} = 2300 \; l/mol/s) \qquad (14)$$

$${}^-H\text{-}Fe\text{-}Fe\text{-}HP^- + HP \rightarrow H\text{-}Fe\text{-}Fe\text{-}HP^- + P^- + H_2 \qquad (k_{f15} = 13500 \; l/mol/s) \qquad (15)$$

$$H\text{-}Fe\text{-}Fe\text{-}HP^- = H\text{-}Fe\text{-}Fe\text{-}H + P^- \qquad (16)$$

$${}^-H\text{-}Fe\text{-}Fe\text{-}H^- \rightarrow {}^-Fe\text{-}Fe^- + H_2 \qquad (17)$$

$$^-\text{H-Fe-Fe-H}^- + \text{HP} \rightarrow {}^-\text{Fe-Fe-H} + \text{H}_2 + \text{P}^- \qquad (18)$$

$$^-\text{H-Fe-Fe-H}^- + \text{HP} \rightarrow \text{H-Fe-Fe-H}^- + \tfrac{1}{2}\,\text{H}_2 + \text{P}^- \qquad (19)$$

$$^-\text{H-Fe-Fe-HP}^- \xrightarrow{\ e^-\ } {}^-\text{H-Fe-Fe-H}^- + \text{P}^- \qquad (20)$$

$$\text{H-Fe-Fe-HP}^- \rightarrow \text{H-Fe-Fe-H} + \text{P}^- \qquad (21)$$

It should be mentioned that it might be better to formulate reaction equations (12) - (15) in terms of H-Fe-Fe-H instead of H-Fe-Fe-HP$^-$. However, this question could not be answered, since it was not possible to commit studies at high scan rates so that the effect of reaction (16) would become visible. Unfortunately, adsorption phenomena on the electrode prevented quantitative studies of the system at sufficiently high scan rates. A simplified mechanistic cycle can be seen in Scheme 53.

The main catalytic species is $^-$H-Fe-Fe(HP)$^-$ and H$_2$ formation follows equation (15) with access of HP or (13) with small amounts of acid. A few more comments have to be given according to the intermediates **I** and **II** (Scheme 53) since their structure is eminent and important for the understanding of the mechanism displayed.
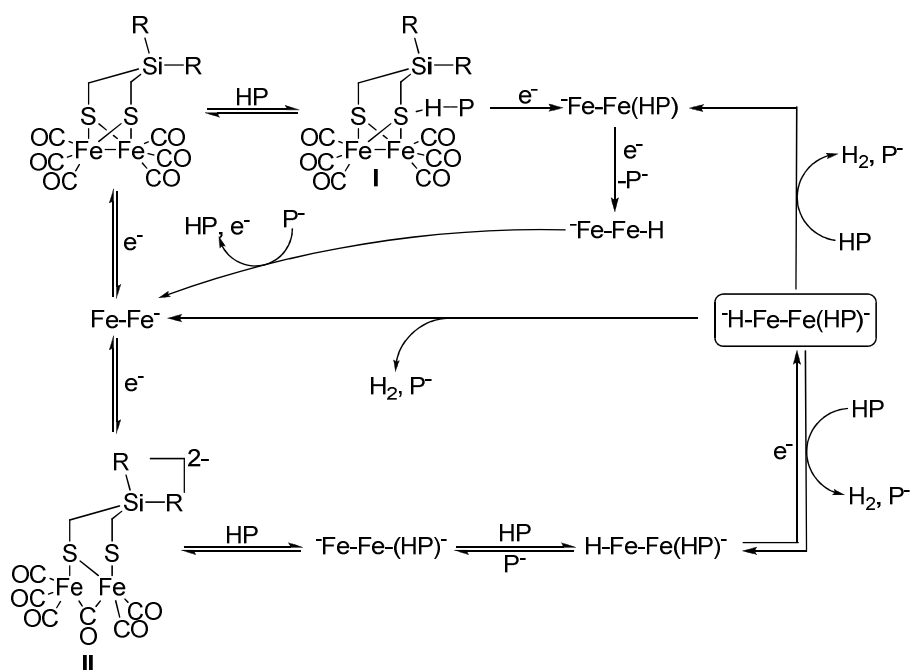
Scheme 53. Tentative mechanism for the H$_2$ development of the silicon-containing [FeFe]-hydrogenase models **114** - **116** with respect to reaction equations (1)-(15). The influence of equation (16) was neglected in this scheme for simplicity.

Structure of I: It was noticed during electrochemical investigations that an "isosbestic" like point appeared in the presence of acid (see Figure 18). Comparable anodic shifts were observed only in the case of functionalized diiron azadithiolato complexes, thus this behaviour can be best interpreted by a protonation of the complex **115** either on the Fe-Fe bond or on the sulphur atoms.

No example of protonation of coordinated sulphur has been reported for [FeFe]-hydrogenase model systems. However, using DFT calculations and photoelectron spectroscopy, Glass *et al.* have shown that for related tin containing [2Fe2S(Sn)] systems the σ(Sn–C) orbital interacts with a 3p(S) orbital.[200] These inductive and hyperconjugative interactions increase the electron density at the sulphur atom. As a direct result the basicity of the sulphur atom increases. Within the course of digital simulations it was possible to reconstruct the "isosbestic" point by taking into account reaction equation (5). Since pivalic acid is a rather weak acid[**] a direct protonation was excluded. On the contrary, an undissociated HP molecule is coordinated to the complex through hydrogen bonds and the splitting of the H-P bond is initiated by the reduction of **115** (either in form of a concerted process or as follow-up reaction).

This theory was further confirmed by IR spectroscopic investigations of the reaction of **115** with the strong acid HBF$_4$. In the course of these investigations it was observed that a strong shift to higher wave numbers appeared after adding acid.[199] Since these initial tests reveal a reaction with acid, ^{1}H NMR spectroscopic investigations were committed to allow a distinction between a protonation on the Fe-Fe bond or the sulphur atom. However, no signal at higher field was obtained (> -1 ppm) which is a requisite evidence for an iron bound hydride.[199] Thus a protonation of the Fe-Fe bond can be excluded.

An additional supporting argument of the high electron density was obtained by quantum chemical calculations. The computed molecule orbital (MO-103) (molecular orbital, energy niveau 103) shown in Figure 20, can be understood as a σ-bonding interaction between the silicon atom Si(1) with its neighbouring carbon atom C(1), and also as a π-bonding interaction between C(1) and the sulphur atom S(1). This type of interaction allows a shift of electron

---

[**] The pK$_a$-value of acetic acid is 22.6 [113] and that of pivalic acid should not be significantly different.
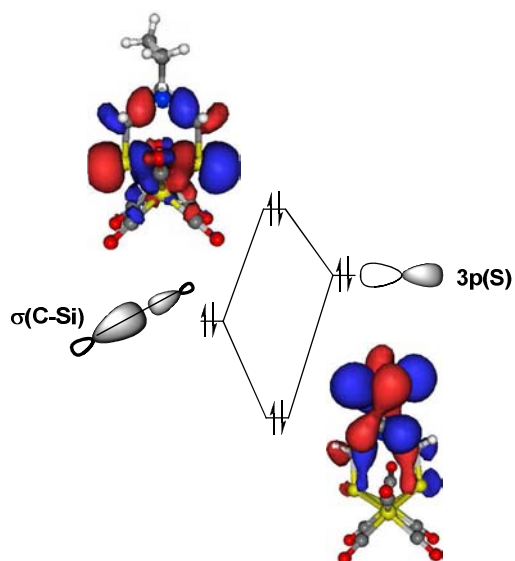
Figure 20. Simplified model for the electronic structure of the Si-C-S fragment. The bonding interaction refers to MO-103 and the anti bonding combination to the HOMO^{-1}.

density from the electropositive silicon atom (EN$_{Pauling}$ = 1.9[201]) to the more electronegative sulphur atom (EN$_{Pauling}$ = 2.58[201]). It is comparable to the β-silicon-effect, which describes the stabilization of a carbocation in beta position to a silyl group by hyperconjugation. In analogy to that, the interaction in **115** can thus be interpreted as an interaction between the σ(Si-C) fragment orbital and a p-orbital of sulphur.

In contrast to the beta-silicon-effect, the p-orbial of sulphur is occupied. The anti-bonding combination of these fragment orbitals results in the HOMO^{-1} (Figure 20, Figure 21) and displays a four-electron interaction. The fragment orbital assigned to the σ(C-Si) bond interacts with the energetically higher p-orbital of sulphur resulting in a binding combination with higher electron probability density located at the C-Si fragment (MO-103). The corresponding anti-bonding interaction in return has a higher electron probability density located at the sulphur. Due to the local C$_s$ symmetry of the molecule, all discussed interactions in the fragment consisting of the atoms Si(1)-C(1)-S(1) also apply for the fragment Si(1)-C(2)-S(2).
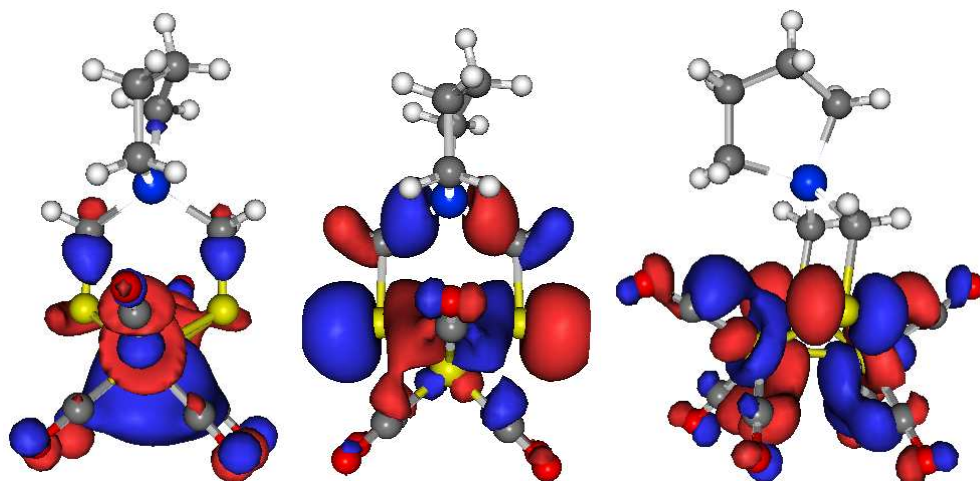
Figure 21. Kohn-Sham orbitals for compound **115** (HOMO - left; HOMO^{-1} - middle; LUMO - right).

Structure of II: Since a two-electron reduction of **115** was proclaimed according to an ECE mechanism, whereby the chemical reaction was assigned to a structural reorganisation, it was believed that a "rotated" state is also formed in the reduced species. It is well known from the investigations of Darensbourg *et al.* that in the presence of electron donating phosphorous ligands the oxidized iron cluster reveals a "rotated" state.[99] However, up to now only little is known about the shape of the reduced states. Since during CV investigations the reduction processes appeared at -1.48 V, sodium amalgam (U$^{\varnothing}$ < -1.8 V depending on the concentration of sodium in mercury[202]) was used for the reduction of compound **115** (Scheme 54) and the reaction was followed by IR spectroscopy.

During treatment of **115** with sodium amalgam a new adsorption band appeared at 1726 cm^{-1} in the IR spectrum and gave hint for a bridging carbonyl. Comparison of the calculated and the experimental IR spectra of **II** reveal good accordance and confirmed the "rotated" state of **II**. It is therefore reasonable to deal with "rotated" states also in the course of reduction processes and not solely for oxidation processes.
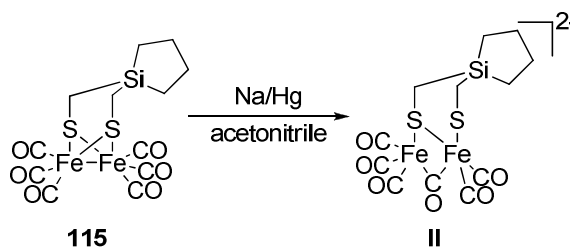
Scheme 54. Reaction of compound **115** with sodium amalgam in acetonitrile.
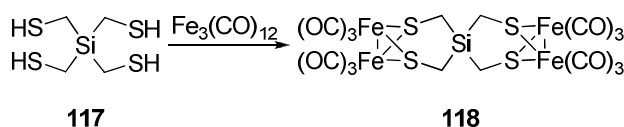
Scheme 55. Reaction of Si(CH$_2$SH)$_4$ (**117**) and Fe$_3$(CO)$_{12}$.

Further reactions were committed with Si(CH$_2$SH)$_4$ (**117**). The reaction of **117** with Fe$_3$(CO)$_{12}$ afforded compound **118** (Scheme 55). Attempts to obtain a [2Fe2S(Si)(SH)$_2$] cluster by varying the amount of Fe$_3$(CO)$_{12}$ exclusively afforded compound **118** in diverging yields.

Efforts to synthesize heteronuclear compounds as described for compound **110** in chapter 2.3 failed, since no platinum complex was accessible *via* the described method. Electrochemical investigations of **118** were performed and reveal no interaction between the two active iron sites (Table 12). It is however reasonable that the properties concerning the protonation and redox behaviour were lost due to a possible electron allocation to four sulphur sites.[199]

To increase the basicity of the iron atoms in the [2Fe2S(Si)] sub-site and to facilitate the formation of hydrides, one carbonyl ligand was selectively exchanged by either cyanide or phosphine ligands. The [FeFe]-hydrogenase model complexes **114** - **116** were reacted with triphenylphosphine and tetraethylammonium cyanide to afford the mono-substituted, asymmetric [2Fe2S(Si)] cluster compounds **119** - **124** (Scheme 56).[203] A selective mono-substituted product was obtained *via* oxidative cleavage of a CO group with trimethylamine-*N*-oxide in acetonitrile and subsequent addition of the phosphine or the cyanide. Structure determination discerned a basal position of the cyanide ligands. In contrast, an apical coordination mode was found for the phosphines.[203]

A comparison of the IR frequencies of the CO stretching vibrations revealed an increasing electron density on the iron atoms according to CO < PPh_3 < CN^- (Table 13), which is notable by decreasing of CO frequencies. This trend was also observed during cyclic voltammetry (Table 14). As already shown for compounds **114** - **116,** the substitution pattern on silicon had no influence on the electrochemistry of these complexes. The reduction potentials clearly indicate that the mono-substituted complexes are easier to reduce than the corresponding complexes **114** - **116**. Thereby, it is noticed that the CN^- substituted complexes reveal the most negative reduction potential. It is somehow surprising that by substitution, the reduction signal becomes irreversible and in the same manner the oxidation signal becomes reversible. It is notable that two closely spaced reduction steps are observed for these compounds. However, unexpected trends arose from the evaluation of the redox potentials.
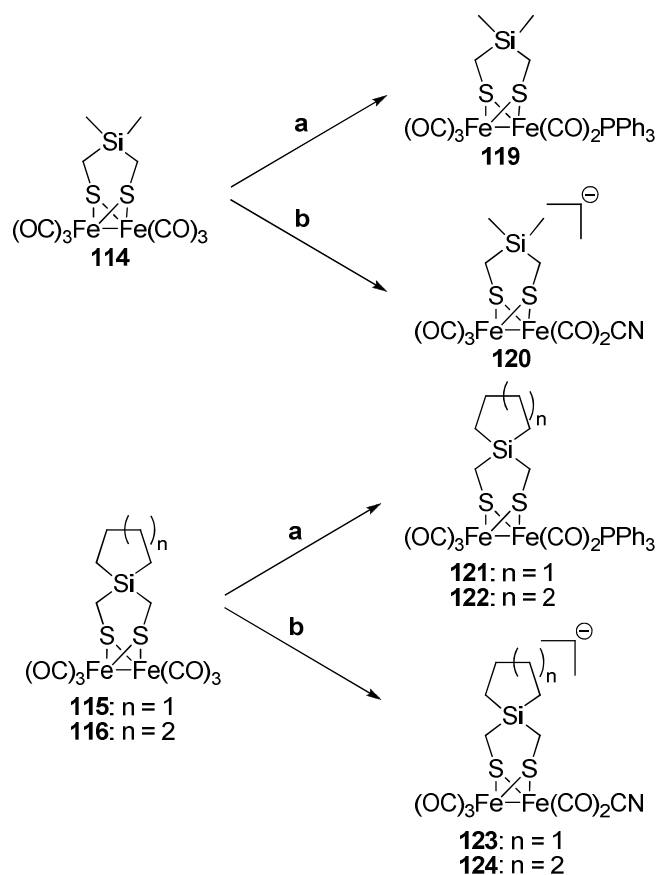
Scheme 56. Synthesis of mono-substituted phosphine and cyanide [2Fe2S(Si)] complexes. a) 1. Me_3NO, acetonitrile; 2. PPh_3. b) 1. Me_3NO, acetonitrile; 2. $Et_4N^+CN^-$.[203]

Table 13. $\tilde{v}$CO and CN$^-$ shifts of complexes **114**, **119**, **120**.[199,203]

Compound	$\tilde{v}_{CO}$ shift	$\tilde{v}_{CN^-}$ shift
114	2074 (vs), 2031 (vs), 1989 (vs)	-
119	2041 (vs), 1981 (vs, b)	-
120	2027 (vs), 1973 (vs)	2088

Table 14. Electrochemical data of **115** and **119** - **124**.[199,203]

Compound	E$_{ox}$ [V]	E$_{red,1}$ [V]
115[a, 199]	+0.81[b]	−1.49 (E$_{pc}$), −1.40 (E$_{pa}$)
119[b]	+0.57 (E_{pa}); +0.44 (E_{pc})	-1.83 (E_{pc})[c]
121[b]	+0.62 (E_{pa}); +0.49 (E_{pc})	-1.80 (E_{pc})[c]
122[b]	+0.61 (E_{pa}); +0.46 (E_{pc})	-1.85 (E_{pc})[c]
124[a]	+0.86 (E_{pa})[c]	-2.04 (E_{pc})[c]

[a] Potentials in V ± 0.01 *vs.* 0.01 M Ag/Ag$^+$ in CH$_3$CN in 0.10 M [*n*-Bu$_4$N][BF$_4$]/CH$_3$CN; [b] Potentials in V ± 0.01 *vs.* 0.01 M Ag/Ag$^+$ in CH$_2$Cl$_2$ in 0.10 M [*n*-Bu$_4$N][BF$_4$]/CH$_3$CN; [c] irreversible wave.

Addition of the σ-donor ligands such as CN$^-$ or PPh$_3$ lead to an increase in electron density around the metal centres which should result in an increase in basicity of the active site. This hypothesis is not completely consistent with all oxidation potential values obtained. The mono-substituted cyano complex **124** experiences an oxidation potential that is more positive than that of the corresponding hexacarbonyl analogues. Therefore, the effect of these ligands on the nature of the HOMO and LUMO must be considered. The addition of a negatively charged ligand may change the location of these orbitals demanding a complicated interpretation of results. Catalytic behaviour is observed for all complexes. However, direct comparison of all six complexes is not possible as a result of the compounds' solubility in different solvents (Table 14).

2.4.2 Hydroxy Functionalized [2Fe2S(Si)] Complexes (*manuscript number 4*)

Inspired by the properties of [2Fe2S(Si)] complexes, hydroxyl functionalized silicon containing complexes were planned. The introduction of hydroxyl functions discloses the possibility of further derivatizations and linking to surfaces. Likewise the type and the spatial arrangement of hydrogen bonds are interesting as it may reflect the enzymatic surrounding and lead to a stabilization of the complexes. In continuation of the investigations on this novel kind of complexes, the hydroxyl functionalized complexes **126** and **128** were synthesized. Thereby, the respective dithiols **125** and **127** were reacted with one equivalent $Fe_3(CO)_{12}$ in boiling toluene and following purification *via* chromatography afforded the complexes **126** and **128** in good yields. The structures of these complexes were confirmed *via* ^1H, ^{13}C NMR, IR spectroscopy as well as mass spectrometry and elemental analysis. Crystal structure analyses revealed the molecular structure of these complexes, whereby strong hydrogen bonds within the molecules were noticed.[204] Cyclic voltammetry was performed to reveal the electrocatalytic properties of the complexes (Table 15). It was noticed that the hydroxyl function had no influence on the catalytic cycle which remained closely the same as reported for compound **115**.

To confirm the ability to act as a building block for novel complexes containing the [2Fe2S(Si)] unit, compound **126** was reacted with the PB-PEO2 compound **66** (Scheme 58). Thus, this reaction afforded the polymer bound complexes **129**, which is currently under investigation to reveal its properties in vesicles.
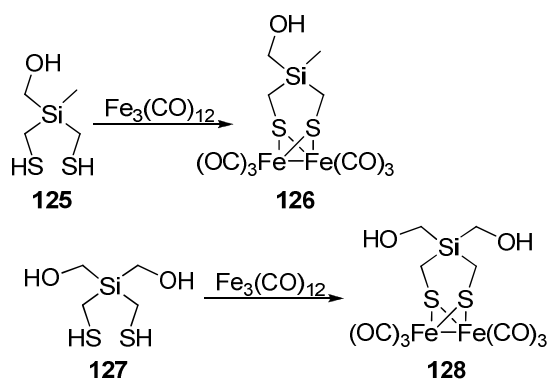
Scheme 57. Hydroxy functionalized [2Fe2S(Si)] complexes.

Table 15 . Electrochemical data of **126** and **128**.[204]

Compound	E_{ox} [V]	$E_{red,1}$ [V]	$E_{red,2}$ [V]
115[199,a]	+0.81[c]	−1.49 (E_{pc}), −1.40 (E_{pa})	-
126[a]	+1.02	−1.57 (E_{pc}), −1.39 (E_{pa})	-
128[b]	+0.82	−1.43 (E_{pc}), −1.36 (E_{pa})	-

[a] Potentials in V ± 0.01 *vs.* 0.01 M Ag/Ag$^+$ in CH$_3$CN in 0.10 M [*n*-Bu$_4$N][BF$_4$]/CH$_3$CN;
[b] Potentials in V ± 0.01 *vs.* 0.01 M Ag/Ag$^+$ in CH$_3$CN in 0.10 M [*n*-Bu$_4$N][BF$_4$]/CH$_3$CN;
[c] irreversible wave.
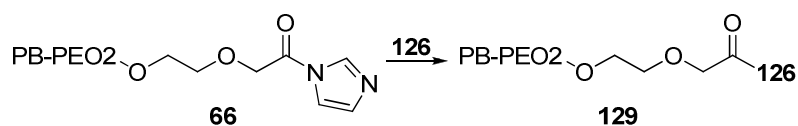
Scheme 58. Synthesis of polymer-attached complex **129** as an ester.

2.4.3 Mixed Valent [FeFe(Si)] Systems (*manuscript number 2* and 4)

Inspired by the investigations of Pickett *et al.*[101,102] concerning mixed-valent hydrogenase models, compound **130** was reacted with $Fe_3(CO)_{12}$ under various reaction conditions. Reaction of the silicon compound **130** with one molar equivalent of $Fe_3(CO)_{12}$ afforded the diiron compound **131** and the tetrairon complex **132** (Scheme 59). The identity of the two compounds was established by NMR studies (^{1}H, ^{13}C, HSQC, H,H-COSY), mass spectrometry, as well as IR spectroscopy, powder diffractometry and Raman studies. Additionally, compound **132** was structurally characterized by single crystal X-ray diffraction.[199] Interestingly, single crystals of **132** were obtained by slow evaporation from both, a solution of **131** and a solution of **132**, dissolved in chloroform. A transformation of **131** into **132** was observed and verified *via* powder X-ray crystallography and thin layer chromatography. Furthermore it was noticed that **132** decomposes in solution within several hours and afford a mixture of iron oxides, iron sulphides and silicates, as substantiated by powder X-ray crystallography.

In agreement to the literature-known complex $[Fe_4\{MeC(CH_2S)_3\}_2(CO)_8]$, compound **132** affords a $Fe^IFe^{II}{\cdots}Fe^{II}Fe^I$ assembly with comparable bond angles and distances. The electrochemistry of compound **132** was investigated in dichloromethane and acetonitrile and compared with the literature-known complex as well as **115** (Table 16).[199] The redox processes of these complexes are solvent-dependent, with an approximately 100 mV negative shift when changing from dichloromethane to acetonitrile. The first reduction wave of $[Fe_4\{MeC(CH_2S)_3\}_2(CO)_8]$ compound appears at a potential that is approximately 140 mV more positive than that of the corresponding process in the related silicon compound **132**. A difference of 100 mV is noted for the second reduction potential. However, comparison of the silicon-based hydrogenase
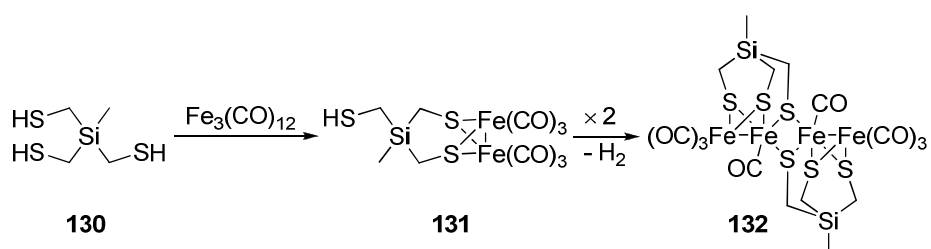
Scheme 59. Reaction cascade towards tetra-nuclear, mixed-valent iron sulphur complex **132**.

Table 16. Electrochemical data for compound **132** and the related carbon compound $[Fe_4\{MeC(CH_2S)_3\}_2(CO)_8]$ in acetonitrile and dichloromethane. All values have been corrected against Ag/Ag^+ reference electrode using the Fc/Fc^+ redox couple as an internal standard.[199]

Compound	E_{ox} [V]	$E_{red,1}$ [V]	$E_{red,2}$ [V]
132 (CH_3CN)[a]	+0.91 and +1.04	-1.35 (E_{pc}), -1.52 (E_{pc})	-2.16[b]
132 (CH_2Cl_2)[a]	+1.44[b]	-1.25 (E_{pc}), -1.43 (E_{pc})	-
$[Fe_4\{MeC(CH_2S)_3\}_2(CO)_8]$[102] (CH_2Cl_2)	-	-1.11 (E_{pc}), -1.48 (E_{pc})	-

[a] Potentials in V ± 0.01 *vs.* 0.01 M Ag/Ag^+ in 0.10 M $[n\text{-}Bu_4N][BF_4]/CH_3CN$; [b] irreversible wave.

analogue with the related carbon-based species suggested that the presence of silicon does not greatly affect the reduction potentials. Subsequent addition of acetic acid revealed hydrogen development from the Fe^IFe^I redox couple at moderate potential (~ –1.8 V).

Since compound **132** offered dihydrogen development at the Fe^IFe^I level at moderate potential, a functionalized complex was planned. Thus a derivatization and linking to surfaces would be possible. For this purpose, compound **133** was reacted with $Fe_3(CO)_{12}$ and afforded the functionalized [4Fe6S] cluster **134** in 12 % yield.[204] Compound **134** was verified by spectroscopic techniques (^1H, ^{13}C, IR) as well as mass spectrometry. However, investigation of the electrochemical features was not possible due to the instability of **134** in solution.
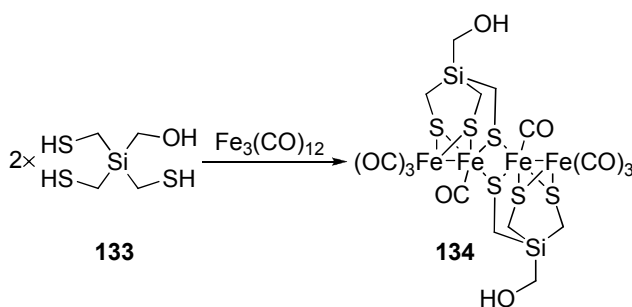
Scheme 60. Synthesis of the functionalized mixed-valent [4Fe6S] complex **134**.[204]

2.4.4 Sterical Demanding [2Fe2S(Si)] Complexes (*manuscript number 5*)

Since Darensbourg *et al.* described the synthesis of model complexes, replicating the mixed-valence H_{ox} state with a rotated iron site the modelling of this feature is in progress.[80h,99] Thereby, the $Fe^I Fe^{II}$ system reveals a vacant coordination site and a semi-bridging CO ligand. It is assumed that the sterical demand of the S-to-S linker and the establishment of asymmetrical bisphosphine complexes stabilize the oxidized rotated form.[100] Since investigations on [2Fe2S(Si)] complexes exhibited different structural and electrochemical behaviour,[199] sterically demanding silicon-containing ligands were synthesized to favour the oxidized or reduced rotated species. In order to investigate the chemical and electrochemical features in the presence of sterically demanding ligands, bis(mercaptomethyl)-diphenylsilane (**135**),[205] bis(benzylthio)-dimethylsilane (**136**)[206] and bis(benzylthio)diphenylsilane (**137**) were synthesized (Scheme 61).

Initial attempts to synthesize compound **136** according to the Grignard-pathway depicted in Scheme 62 failed since the respective dibromide was not isolable. In contrast to compound **136**, the dithiol **137** was obtained *via* this path. Thereby, diphenyldichlorosilane was reacted with two equivalents of benzylmagnesium chloride to give **138** in good yield. Subsequent reaction with NBS afforded *meso*-**139**. The following reaction with potassium thioacetate afforded compound **140,** which was additionally reacted with lithium alanate leading to compound **137**. However, the overall yield was very low (~ 1 %) and the pathway was therefore inacceptable.

A more suitable procedure with an increased yield is displayed in Scheme 63.[206] The dichlorosilane component was reacted with two equivalents of benzylmercaptane in the presence of *n*-butyllithium, whereas compound **A** was generated. Consecutive double Wittig rearrangement by *in situ* treatment of **A** with *tert*-butyllithium and crystallization afforded exclusively the *meso*-forms of **136** and **137**. They were entirely analysed by NMR techniques, mass spectrometry and elemental analysis.
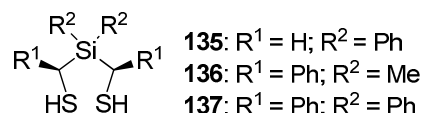
Scheme 61. Sterical demanding dithiols.
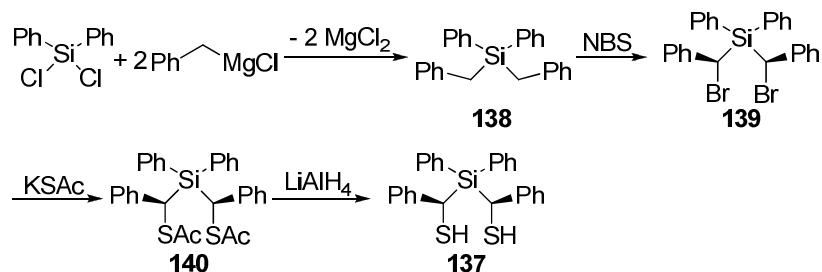
Scheme 62. Synthesis of compound **137** *via* the Grignard way.
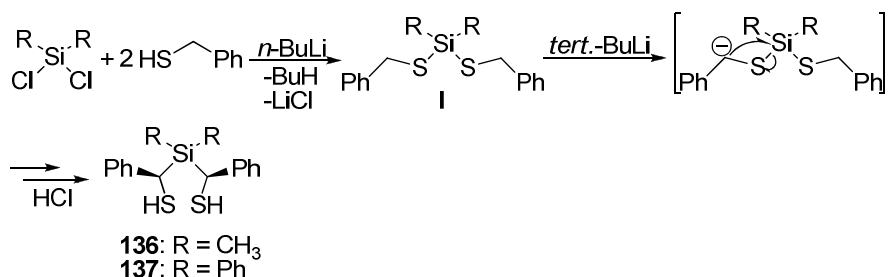
Scheme 63. Double Wittig rearrangement of *in situ* generated compound **A** afforded exclusively the *meso*-**136** and *meso*-**137** after workup.

Subsequent reaction of **135**, **136** and **137**, respectively, with one molar equivalent $Fe_3(CO)_{12}$ afforded the complexes **141** - **143** (Scheme 64).[207] For these hexacarbonyl complexes already a significant rotation of a $Fe(CO)_3$ fragment was observed. This however is strongly dependent on both the substituents R^1 and R^2 (Table 17). Where compound **141** shows a slight increase of the torsion angle OC_{apical}-Fe-Fe-CO_{apical} to 4.13°, the less sterical demanding methyl groups in compound **142** does not induce any rotation of an iron centre. In contrast to these rather "unpretentious" molecules, compound **143** shows up the influence of combining sterical demanding groups for R^1 and R^2. A C_{apical}-Fe-Fe-C_{apical} torsion angle of 18.03° is observed within the molecule. This is the first example with a strong rotation for a hexacarbonyl complex.
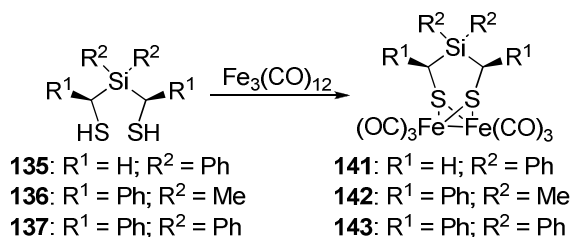
Scheme 64. Synthesis of sterical demanding molecules **141** - **143**.

135: R^1 = H; R^2 = Ph
136: R^1 = Ph; R^2 = Me
137: R^1 = Ph; R^2 = Ph

141: R^1 = H; R^2 = Ph
142: R^1 = Ph; R^2 = Me
143: R^1 = Ph; R^2 = Ph

141: R^1 = H; R^2 = Ph
142: R^1 = Ph; R^2 = Me
143: R^1 = Ph; R^2 = Ph

144: R^1 = H; R^2 = Ph; R' = Ph
145: R^1 = Ph; R^2 = Me; R' = Ph
146: R^1 = Ph; R^2 = Ph; R' = Ph
147: R^1 = H; R^2 = Ph; R' = Me
148: R^1 = Ph; R^2 = Me; R' = Me
149: R^1 = Ph; R^2 = Ph; R' = Me
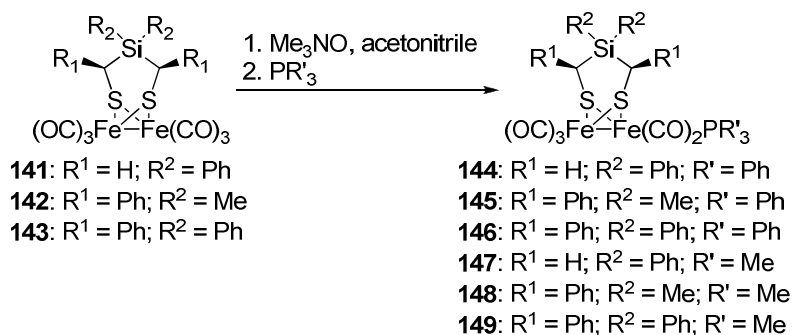
Scheme 65. Substitution *via* oxidative cleavage of CO and subsequent addition of phosphines lead to the mono-substituted complexes **144** - **149**.

Table 17. Torsion angles (OC$_{apical}$)-Fe-Fe-(L$_{apical}$).

compound	Torsion angle α [°]
141	4.13
142	0
143	18.03
144	29.96
146	7.21
147	26.20
148	11.61
(μ-pdt){Fe(CO)$_2$PMe$_3$}$_2$[99]	29

To further increase the sterical demand within the complexes, complexes **141** - **143** were reacted with trimethylamine-*N*-oxide and an excess of triphenyl- or trimethylphosphine. Thereby, exclusively the mono-substituted triphenylphosphine complexes **144** - **146** and trimethylphosphine complexes **147** - **149** were obtained (Scheme 65).

It was possible to obtain crystal structures suitable for single crystal X-ray determination of **144**, **146**, **147** and **148**. A tremendous increase of the OC$_{apical}$-Fe-Fe-P$_{apical}$ torsion angle was noticed for the triphenylphosphine complex **144** (Table 17). It is notable that especially complex **144**
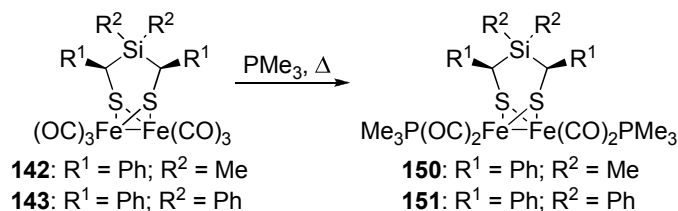
Scheme 66. Reaction of the hexacarbonyl complexes **142** and **143** with trimethylphosphine to reveal the disubstituted complexes **150** and **151**.

reveals an even higher torsion angle than noticed for the disubstituted complex, (μ-pdt){Fe(CO)$_2$PMe$_3$}$_2$.[99] The latter complex is known for the possibility to form the "rotated" structure upon oxidation and the size of the OC$_{apical}$-Fe-Fe-P$_{apical}$ torsion angle can be assumed as a scale for the voluntariness to form a "rotated" state. It is somehow surprising that the OC$_{apical}$-Fe-Fe-CO$_{apical}$ torsion angle decreases by about 11° to 7.21° for compound **146**. Furthermore, the crystal structure of **146** revealed decreased bonding angles (S-C-Si) of 114.8(2) and 118.0(2)°, which is about 4° smaller than for compound **143**.

In addition, reactions of complexes **142** and **143** with trimethylphosphine in boiling toluene afforded the disubstituted complexes **150** and **151** in moderate yields (50 and 34 %, respectively) (Scheme 66). No single crystals suitable for structure determination were obtained so far from complexes **150** and **151**. It is therefore not possible to compare and discuss the torsion angles of these molecules. However, one should expect an increase of the torsion angles and a stabilization of a "rotated" state.

To reveal the formation of the "rotated" state during oxidation, complexes **141** - **151** were reacted with ferrocenium hexafluorophosphate (FcPF$_6$) and the process monitored via IR spectroscopy. No band was observed which could be assigned to a bridging CO ligand and merely a precipitate was formed during the reactions, suggesting a possible decomposition of the complexes. In opposite, upon treatment with sodium/amalgam a bridging CO was verified. Electrochemical investigations of these complexes are currently in progress and will show their ability towards the dihydrogen formation.

2.5 *Influence of the Bridgehead Atoms* (*publication number 5 and manuscript 6*)

Since in the preceding investigations the nature of the S-to-S linker as well as the CO replacement was shown to reveal tremendous influence on the electrochemical properties of the dihydrogen formation, a further going study was focused on the importance of sulphur as a bridgehead atom. It is surprising that in case of [FeNiSe]-hydrogenases, nature incorporates selenium into the active site.[15] Furthermore, selenium is not very rare in organisms and other metabolisms and selenium containing enzymes exist.[208] Related to the [FeFe]-hydrogenase, the incorporation of selenium or the higher homologous tellurium should result in an easier formation of a terminal hydride and higher activity by increasing the electron density on the iron atoms. However, no [FeFe(Se)]-hydrogenase is known up to now.

Inspired by the question of the "Why not?" the two homologous series displayed in Scheme 68 were synthesized and investigated according to their electrocatalytical differences.[209,210] The electrochemical properties in the absence of acid are displayed in Table 18.

The electrochemical data revealed comparable potentials for the reduction behaviour. However, in the presence of acid the catalytic activity for the reduction of protons was shown to be substantially diminished with increasing atom number from sulphur to tellurium. Furthermore, quantum chemical calculations revealed that the formation of a rotated state with a bridging
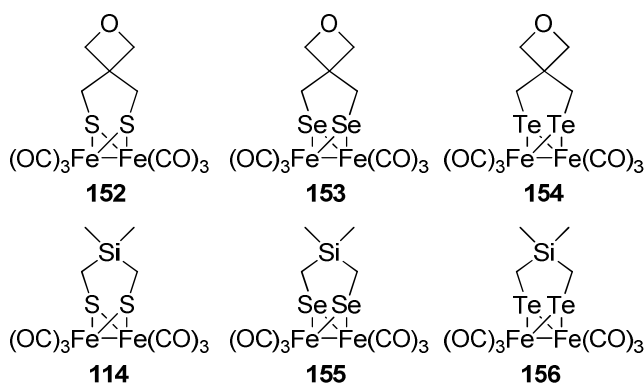
Scheme 67. Homologous series of hydrogenase models containing E-to-E linkers (E = S, Se, Te).

ligand is likewise restricted.[209] Thus this homologous series brings forth a plausible reason for the natural incorporation of sulphur instead of selenium or tellurium. Sulphur offers higher activity towards the formation of dihydrogen due to the preferred formation of the rotated state.

Table 18. Electrochemical data of [2Fe2E] system (E = S, Se, Te).[209,210]

Compound[a]	E_{ox} [V]	$E_{red,1}$ [V]
114	+0.79[b]	−1.48 (E_{pc}), −1.40 (E_{pa})
152	0.810[b]	-1.602[b]
153	0.778[b]	-1.551[b]
154	0.708[b]	-1.535[b]
155	+0.70	-1.51
156	+0.62	-1.51

[a] Potentials in V ± 0.01 *vs.* the ferrocenium/ferrocene couple in CH_3CN in 0.10 M [n-Bu_4N][BF_4]/CH_3CN; [b] irreversible wave.

3 Outlook

Since interesting properties arose during the preparation of this thesis, a small outlook should be given for future possibilities based on this work.

i) Especially the silicon containing [2Fe2S] complexes offered extraordinary properties. In contrast to [2Fe2S(Si)] complexes, no currently described model complex in literature revealed dihydrogen development at three different potentials. Furthermore, the [2Fe2S(Si)] complexes offered high activity towards dihydrogen development at moderate potential.
Inspired by these properties, it would be interesting to investigate the higher homologues of silicon and to establish germanium and tin containing complexes (Scheme 68). The use of these higher homologues should probably enhance these features.
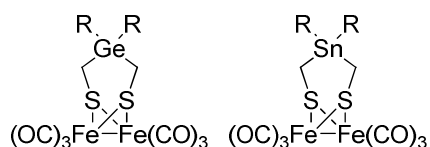
Scheme 68. Desired germanium or tin complexes.

ii) [2Fe2S(Si)] complexes show up interesting properties (sulphur protonation, reduction of protons with a low overpotential, formation of a "rotated state") but the formation of dihydrogen was only possible within electrocatalysis. Therefore, new silicon containing complexes were planned, where the reduction of the [2Fe2S] cluster can be achieved by irradiation (Scheme 69).[211]
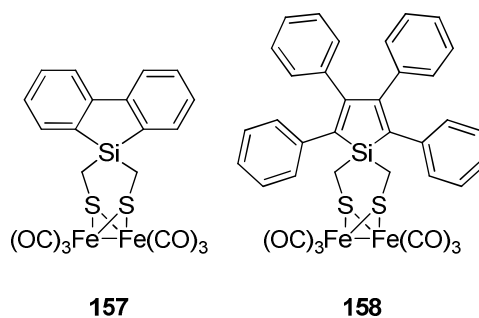
Scheme 69. Desired photoactive [2Fe2S(Si)] complexes.

It is notable that silicon containing heteroles already exist and exhibit extraordinary good properties (low band gaps, non-linear optical properties and thermochroism).[212] In contrast to their carbon analogues, the HOMO of the siloles is lowered by ~ 0.4 eV and the LUMO even more by 1.2 eV.[213] This behaviour can be best described by a good interaction between the π* of the butadiene orbital and the σ* of the silylene orbitals (Scheme 70). This interaction is enforced by the tetrahedral geometry around the silicon atom, whereby the σ* of the silylene and the π* of the butadiene orbitals are parallel to each other.[213,214] In contrast to silicon, a comparable interaction in cyclopentadiene systems is rather not possible due to the energetically high σ*(CH) orbitals.[213] The reduced energy distance ($\sigma^*(b_1)/\pi^*(b_1)$) of the siloles results in both, a shift of the absorption and the fluorescence to an intense blue spectral region.[213,215] Since it was shown that the silicon atom can communicate with the [2Fe2S] cluster *via* hyperconjugation, fluorescence quenching can be expected, similar to that found by Song and co-workers and should allow the establishment of a photocatalytic dihydrogen formation mechanism, similar to that found during cyclic voltammetry.[216] The short linker and the hyperconjugation between σ(Si-C) and 3p(S) should make complexes **157** and **158** very attractive on the way to the photocatalytical formation of dihydrogen due to the effect of fluorescence quenching.

To establish compound **157** the synthesis route shown in Scheme 71 was planned. 1,2-Dibromobenzene was reacted with n-BuLi and afforded 2,2′-dibromobiphenyl (**159**).[217] Further reaction of compound **159** with tetrachlorosilane in the presence of *n*-BuLi afforded 1,1-dichloro-1-silafluorene (**160**).[218] Up to now, no reaction could be established which would afford compound **161**.

$\Delta E_{LUMO} = -1.28$ eV

$\Delta E_{HOMO} = -0.44$ eV
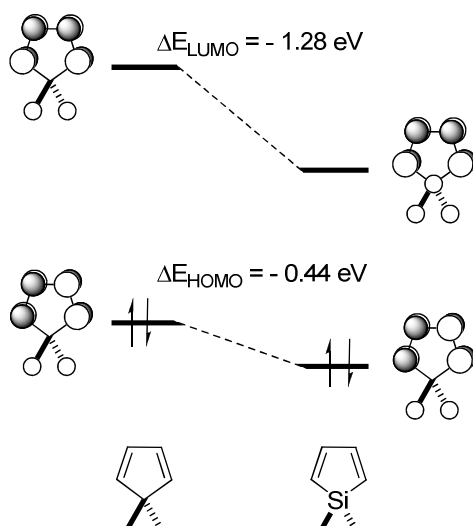
Scheme 70. Relative energy levels of the HOMO and LUMO for cyclopentadiene and silole based on calculations.[213]

Neither the reaction as depicted with n-BuLi and XCH_2Cl (X = Br, I)[199] nor reaction with lithium benzylmercaptane[207] gave the desired compound and exclusively 1,1-dibutyl-1-silafluorene was obtained. Further attempts were commenced by using chloromethylmagnesium chloride, which can be obtained by *in situ* reaction of iodochloromethane and isopropylmagnesium chloride.[219] However, also this treatment did not yield the desired product and merely the starting material was recovered.
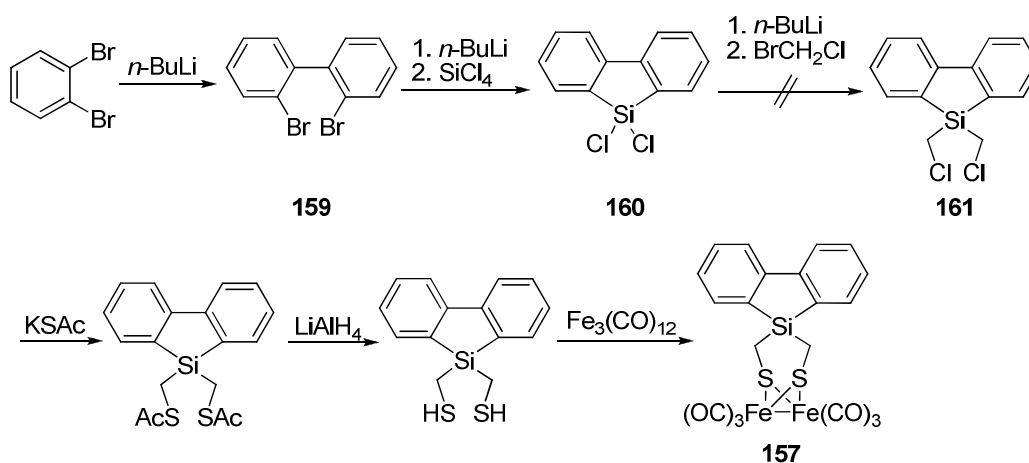
Scheme 71. Initial planned synthesis pathway towards complex **157**.
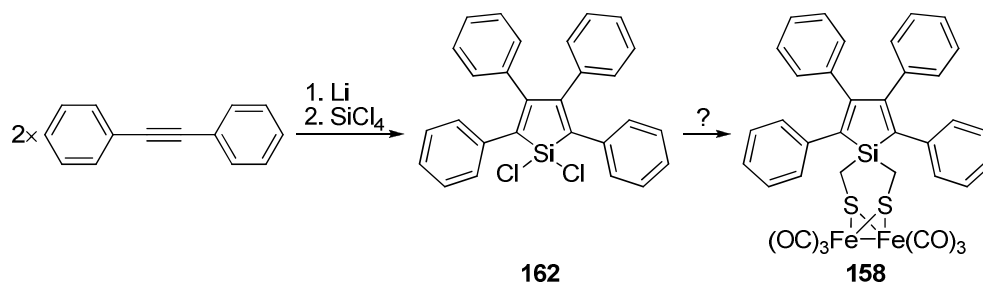
Scheme 72. Reaction pathway *via* the silacyclopentadiene **162** to compound **158** is still not established.

Since the reaction of the dichlorosilanes according to Scheme 71 is not conclusively predictable, the same reaction was tried with 1,1-dichloro-2,3,4,5-tetraphenyl-1-silacyclopentadiene (**162**) (Scheme 71). Unfortunately the same results were obtained as described for compound **161**. Since compound **162** is accessible by the reaction of lithium, diphenylacetylene and tetrachlorosilane in a one-pot procedure within a single step,[220] continuing efforts towards the generation of bischloromethylsilanes are focused on the synthesis of compound **162**.

Thereby two different approaches are currently under investigation: *i*) The formation of 1,1-disodio-2,3,4,5-tetraphenyl-1-silacyclopentadiene[221] and reaction with XCH_2Cl (X = Br, I) and *ii*) the reaction with trimethylsilyldiazomethane or diazomethane.[222]

4 Publications and Documentation of Authorship

4.1 Synthesis and Characterization of Hydroxy-Functionalized Models for the Active Site in Fe-Only-Hydrogenases

Ulf-Peter Apfel, Yvonne Halpin, Helmar Görls, Johannes G. Vos, Bernd Schweizer, Gerald Linti, Wolfgang Weigand, *Chemistry and Biodiversity* **2007**, *4*, 2138 - 2147.

- U.-P. Apfel: Syntheses of all compounds; Manuscript preparation; evaluation of the CV measurements
- Y. Halpin, J. G. Vos: CV measurements; evaluation of the CV measurements
- H. Görls, B. Schweizer: Crystal structure analyses
- G. Linti: Quantum chemical calculations
- W. Weigand: Supervision

4.2 Functionalized Sugars as Ligands towards water soluble [Fe-only] Hydrogenase Models

Ulf-Peter Apfel, Yvonne Halpin, Michael Gottschaldt, Helmar Görls, Johannes G. Vos, Wolfgang Weigand, *Eur. J. Inorg. Chem.* **2008**, *33*, 5112 - 5118.

- U.-P. Apfel: Syntheses of the compounds; Manuscript preparation; Evaluation of the CV measurements
- Y. Halpin, J. G. Vos: CV measurements; evaluation of the CV measurements
- H. Görls: Crystal structure analyses
- M Gottschaldt: Synthesis of β,β-dibromoisopropyl-tetra-*O*-acetyl-β-D-glucopyranoside
- W. Weigand: Supervision

4.3 Oxidation of Diiron and Triiron Sulphurdithiolato Complexes: Mimics for [Fe-only]-hydrogenase's Active Site

Jochen Windhager, Raphael A. Seidel, Ulf-Peter Apfel, Helmar Görls, Gerald Linti, Wolfgang Weigand, *Chemistry and Biodiversity* **2008**, *5*, 2023 - 2041.

- J. Windhager: Syntheses of the compounds; Manuscript preparation
- R. A. Seidel: Assistance in complex preparation
- U.-P. Apfel: Assistance in complex preparation
- G. Linti: Quantum chemical calculations
- H. Görls: Crystal structure analyses
- W. Weigand: Supervision

4.4 Investigation of Amino Acid Containing [FeFe] Hydrogenase Models Concerning Pendant Base Effects

Ulf-Peter Apfel, Christian R. Kowol, Yvonne Halpin, Florian Kloss, Joachim Kübel, Helmar Görls, Johannes G. Vos, Bernhard K. Keppler, Enrico Morera, Gino Lucente, Wolfgang Weigand, *J. Inorg. Biochem.* **2009**, *103*, 1236 - 1244.

- U.-P. Apfel: Syntheses of the compounds except of compound 4; Manuscript preparation; Evaluation of the CV measurements
- C. R. Kowol, B. K. Keppler: CV measurements; Discussion of the manuscript
- Y. Halpin, J. G. Vos: CV measurements
- E. Morera, G. Lucente: Supply with ligand material for initial tests; Synthesis of compound 4
- H. Görls: Crystal structure analyses
- W. Weigand: Supervision

4.5 Preparation and Characterization of Homologous Diiron Dithiolato, Diselenato, and Ditellurato Complexes: [FeFe]-Hydrogenase Models

Mohammad K. Harb, Ulf-Peter Apfel, Joachim Kübel, Helmar Görls, Greg A. N. Felton, Taka Sakamoto, Dennis H. Evans, Richard S. Glass, Dennis. L. Lichtenberger, Mohammad El-Khateeb, Wolfgang Weigand, *Organometallics* **2009**, *28*, 6666 - 6675.

- M. K. Harb: Syntheses of the selenium and tellurium compounds; Manuscript preparation

- U.-P. Apfel: Syntheses of the sulphur compounds; Manuscript preparation

- J. Kübel: Assistant work

- G. A. Felton, T. Sakamoto, D. H. Evans, R. S. Glass, D. L. Lichtenberger: CV measurements, PES measurements, quantum chemical calculations; Manuscript preparation

- M. El-Khateeb: Discussion of the manuscript

- H. Görls: Crystal structure analyses

- W. Weigand: Supervision

4.6 Reaction of $Fe_3(CO)_{12}$ with Octreotide – Chemical, Electrochemical and Biological Investigations

Ulf-Peter Apfel, Manfred Rudolph, Christina Apfel, Christian Robl, Daniel Langenegger, Daniel Hoyer, Bernhard Jaun, Oliver Ebert, Theodor Alpermann, Dieter Seebach, Wolfgang Weigand, *Dalton Trans.* **2010**, *39*, 3065 - 3071.

- U.-P. Apfel: Syntheses of the compounds; Manuscript preparation;

- M. Rudolph: CV measurements; Evaluation of the CV measurements

- C. Apfel, C. Robl: DTA/DSC and powder X-ray crystallographic measurements

- D. Langenegger, D. Hoyer: Affinity tests

- B. Jaun, O. Ebert: Attempts for NMR-structure resolving

- T. Alpermann: Assistant work

- W. Weigand, D. Seebach: Supervision

4.7 Reactions of 7,8-Dithiabicyclo[4.2.1]nona-2,4-diene 7-exo-Oxide with Dodecacarbonyl Triiron Fe$_3$(CO)$_{12}$: A Novel Type of Sulfenato Thiolato Diiron Hexacarbonyl Complexes

Jochen Windhager, Ulf-Peter Apfel, Tomoharu Yoshino, Norio Nakata, Helmar Görls, Manfred Rudolph, Akihiko Ishii, Wolfgang Weigand, *Chemistry Asian Journal* **2010**, DOI: 10.1002/asia.200900733.

- J. Windhager: Syntheses of the compounds; Manuscript preparation

- U.-P. Apfel: Assistance in complex preparation; Manuscript preparation

- T. Yoshino, N. Nakata: Syntheses of the ligands

- H. Görls: Crystal structure analyses

- M. Rudolph: Electrochemical investigations

- A. Ishii, W. Weigand: Supervision

4.8 Unpublished Manuscripts

4.8.1 Synthetic and Electrochemical Studies on [2Fe2S] Complexes containing a 4-Amino-1,2-dithiolane-4-carboxylic acid moiety

Ulf-Peter Apfel, Christian R. Kowol, Enrico Morera, Helmar Görls, Gino Lucente, Bernhard K. Keppler, Wolfgang Weigand, *Eur. J. Inorg. Chem.* **2010**, accepted.

- U.-P. Apfel: Syntheses of the compounds except of compound 10; Manuscript preparation; Evaluation of the CV measurements
- C. R. Kowol, B. K. Keppler: CV measurements; Discussion of the manuscript
- Y. Halpin, J. G. Vos: CV measurements
- E. Morera, G. Lucente: Supply with ligand material for initial tests; Synthesis of compound 10
- H. Görls: Crystal structure analyses
- W. Weigand: Supervision

4.8.2 Models for the Active Site in [FeFe]-hydrogenase with Iron-Bound Ligands Derived from Bis-, Tris-, and Tetrakis(mercaptomethyl)silanes

Ulf-Peter Apfel, Dennis Troegel, Yvonne Halpin, Stefanie Tschierlei, Ute Uhlemann, Michael Schmitt, Jürgen Popp, Helmar Görls, Peter Dunne, Munuswamy Venkatesan, Michael Coey, Manfred Rudolph, Johannes G. Vos, Reinhold Tacke, Wolfgang Weigand, **2010**, submitted.

- U.-P. Apfel: Syntheses of the metal complexes; Manuscript preparation; Analytics; Evaluation of the CV measurements
- Dennis Troegel: Syntheses of the ligands; Manuscript preparation
- Y. Halpin, J. G. Vos: CV measurements
- M. Rudolph: CV measurements and simulation.

- P.Dunne, M. Venkatesan, M. Coey:

  Mossbauer and magnetic measurements

- U. Uhlemann, S. Tschierlei, M. Schmitt, J. Popp:

  RAMAN, DFT calculation

- H. Görls: Crystal structure analyses

- R. Tacke, W. Weigand: Supervision

4.8.3 Influence of the introduction of cyanide and phosphine ligands in multifunctionalized (mercapto-methyl)silanes [FeFe]-hydrogenase model systems

Ulf-Peter Apfel, Yvonne Halpin, Helmar Görls, Johannes G. Vos, Wolfgang Weigand.

- U.-P. Apfel: Syntheses of the metal complexes; Manuscript preparation; Analytics; Evaluation of the CV measurements

- Y. Halpin, J. G. Vos: CV measurements

- H. Görls: Crystal structure analyses

- W. Weigand: Supervision

4.8.4 Hydroxy functionalized (Mercapto-methyl)silanes as ligands for [FeFe]-hydrogenase models

Ulf-Peter Apfel, Dennis Troegel, Yvonne Halpin, Helmar Görls, Johannes G. Vos, Reinhold Tacke, Wolfgang Weigand.

- U.-P. Apfel: Syntheses of the metal complexes; Manuscript preparation; Evaluation of the CV measurements

- D. Troegel   Syntheses of compounds 2-11.

- Y. Halpin, J. G. Vos: CV measurements

- H. Görls: Crystal structure analyses

- R. Tacke, W. Weigand: Supervision

4.8.5 Sterically Demanding Silicon containing Ligands in [FeFe]-hydrogenase Models

Ulf-Peter Apfel, Manfred Rudolph, Joachim Kübel, Helmar Görls, Wolfgang Weigand.

- U.-P. Apfel: Syntheses of the metal complexes; Manuscript preparation;
- M. Rudolph: CV measurements.
- J. Kübel: Assistance in complex preparation
- H. Görls: Crystal structure analyses
- W. Weigand: Supervision

4.8.6 2-Dimethylsilapropanedichalogenolato [2Fe2E(Si)] (E = S, Se, Te) Complexes – [FeFe]-hydrogenase Models

Ulf-Peter Apfel, Helmar Görls, Greg A. N. Felton, Dennis H. Evans, Richard S. Glass, Dennis L. Lichtenberger, Wolfgang Weigand.

- U.-P. Apfel: Syntheses of all compounds; Manuscript preparation;
- G. A. N. Felton: CV measurements.
- H. Görls: Crystal structure analyses
- D. L. Lichtenberger: DFT calculation
- D. H. Evans, R. S. Glass, W. Weigand:

  Supervision

4.9 Presentations

1. U.-P. Apfel, D. Troegel, Y. Halpin, S. Tschierlei, U. Uhlemann, H. Görls, M. Schmitt, J. Popp, P. Dunne, M. Venkatesan, M. Coey, M. Rudolph, J. G. Vos, R. Tacke, W. Weigand, ***Carbon/Silicon switch - a promising approach towards [FeFe]-hydrogenase models***, EUROBIC 10, Thessaloniki/Greece, **2010**.

2. U.-P. Apfel, D. Troegel, Y. Halpin, S. Tschierlei, U. Uhlemann, H. Görls, M. Schmitt, J. Popp, M. Rudolph, J. G. Vos, R. Tacke, W. Weigand, ***Modelle für das aktive Zentrum der [FeFe]-hydrogenase mit Bis-, Tris-, und Tetrakis(mercaptomethyl)silanen***, 6. Koordinationschemie-Treffen, Mainz/Germany, **2010**.

3. W. Weigand, T. Alpermann, U.-P. Apfel, A. Darawsheh, M. Harb, A. Fahr, K. Rüdel, R. Rüger, ***From Iron-sulfur Minerals to [FeFe]-hydrogenase Models***, ICBIC 14, Nagoya/Japan, **2009**.

4. U.-P. Apfel, D. Troegel, Y. Halpin, H. Görls, J. G. Vos, R. Tacke, Wolfgang Weigand, ***Models for the Active Site in [FeFe]-hydrogenase with Multifunctionalized (Mercapto-methyl)silanes***, Organometallic Complexes Containing Sulfur or Selenium Ligands, Aman/Jordan, **2008**.

5. W. Weigand, U.-P. Apfel, J. Windhager, G. Mloston, R. Tacke, D. Troegel, ***Studies on the Reactions of $Fe_2(CO)_9$ and $Fe_3(CO)_{12}$ with Sulfur Rich Heterocycles - Novel Hydrogenase Models***, ISOCS 23, Moskau/Russia, **2007**.

6. W. Weigand, J. Windhager, U.-P. Apfel, M. Rudolph, H. Görls. ***Synthesis of novel model complexes of the active site of the [FeFe]-hydrogenase***, ICBIC 13, Wien/Austria, **2007**.

5 Summary

This thesis provides a detailed investigation on the influences of the S-to-S linkers and the exchange of CO by stronger σ- and π-donating ligands (CN⁻, phosphanes) on the chemical and electrochemical properties of [FeFe]-hydrogenase model complexes. The overall topic was split into four main parts:

1. $ROCH(CH_2S)_2Fe_2(CO)_6$ systems (interaction *via* the S-to-S linker, improvement of water solubility, vesicle systems).

2. [FeFe]-hydrogenase models with amino acidic systems reflecting the natural enzymatic backbone.

3. [2Fe2S(Si)] complexes.

4. The role of sulphur as bridgehead atom in [2Fe2S] systems towards electrocatalytic dihydrogen development.

A short summary will be given for each sequence.

Part 1:

Initial attempts to synthesize [FeFe]-hydrogenase models were based on the fundamental chemistry and electrochemistry of $HOCH(CH_2S)_2Fe_2(CO)_6$. It was noticed that this molecule reveals advantages towards the attachment of further groups onto the hydroxyl function. The most important fact, however, is the electronic segregation of the [2Fe2S] cluster from any attached group R in $ROCH(CH_2S)_2Fe_2(CO)_6$ complexes (R = alkyls, sugars, polymers, peptides) in the presence and absence of acid. It was shown that linkage to a glucose molecule improves the solubility in water and enables dihydrogen formation from water. This is very interesting since recent model complexes only reveal dihydrogen development in acetonitrile and the presence of acids as proton distributor. The use of water as solvent and proton distributor is cheap and allows an easy handling. However, the stability of the sulphur derivative is deficient and the selenium derivative should be preferred. To further diminish solubility and stability problems, new systems were developed with a [2Fe2S] complex incorporated into a vesicle.

This should result in both higher stability and solubility in water. Thereby the fundamental complex, $HOCH(CH_2S)_2Fe_2(CO)_6$, was attempted to be linked to amphiphilic compounds. The attachment of lipids failed due to reactions at the lipidic phosphorous ester. In contrast to this lipidic system, the polymer-attached complexes of $HOCH(CH_2S)_2Fe_2(CO)_6$ were easily accessible *via* the carbonyl diimidazole method. These compounds could be implemented into vesicles and further studies will be necessary to reveal the advantages and disadvantages of hydrogenase models incorporated into vesicles.
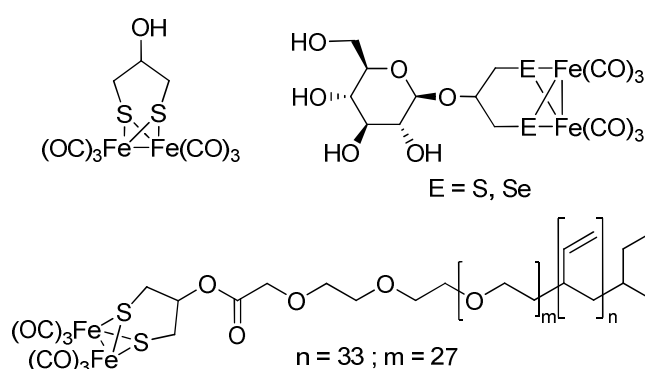
Scheme 73. Representative complexes for part 1.

Part 2:

A second part was focused on the mimic of the enzymatic environment by using amino dithiolanes (*e.g.* 4-amino-4-carboxy-dithiolane). Due to irreconcilable problems during the syntheses of the [2Fe2S] complexes containing a free amine function, the Boc-protected ligand molecules and their respective complexes were established in good yields. Unfortunately, it was impossible to deprotect these complexes with the standard reagents (TFA, thionyl chloride and hydrogen chloride) and the desired complexes were not accessible. A comparable sulphonamide pointed out to be an interesting molecule class due to the high acidity of the sulphonamide group. However, also this molecule reveals an unexpected low reduction potential compared to respective amide complexes and pointed out to be irrelevant as a [FeFe]-hydrogenase model.

Further going studies were focused on the complexation of *α*- and *β*-peptidic moieties with $Fe_3(CO)_{12}$. Interestingly, the more rigid *β*-peptides tended to be instable after coordination and it was not possible to isolate these complexes in analytical pure form. In contrast, the *α*-peptides were accessible in moderate yields. Compared to *β*-peptidic [2Fe2S] complexes the stability was increased and the secondary structure was reserved. This was impressively shown for a $[Fe_2(CO)_6(Sandostatin)]$ complex. Thereby the activity of the complex against the somatostatin receptors ($hsst_{1-5}$) remained closely the same as reported for pure sandostatin. Since the secondary structure is responsible for the high affinity of sandostatin towards the $hsst_{1-5}$ receptors, the secondary structure of the [2Fe2S] complex molecule remains closely the same. The investigations of the electrochemical properties *via* cyclic voltammetry exhibit a strong shift to more negative potentials than compared to related [2Fe2S] systems. Contrary to the high affinity for the somatostatin receptors, the use as a [FeFe]-hydrogenase mimics is dissatisfying.
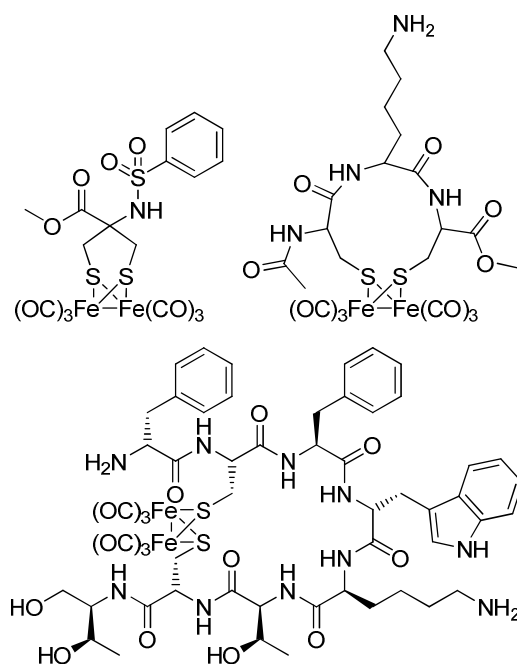
Scheme 74. Selected complexes for the mimic of the enzymatic environment.

Part 3:

Inspired by recent publications in the field of medicinal chemistry as well as the chemistry of odorants and explosives, silicon containing S-to-S linkers were reacted with $Fe_3(CO)_{12}$. The influence of silicon containing dithiols towards novel [FeFe]-hydrogenase models should be

tested according to structural properties and the electro-catalytic development of dihydrogen. Therefore, suitable synthesis procedures towards dimercaptomethyl silanes were established. Two synthesis pathways figured out to give the highest yields. *i*) The reaction of the respective dichlorosilanes with an *in situ* generated chloromethylene carbenoid (derived from bromochloromethane and *n*-BuLi) afforded dichloromethyl silanes, which were converted to the respective dimethylmercaptanes by reaction with potassium thioacetate and following hydrolysis. *ii*) The double Wittig rearrangement was used for the synthesis of sterically demanding [2Fe2S] systems. A dichlorosilane was thereby reacted with benzylmercaptane, whereby a silicon-sulphur bond was erected. Further reaction with *tert*-BuLi lead to deprotonation of the two allylic methylene groups and initialized the rearrangement to afford the bismercaptomethylsilanes after acidic workup. The oxidative addition of these compounds to $Fe_3(CO)_{12}$ lead to the [2Fe2S(Si)] complexes in good yield.

A detailed investigation of the chemical, electrochemical and spectroscopic properties pointed out interesting features arisen by the exchange of carbon by silicon. The possibility of an electrophilic attack on the sulphur bridgehead atoms as well as the tendency to form a rotated state after a two-electron reduction step are important features of these compounds and were proofed by IR, NMR experiments and quantum chemical calculations. Furthermore, these complexes reveal high catalytic activity towards the formation of dihydrogen. The generation of dihydrogen was found to occur *via* three different pathways and a reduced overpotential of about 800 mV was observed for the reduction of acetic acid on a glassy carbon electrode.

Further investigations were focused on the influence of CO exchange to increase of the electron density on the iron centres. However, exchange of CO by CN^- or phosphanes lead to more negative potentials for the dihydrogen generation.
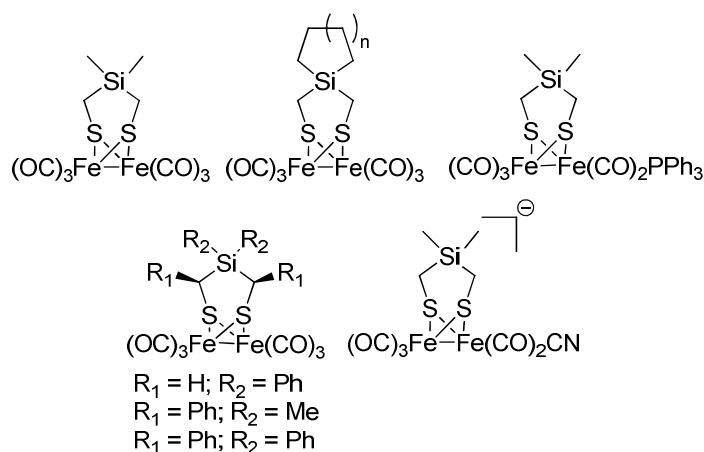
Scheme 75. Representative silicon containing hydrogenase model complexes.

Part 4:

In the last part, the importance of the bridgehead atoms (sulphur in nature) was in the focus of this study. Homologous ligand series with sulphur, selenium and tellurium were synthesized to obtain the respective [2Fe2E] complexes (E = S, Se, Te). Within electrochemical investigations, a shift to more negative potentials for the reduction of protons to dihydrogen was observed according to $E_S > E_{Se} > E_{Te}$. Furthermore, the activity of the dihydrogen generation decreased, visible by the lowered catalytic current.

An explanation for this unexpected behaviour was obtained by quantum chemical calculations and photoelectron spectroscopy. It could be shown that the preference of the reduced species to adopt a rotated structure was markedly diminished. Therefore no terminal hydride could be formed which is important for a fast and effective formation of dihydrogen in [FeFe]-hydrogenase models.

E = S, Se, Te
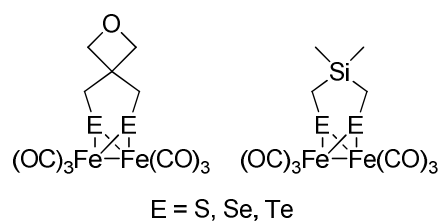
Scheme 76. Homologous hydrogenase complexes containing sulphur, selenium and tellurium

120

Overall, it was possible to synthesize several novel [FeFe]-hydrogenase models. Thereby two water soluble [FeFe]-hydrogenase model complex were synthesized. It was possible to synthesize polymer bound [2Fe2S] complex and the formation of membrane standing hydrogenase models was successfully confirmed. Interested in the features of amino acid and peptide containing [2Fe2S] complexes a series of complexes were synthesized. Electrochemical investigations pointed out that these systems were not able to establish a proton relay between a pendant base and the iron centres. In addition, the peptidic systems tend to be instable in solution and revealed dihydrogen development at very negative potentials.

In contrast, the [2Fe2S(Si)] complexes turned out to be an alternative path towards effective [FeFe]-hydrogenase model complexes. It was shown that substitution of CO with CN^-, or phosphanes, as well as the exchange of sulphur by the higher homologues (Se, Te) lead to unfavourable low reduction potentials and a mindered activity for [2Fe2E] complexes (E = Se, Te).

6 Zusammenfassung

In der vorgestellten Arbeit konnte eine detailierte Darstellung über die Einflüsse und Auswirkungen sowohl von Veränderungen am Dithiolatoliganden als auch der CO Liganden durch bessere σ- und π-Donoren gegeben werden. Dabei gliedert sich die Dissertation in vier verschiedene Teile:

1. Hydroxy-funktionalisierte Systeme (Elektrochemische Eigenschaften von $[HOCH(CH_2S)_2Fe_2(CO)_6]$-Systemen, Verbesserung der Wasserlöslichkeit von [2Fe2S] Komplexen, Einbindung in vesikuläre Systeme)

2. [FeFe]-hydrogenase-Modelle mit aminosäurehaltigen Schwefellinkern ("Nachempfinden der natürlichen Enzym-Umgebung")

3. Siliziumhaltige [2Fe2S] Komplexe

4. Einfluß und Notwendigkeit der Brückenkopfatome für die Wasserstoffgenerierung

Im Folgenden soll eine kurze Zusammenfassung zu den einzelnen Unterthemen gegeben werden.

Teil 1: Der zentrale Bestandteil des ersten Teils dieser Arbeit war die Synthese und Charakterisierung von $HOCH(CH_2S)_2Fe_2(CO)_6$. Ich konnte dabei zeigen, dass trotz des deutlich vergrößerten s-Anteils der C-C Bindung des [2Fe2S] Zentrums als isoliert betrachtet werden kann. Demnach sind die katalytischen Eigenschaften ausschließlich vom [2Fe2S] Zentrum abhängig und nicht von den an OH-Funktionalität angebundenen Gruppen. Derivatisierungen haben demzufolge keinen Einfluß auf die elektrochemischen Eigenschaften. Zunächst erschien dies als Nachteil, da eine elektronische Wechselwirkung über die Dithiolato-Brücke angenommen wurde. Dies erwies sich jedoch als Vorteil, da die Eigenschaften der Modellverbindung (z. B. Lösungsverhalten) ohne Verlust der Katalyseaktivität unabhängig verändert werden können. Zur Verbesserung der Löslichkeit in Wasser wurde $HOCH(CH_2S)_2Fe_2(CO)_6$ an der OH-Gruppe mit Glukose derivatisiert. Als interessantes Ergebnis konnte dabei gefunden werden, dass in diesem Fall Wasser nicht nur als Lösungsmittel,

sondern auch als Protonenquelle dient. Dies ist insofern von Bedeutung, da bisher beschriebene Modellsysteme ausschließlich die Bildung von Wasserstoff in Acetonitril in Gegenwart von Säuren (z. B. Essigsäure) katalysieren. Es muß dabei jedoch ausdrücklich erwähnt werden, dass der Glukose-derivatisierte [2Fe2S] Komplex während der katalytischen Generierung von Wasserstoff nicht stabil ist. Im Gegensatz dazu zeigt der entsprechende Selenkomplex eine erhöhte Stabilität und keinerlei Zersetzung in wässrigem Milieu. Die Wasserstoffgenerierung findet jedoch bei negativerem Elektrodenpotential statt als beim vergleichbaren Schwefelsystem. Ein möglicher Ansatz zur Behebung des Stabilitätsproblems bei den Schwefel-haltigen Verbindungen könnte sich durch das Einbringen der Komplexe in Vesikel ergeben. Dafür wurde $HOCH(CH_2S)_2Fe_2(CO)_6$ mit amphiphilen Verbindungen umgesetzt. Besonders Polymer-basierende Verbindungen eröffneten einen guten Zugang zu solchen vesikulären Systemen. Es konnte gezeigt werden, dass diese Verbindungen Vesikel ausbildeten und so ein Modell für membranständige Hydrogenasen zugänglich war.

Teil 2: Ein weiterer Abschnitt beschäftigte sich mit der Modellierung der enzymatischen Umgebung der [FeFe]-Hydrogenase. Dazu wurden besonders Komplexe des biologisch aktiven Aminodithiolan, 4-Amino-4-carboxy-dithiolan, und dessen Derivate als Liganden für Hydrogenasemodelle untersucht. Jedoch waren trotz zahlreicher Versuche keine Verbindungen mit einer freien Aminogruppe zugänglich. Daraufhin wurden die Aminogruppen Boc-geschützt. In einer anschließenden oxidativen Addition dieser Aminosäurederivate an $Fe_3(CO)_{12}$ konnten die [2Fe2S] Komplexe in guten Ausbeuten erhalten werden. Allerdings ließen sich diese Komplexe bisher nicht mit den üblichen Reagenzien (Trifluoressigsäure, Thionylchlorid, Salzsäure) entschützen. Ein freier Aminkomplex war damit auch über diesen Weg bisher nicht zugänglich.

Weiterführende Untersuchungen waren auf die Komplexierung von *α*- und *β*-Peptiden gerichtet. Interessanterweise tendierten *β*-Peptidkomplexe zum Zerfall, und es war nicht möglich diese in analytisch reiner Form zu erhalten. Im Vergleich dazu konnten die *α*-Peptidkomplexe in guten Ausbeuten isoliert werden und zeigten eine höhere Stabilität als ihre *β*-Peptid-Homologen. Dies ist erstaunlich, da *β*-Peptide normalerweise eine erhöhte Stabilität gegenüber *α*-Peptiden aufweisen.

Anhand des Eisen-hexacarbonylkomplexes mit Sandostatin konnte nachgewiesen werden, dass die Sekundärstruktur des Peptidrückgrades bei α-Peptiden nahezu intakt bleibt. Es wurde dabei gezeigt, dass die Aktivität gegenüber den Somatostatinrezeptoren (hsst$_{1-5}$) nur wenig von der des reinen Sandostatins abweicht. Da die Sekundärstruktur des Sandostatin-Rückgrades großen Einfluß auf die Affinität gegenüber den Somatostatinrezeptoren besitzt und kleinste Abweichungen in der Struktur der Verbindung zu Affinitätsverlust dieser führen, konnte gefolgert werden, dass das entsprechende Peptidgerüst im Komplex nahezu unverändert vorliegt. Im Vergleich zu literaturbekannten Verbindungen wies die Untersuchung der elektrochemischen Eigenschaften des Peptidkomplexes eine deutliche Verschiebung des Reduktionspotentials zu negativeren werten auf. Damit ist dieses System für die Wasserstoffproduktion ungeeignet. Eine solche "negative" Verschiebung des Reduktionspotentials von Protonen zu Wasserstoff konnte bei allen peptidischen Verbindungen beobachtet werden.

Teil 3: Inspiriert durch Literaturbeiträge aus den Bereichen der medizinischen Chemie, von Geruchs- und Sprengstoffen, bei denen eine merkliche Veränderung der chemischen und physikalischen Eigenschaften durch den Austausch von Kohlenstoff gegen Silizium zu beobachten war, wurden Bismercaptomethylsilane synthetisiert und mit $Fe_3(CO)_{12}$ umgesetzt. Elektrochemische Untersuchungen ergaben ein Abweichen des katalytischen Mechanismus der Wasserstoffentstehung gegenüber bekannten Systemen. Im Gegensatz zu diesen Systemen zeichnet sich die hier etablierte Verbindungsklasse durch eine initiale Zweielektronenreduktion und der Ausbildung einer "rotated state - rotierten Struktur" aus. Weiterhin konnte in Gegenwart von Säuren ein vorgelagertes Gleichgewicht beobachtet werden. Es wurde dabei gezeigt, dass es in diesem Gleichgewicht nicht zu einer Ausbildung eines Eisenhydrids kommt, sondern vielmehr zu einer Protonierung der Schwefelbrückenatome.

Im Gegensatz zu den Kohlenstoff- und Stickstoffderivaten zeichnen sich die siliziumhaltigen Systeme durch erhöhte Aktivität und eine deutlich verringerte Überspannung gegenüber der elektrochemischen Wasserstofferzeugung in Gegenwart von schwachen Säuren aus. Es war erstmals möglich, zu zeigen, dass die Wasserstofferzeugung dabei über drei verschiedene Wege geschehen kann.

Auf Grundlage weiterer Substitutionsexperimente konnte beobachtet werden, dass ein Austausch von CO gegen CN⁻ oder Phosphine in Modellsystemen nicht ratsam ist. Dies führt zur Verschiebung der Reduktionspotentiale zu negativeren Werten und somit wiederum zur Erhöhung der Überspannung.

Teil 4: Der letzte Teil dieser Arbeit beschäftigte sich mit der Frage, warum in den natürlich vorkommenden Systemen Schwefel anstelle von Selen eingebaut ist. Insbesondere das höhere Homologe des Schwefels, Selen, ist für sein natürliches Vorkommen in [FeNiSe]-Hydrogenasen bekannt und würde in [FeFe]-hydrogenasen zu einer Erhöhung der Basizität der Eisenzentren führen. Durch Synthese homologer Schwefel-, Selen- und Tellurverbindungen war es erstmals anhand von elektrochemischen Untersuchungen möglich, zu zeigen, dass der Austausch von Schwefel gegen die höheren Homologen kontinuierlich zum Aktivitätsverlust der Wasserstoffgenerierung führt. Dies ist insofern erstaunlich, da eine erhöhte Elektronendichte durch gesteigerte Elektropositivität am Eisen erwartet wurde. Eine Erklärung hierfür lieferten DFT-Berechnungen und Untersuchungen mittels Photoelektronenspektroskopie. Es konnte aufgezeigt werden, dass der Austausch gegen die höheren Homologen dazu führte, dass die reduzierte Spezies deutlich an der Ausbildung eines "rotated state" gehindert wurde. Demzufolge kann *in situ* kein terminales Hydrid generiert werden, welches für eine schnelle und effektive Wasserstoffbildung von großer Bedeutung ist.

Es war möglich, eine Reihe neuartiger Verbindungen herzustellen, welche als [FeFe]-Hydrogenasemodell fungieren können und zur Wasserstoffgenerierung befähigt sind. Besonders die siliziumhaltigen Spezies zeigten interessante neue und vielversprechende Eigenschaften auf.

.

7 Experimental Part

Note: Only syntheses which are not recorded in any manuscript or draft attached will be described within this chapter.

General Procedures. All syntheses were carried out under dry nitrogen or argon atmosphere. The organic solvents used were dried and purified according to standard procedures and stored under dry nitrogen or argon. Chemicals were used as received from Fluka or Acros without further purification. Thin layer chromatography (TLC): Merck silica gel 60 F_{254} plates; detection under UV light at 254 nm. Flash chromatography (FC): Fluka silica gel 60. A Büchi GKR-51 apparatus was used for the bulb-to-bulb distillations. The ^{1}H, ^{13}C{^{1}H} and ^{29}Si{^{1}H} NMR spectra were recorded at 23 °C on a Bruker Avance 200 or Avance 400 NMR spectrometer. Analysis and assignment of the ^{1}H NMR data were supported by ^{1}H,^{1}H COSY, ^{13}C,^{1}H HMQC, and ^{13}C,^{1}H HMBC experiments. Assignment of the ^{13}C{^{1}H} NMR data was supported by DEPT 135, ^{13}C,^{1}H HMQC, and ^{13}C,^{1}H HMBC experiments. Chemical shifts (ppm) were determined relative to internal solvent (^{1}H, ^{13}C), or external TMS (^{29}Si). IR spectra were recorded on a Perkin-Elmer 2000 FT-IR spectrometer. Mass-spectrometric studies (FAB/MS, DEI/MS, ESI/MS) were performed on a SSQ710 Finnigan MAT spectrometer. Elemental analyses (C, H, N, S) were carried out on a Leco CHNS-931 instrument. Halogen determination was performed by titration. A fundamental problem for the elemental analysis of the complexes was remaining solvents within the samples. Even 24 hours treatment in high vacuum did not lead to full removal of the solvent molecules. The amount of solvent was calculated in agreement to ^{1}H NMR spectroscopy. Analytical HPLC was performed using a Merck Hitachi device (Interface: D7000; UV detector (220 nm): L-7400; pump: L-7150 (flowrate 1 mL/min)) with water/ acetonitrile on a Macherey-Nagel C_8-column. Preparative HPLC was performed under the same conditions with a flow rate of 10 mL/min. CD spectroscopy was performed on a Jobin-Yvon-Mark-III spectrometer. Lyophilization was carried out with a Hetosicc cooling condenser.

Synthesis of 1,3-Dithioacetyl-2-methoxy-propane (43)

Allylbromide (20 g, 165.4 mmol) and mercury(II) acetate (30 g, 57.7 mmol) were dissolved in 300 mL methanol and stirred for 10 days at room temperature whereupon a white precipitate was formed. Filtration and removal of the solvent yielded an oily substance to which 400 mL water were added. 20 g (168 mmol) Potassium bromide were added and after cooling to 0 °C, 26.3 g (165 mmol) bromine were slowly dropped into the solution. After 3 hours stirring, the mixture was extracted with 100 mL diethyl ether, followed by washing with water and saturated sodium thiosulphate solution. Removing of the solvent under reduced pressure and bulb-to-bulb distillation (0.06 mbar/ 50 °C) yielded 10.2 g of crude 2-methoxy-1,3-dibrompropane (**42**); MS (DEI): 230 [M]$^+$. Attempts to remove excess of mercury salts failed. Therefore, the crude product was used without further purification for the next step.

Crude 2-methoxy-1,3-dibrompropane (10 g, ~ 40.6 mmol) was dissolved in 120 mL acetone and 20 g (175 mmol) potassium thioacetate were added slowly. After 1 week, the reaction mixture was filtrated and the precipitate was washed with acetone several times. The filtrate was evaporated under reduced pressure. The residue was redissolved in diethyl ether, filtrated and concentrated in vacuo. Bulb-to-bulb distillation (0.15 mbar, 110 °C) afforded 3.3 g (37 %) of a yellow oil. ^{1}H NMR (200 MHz, CDCl$_3$): δ = 3.45-3.33 (m, 4H, C*H* and OC*H$_3$*), 3.06 (d, 4H, SC*H$_2$*CHC*H$_2$*S, ^{3}J$_{H,H}$ = 5.8 Hz), 2.32 (s, 6H, SC(O)C*H$_3$*). ^{13}C NMR (50 MHz, CDCl$_3$): δ = 195.1 (S*C*(O)CH$_3$), 78.6 (*C*H), 57.6 (O*C*H$_3$), 31.7 (*C*H$_2$); 30.5 (SC(O)*C*H$_3$). MS (DEI): *m/z* = 222 [M]$^+$. Anal. calcd. for C$_8$H$_{14}$O$_3$S$_2$: C, 43.22 %; H, 6.35 %; S, 28.85 %. Found: C, 42.58 %; H, 5.85 %; S, 29.18 %.

Synthesis of 1,3-Disulfanyl-2-methoxy-propane (44)

To an ice-cooled solution of 1 g (4.5 mmol) 1,3-dithioacetyl-2-methoxy-propane dissolved in 20 mL methanol, sodium hydroxide (1.44 g, 36 mmol) was added slowly and stirred for 4 days. Afterwards the reaction mixture was neutralized with hydrogen chloride (pH ~ 3) and 100 mL water were added. The solution was extracted three times with 50 mL diethyl ether and the combined organic phases dried with sodium sulphate. Removal of the solvent under reduced pressure followed by bulb-to-bulb distillation (0.34 mbar, 50 °C) afforded 191 mg (31 %) of a yellow oil. ^{1}H NMR (400 MHz, CDCl$_3$): δ = 3.39-3.31 (m, 4H, C*H* and OC*H$_3$*), 2.78-2.71 (m, 4H,

CH_2), 1.43 (t, ^{3}J = 8.4 Hz, 2H, SH). ^{13}C NMR (50 MHz, CDCl$_3$): δ = 82.4 (*C*H), 57.4 (O*C*H$_3$), 26.0 (*C*H$_2$). MS (DEI): m/z = 138 [M]$^+$. Elemental analysis was not performed due to fugacity of the compound.

Synthesis of Hexacarbonyl (μ-2-methoxypropan-1,3-dithiolato-S,S')diiron (45)

2–Methoxypropane–1,3-dithiol (50 mg, 0.362 mmol) and triiron dodecacarbonyl (182 mg, 0.362 mmol) were dissolved in 25 mL toluene and refluxed for 2 hours. After evaporation to dryness, the crude product was purified *via* FC (diethyl ether:hexane = 1:10) yielding 115 mg (76 %) of a red crystalline product. ^{1}H NMR (400 MHz, CDCl$_3$): δ = 3.26 (s, 3H, CH_3), 2.76 (dd, ^{3}J$_{H,H}$ = 3.8 Hz, ^{2}J$_{H,H}$ = 13 Hz, 2H, CH_2), 2.72-2.64 (m, 1H, CH), 1.55-1.49 (m, 2H, SCH_2CHCH_2S). ^{13}C NMR (50 MHz, CDCl$_3$): δ = 207.6/207.3 (CO), 81.5 (*C*H), 56.5 (*C*H$_3$), 26.88 (*C*H$_2$). MS (DEI): m/z = 388 [M-CO]$^+$. IR (KBr, cm^{-1}): 3437 (s), 2926 (s), 2854 (w), 2073(vs), 2030 (vs), 1982 (vs), 1947 (s), 1637 (m), 1384 (m), 1220 (w), 1183 (w), 1086 (s), 953 (w), 611 (m), 584 (s), 563 (s). Anal. calcd. for C$_{10}$H$_8$Fe$_2$O$_7$S$_2$•Et$_2$O: C, 34.31 %; H, 3.70 %; S, 13.08 %. Found: C, 34.20 %; H, 3.69 %; S, 13.52 %.

Synthesis of 2-Methyl-3-brom-propene (46)

A suspension of 10 g (0.11 mol) methylallylchloride and 15 g (0.17 mol) lithium bromide was stirred for 12 hours in 50 mL boiling acetone. To the reaction mixture, 10 mL water were added and the organic fraction was separated from the aqueous phase and dried with magnesium sulphate. Distillation (atm. pressure, 85-87 °C) afforded 3 g (21 %) 2-methyl-3-brom-propene. ^{1}H NMR (200 MHz, CDCl$_3$): δ = 5.10 (m, 1H, *cis*-CH), 4.92 (m, 1H, *trans*-CH), 3.93 (s, 2H, CH_2Br), 1.86 (s, 3H, CH_3). ^{13}C NMR (50 MHz, CDCl$_3$): δ = 141.5 (*C*), 115.7 (*C*H$_2$), 38.0 (*C*H$_2$Br), 19.7 (*C*H$_3$). MS (DEI): m/z = 134 [M]$^+$. The purity was verified *via* GC-MS.

Synthesis of 1,3-Dibrom-2-methyl-2-hydroxy-propane (47)

2-Methyl-3-brom-propene (2 g, 0.015 mol) was dissolved in a mixture of 90 mL dimethylsulfoxide and 0.5 mL water, and cooled to -10 °C. Afterwards, 5.27 g (0.03 mol) *N*-bromsuccinimide was added within 15 minutes in small portions and stirred for an additional hour. The reaction was stopped by adding 50 mL water (visible by bleaching of the solution). Extraction with diethyl ether, washing with a saturated sodium chloride solution afforded the

Experimental Part

---

crude product. Kugelrohr distillation (0.71 mbar, 55 °C) afforded 1.62 g (47 %) 1,3-dibrom-2-methyl-2-hydroxy-propane. ^{1}H NMR (400 MHz, CDCl$_3$): δ = 3.54 (dd, $^2J_{H,H}$ = 13.8 Hz, $^3J_{H,H}$ = 10.4 Hz, 4H, CH_2), 2.38 (s, 1H, OH), 1.47 (s, 3H, CH_3). ^{13}C NMR (100 MHz, CDCl$_3$): δ = 71.0 (C), 40.5 (CH$_2$), 23.2 (CH$_3$). MS (DEI): m/z = 137 [M-CH$_2$Br]$^+$.

Synthesis of 4-Methyl-4-hydroxy-dithiolane (48)

Sodium hydrogensulphide monohydrate (2.05 g, 0.028 mol) was dissolved in 40 mL absolute ethanol and 1,3-dibrom-2-methyl-2-hydroxy-propane (1.6 g, 6.9 mmol) was added. The resulting solution was treated under reflux for 2 hours, whereupon a white precipitate appears. After filtration, 5 mL glacial acetic acid (pH = 5) were added to the filtrate, whereupon a white precipitate was formed. The solution was filtrated, degassed for 1 hour by bubbling argon through the solution and evaporated to dryness. The residue was extracted with 300 mL dichloromethane and after removal of the solvent the residue was purified by distillation (21 mbar, 108-112 °C) and afforded 230 mg (24 %) of 4-methyl-4-hydroxydithiolane as yellow oil. ^{1}H NMR (CDCl$_3$, 400 MHz): δ = 3.04 (s, 3H, CH_3), 1.58 (s, 4H, CH_2). ^{13}C NMR (CDCl$_3$, 100 MHz): δ = 82.4 (C), 50.9 (CH$_2$), 23.5 (CH$_3$). MS (DEI): m/z = 136 [M]$^+$. Elemental analysis was not performed due to impurities of 4-methyl-4-hydroxy-dithiol which could not been separated.

Syntheses of Hexacarbonyl (μ-2-methyl-2-hydroxypropane-1,3-dithiolato-S,S')diiron (49)

In a 100 mL Schlenk-vessel, 100 mg (0.735 mmol) 4-methyl-4-hydroxy-dithiolane were dissolved in 40 mL tetrahydrofurane and refluxed for 1.5 hours. After evaporation, the remaining solid was purified via FC (THF:hexane = 1:3) and gave 48 mg (16 %) of the desired product. ^{1}H NMR (CDCl$_3$, 200 MHz): δ = 2.50 (d, ^2J = 14 Hz, 2H, SCH_AH$_B$), 1.83 (d, ^2J = 14 Hz, 2H, SCH$_A$$H_B$), 1.17 (s, 3H, C$H_3$). ^{13}C NMR (CDCl$_3$, 50 MHz): δ = 207.8 (CO), 69.6 (C), 33.0 (CH$_2$), 30.3 (CH$_3$). MS (DEI): m/z = 416 [M]$^+$, 388 [M-CO]$^+$, 360 [M-2CO]$^+$, 432 [M-3CO]$^+$, 304 [M-4CO]$^+$, 276 [M-5CO]$^+$, 248 [M-6CO]$^+$. IR (Nujol, cm^{-1}): 2073 (vs), 2034 (vs), 1995 (vs). Anal. calcd. for C$_{10}$H$_8$Fe$_2$O$_7$S$_2$•0.25THF: C, 30.44 %; H, 2.63 %; S, 14.78 %. Found: C, 30.44 %; H, 2.32 %; S, 14.48 %.

129

Tris-(hexacabonyl(μ-2-hydroxypropane-1,3-dithiolato-S,S')diiron)-1,3,5-tricarboxylic acid benzol ester (50)

In a round-bottom flask, 42.4 mg (0.16 mmol) 1,3,5-benzentricarboxylic acid were dissolved in 20 mL dichloromethane. After addition of 0.1 mL triethylamine, 200 mg (0.5 mmol) hexacarbonyl (μ-2-hydroxypropane-1,3-dithiolato-S,S')diiron (**40**), dissolved in 5 mL dichloromethane, were added within 5 minutes, whereupon a precipitate was formed. After stirring for additional 2 hours, the solution was filtrated and purified *via* flash chromatography (THF:hexane = 1:1). 256 mg (52 %) of an orange solid were isolated. ^{1}H NMR (400MHz, CDCl$_3$): δ = 8.62 (s, 3H, C$H_{aromatic}$), 4.49 (m, 3H, CH), 2.88 (dd, ^{2}J$_{H,H}$ = 12.8 Hz, ^{3}J$_{H,H}$ = 4.2 Hz, 6H, CH_AH_B), 1.71 (dd collapsing to triplett, 6H, CH$_A H_B$). ^{13}C NMR (50MHz, CDCl$_3$): δ = 207.0 (CO), 162.8 (*C*(O)O), 135.1 (*C*$_{aromatic}$), 130.6 (*C*H$_{aromatic}$), 75.6 (*C*H), 26.9 (*C*H$_2$). MS (DCI-neg): m/z = 1334 [M-CO]$^{-}$. IR(KBr, cm^{-1}): 2958 (m), 2919 (m), 2871 (w), 2083 (vs), 2038 (vs), 2006 (vs), 1977 (vs), 1725 (s), 1232 (s). Anal. calcd. for C$_{36}$H$_{18}$Fe$_6$O$_{24}$S$_6$•THF: C, 33.50 %; H, 1.83 %; S, 13.42 %. Found: C, 33.71 %; H, 1.82 %; S 13.94 %.

Synthesis of Bis-(hexacabonyl (μ-2-hydroxypropane-1,3-dithiolato-S,S')diiron)terephtalic ester (51) and (Hexacabonyl (μ-2-hydroxypropane-1,3-dithiolato-,S')diiron)terephtalic ester (52)

To a solution of 170 mg (0.42 mmol) hexacarbonyl (μ-2-hydroxypropane-1,3-dithiolato-S,S')diiron (**40**) in 40 mL dichloromethane, 35.1 mg (0.21 mmol) terephtalic acid, 57.2 mg (0.42 mmol) hydroxybenzotriazol, 262 mg (1.27 mmol) dicyclohexyl carbodiimide and 0.2 mL triethylamine were added. The resulting mixture was stirred for 5 days at room temperature and purified *via* flash chromatography using toluene. Two different fractions were isolated and analyzed.

Bis-(hexacabonyl (μ-2-hydroxypropane-1,3-dithiolato-S,S')diiron)terephtalic ester (**51**) was obtained in 24 % yield (48 mg) as a red solid. ^{1}H NMR (400 MHz, CDCl$_3$): δ = 7.96 (s, 4H, C$H_{aromatic}$), 4.45 (m, 2H, CH), 2.90 (dd, ^{2}J$_{H,H}$ = 12.8 Hz, ^{3}J$_{H,H}$ = 4.2 Hz, 4H, SCH_AH_B), 1.69 (dd collapsing to a triplett, 4H, SCH$_A H_B$). ^{13}C NMR (100MHz, CDCl$_3$): δ = 206.9 (*C*O), 163.7 (*C*(O)O), 133.4 (*C*$_{aromatic}$), 128.8 (*C*H$_{aromatic}$), 75.0 (*C*H), 26.8 (*C*H$_2$). MS (DEI): m/z = 878 [M-

2CO], 850 [M-3CO], 822 [M-4CO], 794 [M-5CO], 766 [M-6CO], 738 [M-7CO], 710 [M-8CO], 682 [M-9CO], 654 [M-10CO], 626 [M-11CO], 598 [M-12CO]. Anal. calcd. for $C_{26}H_{14}Fe_4O_{16}S_4$: C, 33.43 %, H, 1.51 %; S, 13.73 %. Found: C, 33.41 %; H, 1.60 %; S, 13.50 %. IR(KBr, cm^{-1}): 2077 (vs), 2036 (vs), 1998 (vs), 1721 (s).

(Hexacabonyl (μ-2-hydroxypropane-1,3-dithiolato-,S')diiron)terephtalic ester (**52**) was obtained as red solid (43 mg, 37 %). ^{1}H NMR (200 MHz, CDCl$_3$): δ = 8.26-7.97 (m, 4H, C$H_{aromatic}$), 4.48-4.37 (m, 1H, CH), 2.92 (dd, $^2J_{H,H}$ = 13 Hz, $^3J_{H,H}$ = 4.4 Hz, 2H, SCH_AH$_B$), 1.70 (dd collapsing to triplett, 2H, CH$_A$$H_B$). ^{13}C NMR (100 MHz, CDCl$_3$): δ = 207.1 (CO), 165.6 (C(O)OH), 164.0 (C(O)O), 134.8 (CC(O)O), 132.8 (CC(O)OH), 129.6 (CH$_{aromatic}$), 74.9 (CH), 26.9 (CH$_2$). MS (DEI): m/z = 522 [M-CO], 494 [M-2CO], 466 [M-3CO], 438 [M-4CO], 410 [M-5CO]. IR(KBr, cm^{-1}): 2985 (w), 2078 (vs), 2037 (vs), 1998 (vs), 1720 (vs), 1268 (s), 1100 (s). Anal. calcd. for $C_{17}H_{10}Fe_2O_{10}S_2$•0.4hexane: C, 39.86 %, H, 2.69 %, S, 10.97 %. Found.: C, 39.80 %, H, 2.81 %, S, 10.91 %.

Synthesis of (Hexacabonyl (μ-2-hydroxypropane-1,3-dithiolato-,S')diiron)oleic acid ester (59)

Hexacarbonyl (μ-2-hydroxypropane-1,3-dithiolato-S,S')diiron (**40**) (76 mg, 0.189 mmol) was dissolved in 10 mL dichloromethane. Subsequently, 53 µL (0.378 mmol) triethylamine and 165.3 µL (0.473 mmol) oleoyl chloride were added and the solution stirred 5 days at room temperature. Evaporation of the solution afforded the crude product which was purified by FC (THF:hexane = 1:6) to yield 95 mg (75 %) of a red oil. ^{1}H NMR (200 MHz, CDCl$_3$): δ = 5.34 (m, 2H, CH=CH), 4.29 (m, 1H, SCH$_2$CHCH$_2$S), 4.12 (dd, $^2J_{H,H}$ = 14.3 Hz, $^3J_{H,H}$ = 7.1 Hz, 2H, SCH_AH$_B$), 2.28 (t, $^3J_{H,H}$ = 7.5 Hz, 2H, OC(O)CH_2), 2.00 (m, 4H, CH_2CH=CHCH_2), 1.61 (m, 2H, OC(O)CH$_2$CH_2), 1.27 (m, 22H, remaining CH_2 and SCH$_A$$H_B$), 0.88 (t, $^3J_{H,H}$ = 6.6 Hz, 3H, CH_3). ^{13}C NMR (100 MHz, CDCl$_3$): δ = 207.2 (CO), 173.9 (C(O)O), 129.9, 129.7 (CH=CH), 73.3 (SCH$_2$$CHCH_2$S), 60.1 (S$CH_2$), 34.4 (OC(O)$CH_2$), 31.9 ($CH_2CH_2CH_3$), 29.8, 29.7, 29.5, 29.3, 29.1 (remaining CH$_2$), 27.2, 27.1 (CH$_2$CH=CHCH$_2$), 24.9 (OC(O)CH$_2$$CH_2$), 22.7 ($CH_2CH_3$), 14.1 ($CH_3$). MS (FAB in nba): m/z = 582 [M-3CO]$^+$, 498 [M-6CO]$^+$. IR (pur, cm^{-1}): 3003 (m), 2926 (s), 2854 (s), 2077 (vs), 2037 (vs), 1998 (vs), 1739 (s), 1465 (m). A correct elemental analysis was not obtained.

Generation of the [2Fe2S] Modified Polymer (61)

To a solution of compound **64** (1.12 g, 0.33 mmol), 134 mg (0.33 mmol) of compound **40** were added and the solution stirred for

n = 33 ; m = 27

24 hours at room temperature. Evaporation to dryness followed by dissolving in chloroform and extraction with sodium bicarbonate, brine and water afforded 1.22 g of a red residue. Analyses *via* GPC revealed a mixture of **61** and PB-PEO2. ^{1}H NMR (400 MHz, CDCl$_3$): δ = 5.38 (m, 33H, H7), 4.86 (m, 66H, H8), 3.57 (m, 117H, H9, H10, H11, H12, H13, H14), 2.05 (m, 33H, H6), 1.13 (m, 69H, H2, H3, H5), 0.76 (m, 6H, H1, H4). IR(KBr, cm^{-1}): 3978 (s), 2973 (vs), 2932 (vs), 2077 (vs), 2040 (vs), 2006 (vs), 1767 (s), 1642 (m).

Synthesis of the [2Fe2S] Modified Polymer (62)

To a solution of compound **66** (1.42 g, 0.41 mmol) in 50 mL THF, 723 mg (1.8 mmol) of compound **40** were added and

n = 33 ; m = 27

the solution stirred for 24 hours at room temperature, evaporated to dryness, followed by dissolving in chloroform and extraction with sodium bicarbonate, brine and water. Precipitation in acetone at -95°C afforded 180 mg (11 %) of a red residue. ^{1}H NMR (400 MHz, CDCl$_3$): δ = 5.44 (m, 33H, H7), 4.94 (m, 66H, H8), 3.66 (m, 119H, H9, H10, H11, H12, H13, H14, H15), 2.11 (m, 33H, H6), 1.14 (m, 69H, H2, H3, H5), 0.84 (m, 6H, H1, H4). IR(KBr, cm^{-1}): 3068 (m), 2972 (m), 2923 (vs), 2889 (s), 2077 (s), 2038 (s), 2000 (s), 1751 (m), 1642 (m), 1124 (m), 996 (m), 910 (m).

Reaction of PB-PEO2 with Carbonyldiimidazole (64)

A solution of 2.21 g (0.675 mmol) PB-PEO2 and 3.07 g (18.9 mmol) CDI, dissolved in 60 mL chloroform was stirred for 24 hours at room temperature. The solution was

n = 33 ; m = 27

extracted with water (3 × 20 mL) and the aqueous fractions were extracted with chloroform (3 × 20 mL). The combined organic phases were dried with sodium sulphate and evaporated to dryness. 2.23 g (99%) of compound **64** were obtained as a yellowish resinous compound.

^{1}H NMR (400 MHz, CDCl$_3$): δ = 8.08 (s, 1H, H15), 7.39 (d, $^3J_{H,H}$ = 14.4 Hz, 1H, H13), 7.02 (d, $^3J_{H,H}$ = 14.4 Hz, 1H, H14), 5.40 (m, 33H, H7), 4.87 (m, 66H, H8), 3.59 (m, 112H, H9, H10, H11, H12), 2.06 (m, 33H, H6), 1.14 (m, 69H, H2, H3, H5), 0.77 (m, 6H, H1,H4).

Synthesis of the Carboxylic Acid Modified Polymer (65)

PB-PEO2 (3 g, 0.92 mmol) and chloroacetic acid (0.43 g, 4.84 mmol) were dissolved in 70 mL THF. The solution was titrated with diphenylmethyl potassium and stirred over night.

n = 33 ; m = 27

Subsequently the reaction mixture was extracted with sodium bicarbonate, brine and water. After drying with magnesium sulphate, the reaction mixture was evaporated to dryness to give 2.88 g (94 %) of compound **65**. ^{1}H NMR (400 MHz, CDCl$_3$): δ = 5.45 (m, 33H, H7), 4.94 (m, 66H, H8), 3.99 (s, 2H, H13), 3.65 (m, 112H, H9, H10, H11, H12), 2.12 (m, 33H, H6), 1.14 (m, 69H, H2, H3, H5), 0.77 (m, 6H, H1,H4).

Synthesis of PB-PEO2-C(O)(CDI) (66)

A solution of 2.89 g (0.87 mmol) of compound **65** and 2.82 g (17.35 mmol) CDI, dissolved in 50 mL chloroform was stirred for 24 hours at room temperature. The solution was extracted with water (3 × 20 mL) and the aqueous fractions were extracted with chloroform (3 × 20 mL). The combined organic phases were dried with magnesium sulphate and evaporated to dryness. 2.88 g (97 %) of compound **66** were obtained as a resinous compound. ^{1}H NMR (400 MHz, CDCl$_3$): δ = 7.84 (s, 1H, H15), 7.48 (m, 1H, H13), 7.10 (m, 1H, H14), 5.46 (m, 33H, H7), 4.95 (m, 66H, H8), 3.99 (s, 2H, H13), 3.65 (m, 112H, H9, H10, H11, H12), 2.12 (m, 33H, H6), 1.14 (m, 69H, H2, H3, H5), 0.77 (m, 6H, H1,H4).

n = 33 ; m = 27

Synthesis of 4-(Ditetradecylmethyl)pyridine (67)

A solution of *n*-butyllithium (1.6 mol/L in hexane) was slowly added to a solution of 15.2 mL (0.11 mol) diisopropylamine in 100 mL diethyl ether at -15°C and stirred for 30 min. Subsequently, 5 g (0.54mol) 4-methylpyridine were added and the obtained orange suspension stirred for additional 3 hours. 30.5 g (0.1 mol) tetradecylbromide were added at once and the solution stirred for 20 hours at room temperature. The reaction mixture was washed twice with a

concentrated solution of ammonium chloride and water. Drying with sodium sulphate and evaporation to dryness afforded the crude product. Crystallization from acetone afforded 19.1 g (73%) of a white powder. ^{1}H NMR (200 MHz, CDCl$_3$): δ = 8.45 (d, [3]J$_{H,H}$ = 5.4 Hz, 2H, CHN), 7.03 (d, [3]J$_{H,H}$ = 5.4 Hz, 2H, CHCHN), 2.44 (m, 1H, CH), 1.53 (m, 4H, CH_2CH), 1.22 (m, 48H, CH_2), 0.85 (t, [3]J$_{H,H}$ = 6.4 Hz, 6H, CH_3). ^{13}C NMR (50 MHz, CDCl$_3$): δ = 155.7 ($C_{aromatic}$), 149.5 (CHN), 123.3 (CHCHN), 45.6 (CH), 36.2 (CHCH$_2$), 31.9 (CH$_2$CH$_2$CH$_3$), 29.6, 29.5, 29.3 (CH$_2$), 27.4 (CHCH$_2$$CH_2$), 22.7 ($CH_2CH_3$), 14.1 ($CH_3$). MS (DEI): m/z = 486 [M]$^+$. Anal. calcd. for C$_{34}$H$_{63}$N: C, 84.05 %; H, 13.07 %; N, 2.88%. Found: C, 83.74 %; H, 13.12 %; N, 2.52 %.

Synthesis of 4-(Ditetradecylmethyl)-N-(carboxymethyl)pyridinium bromide (68)

A solution of 5 g (0.01 mol) 4-(ditetradecylmethyl)pyridine (**67**) and 2.84 g (0.02 mol) bromoacetic acid in 100 mL toluene was refluxed for 10 hours. Following evaporation to dryness and two-times crystallization from ethylacetate afforded 2.36 g (38 %) of a white solid. ^{1}H NMR (400 MHz, CDCl$_3$): δ = 16.08 (s, 1H, OH), 9.29 (d, [3]J$_{H,H}$ = 6.4 Hz, 2H, CHN), 7.74 (d, [3]J$_{H,H}$ = 6.4 Hz, 2H, CHC), 6.06 (s, 2H, NCH_2), 2.73 (m, 1H, CH), 1.66 and 1.53 (2m, 4H, CH_2CH), 1.19 (m, 48H, CH_2), 0.82 (t, [3]J$_{H,H}$ = 6.5 Hz, 6H, CH_3). ^{13}C NMR (100 MHz, CDCl$_3$): δ = 166.6 (COOH), 145.8 (CHN), 126.6 (CHCHN), 60.4 (NCH$_2$), 46.5 (CH), 35.4 (CH$_2$CH), 31.8 (CH$_2$CH$_2$CH$_3$), 29.6, 29.3, 27.3 (CH$_2$), 22.6 (CH$_2$CH$_3$), 14.0 (CH$_3$). MS (micro-ESI): m/z = 646 [M+Na]$^+$. MS (FAB in nba): m/z = 545 [M-Br]$^+$. Anal. calcd. for C$_{36}$H$_{66}$BrNO$_2$: C, 69.20 %; H, 10.65 %; N, 2.24 %; Br, 12.79 %. Found: C, 68.89 %; H, 10.72 %; N, 2.09 %; Br, 13.27 %.

Synthesis of 1,3-Dithiobenzylacetone (70)

Under strong cooling, 5.67 g (0.247 mol) sodium were dissolved in 370 mL dry ethanol under an argon atmosphere. Next, the solution was cooled using ice/sodium chloride and 30.74 g (0.247 mmol) benzylmercaptane were added. To this solution, 15 g (0.12 mol) 1,3-dichloroacetone, dissolved in 200 mL ethanol, were dropped in slowly and a white precipitate became visible. After 10 hours stirring at room temperature the solvent was removed and the residue was suspended in 200 mL water and extracted four times with 80 mL diethyl ether. The combined organic phases were again washed with 70 mL water and dried over sodium sulphate. Removal of the solvent afforded 33.31 g (93 %) of 1,3-dithiobenzylacetone as

a yellow oil. ^{1}H NMR (400 MHz, CDCl$_3$): δ = 7.29-7.09 (m, 10H, H$_{aromatic}$), 3.66 (s, 4H, SCH_2Ph), 3.22 (s, 4H, CH_2C(O)CH_2). ^{13}C NMR (50MHz, CDCl$_3$): δ = 199.9 (CO), 137.1 (C). 129.2 (o-CH), 128.5 (m-CH), 126.9 (p-CH), 37.5 (CH$_2$C(O)CH$_2$), 36.1 (SCH$_2$Ph). MS (DEI): m/z = 302 [M]$^+$. IR (KBr, cm^{-1}): 3084 (w), 3061 (m), 3028 (m), 2921 (m), 1951 (w), 1882 (w), 1808 (w), 1701 (vs), 1601 (m), 1583 (w), 1494 (s), 1453 (s), 1406 (m), 1287 (m), 1254 (s), 1186 (m), 1070 (s), 1028 (s). Anal. calcd. for C$_{17}$H$_{18}$OS$_2$: C, 67.51 %; H, 6.00 %; S, 21.20 %. Found: C, 67.49 %; H, 6.05 %; S, 21.12 %.

Synthesis of 1,3-Dithiobenzylacetonoxime (71)

Under an argon atmosphere 32.82 g (0.11 mol) 1,3–dithiobenzylacetone (**70**) and 35.8 g (0.52 mol) hydroxylamine hydrochloride were dissolved in 270 mL ethanol. Subsequently, 55 mL aqueous sodium hydroxide (10 mol/L) were added and the reaction mixture warmed for 2 hours under reflux, followed by addition of 100 mL water. Extraction with 400 mL diethyl ether, drying over sodium sulphate and crystallization from ethanol yielded 24.67 g (71.6%) of a white solid. ^{1}H NMR (400 MHz, CDCl$_3$): δ = 8.81 (s, 1H, OH), 7.31-7.18 (m, 10H, C$H_{aromatic}$), 3.71 (s, 2H, trans-SCH_2Ph), 3.61 (s, 2H, cis-SCH_2Ph), 3.50 (s, 2H, trans-CH_2CN), 3.21 (s, 2H, cis-CH_2CN). ^{13}C NMR (50MHz, CDCl$_3$): δ = 155.5 (CNOH), 137.9/ 137.8 (C$_{aromatic}$), 129.1/128.9 (o-CH$_2$), 128.5 (m-CH$_2$), 127.1/127.0 (p-CH), 37.0 (trans-SCH$_2$Ph), 35.6 (cis-SCH$_2$Ph), 32.6 (cis-CH$_2$CN), 24.8 (trans-CH$_2$CN) [aromatic signals for the cis and trans groups are not exactly assignable from HSQC and HMBC measurements due to the broadness of the cross peaks]. MS (DEI): m/z = 317 [M]$^+$. IR (KBr, cm^{-1}): 3242 (vs), 3052 (m), 3028 (m), 2923 (m), 1945 (w), 1601 (m), 1493 (s), 1450 (s), 1407 (s), 1284 (s), 1250 (m), 1225 (m), 1154 (m), 1070 (m), 1029 (m), 975 (vs), 922 (w), 906 (w), 822 (s), 742 (s), 705 (vs), 618 (m), 562 (w), 477 (m), 456 (w). Anal. calcd. for C$_{17}$H$_{19}$NOS$_2$: C, 64.32 %; H, 6.03 %; N, 4.41 %; S, 20.20 %. Found: C, 64.28 %; H, 6.08 %; N, 4.38 %; S, 20.33 %.

Synthesis of 1,3-Dithiobenzyl-2-aminopropane hydrochloride (72)

In 100 mL diethyl ether, 15 g (47.3 mmol) 1,3-dithiobenzylacetonoxime (**71**) were dissolved and cooled to 10 °C, whereupon lithium alanate (3.75 g, 99 mmol) was added and stirred for 2 hours at 10 °C. After 72 hours stirring at room temperature, the solution was cooled to 0 °C and water

was added dropwise until only a white precipitate remained. The suspension was filtered and the filtration residue washed several times with diethyl ether. The combined organic phases were dried over sodium sulphate and evaporated to dryness. To the remaining yellow oily substance 150 mL hydrogen chloride (10 % in water) were added whereupon a slightly yellow precipitate appeared which was separated, washed with little diethyl ether and crystallized from ethanol. 8.53 g (53 %) 1,3-dithiobenzyl-2-aminopropane hydrochloride (**72**) were obtained as white needles. ^{1}H NMR (200MHz, CD_2Cl_2): δ = 8.63 (s, 2H, NH_2), 7.32–7.19 (m, 10H, C$H_{aromatic}$), 3.70 (s, 4H, SCH_2Ph), 3.61 (m, 1H, CH), 3.00–2.78 (m, 4H, SCH_2CHCH_2S). ^{13}C NMR (50MHz, $CDCl_3$): δ = 138.1 (C$_{aromatic}$), 129.5 (o-CH), 129.0 (m-CH), 127.6 (p-CH), 51.6 (CH), 37.1 (SCH_2Ph). 33.7 (SCH_2CHCH_2S). MS (DEI): m/z = 304 [M-Cl]$^{+}$. IR (KBr, cm^{-1}): 3434 (s), 2907 (vs), 2679 (m), 2592 (m), 2478 (m), 2005 (w), 1957 (w), 1587 (s), 1495 (vs), 1453 (s), 1414 (m), 1377 (m), 1339 (w), 1250 (m), 1193 (m), 1116 (m), 1071 (m), 1031 (w), 985 (w), 926 (w), 801 (w), 774 (m), 705 (vs). Anal. calcd. for $C_{17}H_{22}NS_2Cl$: C, 60.06 %; H, 6.52 %; N, 4.12 %; S, 18.86 %; Cl, 10.43 %. Found: C, 60.06 %; H, 6.49 %; N, 4.10 %; S, 18.87 %, Cl, 10.29 %.

Synthesis of 3-Amino-1,2-dithiolane hydrochloride (74)

1,3-Dithiobenzyl-2-aminopropane hydrochloride (**72**) (2.23 g, 6.58 mmol) was dissolved in 20 mL THF and cooled to -78 °C. Then, 600 mL ammonia was condensed in the same vessel and sodium (676 mg, 29.4 mmol) was added in small portions until the blue colour persisted for 20 minutes. The excess of sodium was destroyed by adding ammonium chloride. By bubbling argon through the solution, the ammonia was evaporated slowly (*caution: danger of explosion*). The small amount of THF was flushed out with the ammonia. The residue was dissolved in 100 mL water and the solution was acidified (pH = 1) using hydrogen chloride (10% in water). The solution was stored at 4 °C whereas a precipitate was formed. After filtration, the filtrate was used for the subsequent reaction. A 0.03 mol/L I_2/KI solution and the filtrate were dropped simultaneously into 10 mL water, so that the colour of the solution became slightly yellow. The end point for the oxidation of the dithiol (**73**) to the disulfane (**74**) was monitored using starch as indicator. Afterwards the pH was increased to pH = 12 with 5 mol/L sodium hydroxide and extracted 5 times with 75 mL chloroform. The combined organic fractions were washed twice

with water and dried over sodium sulphate. Afterwards the organic fraction was extracted with 10% hydrogen chloride until the chloroform phase was colourless. Lyophilization of the aqueous solution afforded 557 mg (54 %) yellow solid. ^{1}H NMR (200 MHz, D$_2$O): δ = 4.52-4.40 (m, 1H, C*H*), 3.39 (dd, ^{2}J = 13.2 Hz, ^{3}J = 5.3 Hz, 2H, C*H*$_A$H$_B$), 3.25 (dd, ^{2}J = 2.6 Hz, 13.2 Hz, ^{3}J = 5.3 Hz, 2H, CH$_A$*H*$_B$). ^{13}C NMR (50 MHz, D$_2$O): δ = 55.4 (*C*H), 41.8 (*C*H$_2$). MS (DEI): *m/z* = 121 [M-HCl]$^+$. IR (KBr, cm^{-1}): 3435 (vs), 2921 (vs), 2560 (m), 2366 (w), 2340 (w), 1973 (m), 1625 (s), 1588 (m), 1489 (s), 1401 (s), 1384 (vs). Anal. calcd. for C$_3$H$_8$ClS$_2$N: C, 22.85 %; H, 5.11 %; N, 8.88 % S, 40.67 %; Cl, 22.48 %. Found: C, 22.49 %; H, 5.00 %; N, 8.62 %; S, 38.47 %; Cl, 22.72 %.

Synthesis of 5,5-Bis[(benzylthio)methyl]hydantoine (80)

3.25 g (0.011 mol) 1,3-dithiobenzylacetone (**70**), 2.09 g (0.032 mol) potassium cyanide and 5.17 g (0.053 mol) ammonium carbonate were dissolved in 30 mL ethanol and 21 mL water. Afterwards the mixture was heated to 120 °C for 24 hours and to 140 °C for 22 hours in a sealed tube. After cooling the solution to room temperature, 100 mL 2 N hydrochloric acid were added (*caution: development of dicyane*) and stirred for 22 hours. The formed precipitate was separated and washed twice with 10 mL water and 10 mL toluene. Crystallization from ethylacetate afforded 2.71 g (23 %) of a golden solid. ^{1}H NMR (200 MHz, DMSO-d$_6$): δ = 10.90 (s, 1H, C(O)N*H*C(O)), 8.07 (s, 1H, CN*H*C(O)), 7.35-7.19 (m, 10H, C*H*$_{aromatic}$), 3.76 (s, 4H, SC*H*$_2$Ph), 2.75 (d, ^{2}J$_{H,H}$ = 14 Hz, 2H, SC*H*$_A$H$_B$C), 2.65 (d, ^{2}J = 14 Hz, 2H, SCH$_A$*H*$_B$C). ^{13}C NMR (50 MHz, DMSO-d$_6$): δ = 175.9 (C*C*(O)NH), 157.0 (NH*C*(O)NH), 138.1, 128.8, 128.4, 126.9 (C$_{aromatic}$), 67.4 (CH$_2$*C*HCH$_2$), 36.6 (S*C*H$_2$Ph), 36.4 (*C*H$_2$CH*C*H$_2$). MS (FAB in nba): *m/z* = 373 [M+H]$^+$. IR (KBr, cm^{-1}): 3375 (s), 3220 (s), 3062(m), 2919 (m), 1762 (s), 1720 (vs), 1494 (m), 1453 (m), 1401 (s). Anal. calcd. for C$_{19}$H$_{20}$N$_2$O$_2$S$_2$: C, 61.26 %; H, 5.41 %; N, 7.52 % S, 17.22 %. Found: C, 61.26 %; H, 5.36 %; N, 7.45 %; S, 17.25 %.

Synthesis of 2,2-Bis(benzylthiomethyl)glycine (81)

5,5-Bis[(benzylthio)methyl]hydantoine (**80**) (2.01 g, 5.4 mmol) was suspended in an aqueous solution of 40 mL 1 N sodium hydroxide and heated to 170 °C for 20 hours in a pressure apparatus at 100 psi. After cooling to 0 °C, the solution was acidified (pH = 5-6) with

6 N hydrochloric acid. The precipitate was separated and crystallized from methanol to give 1.22 g (65 %) brown powder. ^{1}H NMR (200 MHz, DMSO-d$_6$): δ = 7.31-7.19 (m, 10H, C$H$$_{aromatic}$), 3.76 (s, 4H, SC$H_2$Ph), 2.87 (d, ^{2}J$_{H,H}$ = 14 Hz, 2H, SCH_AH$_B$C), 2.75 (d, ^{2}J$_{H,H}$ = 14 Hz, 2H, SC$H_A$$H_B$C). ^{13}C NMR (50 MHz, DMSO-d$_6$): δ = 169.6 (C(O)OH), 138.6, 128.9, 128.3, 126.7 ($C$$_{aromatic}$), 62.4 (CH$_2$$CHCH_2$), 37.4 (S$CH_2$Ph), 36.2 (S$CH_2CHCH_2$S). MS (micro-ESI, positive scan): m/z = 370.1 [M+Na]$^+$. MS (micro-ESI, negative scan): m/z = 346.4 [M-H]$^-$. IR (KBr, cm^{-1}): 3437 (s), 3028(s), 2922 (s), 1636 (s), 1494 (s), 1453 (m), 1368 (s). Anal. calcd. for C$_{18}$H$_{21}$NO$_2$S$_2$: C, 62.21 %; H, 6.09 %; N, 4.03 % S, 18.45 %. Found: C, 61.91 %; H, 5.96 %; N, 3.94 %; S, 18.37 %.

Synthesis of N-Carboxy-2,2-bis(benzylthiomethyl)glycine anhydride (82)

Caution: Gas masks with suitable air filter should be within range and contaminated glassware should be treated with concentrated sodium hydroxide. Likewise, the fumes should be conducted through a concentrated sodium hydroxide solution to destroy gaseous phosgene.

5,5-Bis[(benzylthio)methyl]glycine (**81**) (8.97 g, 25.84 mmol) was dissolved in 300 mL tetrahydrofurane and cooled to 0 °C. To this solution 76 mL phosgene (20 % in toluene) were added slowly. After stirring the solution for 5 hours at room temperature, the solvent was removed by room temperature distillation under reduced pressure using a cooling trap. The residue was dissolved in diethyl ether and filtrated through silica gel. By evaporation to dryness and washing with pentane 8.50 g (88 %) of compound **82** were obtained as white solid. ^{1}H NMR (200 MHz, CDCl$_3$): δ = 7.39-7.26 (m, 10H, C$H$$_{aromatic}$), 3.81 (s, 4H, SC$H_2$Ph), 2.75 (s, 4H, C$H_2$CN). ^{13}C NMR (50 MHz, CDCl$_3$): δ = 170.3 (C(O)O), 151.6 (NHC(O)O), 136.9, 129.0, 128.8, 127.6 (C$_{aromatic}$), 69.1 (CH$_2$$CHCH_2$), 37.6 (S$CH_2$Ph), 36.6 ($CH_2CHCH_2$). MS (FAB in nba): m/z = 374 [M-H]$^+$. IR (KBr, cm^{-1}): 3413 (s), 2923 (s), 2852 (m), 1843 (s), 1775 (vs), 1494 (m), 1453 (m), 1341 (m). Anal. calcd. for C$_{19}$H$_{19}$NO$_3$S$_2$•0.5pentane: C, 63.05 %; H, 6.15 %; N, 3.42 %; S, 15.66 %. Found: C, 63.07 %; H, 6.26 %; N, 3.27 %; S, 15.48 %.

Synthesis of N-Boc-2,2-bis(benzylthiomethyl)-Gly-OMe (83)

To a solution of 8.49 g (0.023 mol) N-carboxy-2,2-bis(benzylthiomethyl)glycine anhydride (**82**) dissolved in 80 mL THF, a solution of 6 g (0.027 mol) di-$tert$-butyl dicarbonate and 4 mL pyridine, dissolved in 80 mL THF, was added slowly at 0 °C and stirred for 45 minutes. After warming up to room temperature, the solution was stirred for another 10 minutes followed by addition of 30 mL methanol and 5.4 mL N-methylmorpholine. The solution was stirred for 21 hours at room temperature and purified via FC (CH_2Cl_2:hexane = 3:2) to yield 8.76 g (83 %) of the desired product. ^{1}H NMR (200 MHz, $CDCl_3$): δ = 7.25-7.14 (m, 10H, C$H_{aromatic}$), 5.86 (s, 1H, NH), 3.66 (s, 3H, OCH_3), 3.64 (s, 4H, SCH_2Ph), 3.46 (d, $^2J_{H,H}$ = 13.5 Hz, 2H, CH_AH$_B$CN), 2.80 (d, $^2J_{H,H}$ = 13.5 Hz, 2H, CH$_A$$H_B$CN), 1.42 (s, 9H, C(C$H_3$)$_3$). ^{13}C NMR (50 MHz, $CDCl_3$): δ = 171.6 (C(O)O), 154.1 (NHC(O)O), 138.1, 128.8, 128.5, 127.1 (C$_{aromatic}$), 79.9 (C(CH$_3$)$_3$), 65.4 (CH$_2$$CHCH_2$), 52.9 (O$CH_3$), 37.2 (S$CH_2$Ph), 36.5 ($CH_2CHCH_2$), 28.4 (C($CH_3$)$_3$). MS (DEI): m/z = 462 [M+H]$^+$, 406 [M-tBu]$^+$, 370 [M-C$_7$H$_7$]$^+$. IR (KBr, cm^{-1}): 3423 (s), 2925 (s), 2853 (m), 1744 (s), 1712 (vs), 1492 (s), 1454 (m), 1326 (m). Anal. calcd. for $C_{24}H_{31}NO_4S_2$: C, 62.44 %; H, 6.77 %; N, 3.03 %; S, 13.89 %. Found: C, 62.61 %; H, 6.88 %; N, 3.09 %; S, 13.75 %.

Synthesis of 4-(N-tert-Butyloxycarbonyl)-amino-1,2-dithiolane-4-carboxylic acid methyl ester/ Boc-Adt-OMe (84)

N-Boc-2,2-bis(benzylthiomethyl)-Gly-OMe (**83**) (3.29 g, 6.94 mmol) was dissolved in 40 mL diethyl ether. Afterwards ammonia (600 mL) was condensed in the same vessel and sodium (755 mg, 32.8 mmol) was added in small portions until the blue colour persisted for 30 minutes. The excess of sodium was destroyed by ammonium chloride visible by decolouration and the ammonia was slowly evaporated by bubbling argon through the solution. The residue was dissolved in 100 mL methanol and neutralized with 2 N hydrochloric acid. To this solution a 0.05 mol/L I$_2$/KI solution was added until controlling reactions with starch, revealed a permanent blue colour. Small excess of iodine was destroyed with sodium thiosulphate. The aqueous solution was extracted with ethylacetate and dried over sodium sulphate. Removal of the solvent and washing with pentane afforded 1.62 g (84 %) of the dithiolane as slightly yellow solid. ^{1}H NMR (200 MHz, $CDCl_3$): δ = 7.30-7.15 (m, 10H, C$H_{aromatic}$), 5.26 (s, 1H, NH), 3.79 (s, 3H, OCH_3), 3.62 (d, $^2J_{H,H}$ = 12.2 Hz, 2H, CH_AH$_B$CN), 3.36 (d, $^2J_{H,H}$ = 12.2 Hz, 2H, CH$_A$$H_B$CN),

1.43 (s, 9H, C(CH_3)$_3$). ^{13}C NMR (50 MHz, CDCl$_3$): δ = 170.9 (C(O)O), 154.1 (NHC(O)O), 133.4, 128.8, 128.5, 127.0 (C$_{aromatic}$), 80.9 (C(CH$_3$)$_3$), 71.3 (CH$_2$CHCH$_2$), 53.6 (OCH$_3$), 47.7 (CH$_2$), 28.1 (C(CH$_3$)$_3$). MS (DEI): m/z = 279 [M]$^+$, 223 [M-tBu]. IR (KBr, cm^{-1}): 2977 (m), 2933 (w), 1737 (s), 1709 (s), 1490 (m), 1136 (s). Anal. calcd. for C$_{10}$H$_{17}$NO$_4$S$_2$: C, 42.99 %; H, 6.13 %; N, 5.01 %; S, 22.95 %. Found: C, 42.83 %; H, 5.96 %; N, 4.84 %; S, 22.18 %.

Synthesis of N-Boc-Met-Adt-OMe (86)

Boc-adt-OMe (**84**) (188 mg, 0.67 mmol) was dissolved in 5 mL methanol and cooled to 0 °C, after which 49 μL (0.67 mmol) thionyl chloride were added. The solution was warmed to 50 °C for 4 hours and evaporated to dryness. Afterwards the residue was dissolved in 2 mL dimethylformamide and cooled to 0 °C. Successive 115 mg (0.85 mmol) HOBt, 163 mg (0.85 mmol) EDC and 186 mg (0.75 mmol) Boc-Met-OH were added and stirred for 20 minutes at 0 °C. After warming to room temperature 1 mL (7.2 mmol) triethylamine was added and stirred for additional 2 days at room temperature. Water (10 mL) was added and the solution was extracted twice with 20 mL ethylacetate. The organic fractions were extracted with water, 10 % citric acid, saturated sodium bicarbonate solution and water and dried over sodium sulphate. Removal of the solvent afforded 789 mg crude product, purified by FC (ethylacetate:hexane = 35:65) to yield 59 mg (22 %) white solid. ^{1}H NMR (200 MHz, CDCl$_3$): δ = 7.06 (s, 1H, NH), 5.13 (d, ^{3}J$_{H,H}$ = 8 Hz, 1H, NHBoc), 4.30 (m, 1H, NCHC(O)), 3.77 (s, 3H, OCH_3), 3.64 (d, ^{2}J$_{H,H}$ = 11.2 Hz, 2H, SCH_AH$_B$), 3.43-3.34 (m, 2H, SCH$_A$$H_B$), 2.59 (t, ^{3}J$_{H,H}$ = 7.2 Hz, 2H, CH_2SCH$_3$), 2.12 (s, 3H, SCH_3), 2.09-1.88 (m, 2H, CH_2CH$_2$SCH$_3$) 1.45 (s, 9H, C(CH_3)$_3$). ^{13}C NMR (50 MHz, CDCl$_3$): δ = 171.4 (C(O)OCH$_3$), 169.9 (C(O)NH), 155.6 (OC(O)NH), 80.5 (C(CH$_3$)$_3$), 70.8 (CH$_2$CCH$_2$), 53.3 (NCHC(O) and OCH$_3$), 47.3, 47.2 (S CH$_2$CCH$_2$S), 30.8 (CH$_2$CH$_2$SCH$_3$), 30.0 (CH$_2$SCH$_3$), 28.3 (C(CH$_3$)$_3$), 15.2 (SCH$_3$).

Synthesis of N-Boc-Met-Adt-Phe-OMe (88)

To a solution of 182 mg (0.44 mmol) N-Boc-Met-Adt-OMe (**86**), dissolved in 2 mL methanol, 1.9 mL NaOH$_{aq}$ (1 mol/L) was added and the solution was stirred for 6 hours at room temperature. After evaporation to dryness, the remaining solid was acidified with 5 mL hydrogen chloride (0.5 mol/L in water) and the organic material was extracted with ethyl acetate. The

organic phase was washed with water, dried with sodium sulphate, evaporated to dryness and dissolved in 4 mL dimethylformamide. Subsequently, 78 mg (0.58 mmol) HOBt, 95 mg (0.50 mmol) EDC, 71 µL (0.51 mmol) triethylamine and 110 mg (0.51 mmol) phenylalanine methylester hydrochloride were added at 0 °C and stirred for 30 min, followed by 16 hours stirring at room temperature. The reaction was stopped by addition of 5 mL water. The reaction solution was extracted twice with 20 mL ethylacetate. The organic fraction was successive washed with water, citric acid (10 % in water), sodium bicarbonate and water. Drying with sodium sulphate and evaporation to dryness afforded the crude product, which was purified via FC (chloroform:ethylacetate = 9:1). 79 mg (32 %) of compound **88** was obtained as white solid. ^{1}H NMR (400 MHz, CDCl$_3$): δ = 7.24 (m, 3H, m-, p-C$H_{aromatic}$), 7.10 (m, 2H, o-C$H_{aromatic}$), 6.92 (s, 1H, NH-adt), 5.14 (d, $^3J_{H,H}$ = 6.4 Hz, 1H, NHBoc), 4.80 (m, 1H, CHC(O)OCH$_3$), 4.19 (m, 1H, CHC(O)NH), 3.68 (s, 3H, OCH_3), 3.45 (m, 4H, SCH_2CCH_2S), 3.16 (dd, $^2J_{H,H}$ = 13.9 Hz, $^3J_{H,H}$ = 5.8 Hz, 1H, CH_AH$_B$Ph), 3.03 (dd, $^2J_{H,H}$ = 13.9 Hz, $^3J_{H,H}$ = 7.2 Hz, 1H, CH$_A$$H_B$Ph), 2.56 (t, $^3J_{H,H}$ = 7 Hz, 2H, CH_2SCH$_3$), 2.08 (m, 4H, SCH_3 and CH_AH$_B$CH$_2$S), 1.89 (m, 1H, CH$_A$$H_BCH_2$S), 1.43 (s, 9H, C(C$H_3$)$_3$). ^{13}C NMR (50 MHz, CDCl$_3$): δ = 171.8 (adt-C(O)NH), 171.6 (C(O)OCH$_3$), 168.9 (CHC(O)NH), 155.8 (OC(O)NH), 135.9, 129.2, 128.5, 127.1 (C$_{aromatic}$), 80.8 (C(CH$_3$)$_3$), 71.6 (SCH$_2$$CCH_2$S), 53.8 ($C$HC(O)OCH$_3$ and CHC(O)NH), 52.3 (OCH$_3$), 46.7, 45.8 (SCH$_2$CCH$_2$S), 37.7 (CH$_2$Ph), 30.2 (CH$_2$CH$_2$S and CH$_2$SCH$_3$), 28.3 (C(CH$_3$)$_3$), 15.2 (SCH$_3$).

Synthesis of N-Boc-Adt-Phe-OMe (90)

To a solution of 224 mg (0.8 mmol) N-Boc-Adt-OMe (**84**) dissolved in 3.5 mL methanol, 1.6 mL sodium hydroxide (1 mol/L in water) were added and the mixture stirred for 6 hours at room temperature. The solution was evaporated to dryness, acidified with 20 mL hydrogen chloride (0.5 mol/L in water) and extracted with ethylacetate. The organic fractions were washed with water and dried with sodium sulphate. Evaporation to dryness afforded 198 mg of N-Boc-Adt-OH and was used without further purification. N-Boc-Adt-OH was dissolved in 4 mL dimethylformamide and 182 mg (0.95 mmol) EDC, 137 mg (1.01 mmol) HOBt, 191 mg (0.89 mmol) phenylalanine methylester hydrochloride and 0.15 mL (1.08 mmol) triethylamine were added consecutively at 0 °C. After 2 days of stirring at room temperature, 10 mL water were added to the reaction mixture. The solution was extracted twice with ethylacetate and the

obtained organic fraction was successive washed with water, citric acid (10 % in water), sodium bicarbonate, water and dried over sodium sulphate. Evaporation to dryness and purification *via* FC (chloroform:ethylacetate = 95:5) afforded 75 mg (22 %) of a white solid. ^{1}H NMR (200 MHz, CDCl$_3$): δ = 7.27 (m, 3H, *m*-, *p*-C$H_{aromatic}$), 7.11 (m, 2H, *o*-C$H_{aromatic}$), 5.19 (s, 1H, NHBoc), 4.88 (m, 1H, CHC(O)OCH$_3$), 3.72 (s, 3H, OCH_3), 3.51 (m 4H, SCH_2), 3.14 (m, 2H, CH$_2$Ph), 1.43 (s, 9H, C(CH$_3$)$_3$). ^{13}C NMR (100 MHz, CDCl$_3$): δ = 171.6 (*C*(O)OCH$_3$), 169.4 (C(O)NH), 154.5 (O*C*(O)NH), 135.7, 129.2, 128.6, 127.2 (*C*$_{aromatic}$), 81.3 (*C*(CH$_3$)$_3$), 71.7 (SCH$_2$*C*CH$_2$S), 53.6 (O*C*H$_3$), 52.4 (*C*HC(O)OCH$_3$), 46.3 (S*C*H$_2$C), 37.9 (*C*H$_2$Ph), 28.2 (C(*C*H$_3$)$_3$).

Synthesis of L-Cystine dimethylester dihydrochloride (97)

Thionyl chloride (1.9 mL, 13.7 mmol) was added slowly to 40 mL methanol. *L*-Cystine (2.5 g, 0.01 mol) was added at once and the reaction mixture was refluxed for 16 hours. The solution was evaporated to dryness and afforded 3.4 g (99%) of compound **97** as a white solid without further purification. ^{1}H NMR (200 MHz, D$_2$O): δ = 4.48 (m, 2H, CH), 3.76 (s, 6H, OCH$_3$), 3.27 (m, 4H, CH$_2$). ^{13}C NMR (50 MHz, D$_2$O): δ = 168.7 (*C*(O)O), 53.5 (*C*H), 51.1 (*C*H$_3$), 35.2 (*C*H$_2$). MS (DEI): *m/z* = 269 [M-2HCl]$^+$. Anal. Calcd. for C$_8$H$_{18}$N$_2$Cl$_2$O$_4$S$_2$: C, 28.15 %; H, 5.32 %; N, 8.21 %; S, 18.79 %; Cl, 20.78 %. Found: C, 27.59 %; H, 5.96 %; N, 7.80 %; S, 18.02 %; Cl, 20.33 %.

Synthesis of N,N'-Bis[(tert-butyloxy)carbonyl]-L-cystine dimethyl ester (98)

L-cystine dimethylester dihydrochloride (**97**) (3.5 g, 0.01 mol) was dissolved in 20 mL sodium hydroxide (1 mol/L in water) and 30 mL dioxane/water (2:1 ratio). The solution was cooled to 0 °C and 5.2 g (0.024 mmol) di-*tert*-butyldicarbonate were added in one portion. After 24 hours stirring at room temperature, the resinous residue was dried in high vacuum. The material was dissolved in 30 mL ethylacetate and the pH was adjusted to 3 with sodium hydrogensulphate. The aqueous layer was extracted twice with 30 mL ethylacetate and the combined organic fractions were washed with brine and water, dried with sodium sulphate and evaporated to dryness. Crystallization from ethylacetate/pentane yielded 3.6 g (77 %) of compound **98**. ^{1}H NMR (200 MHz, CDCl$_3$): δ = 5.37 (d, [3]J$_{H,H}$ = 7.4 Hz, 2H, NH), 4.56 (m, 2H, CH), 3.75 (s, 6H, OCH_3), 3.14 (m, 4H, CH_2), 1.43 (s, 9H, C(CH$_3$)$_3$). ^{13}C NMR (50 MHz, CDCl$_3$): δ = 171.1 (*C*(O)O),

155.0 ($OC(O)NH$), 80.3 ($C(CH_3)_3$), 52.8 (CH), 52.6 (OCH_3), 41.3 (CH_2), 28.3 ($C(CH_3)_3$). MS (DEI): m/z = 468 [M]$^+$. Anal. Calcd. for $C_{18}H_{32}N_2O_8S_2$: C, 46.14 %; H, 6.88 %; N, 5.98 %; S, 13.69 %. Found: C, 46.18 %; H, 7.04 %; N, 5.89 %; S, 13.90 %.

Reaction of N,N'-Bis[(tert-butyloxy)carbonyl]-L-cystine dimethylester with Fe₃(CO)₁₂ (99)

N,N'-Bis[($tert$-butyloxy)carbonyl]-L-cystine dimethyl ester (56 mg, 0.119 mmol) and $Fe_3(CO)_{12}$ (60 mg, 0.1197 mmol) were dissolved in 40 mL THF and refluxed for 20 minutes. Evaporation, followed by FC (THF:hexane = 1:1) yielded 64 mg (72 %) as red solid. ^{1}H NMR (200 MHz, CDCl$_3$): δ = 5.38 (m, 2H, NH), 4.59 (m, 2H, CH), 3.82, 3.81, 3.75 (3·s, 6H, OCH_3, a,e), 2.84, 3.15 (2·m, 4H, SCH_2), 1.44 (s, 9H, CH_3). ^{13}C NMR (50 MHz, CDCl$_3$): δ = 208.3, 207.5, 207.3 (CO), 170.8, 169.9, 169.3 (C(O)O), 154.4 (OC(O)NH), 80.2 (CH), 53.9, 52.4 (OCH$_3$), 41.0, 39.0 (SCH$_2$), 28.9 (C(CH$_3$)$_3$). IR (KBr, cm^{-1}): 2074 (vs), 2038 (vs), 1995 (vs), 1745 (s), 1719 (s).

Synthesis of [(CH₃C(O)Cys-Lys-Cys-NH₂)Fe₂(CO)₆] (101)

Acetyl-Cys-Lys-Cys-OCH$_3$ (23 mg, 0.059 mmol) was dissolved in a mixture of 10 mL toluene and 5 mL methanol. To this solution, $Fe_3(CO)_{12}$ (30 mg, 0.059 mmol) was added and the reaction mixture was stirred for 24 hours at room temperature, whereupon the solution turned red and a black precipitate appeared. The solid was filtered off and methanol was removed under reduced pressure. Subsequently, 10 mL hexane were added and the solution stored for 12 hours at -20 °C whereby 13 mg (33 %) of an orange solid precipitated. NMR investigations were not assignable due to strong line broadening. MS (Micro-ESI in methanol): m/z = 672.0 [M+H]$^+$. IR (KBr, cm^{-1}): 3420 (m), 2985 (m), 2926 (m), 2851 (w), 2076 (vs), 2038 (vs), 1998 (vs), 1671 (s), 1542 (m), 1203 (m), 1137 (m). EA was not obtained due to the small quantity of sample.

Peptide Synthesis. Anchoring of N-Fmoc-Protected β-Amino Acids on Rink Amide AM

General Procedure 1 (GP 1)

Esterification of the Fmoc-protected β^3-amino acid was performed according to reference [223]. The resin was placed in a dried manual SPPS reactor and swelled in dichloromethane (20 mL/g resin) for 1 h. To enable a linking of the amino acid to the resin, the swollen resin was treated according to *GP 2* (*vide infra*). The Fmoc-protected β-amino acid (2.2 eq.), HATU (2.9 eq.) and

DIPEA (4 eq.), dissolved in dimethylformamide (20 mL/g resin) were added under nitrogen atmosphere and mixed by bubbling nitrogen for 6 hours at room temperature. Subsequently, the resin was filtered, washed with dimethylformamide (20 mL/g resin, 5x1 min) and dichloromethane (20 mL/g, 5x1 min). The unreacted NH_2 functions were protected according to *GP 3* (*vide infra*), followed by filtration and washing with dimethylformamide (20 mL/g resin, 5x1 min) and dichloromethane (20 mL/g, 5x1 min). The resin was dried in high vacuum for 24 hours. The resin substitution was determined by measuring the UV/Vis absorbance of the dibenzofulvalene-piperidin adduct. Therefore, two aliquots of the loaded resin were weighed (m_1(resin) and m_2(resin)) and suspended in piperidine (20 % in DMF) in a volumetric flask ($V_1 = V_2 = 10$ mL). After 45 min, the mixtures were transferred into a UV cell. A solution of piperidine (20 % in DMF) served as blank sample. The absorbance was measured at 290 nm. The concentrations (c_1 and c_2) of the benzofulvalene-piperidine adduct in solution were determined using a calibration curve.[224] The loading was determined calculated according to:

$$\text{Loading [mmol/g resin]} = c_n \cdot V_n / \{m_n(\text{resin}) - [\, c_n \cdot V_n \cdot (\text{MW-18})/1000]\}$$

$$(\text{MW} = \text{molecular weight of the Fmoc-protected } \beta\text{-amino acid})$$

The yield for the attachment of Fmoc-protected β-amino acid to the resin was determined according to:

$$\text{Loading yield} = [(\text{Loading}_1 + \text{Loading}_2)/2]/\text{Loading}_{\text{theor}}$$

Fmoc-Deprotection. General Procedure 2 (GP2)

The Fmoc-deprotection was realized using 20 % piperidine in DMF (20 mL/g resin, 2x10 min), DBU:piperidine:DMF (1:1:48) (20 mL/g resin, 3x10 min) and 20 % piperidine in DMF (20 mL/g resin, 1x10 min). Afterwards the resin was washed with DMF (20 mL/g resin, 5x1 min) and dichloromethane (20 mL/g, 5x1 min).

Capping. General Procedure 3 (GP3)

The resin was suspended in DMF (20 mL/g resin) and the unreacted NH_2 groups were reacted with Ac_2O (10 eq.) and DMAP (10 eq.) for 1 hour under nitrogen bubbling. Afterwards, the resin was washed with DMF (20 mL/g resin, 5x1 min) and dichloromethane (20 mL/g, 5x1 min).

Coupling of the β-Amino Acids on Rink Amide AM. General Procedure 4 (GP4)

The Fmoc-deprotection was carried out according to *GP2*. For each additional coupling step, the resin was treated with a solution of the Fmoc-protected β^3-amino acid (3 eq.), HATU (2.9 eq.) and DIPEA (6 eq.), dissolved in DMF (20 mL/g resin). The coupling reaction was monitored by the TNBS test.[225] In case of incomplete coupling the reaction mixture was reacted for another two hours with the Fmoc-protected β^3-amino acid (3 eq.), HATU (2.9 eq.) and DIPEA (6 eq.), dissolved in DMF (20 mL/g resin) and the TNBS test was repeated. After the last coupling, the resin was washed with DMF (20 mL/g resin, 5x1 min) and dichloromethane (20 mL/g, 5x1 min) and dried for 2 h under high vacuum.

Cleavage from Rink Amide AM and Final Deprotection. General Procedure 5 (GP5)

The cleavage of the peptide from the resin and the final deprotection were performed according to reference [223]. Therefore, the resin was treated with a solution of TFA:TIS:water = 95:2.5:2.5 und nitrogen bubbling for 4 hours. Subsequentially, the resin was filtered and washed with TFA (5 mL, 3x1 min). The combined organic fractions were evaporated to dryness and the oily residue was treated with diethyl ether, cooled to 0°C. The formed precipitate was separated and dried under high vacuum for 2 h. The crude peptide was stored at -20°C before purification.

HPLC Analysis and Purification of the β-Peptides. General Procedure 6 (GP6)

RP-HPLC analysis was performed on a *Macherey-Nagel C8* column (Nucleosil 100-5 C_8 (250x4 mm)) by using a linear gradient of A: 0.1 % TFA in water and B: acetonitrile at a flow rate of 1 mL/min with UV detection at 220 nm (t_r = retention time). The crude products were purified by preparative RP-HPLC on a *Macherey-Nagel C8* column (Nucleosil 100-7 C_8 (250x21 mm)) by using a linear gradient of A and B at a flow rate of 10 mL/min with UV detection at 220 nm. Subsequently, the solution was lyophilized to afford the purified peptide.

Formation of the Disulphides. General Procedure 7 (GP7)

In order to remove the acetamidomethyl protection group and to afford a cyclic disulphidic peptide, the peptide was dissolved in methanol (200 mL/mmol) and iodine (33 eq.) was added in once. The mixture was stirred for 9 h under argon atmosphere at room temperature and the

reaction progress was determined by LC-MS. The access of iodine was destroyed using an aqueous solution of ammonium thiosulphate (10 %) and methanol was removed under reduced pressure. After lyophilisation, the crude product was stored at -20 °C before purification.

Synthesis of H-(S)-β³-hPhe-(S)-β³-hVal-(R)-β³-hCys-(S)-β³-hLeu-(S)-β³-hVal-(R)-β³-hCys-(S)-β³-hLeu-(S)-β³-hPhe-OH (104)

304 mg (0.334 mmol) Wang Resin was swelled in 5 mL dichloromethane for 1 h in a dried manual SPPS reactor. Fmoc-(S)-β³-hPhe-OH (671 mg, 1.67 mmol), 0.1 mL (1.26 mmol) methylimidazole and 496 mg (1.67 mmol) MSNT were dissolved in 5 mL DMF and added under nitrogen atmosphere to the resin and mixed by bubbling nitrogen for 4.5 hours. Subsequently, the resin was worked up and analysed according to *GP 1*. The loading was estimated as 82 %. The second amino acid (Fmoc-(S)-β³-hLeu-OH) was coupled according to *GP4* and Fmoc-deprotected according to *GP2*. The third amino acid (Fmoc-(R)-β³-(Acm)hCys-OH) was coupled according to *GP4* and Fmoc-deprotected according to *GP2*. The fourth amino acid (Fmoc-(S)-β³-hVal-OH) was coupled according to *GP4*, capped according to *GP3* and Fmoc-deprotected according to *GP2*. The fifth amino acid (Fmoc-(S)-β³-hLeu-OH) was coupled according to *GP4* and Fmoc-deprotected according to *GP2*. The sixth amino acid (Fmoc-(R)-β³-(Acm)hCys-OH) was coupled according to *GP4* and Fmoc-deprotected according to *GP2*. The seventh amino acid (Fmoc-(S)-β³-hVal-OH) was coupled according to *GP4* and Fmoc-deprotected according to *GP2*. The eighth amino acid (Fmoc-(S)-β³-hPhe-OH) was coupled according to *GP4* and Fmoc-deprotected according to *GP2*.

After drying in high vacuum for 24 hours, the peptide resin was treated according to *GP5*. RP-HPLC purification of crude peptide according to *GP6* (5 min 30 % B; 30-70 % B in 40 min; 70-95 % B in 5 min; 5 min 95 % B; t_r = 28.7 min) afforded 98.8 mg (overall yield: 25 %) of the ACM-protected peptide as a white solid in > 95% purity. MS (HiResMALDI): m/z = 1197.679 [M+H]$^+$, $C_{60}H_{97}N_{10}O_{11}S_2^+$; calcd. 1197.678.

The synthesis of the Acm-deprotected disulphide (98.8 mg, 0.08 mmol) was performed according to *GP7*. The removal of the solvent was followed by purification on Sephadex G-25 (water:methanol = 1:1) and lyophilisation afforded 43.3 mg (overall yield: 13 %) of disulphide

(**104**) as white solid. MS (HiResMALDI): m/z = 1053.589 [M+H]$^+$, $C_{54}H_{84}N_8O_8S_2Na^+$; calcd. 1053.588.

Synthesis of CH$_3$C(O)-(S)-β^3-hAla-(S)-β^3-hPhe-(S)-β^3-hVal-(R)-β^3-hCys-(S)-β^3-hLeu-β^3-(S)-hVal-(R)-β^3-hCys-(S)-β^3-hLeu-(S)-β^3-hPhe-NH$_2$ (105)

The first β-amino acid Fmoc-(S)-β^3-hPhe-OH (283.0 mg, 0.70 mmol) was loaded to Rink Amide AM (213.7 mg) according to *GP1*. The loading was estimated as 73 % and free amino functions were capped according to *GP3*, dried in high vacuum for 12 hours and the resin was Fmoc-deprotected according to *GP2.* The second amino acid (Fmoc-(S)-β^3-hLeu-OH) was coupled according to *GP4* and Fmoc-deprotected according to *GP2*. The third amino acid (Fmoc-(R)-β^3-(Acm)hCys-OH) was coupled according to *GP4* and Fmoc-deprotected according to *GP2*. The fourth amino acid (Fmoc-(S)-β^3-hVal-OH) was coupled according to *GP4*, capped according to *GP3* and Fmoc-deprotected according to *GP2*. The fifth amino acid (Fmoc-(S)-β^3-hLeu-OH) was coupled according to *GP4* for 2 h and Fmoc-deprotected according to *GP2*. The sixth amino acid (Fmoc-(R)-β^3-(Acm)hCys-OH) was coupled according to *GP4* for 2 h and Fmoc-deprotected according to *GP2*. The seventh amino acid (Fmoc-(S)-β^3-hVal-OH) was coupled according to *GP4* for 1.5 h and Fmoc-deprotected according to *GP2*. The eighth amino acid (Fmoc-(S)-β^3-hPhe-OH) was coupled according to *GP4* for 2 h and Fmoc-deprotected according to *GP2*. The ninth amino acid (Fmoc-(S)-β^3-hAla-OH) was coupled according to *GP4* for 3h and Fmoc-deprotected according to *GP2*.

After drying in high vacuum for 24 hours, the peptide resin was treated according to *GP5*. RP-HPLC purification of the crude peptide according to *GP6* was not possible due to the insolubility in both acetonitrile and water. The peptide was soluble in TFA. MS (HiResMALDI): m/z = 1345.7374 [M+Na]$^+$, $C_{66}H_{106}N_{12}O_{12}S_2Na^+$; calcd. 1345.7387.

Due to the solubility problems the crude material (205 mg) was directly treated according *GP7*. Instead of methanol, the material was suspended in 10 mL TFA and 5 mL water and reacted for 5 days, whereupon the solution clarified. However, like for the Acm-protected peptide no purification according to *GP6* was possible for the disulphide. The peptide was extracted with water to remove smaller peptides. Drying in high vacuum for 24 hours afforded 94 mg (overall

yield: 25 %) of compound **105**. MS (HiResMALDI): m/z = 1179.6680 [M+H]$^+$, C$_{60}$H$_{94}$N$_{10}$O$_{10}$S$_2^+$; calcd. 1179.6668.

Synthesis of H-(S)-β^3-hAla-(S)-β^3-hTyr-(S)-β^3-hVal-(R)-β^3-hCys-(S)-β^3-hLeu-β^3-hVal-(R)-β^3-hCys-β^3-hLeu-(S)-β^3-hTyr-NH$_2$ (106)

The first *β*-amino acid Fmoc-(S)-β^3-hTyr(*tert*-butyl)-OH (244.2 mg, 0.52 mmol) was loaded to Rink Amide AM (298.2 mg) according to *GP1*. The loading was estimated as 75 % and free amino functions were capped according to *GP3*, dried in high vacuum for 12 hours and the resin was Fmoc-deprotected according to *GP2.* The second amino acid (Fmoc-(S)-β^3-hLeu-OH) was coupled according to *GP4* and Fmoc-deprotected according to *GP2*. The third amino acid (Fmoc-(R)-β^3-(Acm)hCys-OH) was coupled according to *GP4* and Fmoc-deprotected according to *GP2*. The fourth amino acid (Fmoc-(S)-β^3-hVal-OH) was coupled according to *GP4*, capped according to *GP3* and Fmoc-deprotected according to *GP2*. The fifth amino acid (Fmoc-(S)-β^3-hLeu-OH) was coupled according to *GP4* and Fmoc-deprotected according to *GP2*. The sixth amino acid (Fmoc-(R)-β^3-(Acm)hCys-OH) was coupled according to *GP4* for 3 h. Unreacted amino functions were capped according to *GP3* for 1 hour and Fmoc-deprotected according to *GP2*. The seventh amino acid (Fmoc-(S)-β^3-hVal-OH) was coupled according to *GP4* and Fmoc-deprotected according to *GP2*. The eighth amino acid (Fmoc-(S)-β^3-hTyr-OH) was coupled according to *GP4* for 2.5 h and Fmoc-deprotected according to *GP2*. The ninth amino acid (Fmoc-(S)-β^3-hAla-OH) was coupled according to *GP4* and Fmoc-deprotected according to *GP2*.

After drying in high vacuum for 24 hours, the peptide resin was treated according to *GP5*. RP-HPLC purification of 483.4 mg crude peptide according to *GP6* (5 min 30 % B; 30-60 % B in 25 min; 60-95 % B in 5 min; 1 min 95 % B; t_r = 28.7 min) afforded 66 mg (overall yield: 19.5 %) of the ACM-protected peptide as a white solid in > 95% purity. MS (HiResMALDI): m/z = 1313.7371 [M+H]$^+$, C$_{64}$H$_{105}$N$_{12}$O$_{13}$S$_2^+$; calcd. 1313.7365.

The synthesis of the Acm-deprotected disulphide (66 mg, 0.05 mmol) was performed according to *GP7*. Purification according to *GP6* (5 min 30 % B; 30-60 % B in 25 min; 60-95 % B in 5 min; 1 min 95 % B; t_r = 28.7 min) afforded 23 mg (overall yield: 7.7 %) of disulphide (**106**) as white

solid in > 98 % purity. MS (HiResMALDI): m/z = 1191.6260 $[M+Na]^+$, $C_{58}H_{92}N_{10}O_{11}S_2Na^+$; calcd. 1191.6281. The normalized CD-spectrum of **106** is depicted in Figure 22.

Figure 22. Normalized CD-spectrum of **106** of a 0.2 mM solution in methanol.

Synthesis of Dodecacarbonyl bis(μ,μ'-tetramethylthiolatocarbon)-S,S',S'',S''')tetrairon (108)

$C(CH_2SH)_4$ (**107**) (50 mg, 0.25 mmol) and $Fe_3(CO)_{12}$ (251 mg, 0.5 mmol) were dissolved in 30 mL toluene and refluxed for 2 hours. Flash chromatography with THF:hexan = 1:6 afforded 23 mg (12% yield) of **108**. ^{1}H NMR (200 MHz, $CDCl_3$): δ = 1.42 (s, 4H, CH_2). ^{13}C NMR (50 MHz, $CDCl_3$): δ = 206.9 (CO), 38.4 (C_q), 32.8 (CH_2). MS (DEI): m/z = 756 $[M]^+$, 728 $[M–CO]^+$, 700 $[M–2CO]^+$, 672 $[M–3CO]^+$, 644 $[M–4CO]^+$, 616 $[M–5CO]^+$, 588 $[M–6CO]^+$, 560 $[M–7CO]^+$, 532 $[M–8CO]^+$, 504 $[M–9CO]^+$, 476 $[M–10CO]^+$, 448 $[M–11CO]^+$, 420 $[M–12CO]^+$. IR (KBr): 2925 (m), 2854 (m), 2073 (vs), 2035 (vs), 1992 (vs,br), 1718 (m), 1629 (m), 1459 (m). Anal. Calcd. for $C_{17}H_8Fe_4O_{12}S_4$: C, 27.01 %; H, 1.07 %; S, 15.89 %. Found: C, 27.31 %, H, 1.15 %, S, 16.43 %.

Synthesis of Bis(triphenylphosphin)-2,2-dimercaptomethyl-1,3-propane-dithiolato-platinum(II) (109)

In 30 mL absolute ethanol, 79 mg (0.1 mmol) *bis*(triphenyl-phospino)-platinum(II) chloride and 27.5 mg (0.2 mmol) potassium carbonate were suspended. To this suspension 20 mg (0.1 mmol) $C(CH_2SH)_4$ (**107**) were added and the resulting slightly yellow mixture was stirred for 15 hours at room temperature, whereupon a yellow precipitate appeared. Separation of the precipitate and washing of the solid with ethanol, water and diethyl ether yielded, after drying in

high vacuum for 1 day, 86 mg (94 %) of a yellow solid. ^{1}H NMR (200 MHz, CDCl$_3$): δ = 7.36 (m, 12H, C$H_{aromatic}$), 7.22 (m, 6H, C$H_{aromatic}$), 7.14 (m, 12H, C$H_{aromatic}$), 2.86 (d with Pt-satelites, $^3J_{Pt-H}$ = 57.6 Hz, $^4J_{P-H}$= 7.20 Hz, 4H, P-Pt-S-CH_2), 2.71 (d, 4H, CH_2-SH), 1.15 (t, 2H, CH$_2$-SH). ^{13}C NMR (50 MHz, CDCl$_3$): δ = 134.8/ 130.6/ 129.7/ 127.5 (C$_{aromatic)}$, 45.8 (C), 34.0 (PtSCH$_2$), 23.0 (CH$_2$-SH). ^{31}P{^{1}H}-NMR (81 MHz, CDCl$_3$): δ = 27.19 ($^1J_{P-Pt}$ = 2834 Hz). MS (ESI): m/z = 916 [M-2H]$^+$. Anal. Calcd. for C$_{41}$H$_{40}$P$_2$PtS$_4$: C, 53.60 %; H, 4.39 %; S, 13.96 %. Found: C, 53.66 %, H, 4.65 %, S, 13.71 %.

Synthesis of [Bis(triphenylphosphino)platin(II)-S,S']–[diironhexacarbonyl-S'',S''']-tetra-mercaptomethyl-methane (110)

In a 100 mL Schlenk vessel 163 mg (0.178 mmol) *bis*(triphenylphosphine)-2,2-dimercaptomethyl-1,3-propane-dithiolato-platinum(II) (**109**) and 90 mg (0.178 mmol) Fe$_3$(CO)$_{12}$ were dissolved in 40 mL dichloromethane. The solution was stirred at room temperature for 4.5 hours, whereupon the colour changed from dark green to red. After evaporation to dryness, the crude material was purified *via* column chromatography (CH$_2$Cl$_2$) and washed with pentane to give 44 mg (21 %) of a red solid. ^{1}H NMR (200MHz, CDCl$_3$): δ = 7.41-7.06 (m, 10H, $C_{aromatic}$), 2.86/2.83 (d with Pt satellites, $^3J_{H-Pt}$ = 66.4 Hz, $^4J_{H-P}$ = 6.4 Hz, 4H, CH_2), 2.33 (s, 4H, CH_2). ^{13}C NMR (50 MHz, CDCl$_3$): δ = 207.8 (CO), 134.8/ 130.1/ 127.4 (C$_{aromatic}$), 43.5 (PtSCH$_2$), 38.2 (CH$_2$SFe). ^{31}P NMR (81 MHz, CDCl$_3$): 27.5 ($^2J_{Pt-P}$ = 2852 Hz). MS (FAB in nba): m/z = 1196 [M+H]$^+$, 1028 [M–6CO]$^+$. IR (KBr): 3054 (w), 2959 (m), 2924 (s), 2853 (m), 2069 (vs), 2029 (vs), 1987 (vs), 1636 (m), 1436 (s), 1096 (s). Anal. Calcd. for C$_{47}$H$_{38}$Fe$_2$P$_2$O$_6$S$_4$Pt•0.55pentane: C, 48.10 %; H, 4.09 %; S, 10.25 %. Found: C, 48.37 %; H, 3.64 %; S, 10.38 %.

Synthesis of the [2Fe2S(Si)] Modified Polymer (123)

To a solution of compound **66** (1.46 g, 0.43 mmol), 210 mg (0.46 mmol) of compound **120** were added and the

solution stirred for 24 hours at room temperature. Evaporation to dryness, followed by dissolving in chloroform and extraction with sodium bicarbonate, brine and water afforded 234 mg (14 %) of compound **123** after precipitation in acetone at -95 °C. ^{1}H NMR (400 MHz, CDCl$_3$): δ = 5.45

(m, 33H, H7), 4.95 (m, 66H, H8), 3.67 (m, 114H, H9, H10, H11, H12, H13, H14), 2.11 (m, 33H, H6), 1.20 (m, 73H, H2, H3, H5, H16), 0.84 (m, 6H, H1, H4), 0.00 (s, 3H, H15). IR(KBr, cm^{-1}): 3076 (m), 2972 (m), 2925 (vs), 2074 (vs), 2034 (vs), 2002 (vs), 1750 (m), 1642 (m), 1119 (m), 909 (m).

Synthesis of 2,2'-Dibromobiphenyl (153)

A solution of 15 g (0.064 mol) 1,2-dibromobenzene, dissolved in 100 mL THF, was cooled to -78 °C and 21 mL (0.033 mol) n-butyllithium (1.6 mol/L in hexane) were slowly added within 30 min. Within 24 hours the reaction mixture was allowed to warm up and the reaction mixture was subsequently hydrolyzed at 5 °C with 60 mL hydrogen chloride (0.5 mol/L in water). The solution was extracted three times with 50 mL diethyl ether and the organic fractions were dried with sodium sulphate. Evaporation to dryness and crystallization from ethanol afforded 4.9 g (25 %) white crystals. ^{1}H NMR (200 MHz, CDCl$_3$): δ = 7.65 (m, 2H, C$H_{aromatic}$), 7.29 (m, 6H, CH$_{aromatic}$). ^{13}C NMR (50 MHz, CDCl$_3$): δ = 142.0 (C_qC_q), 132.5 (CHCBr), 130.9 (CHC$_q$), 129.3 (CHCHCBr), 127.1 (CHCHC$_q$), 123.5 (CBr). MS (DEI): m/z = 310 [M]$^+$, 231 [M-Br]$^+$, 152 [M-2Br]$^+$.

Synthesis of 1,1-Dichlorosilafluorene (154)

2,2'-Dibromobiphenyl (**146**) (4.5 g, 0.0145 mol) was dissolved in 50 mL diethyl ether. At -78 °C, 18.75 mL (0.03 mol) n-butyllithium (1.6 mol/L in hexane) were added slowly, whereupon a white precipitate was formed. After stirring for 14 hours at room temperature, the reaction mixture was cooled to -78 °C. To this solution 7.5 mL (0.07 mol) tetrachlorosilane, dissolved in 40 mL diethyl ether, were added and after 3 hours the reaction mixture was allowed to warm up to room temperature. After 19 hours additional stirring at room temperature, the reaction mixture was filtrated and the solvent evaporated off. Bulb-to-bulb distillation (0.08 mbar/ 130 °C) afforded 1.8 g (50 %) of a white crystalline solid. ^{1}H NMR (200 MHz, C$_6$D$_6$): δ = 7.39 (d, $^3J_{H,H}$ = 7.12 Hz, 2H, C$_q$CH), 7.24 (d, $^3J_{H,H}$ = 7.8 Hz, 2H, SiCCH), 7.00 (m, 2H, C$_q$CHCH), 6.86 (m, 2H, SiCCHCH). ^{13}C NMR (50 MHz, C$_6$D$_6$): δ = 145.8 (C_qC_q), 133.1 (SiCCH), 132.8 (C$_q$CHCH), 130.8 (SiC), 129.1 (SiCCHCH), 121.3 (C$_q$$C$H). ^{29}Si NMR (79.5 MHz, C$_6$D$_6$): δ = 8.28. MS (DEI): m/z = 250 [M]$^+$, 215 [M-Cl]$^+$, 152 [M-SiCl$_2$]$^+$.

Synthesis of 1,1-Dichloro-2,3,4,5-tetraphenyl-1-silacyclopentadiene (156)

Precaution: Avoid humidity. Traces of water will change the reaction and will afford exclusively 1,2,3,4-tetraphenyl-cis,cis-butadiene. Lithium should be used as mineral oil suspension. Pieces of lithium will be deactivated very fast and no reaction can be observed.

Diphenylacetylene (15 g, 0.084 mol) and 2.35 g (~ 0.1 mol) lithium (~ 30 % in mineral oil) were suspended in 150 mL thoroughly dried diethyl ether. The suspension was stirred for 4 hours, whereupon most lithium disappeared and the mixture coloured deep red. Subsequently, the reaction mixture was cooled to -78 °C and tetrachlorosilane was added at once. The reaction was allowed to warm up to room temperature within 3 hours and stirred for additional 4 weeks (elongation of time leads to higher yields). The formed precipitate was filtered off and the solution was concentrated to one third under high vacuum. The solution was stored at -20 °C whereupon 4.3 g (23 %) greenish crystals were formed. ^{1}H NMR (200 MHz, CDCl$_3$): δ = 7.55-6.80 (m, 20H, CH). ^{13}C NMR (50 MHz, CDCl$_3$): δ = 154.8, 136.7 (*C*-Si), 135.4, 132.3, 129.5, 129.3, 128.2, 127.8, 127.4, 127.1 (*CH*$_{aromatic}$). ^{29}Si NMR (79.5 MHz, CDCl$_3$): δ = 8.1. MS (DEI): *m/z* = 454 [M]$^+$.

Electrochemistry: Instrumentation and Procedures

Cyclic voltammograms were recorded against a non-aqueous Ag/Ag$^+$ reference electrode (0.1 M [*n*-Bu$_4$N][PF$_6$] and 0.01 M AgNO$_3$ in acetonitrile) and Ag/AgCl using 0.45 M [*n*-Bu$_4$N][BF$_4$] in dichloromethane as supporting electrolyte. A glassy carbon (GC) macroelectrode and a platinum wire were used as the working and auxiliary electrodes, respectively. A solution of 0.05 M [*n*-Bu$_4$N][PF$_6$] (Fluka, electrochemical grade) in acetonitrile (Aldrich, anhydrous, 99.8%) was used as the supporting electrolyte. Electrochemical experiments were carried out using a CHI750C electrochemical bipotentiostat. Prior to each experiment, the electrochemical cell was degassed for at least 10 minutes using argon, and a blanket of argon was maintained throughout. The GC working electrode was prepared by successive polishing with 1.0 and 0.3 micron alumina pastes and sonicated in Millipore water for 5 minutes. All cyclic voltammograms were recorded at a scan rate of 100 mVs^{-1}. In case of the studies of compound **115**, cyclic voltammetric measurements were conducted in 3-electrode technique using a Reference 600 potentiostat (Gamry Instruments, Warminster, USA) which was controlled by *DigiElch 5.R*[226].

This program provides not only routines for the digital simulation of electrochemical experiments but also those for performing the measurements in a consistent way making use of the Gamry Electrochemical Toolkit[TM] library. Unless otherwise stated the experiments were performed in acetonitrile (containing 0.25 M tetra-*N*-ethyl-ammonium-perchlorate) under a blanket of solvent-saturated argon. The ohmic resistance which had to be compensated was determined by measuring the impedance of the system at potentials where the faradaic current was negligibly small. Background correction was accomplished by subtracting the current curves of the blank electrolyte (containing the same concentration of supporting electrolyte) from the experimental CVs. The reference electrode was an Ag/AgCl electrode in acetonitrile containing 0.25 M tetra-*N*-butylammonium chloride. All potentials reported in this thesis refer to the ferrocenium/ferrocene couple which was measured at the end of a series of experiments. The reduction processes for simulation experiments were studied on a hanging mercury drop ($m_{Hg\text{-}drop} \approx 4mg$) produced by the CGME instrument (Bioanalytical Systems, Inc.,West Lafayette, USA).

Quantum Chemical Calculations

The density functional programs provided by the TURBOMOLE 5.71 suite[227] were used for all calculations. The calculations were arranged with the density functional BP86[228,229] in combination with the resolution-of-the-identity (RI) technique[230] as implemented in TURBOMOLE. The BP86 functional is composed of the Becke exchange functional B88[228] and the Perdew correlation functional P86.[229] The preoptimizations of the geometries were done with the basis set SVP.[231] The final structures and frequency calculations were calculated by applying the basis set TZVP[232] The output IR line spectra were convoluted with a Gaussian profile of 15 cm^{-1} width to better match the experimental spectra.

Further quantum chemical calculations were carried out using the DFT (density functional theory) hydride functional Becke3LYP[233], as implemented in the program package Gaussian 03.[234] The used basis sets for the elements are all of 6-311+G(d,p)[235] quality. As it is assumed, that lattice effects to the molecule geometry are negligible, the calculation is carried out as a single point gas phase calculation using the geometry determined from the crystal structure.

Crystal Structure Determination

Compounds were crystallized from solutions in chloroform or dichloromethane by slow evaporation of the solvent at 4 °C. The intensity data were collected on a Nonius Kappa CCD diffractometer using graphite-monochromated Mo-K$_\alpha$ radiation. Data were corrected for Lorentz and polarization effects but not for absorption.[236,237] Crystallographic data as well as structure solution and refinement details are summarized in Table 19 or the manuscripts attached.

The structures were solved by direct methods (SHELXS)[238] and refined by full-matrix least squares techniques against F$_0^2$ (SHELXL-97).[238] All non-hydrogen atoms were refined anisotropically.[238] The hydrogen atoms were included at calculated positions according to the riding model.

Table 19. Crystal Data and Refinement Details for the Crystal Structure Analyses of Compounds **45**, **108** and **110**.

	45	108	110
empirical formula	$C_{10}H_8Fe_2O_7S_2$	$C_{17}H_8Fe_4O_{12}S_4$	$C_{48}H_{39}Cl_3Fe_2O_6P_2PtS_4$
formula mass [g·mol^{-1}]	415.98	755.87	1315.11
collection T [°C]	-90(2)	-90(2)	-90(2)
λ (Mo K$_\alpha$) [Å]	0.71073	0.71073	0.71073
crystal system	monoclinic	orthorhombic	triclinic
space group (No.)	Cc	Iba2 (45)	$P\bar{1}$ (2)
a [Å]	9.1318(9)	17.2326(5)	9.4428(2)
b [Å]	20.914(2)	11.6371(2)	17.9737(6)
c [Å]	8.6091(5)	12.4149(2)	18.0198(6)
α [°]	90	90	118.7760(10)
β [°]	111.213(5)	90	95.286(2)
γ [°]	90	90	100.883(2)
V [Å^3]	1532.8(2)	2489.65(12)	2572.27(13)
Z	4	4	2
ρ_{calcd} [g·cm^{-3}]	1.803	2.017	1.698
μ [mm^{-1}]	2.19	2.68	3.696
$F(000)$	832	1496	1300
crystal dimensions [mm]	0.05 x 0.03 x 0.03	0.05 x 0.05 x 0.04	0.06 x 0.06 x 0.03
2θ range [deg]	2.95-27.47	3.90-27.45	2.25-27.48
index ranges	$-10 \leq h \leq 11$, $-26 \leq k \leq 27$, $-11 \leq l \leq 10$	$-21 \leq h \leq 22$, $-13 \leq k \leq 15$, $-16 \leq l \leq 15$	$-12 \leq h \leq 12$, $-22 \leq k \leq 23$, $-23 \leq l \leq 23$
measured reflections	4863	8458	29241
unique reflections/R_{int}	2891	2782	11756
reflections used	4863	8458	29241
data with $I > 2\sigma(I)$	2125	2640	8920
parameters	191	168	595
S[a]	1.005	1.022	1.026
$R1$ [$I > 2\sigma(I)$][b]	0.0492	0.0190	0.0481
$wR2$ [all data, on F^2][c]	0.0934	0.0427	0.1069
max./min. residual electron density [e·Å^{-3}]	0.612/-0.551	0.272/-0.306	2.226/-2.172

[a] $S = \{\Sigma[w(F_o^2 - F_c^2)^2] / (n - p)\}^{0.5}$; n = no. of reflections; p = no. of parameters; [b] $R1 = \Sigma||F_o| - |F_c|| / \Sigma|F_o|$; [c] $wR2 = \{\Sigma[w(F_o^2 - F_c^2)^2] / \Sigma[w(F_o^2)^2]\}^{0.5}$.

8 Acknowledgements

I would like to thank Professor W. Weigand for the opportunity to work on this very interesting topic. Furthermore, I have to thank him for his generosity. He always gave me the possibility to erect new collaborations, to use old collaborations by myself and to follow my own ideas.

Furthermore I have to thank the Studienstiftung des deutschen Volkes. Without their financial support during my time as a PhD student this work would not exist.

I am also in deep gratitude to Professor D. Seebach. I was very delighted about the invitation to come to Zurich one more time. Without his financial support during the research stay it would not have been affordable to me. I also have to thank him for the scientific discussions. Although I felt like a "little student" in my first exam, it was a big pleasure for me to learn from him. Furthermore, I thank to him for the Sandostatin® he made available for us. In this context, I have to gratefully acknowledge Professor D. Hoyer and his co-workers for Sandostatin® and the biological investigation on the $[Fe_2(CO)_6(Sandostatin®)]$ complex.

Albert Beck: It was nice to learn some new tricks from an "old stager". Thanks for the nice time in Zurich. It was a big pleasure to spend the time in Zurich with my nice colleagues Uros, Krystina and Gildas.

This work would not have been feasible without the help of Professor J. G. Vos, Y. Halpin, Dr. M. Rudolph, Professor Evans, Dr. Greg A. N. Felton as well as Dr. C. Kowol. Without their enthusiasm and willingness to perform the CV measurements, the investigation of the presented compounds would not have been feasible. It was a pleasure to discuss the obtained CV's with them. I am also in deep gratitude to Professor Tacke and Dr. D. Troegel for their collaboration. It was a big pleasure for me to discuss and work with Dennis.

Additionally, I have to thank Professor Coey and his co-workers for the Mössbauer and susceptibility investigations on [2Fe2S(Si)] model complexes.

I am further indebted to Professors D. Gabel and S. Förster as well as their co-workers, especially to Nonio Wolter for the joint laboratory actions and the nice conversations during my stay in Hamburg and Bremen. In this context, I have to give special thanks to my long-time friend Steffen Boob for the free lodging, food and nice atmosphere during my visit to the group of Prof. Gabel.

Curriculum vitae

Ulf-Peter Apfel

Personal Information	Date of birth:	14th March 1984
	Place of birth:	Jena (Germany)
	Marital status:	Unmarried
Academic track record	Since 07/ 2007	Friedrich-Schiller-Universität Jena
		PhD thesis: „Models for the Active Site of the [FeFe]-Hydrogenase"
	10/2002 – 05/2007	Friedrich-Schiller-Universität Jena
		chemistry (diploma)
		title of diploma thesis: „Neuartige Hydrogenasemodelle"
	07/2002	Carl-Zeiss-Gymnasium with mathematic, scientific and technical special classes *(secondary school)*; Jena
Research experience	02/2009 – 03/2009	guest researcher at Swiss Ferderal Institute of Technology Zürich, Switzerland; Group of Prof. Seebach
	01/2007 – 04/2007	guest researcher at Swiss Ferderal Institute of Technology Zürich, Switzerland; Group of Prof. Seebach
	08/2005 – 10/2005	research student at Swiss Ferderal Laboratories for Material Testing and Research, Thun (Switzerland)
Fellowships	Since 2008	Studienstiftung des deutschen Volkes

	2005 – 2007	Studienstiftung des deutschen Volkes
	2002 – 2004	Fonds der Chemischen Industrie
Certificates	07/2005	Quality management in Analytical Chemistry
Awards	2009	Participation in the 59th Meeting of Nobel Laureates, dedicated to Chemistry
	2005	GDCh award "für besondere Leistung in der Vordiplomprüfung"
Memberships	Since 2010	American Chemical Society
	Since 2004	Jungchemiker Forum (JCF/GDCh)
	Since 2002	Förderverein Chemie-Olympiade e.V.
Language skills	German (mother tongue)	
	English (good)	
	Latin (basic)	

_____   Jena,

Ulf-Peter Apfel

Declaration of authorship

I, Ulf-Peter Apfel, declare that this thesis and the work presented herewith is my own and has been generated by me as the result of my own original research.

I confirm that:

1. This work was done mainly while in candidature for a research degree at this University.

2. Where I have consulted the published work of others, this is always clearly attributed.

3. Where I have quoted from the work of others, the source is always given.

4. I have acknowledged all main sources of help.

5. Where the thesis is based on work done by myself jointly with others, I have made clear exactly what was done by others and what I have contributed myself.

6. Parts of this work have been published (see chapter 4).

Ich erkläre, dass ich die vorliegende Arbeit selbständig und unter Verwendung der angegebenen Hilfsmittel, persönlichen Mitteilungen und Quellen angefertigt habe.

_____   Jena,

Ulf-Peter Apfel

[1]   N. Benoved, O. Kesler, *Journal of Power Sources* **2009**, *193*, 454 - 461.

[2]   C. Koroneos, A. Dompros, G. Roumbas, N. Moussiopoulos, *Int. J. Hydrogen Energy* **2004**, *29*, 1443 - 1450.

[3]   R. Cammack, M. Frey, R. Robson, *Hydrogen as a Fuel. Learning from Nature*, London (**2001**).

[4]   M. A. Pena, J. P. Gomez, J. L. G. Fierro, *Appl. Catal. A* **1996**, *144*, 7 - 57; J. A. Armor, *Appl. Catal. A*, **1998**, *176*, 159 - 176; D. L. Trimm, Z. I. Onsan, *Catal. Rev. Sci. Eng.* **2001**, *43*, 31 - 84; R. M. Navarro, M. A. Pena, J. L. G. Fierro, *Chem. Rev.* **2007**, *107*, 3952 - 3991.

[5]   P. A. Pilavachi, A. I. Chatzipanagi, A. I. Spyropoulou, *Int. J. Hydrogen Energy* **2009**, *34*, 5294 - 5303.

[6]   J. M. Ogden, *Annual Review of Energy and the Environment* **1999**, *24*, 227 - 279.

[7]   F. Müller-Langera, E. Tzimas, M. Kaltschmitt, S. Peteves, *Int. J. Hydrogen. Energy* **2007**, *32*, 3797 - 3810:

[8]   R. M. Navarro, M. C. Sanchez-Sanchez, M. C. Alvarez-Galvan, F. del Valle, J. L. G. Fierro, *Energy Environ. Sci.* **2009**, *2*, 35 - 54.

[9]   L. Stryer, *Biochemistry*, 2nd Edition, New York (**1981**), 244 - 246.

[10]   M. W. Adams, E. L. Stiefel, *Science* **1998**, *282*, 1842 - 1843.

[11]   C. Zirngibl, W. Dongen, B. Schwörer, R. Bünau, M. Richter, A. Klein, R. K. Thauer, *Eur. J. Biochem.* **1992**, *208*, 511 - 520.

[12]   E. J. Lyon, S. Shima, G. Buurman, S. Chowdhuri, A. Batschauer, K. Steinbach, R. K. Thauer, *Eur.J.Biochem.* **2004**, *271*, 195 - 204.

[13]   X. Wang, Z. Li, X. Zeng, Q. Luo, D. J. Evans, C. J. Pickett, X. Liu, *Chem.Commun.* **2008**, 3555 - 3557.

[14]   S. Shima, R. K. Thauer, *Chem. Rec.* **2007**, *7*, 37 - 46.

[15]   E. Garcin, X. Vernede, E. C. Hatchikian, A. Volbeda, M. Frey, J. C. Fontecilla-Camps, *Struct. Fold. Des.* **1999**, 557 - 566.

[16]   W. Lubitz, E. Reijerse, M. van Gastel, *Chem. Rev.* **2007**, *107*, 4331 - 4365.

[17]   J. C. Fontecilla-Camps, A. Volbeda, C. Cavazza, Y. Nicolet; *Chem. Rev.* **2007**, *107*, 4273 - 4303.

[18]   D. Das, T. Dutta, K. Nath, S. Meher Kotay, A. K. Das, N. T. Veziroglu, *Current Science* **2006**, *90*, 1627 - 1637

[19]   M. W. Adams, *Biochim. Biophys. Acta* **1990**, *1020*, 115 - 145.

[20]   M. Frey, *ChemBioChem* **2002**, *3*, 153 - 160.

[21]   R. H. Holm, P. Kennepohl, E. I. Solomin, *Chem. Rev.* **1996**, *96*, 2239 - 2314.

[22]   M. W. Adams, L. E. Mortenson, *J. Bio. Chem.* **1984**, *259*, 7045 - 7055.

[23]   G. Voordouw, S. Brenner, *Eur. J. Biochem.* **1985**, *148*, 515 - 520.

[24]   Y. Nicolet, C. Piras, P. Legrand, C. E. Hatchikian, J. C. Fontecilla-Camps, *Structure* **1999**, *7*, 13 - 23.

[25]   J. W. Peters, W. N. Lanzilotta, B. J. Lemon, L. C. Seefeldt, *Science* **1998**, *282*, 1853 - 1858.

[26]   A. J. Pierik, M. Hulstein, W. R. Hagen, S. P. J. Albracht, *Eur. J. Biochem.* **1998**,.*258*, 572 - 578.

[27]   D. H. Paladini, M. A. Musumeci, N. Carrillo, E. A. Ceccarelli, *Biochemistry* **2009**, *48*, 5760 - 5768.

[28]   T. M. van Der Spek, A. F. Arendsen, R. P. Happe, S. Yun, K. A. Bagley, D. J. Stufkens, W. R. Hagen, S. P. J. Albracht, *Eur. J. Biochem.* **1996**, *237*, 629 - 634.

[29]   B. J. Lemon, J. W. Peters, *Biochemistry* **1999**, *38*, 12969 - 12973.

[30]   (a) A. L. De Lacey, C. Stadler, C. Cavazza, E. C. Hatchikian, V. M. Fernandez, *J. Am. Chem. Soc.* **2000**, *122*, 11232 - 11233; (b) W. Roseboom, A. L. De Lacey, V. M. Fernandez, E. C. Hatchikian, S. P. J. Albracht, *J. Biol. Inorg. Chem.* **2006**, *11*, 102 - 118.

[31]   (a) H. Thomann, M. Bernardo, M. W. Adams, *J. Am. Chem. Soc.* **1991**, *113*, 7044 - 7046; (b) R. Williams, R. Cammack, E. C. Hatchikian, *J. Chem. Soc., Faraday Trans.* **1993**, *89*, 2869 - 2872; (c) P. J. Van Dam, E. J. Reijerse, W. R. Hagen, *Eur. J. Biochem.* **1997**, *248*, 355 - 361.

[32]   A. Silakov, B. Wenk, E. Reijerse, S. P. J. Albracht, W. Lubitz, *J. Biol. Inorg. Chem.* **2009**, *14*, 301 - 313.

[33]   A. Silakov, E. J. Reijerse, S. P. J. Albrach, E. C. Hatchikian, W. Lubitz, *J. Am. Chem. Soc.* **1997**, *129*, 11447 - 11458.

[34]   A. L. de Lacey, E. C. Hatchikian, A. Volbeda, M. Frey, J C. Fontecilla-Camps, V. M. Fernandez, *J. Am. Chem. Soc.* **1997**, *119*, 7181 - 7189.

[35]   E. Pilet, Y. Nicolet, C. Mathevon, T. Douki, J. C. Fontecilla-Camps, M. Fontecave, *FEBS lett.* **2009**, *583*, 506 - 511.

[36]   R. P.Happe, W. Roseboom, A. J. Pierik, S. P. J. Albracht, K. A. Bagley, *Nature* **1997**, *385*, 126.

[37]   J. W. Peters, R. K. Szilagyi, A. Naumov, T. Douglas, *FEBS Lett.* **2006**, *580*, 363 - 367.

[38]   A. Paschos, R. S. Glass, A. Böck, *FEBS Lett.* **2001**, *488*, 9 - 12.

[39]   F. Lacroute, A. Pierard, M. Grenson, J. M. Wiame, *J. Gen. Microbiol.* **1965**, *40*, 127 - 142.

[40]   O. Lenz, I. Zebger, J. Hamann, P. Hildebrandt, B. Friedrich, *FEBS Lett.* **2007**, *581,* 3322 - 3326.

[41]   S. Reissmann, E. Hochleitner, H. F. Wang, A. Paschos, F. Lottspeich, R. S. Glass, A. Böck, *Science* **2003**, *299*, 1067 - 1070.

[42]   S. Watanabe, M. Matsumi, T. Arai, H. Atomi, T. Imanaka, K. Miki, *Molec. Cell.* **2007**, *27*, 29 - 40.

[43]   F. Blachier, C. Boutry, C. Bos, D. Tome, *Am. J. Clin. Nutr.* **2009**, *90*, 814S - 821S.

[44]   W. Roseboom, M. Blokesch, A. Böck, S. P. J. Albracht, *FEBS Lett.* **2005**, *579*, 469 - 472.

[45]   R. C. Driesener, M. R. Challand, S. E. McGlynn, E. M. Shepard, E. S. Boyd, J. B. Broderick, J. W. Peters, P. L. Roach, *Angew. Chem.* **2010**, *22*, 1731 –1734.

[46]   M. Blokesch, S. P. J. Albracht, B. F. Matzanke, N. M. Drapal, A. Jacobi, A. Böck, *J. Mol. Biol.* **2004**, *344*, 155 - 167.

[47]   S. P. J. Albracht, W. Roseboom, E. C. Hatchikian, *J. Biol. Inorg. Chem.* **2006**, *11*, 88 – 101.

[48]   (a) G. Wang, M. J. Benecky, B. H. Huynh, J. F. Cline, M. W. Adams, L. E. Mortenson, B. M. Hoffman, E. Münck, *J. Biol. Chem.* **1984**, *259*, 14328 - 14331; (b) C. V. Popescu, E. Münck, *J. Am. Chem. Soc.* **1999**, *121*, 7877 - 7884; (c) F. M. Rusnak, M. W. Adams, L. E. Mortenson, E. Münck, *J. Biol. Chem.* **1987**, *262*, 38 - 41; (d) A. J. Pierik, W. R. Hagen, W. R. Dunham, R. H. Sands, *Eur. J. Biochem.* **1992**, *206*, 705 - 719; (e) E. Münck, C. V. Popescu, *Hyperfine Interact.* **2000**, *126*, 59 - 67.

[49]   A. Silakov, E. J. Reijerse, S. P. J. Albracht, E. C. Hatchikian, W. Lubitz, *J. Am. Chem. Soc.* **2007**, *129,* 11447 - 11458.

[50]   D. S. Patil, B. H. Huynh, S. H. He, H. D. Peck, D. V. Dervartanian, J. Legall, *J. Am. Chem. Soc.* **1988**, *110*, 8533 - 8534.

[51]   A. S. Pereira, P. Tavares, I. Moura, J. J. G. Moura, B. H. Huynh, *J. Am. Chem. Soc.* **2001**, *123*, 2771 - 2782.

[52]   (a) Z. X. Cao, M. B. Hall, *J. Am. Chem. Soc.* **2001**, *123*, 3734 - 3742; (b) Z. P. Liu, P. Hu, *J. Am. Chem. Soc.* **2002**, *124*, 5175 - 5182.

[53]   A. E. Silakov, *Investigation of the active site of the [FeFe]-hydrogenase from Desulfovibrio desulfuricans.* Doctoral Thesis, Heinrich-Heine-Universität Düsseldorf, **2007**.

[54]   W. Lubitz, E. J. Reijerse, M. van Gastel, *Chem. Rev.* **2007**, *107*, 4331 - 4365.

[55]   H. Reihlen, A. von Friedolsheim, W. J. Oswald, *Liebigs Ann. Chem.* **1928**, *465*, 72 - 96.

[56]   W. Hieber, P. Spacu, A*norg. Allg. Chem.* **1937**, *233,* 353 - 364.

[57]   W. Hieber, J. Gruber, *Anorg. Allgem. Chem.* **1958**, *296*, 91 - 103; W. Hieber, C. Scharfenberg, *Ber. Dtsch. Chem. Ges.* **1940**, *73*, 1012 - 1021; W. Hieber, W. Beck, *Z. Anorg. Allg. Chem.* **1960**, *305*, 265 - 273.

[58]   A. Winter, L. Zsolnai, G. Huttner, *Chem. Ber.* **1982**, *115*, 1286 - 1304; A. Winter, L. Zsolnai, G. Huttner, *Naturforsch.,* B **1982**, *37,* 1430 - 1436.

[59]   (a) D. Seyferth, G. B. Womack, J. C. Dewan, *Organometallics* **1985**, *4*, 398 - 400; (b) M. Cowie, R. L. DeKock, T. R. Wagenmaker, D. Seyferth, R. A. Henderson, M. K. Gallagher, *Organometallics* **1989**, *8*, 119 - 132; (c) D. Seyferth, R. S. Henderson, *J. Am. Chem. Soc.* **1979**, *101*, 508 - 509; (d) D. Seyferth, R. S. Henderson, M. K. Gallagher, *J.*

Organomet. Chem. **1980**, *193*, C75 - C78; (e) D. Seyferth, L.-C. Song, R. S. Henderson, *J. Am. Chem. Soc.* **1981**, *103*, 5103 - 5114; (f) C. Chieh, D. Seyferth, L.-C. Song, *Organometallics* **1982**, *1*, 473 - 476; (g) D. Seyferth, R. S. Henderson, L.-C. Song, *Organometallics* **1982**, *1*, 125 - 133; (h) T. C. W. Mak, L. Book, C. Chieh, M. K. Gallagher, L.-C. Song, D. Seyferth, *Inorg. Chim. Acta* **1983**, *73*, 159 - 164; (i) D. Seyferth, G. B. Womack, L.-C. Song, M. Cowie, B. W. Hames, *Organometallics* **1983**, *2*, 928 -930; (j) D. Seyferth, G. B. Womack, M. Cowie, B. W. Hames, *Organometallics* **1984**, *3*, 1891 - 1897; (k) D. Seyferth, R. S. Henderson, L.-C. Song, G. B. Womack, *J.Organomet. Chem.* **1985**, *292*, 9 - 17; (l) D. Seyferth, A. M. Kiwan, *J. Organomet. Chem.* **1985**, *286*, 219 - 223; (m) D. Seyferth, A. M. Kiwan, E. Sinn, *J. Organomet. Chem.* **1985**, *281*, 111 - 118; (n) D. Seyferth, C. M. Archer, *Organometallics* **1986**, *5*, 2572 - 2574; (o) D. Seyferth, G. B. Womack, R. S. Henderson, M. Cowie, B. W. Hames, *Organometallics* **1986**, *5*, 1568 - 1575; (p) J. B. Hoke, J. C. Dewan, D. Seyferth, *Organometallics* **1987**, *6*, 1816 - 1819; (q) D. Seyferth, J. B. Hoke, J. C. Dewan, *Organometallics* **1987**, *6,* 895 - 897; (r) D. Seyferth, G. B. Womack, M. K. Gallagher, M. Cowie, B. W. Hames, J. P. Fackler, A. M. Mazany, *Organometallics* **1987**, *6*, 283 - 294; (s) D. Seyferth, J. B. Hoke, A. L. Rheingold, M. Cowie, A. D. Hunter, *Organometallics* **1988**, *7*, 2163 - 2177; (t) D. Seyferth, G. B. Womack, C. M. Archer, J. C. Dewan, *Organometallics* **1989**, *8*, 430 - 442; (u) D. Seyferth, G. B. Womack, C. M. Archer, J. P. Fackler, D. O. Marler, *Organometallics* **1989**, *8*, 443 - 450; (v) D. Seyferth, C. M. Archer, D. P. Ruschke, M. Cowie, R. W. Hilts, *Organometallics* **1991**, *10*, 3363 - 3380; (w) D. Seyferth, L. L. Anderson, F. Villafane, M. Cowie, R. W. Hilts, *Organometallics* **1992**, *11*, 3262 - 3271; (x) D. Seyferth, L. L. Anderson, W. M. Davis, *J. Organomet. Chem.* **1993**, *459*, 271 - 281; (y) D. Seyferth, J. B. Hoke, J. C.; Dewan, P. Hofmann, M. Schnellbach, *Organometallics* **1994**, *13*, 3452 - 3464. (z) D. Seyferth, D. P. Ruschke, W. M. Davis, *Organometallics* **1994**, *13*, 4695 - 4703.

[60]   "*Gmelin Handbuch der Anorganischen Chemie*", 8th ed., Gmelin Institut für Anorganische Chemie and Springer-Verlag, Berlin (**1978**) Part C1, 77 - 93.

[61]   S. F. A. Kettle, L. E. Orgel, *J. Chem. Soc.*, **1960**, 3890 – 3891.

[62] M. Y. Darensbourg, E. J. Lyon, X. Zhao, P. Georgakaki, *Procl. Natl. Acad. Sci. USA* **2003**, *100*, 3683 - 3688.

[63] E. Drobner, H. Huber, G. Wächtershäuser, D. Rose, K. O. Stetter, *Nature* **1990**, *346*, 742 - 744.

[64] M. Dörr, J. Kässbohrer, R. Grunert, G. Kreisel, W. A. Brand, R. A. Werner,H. Geilmann, C. Apfel, C. Robl, W. Weigand, *Angew. Chem. Int. Ed.* **2003**, *42*, 1540 - 1543.

[65] L. F. Dahl, C. H. Wie, *Inorg. Chem.* **1963**, *2*, 328 - 333.

[66] R. B. King, *J. Am. Chem. Soc.* **1962**, *34*, 2460.

[67] (a) H. Ogino, S. Inomata, H. Tobita, *Chem. Rev.* **1998**, *98*, 2093 - 2121; (b) L.-C. Song, *Trends Organomet. Chem.* **1999**, *3*, 1 - 20; (b) N. S. Nametkin, V. D. Tyurin, M. A. Kukina, *J. Organomet. Chem.* **1978**, *149*, 355 - 370; (c) K. S. Bose, E. Sinn, B. A. Averill, *Organometallics* **1984**, *3*, 1126 - 1129; (c) L.-C. Song, C.-G. Yan, Q.-M. Hu, B.-M. Wu, T. C. W. Mak, *Organometallics* **1997**, *16*, 632 - 635; (d) L.-C. Song, G.-L. Lu, Q.-M. Hu, H.-T. Fan, Y. Chen, J. Sun, *Organometallics* **1999**, *18*, 3258 – 3260; (e) L.-C. Song, G.-L. Lu, Q.-M. Hu, J. Sun, *Organometallics* **1999**, *18*, 5429 - 5431; (e) R. B. King, *J. Am. Chem. Soc.* **1962**, *84*, 2460; (f) R. B. King, T. E. Bitterwolf, *Coord. Chem. Rev.* **2000**, *206–207*, 563 - 579; (g) M. Y. Darensbourg, E. J. Lyon, J. J. Smee, *Coord. Chem. Rev.* **2000**, *206–207*, 533 - 561; (h) L.-C. Song, *Acc. Chem. Res.* **2005**, *38*, 21 - 28; i) M. S. Arabi, R. Mathieu, R. Poilblanc, *J. Organomet. Chem.* **1979**, *177*, 199 - 209; (j) K. Fauvel, R. Mathieu, R. Poilblanc, *Inorg. Chem.* **1976**, *15*, 976 - 978; (k) M. S. Arabi, R. Mathieu, R. Poilblanc, *Inorg. Chim. Acta* **1977**, *23*, L17 - L18; (l) G. Leborgne, D. Grandjean, R. Mathieu, R. Poilblanc, *J. Organomet. Chem.* **1977**, *131*, 429 - 438; (m) R. Mathieu, R. Poilblanc, *J. Organomet. Chem.* **1977**, *142*, 351 - 355; (n) R. Poilblanc, R. *New J. Chem.* **1978**, *2*, 145 - 150; (o) J. J. Bonnet, R. Mathieu, R. Poilblanc, J. A. Ibers, *J. Am. Chem. Soc.* **1979**, *101*, 7487 - 7496; (p) R. Mathieu, R. Poilblanc, P. Lemoine, M. Gross, *J. Organomet. Chem.* **1979**, *165*, 243 - 252; (q) A. Shaver, P. J. Fitzpatrick, K. Steliou, I. S. Butler, *J. Organomet. Chem.* **1979**, *172*, C59 - C62; (r) A. Shaver, P. J. Fitzpatrick, K. Steliou, I. S. Butler, *J. Am. Chem. Soc.* **1979**, *101*, 1313 - 1315; (s) J. J. Bonnet, R. Mathieu, J. A. Ibers, *Inorg. Chem.* **1980**, *19*, 2448 - 2453; (t)

G. Leborgne, R. Mathieu, *J. Organomet. Chem.* **1981**, *208*, 201 - 212; (u) H. Patin, G. Mignani, A. Benoit, J. Y. Lemarouille, D. Grandjean, *Inorg. Chem.* **1981**, *20*, 4351 - 4355; (v) P. V. Broadhurst, B. F. G. Johnson, J. Lewis, P. R. Raithby, *Chem. Commun.* **1982**, 140 - 141; (w) G. Dettlaf, P. Hubener, J. Klimes, E. Weiss, *J. Organomet. Chem.* **1982**, *229*, 63 - 75; (x) E. A. Chernyshev, O. V. Kuzmin, A. V. Lebedev, A. I. Gusev, M. G. Los, N. V. Alekseev, N. S. Nametkin, V. D. Tyurin, A. M. Krapivin, N. A. Kubasova, V. G. Zaikin, *J. Organomet. Chem.* **1983**, *252*, 143 - 148; (y) N. S. Nametkin, B. I. Kolobkov, V. D. Tyurin, A. N. Muratov, A. I. Nekhaev, M. Mavlonov, A. Y. Sideridu, G. G. Aleksandrov, A. V. Lebedev, M. T. Tashev, H. B. Dustov, *J. Organomet. Chem.* **1984**, *276*, 393 - 397; (z) A. I. Nekhaev, S. D. Alekseeva, N. S. Nametkin, V. D. Tyurin, B. I. Kolobkov, G. G. Aleksandrov, N. A. Parpiev, M. T. Tashev, H. B. Dustov, *J. Organomet. Chem.* **1985**, *297*, C33 - C36.

[68]   (a) R. D. Adams, J. Babin, *Inorg. Chem.* **1986**, *25*, 3418 - 3422; (b) W. Gaete, J. Ros, R. Yanez, X. Solans, M. Fontaltaba, *J. Organomet. Chem.* **1986**, *316*, 169 - 175; (c) W. Gaete, J. Ros, R. Yanez, X. Solans, C. Miravitlles, M. Aguilo, *Inorg. Chim. Acta* **1986**, *119*, 55 - 59; (d) S. Lotz, P. H. Vanrooyen, M. M. Vandyk, *Organometallics* **1987**, *6*, 499 - 505; (e) J. Messelhauser, K. U. Gutensohn, I. P. Lorenz, W. J. Hiller, *Organomet. Chem.* **1987**, *321*, 377 - 388; (f) X. T. Wu, K. S. Bose, E. Sinn, B. A. Averill, *Organometallics* **1989**, *8*, 251 - 253; (g) J. L. M. Dillen, M. M. Vandyk, S. Lotz, *J. Chem. Soc., Dalton Trans.* **1989**, 2199 - 2203; (h) A. J. Banister, I. B. Gorrell, W. Clegg, K. A. Jorgensen, *J. Chem. Soc., Dalton Trans.* **1989**, 2229 - 2233; (i) N. Choi, Y. Kabe, W. Ando, *Organometallics* **1992**, *11*, 1506 - 1513; (j) E. Delgado, E. Hernandez, O. Rossell, M. Seco, E. G. Puebla, C. Ruiz, *J. Organomet. Chem.* **1993**, 455 - 177; (k) J. J. Cherng, Y. C. Tsai, C. H. Ueng, G. H. Lee, S. M. Peng, M. Shieh, *Organometallics* **1998**, *17*, 255 - 261; (l) C. Alvarez-Toledano, J. Enriquez, R. A. Toscano, M. Martinez-Garcia, E. Cortes-Cortes, Y. M. Osornio, O. Garcia-Mellado, R. Gutierrez-Perez, R. *J. Organomet. Chem.* **1999**, *577*, 38 - 43; (m) E. Delgado, E. Hernandez, N. Mansilla, F. Zamora, L. A. Martinez- Cruz, *Inorg. Chim. Acta* **1999**, *284*, 14 - 19; (n) W. Imhof, *Organometallics* **1999**, *18*, 4845 - 4855; (n) Z. X. Wang, C. S. Jia, Z. Y. Zhou, X. G. Zhou, *J. Organomet.*

Chem. **1999**, *580*, 201 - 204, (o) R. Hourihane, G. Gray, T. Spalding, T. Deeney, *J. Organomet. Chem.* **2000**, *595*, 191 - 198.

[69] C. Tard, C. J. Pickett, *Chem. Rev.* **2009**, *109*, 2245 - 2274.

[70] (a) A. Le Cloirec, S. P. Best, S. Borg, S. C. Davies, D. J. Evans, D. L. Hughes, C. J. Pickett, *Chem. Commun.* **1999**, 2285 - 2286; (b) E. J. Lyon, I. P. Georgakaki, J. H. Reibenspies, M. Y. Darensbourg, *Angew. Chem., Int. Ed.* **1999**, *38*, 3178 - 3180; (c) M. Schmidt, S. M. Contakes, T. B. Rauchfuss, T. B. *J. Am. Chem. Soc.* **1999**, *121*, 9736 - 9737.

[71] J. D. Lawrence, H. X. Li, T. B. Rauchfuss, M. Benard, M. M. Rohmer, *Angew. Chem., Int. Ed.* **2001**, *40*, 1768 - 1771.

[72] H. X. Li, T. B. Rauchfuss, *J. Am. Chem. Soc.* **2002**, *124*, 726 - 727.

[73] (a) L.-C. Song, Z. Y. Yang, H. Z. Bian, Y. Liu, H. T. Wang, X. F. Liu, Q. M. Hu, *Organometallics* **2005**, *24*, 6126 - 6135; (b) L.-C. Song, Z. Y. Yang, H. Z. Bian, Q. M. Hu, *Organometallics* **2004**, *23*, 3082 - 3084.

[74] J.-F. Capon, S. Ezzaher, F. Gloaguen, F. Y. Pétillon, P. Schollhammer, J. Talarmin, *Chem. Eur. J.* **2008**, *14*, 1954 - 1964.

[75] B. E. Barton, M. T. Olsen, T. B. Rauchfuss, *J. Am. Chem. Soc.* **2008**, *130*, 16834 - 16835.

[76] (a) J. Windhager, M. Rudolph, S. Bräutigam, H. Görls, W. Weigand, *Eur. J. Inorg. Chem.* **2007**, 2748 - 2760; (b) J. Windhager, H. Görls, H. Petzold, G. Mloston, G. Linti, W. Weigand, *Eur. J. Inorg. Chem.* **2007**, 4462 - 4471.

[77] L. C. Song, Z. Y. Yang, Y. J. Hua, H. T.Wang, Y. Liu, Q.-M. Hu, *Organometallics* **2007**, *26*, 2106 - 2110.

[78] (a) Z. Wang, J. H. Liu, C. J. He, S. Jiang, B. Akermark, L. C. Sun, *J. Organomet. Chem.* **2007**, *692*, 5501 - 5507; (b) W. B. Dong, M. Wang, X. Y. Liu, K. Jin, G. H. Li, F. J. Wang, L. C. Sun, *Chem. Commun.* **2006**, 305 - 307; (c) L. Schwartz, G. Eilers, L. Eriksson, A. Gogoll, R. Lomoth, S. Ott, *Chem. Commun.* **2006**, 520 - 522; (d) G. Si, W. G. Wang, H. Y. Wang, C. H. Tung, L. Z. Wu, *Inorg. Chem.* **2008**, *47*, 8101 - 8111; (e) A. J. Justice, M. J. Nilges, T. B. Rauchfuss, S. R. Wilson, L. De Gioia, G. Zampella, *J. Am.*

Chem. Soc. **2008**, *130*, 5293 - 5301; (f) Justice, A. K.; De Gioia, L.; Nilges, M. J.; Rauchfuss, T. B.; Wilson, S. R.; Zampella, G. *Inorg. Chem.* **2008**, *47*, 7405 - 7414; (g) B. E. Barton, T. B. Rauchfuss, *Inorg. Chem.* **2008**, *47*, 2261 - 2263; (h) A. K. Justice, T. B. Rauchfuss, S. R. Wilson, *Angew. Chem., Int. Ed.* **2007**, *46*, 6152 - 5154; (i) J. I. van der Vlugt, T. B. Rauchfuss, S. R. Wilson, *Chem. Eur. J.* **2006**, *12*, 90 - 98; (j) F. Gloaguen, J. D. Lawrence, M. Schmidt, S. R. Wilson, T. B. Rauchfuss, *J. Am. Chem. Soc.* **2001**, *123*, 12518 - 12527; (k) F. Gloaguen, J. D. Lawrence, T. B. Rauchfuss, *J. Am. Chem. Soc.* **2001**, *123*, 9476 - 9477; (l) X. Zhao, I. P. Georgakaki, M. L. Miller, J. C. Yarbrough, M. Y. Darensbourg, *J. Am. Chem. Soc.* **2001**, *123*, 9710 - 9711; (m) F. Gloaguen, J. D. Lawrence, T. B. Rauchfuss, M. Benard, M. M. Rohmer, *Inorg. Chem.* **2002**, *41*, 6573 - 6582; (n) X. Zhao, Y. M. Hsiao, C. H. Lai, J. H. Reibenspies, M. Y. Darensbourg, *Inorg. Chem.* **2002**, *41*, 699 - 708; (o) X. Zhao, I. P. Georgakaki, M. L. Miller, R. Mejia-Rodriguez, C. Y. Chiang, M. Y. Darensbourg, *Inorg. Chem.* **2002**, *41*, 3917 - 3928; (p) D. S. Chong, I. P. Georgakaki, R. Mejia-Rodriguez, J. Samabria-Chinchilla, M. P. Soriaga, M. Y. Darensbourg, *Dalton Trans.* **2003**, 4158 - 4163; (q) R. Mejia-Rodriguez, D. S. Chong, J. H. Reibenspies, M. P. Soriaga, M. Y. Darensbourg, *J. Am. Chem. Soc.* **2004**, *126*, 12004 - 12014; (r) P. Li, M. Wang, C. J. He, G. H. Li, X. Y. Liu, C. N. Chen, B. Akermark, L. C. Sun, *Eur. J. Inorg. Chem.* **2005**, 2506 - 2513; (s) J. I. van der Vlugt, T. B. Rauchfuss, C. M. Whaley, S. R. Wilson, *J. Am. Chem. Soc.* **2005**, *127*, 16012 - 16013; (t) G. A. N. Felton, A. K. Vannucci, J. Z. Chen, L. T. Lockett, N. Okumura, B. J. Petro, U. I. Zakai, D. H. Evans, R. S. Glass, D. L. Lichtenberger, *J. Am. Chem. Soc.* **2007**, *129*, 12521 - 12530; (u) S. Loscher, L. Schwartz, M. Stein, S. Ott, M. Haumann, *Inorg. Chem.* **2007**, *46*, 11094 - 11105; (v) L. Schwartz, P. S. Singh, L. Eriksson, R. Lomoth, S. Ott, *C. R. Chimie* **2008**, *11*, 875 - 889; (w) L.-C. Song, C. G. Li, J. Gao, B. S. Yin, X. Luo, X. G. Zhang, H. L. Bao, Q. M. Hu, *Inorg. Chem.* **2008**, *47*, 4545 - 4553; (x) Z. Wang, W. F. Jiang, J. H. Liu, W. Jiang, Y. Wang, B. Akermark, L. C. Sun, *J. Organomet. Chem.* **2008**, *693*, 2828 - 2834; (y) N. Wang, M. Wang, T. B. Liu, P.; Li, T. T. Zhang, M. Y. Darensbourg, L. C. Sun, *Inorg. Chem.* **2008**, *47*, 6948 - 6955.

[79]   M. T. Olsen, M. Bruschi, L. De Gioia, T. B. Rauchfuss, S. R. Wilson, *J. Am. Chem. Soc.* **2008**, *130*, 12021 - 12030.

[80]   (a) J. W. Tye, J. Lee, H. W. Wang, R. Mejia-Rodriguez, J. H. Reibenspies, M. B. Hall, M. Y. Darensbourg, *Inorg. Chem.* **2005**, *44*, 5550 - 5552; (b) J. F. Capon, S. El Hassnaoui, F. Gloaguen, P. Schollhammer, J. Talarmin, *Organometallics* **2005**, *24*, 2020 - 2022; (c) L. L. Duan, M. Wang, P. Li, Y. Na, N. Wang, L. C. Sun, *Dalton Trans.* **2007**, 1277 - 1283; (d) S. Jiang, J. H. Liu, Y. Shi, Z. Wang, B. Akermark, L. H. Sun, *Polyhedron* **2007**, *26*, 1499 - 1504; (e) T. B. Liu, M. Y. Darensbourg, *J. Am. Chem. Soc.* **2007**, *129*, 7008 - 7009; (f) D. Morvan, J. F. Capon, F. Gloaguen, A. Le Goff, M. Marchivie, F. Michaud, P. Schollhammer, J. Talarmin, J. J. Yaouanc, R. Pichon, N. Kervarec, *Organometallics* **2007**, *26*, 2042 - 2052; (g) C. M. Thomas, M. Y. Darensbourg, M. B. Hall, *J. Inorg. Biochem.* **2007**, *101*, 1752 - 1757; (h) C. M. Thomas, T. B. Liu, M. B. Hall, M. Y. Darensbourg, *Inorg. Chem.* **2008**, *47*, 7009 - 7024; (i) C. M. Thomas, T. B. Liu, M. B. Hall, M. Y. Darensbourg, *Chem. Commun.* **2008**, 1563 - 1565; (j) D. Morvan, J.-F. Capon, F. Gloaguen, F. Y. Pétillon, P. Schollhammer, J. Talarmin, J.-J. Yaouanc, F. Michaud, N. Kervarec, *J. Organomet. Chem.* 2009, *694*, 2801 - 2807.

[81]   (a) S. Ott, M. Kritikos, B. Akermark, L. C. Sun, *Angew. Chem., Int. Ed.* **2003**, *42*, 3285 - 3288; (b) S. Ott, M. Borgstrom, M. Kritikos, R. Lomoth, J. Bergquist, B. Akermark, L. Hammarstrom, L. C. Sun, *Inorg. Chem.* **2004**, *43*, 4683 - 4692; (c) H. Wolpher, M. Borgstrom, L. Hammarstrom, J. Bergquist, V. Sundstrom, S. Stenbjorn, L. C. Sun, B. Akermark, *Inorg. Chem. Commun.* **2003**, *6*, 989 - 991; (d) J. Ekstrom, M. Abrahamsson, C. Olson, J. Bergquist, F. B. Kaynak, L. Eriksson, S. C. Licheng, H. C. Becker, B. Akermark, L. Hammarstrom, S. Ott, S. *Dalton Trans.* **2006**, 4599 - 4606; (e) W. M. Gao, J. H. Liu, W. Jiang, M. Wang, L. H. Weng, B. Åkermark, L. C. Sun, *C. R. Chimie* **2008**, *11*, 915 - 921; (f) L. C. Song, M. Y. Tang, F. H. Su, Q. M. Hu, *Angew. Chem., Int. Ed.* **2006**, *45*, 1130 - 1133; (g) X. Q. Li, M. Wang, S. Zhang, J. X. Pan, Y. Na, J. H. Liu, B. Akermark, L. C. Sun, *J. Phys. Chem. B* **2008**, *112*, 8198 - 8202.

[82]   (a) V. Vijaikanth, J.-F. Capon, F. Gloaguen, P. Schollhammer, J. Talarmin, *Electrochem. Commun.* **2005**, *7*, 427 - 430; (b) K. N. Green, J. L. Hess, C. M. Thomas, M. Y.

Darensbourg, *Dalton trans.*, **2009**, 4344 - 4350; (c) S. K. Ibrahim, X. Liu, C. Tard, C. J. Pickett, *Chem. Commun.* **2007**, 1535 - 1537.

[83] M. T. Olsen, B. E. Barton, T. B. Rauchfuss, *Inorg. Chem.* **2009**, *48*, 7507 - 7509.

[84] J. L. Stanley, Z. M. Heiden, T. B. Rauchfuss, S. R. Wilson, L. De Gioia, G. Zampella, *Organometallics* **2008**, *27*, 119 - 125.

[85] J. W. Tye, M. Y. Darensbourg, M. B. Hall, *J. Mol. Structure: Theochem.* **2006**, *771*, 123 - 128.

[86] S. Jiang, J. Liu, Y. Shi, Z. Wang, B. Akermark, L. Sun, *Dalton trans.* **2007**, 896 - 902.

[87] S. Ezzaher, J. F. Capon, F. Gloaguen, F. Y. Petillon, P. Schollhammer, J Talarmin, *Inorg. Chem.* **2007**, *46*, 3426 - 3428.

[88] (a) M. Rakowski DuBois, D. L. DuBois, *C. R. Chimie* **2008**, *11*, 805 - 817; (b) A. D. Wilson, R. K. Shoemaker, A. Miedaner, J. T. Muckerman, D. L. DuBois, M. Rakowski DuBois, *Proc. Natl. Acad. Sci. U.S.A.* **2007**, *104*, 6951 - 6958; (c) C. J. Curtis, A. Miedaner, R. Ciancanelli, W. W. Ellis, B. C. Noll, M. Rakowski DuBois, D. L. DuBois, *Inorg. Chem.* **2003**, *42*, 216 - 227.

[89] S. Ezzaher, J.-F. Capon, F. Gloaguen, F. Y. Pétillon, P. Schollhammer, J. Tarlamin, N. Kervarec, *Inorg. Chem.* **2009**, *48*, 2 - 4.

[90] P. Li, M. Wang, L. Chen, J. Liu, Z. Zhao, L. Sun, *Dalton trans.* **2009**, 1919 - 1926.

[91] G. Eilers, L. Schwartz, M. Stein, Zampella, G. Zampella, L. De Gioia, S. Ott, R. Lomoth, *Chem. Eur. J.* **2007**, *13*, 7075 - 7084.

[92] L. Duan, M. Wang, P. Li, N. Wang, F. Wang, L. Sun, *Inorg. Chim. Acta* **2009**, *362*, 372 - 376.

[93] C. He, M. Wang, X. Zhang, Z. Wang, C. Chen, J. Liu, B. Akermark, L. Sun, *Angew. Chem. Int., Ed.* **2004**, *43*, 3571 - 3574.

[94] A. K. Jones, B. R. Lichtenstein, A. Dutta, G. Gordon, P. L. Dutton, *J. Am. Chem. Soc.* **2007**, *129*, 14844 - 14845.

[95] X. De Hatten, E. Bothe, K. Merz, I. Huc, N. Metzler-Nolte, *Eur. J. Inorg. Chem.* **2008**, 4530 - 4537.

[96]   M. Razavet, S. C. Davies, D. L. Hughes, C. J. Pickett, *Chem. Commun.* **2001**, 847 - 848.

[97]   C. A. Boyke, T. B. Rauchfuss, S. R. Wilson, M. M. Rohmer, M. Benard, *J. Am. Chem. Soc.* **2004**, *126*, 15151 - 15160.

[98]   (a) M. Razavet, S. J. Borg, S. J. George, S. P. Best, S. A. Fairhurst, C. J. Pickett, C. J. *Chem. Commun.* **2002**, 700 - 701; (b) S. J. George, Z. Cui, M. Razavet, C. J. Pickett, *Chem. Eur. J.* **2002**, *8*, 4037 - 4046.

[99]   M. L. Singleton, N. Bhuvanesh, J. H. Reibenspies, M. Y. Darensbourg, *Angew. Chem., Int. Ed.* **2008**, *47*, 9492 - 9495.

[100]   J. W. Tye, M. B. Hall, M. Y. Darensbourg, *Inorg. Chem.* **2006**, *45*, 1552 - 1559.

[101]   C. Tard, X. M. Liu, D. L. Hughes, C. J. Pickett, *Chem. Commun.* **2005**, 133 - 135.

[102]   M. H. Cheah, C. Tard, S. J. Borg, X. M. Liu, S. K. Ibrahim, C. J. Pickett, S. P. Best, *J. Am. Chem. Soc.* **2007**, *129*, 11085 - 11092.

[103]   S. J. Borg, T. Behrsing, S. P. Best, M. Razavet, X. M. Liu, C. J. Pickett, *J. Am. Chem. Soc.* **2004**, *126*, 16988 - 16999.

[104]   J.-F. Capon, S. Ezzaher, F. Gloaguen, F. Y. Petillon, P. Schollhammer, J. Talarmin, *Chem. Eur. J.* **2008**, *14*, 1954 - 1964.

[105]   (a) J. M. Savariault, J. J. Bonnet, R. Mathieu, J. Galy, *C. R. Acad. Sci., Ser. C* **1977**, *284*, 663 - 665; (b) F. I. Adam, G. Hogarth, I. Richards, *J. Organomet. Chem.* **2007**, *692*, 3957 - 3968 ; (c) C. M. Thomas, O. Rudiger, T. Liu, C. E. Carson, M. B. Hall, M. Y. Darensbourg, *Organometallics* **2007**, *26*, 3976 - 3984; (d) F. J. Wang, M. Wang, X. Y. Liu, K. Jin, W. B. Donga, L. C. Sun, *Dalton Trans.* **2007**, 3812 - 3819.

[106]   F. F. Xu, C. Tard, X. F. Wang, S. K. Ibrahim, D. L. Hughes, W. Zhong, X. R. Zeng, Q. Y. Luo, X. M. Liu, C. J. Pickett, C. J. *Chem. Commun.* **2008**, 606 - 608.

[107]   (a) N. Wang, M. Wang, T. T. Zhang, P. Li, J. H. Liu, L. C. Sun, *Chem. Commun.* **2008**, 5800 - 5802; (b) M.-H. Chiang, Y.-C. Liu, S.-T. Yang, G.-H. Lee, *Inorg. Chem.*, **2009**, *48*, 7604 - 7612.

[108]   A. K. Jones, E. Sillery, S. P. J. Albracht, F. A. Armstrong, *Chem. Commun.* **2002**, 866 - 867.

[109] G. A. N. Felton, C. A. Mebi, B. J. Petro, A. K. Vannucci, D. H. Evans, R. S. Glass, D. L. Lichtenberger, *J. Organomet. Chem.* **2009**, *694*, 2681 - 2699 and references cited therein.

[110] S. J. Borg, J. W. Tye, M. B. Hall, S. P. Best, *Inorg. Chem.* **2007**, *46*, 384 - 394.

[111] J.-F. Capon, F. Gloaguen, F. Y. Petillon, P. Scholhammer, J. Talarmin, *C. R. Chimie* **2008**, *11*, 842 - 851.

[112] C. P. Andrieux, *Pure Appl. Chem.* **1994**, *66*, 2445 - 2450.

[113] I. Kosuke, *Acid-Base Dissociation Constants in Dipolar Aprotic solvents*, Blackwell Scientific Publications: Oxford (**1990**).

[114] S. P. Best, S. J. Borg, J. M. White, M. Razavet, C. J. Pickett, *Chem. Commun.* **2007**, 4348 - 4349.

[115] (a) D. H. Evans, K. M. O'Connell, in: A. J. Bard, *Electroanalytical Chemistry*, Vol. 14, M. Dekker, New York, **1986**, 113; (b) F.Y. Pétillon, P. Schollhammer, J. Talarmin, in: A.J. Bard, M. Stratman, F. Scholz, C.J. Pickett (Eds.), *Encyclopedia of Electrochemistry*, *Inorganic Chemistry*, Vol. 7, Wiley, **2006**, 565 and references therein; (c) B. Zhuang, J. W. McDonald, F. A. Schultz, W. E. Newton, *Organometallics* **1984**, *3*, 943 - 945; (d) B. Zhuang, J. W. McDonald, F. A. Schultz, W. E. Newton, *Inorg. Chim. Acta* **1985**, *99* L29 - L31; (e) D. A. Smith, B. Zhuang, W. E. Newton, J. W. McDonald, F. A. Schultz, *Inorg. Chem.* **1987**, *26*, 2524 - 2531; (f) J. B. Fernandes, L. Q. Zhang, F. A. Schultz, *J. Electroanal. Chem.* **1991**, *297*, 145 - 161; (g) D. Uhrhammer, F. A. Schultz, *J. Phys. Chem. A* **2002**, *106*, 11630 - 11636; (h) J. P. Collman, R. K. Rothrock, R. G. Finke, E. J. Moore, F. Rose-Munch, *Inorg. Chem.* **1982**, *21*, 146 - 156.

[116] X. Hu, B. M. Cossairt, B. S. Brunschwig, N. S. Lewis, J. C. Peters, *Chem. Commun.* **2005**, 4723 - 4725.

[117] S. Ott, M. Kritikos, B. Akermark, L. Sun, R. Lomoth, *Angew. Chem., Int. Ed.* **2004**, *43*, 1006 - 1009.

[118] W. Gao, J. Liu, C. Ma, L. Wenig, K. Jin, C. Chen, B. Akermark, L. Sun, *Inorg. Chim. Acta* **2006**, *359*, 1071 - 1080.

[119] L.-C. Song, J.-H. Ge, X.-F. Liu, L.-Q. Zhao, Q.-M. Hu, *J. Organomet. Chem.* **2006**, *691*, 5701 - 5709.

[120] L.-C. Song, J.-H. Ge, X.-G. Zhang, Y. Liu, Q.-M. Hu, *Eur. J. Inorg. Chem.* **2006**, 3204 - 3210.

[121] (a) J.-F. Capon, S. Ezzaher, F. Gloaguen, F. Y. Pétillon, P. Schollhammer, J. Talarmin, T. Davin, J. E. McGrady, K. W. Muir, *New J. Chem.* **2007**, *31*, 2052 - 2064; (b) C. Greco, G. Zampella, L. Bertini, M. Bruschi, P. Fantucci, L. De Gioia, Inorg. Chem. **2007**, *46*, 108 - 116.

[122] G. R. Stephenson in G. Jaouen, *Bioorganometallics: Biomolecules, Labeling, Medicine*, WILEY-VCH, Weinheim (**2006**), chap 7.

[123] Used literatur for electrochemical thermodynamic: (a) R. Brdicka, *Grundlagen der physikalischen Chemie*, 7th Edition, Berlin (**1968**); (b) G. Wedler, *Lehrbuch der Physikalischen Chemie*, 5th Edition, WILEY-VCH, Weinheim (**2004**); (c) F. Scholz, *Electroanalytical Methods*, 2nd Edition, Springer, Heidelberg, New York (**2005**).

[124] P. T. Kissinger, W. R. Heinemann, *Laboratory techniques in electrctroanalytical chemistry*, Marcel Dekker, New York (**1984**), chap 6.

[125] G. I. Janz, D. J. G. Ives, *Reference electrodes*, Academic Press, New York (**1961**).

[126] (a) A. M. Bond, K. B. Oldham, G. A. Snook, *Anal. Chem.* **2000**, *72*, 3492 - 3496. (b) V. V. Pavlishchuk, A. W. Addison, *Inorg. Chim. Acta* **2000**, *298*, 97 - 102.

[127] U.-P. Apfel, Y. Halpin, H. Görls, J. G. Vos, B. Schweizer, G. Linti, W. Weigand; *Chemistry and Biodiversity* **2007**, *4*, 2138 - 2147.

[128] A. Winter, L. Zsolani, G. Huttner, *Z. Naturforsch.* **1982**, *37B*, 1430 - 1436.

[129] a) L.-C. Song, J. Gao, H.-T. Wang, Y.-J. Hua, H.-T. Fan, X.-G. Zhang, Q.-M. Hu, *Organometallics* **2006**, *25*, 5724 - 5729, b) M.-H. Chiang, Y.-C. Liu, S.-T. Yang, G.-H. Lee, *Inorg. Chem.* **2009**, *48*, 7604 - 7612.

[130] H. A. Bent, *Chem.Rev.* **1960**, 61, 275 - 307.

[131] G. N. Vyas, M. N. Shah, *Org. Synth.,***1963**, *4*, 836.

[132] E. S. West, R. F. Holden, *Org. Synth.* **1955**, *3*, 800.

[133] L. Sattler, M. Altamura, S. Prener, *J. Am. Chem. Soc.* **1935**, *57*, 333 - 334.

[134]   J. H. Brewster, *J. Am. Chem. Soc.* **1951**, *73*, 366 - 370.

[135]   L. A. Carpino, N. W. Rice, E. M. E. Mansour, S. A. Triolo, *J. Org. Chem.* **1984***, 49,* 836 - 842.

[136]   a) R. E. Kent, S. M. McElvain, *Org. Synth.* **1955**, *3*, 490; b) A. C. Cope, E. Ciganek, *Org. Synth.* **1963**, *4*, 339.

[137]   a) A. Hassner, V. Alexanian, *Tetrahedron Lett.* **1978**, *46*, 4475 - 4478; b) B. Neises, W. Steglich, *Angew. Chem., Int. Ed.* **1978**, *17*, 522 - 524; c) M. C. Desai, L. M. Stephens Stramiello, *Tetrahedron Lett.* **1993**, *34*, 7685 - 7688.

[138]   H. A. Staab, W. Rohr, *Newer Methods Prep. Org. Chem.*, Vol. 5*,* Academic Press, New York and London, **1968**, 61 - 108.

[139]   U.-P. Apfel, Y. Halpin, M. Gottschaldt, H. Görls, J. G. Vos, W. Weigand*, Eur. J. Inorg. Chem.* **2008**, *33*, 5112 - 5118.

[140]   L.-C. Song, W. Gao, C.-P. Feng, D.-F. Wang, Q.-M. Hu, *Organometallics*, **2009**, *28*, 6121 - 6130.

[141]   R. R. Schmidt; J. Michel, *J. Carbohydrate Chem.*, **1985**, *4*, 141 - 169.

[142]   M. Horisberger, B. A. Lewis, F . Smith, *Carbohyd. Res.* **1972**, *23*, 175 - 182.

[143]   V. Noireaux, A. Libchaber, *PNAS* **2004**, 101, 17669 - 17674.

[144]   A. Olaru, M. Gheorghiu, S. David, T. Wohland, E. Gheorghiu, *J. Phys. Chem. B* **2009,** *113,* 14369 - 14380

[145]   R. Wick, P. L. Luisi, *Chem. Biol.*, **1996**, *81*, 277 - 265; S. M. Nomura, K. Tsumoto,T. Hamada,K. Akiyoshi, Y. Nakatani, K. Yoshikawa, *ChemBioChem* **2003**, *4*, 1172 - 1775.

[146]   a) M. T. Madigan, J. M. Martinko, J. Parker, *Brock Biology of Microorganisms*, *10th Edition*, Pearson Education Ltd. (London) **2003**; b) R. Pascal, L. Boiteau, B. Forterre, M. Gargaud, A. Lazcano, P. Lopez-Gacia, D. Moreira, M. C. Maurel, J. Pereto, D. Prieur, J. Reisse, *Earth, Moon, and Planets* **2006**, *98*, 153 - 203.

[147]   a) T. R. Johnson, B. E. Mann, I. P. Teasdale, H. Adams, R. Foresti, C. J. Green*,* R. Motterlini*, Dalton Trans.* **2007**, 1500 - 1508; b) W.-Q. Zhang, A. J. Atkin, R. J. Thatcher, A. C. Whitwood, I. J. S. Fairlamb, J. M. Lynam, *Dalton Trans.* **2009**, 4351 - 4358; c) B. E. Mann, R. Motterlini, *Chem. Commun.* **2007**, 4197 - 4208; d) R. Motterlini, P. Sawle,

J. Hammad, S. Bains, R. Alberto, R. Foresti, C. J. Green, *The FASEB Journal* **2005**, *19*, 284 - 286; d) K. L. Haas, K. J. Franz, *Chem. Rev.* **2009**, *109,* 4921 - 4960.

[148] a) S. W. Ryter, J. Alam, A. M. K. Choi, *Physiol. Rev.* **2006**, *86*, 583 - 650; b) T. R. Johnson, B. E. Mann, J. E. Clark, R. Foresti, C. J. Green, R. Motterlini, *Angew. Chem., Int. Ed.* **2003**, *42*, 3722 - 3729.

[149] a) P. G. Rose, *The Oncologist* **2005**, *10*, 205 - 214; b) R. J. Veldman, G. A. Koning, A. van Hell, S. Zerp, S. R. Vink, G. Storm, M. Verheij, W. J. van Blitterswijk, *J. Pharm. Exp Therapeutics* **2005**, *315*, 704 - 710; c) J. M. Chan, L. Zhang, K. P. Yuet, G. Liao, J.-W. Rhee, R. Langer, O. C. Farokhzad, *Biomaterials* **2009**, *30*, 1627 - 1634.

[150] Information from "Rote Liste GmbH" **2009**.

[151] Information from "Rote Liste GmbH" **2009**.

[152] a) W. R. Hargreaves, D. W. Deamer, *Biochemistry* **1978**, *17*, 3759 - 3768; b) D. P. Cistola, J. A. Hamilton, D. Jackson, D. M. Small, *Biochemistry* **1988**, *27,* 1881 - 1888; c) J.M. Gebicki, M. Hicks, *Nature* **1973**, *243*, 232 - 234.

[153] A. D. Bangham, M. M. Standish, J. C. Watkins, *J. Mol. Biol.* **1965**, *13*, 238 - 252.

[154] a) R. Dimova, U. Seifert, B. Pouligny, S. Förster, H.-G. Döbereiner, *Eur. Phys. J. E* **2002**, *7*, 241 - 250; b) S. Förster, *Macromolecules* **2001,** *34,* 4610 - 4623.

[155] U.-P. Apfel, M. Rudolph, C. Apfel, C. Robl, D. Langenegger, D. Hoyer, B. Jaun, M.-O. Ebert, T. Alpermann, D. Seebach, W. Weigand**,** *Dalton Trans.* **2010**, DOI: 10.1039/b921299j.

[156] A. A. P. Meekel, A. Wagenaar, J. Smisterova, Je E. Kroeze, P. Haadsma, B. Bosgraaf, M. C. A. Stuart, A. Brisson, M. H. J. Ruiters, D. Hoekstra, J. B. F. N. Engberts, *Eur. J. Org. Chem.* **2000**, 665 - 673.

[157] In analogy to L. Zhang, F. Liang, L. Sun, Y. Hu, H. Hua, *Synthesis* **2000**, *12*, 1733 - 1737.

[158] T. Schaffran, A. Burghardt, S. Barnert, R. Peschka-Süss, R. Schubert, M. Winterhalter, D. Gabel, *Bioconjugate Chem.* **2009,** *20,* 2190 - 2198.

[159] K. N. Green, J. L. Hess, C. M. Thomas, M. Y. Darensbourg**,** *Dalton Trans.* **2009**, 4344 - 4350

[160] S.-J. Lee, M. Tomizawa, J. E. Casida, *J. Agric. Food Chem.* **2003**, *51,* 2646 - 2652.

[161] M. Kojima, *Yakugaku Zasshi* **1970**, *90*, 670 - 674.

[162] J. W. Pham, I. Radhakrishnan, E. J. Sontheimer, *Nucleic Acids Research* **2004**, *32*, 3446 - 3455.

[163] A. Thalen, G. Claeson, *Arkiv Kemi* **1965**, *24*, 463 - 470.

[164] a) S. Ezzaher, P.-Y. Orain, J.-F. Capon, F. Gloaguen, F. Y. Petillon, T. Roisnel, P. Schollhammer, J. Talarmin, *Chem. Commun.* **2008,** 2547 - 2549, b) A. R. Sadique, W. W. Brennessel, P. L. Holland, *Inorg. Chem.* **2008**, *47*, 784 - 786.

[165] a) G. Bartoli, M. Bosco, A. Giuliani, T. Mecozzi, L. Sambri, E. Torregiani, E. Marcantoni, *J. Org. Chem.* **2002**, *67*, 9111 - 9114; b) O. Keller, W. Keller, G. van Look, G. Wersin, *Org. Synth.* **1984**, *63*, 160.

[166] E. Wünsch, *Methoden der Organischen Chemie*, Vol 15, Thieme, Stuttgart **1975**.

[167] G. L. Stahl, R. Walter, C. W. Smith, *J. Org. Chem.* **1978**, *43*, 2285 - 2286.

[168] S. Salyi, M. Kritikos, B. Akermark, L. Sun, *Chem. Eur. J.* **2003**, *9*, 557 - 560.

[169] P. J. Kocienski, *Protecting Groups*, Thieme, Stuttgart, **1994**.

[170] U.-P. Apfel, C. R. Kowol, Y. Halpin, F. Kloss, J. Kübel, H. Görls, J. G. Vos, B. K. Keppler, E. Morera, G. Lucente, W. Weigand, *J. Inorg. Biochem.* **2009**, *103*, 1236 - 1244.

[171] a) T.-Y. Shen, G. L. Walford, U.S. Patent 3,547,948, **1970**; T.-Y. Shen, G. L. Walford *Chem. Abstr.* **1971**, *75*, 6336j; b) T. Y. Shen, G. L. Walford, U. S. Patent 3,655,692, **1972**; c) T.-Y. Shen, G. L. Walford *Chem. Abstr.* **1972**, *77*, 5331h; d) W. G. Rice, R. R. Schultz, D. C. Baker, L. E. Henderson, PCT Int. Appl. WO 98 01,440, **1998**; e) W. G. Rice, R. R. Schultz, D. C. Baker, L. E. Henderson, *Chem. Abstr.* **1998**, *128*, 123799m; f) A. W. Coulter, J. B. Lombardini, J. R. Sufrin, P. Talalay, *Mol. Pharmacol.* **1974**, *10*, 319 - 334.

[172] D. R. Appleton, B. R. Copp, *Tetrahedron Lett.* **2003**, *44*, 8963 - 8965.

[173] E. Morera, M. Nalli, F. Pinnen, D. Rossia, G. Lucente, *Bioorg. Med. Chem. Lett.* **2000**, *10*, 1585 - 1588.

[174] a) W. D. Fuller, M. P. Cohen, M. Shabankareh, R. K. Blair, *J. Am. Chem. Soc.* **1990**, *112*, 7414 - 7416; b) W. D. Fuller, M. Goodman, F. R. Naider, Y.-F. Zhu, *Biopolymers* **1996**, *40*, 183 - 205.

[175] E. Morera, G. Lucente, G. Ortar, M. Nalli, F. Mazza, E. Gavuzzo, S. Spisani, *Bioorg. Med. Chem.* **2002**, *10*, 147 - 157.

[176] L.-C. Song, J. Yan, Y.-L. Li, D.-F. Wang, Q.-M. Hu, *Inorg. Chem.* **2009**, *48*, 11376 - 11381.

[177] E. Morera, M. Nalli, A. Mollica, M. P. Paradisi, M. Aschi, E. Gavuzzo, F. Mazza, G. Lucente, *J. Peptide Sci.* **2005**, *11*, 104 - 112.

[178] E. Morera, F. Pinnen, G. Lucente, *Org. Lett.* **2002**, *4*, 1139 - 1142.

[179] a) C. Hansch, P. G. Sammes, J. B. Taylor, *Comprehensive Med. Chem.*, Vol. 2, Chapter 7.1, Pergamon Press, Oxford, **1990**; b) P. R. Hanson, D. A. Probst, R. E. Robinson, M. Yau, *Tetrahedron Lett.* **1999**, *40*, 4761 - 4764; c) J. H. McKerrow, M. N. G. James, *Perspectives in Drug Discovery and Design*, Vol. 6, ESCOM Science Publishers: Leiden, **1996**; pp 1 - 120; d) W. R. Roush, S. L. Gwaltney II, J. Cheng, K. A. Scheidt, J. H. McKerrow, E. Hansell, *J. Am. Chem. Soc.* **1998**, *120*, 10994 - 10995.

[180] M. A. Na*via*, *Science* **2000**, *288*, 2132 - 2133.

[181] F. M. Menger, C. L. Johnson, *Tetrahedron* **1967**, *23*, 19 - 27.

[182] A. Agren, U. Hedsten, B. Jonsson, *Acta Chem. Scand.* **1961**, *15*, 1532 - 1544.

[183] M. L. Bender, F. J. Kézdy, B. Zerner, *J. Am. Chem. Soc.* **1963**, *85*, 3017 - 3024.

[184] T. Birchall, R. J. Gillespie, *Can. J. Chem.* **1963**, *41*, 2642 - 2650.

[185] C. H. Hamann, A. Hamnett, W. Vielstich, *Electrochemistry*, Wiley, Weinheim, **2007**.

[186] F. M. Menger, L. Mandell**,** *J. Am. Chem. Soc.* **1967**, *89,* 4424 - 4426.

[187] U.-P. Apfel, M. Rudolph, C. Apfel, C. Robl, D. Langenegger, D. Hoyer, B. Jaun, O. Ebert, T. Alpermann, D. Seebach, W. Weigand, *Dalton trans.* **2010**, accepted.

[188] a) D. Hoyer, G. I. Bell, M. Berelowitz, J. Epelbaum, W. Feniuk, P. P. A. Humphrey, A. M. ONCarroll, Y. C. Patel, A. Schonbrunn, J. E. Taylor, T. Reisine, *Trends Pharmacol. Sci.*, **1995**, *16*, 86 - 88; b) Y. C. Patel, *Frontiers in Neuroendocrinology* **1999**, *20*, 157 - 198; c) D. Hoyer, R. A. Hills, J. Epelbaum, A. J. Harmar, J.-C. Reubi, A. Schonbrunn, J. E.

Taylor, A. Vezzani, *IUPHAR Receptor Database*, **2005** Somatostatin receptors (10.1786/543800763668); d) S. Siehler, C. Nunn, J. Hannon,D. Feuerbach, D. Hoyer, *Mol. Cell. Endocrinol.* **2008**, *286*, 26 - 34; e) M. D. Katz, B. L. Erstad, *Clin. Pharm.* **1989**, *8*, 255 - 273; f) A. Manni, A. E. Boucher, L. M. Demers, H. A. Harvey, A. Lipton, M. A. Simmonds, M. Bartholomew, *J. Steroid Biochem. Mol. Biol.* **1990**, *37*, 1083 - 1087; g) E. A. Kouroumalis, *Chemotherapy* **2001**, *47*, 150 - 161.

[189]   for example see D. Seebach, A. K. Beck, D. J. Bierbaum, *Chemistry and Biodiversity* **2004**, *1*, 1111 - 1239 and references cited herein.

[190]   A. Jacobi, D. Seebach, *Helv. Chim. Acta* **1999**, *82*, 1150 - 1171; M. Rueping, B. Jaun, D. Seebach, *Chem. Commun.* **2000**, 2267 - 2268.

[191]   G. Guichard, S. Abele, D. Seebach, *Helv. Chim. Acta* **1998**, *81*, 187 - 206.

[192]   H. J. Backer, N. Evenhuis, *Rec. Trav. Chim. Belg.* **1937**, *56*, 174 - 180.

[193]   L.-C. Song, X.-N. Fang, C.-G. Li, J. Yan, H.-L. Bao, Q.-M. Hu, *Organometallics* **2008**, *27*, 3225 - 3231.

[194]   a) J. O. Daiss, C. Burschka, J. S. Mills, J. G. Montana, G. A. Showell, I. Fleming, C. Gaudon, D. Ivanova, H. Gronemeyer, R. Tacke, *Organometallics* **2005**, *24*, 3192 - 3199; b) G. A. Showell, M. J. Barnes, J. O. Daiss, J. S. Mills, J. G. Montana, R. Tacke, J. B. H. Warneck, *Bioorg. Med. Chem. Lett.* **2006**, *16*, 2555 - 2558; c) R. Ilg, C. Burschka, D. Schepmann, B. Wünsch, R. Tacke, *Organometallics* **2006**, *25*, 5396 - 5408; d) M. W. Büttner, C. Burschka, J. O. Daiss, D. Ivanova, N. Rochel, S. Kammerer, C. Peluso-Iltis, A. Bindler, C. Gaudon, P. Germain, D. Moras, H. Gronemeyer, R. Tacke, *ChemBioChem* **2007**, *8*, 1688 - 1699; e) R. Tacke, F. Popp, B. Müller, B. Theis, C. Burschka, A. Hamacher, M. U. Kassack, D. Schepmann, B. Wünsch, U. Jurva, E. Wellner, *ChemMedChem* **2008**, *3*, 152 - 164; f) J. B. Warneck, F. H. M. Cheng, M. J. Barnes, J. S. Mills, J. G. Montana, R. J. Naylor, M.-P. Ngan, M.-K. Wai, J. O. Daiss, R. Tacke, J. A. Rudd, *Toxicol. Appl. Pharmacol.* **2008**, *232*, 369 - 375; g) W. P. Lippert, C. Burschka, K. Götz, M. Kaupp, D. Ivanova, C. Gaudon, Y. Sato, P. Antony, N. Rochel, D. Moras, H. Gronemeyer, R. Tacke, *ChemMedChem* **2009**, *4*, 1143 - 1152.

[195]   a) M. W. Büttner, M. Penka, L. Doszczak, P. Kraft, *Organometallics* **2007**, *26*, 1295 - 1298; b) L. Doszczak, P. Kraft, H.-P. Weber, R. Bertermann, A. Triller, H. Hatt, R. Tacke, *Angew. Chem.* **2007**, *119*, 3431 - 3436; c) M. W. Büttner, S. Metz, P. Kraft, R. Tacke, *Organometallics* **2007**, *26*, 3925 - 3929; d) M. W. Büttner, C. Burschka, K. Junold, P. Kraft, R. Tacke, *ChemBioChem* **2007**, *8*, 1447 - 1454; e) M. W. Büttner, J. B. Nätscher, C. Burschka, R. Tacke, *Organometallics* **2007**, *26*, 4835 - 4838; f) R. Tacke, S. Metz, *Chem. Biodiv.* **2008**, *5*, 920 - 941.

[196]   T. M. Klapötke, B. Krumm, R. Ilg, D. Troegel, R. Tacke, *J. Am. Chem. Soc.* **2007**, *129*, 6908 - 6915.

[197]   a) S. Yamaguchi, K. Tamao, *Chem. Lett.* **2005**, *34*, 2 - 7; b) M. Hissler, P. W. Dyer, R. Réau, *Coord. Chem. Rev.* **2003**, 244, 1 - 44; c) S. Yamaguchi, C. Xu, T. Okamoto, *Pure Appl. Chem.* **2006**, *78*, 721 - 730; d) G. Yu, S.-W. Yin, Y.-Q. Liu, J.-S. Chen, X.-J. Xu, X.-B. Sun, D.-G. Ma, X.-W. Zhan, Q. Peng, Z.-G. Shuai, B.-Z. Tang, D.-B. Zhu, W.-H. Fang, Y. Luo, *J. Am. Chem. Soc.* **2005**, *127*, 6335 - 6346; e) K. Tamao, S. Yamaguchi, *J. Organomet. Chem.* **2000**, *611*, 5 - 11; f) L. Ilies, H. Tsuji, Y. Sato, E. Nakamura, *J. Am. Chem. Soc.* **2008**, *130*, 4240 - 4241; g) A. C. Grimsdale, K. L. Chan, R. E. Martin, P. G. Jokisz, A. B. Holmes, *Chem. Rev.* **2009**, *109*, 897 - 1091; h) M. Shimizu, H. Tatsumi, K. Mochida, K. Oda, T. Hiyama, *Chem. Asian J.* **2008**, *3*, 1238 - 1247; n) M. Shimizu, K. Mochida, T. Hiyama, *Angew. Chem., Int. Ed.* **2008**, *47*, 9760 - 9764; o) E. G. Wang, C. Li, W.-L. Zhuang, J.-B. Peng, Y. Cao, *J. Mater. Chem.* **2008**, *18*, 797 - 801; p) T. Matsuda, S. Kadowaki, T. Goya, M. Murakami, *Org. Lett.* **2007**, *9*, *133* - 136.

[198]   A. F. Holleman, E. Wiberg, Lehrbuch der Anorganischen Chemie, 101 Ed., Walter de Gruyter, Berlin and New York, **1995**.

[199]   U.-P. Apfel, D. Troegel, Y. Halpin, S. Tschierlei, U. Uhlemann, M. Schmitt, J. Popp, H. Görls, P. Dunne, M. Venkatesan, M. Coey, M. Rudolph, J. G. Vos, R. Tacke, W. Weigand, submitted.

[200]   R. S. Glass, N. E. Gruhn, E. Lorance, M. S. Singh, N. Y. T. Stessman, U. I. Zakai, *Inorg. Chem.* **2005**, *44*, 5728 - 5737.

[201] D. R. Lide: *CRC handbook of chemistry and physics: A ready-reference book of chemical and physical data.* 87. Aufl. CRC Taylor & Francis, Boca Raton Fla. **2006**.

[202] K. Gut, PhD-Thesis (Prom. Nr. 1990), ETH Zürich **1951**.

[203] U.-P. Apfel, Y. Halpin, H. Görls, J. G. Vos, W. Weigand, manuscript in preparation.

[204] U.-P. Apfel, D. Troegel, Y. Halpin, H. Görls, J. G. Vos, R. Tacke, W. Weigand, manuscript in preparation.

[205] D. Troegel, T. Walter, C. Burschka, R. Tacke, *Organometallics* **2009**, *28,* 2756 - 2761.

[206] J. Zubieta, E. Block, G. Ofori-Okai, K Tang, *Inorg. Chem.* **1990**, *29*, 4595 - 4597.

[207] U.-P. Apfel, M. Rudolph, J. Kübel, W. Weigand, manuscript in preparation.

[208] a) A. C. Shum, J. C. Murphy, *J. Bacteriol.* **1972**, *110*, 447 - 449; b) J. R. Andreesen, L. G. Ljungdahl, *J. Bacteriol.* **1973**, *116*, 867 - 873; c) D. C. Turner, T. C. Stadtman, *Arch. Biochem. Biophys.* **1973**, *154*, 366 - 381; d) L. Flohé, W. A. Gunzler, H. H. Schock, *FEBS Lett.* **1973**, *32*, 132 - 134; e) J. T. Rotruck, A. L. Pope, H. E. Ganther, A. B. Swanson, D. G. Hafeman, W. G. Hoekstra, *Science* **1973**, *179*, 588 - 590; f) J. E. Cone, R. M. Del Rio, J. N. Davis, T. C. Stadtman, *Proc. Natl. Acad. Sci. U.S.A.* **1976**, *73*, 2659 - 2663; g) A. J. Wittwer, T. C. Stadtman, *Arch. Biochem. Biophys.* **1986**, *248*, 540 - 550; h) H. Dobbek, L. Gremer, O. Meyer, R. Huber, *Proc. Natl. Acad. Sci. U. S. A.* **1999**, *96*, 8884 - 8889.

[209] M. K. Harb, U.-P. Apfel, J. Kübel, H. Görls, G. A. N. Felton, T. Sakamoto, D. H. Evans, R. S. Glass, D. L. Lichtenberger, M. El-khateeb, W. Weigand, *Organometallics* **2009**, *28*, 6666 - 6675.

[210] U.-P. Apfel, H. Görls, G. A. N. Felton, D. H. Evans, R. S. Glass, D. L. Lichtenberger, W. Weigand, manuscript in preparation.

[211] S. Rau, B. Schäfer, D. Gleich, E. Anders, M. Rudolph, M. Friedrich, H. Görls, W. Henry, J. G. Vos, *Angew. Chem., Int. Ed.* **2006**, *45*, 6215 - 6218.

[212] a) S. Grigoras, G. C. Lie, T. J. Barton, S. Ijadi-Maghsoodi, Y. Pang, J. Shinar, Z. V. Vardeny, K. S. Wong and S. G. Han, *Synth. Met.* **1992**, *49-50*, 293 - 304; b) G. Frapper, M. Kertész, *Organometallics* **1992**, *11*, 3178 - 3184; c) J. Kürti, P. R. Surján, M. Kertész, G. Frapper, *Synth. Met.* **1993**, *57*, 4338 - 4343; d) Y. Yamaguchi, J. Shioya, *Mol. Eng.*

1993, *2*, 339 - ; e) Y. Yamaguchi, *Mol. Eng.* **1994**, *3*, 311 - 320; e) Y. Yamaguchi, T. Yamabe, *Int. J. Quantum Chem.* **1996**, *57*, 73 - 78; f) Y. Matsuzaki, M. Nakano, K. Yamaguchi, K. Tanaka, T. Yamabe, *Chem. Phys. Lett.* **1996**, *263*, 119 - 125; g) S. Y. Hong, D. S. Marynick, *Macromolecules*, **1995**, *28*, 4991 - 4995; h) S. Y. Hong, S. J. Kwon, S. C. Kim, *J. Chem. Phys.* **1995**, *103*, 1871 - 1877; i) S. Y. Hong, S. J. Kwon, S. C. Kim, D. S. Marynick, *Synth. Met.* **1995**, *69*, 701 - 702; j) S. Y. Hong, S. J. Kwon, S. C. Kim, *J. Chem. Phys.* **1996**, *104*, 1140 - 1146; k) S. Y. Hong, J. M. Song, *Synth. Met.* **1997**, *85*, 1113 - 1114.

[213]   S. Yamaguchi, K. Tamao, *J. Chem. Soc., Dalton trans.* **1998**, 3393 - 3702.

[214]   M. Hissler, P. W. Dyer, R. Réau, *Coord. Chem. Rev.* **2003**, *244*, 1 - 44.

[215]   S. Yamaguchi, C. Xu, T. Okamoto, *Pure Appl. Chem.* **2006**, *78*, 721 - 730.

[216]   L.-C. Song, X.-F. Liu, J.-B. Ming, J.-H. Ge, Z.-J. Xie, Q.-M. Hu, *Organometallics* **2010**, *29*, 610 - 617.

[217]   T. K. Dougherty, K. S. Y. Lau, F. L. Hedberg, *J. Org. Chem. **1983**, 48,* 5280 - 5284.

[218]   Y. Liu, T. C. Stringfellow, D. Ballweg, I. A. Guzei, R. West, *J. Am. Chem. Soc.* **2002**, *124*, 49 - 57.

[219]   D. A. Alonso, L. R. Falvello, B. Mancheno, C. Nájera, M. Tomàs, *J. Org. Chem.* **1996,** *61,* 5004 - 5012.

[220]   P. Jutzi, A. Karl, *J. Organomet. Chem.* **1981**, *214*, 289 - 302.

[221]   W.-C. Joo, J.-H. Hong, S.-B. Choi, H.-E. Son, C. H. Kim, *J.* Organomet. *Chem.* **1990**, *391*, 27 - 36.

[222]   G. Papeo, M. A. Gómez-Zurita Frau, D. Borghi, M. Varasi, *Tetrahedron Lett.* **2005**, *46*, 8635 - 8638.

[223]   Novabiochem 2002/3 catalogue: The Fine Art of Solid Phase Synthesis.

[224]   W. C. Chan, P. D. White, Fmoc Solid Peptide Synthesis: A Practical Approach, Vol. 222, Oxford University Press, Oxford, **2000**.

[225]   W. S. Hancock, J. E. Battersby, Anal. Biochem. 1976, 71, 260 - 264.

[226]   *DigiElch 5.R* developed by M. Rudolph available from http://www.gamry.com/Products/ DigiElch5.htm.

[227] R. Ahlrichs, M. Bär, M. Haser, H. Horn, C. Kolmel, *Chem. Phys. Lett.* **1989**, *162*, 165 - 169.

[228] A. D. Becke, *Phys. Rev. A* **1988**, *38*, 3098 - 3100.

[229] J. P. Perdew, *Phys. Rev. B* **1986**, *33*, 8822 - 8824.

[230] K. Eichkorn, O. Treutler, H. Öhm, M. Häser, R. Ahlrichs, R. *Chem. Phys. Lett.* **1995**, *240*, 283 - 290; K. Eichkorn, F. Weigend, O. Treutler, R. Ahlrichs, *Theor. Chem. Acc.* **1997**, *97*, 119 - 124.

[231] A. Schäfer, H. Horn, R. Ahlrichs, *J. Chem. Phys.* **1992**, 97, 2571 - 2577.

[232] A. Schäfer, C. Huber, R. Ahlrichs, *J. Chem. Phys.* **1994**, 100, 5829 - 5835.

[233] A. D. Becke, *J. Chem. Phys.* **1993***, 98*, 5648 -5652.

[234] Gaussian 03, Revision B.04, M. J. Frisch, G. W. Trucks, H. B. Schlegel, G. E. Scuseria, M. A. Robb, J. R. Cheeseman, J. A. Montgomery, Jr., T. Vreven, K. N. Kudin, J. C. Burant, J. M. Millam, S. S. Iyengar, J. Tomasi, V. Barone, B. Mennucci, M. Cossi, G. Scalmani, N. Rega, G. A. Petersson, H. Nakatsuji, M. Hada, M. Ehara, K. Toyota, R. Fukuda, J. Hasegawa, M. Ishida, T. Nakajima, Y. Honda, O. Kitao, H. Nakai, M. Klene, X. Li, J. E. Knox, H. P. Hratchian, J. B. Cross, C. Adamo, J. Jaramillo, R. Gomperts, R. E. Stratmann, O. Yazyev, A. J. Austin, R. Cammi, C. Pomelli, J. W. Ochterski, P. Y. Ayala, K. Morokuma, G. A. Voth, P. Salvador, J. J. Dannenberg, V. G. Zakrzewski, S. Dapprich, A. D. Daniels, M. C. Strain, O. Farkas, D. K. Malick, A. D. Rabuck, K. Raghavachari, J. B. Foresman, J. V. Ortiz, Q. Cui, A. G. Baboul, S. Clifford, J. Cioslowski, B. B. Stefanov, G. Liu, A. Liashenko, P. Piskorz, I. Komaromi, R. L. Martin, D. J. Fox, T. Keith, M. A. Al-Laham, C. Y. Peng, A. Nanayakkara, M. Challacombe, P. M. W. Gill, B. Johnson, W. Chen, M. W. Wong, C. Gonzalez, and J. A. Pople, Gaussian, Inc., Pittsburgh PA, **2003**

[235] a) A. J. H. Wachters, *J. Chem. Phys.* **1970**, 52, 1033 -1036; b) P. J. Hay, *J. Chem. Phys.* **1977**, *66*, 4377 - 4384; c) A. D. McLean, G. S. Chandler, *J. Chem. Phys.* **1980**, *72*, 5639 - 5648; d) R. Krishnan, J. S. Binkley, R. Seeger, J. A. Pople, *J. Chem. Phys.* **1980**, *72*, 650 - 654; e) T. Clark, J. Chandrasekhar, G. W. Spitznagel, P. v. R. Schleyer,

J. Comp. Chem. **1983**, *4*, 294 - 301; f) M. J. Frisch, J. A. Pople, J. S. Binkley, *J. Chem. Phys.* **1984**, 80, 3265 - 3269.

[236]   COLLECT, Data Collection Software; Nonius B. V., The Netherlands, **1998**.

[237]   Otwinowski, Z.; Minor, W. *Methods Enzymol.* **1997**, *276*, 307 - 326.

[238]   Sheldrick, G. M. *Acta Cryst. Sect. A* **2008**, *64*, 112 - 122.

Attachment

Publications and manuscripts

Synthesis and Characterization of Hydroxy-Functionalized Models for the Active Site in Fe-Only-Hydrogenases

by **Ulf-Peter Apfel**[a]), **Yvonne Halpin**[b]), **Helmar Görls**[a]), **Johannes G. Vos**[b]), **Bernd Schweizer**[c]),
Gerald Linti[d]), and **Wolfgang Weigand***[a])

[a]) Friedrich-Schiller Universität Jena, August Bebel-Strasse 2, D-07743 Jena
(phone: +493641/948160; e-mail: wolfgang.weigand@uni-jena.de)
[b]) School of Chemical Sciences, Dublin City University, Dublin 9, Ireland
[c]) Laboratorium für Organische Chemie, Eidgenössische Technische Hochschule Zürich,
CH-8093 Zürich
[d]) Ruprecht-Karls-Universität Heidelberg, Im Neuenheimer Feld 270, D-69120 Heidelberg

The reactions of DL-1,4-disulfanylbutane-2,3-diol and 1,3-disulfanylpropan-2-ol with dodecacarbonyltriiron have been investigated. As main products, the iron complexes **1** and **2** were isolated and characterized by spectroscopic methods, as well as single crystal X-ray analysis. Additionally, the unusually large bond angles in the dithiolato bridge was investigated *via* density-functional theory (DFT) calculations. Moreover, the electrochemical features have been studied by cyclic voltammetry.

Introduction. – In a time of decreasing natural resources, finding alternative energy sources has become eminently important. Nature uses an easy way to form energy by forming molecular hydrogen. Since the structure of the active site of the Fe-only hydrogenases is known [1], an increasing interest in this field is observed. Inspired by this work, we are interested in the synthesis of new models for Fe-only hydrogenases, which are not based on the typical azadithiolato structure [2]. Fe-Only hydrogenase moieties can be obtained in several of ways (*Scheme 1*).

Scheme 1. *Pathways to Models for [Fe-only]-Hydrogenases*
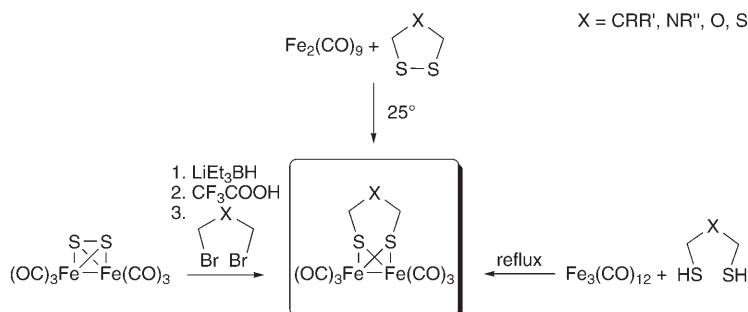
An efficient reaction under mild conditions to dithiolato-bridged complexes is the oxidative addition of nonacarbonyldiirons to cyclic disulfides at room temperature [3]. Another pathway leading to these complexes is the reaction of dodecacarbonyltriirons

with dithiols [4]. The reaction of hexacarbonyldiiron disulfide with LiEt₃BH, CF₃COOH, and a dibromo compounds offers an elegant alternative for the synthesis of these model complexes [5].

By using additional functional groups in the bridge that provide the possibility of forming H-bonds, we intend to simulate the eventual influence of N-containing neighbouring species to the active site of the Fe-only hydrogenase. By using 1,4-disulfanylbutane-2,3-diol [6] and 1,3-disulfanylpropan-2-ol, we aimed at creating two novel model complexes as shown in *Scheme 2*. The reactions of the disulfanyl compounds with dodecacarbonyltriiron in refluxing THF or toluene are presented in this contribution.

Scheme 2. *Potential Model Complexes for [Fe-only]-Hydrogenases*
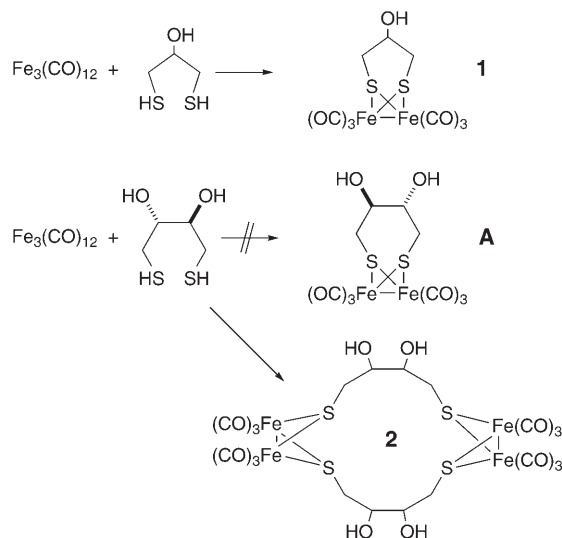
Results and Discussions. – Treatment of 1,3-disulfanlypropan-2-ol with dodeca-carbonyltriiron in toluene (reflux) for 2 h gave only one compound, **1**, in 63% yield. The ¹H-NMR spectrum of **1** shows a *multiplet* at 3.07 ppm, which is assigned to the H-atom next to the OH function, a double *doublet* at 2.89 – 2.72 ppm and 1.54 – 1.42 ppm for the CH₂ groups, and a *doublet* at 1.84/1.81 ppm for the OH group. Based on the ¹H- and ¹³C-NMR spectra, the 2-hydroxypropane-1,3-dithiolato-bridged complex **1** was established. MS Analysis shows a stepwise fragmentation of five CO groups, and the $[M-CO]^+$ peak at *m/z* 373.83 further confirms the structure of compound **1**. Single-crystal X-ray-analysis revealed the proposed structure as depicted in *Fig. 1*. The two Fe-centres are distorted octahedrally, and coordinated by CO ligands and a 2-hydroxy-propane-1,3-dithiolato bridge. An unexpected observation was that the bond angles $S(2)-C(3)-C(2)$, $S(1)-C(1)-C(2)$ and $C(1)-C(2)-C(3)$ are *ca.* 115°. Assuming sp³-hybridization, the angles would be expected to be 109.5°. Also the distances $C(1)-C(2)$ and $C(2)-C(3)$ are slightly shortened (see *Table 1*). In contrast to the calculated
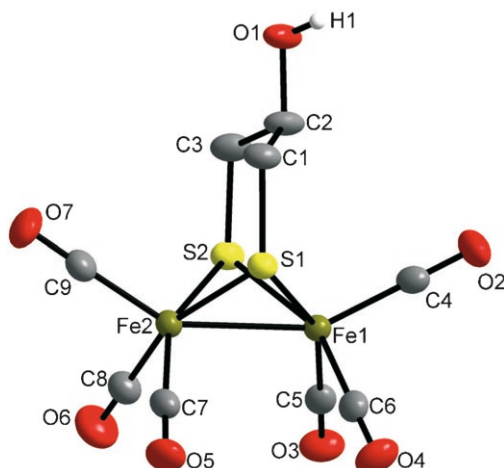
Fig. 1. *Structure of compound* **1** (ellipsoids at the 50% level)

structure, the OH function is arranged in axial position [7]. The molecules of **1**, crystallized in the space group $P2_1/n$, are arranged in a helix (*Fig. 2*).

Table 1. *Bond Lengths* [pm] *and Angles* [°] *for Compound* **1**

Bond lengths			
Fe(1)−Fe(2)	250.39(6)	Fe(2)−S(1)	225.05(8)
Fe(1)−S(1)	225.6(8)	Fe(2)−S(2)	224.77(9)
Fe(1)−S(2)	226.35(8)	Fe(2)−C(7)	180.0(4)
Fe(1)−C(4)	178.8(3)	Fe(2)−C(8)	180.5(3)
Fe(1)−C(5)	180.5(3)	Fe(2)−C(9)	179.8(3)
Fe(1)−C(6)	180.4(3)	C(4)−O(2)	114.5(3)
S(1)−C(1)	182.3(3)	C(5)−O(3)	114.0(4)
S(2)−C(3)	182.9(3)	C(6)−O(4)	113.3(4)
C(1)−C(2)	150.1(4)	C(7)−O(5)	113.9(4)
C(2)−C(3)	148.2(4)	C(8)−O(6)	113.0(4)
C(2)−O(1)	144.4(4)	C(9)−O(7)	114.1(4)
O(1)−H(1)	75.7(0)		
Bond angles			
S(1)−Fe(1)−S(2)	82.2	S(1)−C(1)−C(2)	116.4
S(1)−Fe(2)−S(2)	85.7	S(2)−C(3)−C(2)	115.4
C(1)−C(2)−O(1)	109.4	C(1)−C(2)−C(3)	116.2
C(3)−C(2)−O(1)	106.2		

Within one turn, four molecules are arranged *via* H-bridges, where the O-atoms of the OH groups (O(1)) form the helical backbone. The distance between the O-atoms is *ca.* 2.6 Å, and the pitch is 6.8 Å.

To study the influence of the size of the disulfanyl compound on the arrangement of the resulting complex, we treated DL-1,4-disulfanylbutane-2,3-diol with dodecacarbonyltriiron in boiling THF for 2 h. After workup, besides iron sulfides and oxides one
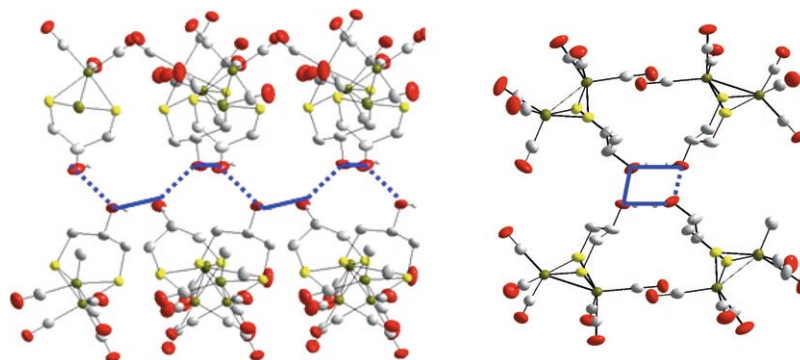
Fig. 2. *Helix backbone of compound* **1**. For a better view, the CO ligands directed to the centre of the helix are omitted.

compound was isolated by column chromatography. After diffusion of hexane into concentrated THF solution, red-brown crystals were obtained after 8 weeks at $-20°$. The ^{1}H-NMR spectrum of the isolated compound shows four *doublets* at 4.70, 4.61, 4.40, and 4.18 ppm, and a broad *multiplet* from 2.87 to 2.28 ppm, which is *not* compatible with the expected structure **A** (*Scheme 2*). The DEI-MS of the isolated compound displayed a peak at *m/z* 780, following stepwise fragmentation of nine CO groups. Based on the ^{1}H-NMR spectrum as well as the DEI-MS the above described reaction has not led to the presumed compound **A**. It is rather indicated that the isolated compound contains more than two Fe(CO)$_3$ moieties, a result that is further confirmed by a single-crystal X-ray analysis. The structural motif is shown in *Fig. 3*. Instead of the binuclear Fe unit in **A** with one dithiolato-1,4-dithiolato bridge, two binuclear ironcarbonyl units are bridged *via* two DL-2,3-dihydroxybutane-1,4-dithiolato bridges, leading to the macrocyclic compound **2**. Such a coordination mode is rare, and an example has recently been published [8].
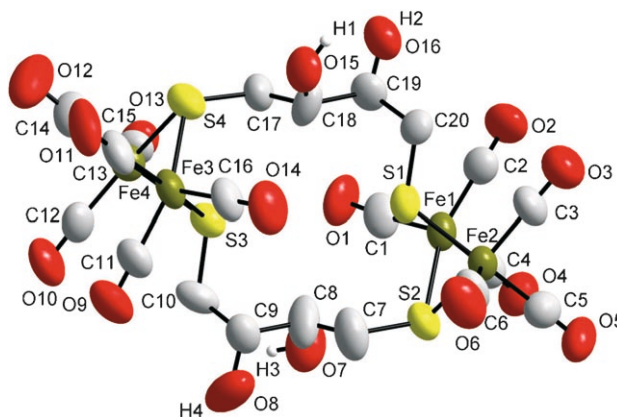

Fig. 3. *One of the two symmetrically independent crystal structures of compound* **2** (ellipsoids at the 50% level)

Quantum-Chemical Calculations. To explain the unusual bonding situation in compound **1**, RT-DFT calculations have been performed (BP-functional def-SV(P) base) using the Turbomole package [9]. The calculated and experimental structures are in good agreement (*Table 2*), implying that the large bond angles S(2)−C(3)−C(2), S(1)−C(1)−C(2), and C(1)−C(2)−C(3) are not a consequence of crystal packing. HOMO and LUMO (*Fig. 4*) are mostly located in the $Fe_2(CO)_6S_2$ part of the molecule. The HOMO^{-1} shows an anti-bonding interaction between C(1)−C(2) and C(3)−C(2) bonds, and the lone pairs at the S-atom. Thus, an influence of the S-atoms to the widening of angles can be excluded. NBO (Gaussian 03) Analysis [10] (*Table 3*) shows that, due to the influence of the O-atom, the p-character of the O(1)−C(2) bond increases, and the p-character of the C(1)−C(2) and C(3)−C(2) bonds is decreasing by the same amount. As a result of this influence, the C(1)−C(2) and C(3)−C(2) bonds are slightly shortened, and the bonding angles are enlarged. Thus, this structural property of compound **1** can be assigned to the rule of *Bent* [11] as to be seen in *Table 3*.

Table 2. *Bond Lengths* [pm] *and Angles* [°] *for* **1** *Resulting from RI-DFT Calculations*

Bond lengths			
Fe(1)−Fe(2)	252.4	Fe(2)−S(1)	229.1
Fe(1)−S(1)	229.2	Fe(2)−S(2)	230.1
Fe(1)−S(2)	229.0	S(1)−C(1)	184.9
Fe−CO	178.0 (average)	S(2)−C(3)	184.9
C(1)−C(2)	152.9	O(1)−H(1)	98.4
C(2)−C(3)	152.9		
C(2)−O(1)	142.5		
Bond angles			
S(1)−Fe(1)−S(2)	85.4	S(1)−C(1)−C(2)	117.4
S(1)−Fe(2)−S(2)	85.8	S(2)−C(3)−C(2)	117.7
C(1)−C(2)−O(1)	110.3	C(1)−C(2)−C(3)	113.5
C(3)−C(2)−O(1)	110.3		

Electrochemistry. To investigate whether the presence of H-bonds influences the catalytic process of the H_2 generation, cyclic voltammograms have been recorded.

The electrochemistry of **1** displays one oxidation and two reduction processes (*1, 2,* and *3* in *Fig. 5*), the potentials of which are listed in *Table 4*. The irreversible anodic wave at +0.85 V is assigned to the $[Fe^IFe^I] \rightarrow [Fe^{II}Fe^I] + e^-$ process, as has been previously proposed for the pdt-bridged diiron complex $[(\mu\text{-pdt})Fe_2(CO)_6]$ (pdt = $S(CH_2)_3S$) by *Darensbourg* and co-workers [12][13].

Two cathodic redox processes have been observed, one of which is quasi-reversible and the second is an irreversible reduction wave. In comparison to compounds **B** and **C** (*Table 4*), as reported by *Sun* and co-workers [12], the redox potential of the cathodic process is shifted to more negative potentials at −1.53 V. This is ascribed to a one-electron process $[Fe^IFe^I] + e^- \rightarrow [Fe^0Fe^I]$. A second reduction peak for similar compounds has been reported [12] for the following process: $[Fe^0Fe^I] + e^- \rightarrow [Fe^0Fe^0]$. For this compound, the irreversible reduction wave at −2.15 V is attributed to this process.
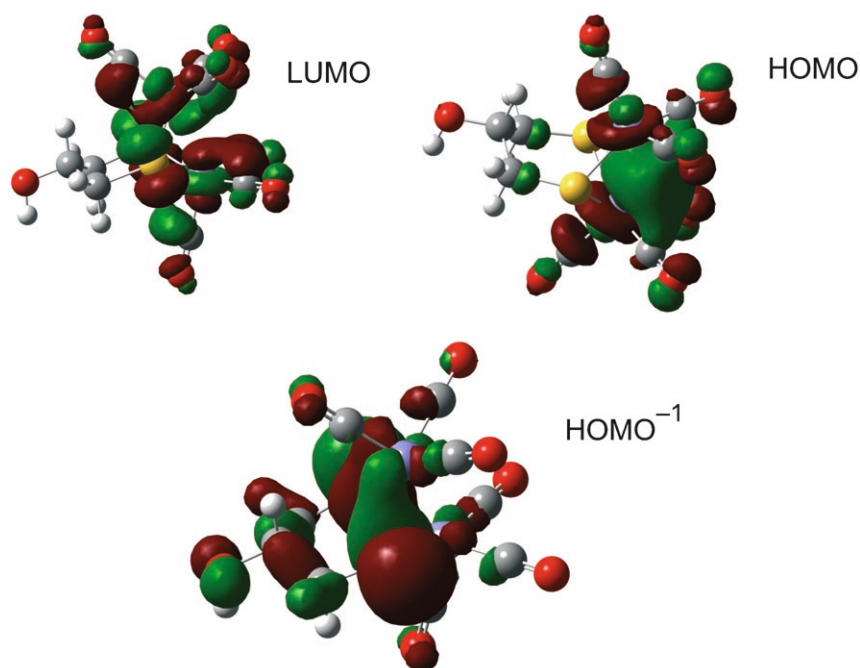
Fig. 4. Kohn–Sham *orbitals for* **1**

Table 3. *s- And p-Bonding Portion at C(2) for Compound* **1** *as Calculated by NBO Analysis*

Hybridization at C(2)	C(1)−C(2)	C(3)−C(2)	O(1)−C(2)
s-Portion	28.15	28.16	20.72
p-Portion	71.85	71.84	79.28

The electrochemistry of compound **1** was studied in the presence of the weak acid AcOH (0–10 mmol) in MeCN to evaluate the potential properties of this compound for catalytic proton reduction (*Fig. 6*). Upon addition of the acid, no anodic shifts in the reduction potential were observed; this remained so for each sequential increment of the acid concentration, with the potential remaining at −1.53 V (*Fig. 7*). The current intensity, however, increased with increasing concentration of the acid.

Unfortunately, the cyclic voltammograms provide no evidence for any influence of the OH group on the H_2 generation. The proposed mechanism for H_2 generation for compound **1** is likely to be the same as described by *Darensbourg* and co-workers [13].

Conclusions. – The present study shows that disulfanyl alkohols and diols react with $Fe_3(CO)_{12}$ by oxidative addition to provided complexes, which can be seen as models for Fe-only hydrogenases. Whereas 1,3-disulfanylpropan-2-ol reacts with $Fe_3(CO)_{12}$ in the usual way to form a dinuclear complex **1**, 1,4-disulfanylbutane-2,3-diol leads, under
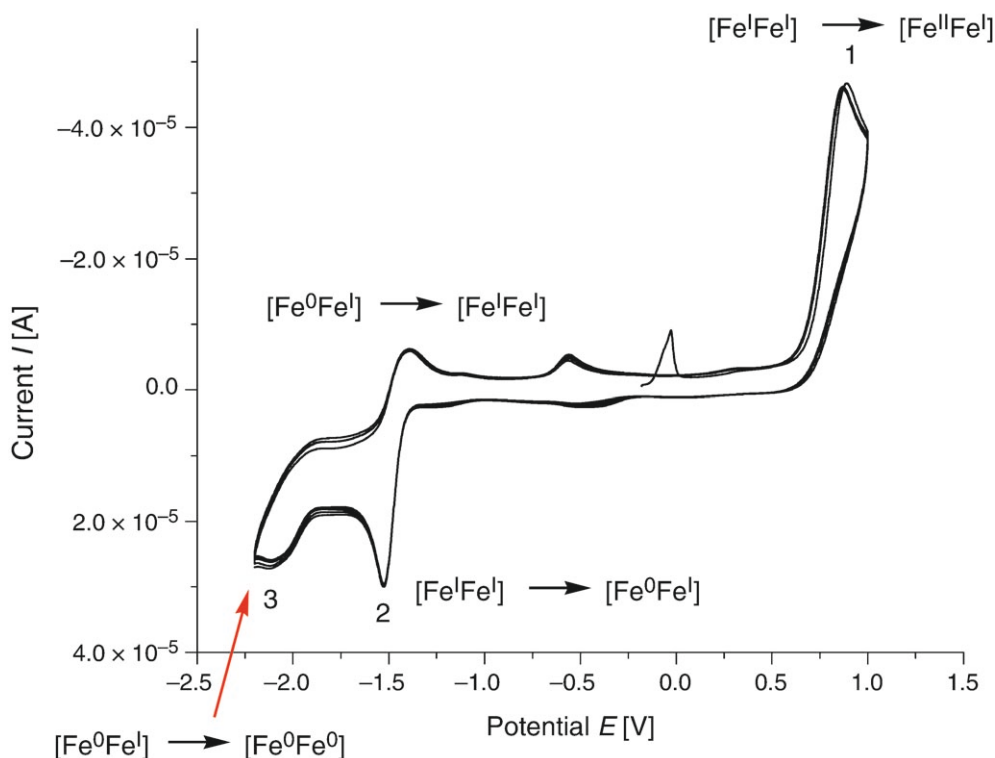
Fig. 5. *Cyclic voltammogram of compound* **1**, *in 0.05M Bu₄NPF₆ in MeCN* vs. *Ag/Ag⁺ reference electrode*

Table 4. *Electrochemical Data of Compound* **1** vs. *Ag/Ag⁺ Reference Electrode*

Compound	E_p^{ox} [V] Fe^I Fe^I/Fe^II Fe^I (irreversible)	E_{pc}, E_{pa} [V] Fe^I Fe^I/Fe^0 Fe^I (irreversible)	E_{pc}, E_{pa} [V] Fe^0 Fe^I/Fe^0 Fe^0
1	+0.85	−1.53 (E_{pc}), −1.42 (E_{pa})	−2.15 (E_{pc})
B [(μ-N-(*para*-Nitrobenzyl)-adt)Fe₂(CO)₆]ᵃ) [13]	+0.78	−1.34 (E_{pc}), −1.28 (E_{pa})	−1.71 (E_{pc}), −1.63 (E_{pa})
C [(μ-N-(*para*-Aminobenzyl)-adt)Fe₂(CO)₆][13]	+0.80	−1.48 (E_{pc}), −1.23 (E_{pa})	
[(μ-pdt)Fe₂(CO)₆]ᵇ) [12]	+0.84	−1.57 (E_{pc}), −1.23 (E_{pa})	−2.11 (E_{pc})

ᵃ) adt = S−CH₂−N(R)−CH₂−S. ᵇ) pdt = S−CH₂−CH₂−CH₂−S.

similar reaction conditions, to a tetranuclear complex **2**. Here, the dithiolato ligands are coordinated to two different Fe₂(CO)₆ moieties.

The DFT calculation for **1** showed that the unexpected bonding situation is not a packing effect, but it is to be attributed to the influence of the O-atom, according to the
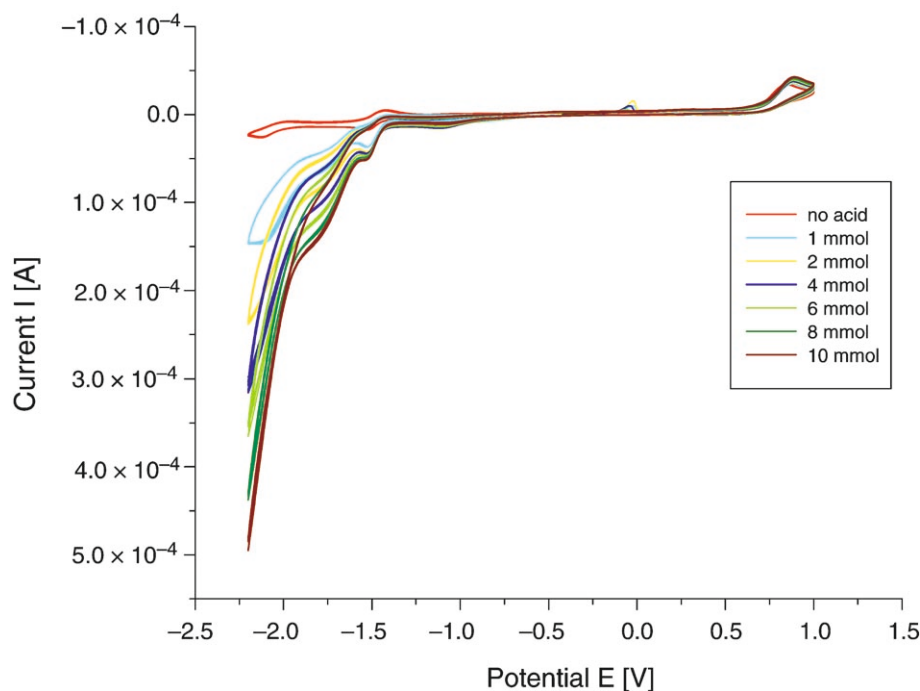
Fig. 6. *Cyclic voltammogram of compound* **1** (1 mmol) *with AcOH* (0–10 mmol)

rule of *Bent*. The cyclic voltammogram in MeCN shows that complex **1** exhibits catalytic properties for H_2 formation, but the OH function does not influence the catalytic cycle.

Experimental Part

General Solvents for syntheses were first dried over KOH and distilled from Na/benzophenone. Chemicals were used as received from *Fluka* and *Acros*. TLC: *Merck* silica gel *60 F_{254}* plates; detection under UV light at 254 nm. FC: *Fluka* silica gel *60*. IR Spectra: *Perkin-Elmer 2000 FT-IR*. NMR Spectra: *Mercury-vx* (^{1}H: 300, ^{13}C: 75 MHz) or *Bruker AVANCE 200* (^{1}H: 200, ^{13}C: 50 MHz) spectrometers.

*Hexacarbonyl (μ-2-hydroxypropane-1,3-dithiolato-*S,S′*)diiron* (**1**). In 20 ml of toluene, 200 mg (1.63 mmol) of 1,3-disulfanylpropan-2-ol and 824 mg (1.63 mmol) of $Fe_3(CO)_{12}$ were dissolved under Ar. The soln. was heated under reflux for 2 h. The resulting red colored soln. was separated from the insoluble precipitate. After removing the solvent, the crude product was purified by flash chromatography (FC; THF/hexane 1:1), and the remaining red solid was dissolved in CH_2Cl_2 and covered with pentane, whereupon 415 mg (63%) of crystals were obtained. IR (KBr): 3258*s*, 2912*w*, 2070v*s*, 2025v*s*, 1986v*s*, 1961v*s*, 1414*m*, 1311*m*, 1218*m*, 1025*s*. ^{1}H-NMR (200 MHz, CDCl$_3$): 3.15–3.02 (*m*, C*H*(OH)); 2.81–2.72 (*dd*, $^3J(H_a,CH) = 13.2$, $^2J(H_a,H_b) = 4.9$, 2 H, C*H*$_a$H$_b$); 1.83 (*d*, $^3J(OH,CH) = 5.6$, OH); 1.56–1.42 (*dd*, $^3J(H_b,CH) = 11.0$, $^2J(H_b,H_a) = 4.9$, 2 H, C*H*$_b$H$_a$). ^{13}C-NMR (50 MHz, CDCl$_3$): 207.4/207.3 (CO); 72.8 (CH); 29.6 (CH$_2$). DEI-MS: 374 ($[M - CO]^+$), 346 ($[M - 2\,CO]^+$), 318 ($[M - 3\,CO]^+$), 290 ($[M - 4\,CO]^+$), 262 ($[M - 5\,CO]^+$), 234 ($[M - 6\,CO]^+$). Anal calc. for C$_9$H$_6$Fe$_2$O$_7$S$_2$ (402): C 26.89, H 1.50, S 15.95; found: C 26.82, H 1.70, S 15.91.
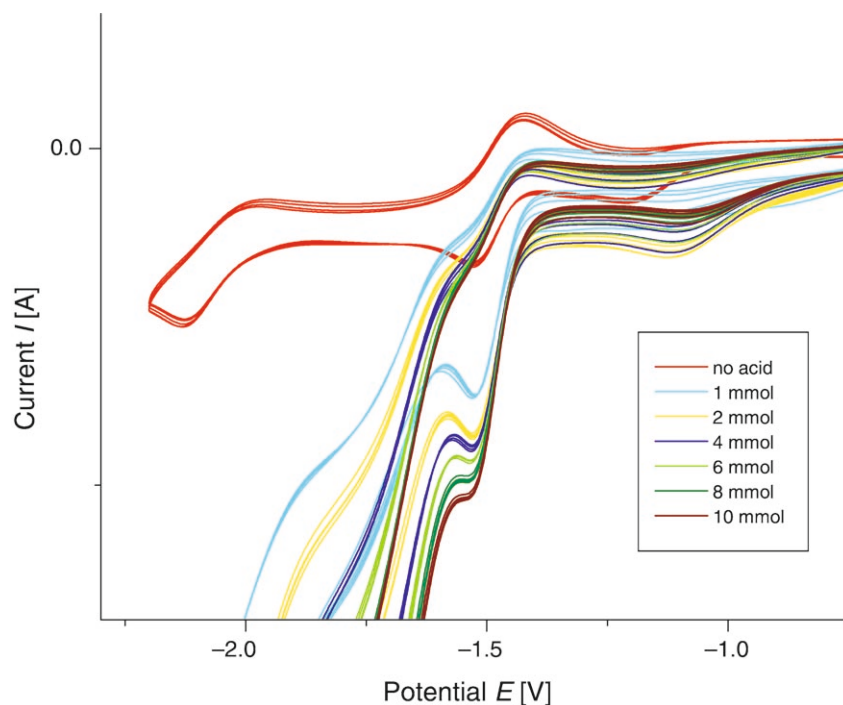
Fig. 7. *Cyclic voltammogram of compound* **1** (1 mmol) *with AcOH* (0–10 mmol), *with emphasis on the catalytic proton reduction in the region of* −1.0 *to* −2.0 *V*

Bis[hexacarbonyl(μ-2,3-dihydroxybutane-1,4-dithiolato-S,S′)diiron] (**2**). In a 100-ml *Schlenk* vessel, 76 mg (0.49 mmol) of DL-1,4-disulfanylbutane-2,3-diol and 248 mg (0.49 mmol) of Fe$_3$(CO)$_{12}$ were dissolved in 20 ml of THF, and the resulting soln. was heated at reflux under Ar for 2 h. Within 2 h, the color of the soln. changed from green to red, and inorg. iron compounds (iron sulfides) precipitated. After evaporation, the crude substance was purified by FC (AcOEt/hexane 1:2): 32 mg (7.6 %) of **2** (mixture of the two diastereoisomers). IR (KBr): 3364s, 2879m, 2068vs, 2026vs, 1963vs, 1384m, 1224m. ^{1}H-NMR ((D$_8$)THF, 300 MHz): 4.70, 4.61, 4.40, 4.18 (4d, ^3J(OH,CH) = 6, 4 OH); 2.88–2.55 (m, CH$_2$−(CH)$_2$−CH$_2$). ^{13}C-NMR ((D$_8$)THF, 300 MHz; mixture of two diastereoisomers): 212.2 (CO); 78.9/78.3 (CH); 44.9/33.7 (CH$_2$). DEI-MS: 780 ([M − 3 CO]), 752 ([M − 4 CO]), 724 ([M − 5 CO]), 696 ([M − 6 CO]), 668 ([M − 7 CO]), 640 ([M − 8 CO]), 612 ([M − 9 CO]), 584 ([M − 10 CO]), 556 ([M − 11 CO]), 528 ([M − 12 CO]). Anal. calc. for 4 C$_{20}$H$_{16}$Fe$_4$O$_{16}$S$_4$·3 C$_4$H$_8$O·H$_2$O (864): C 29.94, H 2.46, S 13.90; found: C 30.44, H 2.92, S 13.69.

Electrochemistry: Instrumentation and Procedures. Cyclic voltammograms were recorded against a non-aqueous Ag/Ag$^+$ reference electrode (0.1M Bu$_4$NPF$_6$ and 0.01M AgNO$_3$ in MeCN). A glassy carbon macro-electrode and a Pt wire were used as the working and auxiliary electrodes, resp. A soln. of 0.05M Bu$_4$NPF$_6$ (*Fluka*, electrochem. grade) in MeCN (*Aldrich*, anh., 99.8%) was used as the supporting electrolyte. Electrochemical experiments were carried out using a *CHI750C* electrochemical bipotentio-stat. Prior to each experiment, the electrochemical cell was degassed for at least 10 min with Ar, and a blanket of Ar was maintained throughout. The glassy-carbon working electrode was prepared by successive polishing with 1.0 and 0.3 μ alumina pastes and sonicated in *Millipore* water for 5 min. All cyclic voltammograms were recorded at a scan rate of 100 mVs^{-1}.

Crystal-Structure Determination for **1**. The intensity data for the compound were collected on a *Nonius KappaCCD* diffractometer, using graphite-monochromated MoK_α radiation. Data were corrected for *Lorentz* and polarization effects, but not for absorption effects [14][15].

The structures were solved by direct methods (SHELXS [16]) and refined by full-matrix least-squares techniques against F_o^2 (SHELXL-97 [17]). The asymmetric unit contains two molecules of the complex, each having no different binding mode. The H-atom of the OH group of molecule **1B** was located by difference *Fourier* synthesis and refined isotropically. All other H-atoms of the structures were included at calculated positions with fixed thermal parameters. XP (*Siemens Analytical X-Ray Instruments*, Inc.) was used for structure representations.

Crystal Data for **1**[1]). $C_9H_6Fe_2O_7S_2 \cdot 0.5\ CH_2Cl_2$, M_r 444.42 g mol^{-1}, red-brown prisms, size $0.06 \times 0.06 \times 0.05$ mm^3, monoclinic, space group P2$_1$/n, $a = 14.8728(2)$, $b = 6.7702(1)$, $c = 32.0661(6)$ Å, $\beta = 101.693(1)°$, $V = 3161.79(9)$ Å^3, $T = -90°$, $Z = 8$, $\rho_{calc.} = 1.867$ g cm^{-3}, $\mu(MoK_\alpha) = 22.93$ cm^{-1}, $F(000) = 1768$, 19082 reflections in $h(-18,17)$, $k(-8,8)$, $l(-35,41)$, measured in the range $1.42° \leq \Theta \leq 27.48°$, completeness $\Theta_{max} = 95.3\%$, 6917 independent reflections, $R_{int} = 0.0433$, 5047 reflections with $F_o > 4\sigma(F_o)$, 393 parameters, 0 restraints, $R_{1obs} = 0.0364$, $wR_{2obs} = 0.0833$, $R_{1all} = 0.0647$, $wR_{2all} = 0.0944$, goodness-of-fit: 0.994, largest difference peak and hole: $0.900/-0.953$ e Å^{-3}.

Crystal Data for **2**[1]). $C_{30}H_{24}Fe_6O_{24}S_6$; C_4H_8O; H_2O, M_r 1386.08 g mol^{-1}, redbrown prism, size $0.28 \times 0.2 \times 0.1$ mm, monoclinic, space group $P21/c$, $a = 13.9020(2)$, $b = 25.5930(4)$, $c = 16.0320(3)$ Å, $\beta = 98.31(1)°$, $V = 5644.2(6)$ Å^3, $T = -40°$, $Z = 4$, $\rho_{calc.} = 1.634$ gcm^{-3}, $\mu(MoK_\alpha) = 0.7107$ Å, $F(000) = 2800$, 20787 reflections in $h(-17,17)$, $k(-31,31)$, $l(-19,19)$, measured in the range $0.998° \leq \Theta \leq 26.022°$, completeness $\Theta_{max} = 99\%$, 11055 independent reflections, $R_{int} = 0.03$, 9070 reflections with $F_o > 4\sigma(F_o)$, structure solved with SIR97 [18], two independent molecules, one completed by crystallographic symmetry centre, THF and H_2O as solvent. Refined with SHELXL97 [19] for non-H-atoms, 619 parameters, 7 restraints, H-atom positions calculated and included in structure factor calculation. $R_{1obs} = 0.11$, $wR_{2obs} = 0.34$, $R_{1all} = 0.13$, $wR_{2all} = 0.34$, goodness-of-fit: 2.4, largest difference peak and hole: 3.9, -1.2 eÅ^{-3} (around Fe-atoms).

REFERENCES

[1] Y. Nicolet, A. L. de Lacey, X. Vernède, V. M. Fernandez, E. C. Hatchikian, J. C. Fontecilla-Camps, *J. Am. Chem. Soc.* **2001**, *123*, 1596; Y. Nicolet, B. J. Lemon, J. C. Fontecilla-Camps, J. W. Peters, *Trends Biochem. Sci.* **2000**, *25*, 138; Y. Nicolet, C. Piras, P. Legrand, C. E. Hatchikian, J. C. Fontecilla-Camps, *Structure* **1999**, *7*, 13.

[2] J. D. Lawrence, H. Li, T. B. Rauchfuss, M. Benard, M.-M. Rohmer, *Angew. Chem., Int. Ed.* **2001**, *40*, 1768; H. Li, T. B. Rauchfuss, *J. Am. Chem. Soc.* **2002**, *124*, 726; S. Ott, M. Kritikos, B. Åkermark, L. Sun, *Angew. Chem., Int. Ed.* **2003**, *42*, 3285.

[3] M. H. Goodrow, W. K. Musker, *Synthesis* **1981**, 457.

[4] L. Song, F. Gong, T. Meng, J. Ge, L. Cui, Q. Hu, *Organometallics* **2004**, *23*, 823; A. Ogilvy, M. Draganjac, T. B. Rauchfuss, S. R. Wilson, *Organometallics* **1988**, *7*, 2084.

[5] D. Seyferth, G. B. Womack, R. S. Henderson, Organometallics **1986**, *5*, 1568; H. Li, T. B. Rauchfuss, *J. Am. Chem. Soc.* **2002**, *124*, 726; c) W. Gao, J. Liu, C. Ma, L. Wang, K. Jin, C. Chen, B. Åkermark, L. S. Sun, *Inorg. Chim. Acta* **2006**, *359*, 1071; S. Jiang, J. Liu, L. Sun, *Inorg. Chem. Commun.* **2006**, *9*, 290; L. Song, M. Tang, F. Su, Q. Hu, *Angew. Chem., Int. Ed.* **2006**, *45*, 1130; L. Song, Z. Yang, H. Bian, Y. Liu, H. Wang, X. Liu, Q. Hu, *Organometallics* **2005**, *24*, 6126.

---

[1]) CCDC-655405 and -655644 contain the supplementary crystallographic data for this paper. These data can be obtained free of charge *via* http://www.ccdc.cam.ac.uk/data_request/cif (or from the *Cambridge Crystallographic Data Centre*, 12 Union Road, Cambridge CB21EZ, UK; fax: +441123336033; e-mail: deposit@ccdc.cam.ac.uk).

[6] A. Winter, L. Zsolani, G. Huttner, *Z. Naturforsch., B: Chem. Sci.* **1982**, *37*, 1430.

[7] J. W. Tye, M. Y. Darensbourg, M. B. Hall, *Inorg.Chem.* **2006**, *45*, 1552.

[8] L. C. Song, Z. Y. Yang, H. Z. Bian, Y. Liu, H. T. Wang, X. F. Liu, Q. M. Hu, *Organometallics* **2006**, *25*, 5724.

[9] K. Eichkorn, O. Treutler, H. Oehm, M. Haeser, R. Ahlrichs, *Chem. Phys. Lett.* **1995**, *242*, 652.

[10] M. J. Frisch, G. W. Trucks, H. B. Schlegel, G. E. Scuseria, M. A. Robb, J. R. Cheeseman, J. A. M. Jr., T. Vreven, K. N. Kudin, J. C. Burant, J. M. Millam, S. S. Iyengar, J. Tomasi, V. Barone, B. Mennucci, M. Cossi, G. Scalmani, N. Rega, G. A. Petersson, H. Nakatsuji, M. Hada, M. Ehara, K. Toyota, R. Fukuda, J. Hasegawa, M. Ishida, T. Nakajima, Y. Honda, O. Kitao, H. Nakai, M. Klene, X. Li, J. E. Knox, H. P. Hratchian, J. B. Cross, C. Adamo, J. Jaramillo, R. Gomperts, R. E. Stratmann, O. Yazyev, A. J. Austin, R. Cammi, C. Pomelli, J. W. Ochterski, P. Y. Ayala, K. Morokuma, G. A. Voth, P. Salvador, J. J. Dannenberg, V. G. Zakrzewski, S. Dapprich, A. D. Daniels, M. C. Strain, O. Farkas, D. K. Malick, A. D. Rabuck, K. Raghavachari, J. B. Foresman, J. V. Ortiz, Q. Cui, A. G. Baboul, S. Clifford, J. Cioslowski, B. B. Stefanov, G. Liu, A. Liashenko, P. Piskorz, I. Komaromi, R. L. Martin, D. J. Fox, T. Keith, M. A. Al-Laham, C. Y. Peng, A. Nanayakkara, M. Challacombe, P. M. W. Gill, B. Johnson, W. Chen, M. W. Wong, C. Gonzalez, J. A. Pople, Gaussian 03, 2003.

[11] H. A. Bent, *Chem. Rev.* **1960**, *61*, 275.

[12] T. Liu, M. Wang, Z. Shi, H. Cui, W. Dong, J. Chen, B. Åkermark, L. Sun, *Chem.–Eur. J.* **2004**, *10*, 4474.

[13] D. Chong, I. P. Georgakaki, R. Mejia-Rodriguez, J. Sanabria-Chinchilla, M. P. Soriaga, M. Y. Darensbourg, *J. Chem. Soc. Dalton Trans.* **2003**, 4158.

[14] COLLECT, Data Collection Software, Nonius B. V., Netherlands, 1998.

[15] Z. Otwinowski, W. Minor, 'Processing of X-Ray Diffraction Data Collected in Oscillation Mode', in Methods in Enzymology, Vol. 276, Macromolecular Crystallography, Part A, Eds. C. W. Carter and R. M. Sweet, pp. 307–326, Academic Press, San Diego 1997.

[16] G. M. Sheldrick, *Acta Crystallogr., Sect. A* **1990**, *46*, 467.

[17] G. M. Sheldrick, SHELXL-97, University of Göttingen, Germany, 1993.

[18] A. Altomare, M. C. Burla, M. Camalli, G. L. Cascarano, C. Giacovazzo, A. Guagliardi, A. G. Moliterni, R. Spagna *J. Appl. Crystallogr.* **1999**, *32*, 115.

[19] G. M. Sheldrick, SHELXL97, Program for the Refinement of Crystal Structures. University of Göttingen, Germany, 1997.

FULL PAPER

Functionalized Sugars as Ligands towards Water-Soluble [Fe-only] Hydrogenase Models

Ulf-Peter Apfel,[a] Yvonne Halpin,[b] Michael Gottschaldt,*[c] Helmar Görls,[a] Johannes G. Vos,*[b] and Wolfgang Weigand*[a]

Dedicated to Professor Jan Reedijk on the occasion of his 65th birthday

Only a small number of water-soluble iron carbonyl type model compounds for the active centre in [Fe-only] hydrogenase are known, and these models are mainly prepared by substitution of one of the CO ligands. In this publication we present new water-soluble models for [Fe-only] hydrogenase that contain a peripherally bound sugar residue. Compounds were prepared in which the 1,3-disulfanyl-2-propyltetra-O-acetyl-β-D-glucopyranoside unit is coordinated to the iron carbonyl core through either a sulfur or a selenium bridgehead atom. Electrochemical results for both types of compounds reveal hydrogen gas evolution from acetic acid and water.

(© Wiley-VCH Verlag GmbH & Co. KGaA, 69451 Weinheim, Germany, 2008)

Introduction

Since the elucidation of the structure of [Fe-only] hydrogenase in *Desulfovibrio desulfuricans* and *Clostridium pasteurianum*,[1] much effort has been devoted to synthesize structural and functional models of its catalytic centre.[2] Because the involvement of a bis(mercaptomethyl)amine bridge at the coordination site of the iron centres is not yet clarified, other dithiolates (SCH_2XCH_2S, $X = CH_2$, O, S) have been studied as bridging ligands in these model complexes.[3] It was shown that an amino functionality was not essential for catalytic activity.[4] Up to now, all model systems exhibit similar problems: too negative potentials for H_2 development from protons (ca. –1.6 V) during electrocatalysis and insolubility in water. The use of sugar residues should strongly increase the hydrophilicity and should allow hydrogen gas formation in aqueous systems, which is sparsely known in the literature.[5] Water would provide the advantage to serve as both the solvent and the proton source, as is the case under physiological conditions. The advantages for the use of sugars, therefore, are self evident. Bound to a metal centre, sugars are able to improve water solubility, and additionally, they may create hydrogen bonds, which may have an influence on the catalytic cycle of hydrogen gas evolution. To form complexes with a [2Fe2S] unit like in natural hydrogenase, it is necessary to introduce sulfur into the ligand molecule. Another important aspect of these studies is clarification of the role of the sulfur bridgehead atoms observed in natural systems. In this study, the more electropositive homologous selenium was incorporated to produce compounds with [2Fe2Se] moieties, and these compounds were compared with their [2Fe2S] sulfur analogues. Only a very small number of [2Fe2Se] complexes are known.[6]

Results and Discussion

The synthetic approach taken in the synthesis of both the sulfur- and selenium-containing model compounds is shown in Scheme 1. Starting from β,β′-dibromoisopropyltetra-O-acetyl-β-D-glucopyranoside (**1**),[7] thioacetate **2** was synthesized in 49% yield by treatment with an excess amount of potassium thioacetate at room temperature.[8] The usual way to deprotect the thioacetate groups with sodium hydroxide[9] would result in deprotection of the sugar hydroxy groups and is therefore not applicable to obtain dithiol **3**. Selective cleavage of the *S*-acetyl groups could be realized by treatment of **2** with hydrazine and acetic acid in dimethylformamide over a period of 4 d by stirring at room

[a] Institut für Anorganische und Analytische Chemie, Friedrich-Schiller Universität Jena,
August-Bebel-Straße 2, 07743 Jena, Germany
Fax: +49-3641-948102
E-mail: wolfgang.weigand@uni-jena.de
[b] Solar Energy Conversion SRC, School of Chemical Sciences, Dublin City University,
Dublin 9, Ireland
E-mail: han.vos@dcu.ie
[c] Institut für Organische und Makromolekulare Chemie, Friedrich-Schiller Universität Jena,
Humboldtstraße 10, 07743 Jena, Germany
E-mail: Michael.Gottschaldt@uni-jena.de
📃 Supporting information for this article is available on the WWW under http://www.eurjic.org or from the author.
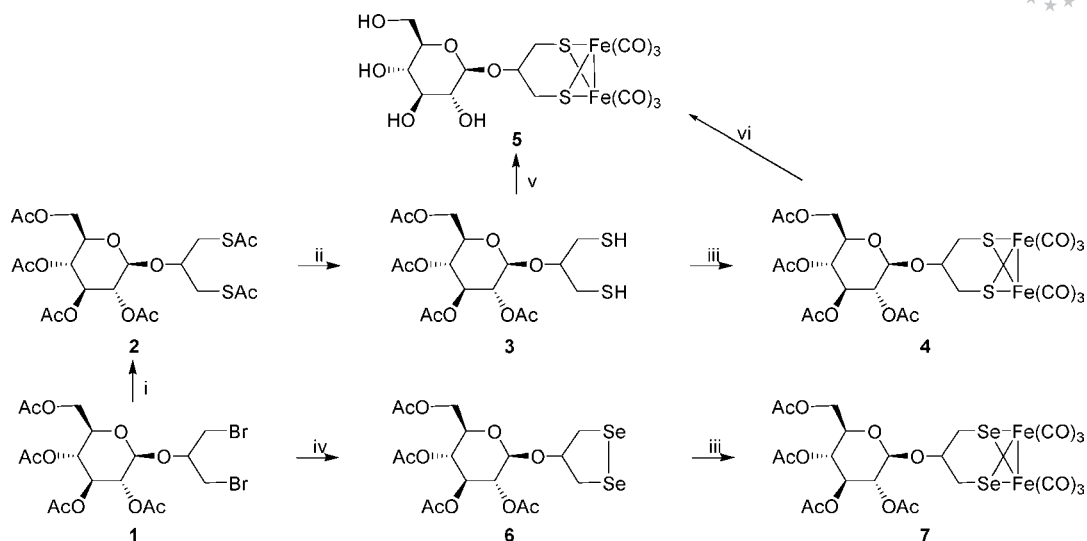
Scheme 1. Synthesis of the sugar-substituted iron carbonyl complexes by starting from dibromide **1**. Reagents and conditions: (i) KSAc, acetone; (ii) $N_2H_4 \cdot 2H_2O$/HOAc; (iii) $Fe_3(CO)_{12}$, toluene; (iv) Na_2Se_2, ethanol/thf; (v) 1. NaOMe, 2. $Fe_3(CO)_{12}$; (vi) NaOMe.

temperature to yield dithiol **3** in 59%.[10] After treatment of 1,3-disulfanyl-2-propyl-tetra-*O*-acetyl-β-D-glucopyranoside (**3**) with $Fe_3(CO)_{12}$ in toluene under reflux conditions[11] only one compound could be isolated. The ^{1}H NMR spectrum of **4** shows two doublets at 2.89–2.85 and 2.69–2.65 ppm and a pseudo triplet (doublet of doublets) at 1.56–1.41 ppm. ^{1}H,^{1}H-COSY measurements suggest that these signals can be assigned to the diastereotopic methylene protons adjacent to the thiolato groups. Two resonances are visible for the methylene carbon atoms in the ^{13}C NMR spectrum at δ = 28.5 and 27.2 ppm. Mass spectrometry shows a stepwise fragmentation of three CO groups and two iron atoms. The [M – 3CO]$^+$ peak at *m/z* = 648 further confirms the structure of compound **4**.

By diffusion of pentane into a dichloromethane solution of complex **4** crystals suitable for X-ray single-crystal structure analysis could be obtained (Figure 1). Compound **4** crystallized in the noncentrosymmetric space group *P*2$_1$. The two Fe centres are distorted octahedrally and coordinated by CO ligands and a 1,3-ditholato-2-propyltetra-*O*-acetyl-β-D-glucopyranoside bridge. The angles C1–C2–C3, S1–C1–C2 and S2–C3–C2 are around 115°, which is unexpectedly high in comparison to a regular sp^3 hybridized atom (109.5°). An explanation for this is given in the literature and can be described by the *Rule of Bent*.[12,13] Also, the distances C1–C2 and C2–C3 are slightly shortened (Table 1). The sugar ring exhibits a chair conformation and is arranged in the axial position to the [2Fe2S] centre.

Treatment of compound **4** with sodium methoxide in methanol led to deprotected complex **5**, which decomposes within hours in protic solvents. Additionally, **3** was deprotected by treatment with sodium methoxide in methanol and converted into **5** with $Fe_3(CO)_{12}$ by heating at reflux in thf for 2 h to give a red-coloured product that is soluble in water and methanol. ^{1}H NMR spectroscopy and mass spectrometry indicate that compound **5** was formed. To prepare selenium-containing sugar complex **7**, dibromide **1** was
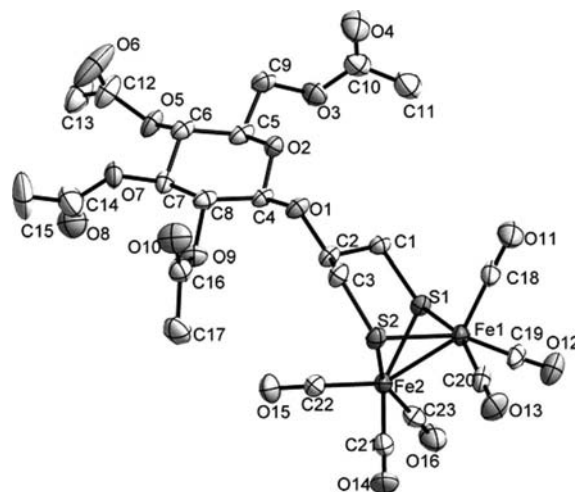

Figure 1. ORTEP view (50% probability) of one of the molecules in the structure of **4**. Hydrogen atoms are omitted for clarity.

Table 1. Selected bond lengths [Å] and angles [°] for compound **4**.

Fe1–Fe2	2.5150(10)	C1–C2	1.487(8)
Fe1–S1	2.2480(16)	C2–C3	1.507(8)
Fe1–S2	2.2554(17)	S1–C1	1.832(5)
Fe2–S1	2.2730(16)	S2–C3	1.829(5)
Fe2–S2	2.2571(17)	C2–O1	1.435(6)
S1–Fe1–S2	85.12(6)	C1–C2–C3	114.1(5)
S1–Fe2–S2	84.59(6)	C1–C2–O1	110.2(4)
S1–C1–C2	114.4(4)	C3–C2–O1	105.4(4)
S2–C3–C2	115.8(4)		

treated with sodium diselenide, freshly prepared from sodium borohydride and selenium in ethanol, to give **6** in 30% yield.[14] Reaction of **6** with $Fe_3(CO)_{12}$ gave complex **7** as a red solid. The structure as drawn in Scheme 1 was confirmed by ^{1}H, ^{13}C and ^{77}Se{^{1}H} NMR spectroscopic measurements. Comparison of the proton resonances of com-

U.-P. Apfel, Y. Halpin, M. Gottschaldt, H. Görls, J. G. Vos, W. Weigand

pound **4** and **7** reveal no important differences. The ^{13}C NMR spectra differ for the resonances of the methylene carbon atoms. The carbon resonances of **7** are found at higher field ($\Delta\delta \approx 10$ ppm) relative to those of **4** and are shifted from 28.5/27.2 ppm in **4** to 17.9/16.4 ppm in **7**, caused by the higher shielding of the carbon nucleus by the more electropositive selenium. Additionally, the [M]$^+$ peak at $m/z = 850.6$ in the ESI-MS and the CO bands between 2069 and 1991 cm^{-1} in the IR spectrum support the structure. Deprotection of **7** was carried out in situ as outlined below. According to the ^{1}H and ^{13}C NMR spectra, no epimerization of a β- to α-glycoside was observed.

Electrochemistry

Sulfur-Containing Complexes

Cyclic voltammetry of compound **4** exhibits one irreversible anodic process and several cathodic processes (Figure S1). The iron centres undergo an irreversible oxidation, $E_{pa} = +1.09$ V, which is assigned to the [Fe^{I}Fe^I] → [Fe^{II}Fe^I] + e$^-$ process, as described for the propylendithiolato (PDT)-bridged diiron complex [(μ-PDT)Fe$_2$(CO)$_6$].[12,15,16] The first cathodic wave observed ($E_{pc} = -1.50$ V) is attributed to the [Fe^{I}Fe^I] + e$^-$ → [Fe^{0}Fe^I] process. The second cathodic wave with a reduction potential of –1.89 V may be ascribed to the [Fe^{0}Fe^I] + e$^-$ → [Fe^{0}Fe^0] process, as was reported for similar compounds.[16]

To investigate the catalytic proton reduction ability of **4**, cyclic voltammetry was studied in the presence of a weak acid (HOAc, 1–10 mmol in acetonitrile; Figure 2). An increase in the current intensities of the reduction potentials upon addition of an acid is a characteristic feature for a catalytic electrochemical process, and in these cases the formation of hydrogen gas. As previously reported in the literature, other compounds that facilitate catalytic proton reduction exhibited a positive shift in their reduction potential upon addition of acetic acid.[13] No positive shift was observed for **4**. The peak current, however, experienced a substantial increase with the first aliquot of acid (1 mmol), whereas each increment thereafter led only to a slight increase in current. An irreversible wave of low intensity was observed ($\approx$–1.23 V) after the initial addition of acid and experiences a slight increase in current with increments of HOAc thereafter.

An equimolar amount of sodium methoxide (NaOCH$_3$) was added to deprotect the sugar hydroxy groups in compound **4** by standard deacylation (Scheme 1, step vi) to yield **5**, and this enabled the in situ investigation of the free sugar in the CV cell.[17] Sodium methoxide is a redox inactive compound. It exhibits poor solubility in acetonitrile, and as a result of this, it was previously dissolved in a minimal amount of methanol and added to the solution prior to HOAc addition. No shift in potential was observed and the reversibility of the process remained the same (Figure S2). A broad cathodic wave is observed in the spectrum at approximately –1.5 V with a current intensity that weakens with every successive voltage cycle. A return wave is
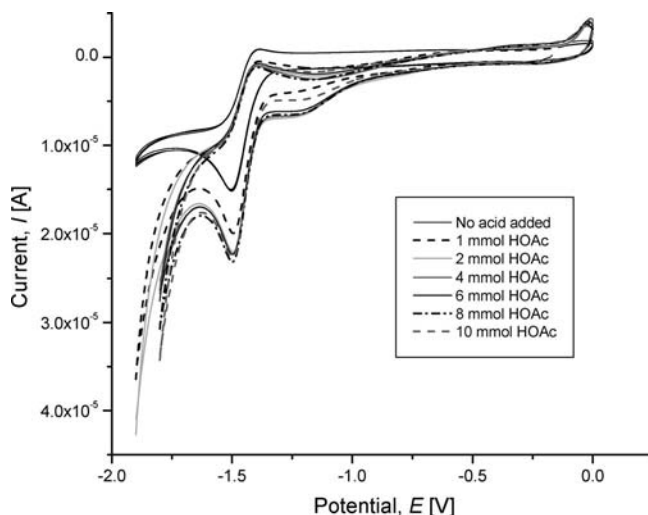
Figure 2. Cyclic voltammograms of **4** (1 mmol) with HOAc (0–10 mmol) in acetonitrile (vs. Ag/Ag$^+$ reference electrode).

observed for this process, which reached a stable state after the third cycle. A decrease in the current intensity of the first reduction was observed when 1 mmol of acid was added. However, with each sequential increment of HOAc the current intensity of the deprotected sugar reduction experienced a steady increase, which may suggest an electrochemical catalytic process (Figure 3). There was no anodic shift in the reduction potential. The weak, broad cathodic wave seen in Figure 3 disappears with the addition of the acid.
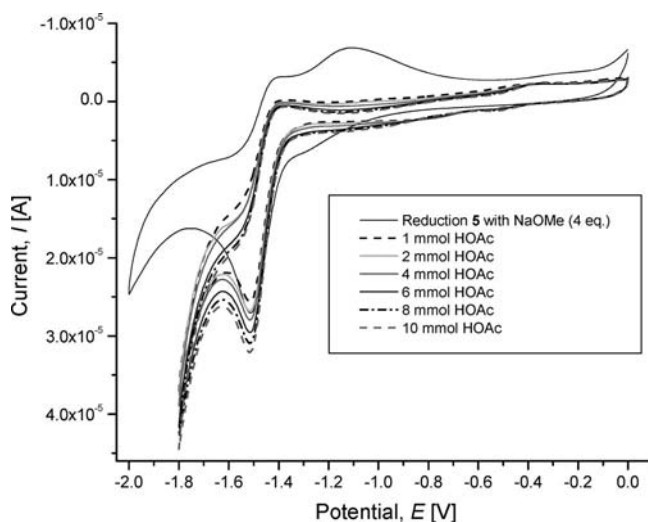
Figure 3. Cyclic voltammograms of **5** (1 mmol) with HOAc (0–10 mmol) in acetonitrile (vs. Ag/Ag$^+$ reference electrode).

Following the addition of HOAc to the complex and investigation of the catalytic proton reduction, a 5:1 mixture of water/acetonitrile (ACN) was added to the solution to examine any changes in the voltage in the electrochemistry. As a result of adding water the current intensity increased and led to a shift in the reduction potential at –1.5 to –1.6 V. Complex **5** was not stable in protic solvents such as methanol and water. This can be seen in the CV (Figure 4).

By adding 4.5 mL of H_2O/ACN (5:1) the reduction potential at –1.5 V, typical for the reduction of Fe^IFe^I to Fe^0Fe^I, disappeared, which indicates the decomposition of **5**.
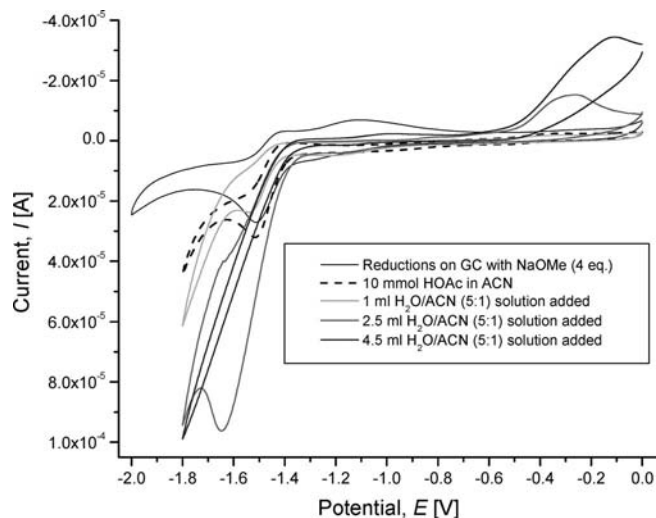

Figure 4. Cyclic voltammograms of **5** detailing the effect of H_2O on the catalytic proton reduction.

Selenium-Containing Complexes

Selenium analogue compound **7** undergoes an irreversible oxidation at +0.97 V, exhibiting a cathodic shift of 120 mV relative to the oxidation potential of **4**. A cathodic wave was observed at –1.46 V, which is attributed to the $[Fe^IFe^I] + e^- \rightarrow [Fe^0Fe^I]$ process. A second reduction wave is observed, $E_{pc} = -2.02$ V, which can be ascribed to the $[Fe^0Fe^I] + e^- \rightarrow [Fe^0Fe^0]$ process (Figure S3).

The catalytic proton reduction of **7** was investigated through the addition of HOAc (Figure 5). As observed for **4**, the reduction potential of the selenium analogue does not shift anodically. Following the addition of 1 mmol of acid, an increase in the peak current at –1.5 V was ob-
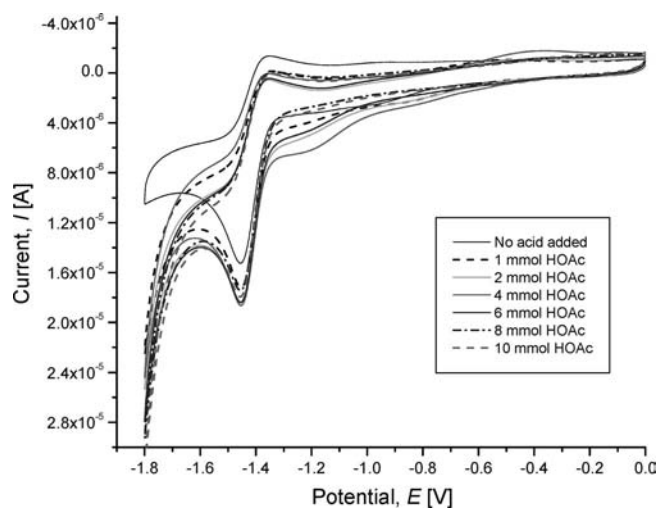
served, which slightly increased with additional aliquots of HOAc. This rise in the current (ca. –1.8 V) suggests catalytic H_2 development.

Compound **7** was treated with sodium methoxide to yield the deprotected sugar complex in analogy to **5** as a precursor molecule of a potential water-soluble hydrogenase model. The cyclic voltammetry of the deprotected sugar complex showed behaviour similar to that of **5**. Again no positive or negative shift was observed, and the reversible process remained the same (Figure S4). A broad anodic wave appeared, but it disappeared after the addition of HOAc. The influence of the added acetic acid was studied and evidence for H_2 development at –1.8 V was found (Figure 6).
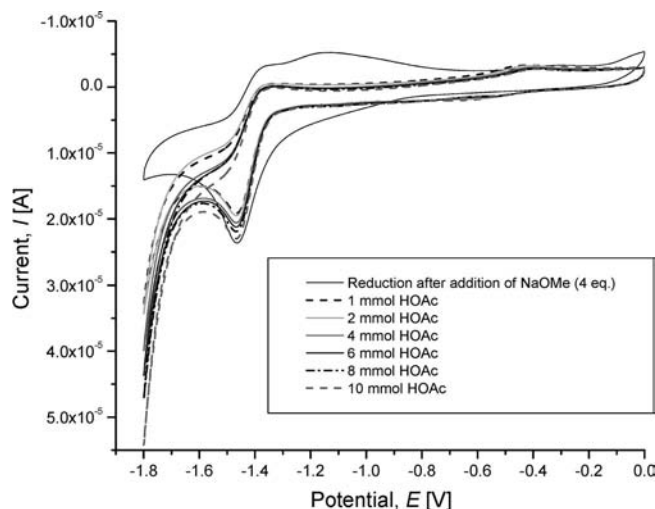

Figure 6. Cyclic voltammograms of the deprotected selenium complex (1 mmol) with HOAc (0–10 mmol) in acetonitrile (vs. Ag/Ag^+ reference electrode).

To investigate the electrochemical properties in water, a mixture of H_2O/ACN (5:1) was added to the deprotected selenium complex. With this, a large increase in the signal
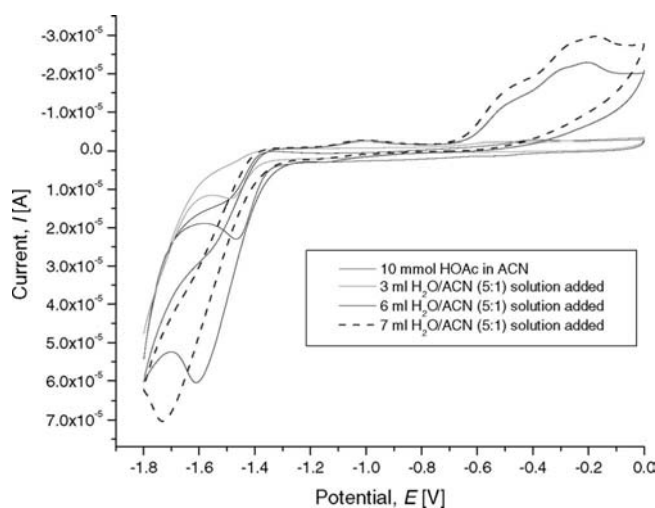

Figure 5. Cyclic voltammograms of **7** (1 mmol) with HOAc (0–10 mmol) in acetonitrile (vs. Ag/Ag^+ reference electrode).

Figure 7. Cyclic voltammograms of the deprotected selenium complex detailing the effect of H_2O on the catalytic proton reduction.

intensity at –1.4 V and an intensive negative shift of this peak potential of approximately 250 mV (Figure 7) was observed.

Comparison of the Electrocatalytic Results

The oxidation potential of **7** for the $Fe^IFe^I \rightarrow Fe^{II}Fe^I$ process experiences a cathodic shift of 120 mV relative to that of **4**. The iron centres in **7** are more easily reduced than those in **4**, as suggested by the positive shift of 40 mV for the first reduction process, $Fe^IFe^I \rightarrow Fe^0Fe^I$, in the selenium analogue, whereas the second reduction occurs at a potential that is 130 mV more negative than the corresponding process in the sulfur compound (Table 2).

Table 2. Electrochemical data for **4** and **7** in acetonitrile (vs. Ag/Ag$^+$ reference electrode).

	$E_{p(ox,irr)}$ [V] $Fe^IFe^I/Fe^{II}Fe^I$	E_{pc}, E_{pa} [V] Fe^IFe^I/Fe^0Fe^I	$E_{pc} - E_{pa}$ Separation [mV]	E_{pc}, E_{pa} [V] Fe^0Fe^I/Fe^0Fe^0
4	+1.09	–1.50 (E_{pc}) –1.39 (E_{pa})	110	–1.89 (E_{pc})
7	+0.97	–1.46 (E_{pc}) –1.36 (E_{pa})	100	–2.02 (E_{pc})

Deprotection of **4** and **7** with NaOMe leads to a new broad anodic wave, which disappears when adding acid. All complexes show a consequent increase in peak current for the $Fe^IFe^0 \rightarrow Fe^0Fe^0$ process with each aliquot of acetic acid, suggesting electrocatalytic hydrogen gas development.

In contrast to complex **5**, the deprotected Se compound was stable in solution even after adding 7 mL of a mixture of water/acetonitrile (5:1) to the acidic complex solution; a fact that must be ascribed by the influence of the selenium atoms. As a result of the more electropositive selenium, the iron atoms become more electron rich, leading to stronger π backbonding with the CO ligands. As a direct consequence, IR wavenumbers for the CO ligand slightly decrease.

Conclusions

Two new ligands based on tetra-*O*-acetyl-β-D-glucopyranosides **3** and **6** and the corresponding diiron complexes **4** and **7** were synthesized and characterized. No epimerization was observed. Complexes **4** and **7** show similar behaviour during electrochemical investigation and exhibit catalytic properties for H$_2$ formation. Deprotection of complexes **4** and **7** with NaOMe leads to the water-soluble complexes. It was thereby recognized that the deprotected selenium complex is more stable in aqueous solution than the sulfur compound. The presence of selenium offers higher activity towards H$_2$ development, but it occurs at lower potentials than the corresponding sulfur complexes. The sugar residue was found to have no notable influence on the catalytic cycle; instead, it changes the solubility properties of the complexes.

Experimental Section

General Procedures: Solvents for the syntheses were first dried with KOH and distilled from sodium/benzophenone. Chemicals were

used as received from Fluka and Acros without further purification. 1,3-dibromo-2-propyl-β-D-glucopyranoside was synthesized by following literature procedures.[7] Thin-layer chromatography (TLC) was performed on Merck silica gel 60 F$_{254}$ plates (detection under UV light at 254 nm); flash chromatography (FC) was performed on Fluka silica gel 60. ^{1}H, ^{13}C and ^{77}Se{^{1}H} NMR spectra were recorded with a Bruker 400 MHz instrument. IR spectra were recorded with a Perkin–Elmer 2000 FTIR. Mass spectrometry was performed with an SSQ710 Finnagen MAT. All reactions were carried out under an argon atmosphere.

1,3-Dithioacetyl-2-propyltetra-*O*-acetyl-β-D-glucopyranoside (2): To a 50-mL round-bottomed flask containing 1,3-dibromo-2-propyltetra-*O*-acetyl-β-D-glucopyranoside (**1**; 500 mg, 0.836 mmol) dissolved in acetone (20 mL) was added potassium thioacetate (430 mg, 3.762 mmol). The solution was stirred for 1 week at room temperature, and the resulting precipitate was filtered off. The filtrate was evaporated to dryness and purified by FC (ethyl acetate/hexane, 1:1) to yield a white precipitate (220 mg, 49%). R_f = 0.63 (ethyl acetate/hexane, 1:1). ^{1}H NMR (400 MHz, CDCl$_3$): δ = 5.19–5.14 (m, 1 H, 3-H), 5.05–5.00 (m, 1 H, 4-H), 4.95–4.90 (m, 1 H, 2-H), 4.63 (d, $^3J_{1,2}$ = 8 Hz, 1 H, 1-H), 4.23–4.12 (m, 2 H, 6-H, 6'-H), 3.75–3.70 [m, 2 H, 5-H and SCH$_2$-C*H*(O)-CH$_2$S], 3.15–2.87 [4 m, 4 H, SC*H$_2$*-CH(O)-C*H$_2$*S], 2.31/2.30 (2 s, 6 H, CH$_3$-S-acetyl), 2.05/2.03/1.99/1.97 (4 s, 12 H, CH$_3$-acetyl) ppm. ^{13}C NMR (50 MHz, CDCl$_3$): δ = 195.1/194.8 (*C*O-S-acetyl), 170.6/170.2/169.4/169.2 (*C*O-acetyl), 101.0 (C-1), 79.3 (C-5), 72.8 (C-3), 71.9 [S*C*H$_2$-CH(O)-CH$_2$S], 71.2 (C-2), 68.4 (C-4), 61.9 (C-6), 32.9/32.3 [S*C*H$_2$-CH(O)-*C*H$_2$S], 30.5 (*C*H$_3$-S-acetyl), 20.7 (*C*H$_3$-acetyl) ppm. MS (Micro-ESI): m/z = 561.1 [M + Na]$^+$. IR (KBr): $\tilde{\nu}$ = 2954 (m), 2877 (m), 1747 (vs), 1690 (vs), 1431 (m), 1378 (s), 1232 (vs) cm^{-1}. C$_{22}$H$_{32}$O$_{11}$S$_2$ (538.12): calcd. C 46.83, H 5.61, S 11.91; found C 46.93, H 5.81, S 11.70.

1,3-Disulfanyl-2-propyltetra-*O*-acetyl-β-D-glucopyranoside (3): To a solution of **2** (1 g, 1.878 mmol) dissolved in dimethylformamide (40 mL) was added hydrazine dihydrate (0.329 g, 6.588 mmol). After stirring for 10 min, acetic acid (380 µL, 6.588 mmol) was added, and the resulting solution was stirred until TLC showed no remaining starting material (usually 4 d). Water was added, and the resulting precipitate was dissolved in ethyl acetate. The organic phase was separated, washed with water and dried with sodium sulfate. Evaporation of the solvent and recrystallization from ethyl acetate/pentane gave compound **3** (508 mg, 60%) as a white powder. ^{1}H NMR (400 MHz, CDCl$_3$): δ = 5.24–5.16 (m, 1 H, 3-H), 5.07–5.00 (m, 1 H, 4-H), 4.98–4.92 (m, 1 H, 2-H), 4.78 (m, 2 H, S*H*), 4.61 (d, $^3J_{1,2}$ = 8 Hz, 1 H, 1-H), 4.21–4.16 (m, 2 H, 6-H), 3.69 (m, 1 H, 5-H), 3.26–3.08 [m, 5 H, SC*H$_2$*-CH(O)-C*H$_2$*S and SCH$_2$-C*H*(O)-CH$_2$S], 2.07/2.02/2.01/1.98 (4 s, 12 H, CH$_3$-acetyl) ppm. ^{13}C NMR (50 MHz, CDCl$_3$): δ = 170.6/170.3/169.3/169.2 (*C*O-acetyl), 101.9 (C-1), 83.5 (C-5), 72.5 (C-3), 72.1 [S*C*H$_2$-CH(O)-CH$_2$S], 71.0 (C-2), 68.3 (C-4), 62.1 (C-6), 44.82/44.83 [S*C*H$_2$-CH(O)-*C*H$_2$S], 20.7 (*C*H$_3$-acetyl) ppm. MS (FAB): m/z (%) = 452 [M – 2H]$^+$. IR (KBr): $\tilde{\nu}$ = 2925 (s), 2855 (m), 1755 (vs), 1654 (m), 1432 (m), 1369 (s), 1222 (vs), 1042 (vs) cm^{-1}. Elemental analysis was not obtained.

Hexacarbonyl(1,3-disulfanyl-2-propyltetra-*O*-acetyl-β-D-glucopyranoside)diiron (4): A solution of **3** (63 mg, 0.139 mmol) and Fe$_3$(CO)$_{12}$ (71 mg, 0.139 mmol) dissolved in thf (20 mL) was heated at reflux for 30 min. After cooling to room temperature, the solvent was evaporated, and crude complex **4** was purified by FC (ethyl acetate/hexane, 1:1) to yield of red solid (25 mg, 25%). Single crystals suitable for X-ray crystallography were obtained by diffusion of pentane into a solution of **4** in dichloromethane. R_f = 0.72 (ethyl acetate/hexane, 1:1). ^{1}H NMR (400 MHz, CDCl$_3$): δ = 5.15–5.10

(m, 1 H, 3-H), 5.05–4.96 (m, 1 H, 4-H), 4.85–4.81 (m, 1 H, 2-H), 4.47 (d, $^3J_{1,2}$ = 7.6 Hz, 1 H, 1-H), 4.21–4.09 (m, 2 H, 6-H), 3.65 (m, 1 H, 5-H), 3.04 [m, 1 H, SCH$_2$-CH(O)-CH$_2$S], 2.89/2.85, [d, ^3J = 8 Hz, 1 H, SCH_2-CH(O)-CH$_2$S] 2.69/2.65 [d, ^3J = 8 Hz, 1 H, SCH$_2$-CH(O)-CH_2S], 1.56–1.41 [m, 2 H, SCH_2-CH(O)-CH_2S], 2.15/1.99.1.96 (3 s, 12 H, CH$_3$-acetyl) ppm. ^{13}C NMR (50 MHz, CDCl$_3$): δ = 207.4 (CO), 170.6/170.1/169.3/169.1 (CO-acetyl), 99.9 (C-1), 80.8 [SCH$_2$-CH(O)-CH$_2$S], 72.5 (C-3), 72.2 (C-5), 68.2 (C-4), 61.8 (C-6), 28.5/27.2 [SCH$_2$-CH(O)-CH$_2$S], 20.6 (CH$_3$-acetyl) ppm. MS (DEI): m/z = 648 [M – 3CO]$^+$, 620 [M – 4CO]$^+$, 592 [M – 5CO]$^+$, 452 [M – 2Fe – 6CO]$^+$. IR (KBr): $\tilde{\nu}$ = 2955 (m), 2925 (m), 2854 (m), 2077 (vs), 2036 (vs), 1995 (vs), 1757 (s), 1227 (s) cm^{-1}. C$_{23}$H$_{24}$Fe$_2$O$_{16}$S$_2$ (731.92): calcd. C 37.73, H 3.30, S 8.76; found C 37.71, H 3.25, S 8.17.

Hexacarbonyl(1,3-dithiolato-2-propyl-β-D-glucopyranoside)diiron (5)

Method A: To a solution of compound **4** (5 mg, 8.867 mmol) dissolved in methanol (1 mL) was added a catalytic amount of sodium methoxide, and the mixture was stirred for 2 h. The resulting solution was evaporated and used directly for NMR and MS analysis.

Method B: To a solution of **3** (41 mg, 0.091 mmol) dissolved in methanol (5 mL) and dichloromethane (1 mL) was added sodium methoxide (100 mg), and the mixture was stirred for 72 h. The solvent was evaporated, and the remaining solid was dissolved in thf (40 mL); Fe$_3$(CO)$_{12}$ (46 mg, 0.091 mmol) was then added. After 30 min under reflux, the formed precipitate was filtered off, and the solvent was evaporated to dryness. The remaining solid was dissolved in methanol, and the solution was separated from solid particles. After evaporation, **5** (22 mg, 53.2%) was obtained as a red solid. ^{1}HNMR (200 MHz, D$_2$O): δ = 5.03 (m, 1 H, 1-H), 3.80–3.25 [m, 11 H, 2-H, 3-H, 4-H, 5-H, 6-H, SCH$_2$-CH(O)-CH$_2$S] ppm. MS (FAB): m/z = 587 [M + Na]$^+$.

1,3-Diselenolan-2-propyltetra-O-acetyl-β-D-glucopyranoside (6): To sodium borohydride (88 mg, 2.3 mmol) and selenium (184 mg, 2.3 mmol) was added absolute ethanol (6 mL) whilst stirring. The resulting suspension was heated at reflux for 1 h and a red solution was obtained. The solution was then cooled to 0 °C and **1** (453 mg, 0.757 mmol) dissolved in absolute ethanol (20 mL) and thf (5 mL) was slowly added. The suspension was stirred for an additional 24 h. Water (15 mL) are added, and a red solid precipitated. After filtration, the separated solid was washed again with dichloromethane (2×). The solvent was evaporated, and crude product **6** was purified by FC (ethyl acetate/hexane, 1:1) to yield **6** (123 mg, 30%) as a slightly brown solid. R_f = 0.37 (ethyl acetate/hexane, 1:1). ^{1}H NMR (400 MHz, CDCl$_3$): δ = 5.19–5.16 (m, 1 H, 3-H), 5.08–5.01 [m, 1 H, 4-H and SeCH$_2$-CH(O)-CH$_2$Se], 4.98–4.94 (m, 1 H, 2-H), 4.64 (d, $^3J_{1,2}$ = 8 Hz, 1 H, 1-H), 4.24–4.12 (m, 2 H, 6-H), 3.71–3.67 (m, 1 H, 5-H), 3.44–3.26 [m, 4 H, SeCH_2-CH(O)-CH_2Se], 2.07/2.04/2.01/1.99 (4 s, 12 H, CH$_3$-acetyl) ppm. ^{13}C NMR (50 MHz, CDCl$_3$): δ = 170.6/170.2/169.3/169.2 (CO-acetyl), 99.2 (C-1), 85.5 [SeCH$_2$-CH(O)-CH$_2$Se], 72.5 (C-3), 72.1 (C-5), 71.2 (C-2), 68.3 (C-4), 61.9 (C-6), 35.3/33.2 [SeCH$_2$-CH(O)-CH$_2$Se], 20.7 (CH$_3$-acetyl) ppm. ^{77}Se{^{1}H} NMR (76 MHz, CDCl$_3$): δ = 261.7, 238.3 ppm. MS (ESI): m/z = 571 [M + Na]$^+$. IR (KBr): $\tilde{\nu}$ = 2940 (m), 1755 (vs), 1637 (m), 1431 (m), 1368 (s), 1230 (vs), 1041 (vs), 908 (m) cm^{-1}. C$_{17}$H$_{24}$O$_{10}$Se$_2$ (547.97): calcd. C 37.38, H 4.43; found C 37.88, H 4.43.

Hexacarbonyl(1,3-diselenolanolato-2-propyltetra-O-acetyl-β-D-glucopyranoside)diiron (7): Compound **6** (50 mg, 0.091 mmol) and Fe$_3$(CO)$_{12}$ (46 mg, 0.091 mmol) were dissolved in thf (20 mL) and stirred in a 50-mL Schlenk vessel. After 2 h under reflux, the solvent was evaporated, and the remaining solid was purified by FC (ethyl acetate/hexane, 1:1) to afford **7** (55 mg, 73%) as a red solid.

R_f = 0.55 (ethyl acetate/hexane, 1:1). ^{1}H NMR (400 MHz, CDCl$_3$): δ = 5.15–5.11 (m, 1 H, 3-H), 5.01–4.96 (m, 1 H, 4-H), 4.86–4.81 (m, 1 H, 2-H), 4.48 (d, $^3J_{1,2}$ = 7.6 Hz, 1 H, 1-H), 4.20–4.08 (m, 2 H, 6-H), 3.65 (m, 1 H, 5-H), 2.95–2.71/1.61–1.44 [2 m, 5 H, SeCH_2-CH(O)-CH_2Se], 2.08/1.99.1.96 (3 s, 12 H, CH$_3$-acetyl) ppm. ^{13}C NMR (50 MHz, CDCl$_3$): δ = 208.6 (CO), 170.5/170.1/169.3/169.1 (CO-acetyl), 99.5 (C-1), 80.6 [SeCH$_2$-CH(O)-CH$_2$Se], 72.5 (C-3), 72.2 (C-5), 71.1 (C-2), 68.2 (C-4), 61.8 (C-6), 20.6 (CH$_3$-acetyl), 17.9/16.4 [SeCH$_2$-CH(O)-CH$_2$Se] ppm. ^{77}Se{^{1}H} NMR (76 MHz, CDCl$_3$): δ = 209.3 (br.) ppm. MS (ESI): m/z = 850.6 [M + Na]$^+$. IR (KBr): $\tilde{\nu}$ = 2926 (m), 2855 (m), 2069 (vs), 2029 (vs), 1991 (vs), 1757 (vs), 1637 (m), 1436 (m), 1370 (s) cm^{-1}. C$_{23}$H$_{24}$Fe$_2$O$_{16}$Se$_2$ (827.81): calcd. C 33.44, H 2.93; found C 32.96, H, 2.42.

Electrochemical Procedure: Cyclic voltammograms were recorded against a nonaqueous Ag/Ag$^+$ reference electrode (0.1 M nBu$_4$NPF$_6$ and 0.01 M AgNO$_3$ in CH$_3$CN). A glassy carbon (GC) macroelectrode and a platinum wire were used as the working and auxiliary electrodes, respectively. A solution of 0.05 M nBu$_4$NPF$_6$ (Fluka, electrochemical grade) in acetonitrile (Aldrich, anhydrous, 99.8%) was used as the supporting electrolyte. Electrochemical experiments were carried out by using a CHI750C electrochemical bipotentiostat. Prior to each experiment, the electrochemical cell was degassed for at least 10 min by using argon and a blanket of argon was maintained throughout. The GC working electrode was prepared by successive polishing with 1.0 and 0.3 micron alumina pastes and sonicated in Millipore water for 5 min. All cyclic voltammograms were recorded at a scan rate of 100 mVs^{-1}.

Crystal Structure Determination: The intensity data for the compound were collected with a Nonius KappaCCD diffractometer by using graphite-monochromated Mo-K_α radiation. Data were not corrected for Lorentz and polarization effects, but for absorption effects.[18,19] The structure was solved by direct methods (SHELXS[20]) and refined by full-matrix least-squares techniques against F_o^2 (SHELXL-97[21]). All hydrogen atoms of the structures were included at calculated positions with fixed thermal parameters. XP (SIEMENS Analytical X-ray Instruments, Inc.) was used for structure representations.

Crystal Data for 4: C$_{23}$H$_{24}$Fe$_2$O$_{16}$S$_2$, M_r = 732.24 gmol^{-1}, brown prism, size $0.04 \times 0.04 \times 0.03$ mm^3, monoclinic, space group $P2_1$, a = 9.4890(4) Å, b = 6.8110(3) Å, c = 23.5479(9) Å, β = 93.422(2)°, V = 1519.18(11) Å^3, T = –90 °C, Z = 2, $\rho_{\text{calcd.}}$ = 1.601 gcm^{-3}, μ(Mo-K_α) = 11.64 cm^{-1}, F(000) = 748, 8761 reflections in h(–9/12), k(–8/7), l(–30/30), measured in the range 2.15° ≤ Θ ≤ 27.53°, completeness $\Theta_{\max}$ = 97.4%, 5943 independent reflections, R_{int} = 0.0806, 4692 reflections with $F_o > 4\sigma(F_o)$, 392 parameters, 1 restraints, R_{1obs} = 0.0598, wR_{2obs} = 0.1323, R_{1all} = 0.0825, wR_{2all} = 0.1440, GOOF = 1.037, Flack parameter: –0.02(3), largest difference peak and hole: 0.697/–0.485 e Å^{-3}.

CCDC-683744 (for **4**) contains the supplementary crystallographic data for this paper. These data can be obtained free of charge from The Cambridge Crystallographic Data Centre via www.ccdc.cam. ac.uk/data_request/cif.

Supporting Information (see footnote on the first page of this article): Additional cyclic voltammogram traces.

Acknowledgments

[1] a) Y. Nicolet, A. L. de Lacey, X. Vernède, V. M. Fernandez, E. C. Hatchikian, J. C. Fontecilla-Camps, *J. Am. Chem. Soc.* **2001**, *123*, 1596–1601; b) Y. Nicolet, B. J. Lemon, J. C. Fontecilla-Camps, J. W. Peters, *Trends Biochem. Sci.* **2000**, *25*, 138–143; c) Y. Nicolet, C. Piras, P. Legrand, C. E. Hatchikian, J. C. Fontecilla-Camps, *Structure* **1999**, *7*, 13–23; d) E. C. Hatchikian, N. Forget, V. M. Fernandez, R. Williams, R. Cammack, *Eur. J. Biochem.* **1992**, *209*, 357–365.

[2] a) J. D. Lawrence, H. Li, T. B. Rauchfuss, M. Benard, M. M. Rohmer, *Angew. Chem. Int. Ed.* **2001**, *40*, 1768–1771; b) T. Liu, M. Wang, Z. Shi, H. Cui, W. Dong, J. Chen, B. Akermark, L. Sun, *Chem. Eur. J.* **2004**, *10*, 4474–4479.

[3] a) W. Gao, J. Liu, C. Ma, L. Weng, K. Jin, C. Chen, B. Akermark, L. Sun, *Inorg. Chim. Acta* **2006**, *359*, 1071–1080; b) L. C. Song, J. Gao, H. T. Wang, Y. J. Hua, H. T. Fan, X. G. Zhang, Q. M. Hu, *Organometallics* **2006**, *25*, 5724–5729; c) M. Razavet, S. C. Davies, D. L. Hughes, J. E. Barclay, D. J. Evans, S. A. Fairhorst, X. Liu, C. J. Picket, *Dalton Trans.* **2003**, 586–595; d) F. Xu, C. Tard, X. Wang, S. K. Ibrahim, D. L. Hughes, W. Zhang, X. Zeng, Q. Luo, X. Liu, C. J. Pickett, *Chem. Commun.* **2008**, 606–608; e) P. I. Volkers, T. B. Rauchfuss, *J. Inorg. Biochem.* **2007**, *101*, 1748–1751; f) J. Windhager, M. Rudolph, S. Bräutigam, H. Görls, W. Weigand, *Eur. J. Inorg. Chem.* **2007**, 2748–2760.

[4] a) C. Greco, G. Zampella, L. Bertini, M. Bruschi, P. Fantucci, L. De Goia, *Inorg. Chem.* **2007**, *46*, 108–116; b) M. H. Cheah, S. J. Borg, S. P. Best, *Inorg. Chem.* **2007**, *46*, 1741–1750.

[5] Y. Na, M. Wang, K. Jin, R. Zhang, L. Sun, *J. Organomet. Chem.* **2006**, *691*, 5045–5051.

[6] a) W. Hieber, J. Gruber, *Z. Anorg. Allg. Chem.* **1958**, *296*, 91–103; b) S. Gao, J. Fan, S. Sun, X. Peng, X. Zhao, J. Hou, *Dalton Trans.* **2008**, *16*, 2128–2135; c) D. Seyferth, R. S. Henderson, *J. Organomet. Chem.* **1981**, *204*, 333–343.

[7] a) H. W. Coles, M. L. Doods, F. H. Bergeim, *J. Am. Chem. Soc.* **1938**, *60*, 1167–1168; b) Y. Mikata, Y. Shinohara, K. Yoneda, Y. Nakamura, K. Esaki, M. Tanahashi, I. Brudzinska, S. Hirohara, M. Yokoyama, K. Mogami, T. Tanase, T. Kitayama, K. Takashiba, K. Nabeshima, R. Takagi, M. Takatani, T. Okamoto, I. Kinoshita, M. Doe, A. Hamazawa, M. Morita, F. Nishida, T. Sakakibara, C. Orvig, S. Yano, *J. Org. Chem.* **2001**, *66*, 3783–3789.

[8] N. S. Johary, L. N. Owen, *J. Chem. Soc.* **1955**, 1302–1307.

[9] L. W. C. Miles, L. N. Owen, *J. Chem. Soc.* **1952**, 2943–2946.

[10] S. Salyi, M. Kritikos, B. Akermark, L. Sun, *Chem. Eur. J.* **2003**, *9*, 557–560.

[11] L. Song, F. Gong, T. Meng, J. Ge, L. Cui, Q. Hu, *Organometallics* **2004**, *23*, 823–831.

[12] U.-P. Apfel, Y. Halpin, H. Görls, J. G. Vos, B. Schweizer, G. Linti, W. Weigand, *Chem. Biodiversity* **2007**, *4*, 2138–2148.

[13] H. A. Bent, *Chem. Rev.* **1961**, *61*, 275–311.

[14] M. Schmidt, U. Görl, *Angew. Chem.* **1987**, *99*, 917–918.

[15] T. Liu, M. Wang, Z. Shi, H. Cui, W. Dong, J. Chen, B. Akermark, L. Sun, *Chem. Eur. J.* **2004**, *10*, 4474–4479.

[16] D. Chong, I. P. Georgakaki, R. Mejia-Rodriguez, J. Sanabria-Chinchilla, M. P. Soriaga, M. Y. Darensbourg, *Dalton Trans.* **2003**, 4158–4163.

[17] M. Jacobsson, U. Ellervik, *Tetrahedron Lett.* **2002**, *43*, 6549–6552.

[18] B. V. Nonius, *COLLECT*, Data Collection Software, Netherlands, **1998**.

[19] Z. Otwinowski, W. Minor, "Processing of X-ray Diffraction Data Collected in Oscillation Mode" in *Methods in Enzymology Vol. 276: Macromolecular Crystallography, Part A* (Ed.: C. W. Carter, R. M. Sweet), Academic Press, San Diego, **1997**, pp. 307–326.

[20] G. M. Sheldrick, *Acta Crystallogr., Sect. A* **1990**, *46*, 467–473.

[21] G. M. Sheldrick, *SHELXL-97*, University of Göttingen, Germany, **1993**.

SUPPORTING INFORMATION

Title: Functionalized Sugars as Ligands towards Water-Soluble [Fe-only] Hydrogenase Models
Author(s): Ulf-Peter Apfel, Yvonne Halpin, Michael Gottschaldt,* Helmar Görls, Johannes G. Vos,* Wolfgang Weigand*
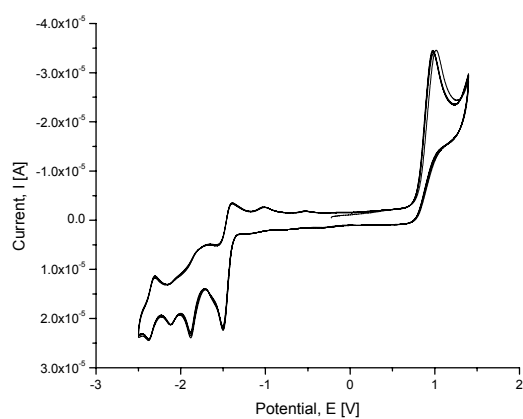**Ref. No.:** I200800720

Figure S1. Cyclic voltammogram of **4**, on a glassy carbon electrode, in 0.05 M nBu$_4$NPF$_6$ in acetonitrile versus Ag/Ag$^+$ reference electrode.

Figure S2. Cyclic voltammograms showing the effect of NaOCH$_3$ on the reduction potential of **4**, on a glassy carbon electrode in 0.05 M nBu$_4$NPF$_6$ in acetonitrile versus Ag/Ag$^+$ reference electrode. The different traces represent changes after each electrochemical cycle.

Figure S3. Cyclic voltammogram of **7**, on a glassy carbon electrode, in 0.05 M nBu₄NPF₆ in acetonitrile versus Ag/Ag⁺ reference electrode.
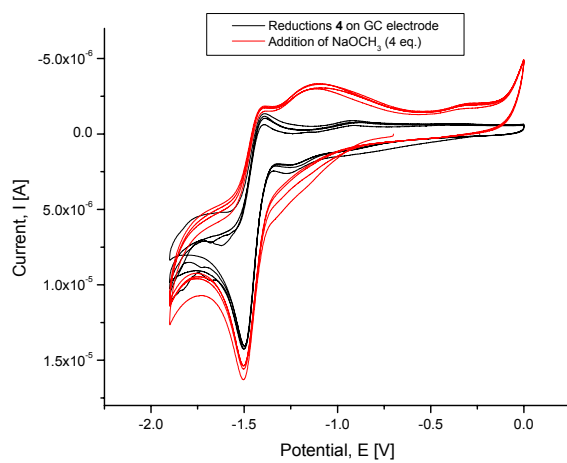

Figure S4. Cyclic voltammograms showing the effect of NaOMe on the reduction potential of **7**, on a glassy carbon electrode in 0.05 M nBu₄NPF₆ in acetonitrile versus Ag/Ag⁺ reference electrode. The different traces represent changes after each electrochemical cycle.
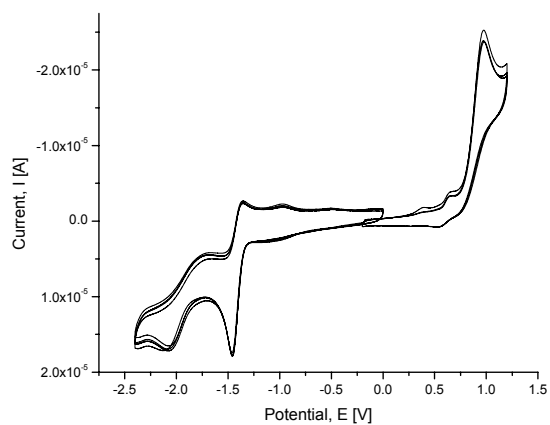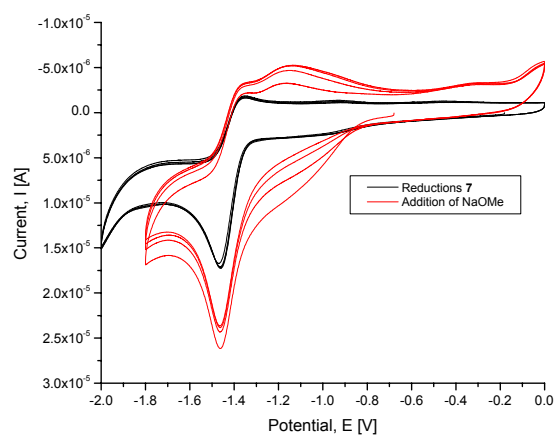
Oxidation of Diiron and Triiron Sulfurdithiolato Complexes: Mimics for the Active Site of [FeFe]-Hydrogenase

by **Jochen Windhager**[a]), **Raphael A. Seidel**[a]), **Ulf-Peter Apfel**[a]), **Helmar Görls**[a]), **Gerald Linti***[b]), and **Wolfgang Weigand***[a])

[a]) Friedrich-Schiller-Universität Jena, Institut für Anorganische und Analytische Chemie, August-Bebel-Strasse 2, D-07743 Jena (phone: +49-3641-948160; e-mail: wolfgang.weigand@uni-jena.de)
[b]) Ruprecht-Karls-Universität Heidelberg, Anorganisch-Chemisches Institut, Im Neuenheimer Feld 270, D-69120 Heidelberg (fax: +49-6221-546617; e-mail: gerald.linti@aci.uni-heidelberg.de)

Dedicated to Professor *Helga Dunken*

The oxidation of the hexacarbonyl(1,3-dithiolato-S,S')diiron complexes **4a**–**4c** with varying amounts of dimethyldioxirane (DMD) was systematically studied. The chemoselectivity of the oxidation products depended upon the substituent R (R = H, Me, 1/2 $(CH_2)_5$). For R = H, four oxidation products, **6a**–**6d**, have been obtained. In the case of R = Me, three products, **7a**–**7c**, were formed, and for R = 1/2 $(CH_2)_5$, only complex **8** was observed. These observations are due to steric and electronic effects caused by the substituent R. Additionally, oxidation of the triiron complex **5** with DMD was performed to yield the products **9a** and **9b**. X-Ray diffraction analyses were performed for **6a**–**6d**, **7a**, and **7c**, as well as for **9a** and **9b**. The electronic properties were determined by density-functional theory (DFT) calculations.

Introduction. – The oxidative addition of Pt^0 complexes to cyclic disulfides received significant attention during the last years [1]. Recently, we have investigated reactions of 1,2,4-trithiolanes with Pt^0 complexes leading to the insertion of the Pt^0 complex fragment along the S−S bond [2]. We have also shown that the 1,2,4-trithiolane can oxidatively be added to $Fe_2(CO)_9$ to give the sulfurdithiolato (sdt) diiron complex $[Fe_2(CO)_6(\mu\text{-}SCH_2SCH_2S\text{-}\mu)]$ as well as $[Fe_2(CO)_6(\mu\text{-}SCH_2S\text{-}\mu)]$ [3a][3b][4a]. Very recently and independently, similar reactions of $Fe_3(CO)_{12}$ and 1,2,4-trithiolane leading to sulfurdithiolato (sdt) diiron complex have been reported [3c].

Since the first X-ray structure determination of the [FeFe]-hydrogenase has been published [5], numerous model compounds [6] suitable as active site of the enzyme such as propanedithiolato (pdt) diiron derivatives [6a–6d], azadithiolato (adt) diiron derivatives [6e–6g], and the oxadithiolato (odt) diiron derivatives were described (*Fig. 1*) [6f][6i][6l].
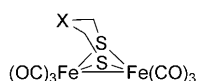

Fig. 1. *Model complexes of the active site of the [FeFe]-hydrogenase with X =* CH_2, *NH, O, and S*

Lorenz and co-workers prepared ethane-1,2-sulfenatothiolato complex **1**, which can be considered as the first oxidized hydrogenase's active-site analogue [3f]. Very recently, we have also shown the preparation of sulfenatothiolato and disulfenato

Investigation of amino acid containing [FeFe] hydrogenase models concerning pendant base effects

Ulf-Peter Apfel [a], Christian R. Kowol [b], Yvonne Halpin [c], Florian Kloss [a], Joachim Kübel [a], Helmar Görls [a], Johannes G. Vos [c], Bernhard K. Keppler [b], Enrico Morera [d], Gino Lucente [d,*], Wolfgang Weigand [a,*]

[a] *Institute for Inorganic and Analytical Chemistry, Friedrich-Schiller University Jena, August-Bebel-Str. 2, D-07743 Jena, Germany*
[b] *University of Vienna, Institute of Inorganic Chemistry, Währingerstr. 42, A-1090 Vienna, Austria*
[c] *Solar Energy Conversion SRC, School of Chemical Sciences, Dublin City University, Dublin 9, Ireland*
[d] *Dpt. di Chimica e Tecnologie del Farmaco, "Sapienza" Università di Roma, P.le A. Moro 5, 00185 Roma, Italy*

ARTICLE INFO

ABSTRACT

The present investigations deal with the modeling of the peptide surrounding of [FeFe] hydrogenase using amine containing disulphides to simulate possible influences of the amino acid lysine (K237) on the electrochemical and electrocatalytic properties of biomimetic compounds based on [Fe2S2] moieties. $Fe_3(CO)_{12}$ was reacted with Boc-4-amino-1,2-dithiolane, Boc-Adt-OMe (Adt = 4-amino-1,2-dithiolane-4-carboxylic acid, Boc = *tert*-butoxycarbonyl) and Boc-Adp *tert*-butyl ester (Adp = (*S*)-2-amino-3-(1,2-dithiolan-4-yl)propionic acid) to elongate the Fe···N distance in comparison to the well known $[Fe_2\{(SCH_2)_2NR\}(CO)_6]$ model complexes. Efforts to deprotect the complexes containing Boc-4-amino-1,2-dithiolane with trifluoroacetic acid result in the formation of $[Fe_3(\mu^3\text{-}O)(\mu\text{-}O_2C_2F_3)_6(OC_4H_8)_2(H_2O)]$. The novel [2Fe2S] complexes are characterized using spectroscopic, electrochemical techniques and X-ray diffraction studies.

© 2009 Elsevier Inc. All rights reserved.

1. Introduction

For some decades, it has been known that [FeFe] hydrogenase can efficiently form dihydrogen from protons. However, the mechanism for H_2 development has not been established and no model complex reported to date shows electrochemical properties like those observed in natural systems. Since the elucidation of the [Fe2S2] cluster as the active site in [FeFe] hydrogenase [1–3], the question has focused on the nature of the S–S linker and on the catalytic pathway of this organometallic active site and is under investigation of many research groups [4–12]. Based on X-ray analyses of the protein, three different kinds of linkers are possible: 1,3-propanethiolate [$(SCH_2)_2CH_2$], azadithiolate [$(SCH_2)_2NR$] and oxadithiolate [$(SCH_2)_2O$] [13,14]. In particular the amino group containing azadithiolate linker is interesting since DFT calculations and cyclic voltammetry measurements of [FeFe] hydrogenase models have shown that the

amino moiety may influence the catalytic mechanism by acting as an initial protonation site [9,15–20].

Subsequently, this proton is directed to the iron centre where it reacts with a hydride bound to the [Fe^IFe^II] core. This species is generated by reaction of a proton with a [Fe^0Fe^I] precursor. However, electrochemical investigations of $[Fe_2\{(SCH_2)_2NR\}(CO)_6]$ model compounds do not show a significant positive shift of the redox potential at which H_2 formation is observed. Apart from the influence of the amino moiety in the S–S linker, the protein layer surrounding of the active site of [FeFe] hydrogenase is also expected to impact on the catalytic mechanism and redox potential of the natural enzyme, especially during the transfer of protons. It is known that the alkylic amino function of the amino acid lysine (K237) is only 440 pm away from the distal iron of the [Fe2S2] cluster and can therefore serve as a possible proton source or relay [2,15]. This raises the question of the existence of a possible proton transfer from lysine or the S–S linker to the [Fe2S2] moiety during the catalytic cycle of [FeFe] hydrogenase. So far only little attention has been devoted towards mimicking the enzymatic environment of the H-cluster. To our best knowledge, only two examples are known in literature containing the naturally occurring amino acid cysteine as ligand for [FeFe] hydrogenase model complexes [21,22].

* Corresponding authors. Tel.: +49 3641 948160; fax: +49 3641 948102 (W. Weigand), tel.: +39 649913626 (G. Lucente).
E-mail addresses: gino.lucente@uniroma1.it (G. Lucente), wolfgang.weigand@uni-jena.de (W. Weigand).

Herein we report about novel [FeFe] hydrogenase model complexes where the Fe···N distance is increased with respect to the value of 345 pm reported by Rauchfuss et al. [23] for complexes of the type [Fe$_2${(SCH$_2$)$_2$NR}(CO)$_6$] to reflect the structural and electrochemical features of lysine (K237). This modification as aimed at investigating, whether the proton relay is established by an assumed azadithiolato linker or a pendant amino moiety of lysine. [Fe2S2] clusters are reported containing 4-amino-1,2-dithiolane and its Boc protected analogue (**1** and **2**) [24], Boc-Adt-OMe (Adt = 4-amino-1,2-dithiolane-4-carboxylic acid) (**3**) [25] and Boc-Adp *tert*-butyl ester (Adp = (*S*)-2-amino-3-(1,2-dithiolan-4-yl)propionic acid) (**4**) [26] (Scheme 1). The structural and catalytic properties of the compounds were investigated by spectroscopic, X-ray diffraction and electrochemical studies.

2. Experimental

2.1. Materials and methods

Toluene and THF were dried over KOH and distilled from sodium/benzophenone. Chemicals were received from Fluka or Acros and used without further purification. 4-Amino-1,2-dithiolane hydrochloride (**1**·HCl) [24], Boc-Adt-OMe (**3**) [25] and Boc-Adp *tert*-butyl ester (**4**) [26] were synthesized following literature procedures. All reactions were carried out under an argon atmosphere. Thin layer chromatography (TLC) was performed on Merck silica gel 60 F$_{254}$ plates (detection under UV light at 254 nm) and FC (flash chromatography) on Fluka silica gel 60. ^{1}H NMR and ^{13}C{^{1}H} NMR spectra were recorded on a Bruker AVANCE 200 MHz or 400 MHz spectrometer, whereby the splitting of proton resonances are defined s (singlet), d (doublet) and m (multiplet). Infrared spectra were obtained from KBr pellets with a Perkin–Elmer 2000 FT-IR instrument. The intensity of the signals is assigned as vs (very strong), s (strong), m (medium) and w (weak). EPR spectra were recorded on a Bruker ESP 300E EPR-spectrometer. Electron impact mass spectrometry was carried out at 70 eV with a Finnigan SSQ710 using desorption electron ionisation (DEI) mode. Expected and experimental isotope distributions were compared.
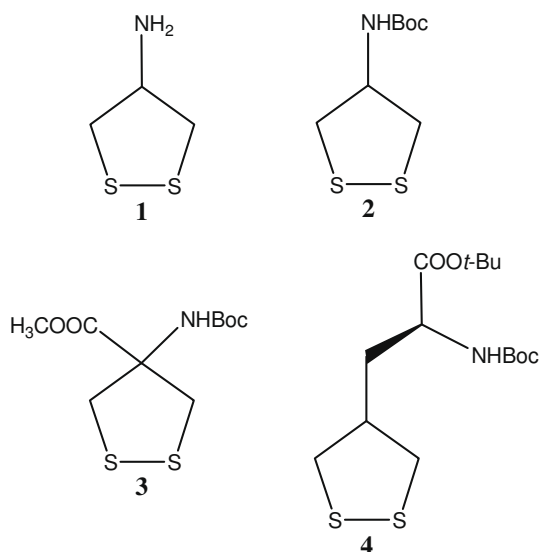
Scheme 1. Ligand molecules for mimicking of lysine (K237) in the [FeFe] hydrogenase.

2.2. Synthesis of ligands and complexes

2.2.1. tert-Butyl 1,2-dithiolan-4-yl carbamate (2)

4-Amino-1,2-dithiolane hydrochloride (527 mg, 3.36 mmol) was suspended in THF (10 mL) and di-*tert*-butyl dicarbonate (879 mg, 4.03 mmol), dissolved in THF (20 mL) and pyridine (20 mL), was slowly added at 0 °C. After 1 h at 0 °C the solution was stirred at room temperature for additional 24 h, followed by the addition of 10 mL water. The solution was extracted with dichloromethane and the combined organic phases were separated, dried with sodium sulphate, evaporated to dryness and recrystallized from dichloromethane/pentane (1:10). Yield: 310 mg (42%) as a pale yellow solid. Anal. calcd. for C$_8$H$_{15}$O$_2$S$_2$N·0.3 THF: C, 45.48%; H, 7.22%; N, 5.76% S, 26.39%. Found: C, 45.7%; H, 7.1%; N, 5.8%; S, 26.8%. ^{1}H NMR (CDCl$_3$, 200 MHz): δ 4.94 (m, 2H, N*H* and C*H*), 3.24–3.05 (m, 4H, C*H$_2$*), 1.43 (s, 9H, C*H$_3$*). ^{13}C NMR (CDCl$_3$, 100 MHz): δ 56.4 (*C*H$_2$CHCH$_2$), 44.9 (CH$_2$*C*HCH$_2$), 28.3 (C(*C*H$_3$)$_3$). MS (DEI): *m/z* 221, [M]$^+$, 166 [M−*t*Bu]$^+$. IR spectrum in KBr, cm^{-1} (selected bands): 3355 (s), 2925 (s), 2854 (m), 1679 (vs), 1523 (s), 1368 (s), 1168 (s).

2.2.2. [{(μ-SCH$_2$)$_2$CHNHBoc}Fe$_2$(CO)$_6$] (5)

tert-Butyl 1,2-dithiolan-4-yl carbamate (**2**) (25 mg, 0.11 mmol) and Fe$_3$(CO)$_{12}$ (57 mg, 0.11 mmol) were dissolved in THF (30 mL) and refluxed for 1 h. After removing the solvent under reduced pressure, the crude product was purified by FC (diethylether/hexane = 1:1). Yield: 31 mg (55%, R_f = 0.3) as a red powder. Anal. calcd. for C$_{14}$H$_{15}$Fe$_2$O$_8$S$_2$N·0.1THF: C, 34.03%; H, 3.13%; N, 2.76% S, 12.62%. Found: C, 34.4%; H, 2.7%; N, 2.6%; S, 11.9%. ^{1}H NMR (CDCl$_3$, 200 MHz): δ 4.49 (m, 1H, N*H*), 3.09 (m, 1H, C*H*), 2.74 (d, ^2J = 11 Hz, 2H, 2 × CH$_A$*H$_B$*), 1.39 (m, 11H, C*H$_3$* and 2 × C*H$_A$*H$_B$). ^{13}C NMR (CDCl$_3$, 50 MHz): δ 207.3 (C≡O), 153.7 (*C*(O)O), 80.4 (C(*C*H$_3$)$_3$), 53.0 (CH$_2$*C*HCH$_2$), 29.7 (*C*H$_2$CHCH$_2$), 28.2 (C(*C*H$_3$)$_3$). MS (DEI): 445 [M−2CO]$^+$, 417 [M−3CO]$^+$, 389 [M−4CO]$^+$, 361 [M−5CO]$^+$, 333 [M−6CO]$^+$. IR spectrum in KBr, cm^{-1} (selected bands): 3442 (s), 2982 (s), 2077 (m), 2077 (vs), 2000 (vs), 1687 (s), 1369 (s), 1166 (s).

2.2.3. [{(μ-SCH$_2$)$_2$C(C(O)OCH$_3$)(NHBoc)}Fe$_2$(CO)$_6$] (6)

Boc-Adt-OMe (**3**) (16.3 mg, 0.06 mmol) and Fe$_3$(CO)$_{12}$ (30 mg, 0.06 mmol) were dissolved in dry toluene (20 mL). The solution was heated at reflux for 30 min followed by the removal of the solvent under reduced pressure. The remaining material was purified by FC (THF/hexane = 1:3). Yield: 30 mg (92%) as a red solid. Anal. calcd. for C$_{16}$H$_{17}$Fe$_2$O$_{10}$S$_2$N·0.8THF: C, 37.39%; H, 3.82%; N, 2.27% S, 10.40%. Found: C, 38.0%; H, 3.4%; N, 2.3%; S, 10.0%. ^{1}H NMR (CDCl$_3$, 200 MHz): δ 4.47 (s, 1H, N*H*), 3.67 (s, 3H, OC*H$_3$*), 2.94 (d, ^2J = 13.6 Hz, 2H, 2 × CH$_A$*H$_B$*), 2.27 (d, ^2J = 14.4 Hz, 2H, 2 × C*H$_A$*H$_B$), 1.40 (s, 9H, C(C*H$_3$*)$_3$). ^{13}C NMR (CDCl$_3$, 50 MHz): δ 207.2/206.8 (C≡O), 171.7 (*C*(O)OCH$_3$), 154.4 (NH*C*(O)), 81.1 (*C*(CH$_3$)$_3$), 61.2 (CH$_2$*C*CH$_2$), 53.3 (O*C*H$_3$), 28.1 (C(*C*H$_3$)$_3$), 27.1 (*C*H$_2$CCH$_2$). MS (DEI): 503 [M−2CO]$^+$, 475 [M−3CO]$^+$, 447 [M−4CO]$^+$, 419 [M−5CO]$^+$, 391 [M−6CO]$^+$. IR spectrum in KBr, cm^{-1} (selected bands): 3442 (s), 2929 (m), 2076 (vs), 2038 (vs), 2000 (vs), 1709 (s).

2.2.4. [{(μ-SCH$_2$)$_2$CCH$_2$C(C(O)Ot-Bu)(NHBoc)}Fe$_2$(CO)$_6$] (7)

Boc-Adp *tert*-butyl ester (**4**) (33 mg, 0.09 mmol) and Fe$_3$(CO)$_{12}$ (48 mg, 0.09 mmol) were dissolved in dry toluene (20 mL) and refluxed for 2 h. After evaporation of the solvent under reduced pressure the crude product was purified via FC (ethyl acetate/hexane = 1:2). Yield: 35 mg (63%, R_f = 0.7) as an orange powder. Anal. calcd. for C$_{21}$H$_{27}$Fe$_2$O$_{10}$S$_2$N·THF: C, 42.81%; H, 5.03%; N, 2.00% S, 9.14%. Found: C, 43.0%; H, 5.2%; N, 2.1%; S, 9.9%. Although the analyses data for "S" are somewhat unsatisfactory, the MS (DEI) results and other spectroscopic analysis data are consistent

with the formula. ^{1}H NMR (CDCl$_3$, 200 MHz): δ 4.92 (d, ^{3}J = 7.4 Hz, 1H, N*H*), 4.09 (m, 1H, C*H*C(O)O), 2.83 (d, ^{2}J = 8.8 Hz, 2H, 2 × SC*H*$_A$H$_B$), 2.55 (d, ^{2}J = 9.2 Hz, 2H, 2 × SCH$_A$*H*$_B$), 1.43 (m, 21H, C(C*H*$_3$)$_3$, CHC*H*$_2$CH and C*H*). ^{13}C NMR (CDCl$_3$, 50 MHz): δ 207.7/207.5 (*C*≡O), 171.3 (*C*(O)OC(CH$_3$)$_3$), 155.4 (NH*C*(O)), 82.6 (C(O)O*C*(CH$_3$)$_3$), 80.2 (NHC(O)O*C*(CH$_3$)$_3$), 50.9 (*C*HC(O)O), 39.9 (*C*HCH$_2$CH), 29.7/27.1 (*C*H$_2$CHCH$_2$), 28.2 (C(O)OC(*C*H$_3$)$_3$), 28.1 (NHC(O)OC(*C*H$_3$)$_3$). MS (DEI): 629 [M]$^+$, 573 [M−*t*Bu]$^+$, 545 [M−*t*Bu-CO]$^+$, 517 [M−*t*Bu-2CO]$^+$, 489 [M−*t*Bu-3CO]$^+$, 461 [M−*t*Bu−4CO]$^+$. IR spectrum in KBr, cm^{-1} (selected bands): 3432 (s), 2980 (m), 2930 (m), 2074 (vs), 2034 (vs), 1995 (vs), 1715 (s, broad).

2.2.5. [Fe$_3$(μ^3-O)(μ-O$_2$C$_2$F$_3$)$_6$(OC$_4$H$_8$)$_2$(H$_2$O)] (8)

2.2.5.1. Method A.
Under an argon atmosphere **5** (34 mg, 0.07 mmol) was dissolved in trifluoroacetic acid (0.1 mL) and dichloromethane (10 mL). The solution was stirred at room temperature for 24 h and the dichloromethane was removed under reduced pressure. The residue was redissolved in THF under atmospheric conditions. After filtration, the solution was treated with pentane, whereupon dark red crystals were obtained after two days. Yield: 12 mg (17%).

2.2.5.2. Method B.
Fe$_3$(CO)$_{12}$ (50 mg, 0.10 mmol) was dissolved in dichloromethane (20 mL) resulting in a dark green solution. Under an argon atmosphere, trifluoroacetic acid (0.1 mL) was added and the solution was refluxed at 40 °C for 4 h, followed by addition of THF (5 mL). The solution was allowed to evaporate at atmospheric conditions, whereby the colour turned into red and red crystals appeared. The crystals were filtered off and washed with hexane. Yield: 21 mg (20%). Anal. calcd. for C$_{20}$H$_{18}$Fe$_3$O$_{16}$F$_{18}$: C, 23.46%; H, 1.77%. Found: C, 23.74%; H, 2.55%. Despite the somewhat unsatisfactory analysis data for "H", the MS (DEI) results and other spectroscopic analysis data reasonably support the formula. MS (DEI): 1006 [M−H$_2$O]$^+$, 934 [M−H$_2$O−THF]$^+$, 862 [M−H$_2$O−2THF]$^+$, 749

[M−H$_2$O−2THF−TFA]$^+$. IR spectrum in KBr, cm^{-1} (selected bands): 3417 (s, br), 2980 (m), 1696 (s), 1469 (m), 1204 (vs), 1161 (s), 855 (m), 795 (m), 728 (s).

2.3. Electrochemistry

Cyclic voltammograms were measured in a three-electrode cell using a 2.0 mm-diameter glassy carbon disc working electrode, a platinum auxiliary electrode, and a Ag|Ag$^+$ reference electrode containing 0.01 M AgNO$_3$ and 0.1 M [*n*-Bu$_4$N][BF$_4$]. Measurements were performed at room temperature in 0.10 M [*n*-Bu$_4$N][BF$_4$]/CH$_3$CN solution using an EG & G PARC 273A potentiostat/galvanostat. Deaeration of solutions was accomplished by passing a stream of argon through the solution for 5 min prior to the measurement and then maintaining a blanket atmosphere of argon over the solution during the measurement. To control the stability of the reference electrode ferrocene was used as an internal standard ($E_{½}$ = +0.087 vs. 0.01 M AgNO$_3$ and 0.1 M [*n*-Bu$_4$N][BF$_4$] in CH$_3$CN) [27,28].

2.4. Structure determinations

The intensity data for the compounds were collected on a Nonius Kappa CCD diffractometer using graphite-monochromated Mo K$_\alpha$ radiation. Data were corrected for Lorentz and polarization effects but not for absorption effects [29,30]. Crystallographic data as well as structure solution and refinement details are summarized in Table 1.

The structures were solved by direct methods (SHELXS) [31] and refined by full-matrix least squares techniques against F_o^2 (SHELXL-97) [32]. All hydrogen atom positions were included at calculated positions with fixed thermal parameters. All non-hydrogen atoms were refined anisotropically [32]. XP (SIEMENS Analytical X-ray Instruments, Inc.) was used for structure representations.

3. Results and discussion

3.1. Synthesis and characterization of the metal complexes

During the treatment of 4-amino-1,2-dithiolane hydrochloride (**1**·HCl) with Fe$_3$(CO)$_{12}$ in boiling toluene the colour of the solution changed from dark green to deep red, but all attempts to isolate a type [Fe2S2] complex were unsuccessful. In every case only a non-soluble dark brown precipitate was obtained, suggesting decomposition of the product. One possible explanation for the decomposition is the presence of the free amino group, as the amino-function itself is able to coordinate to iron [33,34] and may form an instable assembly under these conditions. Accordingly, the ligand was protected (**2**) using di-*tert*-butyl dicarbonate [(Boc)$_2$O] (Scheme 1) [35]. This protection should provide a fast and clean cleavage using trifluoroacetic acid, without reactions to the [Fe2S2] core [36]. Reaction of **2** with Fe$_3$(CO)$_{12}$ in boiling THF afforded complex **5** as a red powder in 55% yield (Scheme 2).

The ^{1}H NMR spectrum of **5** recorded in CDCl$_3$ solution showed one multiplet at 4.49 ppm for the NH proton and another one at 3.09 ppm for the CH proton. HSQC (heteronuclear single quantum coherence) and $^{1}H,^{1}H$-COSY (correlation spectroscopy) experiments revealed two signals for the methylene protons at 2.74 and 1.39 ppm, whereas the latter is overlapped by a singlet of the methyl group protons. The DEI mass spectrum of complex **5** showed a peak at m/z 445 due to [M−2CO]$^+$, followed by stepwise fragmentation of further four C≡O groups. By diffusion of pentane into a solution of **5** in chloroform, single crystals suitable for X-ray diffraction studies were obtained (Fig. 1). Compound **5** comprises

Table 1
Crystal data and refinement details for the X-ray structure determinations.

Compound	5	6	8
Formula	C$_{14}$H$_{15}$Fe$_2$NO$_8$S$_2$	C$_{16}$H$_{17}$Fe$_2$NO$_{10}$S$_2$	C$_{20}$H$_{18}$F$_{18}$Fe$_3$O$_{16}$
fw (g mol^{-1})	501.11	559.15	1023.89
T (°C)	−90(2)	−90(2)	−90(2)
Crystal system	Triclinic	Triclinic	Triclinic
Space group	P$\bar{1}$	P$\bar{1}$	P$\bar{1}$
a (Å)	10.9006(4)	8.4548(6)	9.1293(4)
b (Å)	13.2284(4)	11.5208(9)	12.8614(5)
c (Å)	15.2868(4)	12.9106(7)	16.4181(7)
α (°)	89.385(2)	116.146(4)	95.750(2)
β (°)	80.205(2)	90.334(4)	106.064(2)
γ (°)	70.539(2)	99.919(3)	99.322(3)
V (Å^3)	2045.58(11)	1107.25(13)	1806.50(13)
Z	4	2	2
ρ (g cm^{-3})	1.627	1.677	1.882
μ (cm^{-1})	16.61	15.5	13.46
Measured data	14626	8050	12998
Data with $I > 2\sigma(I)$	7342	3191	5697
Unique data/R_{int}	9313/0.0254	5002/0.0531	8164/0.0295
wR_2 (all data, on F^2)[a]	0.0717	0.1226	0.2222
R_1 ($I > 2\sigma(I)$)[a]	0.0307	0.0502	0.0792
s[b]	0.926	0.999	1.007
Res. Dens./e Å^{-3}	0.347/−0.321	0.456/−0.520	1.812/−0.882
Absorption method	None	None	None
CCDC no.	720323	720324	720325

[a] Definition of the R indices: $R_1 = (\sum \|F_o| - |F_c\|)/\sum |F_o|$ $wR_2 = \left\{ \sum \left[w\left(F_o^2 - F_c^2\right)^2 \right] \Big/ \sum \left[w\left(F_o^2\right)^2 \right] \right\}^{1/2}$ with $w^{-1} = \sigma^2(F_o^2) + (aP)^2$.

[b] $s = \left\{ \sum \left[w\left(F_o^2 - F_c^2\right)^2 \right] \Big/ (N_o - N_p) \right\}^{1/2}$.
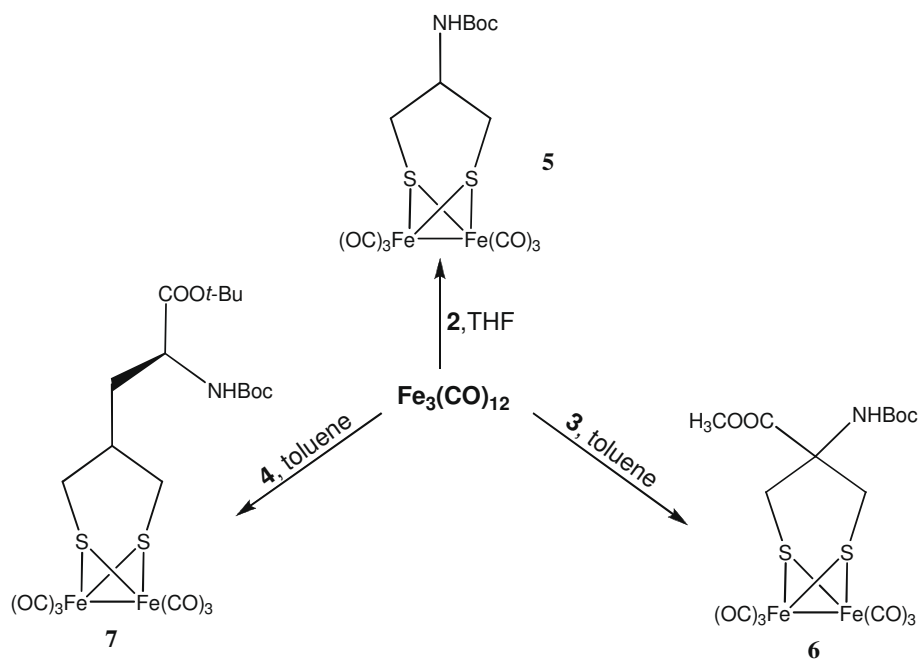
Scheme 2. Novel [FeFe] hydrogenase model complexes.
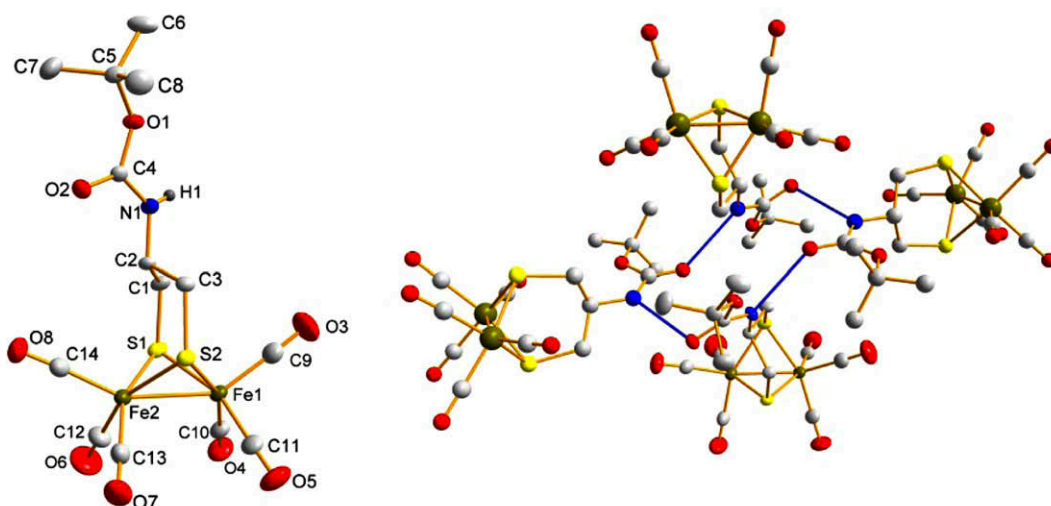
Fig. 1. (Left) One of two independent molecules of **5** with thermal ellipsoids set at the 50% probability level. (Right) Hydrogen bonds between the independent molecules of **5**.

two crystallographically independent molecules, differing in axial and equatorial assembly of the *tert*-butyloxycarbonyl group. As expected each iron centre suggests octahedral geometry and is coordinated by three carbonyl groups, two bridging sulphurs and one

Table 2
Selected bond distances and angles for compound **5**.

Bond lengths (pm)			
Fe(1)–Fe(2)	250.48(4)	S(2)–C(3)	182.5(2)
Fe(1)–S(1)	225.18(7)	C(1)–C(2)	152.0(3)
Fe(1)–S(2)	226.50(6)	C(2)–C(3)	151.6(3)
S(1)–C(1)	182.9(2)	C(2)–N(1)	146.5(3)
Bond angles (°)			
S(1)–Fe(1)–S(2)	85.25(2)	S(2)–C(3)–C(2)	114.97(15)
S(1)–Fe(2)–S(2)	85.47(2)	C(1)–C(2)–C(3)	112.9(2)
S(1)–C(1)–C(2)	117.03(16)	N(1)–C(2)–C(1)	108.17(19)

iron centre. The Fe–Fe distance is 250.48(4) pm (Table 2). The Fe···N distance is 492 pm, whereas the amine function occupies an Fe(2)–C(2)–N(1) angle of 172.14° and is therefore not directed towards the iron core.

The two crystallographically independent molecules form intermolecular hydrogen bonds so that four molecules are arranged in a ring shaped assembly (Fig. 1). The intermolecular hydrogen bonds are of the type N(1)–H(1)···O(2) with two different distances between N(1)···O(2) of 302 and 289 pm. Stirring complex **5** and trifluoroacetic acid in 2-, 10- and 80-fold excess in dichloromethane should lead to deprotection of the *tert*-butyloxycarbonyl group providing the amine complex, as described by Sun et al. [36] However, the expected complex was not obtained. Treatment with hydrochloric acid or thionylchloride also did not result in deprotection. In every case no conversion of the starting complex was observable by TLC over a 5 day period. Using trifluoroacetic acid in
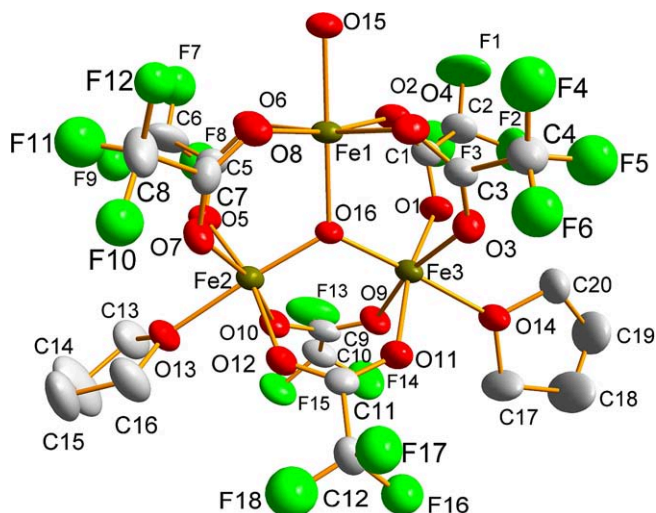
Fig. 2. Reaction product **8** of compound **5** and trifluoroacetic acid under air (thermal ellipsoids set at 50% probability level).

THF under atmospheric conditions resulted in a large amount of starting material and a small amount of a dark red solid. ^{1}H NMR and ^{13}C NMR spectra of the dark red solid show no signals in CDCl$_3$, but DEI mass spectrometry provides a signal at m/z 1006. Via single crystal X-ray analysis the structure was determined to be a trinuclear iron complex (**8**, Fig. 2 and Scheme 3), with a (Fe^{III})$_2$Fe^{II} core in analogy to Fe$_3$(μ^3-O)(Cl$_3$CC(O)O)$_6$(DMF)(THF)$_2$ [37]. The three iron atoms exhibit an octahedral coordination sphere and are connected jointly by two bridging trifluoroacetates and one μ^3-bridged O^{2-} atom. In addition, a two iron(III) ions are coordinated by a THF molecule, whereas the iron(II) ion is coordinated by a water molecule. The three iron atoms and the μ^3-bridged O^{2-} form a trigonal planar coordination sphere, with a Fe–O distance of 186.4(4) and 186.2(4) pm for the two iron(III) atoms bearing the THF ligands and an increased distance of 202.4(4) pm for the iron(II) coordinated to the water molecule.

Further investigations with EPR spectroscopy showed an axial signal with two g-values of 2.217 and 2.0063 indicating an iron(III) low spin configuration. The origin of the μ^3-oxygen atom was unexpected and therefore Fe$_3$(CO)$_{12}$ was treated with trifluoroacetic acid in THF/dichloromethane under an argon atmosphere. No reaction could be observed. Interestingly, compound **8** is obtained only in the presence of air. We suggest that the μ^3-oxygen atom comes from atmospheric molecular oxygen, which is in agreement with results found by Zacchini and co-workers for the compound

Fe$_3$(μ^3-O)(Cl$_3$CC(O)O)$_6$(DMF)(THF)$_2$ [37]. In contrast to the literature reports the iron(III) or iron(II) starting species was a low valence iron species (Fe^{I}Fe^I or all-Fe^0) [38,39].

Compound **6** was obtained as red solid in 92% yield by reaction of Boc-Adt-OMe (**3**) and Fe$_3$(CO)$_{12}$ in dry toluene. The ^{1}H NMR spectrum of compound **6** shows a singlet at 4.47 ppm for the amide function and at 3.67 ppm for the methoxy group, two doublets in the region of 2.97–2.23 ppm for the diastereotopic methylene protons and a singlet at 1.40 ppm for the methyl protons of the *tert*-butyl group. The ^{13}C NMR spectrum and the DEI mass spectrum with a peak at m/z 503, attributed to [M−2CO]$^+$ and additional peaks due to the stepwise loss of four C≡O groups further confirm the proposed structure to complex **6**. Single crystals suitable for structure determination were obtained by slow evaporation of a concentrated solution of compound **6** in toluene at 4 °C. The molecular structure is shown in Fig. 3 and selected bond distances and angles in Table 3.

As anticipated, the Boc-protected amino function of **6** reveals an endo position (Fig. 3) to the [Fe2S2] core and not the ester group. The distance N(1)···Fe(2) is 357.93 pm and should allow interaction of an iron bonded hydride with the amide function during electrocatalysis. The molecules are arranged as dimers caused by two intermolecular hydrogen bonds of the type N(1)–H(1)···O(3) with an N(1)···O(3) distance of 294.8 pm.

An additional methylene group between the dithiolane ring and the α-carbon of the amino acid part (see Scheme 1, compound **4**) should lead to a more increased distance between the amine group and the iron core. Therefore, Boc-Adp *tert*-butyl ester (**4**) was used for reaction with Fe$_3$(CO)$_{12}$ resulting in compound **7** in 63% yield. The ^{1}H NMR spectrum of compound **7** showed a doublet at 4.92 ppm assigned to the amide proton resonance and a multiplet at 4.09 ppm for the α-carbon proton of the amino acid moiety. Two doublets in the area 2.85–2.52 ppm display the resonances for the diastereotopic methylene protons and a multiplet, overlapped by a singlet, was observed at 1.42 ppm and was assigned to the *tert*-butyl group, the β-CH$_2$ and the γ-CH protons, which is in agreement with the ^{1}H,^{1}H-COSY and HSQC spectra. Additionally, the mass spectrum of **7** shows a peak at m/z 629, which can be assigned to the [M]$^+$ molecular ion. Attempts to grow X-ray quality crystals always resulted in an amorphous powder.

3.2. Electrochemistry

The electrochemical properties of complexes **5**–**7** were investigated using cyclic voltammetry to determine their capacity to act as a catalyst for dihydrogen development and to obtain evidence for a possible proton relay between the amine based NH-function
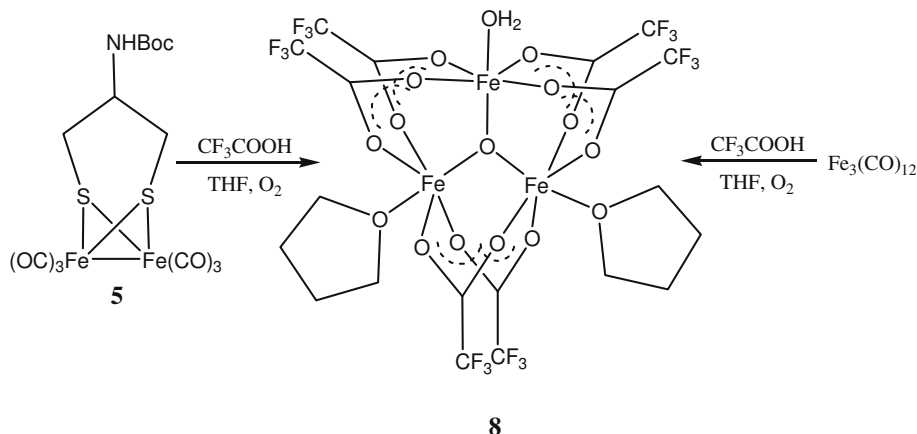
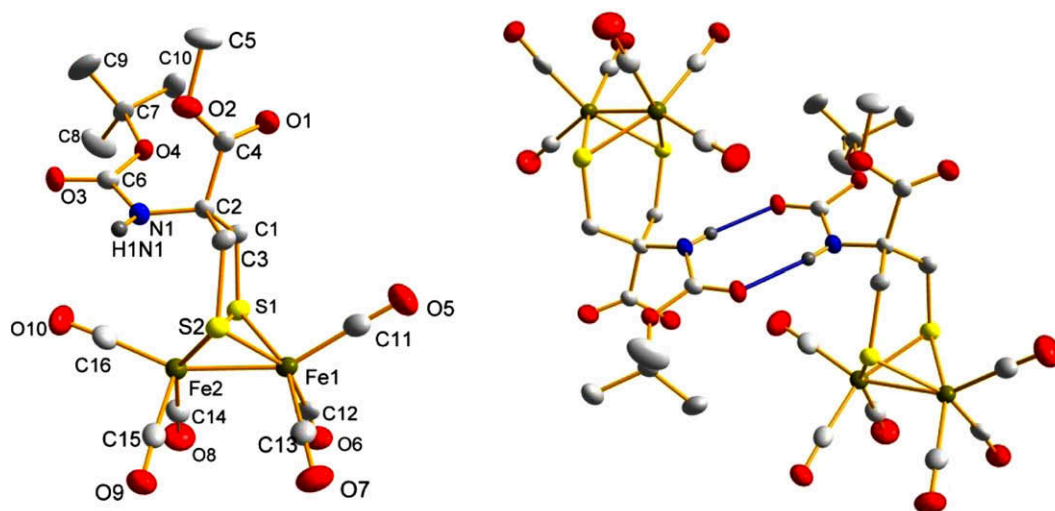**Scheme 3.** Reaction pathways to synthesize compound **8**.

Fig. 3. Molecular structure of compound **6** (left) and its intermolecular hydrogen bonding interactions (right) (thermal ellipsoids set at 50% probability level).

Table 3
Selected bond distances and angles for compound **6**.

Bond lengths (pm)			
Fe(1)–Fe(2)	249.86(8)	S(2)–C(3)	182.4(4)
Fe(1)–S(1)	225.96(12)	C(1)–C(2)	153.1(5)
Fe(1)–S(2)	225.63(11)	C(2)–C(3)	153.0(5)
S(1)–C(1)	181.8(4)	C(2)–N(1)	146.1(5)
Bond angles (°)			
S(1)–Fe(1)–S(2)	84.12(4)	S(2)–C(3)–C(2)	119.1(3)
S(1)–Fe(2)– S(2)	84.06(4)	C(1)–C(2)–C(3)	113.0(3)
S(1)–C(1)–C(2)	120.4(3)	N(1)–C(2)–C(1)	112.7(3)

and the distal iron. Following a cathodic scan of **5** (Fig. 4) starting from +0.3 V vs. 0.01 M Ag/Ag$^+$ in acetonitrile, the cyclic voltammogram showed an nearly irreversible one electron reduction peak at $E_p^{red} = -1.51$ V, which can be assigned to the [Fe^{I}Fe^I] → [Fe^{I}Fe^0] redox process and a further small irreversible reduction at $E_p^{red} = -2.04$ V attributed to the [Fe^{I}Fe^0] → [Fe^{0}Fe^0] process [44]. Reversal of the scan displayed a small irreversible oxidation at −0.53 V and a one electron oxidation at $E_p^{ox} = +0.92$ V. The latter can be ascribed to the [Fe^{I}Fe^I] → [Fe^{I}Fe^{II}] redox process in accordance with the literature (see Fig. 4) [44,40]. The second cycle showed the same signals as the first one, except an additional small irreversible reduction peak at −0.66 V (see Fig. 4). This signal appeared only after the previous oxidation of [Fe^{I}Fe^I] → [Fe^{I}Fe^{II}]. Thus, this signal was assigned as the reduction of an unknown [Fe^{II}-Fe^I] species.

To investigate the electrocatalytical dihydrogen formation properties, cyclic voltammetry was recorded as function of the acetic acid concentration (Fig. 5). In these experiments no shift in the potential of the reduction of [Fe^{I}Fe^I] → [Fe^{I}Fe^0] was observed. This indicates that no protonation occurs at this stage and therefore no proton relay between the amino-function and the distal iron was established, as described in literature [41,42,43]. However, at more negative potentials the current increased dramatically and was in proportion to the amount of acetic acid added, indicating the electrocatalytical formation of dihydrogen (Fig. 5). Thus, the electrochemical pathway can be explained as an ECCE mechanism ([Fe^{I}Fe^I] + e$^-$ → [Fe^{I}Fe^0]$^-$ + H$^+$ → [Fe^{II}Fe^{I}H$^-$] + H$^+$ → [Fe^{II}Fe^I(η^2-H$_2$)]$^+$ + e$^-$ → [Fe^{I}Fe^I] + H$_2$) [40,44]. Since reduction of AcOH is observed at about −2.5 V in
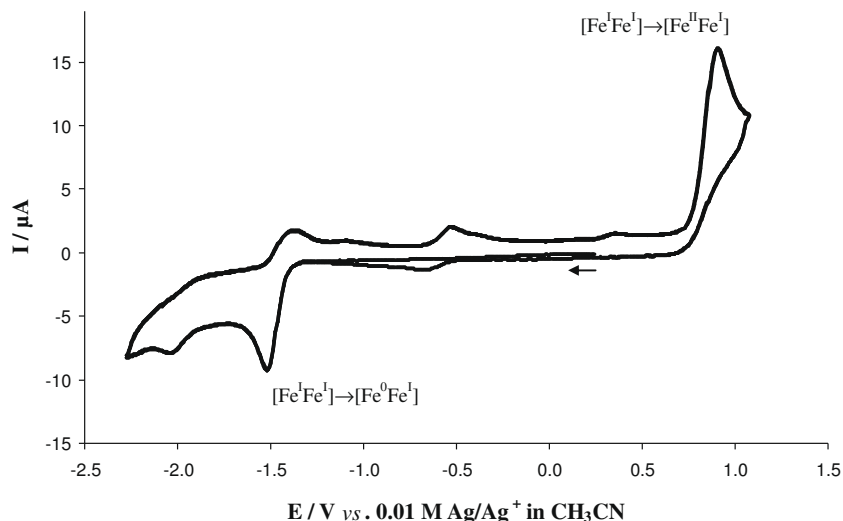
Fig. 4. Cyclic voltammogram of complex **5** in CH$_3$CN solution containing 0.10 M [n-Bu$_4$N][BF$_4$] at a scan rate of 0.10 V s^{-1} using a glassy carbon working electrode.
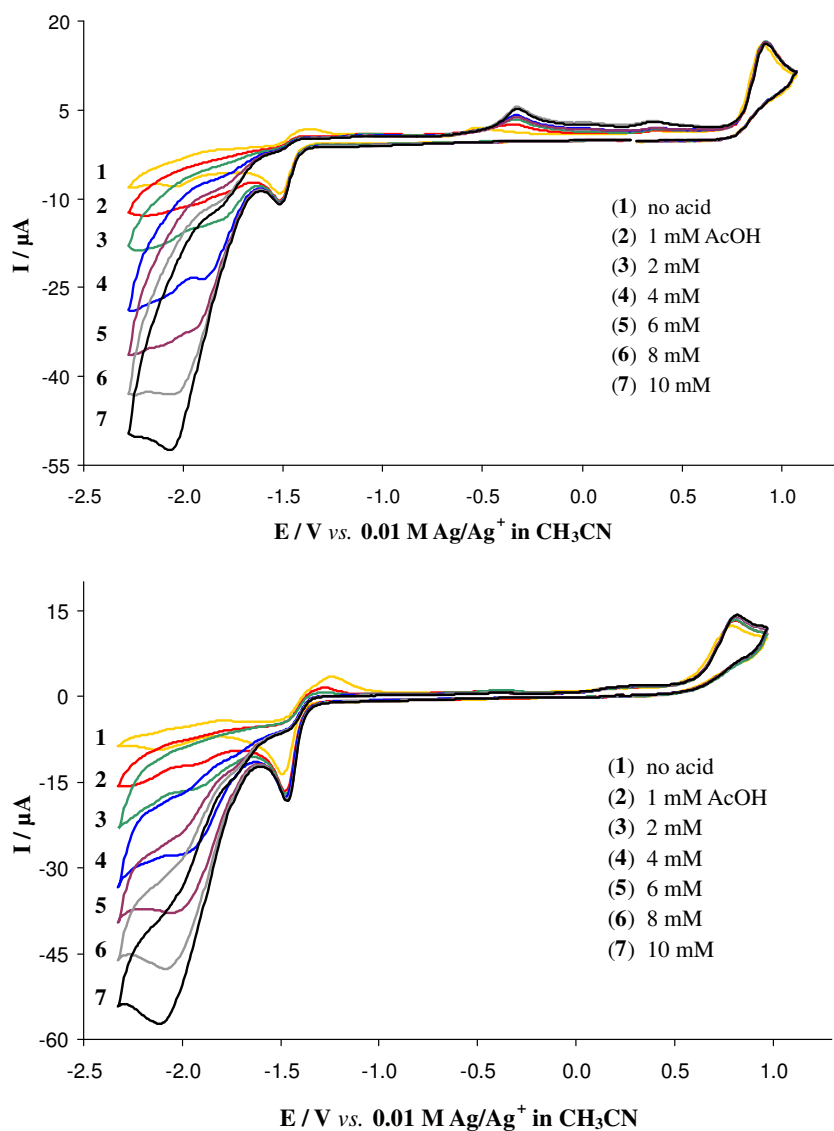
Fig. 5. Cyclic voltammograms (first cycle) of compound **5** (above) and **6** (below) with addition of AcOH (0–10 mmol) in acetonitrile (vs. 0.01 M Ag/Ag$^+$ in CH$_3$CN).
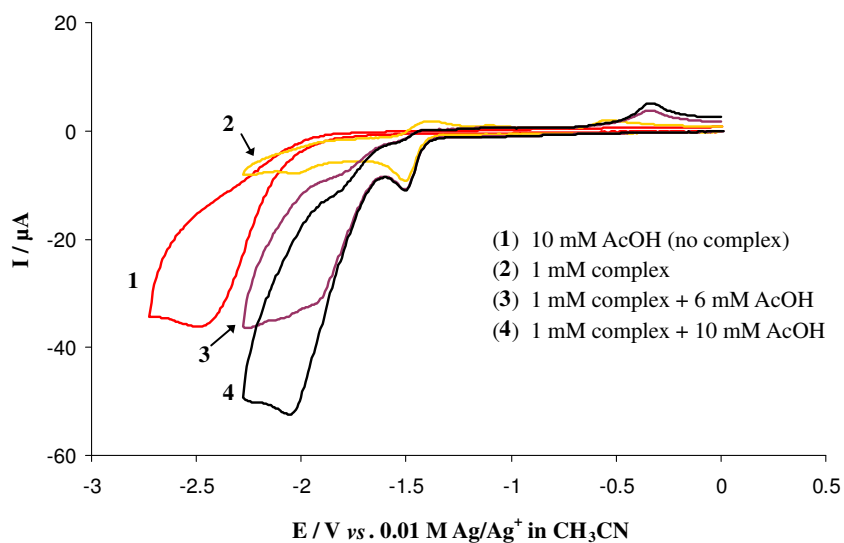
Fig. 6. Comparison of the reduction potential of HOAc alone (1, red) and in the presence of complex **5**. (For interpretation of the references to colour in this figure legend, the reader is referred to the web version of this article.)

Table 4
Electrochemical data[a] of complexes **5**–**7**.

Compound	$E_p/[Fe^IFe^I]/[Fe^0Fe^I]$	$E_p/[Fe^0Fe^I]/[Fe^0Fe^0]$	$E_p/[Fe^IFe^I]/[Fe^{II}Fe^I]$
5	−1.51[b]	−2.04[b]	+0.92[b]
6	−1.47[b]	−2.09[b]	+0.81[b]
7	−1.52 [b]	−2.15	+0.91[b]

[a] Potentials in $V \pm 0.01$ vs. 0.01 M Ag/Ag$^+$ in CH$_3$CN in 0.10 M [n-Bu$_4$N][BF$_4$]/CH$_3$CN.
[b] Irreversible waves.

acetonitrile, the electrocatalysed dihydrogen formation occurs at a potential that is ∼400 mV more positive (Fig. 6).

The cyclic voltammogram of complex **6** in CH$_3$CN exhibits the two irreversible [Fe^{I}Fe^I] → [Fe^{I}Fe^0] and [Fe^{I}Fe^0] → [Fe^{0}Fe^0] redox processes at $E_p^{red} = -1.47$ V and -2.09 V vs. 0.01 M Ag/Ag$^+$, respectively. After reversal of the scan, an oxidation peak at -1.25 V occurred, 220 mV more positive than the original [Fe^{I}Fe^I] → [Fe^{I}Fe^0] reduction potential, suggesting that this signal is not the simple re-oxidation of [Fe^{I}Fe^0] but more than likely the result of a previous chemical reaction. A possible explanation of this signal is the oxidation of a rapidly generated thermodynamically stable [Fe^{I}Fe^0] complex with either a bridging C≡O ligand [45] or the rotation of an iron center [42,46,47]. The only other signal observed is the oxidation [Fe^{I}Fe^I] → [Fe^{I}Fe^{II}] process, which takes place at +0.81 V. Upon addition of AcOH, similar to complex **5**, no shift in the reduction signal of [Fe^{I}Fe^I], but the disappearance of the oxidation signal at -1.25 V was observed. A continuous increase of the peak current after addition of AcOH at -2.1 V suggests catalytical dihydrogen development for complex **6** (Fig. 5).

The cyclic voltammogram of compound **7** exhibits similar redox processes as compound **6** (Table 4), with the exception that the first reduction of [Fe^{I}Fe^I] → [Fe^{I}Fe^0] is quasi-reversible with a peak-to-peak separation of 100 mV and a E_p^{red} potential of -1.52 V (Fig. S1). Upon addition of AcOH, compound **7** exhibits the same properties as discussed above for compounds **5** and **6** (Fig. S2).

4. Conclusions

Starting from the disulphides **2**–**4** and Fe$_3$(CO)$_{12}$, three novel [FeFe] hydrogenase model complexes were synthesized. The structural properties of complexes **5**–**7** reveal the basic [Fe2S2] subunit and a variable NH···Fe distance. In contrast to [Fe$_2${(S-CH$_2$)$_2$NR}(CO)$_6$], the NH···Fe distance is increased and therefore the complexes **5**–**7** can serve as structural models for the adjacent lysine (K237). Investigation of the electrochemical properties of compounds **5**–**7** showed catalytic H$_2$ development. Although structural features of an adjacent lysine in [FeFe] hydrogenase are present, the weak acid, HOAc, was not strong enough to protonate the amide NH-function and to establish a proton relay. Attempts to increase the basicity of the nitrogen atoms failed as the free amine was not accessible. Trials to generate complexes with a free NH$_2$ group, by treatment of the free amines with Fe$_3$(CO)$_{12}$, only lead to decomposition products. Likewise the deprotection of the *tert*-butyloxycarbonyl groups in complexes **5**–**7** via treatment with trifluoroacetic acid, hydrogen chloride or thionylchloride treatment failed. In case of compound **5**, it was possible to isolate and characterize the decomposition product. It was found that a trinuclear Fe(III)/(II) complex was formed with a μ^3-oxo ligand. Further experiments with Fe$_3$(CO)$_{12}$ and trifluoroacetic acid under atmospheric conditions suggest an activation of dioxygen.

However, these experiments do not provide sufficient indices towards an adjacent lysine mechanism, it is important to continue the experiments to form a free amino group with an increased Fe···N distance, as discussed above, and to compare these results with those found for [Fe$_2${(SCH$_2$)$_2$NR}(CO)$_6$] complexes.

5. Abbreviations

Adt	4-amino-1,2-dithiolane-4-carboxylic acid
Adp	(S)-2-amino-3-(1,2-dithiolan-4-yl)propionic acid
Boc	tert-butoxycarbonyl
DEI	desorption electron ionisation
DFT	density functional theory
DMF	dimethylformamide
TFA	trifluoroacetic acid
THF	tetrahydrofurane
TLC	thin layer chromatography
FC	flash chromatography

Appendix A. Supplementary material

Supplementary data associated with this article can be found, in the online version, at doi:10.1016/j.jinorgbio.2009.07.005.

References

[1] Y. Nicolet, B.J. Lemon, J.C. Fontecilla-Camps, J.W. Peters, Trends Biochem. Sci. 25 (2000) 138–143.
[2] Y. Nicolet, C. Piras, P. Legrand, E.C. Hatchikian, J.C. Fontecilla-Camps, Structure 7 (1999) 13–23.
[3] J.W. Peters, W.N. Lanzilotta, B.J. Lemon, L.C. Seefeldt, Science 282 (1998) 1853–1858.
[4] E.J. Lyon, I.P. Georgakaki, J.H. Reibenspies, M.Y. Darensbourg, Angew. Chem. Int. Ed. 38 (1999) 3178–3180.
[5] A. Le Cloirec, S.P. Best, S. Borg, S.C. Davies, D.J. Evans, D.L. Hughes, C.J. Pickett, Chem. Commun. (1999) 2285–2286.
[6] U.-P. Apfel, Y. Halpin, M. Gottschaldt, H. Görls, J.G. Vos, W. Weigand, Eur. J. Inorg. Chem. 33 (2008) 5112–5118.
[7] J. Windhager, H. Gorls, H. Petzold, G. Mloston, G. Linti, W. Weigand, Eur. J. Inorg. Chem. (2007) 4462–4471.
[8] U.-P. Apfel, Y. Halpin, H. Görls, J.G. Vos, B. Schweizer, G. Linti, W. Weigand, Chem. Biodivers. (2007) 2138–2147.
[9] B.E. Barton, T.B. Rauchfuss, Inorg. Chem. 47 (2008) 2261–2263.
[10] L.-C. Song, Z.-Y. Yang, H.-Z. Bian, Q.-M. Hu, Organometallics 23 (2004) 3082–3084.
[11] J. Windhager, M. Rudolph, S. Bräutigam, H. Görls, W. Weigand, Eur. J. Inorg. Chem. (2007) 2748–2760.
[12] L.-C. Song, Z.Y. Yang, Y.J. Hua, H.T. Wang, Y. Liu, Q.-M. Hu, Organometallics 26 (2007) 2106–2110.
[13] Y. Nicolet, A.L. de Lacey, X. Vernde, V.M. Fernandez, E.C. Hatchikian, J.C. Fontecilla-Camps, J. Am. Chem. Soc. 123 (2001) 1596–1601.
[14] J.L. Nehring, D.M. Heinekey, Inorg. Chem. 42 (2003) 4288–4292.
[15] Z.-P. Liu, P. Hu, J. Chem. Phys. 117 (2002) 8177–8180.
[16] J.-H. Fan, M.B. Hall, J. Am. Chem. Soc. 123 (2001) 3828–3829.
[17] T. Liu, M. Wang, Z. Shi, H. Cui, W. Dong, J. Chen, B. Akermark, L. Sun, Chem. Eur. J. 10 (2004) 4474–4479.
[18] Y. Nicolet, C. Cavazza, J.C. Fontecilla-Camps, J. Inorg. Biochem. 91 (2002) 1–8.
[19] P. Li, M. Wang, L. Chen, J. Liu, Z. Zhao, L. Sun, Dalton Trans. (2009) 1919–1926.
[20] S. Ezzaher, J.-F. Capon, F. Gloaguen, F.Y. Pétillon, P. Schollhammer, J. Talarmin, Inorg. Chem. 48 (2009) 2–4.
[21] C. He, M. Wang, X. Zhang, Z. Wang, C. Chen, J. Liu, B. Akermark, L. Sun, Angew. Chem. Int. Ed. 43 (2004) 3571–3574.
[22] X. de Hatten, E. Bothe, K. Merz, I. Huc, N. Metzler-Nolte, Eur. J. Inorg. Chem. (2008) 4530–4537.
[23] J.D. Lawrence, H. Li, T.B. Rauchfuss, M. Benard, M.-M. Rohmer, Angew. Chem. Int. Ed. 40 (2001) 1768–1771.
[24] W. Pham, I. Radhakrishnan, E.J. Sontheimer, Nucleic Acids Res. 32 (2004) 3446–3455.
[25] E. Morera, G. Lucente, G. Ortar, M. Nalli, F. Mazza, E. Gavuzzo, S. Spisani, Bioorg. Med. Chem. 10 (2002) 147–157.

[26] E. Morera, F. Pinnen, G. Lucente, Org. Lett. 4 (2002) 1139–1142.

[27] V.V. Pavlishchuk, A.W. Addison, Inorg. Chim. Acta 298 (2000) 97–102.

[28] D.C. Coomber, D.J. Tucker, A.M. Bond, J. Electroanal. Chem. 426 (1997) 63–73.

[29] COLLECT, Data Collection Software, B.V. Nonius, Netherlands, 1998.

[30] Z. Otwinowski, C.W. Minor, R.M. Sweet, Methods Enzymol. 276 (1997) 207–326.

[31] G.M. Sheldrick, Acta Crystallogr. Sec. A 46 (1990) 467–473.

[32] G.M. Sheldrick, SHELXL-97 (Release 97-2), University of Göttingen, Germany, 1993.

[33] S. Ezzaher, P.-Y. Orain, J.-F. Capon, F. Gloaguen, F.Y. Petillon, T. Roisnel, P. Schollhammer, J. Talarmin, Chem. Commun. (2008) 2547–2549.

[34] A.R. Sadique, W.W. Brennessel, P.L. Holland, Inorg. Chem. 47 (2008) 784–786.

[35] G. Bartoli, M. Bosco, A. Giuliani, T. Mecozzi, L. Sambri, E. Torregiani, E. Marcantoni, J. Org. Chem. 67 (2002) 9111–9114.

[36] S. Salyi, M. Kritikos, B. Akermark, L. Sun, Chem. Eur. J. 9 (2003) 557–560.

[37] F. Marchetti, B. Melai, G. Pampaloni, S. Zacchini, Inorg. Chem. 46 (2007) 3378–3384.

[38] M.K. Johnson, R.D. Cannon, D.B. Powell, Spectrochim. Acta, Part A 38 (1982) 307–315.

[39] M. Yazdanbakhsh, M.H. Alizadeh, H.Z. Khorramdel, W. Frank, Z. Anorg. Allg. Chem. 633 (2007) 1193–1198.

[40] L.-C. Song, H.-T. Wang, J.-H. Ge, S.-Z. Mei, J. Gao, L.-X. Wang, B. Gai, L.-Q. Zhao, J. Yan, Y.-Z. Wang, Organometallics 27 (2008) 1409–1416.

[41] G. Si, W.-G. Wang, H.-Y. Wang, C.-H. Tung, L.-Z. Wu, Inorg. Chem. 47 (2008) 8101–8111.

[42] B.E. Barton, M.T. Olsen, T.B. Rauchfuss, J. Am. Chem. Soc. 130 (2008) 16834–16835.

[43] J.-F. Capon, S. Ezzaher, F. Gloaguen, F.Y. Pétillon, P. Schollhammer, J. Talarmin, Chem. Eur. J. 14 (2008) 1954–1964.

[44] D. Chong, I.P. Georgakaki, R. Mejia-Rodriguez, J. Sanabria-Chinchilla, M.P. Soriaga, M.Y. Darensbourg, Dalton Trans. (2003) 4158–4163.

[45] J.-F. Capon, F. Gloaguen, F.Y. Petillon, P. Schollhammer, J. Talarmin, C.R. Chimie 11 (2008) 842–851.

[46] C.M. Thomas, T. Liu, M.B. Hall, M.Y. Darensbourg, Chem. Commun. (2008) 1563–1565.

[47] M.L. Singleton, B. Bhuvanesh, J.H. Reibenspies, M.Y. Darensbourg, Angew. Chem. Int. Ed. 47 (2008) 9492–9495.

ORGANOMETALLICS

Preparation and Characterization of Homologous Diiron Dithiolato, Diselenato, and Ditellurato Complexes: [FeFe]-Hydrogenase Models

Mohammad K. Harb,[†] Ulf-Peter Apfel,[†] Joachim Kübel,[†] Helmar Görls,[†]
Greg A. N. Felton,[‡] Taka Sakamoto,[‡] Dennis H. Evans,*[‡] Richard S. Glass,*[‡]
Dennis L. Lichtenberger,*[‡] Mohammad El-khateeb,[§] and Wolfgang Weigand*[†]

[†]*Institut für Anorganische und Analytische Chemie, Friedrich-Schiller-Universität Jena, August-Bebel-Strasse 2, 07743 Jena, Germany,* [‡]*Department of Chemistry and Biochemistry, The University of Arizona, Tucson, Arizona 85721, and* [§]*Chemistry Department, Jordan University of Science and Technology, 22110 Irbid, Jordan*

Received July 30, 2009

In order to elucidate the influence of the bridging chalcogen atoms in hydrogenase model complexes, diiron dithiolato, diselenolato, and ditellurolato complexes have been prepared and characterized. Treatment of $Fe_3(CO)_{12}$ with 3,3-bis(thiocyanatomethyl)oxetane (**1**) or a mixture of 2-oxa-6,7-dithiaspiro[3.4]octane (**2a**) and 2-oxa-6,7,8-trithiaspiro[3.5]nonane (**2b**) in toluene at reflux afforded the model compound $Fe_2(\mu\text{-}S_2C_5H_8O)(CO)_6$ (**3**). The analogous diselenolato and ditellurolato complexes, $Fe_2(\mu\text{-}Se_2C_5H_8O)(CO)_6$ (**4**) and $Fe_2(\mu\text{-}Te_2C_5H_8O)(CO)_6$ (**5**), were obtained from the reaction of $Fe_3(CO)_{12}$ with 2-oxa-6,7-diselenaspiro[3.4]octane (**6**) and 2-oxa-6,7-ditelluraspiro-[3.4]octane (**7**), respectively. Compounds **3**−**5** were characterized by spectroscopic techniques (NMR, IR, photoelectron spectroscopy), mass spectrometry, single-crystal X-ray analysis, and computational modeling. The electrochemical properties for the new compounds have been studied to assess their ability to catalyze electrochemical reduction of protons to give dihydrogen, and the catalytic rate is found to decrease on going from the sulfur to selenium to tellurium compounds. In the series **3**−**5** the reorganization energy on going to the corresponding cation decreased from **3** to **4** to **5**. Spectroscopic and computational analysis suggests that the increasing size of the chalcogen atoms from S to Se to Te increases the Fe−Fe distance and decreases the ability of the complex to form the structure with a rotated $Fe(CO)_3$ group that has a bridging carbonyl ligand and a vacant coordination site for protonation. This effect is mirrored on reduction of **3**−**5** in that the rotated structure with a bridging carbonyl, which creates a vacant coordination site for protonation, is disfavored on going from the S to Se to Te complexes.

Introduction

The natural energy resources predominantly used today are diminishing, and their continued use has become more harmful for the environment. Therefore, efforts to develop alternative energy resources and fuels have become major goals for the scientific community. Dihydrogen is one of the future fuels that causes no deleterious products for the environment.[1−5] Efficient production of dihydrogen in good yield has become a challenge, and there has been much research aimed at overcoming this challenge.[6−12] Biomimetic catalysts, shown in Scheme 1a,[13−29] are based on the active site of [FeFe]-hydrogenases[5,30−34] (the identity of X in the enzyme is still unclear).[34−41] Recently, diiron complexes containing diselenolato ligands have been prepared and

---

*Corresponding authors. E-mail: dhevans@email.arizona.edu; rglass@u.arizona.edu; dlichten@email.arizona.edu; c8wewo@uni-jena.de.
(1) Melis, A.; Zhang, L.; Forestier, M.; Ghirardi, M. L.; Seibert, M. *Plant Physiol.* **2000**, *122*, 127.
(2) Cammack, R.; Frey, M.; Robson, R. *Hydrogen as a Fuel: Learning from Nature*; Taylor & Francis: London, 2001.
(3) Woodward, J.; Orr, M.; Cordray, K.; Greenbaum, E. *Nature* **2000**, *405*, 1014.
(4) Coontz, R.; Hanson, B. *Science* **2004**, *305*, 957.
(5) Shima, S.; Pilak, O.; Vogt, S.; Schick, M.; Stagni, M. S.; Meyer-Klaucke, W.; Warkentin, E.; Thauer, R. K.; Ermler, U. *Science* **2008**, *321*, 572.
(6) Zhang, Y. H. P.; Evans, B. R.; Mielenz, J. R.; Hopkins, R. C.; Adams, M. W. W. *PLoS ONE* **2007**, *2*, e456.

(7) Antal, M. J.; Allen, S. G.; Schulman, D.; Xu, X.; Divilio, R. J. *Ind. Eng. Chem. Res.* **2000**, *39*, 4040.
(8) Hallenbeck, P. C.; Benemann, J. R. *Int. J. Hydrogen Energy* **2002**, *27*, 1185.
(9) Cortright, R. D.; Davda, R. R.; Dumesic, J. A. *Nature* **2002**, *418*, 964.
(10) Huber, G. W.; Shabaker, J. W.; Dumesic, J. A. *Science* **2003**, *300*, 2075.
(11) Deluga, G. A.; Salge, J. R.; Schmidt, L. D.; Verykios, X. E. *Science* **2004**, *303*, 993.
(12) Adams, M. W. W.; Stiefel, E. I. *Science* **1998**, *282*, 1842.
(13) Zhao, X.; Georgakaki, I. P.; Miller, M. L.; Yarbrough, J. C.; Darensbourg, M. Y. *J. Am. Chem. Soc.* **2001**, *123*, 9710.
(14) Zhao, X.; Chiang, C.; Miller, M. L.; Rampersad, M. V.; Darensbourg, M. Y. *J. Am. Chem. Soc.* **2003**, *125*, 518.
(15) Gloaguen, F.; Lawrence, J. D.; Rauchfuss, T. B. *J. Am. Chem. Soc.* **2001**, *123*, 9476.
(16) Lyon, E. J.; Georgakaki, I. P.; Reibenspies, J. H.; Darensbourg, M. Y. *J. Am. Chem. Soc.* **2001**, *123*, 3268.
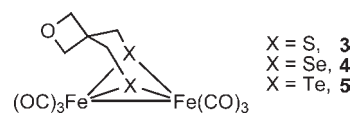
---

a) X = CH₂, O, NH, S

b) X = NPh, CH₂, Se, CHO(Sugar)
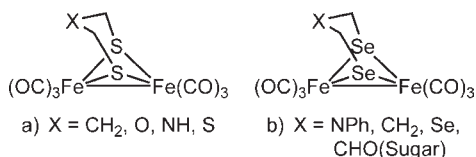
characterized (Scheme 1b), and their ability to catalyze H_2 production from acids was evaluated.[42–45]

Photoelectron spectroscopy and theoretical calculations revealed that the reorganization energy of $Fe_2(\mu$-Se_2-$C_3H_5CH_3)(CO)_6$ is substantially lower than that for analogous complexes with Fe_2S_2 cores.[44] This effect, which may lead to faster electron transfer with complexes containing Fe_2Se_2 rather than Fe_2S_2 cores, has not yet been investigated in detail. On the basis of these observations, we have now

(17) Lawrence, J. D.; Li, H.; Rauchfuss, T. B.; Benard, M.; Rohmer, M. *Angew. Chem., Int. Ed.* **2001**, *40*, 1768.

(18) Razavet, M.; Davies, S. C.; Hughes, D. L.; Barclay, J. E.; Evans, D. J.; Fairhurst, S. A.; Liu, X.; Pickett, C. J. *J. Chem. Soc., Dalton Trans.* **2003**, 586.

(19) Linck, R. C.; Rauchfuss, T. B. In *Synthetic models for bioorganometallic reaction centers*; Bioorganometallics; Wiley-VCH Verlag GmbH & Co.: Weinheim, Germany, 2006; p 403.

(20) Li, H.; Rauchfuss, T. B. *J. Am. Chem. Soc.* **2002**, *124*, 726.

(21) Tard, C.; Liu, X.; Ibrahim, S. K.; Bruschi, M.; De Gioia, L.; Davies, S. C.; Yang, X.; Wang, L.; Sawers, G.; Pickett, C. J. *Nature* **2005**, *433*, 610.

(22) Song, L.-C.; Yang, Z. Y.; Bian, H. Z.; Hu, Q. M. *Organometallics* **2004**, *23*, 3082.

(23) Seyferth, D.; Henderson, R. S.; Song, L.-C. *Organometallics* **1982**, *1*, 125.

(24) Windhager, J.; Rudolph, M.; Bräutigam, S.; Görls, H.; Weigand, W. *Eur. J. Inorg. Chem.* **2007**, 2748.

(25) Windhager, J.; Goerls, H.; Petzold, H.; Mloston, G.; Linti, G.; Weigand, W. *Eur. J. Inorg. Chem.* **2007**, 4462.

(26) Song, L.-C.; Yang, Z. Y.; Bian, H. Z.; Liu, Y.; Wang, H. T.; Liu, X. F.; Hu, Q. M. *Organometallics* **2005**, *24*, 6126.

(27) Tard, C.; Pickett, C. *J. Chem. Rev.* **2009**, *109*, 2245.

(28) Windhager, J.; Seidel, R. A.; Apfel, U.; Görls, H.; Linti, G.; Weigand, W. *Chem. Biodiversity* **2008**, *5*, 2023.

(29) Ott, S.; Kritikos, M.; Åkermark, B.; Sun, L. *Angew. Chem., Int. Ed.* **2003**, *42*, 3285.

(30) Albracht, S. P. J. *Biochim. Biophys. Acta, Bioenerg.* **1994**, *1188*, 167.

(31) Graf, E.; Thauer, R. K. *FEBS Lett.* **1981**, *136*, 165.

(32) Cammack, R.; Patil, D.; Aguirre, R.; Hatchikian, E. C. *FEBS Lett.* **1982**, *142*, 289.

(33) Wang, G.; Benecky, M.; Huynh, B.; Cline, J.; Adams, M.; Mortenson, L.; Hoffman, B.; Munck, E. *J. Biol. Chem.* **1984**, *259*, 14328.

(34) Adams, M. W.; Mortenson, L. E. *J. Biol. Chem.* **1984**, *259*, 7045.

(35) Chen, J.; Mortenson, L. E. *Biochim. Biophys. Acta, Protein Struct.* **1974**, *371*, 283.

(36) Chen, J.; Blanchard, D. K. *Biochim. Biophys. Res. Commun.* **1978**, *84*, 1144.

(37) Glick, B. R.; Martin, W. G.; Martin, S. M. *Can. J. Microbiol.* **1980**, *26*, 1214.

(38) Adams, M. W. W.; Mortenson, L. E. *Biochim. Biophys. Acta, Bioenerg.* **1984**, *766*, 51.

(39) Fauque, G.; Peck, H. D.Jr.; Moura, J. J. G.; Huynh, B. H.; Berlier, Y.; DerVartanian, D. V.; Teixeira, M.; Przybyla, A. E.; Lespinat, P. A. *FEMS Microbiol. Rev.* **1988**, *54*, 299.

(40) Adams, M. W. *Biochim. Biophys. Acta* **1990**, *1020*, 115.

(41) Hatchikian, E. C.; Forget, N.; Fernandez, V. M.; Williams, R.; Cammack, R. *Eur. J. Biochem.* **1992**, *209*, 357.

(42) Gao, S.; Fan, J.; Sun, S.; Peng, X.; Zhao, X.; Hou, J. *Dalton Trans.* **2008**, 2128.

(43) (a) Song, L.-C.; Gai, B.; Wang, H.; Hu, Q. *J. Inorg. Biochem.* **2009**, *103*, 805. (b) Song, L.-C.; Gao, W.; Feng, C.-P.; Wang, D.-F.; Hu, Q.-M. *Organometallics* **2009**, *28*, 6121.

(44) Harb, M. K.; Niksch, T.; Windhager, J.; Görls, H.; Holze, R.; Lockett, L. T.; Okumura, N.; Evans, D. H.; Glass, R. S.; Lichtenberger, D. L.; El-khateeb, M.; Weigand, W. *Organometallics* **2009**, *28*, 1039.

(45) Apfel, U.; Halpin, Y.; Gottschaldt, M.; Görls, H.; Vos, J. G.; Weigand, W. *Eur. J. Inorg. Chem.* **2008**, *2008*, 5112.

X = S, **3**
X = Se, **4**
X = Te, **5**

extended our studies also to the preparation of complexes containing ditellurolato ligands. In the present publication, the preparation of oxetane-containing dithiolato, diselenolato, and ditellurolato diiron complexes is reported (Scheme 2). The ability of these complexes to catalyze the formation of molecular hydrogen from weak acids is presented and compared with related systems. To compare S, Se, and Te analogues, it is important to have the same substitution pattern except for the chalcogen in each complex. This was achieved by synthesizing the homologous series **3–5** shown in Scheme 2. The oxetane ring allows the five-membered ring to which it is attached to be stable for all three 1,2-dichalcogenolanes. These precursors to the desired complexes do not polymerize, as is readily seen with the unsubstituted compounds.

Experimental Section

General Comments. All reactions were carried out under an argon atmosphere with standard Schlenk techniques. THF, toluene, and hexane were dried and distilled prior to use according to standard methods. The ^{1}H, ^{13}C{^{1}H}, ^{77}Se{^{1}H}, and 2D NMR (^{1}H,^{1}H COSY, ^{1}H,^{13}C HSQC, ^{1}H,^{77}Se HMBC) spectra were recorded on either a Bruker AVANCE 200 or 400 MHz spectrometer using the solvent residual peak or a concentrated solution of SeO_2 in D_2O as reference. The ^{77}Se chemical shifts are reported relative to neat Me_2Se [$\delta(Me_2Se) = \delta(SeO_2) + 1302.6$ ppm].[46] The ^{125}Te chemical shift was measured versus external PhTeTePh and converted to that versus Me_2Te.[47] Mass spectra were recorded on a Finnigan MAT SSQ 710 instrument. IR spectra were measured as KBr disks on a Perkin-Elmer System 2000 FT-IR spectrometer and in Nujol on a Thermo Nicolet Avatar ESP 380 FT-IR spectrometer utilizing the OMNIC version 6.1 software. Elemental analyses were performed with a LECO CHNS-932 apparatus. Silica gel 60 (0.015–0.040 mm) was used for column chromatography, and TLC was done using Merck TLC aluminum sheets (silica gel 60 F254). 3,3-Bis(thiocyanatomethyl)oxetane[48] (**1**), a 2-oxa-6,7-dithiaspiro[3.4]octane (**2a**) and 2-oxa-6,7,8-trithiaspiro[3.5]-nonane (**2b**) mixture,[48] 2-oxa-6,7-disellenaspiro[3.4]octane[49] (**6**), and 2-oxa-6,7-ditelluraspiro[3.4]octane[50] (**7**) were prepared according to literature protocols. $Fe_3(CO)_{12}$ purchased from Aldrich, solvents from Fisher Scientific, and other chemicals from Acros were used without further purification. Yield calculations were based on substoichiometric utilized chemicals or on $Fe_3(CO)_{12}$ for the diiron complexes.

Synthesis of $Fe_2(\mu$-$S_2C_5H_8O)(CO)_6$ (3). **Method A.** A solution of $Fe_3(CO)_{12}$ (140 mg, 0.28 mmol) and **1** (56 mg, 0.28 mmol) in toluene (25 mL) was heated under reflux for one hour. The resulting dark red mixture was evaporated to dryness under reduced pressure. The obtained solid was redissolved in a

(46) Burns, R. C.; Collins, M. J.; Gillespie, R. J.; Schrobilgen, G. J. *Inorg. Chem.* **1986**, *25*, 4465.

(47) Granger, P.; Chapelle, S.; McWhinnie, W. R.; Al-Rubaie, A. *J. Organomet. Chem.* **1981**, *220*, 149.

(48) Campbell, T. W. *J. Org. Chem.* **1957**, *22*, 1029.

(49) Günther, W. H.; Salzman, M. N. *Ann. N.Y. Acad. Sci.* **1972**, *192*, 25.

(50) Lakshmikantham, M. V.; Cava, M. P.; Gunther, W. H. H.; Nugara, P. N.; Belmore, K. A.; Atwood, J. L.; Craig, P. *J. Am. Chem. Soc.* **1993**, *115*, 885.

minimum amount of CH_2Cl_2 and column chromatographed. From the major red fraction, which was eluted with THF/hexane (1:3), **3** was obtained as a red solid (56 mg, 47%).

Method B. Twenty-five milligrams of the 2-oxa-6,7-dithiaspiro[3.4]octane and 2-oxa-6,7,8-trithiaspiro[3.5]nonane mixture (**2a** and **2b**) and $Fe_3(CO)_{12}$ (85 mg, 0.169 mmol) were dissolved in 20 mL of toluene and heated under reflux for 1.5 h. Evaporation and column chromatography (THF/hexane, 1:3) gave 36 mg (50%) of the red crystalline product **3**. Anal. Calcd for $C_{11}H_8Fe_2O_7S_2 \cdot 1$hexane: C, 32.34; H, 2.29, S, 14.56. Found: C, 32.27; H, 2.31, S, 14.16. IR $\nu_{C\equiv O}$ cm^{-1}: (KBr disk) 2076 (vs), 2033 (vs), 1997 (vs, sh), (Nujol) 2077 (s), 2036 (vs), 2008 (s), 1993 (s), 1982 (m). ^{1}H NMR (200 MHz, CDCl$_3$): δ 4.28 (s, 4H, (CH$_2$)$_2$O), 2.48 (s, 4H, 2SCH$_2$). ^{1}H NMR (200 MHz, -50 °C, CDCl$_3$): δ 4.28 (s, 4H, (CH$_2$)$_2$O), 3.07 (d, $^2J_{H,H}$ = 8.8 Hz, 2H, SCH_AH$_B$ and SCH_CH$_D$), 1.81 (d, $^2J_{H,H}$ = 8.8 Hz, 2H, SCH$_A$$H_B$ and SCH$_C$$H_D$). ^{13}C NMR (50 MHz, CDCl$_3$): δ 207.1 (CO), 82.2 ((CH$_2$)$_2$O), 42.2 (C$_q$), 30.3 (2SCH$_2$). DEI-MS (*m/z*): 428 (M$^+$), 400 (M$^+$ $-$ CO), 372 (M$^+$ $-$ 2CO), 344 (M$^+$ $-$ 3CO), 316 (M$^+$ $-$ 4CO), 288 (M$^+$ $-$ 5CO), 260 (M$^+$ $-$ 6CO).

Synthesis of Fe$_2$(μ-Se$_2$C$_5$H$_8$O)(CO)$_6$ (4). A solution of Fe$_3$(CO)$_{12}$ (101 mg, 0.2 mmol) and **5** (49 mg, 0.2 mmol) in THF (50 mL) was heated at reflux for one hour. The resulting mixture was evaporated to dryness in vacuo. The obtained solid was suspended in a minimum amount of hexane and chromatographed on silica gel, eluting with CH_2Cl_2/hexane (1:3). From the major red fraction, **4** was obtained as a red solid (73 mg, 70%). Single crystals were obtained from hexane solution. Mp: 169$-$170 °C. Anal. Calcd for C$_{11}$H$_8$Fe$_2$O$_7$Se$_2$: C, 25.32; H, 1.55. Found: C, 25.14; H, 1.66. IR $\nu_{C\equiv O}$ cm^{-1}: (KBr disk) 2068 (vs), 2025 (vs), 1988 (vs) cm^{-1}, (Nujol) 2070 (s), 2029 (vs), 2000 (s), 1989 (s), 1977 (m). ^{1}H NMR (200 MHz, CDCl$_3$): δ 4.26 (s, 4H, (CH$_2$)$_2$O), 2.52 (s, 4H, 2SeCH2). ^{1}H NMR (200 MHz, -50 °C, CDCl$_3$): δ 4.26 (s, 4H, (CH$_2$)$_2$O), 3.15 (d, $^2J_{H,H}$ = 10.2 Hz, 2H, SeCH_AH$_B$ and SeCH_CH$_D$), 1.89 (d, $^2J_{H,H}$ = 10.2 Hz, 2H, SeCH$_A$$H_B$ and SeCH$_C$$H_D$). ^{13}C NMR (50 MHz, CDCl$_3$): δ 208.2 (CO), 81.8 ((CH$_2$)$_2$O), 42.2 (C$_q$), 21.5 (2SeCH$_2$). ^{77}Se$\{^1$H$\}$ NMR (76 MHz, CDCl$_3$): δ 107 ppm. DEI-MS (*m/z*): 524 (M$^+$), 496 (M$^+$ $-$ CO), 468 (M$^+$ $-$ 2CO), 440 (M$^+$ $-$ 3CO), 411 (M$^+$ $-$ 4CO), 384 (M$^+$ $-$ 5CO), 356 (M$^+$ $-$ 6CO).

Synthesis of Fe$_2$(μ-Te$_2$C$_5$H$_8$O)(CO)$_6$ (5). Complex **5** was prepared, separated, and recrystallized by a procedure similar to that of **4**. The reaction of Fe$_3$(CO)$_{12}$ (101 mg, 0.2 mmol) with **6** (68 mg, 0.2 mmol) was carried out in THF. Yield: 82 mg (66%). Mp: 175$-$176 °C. Anal. Calcd for C$_{11}$H$_8$Fe$_2$O$_7$Te$_2 \cdot$0.25hexane: C, 23.44; H, 1.81. Found: C, 23.24; H, 1.99. IR $\nu_{C\equiv O}$ cm^{-1}: (KBr disk) 2055 (s), 2012 (vs), 1971 (vs) cm^{-1}, (Nujol) 2058 (s), 2020 (vs), 1990 (s), 1982 (s), 1969 (m). ^{1}H NMR (200 MHz, CDCl$_3$): δ 4.23 (s, 4H, (CH$_2$)$_2$O), 2.66 (s, 4H, 2TeCH$_2$). ^{1}H NMR (200 MHz, -50 °C, CDCl$_3$): δ 4.48 (s, 2H, CH$_{2A}$O), 4.04 (s, 2H, CH$_{2B}$O) 3.22 (s, 2H, TeCH_AH$_B$ and TeCH_CH$_D$), 2.12 (s, 2H, TeCH$_A$$H_B$ and TeCH$_C$$H_D$). ^{13}C NMR (50 MHz, CDCl$_3$): δ 210 (CO), 80.2 ((CH$_2$)$_2$O), 42.3 (C$_q$), 4.2 (2TeCH$_2$). ^{125}Te NMR (158 MHz, CDCl$_3$): δ 197. DEI-MS (*m/z*): 620 (M$^+$), 496, 564 (M$^+$ $-$ 2CO), 508 (M$^+$ $-$ 4CO), 452 (M$^+$ $-$ 6CO).

Crystal Structure Determination. The intensity data for the compounds were collected on a Nonius KappaCCD diffractometer, using graphite-monochromated Mo Kα radiation. Data were corrected for Lorentz and polarization effects, but not for absorption effects.[51,52] The structures were solved by direct methods (SHELXS)[53] and refined by full-matrix least-squares techniques against F_o^2 (SHELXL-97).[54] All hydrogen atoms were included at calculated positions with fixed thermal

parameters. All non-hydrogen atoms were refined anisotropically. XP (SIEMENS Analytical X-ray Instruments, Inc.) was used for structure representations.

Electrochemical Measurements. Instrumentation and the source and treatment of solvent and supporting electrolyte have been reported earlier.[55] All potentials are reported versus the potential of the ferrocenium/ferrocene (Fc$^+$/Fc) couple measured in acetonitrile. The voltammetric experiments were conducted at 298 K, using $\sim$1.0 mM of each compound in acetonitrile containing 0.10 M Bu$_4$NPF$_6$ on a glassy carbon working electrode (GCE), under an Ar atmosphere. The area of the GCE was determined to be 0.0707 cm^2 from cyclic voltammetric studies of the oxidation of ferrocene in acetonitrile using 2.5×10^{-5} cm^2/s as its diffusion coefficient.[55]

Photoelectron Spectroscopy. Photoelectron spectra were recorded using an instrument that features a 36 cm radius hemispherical analyzer (McPherson),[56] with custom-designed photon source, sample cells, detection and control electronics, calibration, and data analysis as described previously.[57] In the figures of the photoelectron spectra, the spectra obtained with the He I source photons are represented by the solid black lines, and the spectra obtained with the He II source photons are represented with the red dashed lines. The He II spectra are scaled to match the low ionization energy intensities in the He I spectra for visual comparison of the change in relative intensity at higher ionization energies. All samples sublimed cleanly, with no visible changes in the spectra during data collection after initial observation of ionizations from the diiron complex. The sublimation temperatures for the compounds (in °C, at 10^{-5} Torr) were as follows: complex **3**, 90$-$110; **4**, 100$-$110; **5**, 110$-$120.

Density Functional Theory (DFT) Calculations. Computational methods have been developed previously for this class of diiron hexacarbonyl systems with S and Se heteroatoms in the bridging positions and validated by their ability to account for structures, adiabatic ionization energies, carbonyl stretching frequencies, pK_a values, oxidation and reduction potentials, and other electrochemical parameters, as well as metal$-$metal and pertinent metal$-$ligand bond energies.[44,58$-$60] Density functional theory calculations were carried out with the Amsterdam density functional (ADF2006.01d) package.[61,62] Geometry optimizations and frequency calculations (with no imaginary frequencies in the final geometries) were carried out using the VWN functional with the Stoll correction implemented.[63] All electronic energies were obtained with the OPBE functional.[64] Comparison of the OPBE functional to other common functionals found it to be the best for the prediction of nuclear

(51) Nonius, B. V. *COLLECT, Data Collection Software*, **1998**.

(52) Otwinowski, Z.; Minor, W. In *Processing of X-ray diffraction data collected in oscillation mode*; Carter, C. W., Jr., Ed.; Methods in Enzymology; Academic Press: New York, 1997; Vol. *276*, pp 307$-$326.

(53) Sheldrick, G. M. *Acta Crystallogr., Sect. A* **1990**, *46*, 467.

(54) Sheldrick, G. M. *SHELXL-97 (Release 97-2)*; **1997**.

(55) Macías-Ruvalcaba, N. A.; Evans, D. H. *J. Phys. Chem. B* **2005**, *109*, 14642.

(56) Siegbahn, K.; Nordling, C.; Fahlman, A.; Nordberg, R.; Hamrin, K.; Hedman, J.; Johansson, G.; Bergmark, T.; Karlsson, S. E.; Lindgren, I.; Lindberg, B. *Nova Acta Regiae Societatis Scientiarum Upsaliensis* **1967**, *20*, 282.

(57) Cranswick, M. A.; Dawson, A.; Cooney, J. J. A.; Gruhn, N. E.; Lichtenberger, D. L.; Enemark, J. H. *Inorg. Chem.* **2007**, *46*, 10639.

(58) Felton, G. A. N.; Vannucci, A. K.; Chen, J.; Lockett, L. T.; Okumura, N.; Petro, B. J.; Zakai, U. I.; Evans, D. H.; Glass, R. S.; Lichtenberger, D. L. *J. Am. Chem. Soc.* **2007**, *129*, 12521.

(59) Petro, B. J.; Vannucci, A. K.; Lockett, L. T.; Mebi, C.; Kottani, R.; Gruhn, N. E.; Nichol, G. S.; Goodyer, P. A. J.; Evans, D. H.; Glass, R. S.; Lichtenberger, D. L. *J. Mol. Struct.* **2008**, *890*, 281.

(60) Felton, G. A. N.; Vannucci, A. K.; Okumura, N.; Lockett, L. T.; Evans, D. H.; Glass, R. S.; Lichtenberger, D. L. *Organometallics* **2008**, *27*, 4671.

(61) Te Velde, G.; Bickelhaupt, F. M.; Baerends, E. J.; Fonseca Guerra, C.; Van Gisbergen, S. J. A.; Snijders, J. G.; Ziegler, T. *J. Comput. Chem.* **2001**, *22*, 931.

(62) *ADF2006.01d, SCM*, Theoretical Chemistry, Vrije Universiteit: Amsterdam, The Netherlands, 2006.

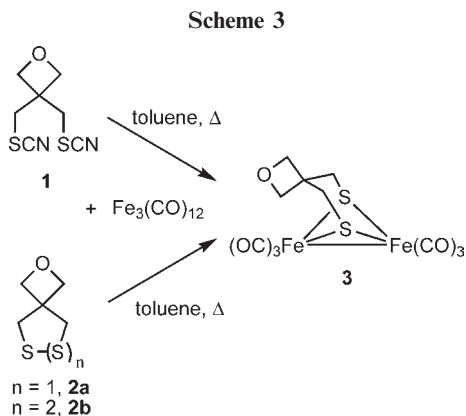(63) Stoll, H.; Pavlidou, C. M. E.; Preuss, H. *Theor. Chim. Acta* **1978**, *49*, 143.

(64) Swart, M.; Ehlers, A. W.; Lammertsma, K. *Mol. Phys.* **2004**, *102*, 2467.

Scheme 3

Scheme 4

Y= Se (**6**)   Y= Se (**4**)
Y= Te (**7**)   Y= Te (**5**)

magnetic constants[65] and the only functional to correctly predict the spin states of seven different iron complexes.[64] All calculations utilized a triple-ζ Slater-type orbital (STO) basis set with one polarization function (TZP) for H, C, O, Fe, S, and Se and two polarization functions (TZ2P) for Te. Relativistic effects by the zero-order regular approximation (ZORA)[66,67] were also applied during all calculations. The frozen core approximation was used for the inner core of all atoms. The theoretical stretching frequencies and IR absorption intensities for all species were calculated analytically with the same computing method as described above and scaled by a factor of 1.002. For the simulated IR spectra in the figure the linewidths are adjusted by a constant factor to approximate the linewidths in the experimental spectra. Figures of the optimized geometries and molecular orbital plots were created with Molekel.[68]

Results and Discussion

Treatment of $Fe_3(CO)_{12}$ with bisthiocyanate **1** in toluene under reflux for one hour afforded the diiron dithiolato complex $Fe_2(\mu-S_2C_5H_8O)(CO)_6$ (**3**). Moreover, complex **3** also was prepared from the reaction of $Fe_3(CO)_{12}$ with an inseparable 1:1 mixture of **2a** and **2b**[48] in toluene under reflux conditions for one and a half hour in 50% yield (Scheme 3).

The analogous diselenolato and ditellurolato complexes $Fe_2(\mu-Se_2C_5H_8O)(CO)_6$ (**4**) and $Fe_2(\mu-Te_2C_5H_8O)(CO)_6$ (**5**) were synthesized from the reaction of $Fe_3(CO)_{12}$ with 2-oxa-6,7-diselenaspiro[3.4]octane (**6**) or 2-oxa-6,7-ditelluraspiro[3.4]octane (**7**), respectively. These reactions were carried out in THF (Scheme 4).

Compounds **3**−**5** are air-stable in the solid state and for several hours in solution. These products were characterized by IR spectroscopy, multinuclear NMR spectroscopy, mass

spectrometry, elemental analysis, X-ray crystallography, and photoelectron spectroscopy.

The room-temperature ^{1}H NMR spectra of **3**−**5** display two singlets at 2.48 and 4.28 (**3**), 2.52 and 4.26 (**4**), and 2.66 and 4.23 (**5**) ppm for the two different methylene groups YCH_2 (Y = S, Se, Te) and CH_2O, respectively. Upon cooling to −50 °C, the resonance signals of the more shielded methylene groups in **3** and **4** split into AB spin systems, since ring flipping of the three-carbon bridge is frozen out and the hydrogen atoms of YCH_2 (Y = S, Se) are now nonequivalent. The low-temperature (−50 °C) ^{1}H NMR spectrum of **5** displays two unresolved signals of an AB spin system corresponding to the diastereotopic protons at $TeCH_2$, as well as two broad singlets for the CH_2OCH_2 group. The $^{13}C\{^1H\}$ NMR spectra of **3**−**5** exhibit three resonances at 82.2, 42.2, and 30.3 (**3**), 81.8, 42.2, and 21.5 (**4**), and 80.2, 42.3, and 4.2 (**5**) for CH_2O, C_q, and YCH_2 (Y = S, Se, Te). The ^{13}C resonance of $TeCH_2$ in **5** is significantly shifted to high field ($\Delta\delta(S,Te)$ = 26.1, $\Delta\delta(Se,Te)$ = 17.3), which could be attributed to the "heavy atom" effect.[69] One signal is observed at 107 ppm in the $^1H,^{77}Se$ HMBC NMR spectrum of **4**, indicating equivalent Se atoms. This resonance is shifted to higher field compared to that of the propanediselenolato (PDS) model complex (145 ppm).[43,44] The mass spectra of **3**−**5** showed the molecular ion peaks and the elimination of six CO ligands sequentially.

The IR spectra of complexes **3**−**5** (KBr disk) exhibit three strong absorption bands in the regions 1997−2076 for **3**, 1988−2068 for **4**, and 1971−2055 cm^{-1} for **5**. When comparing the spectra, it can be seen that the CO absorption bands are shifted to lower frequencies from **3** to **5**, which can be explained by the increasing back-donation to CO caused by rising donor ability from S to Te. These data are within the same ranges as those observed for propanedithiolato (PDT),[70] PDS,[43,44] and propaneditellurolato (PDTe)[71] complexes.

The X-ray diffraction analyses reveal the proposed structures of **3**−**5** as shown in Figures 1−3 and Table 1. The central 2Fe2Y (Y = S, Se, Te) moieties of **3**−**5** are in the butterfly conformation and the geometry around the iron atoms is similar to that reported for PDT, PDS, and PDTe complexes.[43,44,70,71] The Fe−Fe bond distances in **3**−**5** are 2.4923(3), 2.5367(19), and 2.6322(11) Å, respectively, a trend attributed to the increase of atomic sizes from S to Te. The Fe−S, Fe−Se, and Fe−Te bond lengths are comparable to those reported for PDT, PDS, and PDTe complexes.[43,44,70,71] Moreover an increase of the bonding angle X−C1−C2 (X = S, Se, Te) is visible (**3**: 117.76(12)°, **4**: 118.2(6)°, **5**: 118.5(4)°). These values are unexpectedly high in comparison to a regular sp^3-hybridized atom (109.5°). An explanation for this is given in the literature and can be described by the rule of Bent.[72,73]

It is noteworthy that the Fe−CO bond lengths {average lengths: 1.800 Å (**3**), 1.793 Å (**4**), 1.785 Å (**5**)} are slightly decreasing from **3** to **5** due to the increasing electron density at the Fe atoms caused by more back-donation ability from S

(65) Zhang, Y.; Lin, H.; Truhlar, D. G. *J. Chem. Theory Comput.* **2007**, *3*, 1378.

(66) van Lenthe, E.; Ehlers, A.; Baerends, E. J. *J. Chem. Phys.* **1999**, *110*, 8943.

(67) van Lenthe, E.; Baerends, E. J.; Snijders, J. G. *J. Chem. Phys.* **1993**, *99*, 4597.

(68) Portmann, S.; Luthi, H. P. *Chimia* **2000**, *54*, 766.

(69) Kalabin, G. A.; Bzhezovskii, V. M.; Kushnarev, D. F.; Proidakov, A. G. *Zh. Org. Khim* **1981**, *17*, 1143.

(70) Lyon, E. J.; Georgakaki, I. P.; Rabenspies, J. H.; Darensbourg, M. Y. *Angew. Chem., Int. Ed.* **1999**, *38*, 3178.

(71) Shieh, M.; Shieh, M. H. *Organometallics* **1994**, *13*, 920.

(72) Apfel, U.; Halpin, Y.; Görls, H.; Vos, J. G.; Schweizer, B.; Linti, G.; Weigand, W. *Chem. Biodiversity* **2007**, *4*, 2138.

(73) Bent, H. A. *Chem. Rev.* **1961**, *61*, 275.
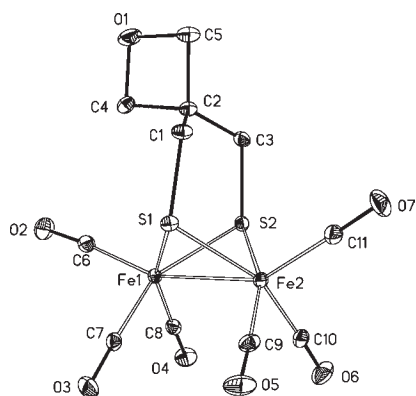
Figure 1. ORTEP drawing of $Fe_2(\mu\text{-}S_2C_5H_8O)(CO)_6$ (**3**) with thermal ellipsoids set at the 50% probability level (hydrogen atoms were omitted for clarity). Selected distances [Å] and angles [deg]: Fe1−Fe2 2.4923(3), Fe1−S1 2.2682(5), Fe1−S2 2.2676(5), Fe2−S1 2.2578(5), Fe2−S2 2.2600(5), Fe1−S1−Fe2 66.826(14), Fe1−S2−Fe2 66.799(14), S1−Fe1−S2 84.279(17), S1−Fe2−S2 84.690(17).
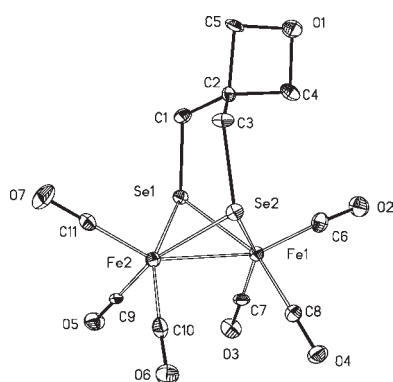
Figure 2. ORTEP drawing of $Fe_2(\mu\text{-}Se_2C_5H_8O)(CO)_6$ (**4**) with thermal ellipsoids set at the 50% probability level (hydrogen atoms were omitted for clarity). Selected distances [Å] and angles [deg]: Fe1−Fe2 2.5367(19), Fe1−Se1 2.3813-(15), Fe1−Se2 2.3824(14), Fe2−Se1 2.3753(16), Fe2−Se2 2.3823(17), Fe1−Se1−Fe2 64.46(5), Fe1−Se2−Fe2 64.34(5), Se1−Fe1−Se2 85.61(5), Se1−Fe2−Se2 85.74(6).

Figure 3. ORTEP drawing of $Fe_2(\mu\text{-}Te_2C_5H_8O)(CO)_6$ (**5**) with thermal ellipsoids set at the 50% probability level (hydrogen atoms were omitted for clarity). Selected distances [Å] and angles [deg]: Fe1−Fe2 2.6322(11), Fe1−Te1 2.5435(8), Fe1−Te2 2.5344(8), Fe2−Te1 2.5317(8), Fe2−Te2 2.5384(7), Fe1−Te1−Fe2 62.48(3), Fe1−Te2−Fe2 62.52(2), Te1−Fe1−Te2 86.92(3), Te1−Fe2−Te2 87.09(2).
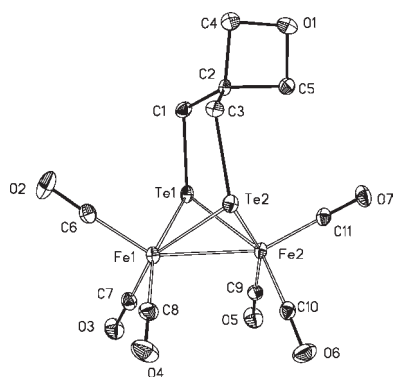
Table 1. Crystal Data and Refinement Details for the X-Ray Structure Determinations of the Compounds 3, 4, and 5

	3	**4**	**5**
formula	$C_{11}H_8Fe_2\text{-}O_7S_2$	$C_{11}H_8Fe_2\text{-}O_7Se_2$	$C_{11}H_8Fe_2\text{-}O_7Te_2$
fw	427.99	521.79	619.07
T/°C	−90(2)	−90(2)	−90(2)
cryst syst	triclinic	triclinic	triclinic
space group	$P\bar{1}$	$P\bar{1}$	$P\bar{1}$
a/Å	8.7511(3)	8.7942(7)	7.7877(4)
b/Å	9.3583(4)	9.4877(11)	9.0734(4)
c/Å	10.2267(3)	10.3124(13)	12.6096(6)
α/deg	100.509(2)	100.635(7)	101.493(2)
β/deg	91.881(2)	92.451(7)	95.493(2)
γ/deg	110.795(2)	110.565(7)	110.171(3)
V/Å^3	765.48(5)	786.33(15)	806.39(7)
Z	2	2	2
ρ/g·cm^{-3}	1.857	2.204	2.550
μ/cm^{-1}	21.95	65.01	53.72
measd data	5538	5339	5678
data with $I > 2\sigma(I)$	3198	1946	2893
unique data/R_{int}	3484/0.0231	3540/0.0868	3644/0.0364
wR_2 (all data, on F^2)^a	0.0636	0.1352	0.0860
R_1 ($I > 2\sigma(I)$)^a	0.0246	0.0655	0.0378
s^b	1.021	1.004	1.046
res dens/e·Å^{-3}	0.420/−0.414	0.989/−1.183	0.785/−1.366
absorpt method	none	none	none
CCDC no.	723576	723577	723578

$^a R_1 = (\sum||F_o|-|F_c||)/\sum|F_o|$, $wR_2 = \{\sum[w(F_o^2 - F_c^2)^2]/\sum[w(F_o^2)^2]\}^{1/2}$ with $w^{-1} = \sigma^2(F_o^2) + (\alpha P)^2$. $^b s = \{\sum[w(F_o^2 - F_c^2)^2]/(N_o - N_p)\}^{1/2}$.
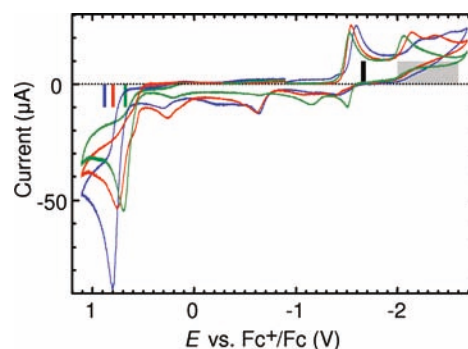
Figure 4. Background-corrected voltammograms of 1.01 mM **3** (blue), 1.00 mM **4** (red), and 1.00 mM **5** (green) in acetonitrile with 0.10 M tetrabutylammonium hexafluorophosphate at glassy carbon (0.10 V/s; scan segments: −0.9 to −2.7 V; −2.7 to +1.1 V; +1.1 to −0.9 V; argon purged). The bars on the zero current axis represent the oxidation and reduction potentials obtained from DFT computations. The colored bars are the calculated oxidation potentials for each respective molecule, the black bar is the range of calculated first reduction potentials for all three molecules, and the gray bar represents the range of calculated second reduction potentials for a variety of final geometries.

to Te. This observation is consistent with the CO band shifts to lower frequencies from **3** to **5** in their IR spectra.

Electrochemical Investigations. Cyclic voltammograms (CV) of **3**−**5** were recorded in order to observe the electrochemically induced reduction and oxidation properties of this family of compounds and to assess their ability to catalyze the reduction of weak acids to form dihydrogen. Comparison of a wide potential range of CV data, Figure 4, for all three compounds shows some broadly similar processes.
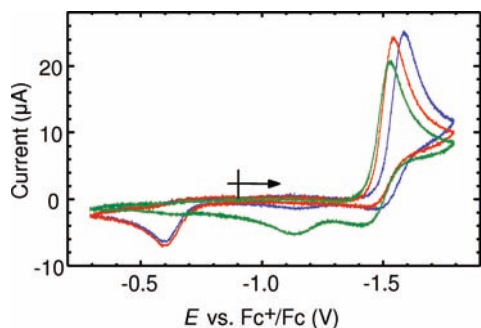
Figure 5. Background-corrected voltammograms of 1.01 mM **3** (blue), 1.00 mM **4** (red), and 1.00 mM **5** (green) in acetonitrile with 0.10 M tetrabutylammonium hexafluorophosphate at glassy carbon (0.10 V/s; scan segments: −0.9 to −1.8 V; −1.8 to −0.3 V; −0.3 to −0.9 V; argon purged).

A primary one-electron reduction with a peak potential around −1.55 V is observed followed by a less distinct second reduction feature at least a further 600 mV more negative. The conclusion that the reduction peak corresponds to a one-electron process is based on comparison of the peak height with that of other known one-electron processes, such as the oxidation of ferrocene, measured under the same conditions. For information about the electronic structure of the one-electron reduction product, see section "Electronic Structure and Observed Properties" below. Strong irreversible oxidation peaks are seen between 0.70 and 0.80 V. Small oxidation peaks are observed for compounds **3** and **4** at −0.60 V but only following an initial scan through the primary reduction peak (see SI-1 and SI-4), suggesting that this feature is due to the oxidation of a species formed upon reduction of the initial compound (this feature is largest at slow scan rates, suggesting that it is due to a species formed in a slow reaction following the initial reduction, SI-2 and SI-5). All three compounds have a degree of chemical reversibility to the primary reduction feature at the larger scan rates (see SI-2, SI-5, and SI-8). At 0.1 V/s, as in Figures 4 and 5, only the Te compound, **5**, shows distinct reversibility. There is a small positive shift, ~70 mV, in the primary reduction peak potential as S is changed to Se and to Te (from Figure 5: $E_{p,red}$ = −1.602 V (**3**), −1.551 V (**4**), and −1.535 V (**5**)). The second more negative reduction peak is chemically irreversible for all three compounds. The anodic peak potentials span a range of ~100 mV, with the Te compound being the most easily oxidized and S most difficult (from Figure 4: $E_{p,ox}$ = 0.810 V (**3**), 0.778 V (**4**), and 0.708 V (**5**)). The finding that the Te compound, **5**, is both the easiest to reduce and the easiest to oxidize is surprising, although the magnitudes of the shifts are fairly small. The oxidation peak is chemically irreversible for all three compounds.

Catalysis of the reduction of weak acids by compounds **3**−**5** was tested with additions of acetic acid to acetonitrile solutions (see Figures 6, 7, SI-3, SI-6, SI-9, and SI-10). The response with a 5-fold excess of acid shows some catalysis, indicated by enhanced current in a region where neither the catalyst nor the acid alone are reduced.[58] There is evidence of modest catalysis in this region, most strongly for **3**, with enhanced current around −2.0 V. The feature is broad and not well-defined, so that determination of the overpotential is imprecise but can be considered to be at least 0.5 V (using the standard potential for reduction of acetic acid,
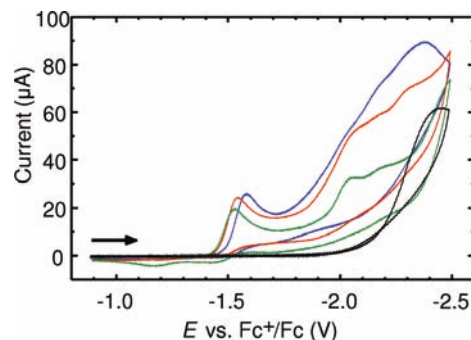
Figure 6. Background-corrected voltammograms of 1.01 mM **3** + 5 mM acetic acid (blue), 1.00 mM **4** + 5 mM acetic acid (red), 1.00 mM **5** + 5 mM acetic acid (green), and 5 mM acetic acid only (black) in acetonitrile with 0.10 M tetrabutylammonium hexafluorophosphate at glassy carbon (0.10 V/s, argon purged); scan: −0.9 to −2.5 V and return to −0.9 V.
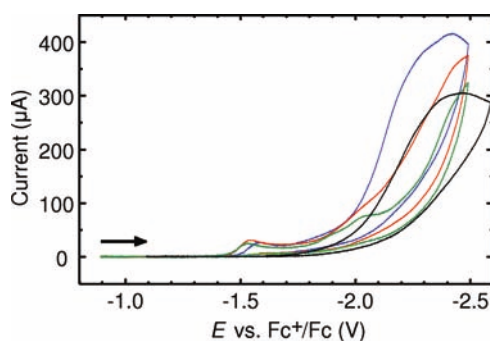
Figure 7. Background-corrected voltammograms of 1.01 mM **3** + 50 mM acetic acid (blue), 1.00 mM **4** + 50 mM acetic acid (red), 1.00 mM **5** + 50 mM acetic acid (green), and 50 mM acetic acid only (black) in acetonitrile with 0.10 M tetrabutylammonium hexafluorophosphate at glassy carbon (0.10 V/s, argon purged); scan: −0.9 to −2.5 V and return to −0.9 V.

−1.46 V).[74] There is little enhancement for **5**, where most of the extra current with 5 mM acid is likely due to the direct reduction of acetic acid on glassy carbon. Compound **4** (Se) represents a case intermediate between compounds **3** (S) and **5** (Te). Figure 7 shows the response with a much larger acid excess, 50:1, wherein any catalytic current is mostly swamped by direct reduction. The addition of acetic acid to these compounds does not lead to growth in the height of the primary reduction peak; such growth was not expected, as this would represent an extremely low overpotential of ~0.10 V. due to the direct reduction of acetic acid on glassy carbon. Compound **4** (Se) represents a case intermediate between compounds **3** (S) and **5** (Te). Figure 7 shows the response with a much larger acid excess, 50:1, wherein any catalytic current is mostly swamped by direct reduction.

Photoelectron Spectroscopy. The He I and He II gas-phase ultraviolet photoelectron spectra of the molecules containing chalcogens S through Te are shown in Figure 8. The general assignment of the ionizations is based on previously reported analogous compounds.[44] The displayed spectrum contains ionizations from the Fe-based metal 3d-orbitals,

(74) Felton, G. A. N.; Glass, R. S.; Lichtenberger, D. L.; Evans, D. H. *Inorg. Chem.* **2006**, *45*, 9181. Corrections: Felton, G. A. N.; Glass, R. S.; Lichtenberger, D. L.; Evans, D. H. *Inorg. Chem.* **2007**, *46*, 5126. Felton, G. A. N.; Glass, R. S.; Lichtenberger, D. L.; Evans, D. H. *Inorg. Chem.* **2007**, *46*, 8098.
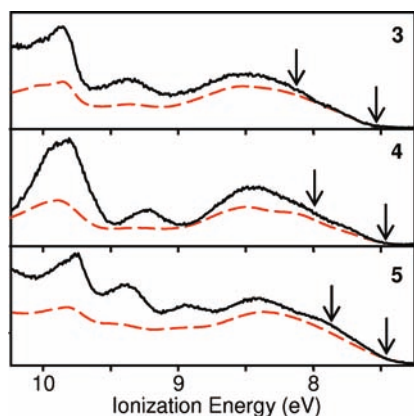
**Figure 8.** He I (black solid line) and He II (red dashed line) photoelectron spectra of oxetane molecules. The arrows around 7.5 eV indicate the DFT-calculated adiabatic ionization energy for each molecule. The arrows around 8 eV indicate the DFT-calculated vertical ionization energy for each molecule.

Figure 9. First ionization bands of molecules **3−5** in the He I photoelectron spectra. The brackets indicate the region of onset of ionization intensity, which approximates the adiabatic ionization energy for the molecules.

chalcogen-based valence p-orbitals, and O-based 2p-orbitals. The metal d-based ionizations include a formal metal–metal bond of the diiron center and the three occupied d-orbitals of each Fe center that are involved in back-bonding to the carbonyl ligands. The chalcogen-based and O-based valence p-orbital ionizations are expected to be observed in the high ionization energy side of this region based on previously reported photoelectron spectra of chalcogen-[75−77] and oxetane-[78,79]containing organometallic compounds.

The first broad ionization profile, shown in more detail in Figure 9, contains the predominantly Fe d-based ionizations and ranges up to about 9 eV for the S- and Se-containing molecules and up to about 8.7 eV for the Te-containing molecule. This band has a weak shoulder on the low ionization energy side corresponding to ionization from the HOMO of the molecule, calculated to be predominantly the Fe–Fe σ-bond (vide infra), with an adiabatic ionization energy approximately in the region indicated by the onset of ionization intensity around 7.5 eV. The estimated shift of the adiabatic ionization energy from molecule **3** to molecule **5** based on these spectra is 0.1 eV, which is the same as the observed shift in oxidation potentials reported above.

The second and third distinct ionization bands (shown in Figure 8), ranging from about 9.0 to 9.5 eV, are chalcogen based, and above 10.0 eV are O p-based ionizations. The additional identifiable band in this region of the spectrum of **5** is most likely the consequence of spin−orbit effects for the heavy tellurium atom. Compared to the ionizations observed in the He I spectra, these chalcogen-based ionizations exhibit substantially decreased intensity relative to the Fe d-based ionizations when the higher-energy He II excitation was used. The probability of ionization from a chalcogen p-orbital falls by an average factor of 10 from He I to He II excitation, while the probability of O p-orbital and Fe
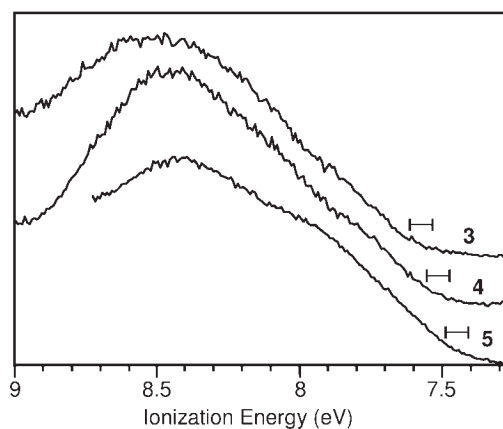
d-orbital ionizations increases by almost a factor of 2 based on theoretical partial photoionization cross-sections of the atoms.[80] However, the relative intensity changes observed in the photoelectron spectra are much less in magnitude than the theoretical values predicted for pure atomic orbital ionizations. This suggests substantial mixing of chalcogen character with iron d orbital and oxygen p orbital character. The energies of these ionizations visibly decrease with substitution from S to Se to Te, as expected from the decreasing electronegativity of the atoms and the decreasing inherent stability of the atomic orbitals.

Electronic Structure and Observed Properties. Density functional theory calculations of these oxetane compounds have been carried out to provide further information on how the electronic structure and properties of the molecules are altered as the chalcogen is changed from S to Se to Te. A computational methodology has been developed previously for [FeFe]-hydrogenase mimics that shows good agreement between calculated and experimental results.[44,58−60] This is the first test of the computational model to account for the properties of a mimic with tellurium atoms in the bridging positions. Optimized geometries and comparisons with the crystal structures are provided in the Supporting Information. For the S- and Se-containing molecules **3** and **4** the calculated Fe−Fe and Fe−chalcogen bond distances are within 0.025 Å of those obtained from crystal structures (see SI). For the Te-containing molecule **5** the optimized Fe−Fe distance is 0.05 Å shorter than the crystal structure distance, and the Fe−Te distance is about 0.07 Å longer than the crystal structure distance. There was some concern about additional relativistic effects or other limitations of the basis set or model for the heavy tellurium atoms, but this was not found to be an issue for the electron distribution or the spectroscopic and thermodynamic properties of the molecule, as evidenced by agreement with the carbonyl stretching frequencies, molecular ionization energies, and oxidation and reduction potentials. It was noted that geometry optimization was much more difficult for the Te-containing molecule because of a fairly flat potential energy surface, perhaps due to the larger and softer tellurium atoms, leading to larger differences in the calculated distances from

(75) Guillemin, J. C.; Bajor, G.; Riague, E.; Khater, B.; Veszpremi, T. *Organometallics* **2007**, *26*, 2507.

(76) Cozzolino, A. F.; Gruhn, N. E.; Lichtenberger, D. L.; Vargas-Baca, I. *Inorg. Chem.* **2008**, *47*, 6220.

(77) Cranswick, M. A.; Gruhn, N. E.; Oorhles-Steele, O.; Ruddick, K. R.; Burzlaff, N.; Schenk, W. A.; Lichtenberger, D. L. *Inorg. Chim. Acta* **2008**, *361*, 1122.

(78) Roszak, S.; Kaufman, J. J.; Koski, W. S.; Barreto, R. D.; Fehlner, T. P.; Balasubramanian, K. *J. Phys. Chem.* **1992**, *96*, 7226.

(79) Mollere, P. D. *Tetrahedron Lett.* **1973**, *14*, 2791.

(80) Yeh, J. J.; Lindau, I. *At. Data Nucl. Data Tables* **1985**, *32*, 1.
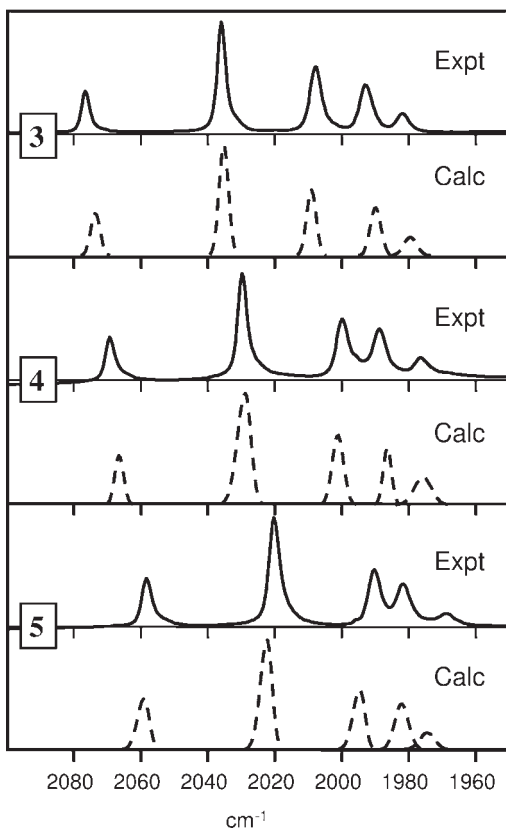
Figure 10. Comparison of the experimental IR spectra (in Nujol) in the carbonyl stretching region (solid lines) with calculated IR spectra (dashed lines) for each of the oxetane molecules.

Figure 11. Calculated neutral and cation structures of **3**.

experiment, but not to significantly larger differences in the calculated energy quantities.

The carbonyl stretching frequencies are an energy measure sensitive to the electron distribution in the molecules, and the intensities of the normal mode absorptions are sensitive to the molecular geometry and carbonyl coupling. The calculated and observed spectra are compared in Figure 10. The average difference in the calculated and experimental frequencies is less that 0.2%, and the relative absorption intensities are in good agreement. As mentioned previously, the decrease in carbonyl stretching frequencies from **3** to **4** to **5** indicates an incre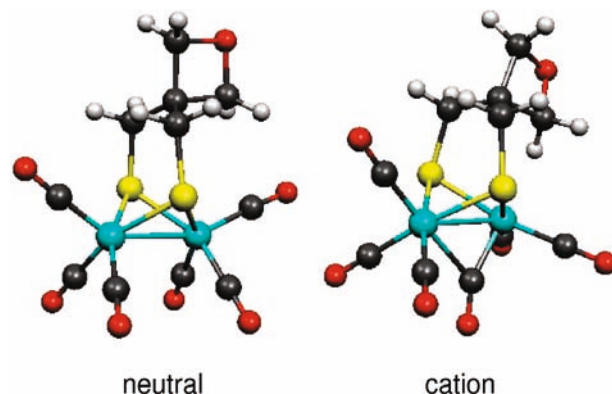ase of electron richness at the diiron core of the molecule from S to Se to Te. The trend is as expected considering the changes in electronegativity from S to Se to Te. The increasing donor ability from S to Se to Te is evidenced by the increasing positive charge on these atoms. Based on Voronoi deformation densities, which are less sensitive to basis sets than Mulliken population analysis,[81] the electron density in the vicinity of the chalcogen decreases by 0.06 e^- from S to Se and another 0.09 e^- from Se to Te. Much of the charge is transferred to the carbonyls, and the corresponding increases in electron density in the vicinity of the Fe atoms are 0.02 and 0.04 e^-.

The agreement of the calculations with the experimental ionization energies is also very good. The arrows in Figure 8 indicate the adiabatic and vertical ionization energies as calculated by the ΔSCF energy between the neutral molecule

and the positive ion. The calculated first vertical ionization energies, for which the structures of the positive ions are constrained to the optimized structures of the neutral molecules, are able to account for the shift of the primary ionization band intensity to lower energy from S to Se to Te substitution. Calculated adiabatic ionization energies, for which the structures of the positive ions are optimized to their global minima, are close to the experimental onset energies of the first ionization bands, indicated by the arrows near 7.5 eV in Figure 8. In each case the global minimum structure of the cation in the gas phase has a semibridging carbonyl ligand, as shown in Figure 11. This general arrangement of the carbonyl ligands, which has been has been the subject of much attention,[59,82−87] has been termed the "rotated" structure because it can be viewed as an approximate 60° rotation of one $Fe(CO)_3$ group. This rotated structure creates a vacant axial coordination site on the Fe center analogous to the active site of [FeFe]-hydrogenase.[19,21,23,88,89]

The cation reorganization energy for each molecule was calculated as the energy difference of the optimized semibridged rotated structure of the cation shown in Figure 11 (corresponding to the adiabatic ionization energy) from the energy of the cation calculated with the nonbridged frozen structure of the neutral molecule (corresponding to the vertical ionization energy). Reorganization energies are calculated to be 0.59 eV for **3**, 0.53 eV for **4**, and 0.42 eV for **5**. Substantial reduction of reorganization energy was calculated with increasing atomic radii of the chalcogen, favoring increasing electron transfer rates from S- to Te-containing molecule. The decrease in the reorganization energy was not as great as observed from S to Se in [μ-Se(CH_2)_2-CHCH_3Se][Fe(CO)_3]_2, where the energies decreased from 0.65 to 0.45 eV.[44] Interestingly, although the vertical ionizations shift significantly to lower energy with the heavier chalcogens, reflecting their greater donor ability, the reorganization energies also decrease down the series, and the

(81) Guerra, C. F.; Handgraaf, J. W.; Baerends, E. J.; Bickelhaupt, F. M. *J. Comput. Chem.* **2004**, *25*, 189.

(82) van der Vlugt, J. I.; Rauchfuss, T. B.; Whaley, C. M.; Wilson, S. R. *J. Am. Chem. Soc.* **2005**, *127*, 16012.
(83) Justice, A. K.; Zampella, G.; DeGioia, L.; Rauchfuss, T. B.; vanderVlugt, J. I.; Wilson, S. R. *Inorg. Chem.* **2007**, *46*, 1655.
(84) Justice, A. K.; Zampella, G.; Gioia, L. D.; Rauchfuss, T. B. *Chem. Commun.* **2007**, 2019.
(85) Justice, A. K.; Rauchfuss, T. B.; Wilson, S. R. *Angew. Chem., Int. Ed.* **2007**, *46*, 6152.
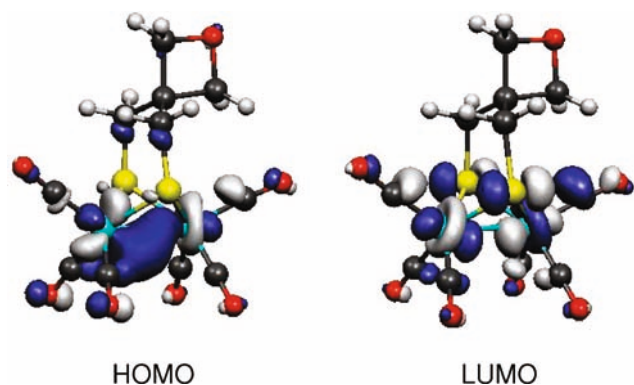(86) Liu, T.; Darensbourg, M. Y. *J. Am. Chem. Soc.* **2007**, *129*, 7008.
(87) Thomas, C. M.; Darensbourg, M. Y.; Hall, M. B. *J. Inorg. Biochem.* **2007**, *101*, 1752.
(88) Peters, J. W. *Curr. Opin. Struct. Biol.* **1999**, *9*, 670.
(89) Nicolet, Y.; Piras, C.; Legrand, P.; Hatchikian, C.; Fontecilla-Camps, J. C. *Struct. Fold Des.* **1999**, *7*, 13.

Figure 12. Highest occupied and lowest unoccupied orbitals of **3**.

consequence of the combination of these effects is that there is little shift, only about 0.1 eV overall, in the adiabatic ionization energies, as also seen in the oxidation potentials.

The trend in ionization energies and reorganization energies shows that as the bridging atoms change from S to Se to Te, the cations gain less stabilization in forming the "rotated" structures with the bridging carbonyls. This is counter to the usual expectation that as electron richness at the metal center increases, as shown by the carbonyl stretching frequencies for these molecules, the bridging carbonyl should become more favored because of its greater ability to withdraw and stabilize the electron density. The other important factor in these molecules is that as the chalcogen atoms become larger down the series, there is a corresponding increase in the Fe–Fe distance, such that the bridging carbonyl becomes less effective at favoring the rotated structure. The relative stability of the rotated structure is important to the reduction chemistry and catalysis discussed below.

From plots of the Kohn–Sham orbitals of the HOMO and LUMO, shown in Figure 12, the HOMO is primarily the metal–metal bonding interaction with delocalization of electron density to the carbonyl ligands. The tilt of the oxetane imparts some asymmetry to the HOMO. The LUMO consists mainly of the metal–metal antibonding interaction with some metal–chalcogen antibonding interaction of chalcogen p-orbitals.

The Kohn–Sham orbitals corresponding to the ionizations from 9.0 to 9.5 eV (see SI for orbital plots) were found to contain substantial chalcogen p-orbital character (HOMO−8 to HOMO−10). This is in agreement with the relative intensity of the ionizations observed in He I/He II photoelectron spectra. Also, the orbital (HOMO−11) above 9.5 eV is calculated to contain O 2p character. In addition to the above, mixing of chalcogen orbital characters with Fe and O orbital characters is consistent with the mixing suggested by the He I/He II photoelectron data.

The calculated oxidation and reduction potentials are displayed with the observed cyclic voltammograms in Figure 4. The calculated oxidation potentials that are shown correspond to cation structures without a bridging carbonyl ligand, similar to the neutral molecule. The good agreement between calculated and observed oxidation potentials and their trends suggests that the structures without bridging carbonyl ligands are favored in acetonitrile solution on the time scale of these experiments. Calculated oxidation potentials with a bridging carbonyl ligand in the cation structure

gave oxidation potentials in the range 0.51−0.67 V, which agreed less well with experiment, although such structures cannot be ruled out with confidence on this basis.

Various structures also were explored for the anions of these molecules obtained by reduction. For the sulfur-containing molecule **3** the free energy of the structure with the rotated iron center and semibridging carbonyl is calculated to be the same (within 0.01 eV) as the free energy of the structure with the unrotated iron center. For the selenium-containing molecule **4** the free energy of the rotated structure is calculated to be 0.1 eV higher than the unrotated structure, and for the tellurium-containing molecule **5** the difference in free energy between these structures increases again to 0.2 eV. The global minimum structure for the dianions of all three molecules has a bridging carbonyl, along with one broken Fe−chalcogen bond, as found in the study of the corresponding benzenedithiolato[58] and ethanedithiolato[90] complexes. The decreasing favorability of the rotated structures in the anions from S to Se to Te parallels the observed increase in reversibility of the reduction of the Te molecule and the decrease in the rate of reduction of protons to hydrogen observed down this series. Previously, the rate of rotation of the Fe(CO)$_3$ unit has been correlated with the rate of cyanide substitution for carbonyl by an associative mechanism.[28,91] Similarly, these observations strongly indicate that the catalytic reduction of protons by these molecules is promoted by transformation to the rotated structure with the bridging carbonyl to open up the site for protonation and subsequent production of hydrogen.

Conclusion

Diiron dithiolato, diselenolato, and ditellurolato compounds containing an oxetane ring have been prepared in good yields as [FeFe]-hydrogenase models. The oxetane ring remarkably stabilizes the cyclic diselenium and ditellurium precursor compounds, which provides the opportunity to synthesize the homologous S, Se, and Te series **3−5**. The objective of this paper was to determine the basis for the difference in reorganization energy of 2Fe2Y (Y = S, Se, and Te) cores. Overall the electronic effects of substitution from S to Se to Te are small. The increasing donor ability of these bridge atoms, as reflected in both the decreasing carbonyl stretching frequencies and the decreasing vertical ionization energies, is compensated by the decreasing reorganization energies such that the adiabatic ionization energies and the electrochemical oxidation potentials occur within narrow energy ranges. The first reduction potentials occur in a similarly small range. However, despite these small changes in potentials, the rate of catalytic reduction of protons to hydrogen is substantially diminished from S to Se to Te. Also diminished is the calculated favorability of the anions to adopt the rotated structures with a bridging carbonyl ligand, which creates an open coordination site on an iron atom for protonation. The increasing size of the chalcogen atoms and the corresponding increasing distance between the iron atoms are likely factors in disfavoring the bridging carbonyl structures.

(90) Felton, G. A. N.; Petro, B. J.; Glass, R. S.; Lichtenberger, D. L.; Evans, D. H. *J. Am. Chem. Soc.* **2009**, *131*, 11290.
(91) Darensbourg, M. Y.; Lyon, E. J.; Zhao, X.; Georgakaki, I. P. *Proc. Natl. Acad. Sci. U.S.A.* **2003**, *100*, 3683.

Supporting Information Available: Crystallographic data (excluding structure factors) have been deposited with the Cambridge Crystallographic Data Centre as supplementary publication CCDC-723576 for $Fe_2(\mu\text{-}S_2C_5H_8O)(CO)_6$ (**3**), CCDC-723577 for $Fe_2(\mu\text{-}Se_2C_5H_8O)(CO)_6$ (**4**), and CCDC-723578 for $Fe_2(\mu\text{-}Te_2C_5H_8O)(CO)_6$ (**5**). Copies of the data can be obtained free of charge on application to CCDC, 12 Union Road, Cambridge CB2 1EZ, UK [e-mail: deposit@ccdc.cam.ac.uk]. Supporting Information contains sample input files for calculations, optimized Cartesian coordinates and total energies for all structures, pictures of molecular structures and frontier orbitals, comparison of experimental and calculated geometries, calculated oxidation and reduction potentials, and CV diagrams. This material is available free of charge via the Internet at http://pubs.acs.org.

This paper is published as part of a *Dalton Transactions* themed issue on:

Bioinspired Catalysis

Guest Editor Seiji Ogo
Kyushu University, Japan

Published in issue 12, 2010 of *Dalton Transactions*

Image reproduced with permission of Seiji Ogo

Articles published in this issue include:

PERSPECTIVES:

Mimicking Nitrogenase
Ian Dance
Dalton Trans., 2010, DOI: 10.1039/b922606k

Dual functions of NifEN: insights into the evolution and mechanism of nitrogenase
Yilin Hu, Aaron W. Fay, Chi Chung Lee, Jared A. Wiig and Markus W. Ribbe
Dalton Trans., 2010, DOI: 10.1039/b922555b

Quest for metal/NH bifunctional biomimetic catalysis in a dinuclear platform
Takao Ikariya and Shigeki Kuwata
Dalton Trans., 2010, DOI: 10.1039/b927357c

COMMUNICATION:

Chemiluminescence enhancement and energy transfer by the aluminium(III) complex of an amphiphilic/bipolar and cell-penetrating corrole
Atif Mahammed and Zeev Gross
Dalton Trans., 2010, DOI: 10.1039/b916590h

Visit the *Dalton Transactions* website for more cutting-edge inorganic and bioinorganic research
www.rsc.org/dalton

Reaction of Fe₃(CO)₁₂ with octreotide—chemical, electrochemical and biological investigations

Ulf-Peter Apfel,[a] Manfred Rudolph,[a] Christina Apfel,[a] Christian Robl,[a] Daniel Langenegger,[b] Daniel Hoyer,[b] Bernhard Jaun,[c] Marc-Olivier Ebert,[c] Theodor Alpermann,[a] Dieter Seebach*[c] and Wolfgang Weigand*[a]

In search for peptidic [FeFe] hydrogenase mimics, the cyclic disulfide Sandostatin® (octreotide) was allowed to react with Fe₃(CO)₁₂. An octreotide-Fe₂(CO)₆ complex was isolated and characterized spectroscopically as well as by elemental and thermochemical analysis. The complex catalyzes the electrochemical reduction of H⁺ to H₂. It is suggested by radioligand binding assays that the complex retains much of the binding affinity for the somatostatin hsst₁₋₅ receptors of octreotide.

Introduction

Since the active site of [FeFe] hydrogenase from *Clostridium pasteurianum*[1] and from *Desulfovibrio desulfuricans*[2] was characterized (Scheme 1), vigorous activities commenced with the aim to mimic the structural and electrochemical properties of the active site [Fe2S2] cluster.[3]
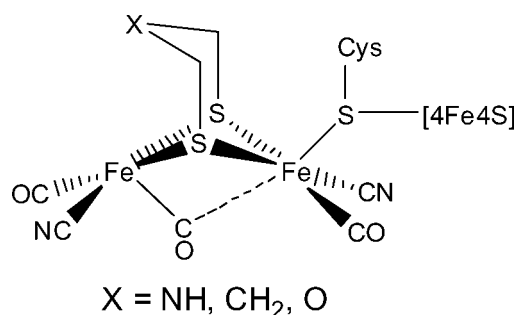
Scheme 1 Active site of [FeFe] hydrogenase with a semibridging CO ligand and a vacant coordination site at the distal iron atom.

Specific features of the active site have been reproduced in model complexes, namely *i*) the "rotated" geometry of the active site, *i.e.* formation of a bridging or semi-bridging C≡O ligand and a vacant coordination site at the distal iron atom,[4] *ii*) the formation of terminal hydrides during catalysis,[5] *iii*) the applicability of water as a solvent and proton source,[6] *iv*) establishment of an electron cascade towards the [Fe2S2] subunit,[7] and *v*) the establishment of a proton relay between the distal iron and an adjacent base.[8] Less attention was directed towards the use of

amino-acid derivatives for mimicking the enzymatic environment until now; some examples (**1-4**) are shown in Scheme 2.[9]
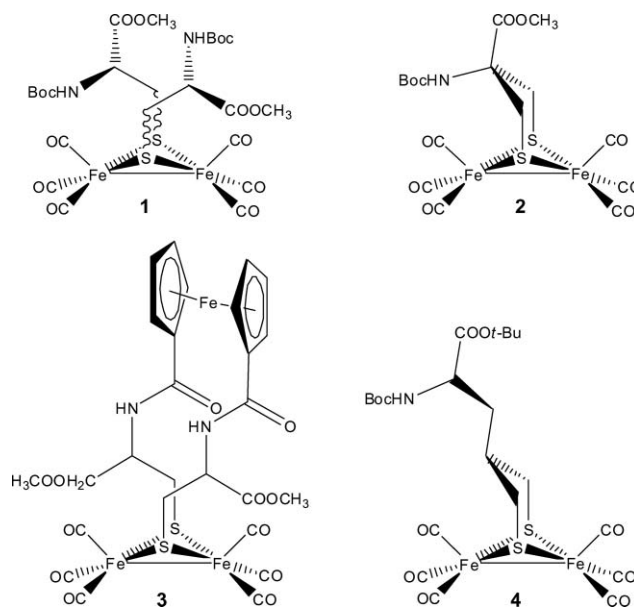

Scheme 2 [FeFe] hydrogenase models containing amino acids.[9]

Following our continued interest in somatostatin mimics[10] we have now investigated the reaction of Fe₃(CO)₁₂ with the macrocyclic peptidic disulfide Sandostatin® (octreotide **5**, Scheme 3) and studied the chemical, electrochemical and biological properties of the resulting product. In comparable conversions, Kolane *et al.*[11] and Sadler *et al.*[12] were able to insert Tc and Pt into the (S,S)-bond of octreotide under mild conditions. Octreotide **5** itself, is well known as a somatostatin (SRIF₁₄, somatotropin-releasing inhibiting factor) analogue; it binds to the five human somatostatin receptors hsst₁₋₅, with affinities ranging from 0.8 nM (hsst₂) to 1.7 μM (hsst₄).[13] It inhibits the release of the growth hormone somatotropin, with an activity that is 70 times higher than that of the natural hormone somatostatin.[14,15] Octreotide derivatives are used in diagnosis and therapy of endocrinic and gastro entero pancreatic tumours, breast and prostate cancers.[15,16]

[a]Institut für anorganische und analytische Chemie, Friedrich-Schiller Universität, August-Bebel-Straße 2, 07751, Jena, Germany. E-mail: wolfgang.weigand@uni-jena.de; Fax: +49 3641 948102; Tel: +49 3641 948160
*[b]Psychiatry Neuroscience Research, Novartis Institutes for Biomedical Research, Postfach, CH-4002, Basel*
[c]Eidgenössische Technische Hochschule Zürich, Departement Chemie und Angewandte Biowissenschaften, Laboratorium für Organische Chemie, Wolfgang-Pauli-Strasse 10, Hönggerberg, HCI, CH-8093, Zürich. E-mail: seebach@org.chem.ethz.ch
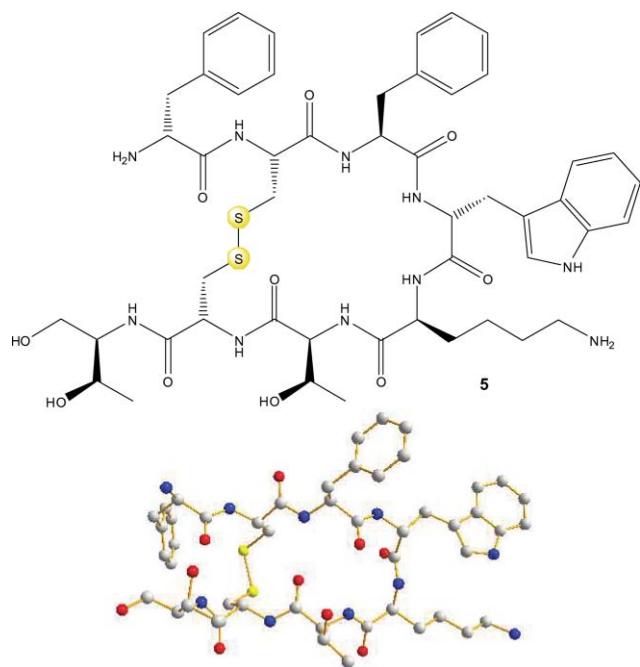
Scheme 3 Molecular formula of Sandostatin® (**5**) and one of its X-ray structures[20] (the C–S–S–C torsion angles in the three independent molecules of the unit cell are 94, 107 and 117°).

Beside the use of octreotide **5** as ligand for a [FeFe]-hydrogenase model complex, it would be interesting to investigate the affinities of the resulting complex towards the somatostatin receptors to reveal its biological and chemical diversity. To the best of our knowledge, a metal-carbonyl complex was first used as a biologically active substance (for immunoassays) in the case of the estrogen mimic **6** (Scheme 4),[17] which binds selectively to estrogen receptors in target tissue and can be detected *via* FT-IR spectroscopy.[18,19]
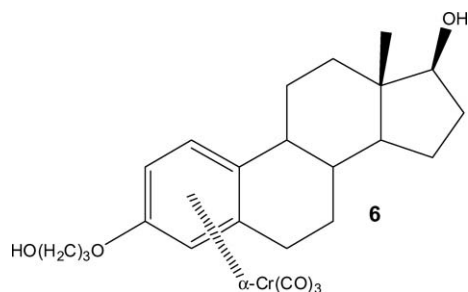
**Scheme 4** FT-IR Detectable organometallic hormone derivative.

This study brings forth a novel [2Fe2S] complex with a peptidic moiety, which can serve as a [FeFe] hydrogenase model. Additionally, the ability to bind to the somatostatin receptors would eventually allow the establishment of a new class of CO-releasing molecules (CORM) or molecules for immunoassays.

Results and discussion

Synthesis and characterization of the iron complex 7

Treatment of octreotide **5** (as an acetate salt) with four equivalents of dodecacarbonyltriiron ($Fe_3(CO)_{12}$) in a 3 : 1 mixture of methanol

and toluene afforded the iron complex **7**, which was isolated as an amorphous orange solid in 39% yield (Scheme 5).
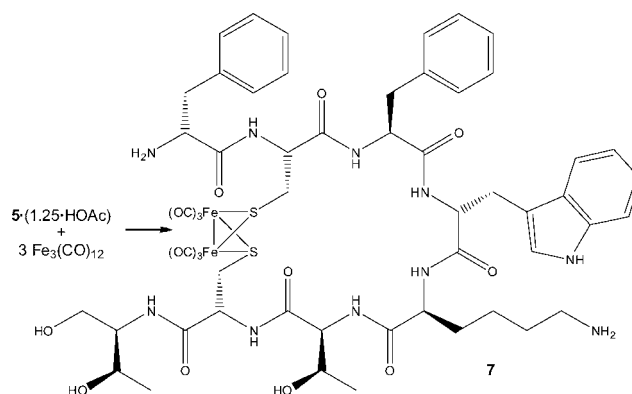
Scheme 5 Reaction of octreotide **5** with excess $Fe_3(CO)_{12}$ to form complex **7** of insertion into the (S,S)-bond.

Compound **7** is air-sensitive in pure methanol and undergoes rearrangement and decomposition, which become evident in the course of NMR measurements and DTA/DSC experiments. The identity of **7** was verified by elemental analysis, NMR, MS and IR studies. Mass spectrometry (micro-ESI) afforded the $[M]^+$ peak at m/z 1298.7, and elemental analysis was correct within *ca.* 0.3% for the composition [**7**·3AcOH·MeOH]. Additionally, the iron content was determined spectrophotometrically with 1,10-phenantroline (calcd.: 7.4%; found: 8.3 ± 0.7%).[21] IR spectroscopy provides additional confirmation for the structure of compound **7**: three v_{CO} bands are visible between 2075 and 1997 cm^{-1} (Fig. 1), which are in good accordance to the CO vibrations observed for complexes **1-4** (Table 1).

To prevent decomposition and oxidation, a sample of **7** for NMR in degassed CD$_3$OH was dissolved and filtered inside a dry-box (<5 ppm O$_2$) into an NMR-tube fitted with a Young-valve. Nevertheless, the ^{1}H NMR spectrum at both 5 °C and 15 °C showed strongly broadened lines, presumably due to contamination with paramagnetic components. This made detailed signal assignment *via* the measured 2D-correlation data impossible and precluded the planned full 3D-solution structure determination by NMR. Repeated measurements at 15 °C, with intervals of several hours in between, showed only very minor changes of the spectrum of **7** with time. A comparison of the ^{1}H NMR spectra at 15 °C of **5**[22] and **7** is displayed in Fig. 2. The solvent OH signal was suppressed by presaturation.

Further characterisation of compound **7** by simultaneous thermal analysis (employing a Netzsch STA 429 equipment) was carried out in the range of room temperature and 400 °C with a heating rate of 5 K min^{-1} in an argon atmosphere (Fig. 3).

Table 1 Comparison of the IR data of complex **7** with literature known amino acid complexes **1-4**

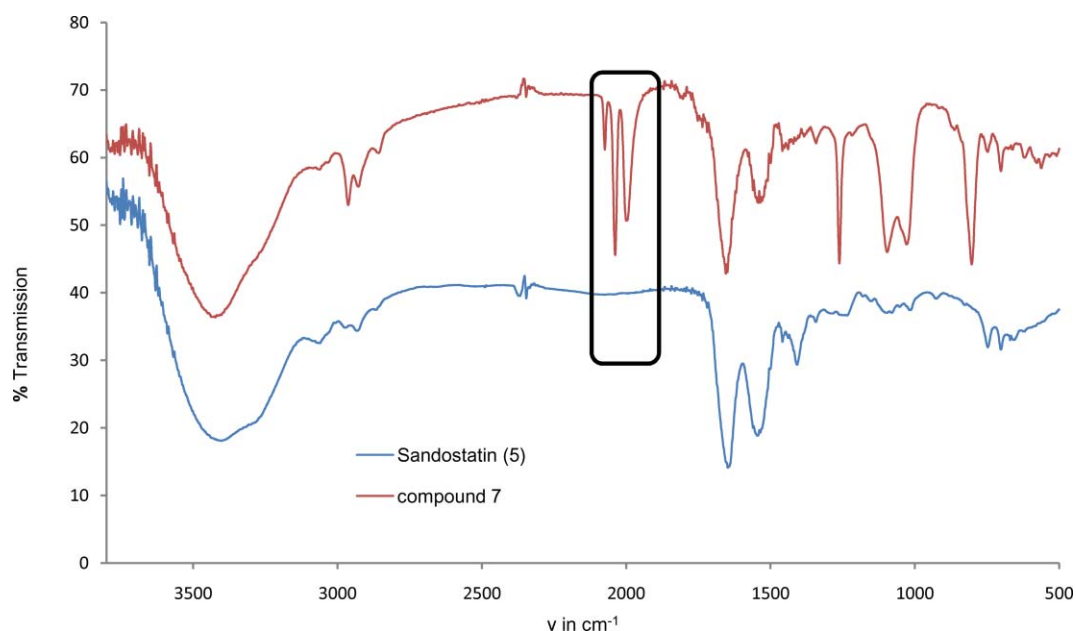| Compound	v_{CO} in cm^{-1}
1[9a]	2073, 2036, 1994
2[9c]	2076, 2038, 2000
3[9b]	2077, 2040, 2000
4[9c]	2074, 2034, 1995
7	2074, 2037, 1997

Fig. 1 IR Spectra of octreotide (**5**) (blue) and compound **7** (red). The v_{CO} frequencies are highlighted in the black box.
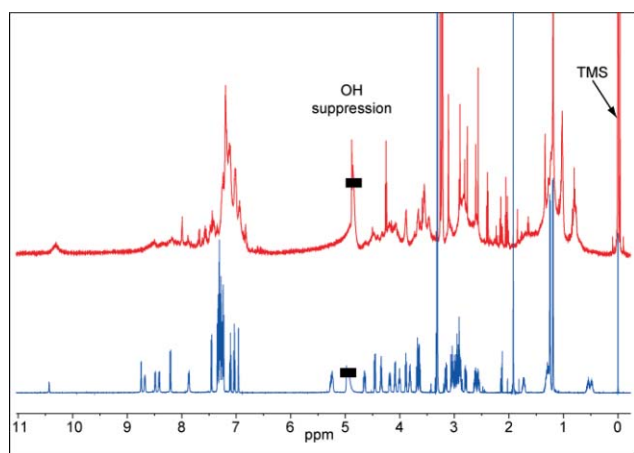

Fig. 2 ^{1}H-NMR spectra (600 MHz) in CD$_3$OH at 15 °C of octreotide (**5**) (blue) and compound **7** (red).

An initial weight loss of 2.1% is completed at 62 °C and can be assigned to the loss of one molecule of methanol per formula unit (calcd. 2.1%). The succeeding weight losses of 3.3% and 8.4% occurring up to 192 °C are compatible with the evolution of three molecules of acetic acid per formula unit (calcd. 4.0% and 7.9%). A further weight loss takes place between 192 and 273 °C when CO is released, which has also been verified by IR spectroscopy (calcd. 11.1%, found 11.8%). The final weight loss is due to further degradation of the molecule. This thermal degradation is an exothermic reaction yielding a residue, which was investigated by X-ray powder diffraction and is a mixture of various components, including iron oxide and iron sulfide.

Electrochemistry

The electrochemistry of compound **7** was studied in DMF by cyclic voltammetry and (cyclic) square wave voltammetry.

Unfortunately, the solubility of **7** is bad in DMF and even worse in the other aprotic solvents normally used for conducting electrochemical experiments. For this reason a saturated solution of unknown concentration was used in all experiments and the results will be described only in a qualitative way.

Fig. 4 shows the cyclic voltammetric reduction of compound **7** in DMF. The main process (accompanied by two irreversible pre-waves which appear at about −1.5 V and −1.75 V, respectively) is observed in the potential range between −2.5 V and −2.7 V. The square wave voltammogram shown in Fig. 5 reveals that the shape of the CV peak associated with this process results from a superposition of two overlapped reduction steps. The first one is a reversible reduction with a half-wave potential of about −2.47 V and a half-peak width that points to a one-electron process. It is followed by an irreversible step which is not visible in the square wave experiment due to the better discrimination between reversible and irreversible processes achieved by this technique. However, because of the unknown saturation concentration of compound **7** in DMF, it was neither possible to determine the diffusion coefficient of the compound nor the exact number of electrons involved in the reversible reduction step.

With respect to the relative high negative potential where the reversible reduction of compound **7** proceeds (compared to other compounds such as Fe$_2$(CO)$_6$(pdt) (pdt = propandithiolato)[23] it is not surprising that the current is increased when adding acetic acid to the sample. However, the catalytic current (measured by square wave voltammetry) starts already at about −2.15 V and grows in an unspecific way (*i.e.* almost linearly) when the electrode potential becomes more negative. That means, the starting potential of the catalytic hydrogen generation lies amid the plateau of the second pre-wave (see Fig. 4) and is still far from the potential were the reversible reduction process occurs. It is therefore hardly possible to make any statement about the mechanism of the proton reduction in the presence of **7** or the species involved in this process.
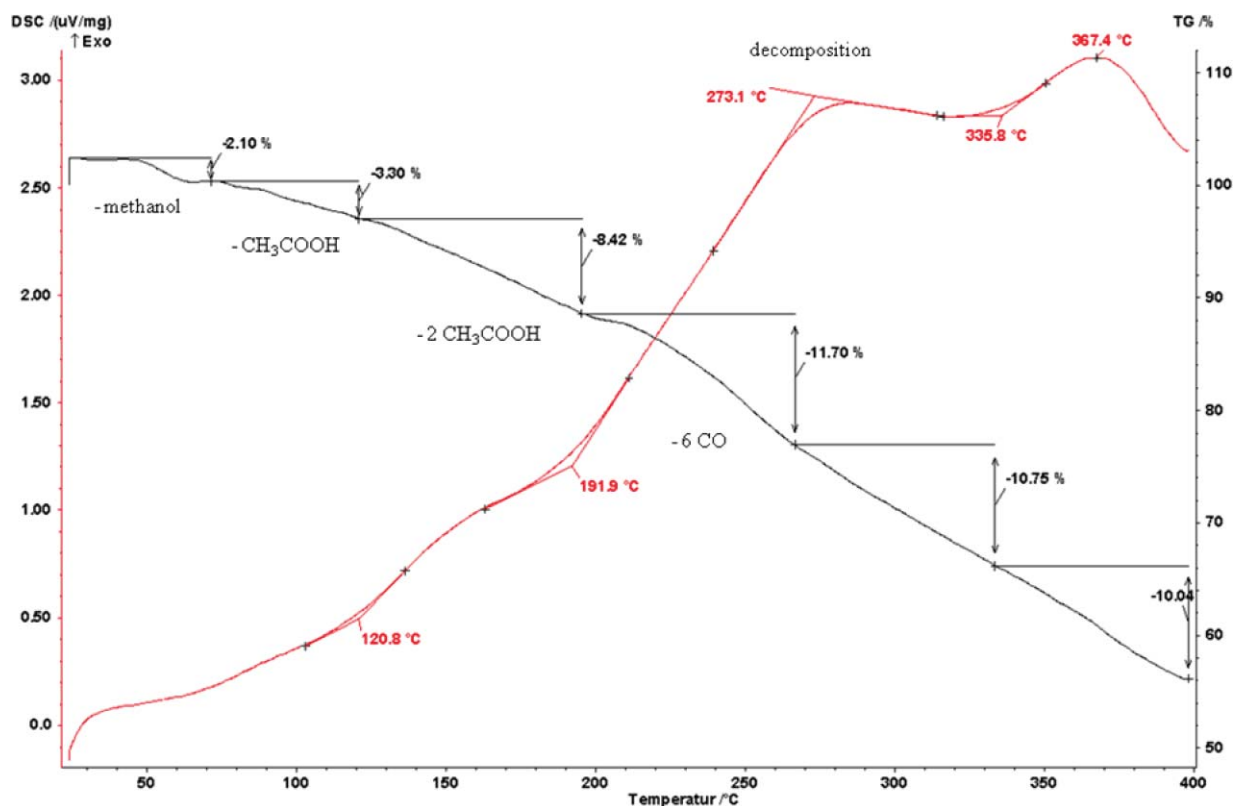
Fig. 3 Differential Scanning Calorimetry (DSC, red) and Thermogravimetry (TG, black) curves of compound [7·3AcOH·MeOH].
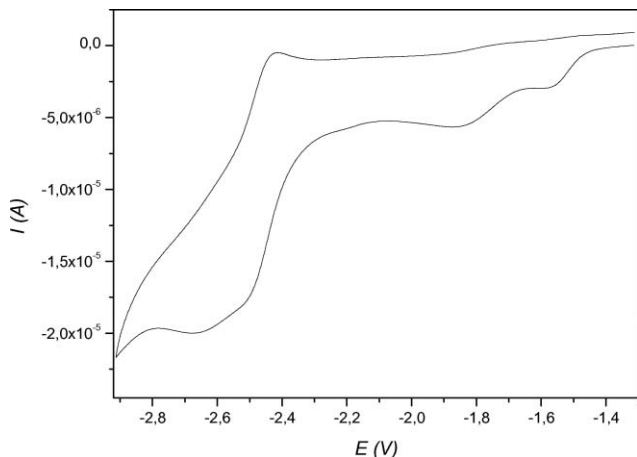
Fig. 4 Cyclic voltammetric reduction of compound **7** in DMF using a scan rate of *1 V/s.*

Biological tests

Measurements of the affinities of compound **7** for the five human somatostatin receptors hsst$_{1-5}$ were carried out as previously described by us.[10] As can be seen from the data listed in Table 2 all affinities are equivalent or at most by one order of magnitude lower in the measurements done with solutions of the complex **7** as compared to octreotide **5**.
This is surprising for two reasons.
i) With most octreotide derivatives, analogs, or mimics the affinity patterns differ from that of octreotide itself, while here all five values differ at most a factor of 10. This would be compatible
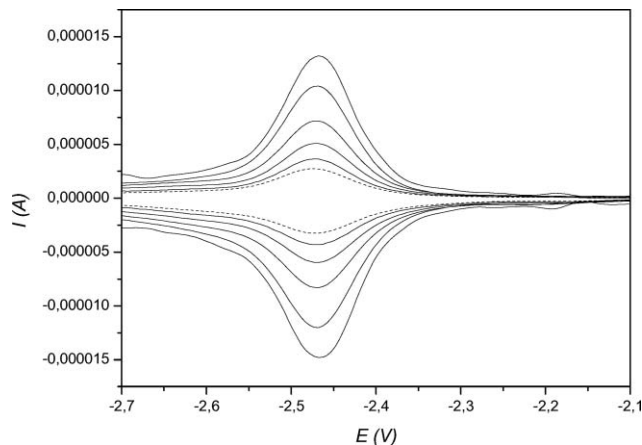
Fig. 5 Square wave voltammograms for the reduction of **7** in DMF using square wave frequencies of *25* (dashed line), *50, 100, 200, 428 and 750 Hz.*.

with partial decomposition of **7** to give *ca.* 10% octreotide **5** when the stock solution is freshly prepared (see Experimental Section). However, in this case a slow decomposition would have been noticed, because the stock solution was used over a period of time for preparing series of diluted solutions, and the assays were repeated three to four times each (see Table 2).

ii) The similarity of the affinities of the iron complex **7** and of octreotide **5** would indicate that there is no significant structural change by insertion of Fe$_2$(CO)$_6$ into the (S,S)-bond. As outlined in Scheme 6, the torsion angle CH$_2$–S–S-CH$_2$ is ≥ 94° (*cf.* Scheme 3), whereas the virtual C–S···S–C dihedral angles in [Fe2S2] clusters[24] are either 0° or close to 180°, which would
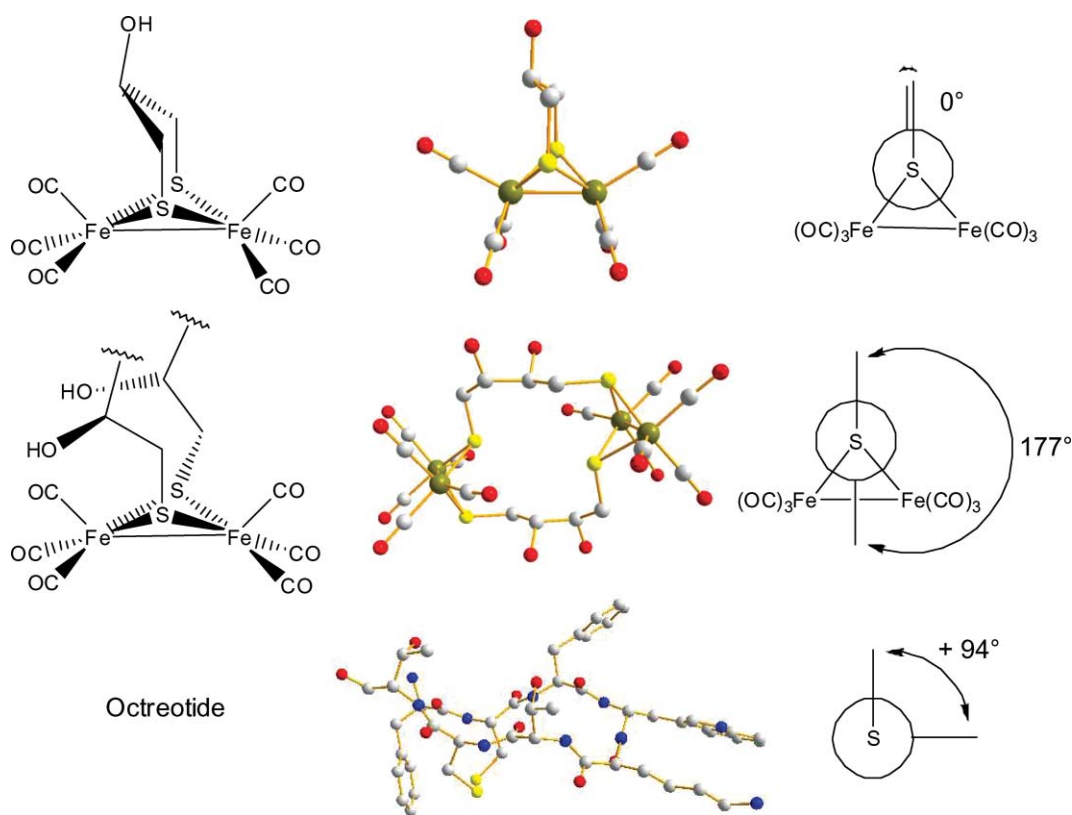
Scheme 6 Virtual C–S···S–C dihedral angles in [Fe2S2] carbonyl complexes and torsion angle CH_2–S–S–CH_2 in octreotide (*cf.* Scheme 3).

Table 2 Affinities measured with octreotide (**5**) and compound **7**. Radioligand binding assay (competition of the specific binding of [^{125}I]-LTT-SRIF$_{28}$) with the five known human somatostatin receptors (hsst$_{1-5}$) expressed in Chinese Hamster Lung Fibroblasts. The numbers in parentheses are the independent determinations, from which the pK_D values were calculated (pK_D = −logM ± SEM). For details see [10] and references cited therein

Affinity (pK_D)		
Octreotide	receptor type	octreotide $Fe_2(CO)_6$ derivative **7**
$6.46 \pm 0.04(18)$	hSST-1	$6.17 \pm 0.06(3)$
$9.21 \pm 0.04(16)$	hSST-2	$8.34 \pm 0.03(4)$
$7.69 \pm 0.04(18)$	hSST-3	$7.07 \pm 0.13(4)$
$6.08 \pm 0.08 (12)$	hSST-4	$6.00 \pm 0.03(3)$
$7.79 \pm 0.04(17)$	hSST-5	$7.02 \pm 0.07(3)$

be expected to lead to considerable backbone distortions of the macrocyclic ring and thus to larger affinity differences as compared to octreotide.

Conclusion

Insertion of diironhexacarbonyl into the (S,S)-bond of sandostatin® (octreotide **5**) leads to a peptidic iron-sulfur cluster **7**, which can be fully characterized (IR, NMR, MS, elemental analysis, thermoanalysis). Albeit compound **7** is not quite stable in solution, it could be used for catalysis of electrochemical hydrogen formation ([FeFe] hydrogenase model) in DMF and for affinity assays for the somatostatin receptors hsst$_{1-5}$. The affinities were surprisingly high in spite of the fact that the iron carbonyl insertion

must lead to major distortions of the macrocylic backbone. With the caveat that there may be (partial) decomposition of the iron-carbonyl complex **7** in the experiments performed in solution we have, for the first time, demonstrated catalytic hydrogen formation with a peptidic [Fe2S2] cluster; furthermore it is indicated by preliminary results that this sandostatin® derived cluster has affinity for the somatostatin receptors. Further investigations (of electrolysis and biological tests under different conditions, crystallization, use of stabilizing Fe-ligands, CO release in solution *etc.*) will provide additional information about the properties of the unique complex **7**.

Experimental section

General

Toluene and hexane were dried over KOH and distilled from sodium/benzophenone. Methanol was dried over CaH_2 and distilled. TLC: Merck silica gel 60 F254 plates were used to monitor the reaction; detection under UV light at 254nm. ^{1}H NMR (of **5** and **7** at 15° C) as well as ^{13}C-NMR, DQF-COSY, TOCSY [t_m = 80 ms], HSQC, HMBC, ROESY [t_m = 300 ms] spectra of **7** were measured at 5° and 15 °C in CD_3OH on a Bruker AVANCE III spectrometer (600MHz; 5 mm DCH cryoprobe) with solvent OH suppression by presaturation. $Fe_3(CO)_{12}$ was used as received from Acros. IR spectra were recorded on a *Perkin-Elmer 2000 FT-IR*. Mass spectrometry (micro-ESI in $CHCl_3$–methanol) was performed on a *SSQ710 Finnigen MAT*. Expected and experimental isotopic distributions were compared.

Preparation of [(octreotide)Fe₂(CO)₆]

$Fe_3(CO)_{12}$ (58 mg, 0.155 mmol) were dissolved in toluene (20 mL). To this solution 39 mg (0.036 mmol) of the peptide, dissolved in methanol (60 mL), was added. Within 4 h stirring at room temperature and argon atmosphere the colour changed from green to red, whereupon the solvent was removed. The oily substance was washed with hexane and dichloromethane to remove excess of $Fe_3(CO)_{12}$. To get rid of possible inorganic contaminations, the residue was dissolved in methanol, the solution filtered off and evaporated to dryness. A red powder (21 mg, 39%) was obtained and identified as $Fe_2(CO)_6$-sandostatin complex. MS (micro-ESI in $CHCl_3$–methanol): 1298.7 [M]⁺, 1321.7 [M+Na]⁺. IR (KBr, cm⁻¹): 3422 (vs), 2963 (m), 2929 (m), 2074 (vs), 2037 (vs), 1997 (vs), 1663 (vs), 1517 (s), 1457 (m), 1340 (m), 1230 (m), 1098 (m), 755 (m), 701 (m), 617 (m), 560 (m). Anal. calcd. for $C_{55}H_{66}Fe_2O_{16}S_2N_{10} + 3CH_3COOH + CH_3OH$: C, 49.28%; H, 5.47%; N, 9.27%; S, 4.24%; Fe, 7.4%. Found: C, 48.92%; H, 5.56%; N, 9.63%; S, 4.71%; Fe, $8.3 \pm 0.7\%$.

Electrochemistry: Instrumentation and procedures

Cyclic voltammetric measurements were conducted in 3-electrode technique using a Reference 600 potentiostat (Gamry Instruments, Warminster, USA). The instrument was controlled by a special build of *DigiElch 5*.[25] This program provides not only routines for the digital simulation of electrochemical experiments but also those for performing the measurements in a consistent way making use of the Gamry Electrochemical Toolkit™ library.

The experiments were performed in DMF (containing 0.25M tetra-*N*-butylammonium-perchlorate) under a blanket of solvent-saturated argon. The ohmic resistance, which had to be compensated for, was determined by measuring the impedance of the system at potentials where the faradaic current was negligibly small. Background correction was accomplished by subtracting the current curves of the blank electrolyte (containing the same concentration of supporting electrolyte) from the experimental CVs. The reference electrode was an Ag/AgCl electrode in acetonitrile containing 0.25M tetra-*N*-butylammonium chloride. The potentials reported in this paper refer to the ferrocenium/ferrocene couple which was measured at the end of each experiment.

The reduction of complex **7** was investigated using a hanging mercury drop ($m_{Hg-drop} \approx 4~mg$) produced by the CGME instrument (Bioanalytical Systems, Inc.,West Lafayette, USA) as working electrode. No oxidation of compound **7** was obtained in DMF on a platinum disk working electrode.

Affinity measurements

A stock solution of compound **7** was prepared by dissolution of 2 mg in 104 µL H_2O/50 µL "cocktail" [a mixture of *N*-methyl-pyrrolidone (NMP), acetic acid and Tween20 (polyoxyethylene sorbitane monolaurate) 5 : 1 by volume]; no insoluble residue was noticed, and the solution remained clear for the entire duration of the measurements. The stock solution was kept in a refrigerator and removed only temporarily for the preparation of dilution series. Air was not excluded from the solutions before affinity measurements. The binding assays were obtained as described previously[10] and the results are collected in.

Briefly, 150 µL of membranes of CCL39 cells expressing recombinant human somatostatin receptors were incubated with 50 µL of [¹²⁵I]-SRIF28, in binding assay buffer containing $MgCl_2$ (5 mM) and the protease inhibitor bacitracin (5 µg mL⁻¹), and either 50 µL binding assay buffer (total binding) or with 50 µL of various concentrations of test compounds. Nonspecific binding was determined in the presence of 50 µL SRIF28 (1 µM). After 1 h at room temperature, the incubation was terminated by vacuum filtration through glass fibre filters pre-soaked in 0.3% (w/v) polyethyleneimine. The filters were rinsed twice with 5 mL of ice cold 10 mM Tris/HCl buffer, pH 7.4, and dried. Bound radioactivity was measured in a γ-counter (80% counting efficiency). Data were analyzed by non-linear regression curve fitting. The data are expressed as mean pK_D (–log M) values of at least 3 independent determinations performed in triplicates.

Acknowledgements

Notes and references

1 J. W. Peters, W. N. Lanzilotta, B. J. Lemon and L. C. Seefeldt, *Science*, 1998, **282**, 1853.
2 Y. Nicolet, C. Piras, P. Legrand, C. E. Hatchikian and J. C. Fontecilla-Camps, *Structure*, 1999, **7**, 13.
3 L. Schwartz, L. Eriksson, R. Lomoth, F. Teixidor, C. Viñas and S. Ott, *Dalton Trans.*, 2008, 2379; Z. Yu, M. Wang, P. Li, W. Dong, F. Wang and L. Sun, *Dalton Trans.*, 2008, 2400; S. Ezzaher, P.-Y. Orain, J.-F. Capon, F. Gloaguen, F. Y. Pétillon, T. Roisnel, P. Schollhammer and J. Talarmin, *Chem. Commun.*, 2008, 2547; P. Li, M. Wang, J. Pan, L. Chen, N. Wang and L. Sun, *J. Inorg. Biochem.*, 2008, **102**, 952; L.-C. Song, H.-T. Wang, J.-H. Ge, S.-Z. Mei, J. Gao, L.-X. Wang, B. Gai, L.-Q. Zhao, J. Yan and Y.-Z. Wang, *Organometallics*, 2008, **27**, 1409; T. Liu, M. Wang, Z. Shi, H. Cui, W. Dong, J. Chen, B. Akermark and L. Sun, *Chem.–Eur. J.*, 2004, **10**, 4474; L.-C. Song, J. Gao, H.-T. Wang, Y.-J. Hua, H.-T. Fan, X.-G. Zhang and Q.-M. Hu, *Organometallics*, 2006, **25**, 5724; C. Greco, G. Zampella, L. Bertini, M. Bruschi, P. Fantucci and L. De Goia, *Inorg. Chem.*, 2007, **46**, 108; W. Gao, J. Ekstöm, J. Liu, C. Chen, L. Eriksson, L. Weng and B. Åkermark, *Inorg. Chem.*, 2007, **46**, 1981.
4 M. L. Singleton, N. Bhuvanesh, J. H. Reibenspies and M. Y. Darensbourg, *Angew. Chem., Int. Ed.*, 2008, **47**, 9492.
5 B. E. Barton and T. B. Rauchfuss, *Inorg. Chem.*, 2008, **47**, 2261.
6 U.-P. Apfel, Y. Halpin, M. Gottschaldt, H. Görls, J. G. Vos and W. Weigand, *Eur. J. Inorg. Chem.*, 2008, 5112; Y. Na, M. Wang, K. Jin, R. Zhang and L. Sun, *J. Organomet. Chem.*, 2006, **691**, 5045.
7 L.-C. Song, L.-X. Wang, M.-Y. Tang, C.-G. Li, H.-B. Song and Qing-Mei Hu, *Organometallics*, 2009, **28**, 3834; C. Tard, X. M. Liu, S. K. Ibrahim, M. Bruschi, L. De Gioia, S. C. Davies, X. Yang, L. S. Wang, G. Sawers and C. J. Pickett, *Nature*, 2005, **433**, 610.
8 J. D. Lawrence, H. Li, T. B. Rauchfuss, M. Benard and M.-M. Rohmer, *Angew. Chem., Int. Ed.*, 2001, **40**, 1768; P. Li, M. Wang, L. Chen, J. Liu, Z. Zhao and L. Sun, *Dalton Trans.*, 2009, 1919; S. Ezzaher, J.-F. Capon, F. Gloaguen, F. Y. Pétillon, P. Schollhammer and J. Talarmin, *Inorg. Chem.*, 2009, **48**, 2.
9 (*a*) C. He, M. Wang, X. Zhang, Z. Wang, C. Chen, J. Liu, B. Akermark and L. Sun, *Angew. Chem., Int. Ed.*, 2004, **43**, 3571; (*b*) X. de Hatten, E. Bothe, K. Merz, I. Huc and N. Metzler-Nolte, *Eur. J. Inorg. Chem.*, 2008, 4530; (*c*) U.-P. Apfel, C. R. Kowol, Y. Halpin, F. Kloss, J. Kübel, H. Görls, J. G. Vos, B. K. Keppler, E. Morera, G. Lucente and W. Weigand, *J. Inorg. Biochem.*, 2009, **103**, 1236; (*d*) A. K. Jones, B. R. Lichtenstein, A. Dutta, G. Gordon and P. L. Dutton, *J. Am. Chem. Soc.*, 2007, **129**, 14844.
10 D. Seebach, E. Dubost, R. I. Mathad, B. Jaun, M. Limbach, M. Löwneck, O. Flögel, J. Gardiner, S. Capone and A. K. Beck, *Helv.*

Chim. Acta, 2008, **91**, 1736; S. Capone, I. Kieltsch, O. Flögel, G. Lelais, A. Togni and D. Seebach, *Helv. Chim. Acta*, 2008, **91**, 2035; D. Seebach, H. Widmer, S. Capone, R. R. Ernst, T. Bremi, I. Kieltsch, A. Togni, D. Monna, D. Langenegger and D. Hoyer, *Helv. Chim. Acta*, 2009, **12**, 2577.

11 H. Kolan, J. H. Li and M. L. Thakur, *Peptide Research*, 1996, **9**, 144.

12 V. P. Munk, S. Fakih, P. del Socorro Murdoch and P. J. Sadler, *J. Inorg. Biochem.*, 2006, **100**, 1946.

13 D. Hoyer, G. I. Bell, M. Berelowitz, J. Epelbaum, W. Feniuk, P. P. A. Humphrey, A. M. ONCarroll, Y. C. Patel, A. Schonbrunn, J. E. Taylor and T. Reisine, *Trends Pharmacol. Sci.*, 1995, **16**, 86; Y. C. Patel, *Frontiers in Neuroendocrinology*, 1999, **20**, 157; D. Hoyer, R. A. Hills, J. Epelbaum, A. J. Harmar, J.-C. Reubi, A. Schonbrunn, J. E. Taylor, A. Vezzani, *IUPHAR Receptor Database*, 2005 Somatostatin receptors (10.1786/543800763668); S. Siehler, C. Nunn, J. Hannon, D. Feuerbach and D. Hoyer, *Mol. Cell. Endocrinol.*, 2008, **286**, 26.

14 M. D. Katz and B. L. Erstad, *Clin. Pharm.*, 1989, **8**, 255.

15 A. Manni, A. E. Boucher, L. M. Demers, H. A. Harvey, A. Lipton, M. A. Simmonds and M. Bartholomew, *J. Steroid Biochem. Mol. Biol.*, 1990, **37**, 1083.

16 E. A. Kouroumalis, *Chemotherapy*, 2001, **47**, 150.

17 A. Vessières, S. Top, A. A. Ismail, I. S. Butler, M. Loüer and G. Jaouen, *Biochemistry*, 1988, **27**, 6659.

18 G. Jaouen, A. Vessières, S. Top, A. A. Ismail and I. S. Butler, *J. Am. Chem. Soc.*, 1985, **107**, 4778.

19 A. Varenne, A. Vessières, P. Brossier and G. Jaouen, *Res. Commun. Chem. Pathol. Pharmacol.*, 1994, **84**, 81.

20 E. Pohl, A. Heine and G. M. Sheldrick, *Acta Crystallogr., Sect. D: Biol. Crystallogr.*, 1995, **51**, 48.

21 The amount of iron was determined spectrophotometrically with 1,10-phenantroline *via* standard addition procedure. A sample of compound **7** (0.9 mg) was oxidized with excess of conc. nitric acid and diluted to 10 mL with water. Subsequently, 1 mL of this solution was added to 0.5 mL aqueous hydroxylamine (320 mg mL^{-1}). A respective amount (20, 40, 100 µL) of stock solution (FeCl$_2$·4H$_2$O; 125 mg L^{-1}) as well as 5 mL 1,10-phenantroline (aq./1 g L^{-1}), 0.1 mL conc. ammonia and 6 mL sodium acetate (aq./1.2 mol L^{-1}) were added. Absorption was measured at 508 nm.

22 C. Wynants, G. van Binst and H. R. Loosli, *Int. J. Peptide Protein Res.*, 1985, **25**, 608; C. Wynants, G. van Binst and H. R. Loosli, *Int. J. Peptide Protein Res.*, 1985, **25**, 615; H. Widmer, A. Widmer and W. Braun, *J. Biomol. NMR*, 1993, **3**, 307.

23 A. Darchen, H. Mousser and H. Patin, *J. Chem. Soc., Chem. Commun.*, 1988, 968; G. A. N. Felton, C. A. Mebi, B. J. Petro, A. K. Vannucci, D. H. Evans, R. S. Glass and D. L. Lichtenberger, *J. Organomet. Chem.*, 2009, **694**, 2681.

24 U.-P. Apfel, Y. Halpin, H. Görls, J. G. Vos, B. Schweizer, G. Linti and W. Weigand, *Chem. Biodiversity*, 2007, **4**, 2138.

25 *DigiElch 5.0* by Manfred Rudolph, available on http://www.elchsoft.com.

Reactions of 7,8-Dithiabicyclo[4.2.1]nona-2,4-diene 7-*exo*-Oxide with Dodecacarbonyl Triiron Fe₃(CO)₁₂: A Novel Type of Sulfenato Thiolato Diiron Hexacarbonyl Complexes

Jochen Windhager,[a] Ulf-Peter Apfel,[a] Tomoharu Yoshino,[b] Norio Nakata,[b] Helmar Görls,[a] Manfred Rudolph,*[a] Akihiko Ishii,*[b] and Wolfgang Weigand*[a]

Dedicated to Prof. Juzo Nakayama

Abstract: The reaction of $Fe_3(CO)_{12}$ (**13**) with 7,8-dithiabicyclo[4.2.1]nona-2,4-diene 7-*exo*-oxide (**12**) yields the sulfenato-thiolato complex **14**, which is used as starting material for further reactions. The disulfenato complex **17** is obtained by using one equivalent of dimethyldioxirane (DMD), and the monoep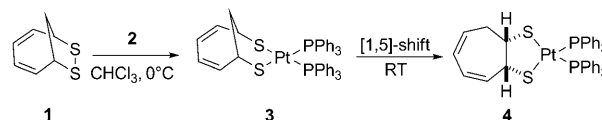oxide **18** is prepared by the oxidation of **14** with an excess of DMD. Complex **14** can be converted to the monophosphine complexes **19a** and **19b** by subsequent substitution of one CO ligand using trimethylaminoxide Me_3NO and triphenylphosphine PPh_3. Additional substitution reactions are done with **17** by using acetonitrile as a ligand to form **20a** and **20b**. In the electrochemical part of the paper, the reactions of the reduced iron species **14**, **15**, **17**, and **19a** are studied.

Keywords: carbonyl ligands · electrochemistry · iron · oxidation · reduction

Introduction

The oxidative addition of cyclic disulfide compounds along the sulfur–sulfur bond to platinum(0) complexes is of current interest.[1–12] Recently, we reported the reaction of the cyclic disulfide 7,8-dithiabicyclo[4.2.1]nona-2,4-diene (**1**) with $[(Ph_3P)_2Pt(\eta^2\text{-}C_2H_4)]$ (**2**),[11] which afforded the corresponding product **3**. Interestingly, the isolated complex **3** showed a [1,5]-rearrangement to form the (dithiolato)platinum(II) complex **4** in high yields (Scheme 1).[11]

[a] Dr. J. Windhager, U.-P. Apfel, Dr. H. Görls, Dr. M. Rudolph,
Prof. Dr. W. Weigand
Institut für Anorganische und Analytische Chemie
Friedrich-Schiller-Universität Jena
August-Bebel-Strasse 2, 07743 Jena (Germany)
Fax: (+49) 3641-948102
E-mail: c8wewo@uni-jena.de

[b] T. Yoshino, Dr. N. Nakata, Prof. Dr. A. Ishii
Department of Chemistry
Graduate School of Science and Engineering
Saitama University
Saitama, Saitama 338-8570 (Japan)
Fax: (+81) 48-858-3700
E-mail: ishiiaki@chem.saitama-u.ac.jp

Supporting information for this article is available on the WWW under http://dx.doi.org/10.1002/asia.200900733.

Scheme 1. [1,5]-Rearrangement of **3** to form (dithiolato)platinum(II) complex **4**.

We have also reported the oxidative addition of cyclic thiosulfinates, for example, dithiane 1-oxide **5** with **2** leading to (sulfenato-thiolato)platinum(II) complex **6** (Scheme 2).[2–7]
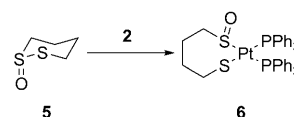
Scheme 2. Formation of (sulfenato-thiolato)platinum(II) complex **6**.

The three-membered cyclic thiosulfinates, dithiirane 1-oxides **7**, showed a similar reactivity, forming the corresponding four-membered (sulfenato-thiolato) platinum(II) complexes **8** in high yields (Scheme 3).[8,9] Alternatively, *S*-oxides of (dithiolato)platinum(II) complexes can also be prepared by photo-oxidation with molecular oxygen[13–15] or

These are not the final page numbers! ⤳⤳

FULL PAPER

Synthetic and Electrochemical Studies on [2Fe2S] Complexes containing a 4-Amino-1,2-dithiolane-4-carboxylic acid moiety

Ulf-Peter Apfel,[a] Christian R. Kowol,[b] Enrico Morera,[c] Helmar Görls, [a] Gino Lucente,[c] Bernhard K. Keppler,[b] and Wolfgang Weigand[*a]

In search for novel [FeFe] hydrogenase model systems, several di- and tripeptides containing a 4-amino-1,2-dithiolane-4-carboxylic acid (Adt) moiety or *N*-benzenesulfonyl-Adt-OMe were reacted with $Fe_3(CO)_{12}$. The resulting [FeFe] complexes were characterized by ^1H and ^{13}C NMR spectroscopy, mass spectrometry and elemental analysis.

All complexes were investigated by cyclic voltammetry and the ability to catalyze the reduction of protons to dihydrogen as a function of acid concentration was studied in different solvents.

(' WILEY-VCH Verlag GmbH & Co. KGaA, 69451 Weinheim, Germany, 2007)

Introduction

Since the active site of the [FeFe] hydrogenase was elucidated by Peters *et al.*[1] and Fontecilla-Camps *et al.*[2] vigorous efforts were undertaken to model the active site of this enzyme. Numerous model complexes are known and recent progress could be observed in the mimicry of specific features of the active site of [FeFe] hydrogenase. Especially, the formation of the "rotated" state (formation of a bridging CO ligand and a vacant coordination site on one iron center),[3] the formation of terminal hydrides during catalysis,[4] the establishment of an electron cascade towards the [2Fe2S] subunit,[5] as well as the influence of a proton shuffle from an adjacent base towards the iron centres during the electrocatalytic dihydrogen formation[6] are in the focus of many research groups. However, so far minor attention was directed towards the use of amino acid containing derivatives mimicking the enzymatic environment.[7] In continuation of our efforts on [2Fe2S] complexes including an amino acid moiety, 4-amino-1,2-dithiolane-4-carboxylic acid (Adt) derivatives were selected as coordinating ligands. Adt exhibits a dithiolane ring in α-position and was exclusively known as a synthetic building block for a long time.[8] But in 2003 the carboxamide derivative of this conformationally restricted dithiolane was found in a natural occurring dibrominated indole enamide termed Kottamide E (Scheme 1) which was isolated from the ascidian *Pycnoclavella kottae*.[9]

Since reaction of iron carbonyls and dithiolanes generates stable double chair conformation complexes, Adt could be an ideal precursor molecule for hydrogenase models, offering an internal base, the capability to form non-covalent interactions via the functional group of the side chain[10] and a variety of possible derivatisations.

___

[a]   Institut für Anorganische und Analytische Chemie, Friedrich-Schiller Universität Jena, August-Bebel-Straße 2, 07743 Jena, Germany, Fax: (+49) 3641 948102, E-mail: wolfgang.weigand@uni-jena.de
[b]   University of Vienna, Institute of Inorganic Chemistry, Währingerstr. 42, A-1090 Vienna, Austria
[c]   Dpt. di Chimica e Tecnologie del Farmaco, "Sapienza" Università di Roma , P.le A. Moro 5, 00185 Roma, Italy

(Insert Scheme 1 here.)

Scheme 1. Kottamide E, containing the carboxamide of 4-amino-1,2-dithiolane-4-carboxylic acid (Adt).

However, initial attempts with Adt containing [FeFe] model complexes revealed no influences of the pendant base on the catalytic.[7c] Thus, novel Adt derivatives with additional functional groups were synthesized. A methionine and/or phenylalanine or proline moiety was coupled to the Adt residue, thus building up di- and tripeptidic ligands (Scheme 2). Furthermore a *N*-sulphonyl derivative of Adt, offering an acidic NH proton, has been also examined (Scheme 2). All dithiolane ligands were reacted with $Fe_3(CO)_{12}$ to afford the corresponding [2Fe2S] complexes, which were investigated according their ability to act as [FeFe] hydrogenase model complex via cyclic voltammetry. In addition the electrocatalytical properties in different aprotic solvents were compared.

Results and discussion

The reaction of Boc-Adt-OMe (**1**) with thionylchloride generates the free amine, which was *in situ* reacted with 1-(3-dimethylaminopropyl)-3-ethylcarbodiimide hydrochloride (EDC), 1-hydroxybenzotriazole (HOBt) and *N-tert*-butoxycarbonyl-L-methionine to afford the dipeptide **2** (Scheme 2).[12] This molecule possesses a thioether group, which basically enables the formation of [2Fe3S] clusters. The reaction of **2** with $Fe_3(CO)_{12}$ under reflux conditions results in complex **3** in moderate yield of 52 %. One- and two-dimensional ^1H and ^{13}C NMR spectra, the *m/z* values and isotopic distribution of mass spectrometry as well as elemental analysis revealed the molecular structure of compound **3**. However, no coordination of the methionine sulphur to the iron centre could be observed either by thermal treatment or by reaction of **3** with trimethylamine-*N*-oxide which should force an oxidative cleavage of a CO group[11] and facilitate the coordination of the thioether group.

Scheme 2. Adt containing ligands and products of the reaction with Fe$_3$(CO)$_{12}$.

Thus compound **2** was treated with sodium hydroxide generating the carboxylic acid, which was used without further purification for the conversion into the tripeptide Boc-Met-Adt-Phe-OMe (**4**) via standard esterification procedures using EDC, HOBt and L-phenylalanine methyl ester.[12] Subsequent reaction of **4** with Fe$_3$(CO)$_{12}$ afforded the respective complex **5**. According to the above procedures also the dipeptide Boc-Adt-Phe-OMe (**6**) and its corresponding [FeFe] complex **7** were synthesized. Additionally complexes **3**, **5** and **7** were treated with trifluoroacetic acid (TFA) to achieve *N*-Boc-deprotection, however no reaction was observed and no complexes containing a free amino group could be obtained. Thus, we decided to examine the properties of the ligand Boc-Pro-Adt-OMe **8** (Scheme 2) in which, unlike models **2**, **4** and **6**, linear side chains are not present. Dipeptide **8**, due to the presence of two consecutive cyclic aminoacids,[13] should prefer a compact folded backbone conformation with reduced side chain steric interference and distinct interaction capability. N-Boc proline was reacted with H-Adt-OMe to give **8** in moderate yield (47%). Single crystals for X-ray diffraction analysis were obtained by slow evaporation of a solution of **8** in chloroform (Figure 1).

Figure 1. Molecular structure of **8** with thermal ellipsoids at 50 % probability level (hydrogen atoms are omitted for clarity).

Compound **8** is co-crystallized with chloroform and confirms the expected molecular structure. Studying the bond lengths and angles in the Adt-part, some interesting features become obvious. The dithiolane ring exhibits two different C–S bond distances of 178.8(5) and 182.3(6) pm as well as two different C–S–S angles of 92.66(19) and 90.20(19)° (Table 1). Comparison of the torsion angle C–S–S–C of **1** and **8** revealed an increase from 31.50 to 44.97°, whereas the S–S distance is unchanged at 205.6(3) and 204.6(3) pm, respectively.[12] These data are very similar to Boc-Adt-Adt-NHMe, where the torsion angle (C–S–S–C) is 42.6° and sterical reasons have been suggested for the distortion of the dithiolane ring.[13]

Table 1. Selected bond angles [°] and distances [pm] of compound **8**.

S(1)–S(2)	204.6(3)	C(2)–C(14)	154.0(7)
S(1)–C(1)	178.8(5)	C(2)–N(1)	147.0(5)
S(2)–C(3)	182.3(6)	C(4)–N(1)	132.2(7)
C(1)–C(2)	154.5(7)	C(4)–O(1)	123.7(6)
C(2)–C(3)	155.6(7)	C(4)–C(5)	154.4(6)
N(2)–C(9)	132.1(6)	C(5)–N(2)	145.2(6)
S(1)–S(2)–C(3)	92.66(19)	C(1)–C(2)–N(1)	108.3(4)
S(2)–S(1)–C(1)	90.20(19)	C(1)–C(2)–C(14)	107.7(4)
S(1)–C(1)–C(2)	107.8(3)	N(1)–C(2)–C(14)	108.8(4)
S(2)–C(3)–C(2)	109.7(4)	C(2)–N(1)–C(4)	121.0(4)
C(1)–C(2)–C(3)	110.3(4)	N(1)–C(4)–C(5)	115.0(4)
C(4)–C(5)–N(2)	111.2(4)		

Unfortunately, all attempts to get single crystals of any [FeFe] model complex were unsuccessful. Reaction of **8** with Fe$_3$(CO)$_{12}$

resulted in complex **9** in good yields (65 %), but again the deprotection of the peptide with standard reagents (TFA, thionylchloride, hydrogen chloride) failed. Attempts to deprotect the dipeptide **8** with TFA and subsequent reaction with Fe$_3$(CO)$_{12}$ resulted in a mixture of species which could not been separated.

A different approach was committed using a sulphonyl group bound to the Adt-OMe residue. Sulphonamides have been known as the largest class of antimicrobial agents for a long period and have shown to be irreversible inhibitors of cysteine proteases.[14] Beside the importance for medicinal chemistry,[15] the electron withdrawing properties of the sulphonyl group results in an acidic NH proton, which can be deprotonated under mild conditions.[16] This was impressively confirmed by kinetic studies of the hydrolysis of *p*-nitrophenyl-*o*-methansulphonamidobenzoate[17] (pK$_a$ = 8.41 in acetonitrile) and *p*-nitrophenyl-*p*-methansulphonamidobenzoate[18] (pK$_a$ = 7.34 in acetonitrile). Thus a proton shift from the sulphone NH to the iron centres becomes rather possible. Inspired by these properties, the dipeptide **10** was synthesized and reacted with Fe$_3$(CO)$_{12}$ in toluene affording complex **11** in good yield (83%) as an air and moisture stable red solid. To validate a possible influence of the sulphonamide group towards the catalytic mechanism, NMR investigations were performed in the presence of CD$_3$COOD. A decrease of the NH resonance at 5.71 ppm should be observed due to a proton exchange by deuterium. This can either occur via a S$_N$2 mechanism similar to that discussed by Mandell *et al.* (Scheme 3)[19] or dissociation of the N-H bond and subsequent deuteration. However, no change in the NMR resonance could be observed, in agreement with IR measurements with and without acetic acid.

Scheme 3. Hypothetic mechanistic pathway for the desired protonation of the [FeFe] core.

Electrochemistry

The cyclic voltammograms of the [FeFe] metal complexes **3**, **5**, **7**, **9** and **11** were recorded in order to observe the electrochemically induced reduction and oxidation properties of these compounds and to assess their ability to catalyze the formation of dihydrogen from weak acids. A comparision of the electrochemical data is shown in Table 2.

Table 2. Electrochemical data[a] of the iron complexes.

Compound	E$_p$/[Fe^{I}Fe^I]/ [Fe^{II}Fe^I]	E$_p$/[Fe^{I}Fe^I]/ [Fe^{0}Fe^I]	E$_p$/[Fe^{0}Fe^I]/ [Fe^{0}Fe^0]
Fe$_2$(CO)$_6$(Boc-Adt-OMe)[7c]	+0.81[b]	–1.47[b]	–2.09[b]
3	+0.98[b]	–1.52[b]	–1.76[b]
5	+0.95[b]	–1.57[b]	n/a
7	+0.71[b] and +0.94[b,c]	–1.51[b]	–1.89[b]
9	+0.8[b] and +0.97[b,c]	–1.48[b]	–1.81[b]
11	+0.8[b] and +1.0[b,c]	-1.48[b]	–1.72[b]

[a] Potentials in V ± 0.01 *vs*. 0.01 M Ag/Ag$^+$ in CH$_3$CN in 0.10 M [*n*-Bu$_4$N][BF$_4$]/CH$_3$CN; [b] irreversible wave; [c] further oxidation to the [Fe^{II}Fe^{II}] state.

Complexes **3**, **5**, **7**, **9** and **11** show quite similar electrochemical properties (Table 1) and as representative a detailed description will be given for compound **9**. Following a cathodic scan of complex **9** (Figure 2) starting at 0.00 V vs. 0.01 M Ag/Ag$^+$ in CH$_3$CN, the cyclic voltammogram reveals an irreversible reduction peak at $E_{p,red}$ = –1.48 V attributable to [Fe^{I}Fe^I]→[Fe^{I}Fe^0]$^-$. This irreversible signal suggests an EC mechanism where the Fe^{I}Fe^I state is transferred into [Fe^{I}Fe^0]$^-$ by a one electron reduction and is followed by a fast change of the bonding properties within the molecule, which is in good agreement with literature results.[20] This change of bonding properties can be best described by the cleavage of the Fe–Fe bond and/or the appearance of a bridging carbonyl molecule.[20,21] At –1.81 V a further small irreversible reduction wave can be observed, attributed to the [Fe^{I}Fe^0]→[Fe^{0}Fe^0]$^{2-}$ process in accordance with Fe$_2$(CO)$_6$(Boc-Adt-OMe)[7a]. After reversal of the scan, an oxidation peak at –1.23 V occurs, 250 mV more positive than the [Fe^{I}Fe^I]→[Fe^{I}Fe^0]$^-$ reduction potential, suggesting that this signal is not the simple re-oxidation of [Fe^{I}Fe^0]$^-$ but the oxidation of the rapidly formed reaction product. At ~ +0.8–1.0 V the oxidation of [Fe^{I}Fe^I] can be observed. In addition, in the case of complex **7** and **9** a second well separated oxidation wave occurs, which can be ascribed to the [Fe^{I}Fe^{II}]$^+$→[Fe^{II}Fe^{II}]$^{2+}$ processes.

(Insert Figure 2 here.)

Figure 2. Cyclic voltammograms of complex **9** (1mM) in the presence of different concentrations of acetic acid.

In the presence of acetic acid (HOAc) the initial reduction potential at –1.48 V remains constant (Figure 2). Thus prior to the reduction no protonation of compound **9** takes place (equally for **3**, **5**, **7** and **11**), suggesting no involvement of the amide groups of the ligand as a proton donor. However, with continuously addition of acetic acid a steadily increasing current at around –2.2 V emerged, indicating the electrocatalytic formation of dihydrogen.[22] In agreement to literature, the second reduction step to [Fe^{0}Fe^0]$^{2-}$ is followed by two protonations leading to the generation of dihydrogen and the simultaneous regeneration of the initial [Fe^{I}Fe^I] state (Scheme 4).[22a]

(Insert Scheme 4 here.)

Scheme 4. Catalytic mechanisms in the presence of a weak (blue) and strong acids (black). The E_p values are taken from compound **9**.

Using trifluoroacetic acid (TFA, pK_a = 12.65 in CH$_3$CN)[23] instead of acetic acid (pK_a = 22.6 in CH$_3$CN)[23] again no shift of the [Fe^{I}Fe^I]→[Fe^{I}Fe^0]$^-$ reduction potential could be observed (Figure 3), confirming the synthetic experience that TFA is not able to remove the Boc protecting group from the proline nitrogen. Nevertheless the cyclic voltammograms (Figure 3) are strongly altered compared to that using HOAc. It is known that in contrast to weak acids[22] the one-electron reduction product [Fe^{0}Fe^I] can react very fast with protons from strong acids like TFA to give a [{H$^-$}Fe^{II}Fe^I] assembly (Scheme 4).[22b] For small TFA concentrations (< 4 mM) the further reduction to [HFe^{I}Fe^I] is followed by a second protonation ([{H$_2$}Fe^{I}Fe^I]), resulting in the release of dihydrogen at around –1.6 V. Thus, in principle, an ECEC mechanism is suggested in the presence of TFA (< 4 mM) in accordance to the results found by Pickett et al.[24] At higher concentrations of TFA (> 4 mM) a new catalytic reduction signal can be observed, which continuously shifts to more negative potentials, ending up at –1.86 V at 10 mM TFA. This behaviour

can be explained by a further reduction of [{H$_2$}Fe^{I}Fe^I] resulting in the formation of dihydrogen and regeneration of [Fe^{0}Fe^I]$^-$ (Scheme 4).[24]

(Insert Figure 3 here.)

Figure 3. Cyclic voltammograms of complex **9** (1 mM) in the presence of different concentrations of trifluoroacetic acid.

To get further information about the parameters affecting the potential for the formation of dihydrogen and the redox properties of the [FeFe] complexes, cyclic voltammetry measurements of complex **9** were repeated in the aprotic solvents dimethylformamide (DMF), dimethylsulfoxide (DMSO) and dichlormethane (CH$_2$Cl$_2$) in the presence of 5 and 10 mmol HOAc. To allow comparison with the data obtained in CH$_3$CN, first the reduction potentials of HOAc in the respective solvents were investigated without presence of the complex (Table 3). In contrast to the strong reduction signal of acetic acid at around –2.3 V in CH$_3$CN, the respective spectra in DMF and DMSO revealed almost no dihydrogen development up to –2.7 and –2.9 V vs 0.01 M Ag/Ag$^+$ in CH$_3$CN, respectively, near to the solvent cut off potentials. In the case of CH$_2$Cl$_2$ a small reduction peak at around –2.1 V can be observed (solvent cut off at around –2.2 V).

Table 3. Comparison of electrochemical reduction of HOAc in different solvents in the absence and in the presence of complex **9**

Solvent	E_p (H$^+$/H$_2$)/[V]	E_p (H$^+$/H$_2$) in the presence of **9**/[V]
CH$_3$CN	–2.3	shoulder at –2.1
DMF	< –2.7	no distinct reduction peak
DMSO	< –2.9	no distinct reduction peak
CH$_2$Cl$_2$	–2.1	shoulder at –2.1

[a] Potentials in V *vs.* 0.01 M Ag/Ag$^+$ in CH$_3$CN containing 0.10 M [*n*-Bu$_4$N][BF$_4$] as supporting electrolyte

Without addition of HOAc the redox potential of the [Fe^{I}Fe^I]→[Fe^{I}Fe^0]$^-$ reduction of complex **9** remains closely the same in all investigated solvents. Addition of 5 mmol HOAc in DMF solution of **9** results in a continuous increase of the current starting at ~ –2.0 V, but not in a distinct reduction signal (Figure 4). Furthermore, the intensity of the catalytic current only slightly increases from 5 to 10 equivalents of acetic acid and nearly no difference could be observed between 10 and 15 mmol HOAc. Using DMSO as the solvent, a similar behaviour as in DMF was observed, again with no correlation of the HOAc amount added and the catalytic current. In CH$_2$Cl$_2$ solution a shoulder at around –2.1 V for the catalytic transformation of protons to dihydrogen can be observed (Figure 4) and a stepwise increase of the catalytic current. Thus for the characterisation of the electrocatalytical properties, only CH$_2$Cl$_2$ is comparable to CH$_3$CN, however with the limitation that the cutoff potential is far more positive at around –2.2 V vs 0.01 M Ag/Ag$^+$ in CH$_3$CN.

(Insert Figure 4 here.)

Figure 4. Cyclic voltammograms of complex **9** (1 mM) in the presence of acetic acid in DMF (top) and CH$_2$Cl$_2$ (bottom).

Conclusion

Diiron dithiolato compounds containing a 4-amino-1,2-dithiolane-4-carboxylic acid (Adt) moiety have been prepared in good yields as [FeFe]-hydrogenase model compounds. The novel di- and tripeptidic complexes show no influence of the *N*-Boc protected amino acid backbone towards the formation of dihydrogen in the presence of acetic acid or trifluoro acetic acid. This behaviour was also observed in the case of a sulphonamide complex, containing an acidic NH proton. A comparative study of the electrochemical properties of compound **9** in DMSO, DMF, CH_2Cl_2 and CH_3CN revealed a very similar response of the complex itself, but the activity of the dihydrogen formation strongly depends on the solvent. Only in the case of CH_2Cl_2 the catalytical current of dihydrogen formation is comparable with that of the standard solvent CH_3CN, whereas DMF and DMSO appear not suitable for the characterisation of the electrocatalytical properties of [2Fe2S] complexes.

Experimental Section

All reactions were carried out under an argon atmosphere. Toluene and THF were dried over KOH and distilled from sodium/benzophenone. Chemicals were received from Fluka or Acros and used without further purification. **1**, **2**, **4** and **6** as well as Boc-Pro-OH were synthesized following literature procedures.[12,25] Thin layer chromatography (TLC) was performed on Merck silica gel 60 F254 plates (detection under UV light at 254 nm) and FC (flash chromatography) on Fluka silica gel 60. ^{1}H NMR and ^{13}C{^{1}H} NMR spectra were recorded on a Bruker AVANCE 200 MHz or 400 MHz spectrometer, whereby the splitting of proton resonances are defined with s (singlet), d (doublet), t (triplet) and m (multiplet). Chemical shifts are given in parts per million with reference to internal $CHCl_3$ or $SiMe_4$. Infrared spectra were obtained from KBr pellets with a Perkin-Elmer 2000 FT-IR instrument or Perkin-Elmer 983 spectrophotometer. The intensity of the signals is assigned as vs (very strong), s (strong), m (medium) and w (weak). Electron impact mass spectrometry was carried out at 70 eV with a Finnigan SSQ710 or Q-TOF Micro instrument (Micromass, Waters) using desorption electron ionisation (DEI), fast atom bombardment (FAB) or electron spray ionisation (ESI) mode. Expected and experimental isotope distributions were compared. Elemental analyses (C, H, N, S) were carried out on a LECO CHNS-931 instrument or on a Fisons EA-1108 apparatus. Prior to the determination of the elemental analyses, all substances were dried in high vacuum for at least one day and the remaining amounts of hexane are in accordance with ^{1}H NMR spectroscopy.

Synthesis of [(Boc-Met-Adt-OMe)Fe$_2$(CO)$_6$] (3): Boc-Met-Adt-OMe (**2**) (25 mg, 0.061 mmol) and Fe$_3$(CO)$_{12}$ (31 mg, 0.061 mmol) were dissolved in dry toluene (20 mL) and refluxed for 30 min. The solvent was evaporated under reduced pressure and the crude product was purified via FC (THF : hexane = 1:3). Yield: 22 mg (52%) as a red solid. ^{1}H NMR (200 MHz, CDCl$_3$): δ = 6.82 (m, 1H, N*H*Boc), 4.90 (d, $^3J_{H,H}$ = 8.2 Hz, 1H, N*H*-Adt), 4.30 (m, 1H, C*H*), 3.66 (s, 3H, OC*H$_3$*), 3.06 and 2.77 (2 d, $^2J_{H,H}$ = 14.2 Hz, 2H, CC*H$_A$H$_B$*S), 2.52 (t, $^3J_{H,H}$ = 7.1 Hz, 2H, C*H$_2$*SCH$_3$), 2.40 and 2.27 (2 d, $^2J_{H,H}$ = 13.4 Hz, 2H, CCH$_A$*H$_B$*S), 2.11 (s, 3H, SC*H$_3$*), 2.02-1.83 (m, 2H, C*H$_2$*CH) 1.41 (s, 9H, C(C*H$_3$*)$_3$). ^{13}C NMR (50 MHz, CDCl$_3$): δ = 207.2 (CO), 172.0 (*C*(O)OCH$_3$), 170.7 (*C*(O)NH), 156.2 (*t*-BuO*C*(O)NH), 80.7 (*C*(CH$_3$)$_3$), 61.5 (S*C*H$_2$CCH$_2$S), 53.4 (O*C*H$_3$), 53.1 (*C*HNHBoc), 30.3 (*C*H$_2$CH), 30.0 (S*C*H$_2$C*C*H$_2$S), 29.7 (*C*H$_2$SCH$_3$), 28.3 (C(*C*H$_3$)$_3$), 15.2 (S*C*H$_3$). MS (FAB in *meta*-nitrobenzyl alcohol): 691 [M+H]$^+$. IR (KBr, cm^{-1}): 3423m, 2960m, 2924m, 2853m, 2076vs, 2036vs, 1996vs, 1740s, 1686s. Anal. calcd. for C$_{21}$H$_{26}$Fe$_2$O$_{11}$S$_3$N$_2$·1.7hexane: C,

44.78%; H, 6.00%; N, 3.35% S, 11.50%. Found: C, 44.56%; H, 6.19%; N, 3.42%; S, 11.76%.

Synthesis of [(Boc-Met-Adt-Phe-OMe)Fe$_2$(CO)$_6$] (5): Boc-Met-Adt-Phe-OMe (**4**) (44 mg, 0.081 mmol) and Fe$_3$(CO)$_{12}$ (41 mg, 0.081 mmol) were dissolved in dry THF (40 mL) and refluxed for 45 min. The solvent was evaporated under reduced pressure and the crude product was purified via FC (THF : hexane = 1:1). Yield: 29 mg (42%) as a red solid. ^{1}H NMR (400 MHz, CDCl$_3$): δ = 7.71–7.14 (m, 5H, H$_{aromatic}$), 6.98 (s, 1H, N*H*-Adt), 5.09 (m, 1H, N*H*Boc), 4.84 (m, 1H, C*H*C(O)OCH$_3$), 4.71 (m, 1H, C*H*NHBoc), 4.22 (s, 3H, OC*H$_3$*), 3.71 (m, 4H, SC*H$_2$*C), 3.49 (m, 2H, C*H$_2$*Ph), 3.12 (m, 2H, C*H$_2$*SCH$_3$), 2.58 (m, 2H, C*H$_2$*CH$_2$S), 2.10 (s, 3H, SC*H$_3$*), 1.49 (s, 9H, C(C*H$_3$*)$_3$). [13]C (100 MHz, CDCl$_3$): δ = 207.3 (CO), 171.5 (*C*(O)OCH$_3$), 167.7 (*C*HC(O)NH), 155.9 (O*C*(O)NH), 132.3, 130.8, 129.9, 128.2 (*C*$_{aromatic}$), 80.8 (*C*(CH$_3$)$_3$), 68.1 (S*C*H$_2$CCH$_2$S), 53.8 (*C*HCH$_2$Ph), 53.6 (*C*HNHBoc), 52.3 (O*C*H$_3$), 37.9 (*C*H$_2$Ph), 30.3 (S*C*H$_2$CH$_2$CH), 30.2 (S*C*H$_2$C*C*H$_2$S), 29.3 (*C*H$_2$SCH$_3$), 28.2 (C(*C*H$_3$)$_3$), 15.2 (S*C*H$_3$). MS (Micro-ESI in CHCl$_3$/CH$_3$OH): 860 [M+Na]$^+$. IR (KBr, cm^{-1}): 3418s, 2955m, 2924s, 2850m, 2074vs, 2035vs, 1989vs, 1931w, 1693vs, 1514m, 1504m. Anal. calcd. for C$_{30}$H$_{35}$Fe$_2$O$_{12}$S$_3$N$_3$·0.5hexane: C, 45.01%; H, 4.81%; N, 4.77% S, 10.92%. Found: C, 45.11%; H, 4.98%; N, 4.62%; S, 11.05%.

Synthesis of [(Boc-Adt-Phe-OMe)Fe$_2$(CO)$_6$] (7): Boc-Adt-Phe-OMe (**6**) (25 mg, 0.059 mmol) and Fe$_3$(CO)$_{12}$ (30 mg, 0.059 mmol) were dissolved in dry toluene (20 mL) and the dark green solution was stirred under reflux for 30 min. The solvent was evaporated under reduced pressure and the crude product was purified via FC (THF : hexane = 1:3). Yield: 28 mg (67%) as a red solid. ^{1}H NMR (200 MHz, CDCl$_3$): δ = 7.24–6.96 (m, 5H, H$_{aromatic}$), 6.64 (d, $^3J_{H,H}$ = 7.8 Hz, 1H, N*H*CH), 4.69 (m, 2H, N*H*Boc and NHC*H*), 3.66 (s, 3H, OC*H$_3$*), 3.04 (d, $^3J_{H,H}$ = 4.4 Hz, 2H, CHC*H$_2$*), 2.92 and 2.76 (2 d, $^2J_{H,H}$ = 14 Hz, 2H, C*H$_A$H$_B$*S), 2.40 and 2.20 (2 d, $^2J_{H,H}$ = 14.6 Hz, 2H, CH$_A$*H$_B$*S), 1.41 (s, 9H, C(C*H$_3$*)$_3$. ^{13}C NMR (50 MHz, CDCl$_3$): δ = 207.0/206.6 (CO), 171.5 (*C*(O)NH), 170.7 (*C*(O)OCH$_3$), 153.3 (*t*-BuO*C*(O)NH), 135.5/129.2/127.2/125.5 (*C*$_{aromatic}$), 81.8 (*C*(CH$_3$)$_3$), 61.6 (S*C*H$_2$CCH$_2$S), 53.4 (NH*C*H), 52.4 (O*C*H$_3$), 37.9 (CH*C*H$_2$), 30.3 (S*C*H$_2$C*C*H$_2$S), 28.1 (C(*C*H$_3$)$_3$). MS (Micro-ESI in CHCl$_3$): 729 [M+Na]$^+$. IR (KBr, cm^{-1}): 3371m, 3315m, 2955m, 2927m, 2855w, 2074vs, 2036vs, 2000vs, 1750s, 1690s, 1649s. Anal. calcd. for C$_{25}$H$_{26}$Fe$_2$O$_{11}$S$_2$N$_2$·0.6hexane: C, 45.32%; H, 4.57%; N, 3.70% S, 8.46%. Found: C, 45.46%; H, 4.56%; N, 3.42%; S, 8.10%.

Synthesis of Boc-Pro-Adt-OMe (8): To a solution of Boc-Adt-OMe (**1**) (500 mg, 1.79 mmol) in methanol (10 mL) at 0 °C was added thionylchloride (130 µL). The solution was heated up to 50 °C and stirred for 6 h, followed by removal of the solvent under reduced pressure. The remaining residue (HCl·H-Adt-OMe) was dissolved in dimethylformamide (10 mL) at 0°C and 1-hydroxybenzotriazole (HOBt) (306 mg, 2.26 mmol), 1-(3-dimethylaminopropyl)-3-ethylcarbodiimide hydrochloride (EDC) (380 mg (1.98 mmol) and Boc-Pro-OH (488 mg, 2.26 mmol) were added. After 20 min at 0°C triethylamine (0.32 mL, 2.30 mmol) was added and the solution was stirred for additional 17 h at room temperature. Water (3 mL) was added and after 30 min the solution was twice extracted with ethylacetate (20 mL). The combined organic phases were extracted with 10% citric acid, saturated NaHCO$_3$ and water. After drying the solution with Na$_2$SO$_4$ and evaporation of the solvent under reduced pressure, the crude product was purified via FC (ethylacetate : hexane = 35:65). Yield: 318 mg (47%) as a white solid. ^{1}H NMR (400 MHz, CDCl$_3$): δ = 7.95 (s, 1H, N*H*), 4.29 (m, 1H, C*H*), 3.74 (s, 3H, OC*H$_3$*), 3.52 (m, 2H, NC*H$_2$*), 3.33 (m, 4H, SC*H$_2$*CC*H$_2$*S), 2.32–2.01 (m, 1H, CHC*H$_2$*CH$_2$), 1.85 (m, 3H, CHC*H$_2$*CH$_2$ and CHCH$_2$C*H$_2$*), 1.45 (s,

9H, C(CH$_3$)$_3$). ^{13}C NMR (100 MHz, CDCl$_3$): δ = 172.1 (C(O)OCH$_3$), 170.1 (CONH), 155.8 (t-BuOCONH), 80.8 (C(CH$_3$)$_3$), 70.7 (SCH$_2$CCH$_2$S), 60.1 (CH), 53.2 (OCH$_3$), 47.6 (NCH$_2$), 47.0 (SCH$_2$CCH$_2$S), 30.8 (CHCH$_2$CH$_2$), 28.3 (C(CH$_3$)$_3$), 24.3 (CHCH$_2$CH$_2$). MS (DEI): 376 [M]$^+$. IR (KBr, cm^{-1}): 3274s, 3219s, 3054m, 2975s, 2877m, 1748s, 1682s, 1543s, 1479m, 1424s, 1289s. Anal. calcd. for C$_{15}$H$_{24}$O$_5$S$_2$N$_2$: C, 47.85%; H, 6.43%; N, 7.44% S, 17.03%. Found: C, 48.05%; H, 6.69%; N, 7.17%; S, 17.04%.

Synthesis of [(Boc-Pro-Adt-OMe)Fe$_2$(CO)$_6$] (9): Boc-Pro-Adt-OMe (8) (103 mg, 0.27 mmol) and Fe$_3$(CO)$_{12}$ (138 mg, 0.27 mmol) were dissolved in dry toluene (40 mL) and refluxed for 90 min. The solvent was evaporated under reduced pressure and the crude product was purified via FC (THF : hexane 1:1). Yield: 116 mg (65%) as a red solid. ^{1}H NMR (200 MHz; CDCl$_3$): δ = 7.89 (s, 1H, NH), 4.38 (m, 1H, CH), 3.62 (s, 3H, OCH$_3$), 3.28 (m, 2H, NCH$_2$), 2.57 (m, 2H, SCH$_A$H$_B$), 2.24 (m, 3H, SCH$_A$H$_B$ and CHCH$_2$CH$_2$), 1.85 (m, 3H, CHCH$_2$CH$_2$ and CHCH$_2$CH$_2$), 1.47 (s, 9H, C(CH$_3$)$_3$). ^{13}C NMR (50 MHz, CDCl$_3$): δ = 207.3 (CO), 172.4 (C(O)OCH$_3$), 171.1 (C(O)NH), 156.6 (t-BuOCONH), 80.7 (C(CH$_3$)$_3$), 61.6 (SCH$_2$CCH$_2$S), 59.2 (CH), 53.2 (OCH$_3$), 46.7 (NCH$_2$), 29.4 (SCH$_2$CCH$_2$S), 26.3 (C(CH$_3$)$_3$), 24.6 (CHCH$_2$CH$_2$), 22.3 (CHCH$_2$CH$_2$). MS (Micro-ESI in CH$_2$Cl$_2$/CH$_3$OH): 679 [M+Na]$^+$. IR (KBr, cm^{-1}): 2966w, 2930w, 2867w, 2076vs, 2036vs, 1999vs, 1742m, 1639m, 1410m. Anal. calcd. for C$_{21}$H$_{24}$Fe$_2$O$_{11}$S$_2$N$_2$·0.3hexane: C, 40.15%; H, 4.17%; N, 4.11% S, 9.40%. Found: C, 40.24%; H, 4.21%; N, 4.06%; S, 9.30%.

Synthesis of N-Benzenesulfonyl-Adt-OMe (10): To a solution of Boc-Adt-OMe (1) (64 mg, 0.23 mmol) in dry MeOH (1.5 mL) at 0 °C, thionyl chloride (17 µL, 0.23 mmol) was added. The solution was heated up to 50 °C and stirred for 3 h. Removal of the solvent under reduced pressure afforded H-Adt-OMe·HCl (50 mg), which was used in the next step without further purification. H-Adt-OMe·HCl was suspended in dry CH$_2$Cl$_2$ (2 mL) and benzenesulfonylchloride (36 µL, 0.28 mmol) and triethylamine (0.11 mL, 0.79 mmol) were added. The mixture was stirred at room temperature for 24 h and subsequently 4 h at 40 °C. After evaporation of the solvent under reduced pressure, the residue was purified on silica gel (3 g) using CH$_2$Cl$_2$ as eluent. Yield: 38 mg (51%) as a white solid. ^{1}H NMR (400 MHz, CDCl$_3$) δ = 7.52–7.94 (5H, m, H$_{aromatic}$), 5.71 (1H, s, NH), 3.67 (3H, s, OCH$_3$), 3.61 (2H, d, $J_{H,H}$ = 12.0 Hz, 2 x SCH$_A$H$_B$), 3.42 (2H, d, $J_{H,H}$ = 12.0 Hz, 2 x SCH$_A$H$_B$); ^{13}C NMR (100 MHz, CDCl$_3$) δ = 141.2, 133.1, 129.1, 127.1 (C$_{aromatic}$), 73.5 (SCH$_2$CCH$_2$S), 53.4 (OCH$_3$), 47.3 (SCH$_2$CCH$_2$S). MS (ESI): 342 [M+Na]$^+$. IR (KBr, cm^{-1}) 3250m, 3226s, 1747vs, 1453s, 1324m, 1295s, 1154s, 1087s. Anal. calcd. for C$_{11}$H$_{13}$NO$_4$S$_3$: C, 41.36; H, 4.10; N, 4.39; S, 30.12. Found: C, 41.31; H, 4.11; N, 4.42; S 30.16.

Synthesis of [(N-Benzenesulfonyl-Adt-OMe)Fe$_2$(CO)$_6$] (11): N-Benzenesulfonyl-Adt-OMe (10) (7 mg, 0.022 mmol) and Fe$_3$(CO)$_{12}$ (12 mg, 0.022 mmol) were dissolved in dry toluene (20 mL) and refluxed for 1.5 h. The solvent was evaporated under reduced pressure and the dark brown crude product was purified using FC (THF : hexane = 1:3). Yield: 11 mg (83%) of a red solid. ^{1}H NMR (200 MHz, CDCl$_3$): δ = 7.79–7.58 (m, 5H, H$_{aromatic}$), 3.67 (s, 1H, NH), 3.52 (s, 3H, OCH$_3$), 2.71 (d, $^2J_{H,H}$ = 14.8 Hz, 2H, SCH$_A$H$_B$), 2.53 (d, $^2J_{H,H}$ = 14.8 Hz, 2H, SCH$_A$H$_B$). ^{13}C NMR (50 MHz, CDCl$_3$): δ = 207.0/206.7 (CO), 169.3 (C(O)OCH$_3$), 139.9/133.4/129.2/127.7 (C$_{aromatic}$), 63.6 (SCH$_2$CCH$_2$S), 53.6 (CH$_3$), 27.8 (SCH$_2$CCH$_2$S). MS (DEI): 543 [M−2CO]$^+$, 515 [M−3CO]$^+$, 487 [M−4CO]$^+$, 459 [M−5CO]$^+$, 431 [M−6CO]$^+$. IR (KBr, cm^{-1}): 3431s, 3066w, 2955m, 2922m, 2852m, 2077vs, 2036vs, 2002vs, 1743s.

Electrochemistry: Cyclic voltammograms were measured in a three-electrode cell using a 2.0 mm-diameter glassy carbon disc working electrode, a platinum auxiliary electrode, and a Ag|Ag$^+$ reference electrode containing 0.01 M AgNO$_3$/CH$_3$CN. The solvent contains 0.1 M [n-Bu$_4$N][BF$_4$] as the supporting electrolyte. Measurements were performed at room temperature using an EG & G PARC 273A potentiostat/galvanostat. Deaeration of solutions was accomplished by passing a stream of argon through the solution for 5 min prior to the measurement and then maintaining a blanket atmosphere of argon over the solution during the measurement. To control the stability of the reference electrode ferrocene was used as an internal standard ($E_{1/2}$ = +0.087 vs. 0.01 M AgNO$_3$ in CH$_3$CN).[27]

Structure Determinations: The intensity data for the compounds were collected on a Nonius Kappa CCD diffractometer using graphite-monochromated Mo-K$_\alpha$ radiation. Data were corrected for Lorentz and polarization effects but not for absorption effects.[28,29]

*Crystal Data for **8**:* C$_{15}$H$_{24}$N$_2$O$_5$S$_2$·2CHCl$_3$, M$_r$ = 615.22 gmol^{-1}, colourless prism, size 0.05 x 0.05 x 0.04 mm^3, monoclinic, space group P2$_1$, a = 9.2374(4), b = 11.6975(7), c = 13.6656(6) Å, β = 106.68(3)°, V = 1414.47(22) Å^3, T= -90 °C, Z = 2, ρ_{calcd} = 1.444 gcm^{-3}, µ (Mo-K$_\alpha$) = 7.84 cm^{-1}, F(000) = 632, 9433 reflections in h(−11/11), k(−14/15), l(−17/15), measured in the range 2.89° $\leq \Theta \leq$ 27.48°, completeness Θ_{max} = 99.3%, 5786 independent reflections, R$_{int}$ = 0.0503, 3857 reflections with F$_o$ > 4σ(F$_o$), 307 parameters, 1 restraints, R1$_{obs}$ = 0.0677, wR$^2_{obs}$ = 0.1713, R1$_{all}$ = 0.1076, wR$^2_{all}$ = 0.1970, GOF = 1.007, Flack-parameter −0.14(10), largest difference peak and hole: 1.218 /−0.693 e Å^{-3}.

The structures were solved by direct methods (SHELXS)[30] and refined by full-matrix least squares techniques against Fo^2 (SHELXL-97).[31] All hydrogen atom positions were included at calculated positions with fixed thermal parameters. All non-hydrogen atoms were refined anisotropically.[31] XP (SIEMENS Analytical X-ray Instruments, Inc.) was used for structure representations.

Supporting Information (see footnote on the first page of this article): Crystallographic data (excluding structure factors) has been deposited with the Cambridge Crystallographic Data Centre as supplementary publication CCDC-775460 for **8**. Copies of the data can be obtained free of charge on application to CCDC, 12 Union Road, Cambridge CB2 1EZ, UK [E- mail: deposit@ccdc.cam.ac.uk].

[1] J. W. Peters, W. N. Lanzilotta, B. J. Lemon, L. C. Seefeldt, *Science* **1998**, *282*, 1853-1858.

[2] Y. Nicolet, C. Piras, P. Legrand, C. E. Hatchikian, J. C. Fontecilla-Camps, *Structure* **1999**, *7*, 13-23.

[3] M. L. Singleton, N. Bhuvanesh, J. H. Reibenspies, M. Y. Darensbourg, *Angew. Chem. Int. Ed.* **2008**, *47*, 9492-9495.

[4] B. E. Barton, T. B. Rauchfuss, *Inorg. Chem.* **2008**, *47*, 2261-2263.

[5] a) L.-C. Song, L.-X. Wang, M.-Y. Tang, C.-G. Li, H.-B. Song, Qing-Mei Hu, *Organometallics*, **2009**, 3834-3841; b) C. Tard, X. M. Liu, S. K. Ibrahim, M. Bruschi, L. De Gioia, S. C. Davies, X. Yang, L. S. Wang, G. Sawers, C. J. Pickett, *Nature* **2005**, *433*, 610-613.

[6] a) J. D. Lawrence, H. Li, T. B. Rauchfuss, M. Benard, M.-M. Rohmer, *Angew. Chem. Int. Ed.* **2001**, *40*, 1768-1771; b) P. Li, M. Wang, L. Chen, J. Liu, Z. Zhao, L. Sun, *Dalton Trans.* **2009**, 1919-

1926; c) S. Ezzaher, J.-F. Capon, F. Gloaguen, F. Y. Pétillon, P. Schollhammer, J. Talarmin, *Inorg. Chem.* **2009**, *48*, 2-4; d) W. Gao, J. Sun, T. Akermark, M. Li, L. Eriksson, L. Sun, B. Akermark, *Chem. Eur. J.* **2010**, *16*, 2537-2546.

[7] a) C. He, M. Wang, X. Zhang, Z. Wang, C. Chen, J. Liu, B. Akermark, L. Sun, *Angew. Chem.Int. Ed.* **2004**, *43*, 3571-3574; b) X. de Hatten, E. Bothe, K. Merz, I. Huc, N. Metzler-Nolte, *Eur. J. Inorg. Chem.* **2008**, 4530-4537; c) U.-P. Apfel, C. R. Kowol, Y. Halpin, F. Kloss, J. Kübel, H. Görls, J. G. Vos, B. K. Keppler, E. Morera, G. Lucente, W. Weigand, *J. Inorg. Biochem.* **2009**, *103*, 1236-1244; d) A. K. Jones, B. R. Lichtenstein, A. Dutta, G. Gordon, P. L. Dutton, *J. Am. Chem. Soc.* **2007**, *129*, 14844-14845; e) U.-P. Apfel, M. Rudolph, C. Apfel, C. Robl, D. Langenegger, D. Hoyer, B. Jaun, O. Ebert, T. Alpermann, D. Seebach, W. Weigand, *Dalton Trans.* **2010**, *39*, 3065-3071.

[8] a) T.-Y. Shen, G. L. Walford, U.S. Patent 3,547,948, 1970; T.-Y. Shen, G. L. Walford *Chem. Abstr.* **1971**, *75*, 6336j; b) T. Y. Shen, G. L. Walford, U. S. Patent 3,655,692, **1972**; c) T.-Y. Shen, G. L. Walford *Chem. Abstr.* **1972**, *77*, 5331h; d) W. G. Rice, R. R. Schultz, D. C. Baker, L. E. Henderson, PCT Int. Appl. WO 98 01,440, **1998**; e) W. G. Rice, R. R. Schultz, D. C. Baker, L. E. Henderson, *Chem. Abstr.* **1998**, *128*, 123799m; f) A. W. Coulter, J. B. Lombardini, J. R. Sufrin, P. Talalay, *Mol. Pharmacol.* **1974**, *10*, 319-334.

[9] D. R. Appleton, B. R. Copp, *Tetrahedron Lett.* **2003**, *44*, 8963-8965.

[10] E. Morera, M. Nalli, F. Pinnen, D. Rossi, G. Lucente, *Bioorg. Med. Chem. Lett.* **2000**, *10*, 1585-1588.

[11] a) L.-C. Song, J. Yan, Y.-L. Li, D.-F. Wang, Q.-M. Hu, *Inorg. Chem.* **2009**, *48*, 11376-11381; b) L.-C. Song, H.-T. Wang, J.-H. Ge, S.-Z. Mei, J. Gao, L.-X. Wang, B. Gai, L.-Q. Zhao, J. Yan, Y.-Z. Wang, *Organometallics*, **2008**, *27*, 1409-1416.

[12] E. Morera, G. Lucente, G. Ortar, M. Nalli, F. Mazza, E. Gavuzzo, S. Spisani, *Bioorg. Med. Chem.* **2002**, *10*, 147–157.

[13] E. Morera, M. Nalli, A. Mollica, M. Paglialunga Paradisi, M. Aschi, E. Gavuzzo, F. Mazza, G. Lucente, J. Peptide Sci. **2005**, *11*, 104-112.

[14] a) C. Hansch, P. G. Sammes, J. B. Taylor, *Comprehensive Med. Chem.*; Pergamon Press: Oxford, **1990**; Vol. 2, Chapter 7.1; b) P. R. Hanson, D. A. Probst, R. E. Robinson, M. Yau, *Tetrahedron Lett.* **1999**, *40*, 4761-4764; c) J. H. McKerrow, M. N. G. James, *Perspectives in Drug Discovery and Design*; P. S. Anderson, G. L. Kenyon, G. R. Marshall, ESCOM Science Publishers: Leiden, **1996**; Vol. 6, pp 1-120; d) W. R. Roush, S. L. Gwaltney II, J. Cheng, K. A. Scheidt, J. H. McKerrow, E. Hansell, *J. Am. Chem. Soc.* **1998**, *120*, 10994-10995.

[15] M. A. Navia, *Science* **2000**, *288*, 2132-2133.

[16] F. M. Menger, C. L. Johnson, *Tetrahedron* **1967**, *23*, 19-27.

[17] A. Agren, U. Hedsten, B. Jonsson, *Acta Chem. Scand.* **1961**, *15*, 1532-1544.

[18] M. L. Bender, F. J. Kézdy, B. Zerner, *J. Am. Chem. Soc.* **1963**, *85*, 3017-3024.

[19] F. M. Menger, L. Mandell**,** *J. Am. Chem. Soc.* **1967**, *89,* 4424-4426.

[20] M. K. Harb, U.-P. Apfel, J. Kübel, H. Görls, G. A. N. Felton, T. Sakamoto, D. H. Evans, R. S. Glass, D. L. Lichtenberger, M. El-khateeb, W. Weigand, *Organometallics* **2009**, *28*, 6666-6675.

[21] U.-P. Apfel, D. Troegel, Y. Halpin, S. Tschierlei, U. Uhlemann, M. Schmitt, J. Popp, H. Görls, P. Dunne, M. Venkatesan, M. Coey, M. Rudolph, J. G. Vos, R. Tacke, W. Weigand, manuscript in preparation.

[22] a) D. S. Chong, I. P. Georgakaki, R. Mejia-Rodriguez, J. Samabria-Chinchilla, M. P. Soriaga, M. Y. Darensbourg, *Dalton Trans.* **2003**, 4158-4163; b) J.-F. Capon, S. Ezzaher, F. Gloaguen, F. Y. Petillon, P. Schollhammer, J. Talarmin, *Chem. Eur. J.* **2008**, *14*, 1954-1964; c) J. Windhager, M. Rudolph, S. Bräutigam, H. Görls, W. Weigand, *Eur. J. Inorg. Chem.* **2007**, 2748-2760;

[23] I. Kosuke, Acid-Base Diss*ociation Constants in Dipolar Aprotic solvents*, Blackwell Scientific Publications: Oxford (**1990**).

[24] S. J. Borg, T. Behrsing, S. P. Best, M. Razavet, X. M. Liu, C. J. Pickett, *J. Am. Chem. Soc.* **2004**, *126*, 16988-16999.

[25] G. Bartoli, M. Bosco, A. Giuliani, T. Mecozzi, L. Sambri, E. Torregiani, E. Marcantoni, *J. Org. Chem.* **2002**, *67*, 9111-9114.

[26] V. V. Pavlishchuk, A. W. Addison, *Inorg. Chim. Acta* **2000**, 298, 97-102.

[27] COLLECT, Data Collection Software, B. V. Nonius, Netherlands, **1998**.

[28] Z. Otwinowski, C. W. Minor, R. M. Sweet, *Methods. Enzymol.* **1997**, *276*, 207-326.

[29] G. M. Sheldrick, *Acta Crystallogr. Sect. A* **1990**, *46*, 467-473.

[30] G. M. Sheldrick, SHELXL-97 (Release 97-2), University of Göttingen, Germany, **1993**.

The synthesis of [FeFe]-hydrogenase model complexes, carrying an amino acid containing ligand and their electrochemical properties are reported.
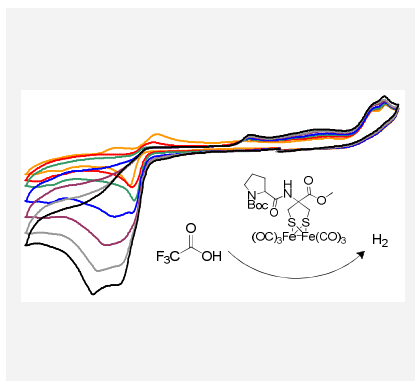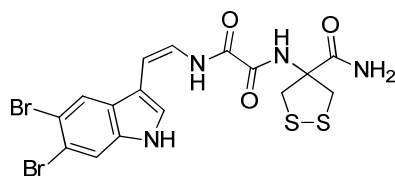
U.-P. Apfel, C. R. Kowol, E. Morera, H. Görls, G. Lucente, B. K. Keppler, W. Weigand[*] **. Page No. Page No.**

Synthetic and Electrochemical Studies on [2Fe2S] Complexes containing a 4-Amino-1,2-dithiolane-4-carboxylic acid moiety
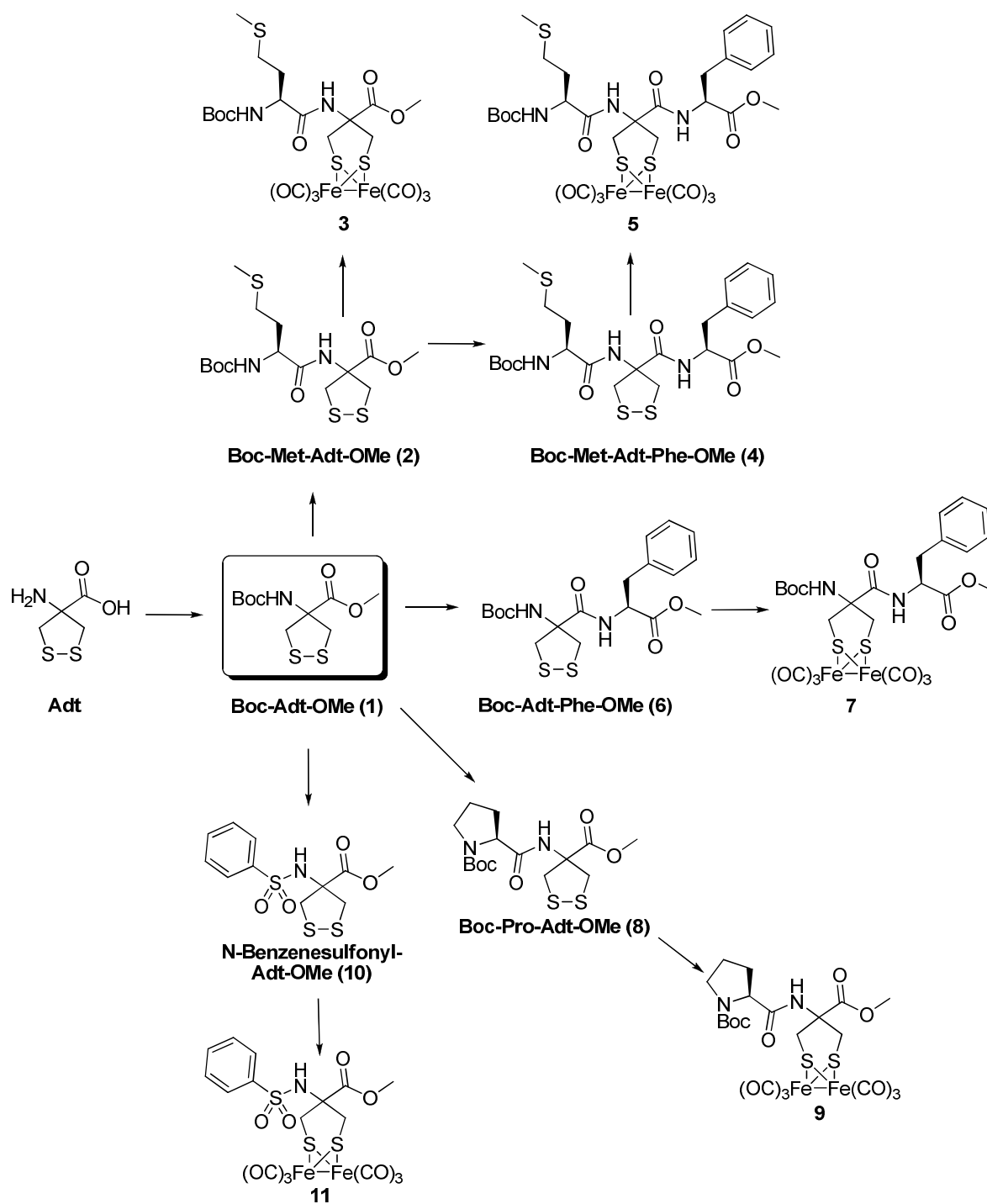
Scheme 1:

Scheme 2:

Scheme 3:
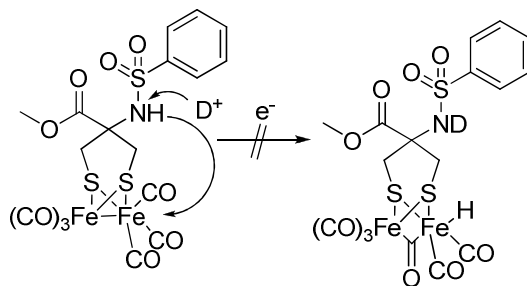
Scheme 4:
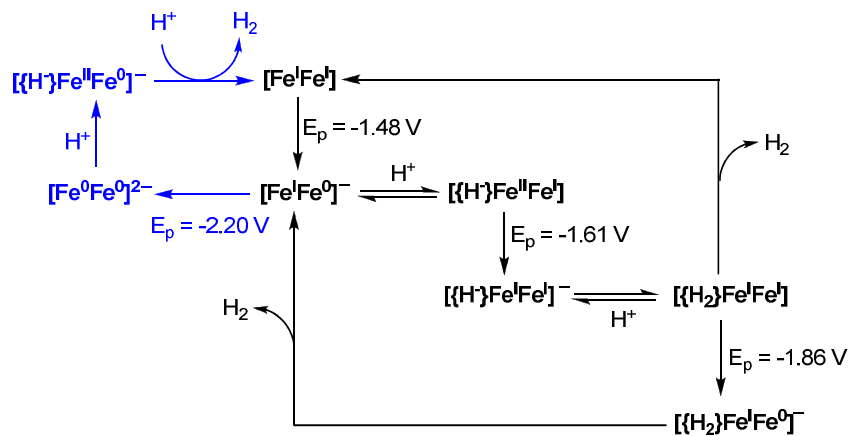
Figure 1:
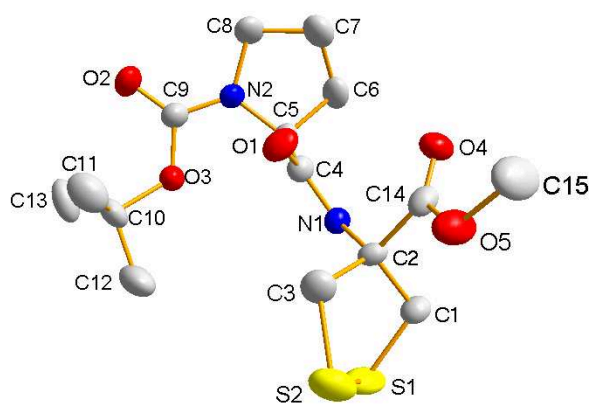
Figure 2:
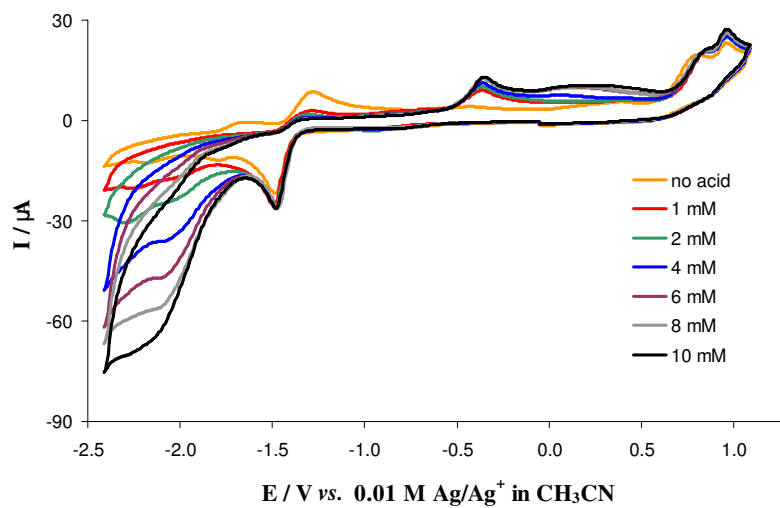
Figure 3:
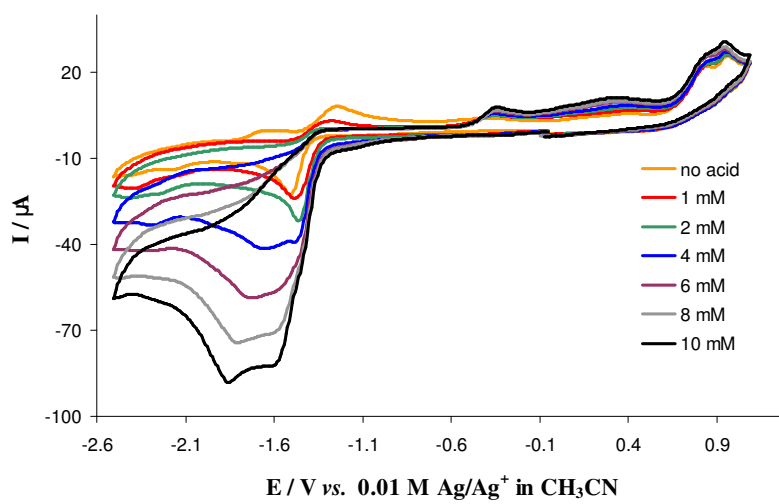
Figure 4:
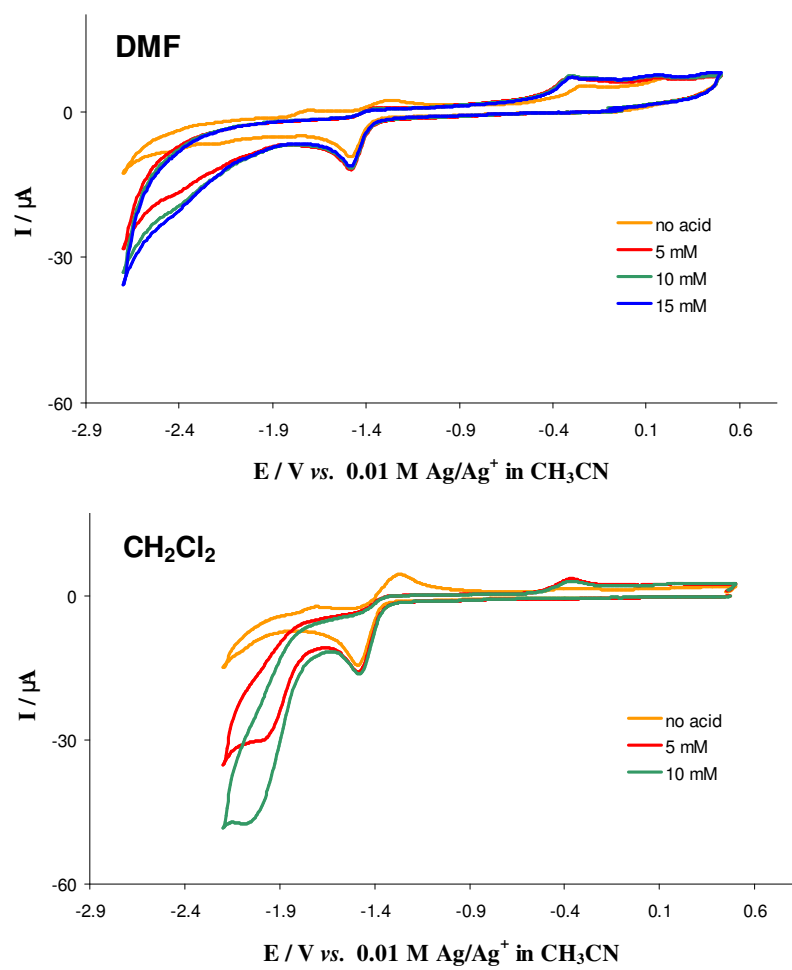
Models for the Active Site in [FeFe] Hydrogenase with Iron-Bound Ligands Derived from Bis-, Tris-, and Tetrakis(mercaptomethyl)silanes

Ulf-Peter Apfel, Dennis Troegel, Yvonne Halpin, Stefanie Tschierlei, Ute Uhlemann, Michael Schmitt, Jürgen Popp, Helmar Görls, Peter Dunne, Munuswamy Venkatesan, Michael Coey, Manfred Rudolph, Johannes G. Vos, Reinhold Tacke, Wolfgang Weigand.
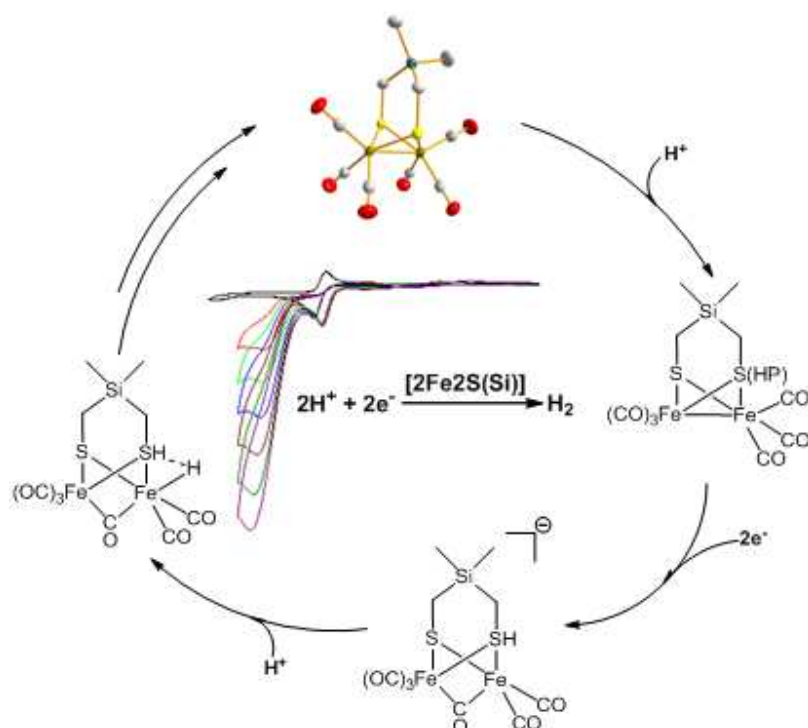
Models for the Active Site in [FeFe] Hydrogenase with Iron-Bound Ligands Derived from Bis-, Tris-, and Tetrakis(mercaptomethyl)silanes

Ulf-Peter Apfel,[‡] Dennis Troegel,[§] Yvonne Halpin,[†] Stefanie Tschierlei,[††] Ute Uhlemann,[††] Helmar Görls,[‡] Michael Schmitt,[††] Jürgen Popp,[††] Peter Dunne,[#] Munuswamy Venkatesan,[#] Michael Coey,[*,#] Manfred Rudolph,[*,‡] Johannes G. Vos,[*,†] Reinhold Tacke,[*,§] Wolfgang Weigand[*,‡]

[‡] *Institut für Anorganische und Analytische Chemie, Friedrich-Schiller-Universität Jena, August-Bebel-Straße 2, D-07743 Jena, Germany,* [§] *Institut für Anorganische Chemie, Universität Würzburg, Am Hubland, D-97074 Würzburg, Germany,* [†] *Solar Energy Conversion SRC, School of Chemical Sciences, Dublin City University, Dublin 9, Ireland,* [††] *Institut für Physikalische Chemie, Friedrich-Schiller-Universität Jena, Helmholtzweg 4, D-07743 Jena, Germany, Institut für Photonische Technologien, Friedrich-Schiller-Universität Jena, Albert-Einstein-Straße 9, D-07745 Jena, Germany, and* [#] *SFI-Trinity Nanoscience Laboratory, Physics Department, Trinity College, Dublin 2, Ireland*

[*] To whom correspondence should be addressed. E-mail:; jcoey@tcd.ie (M.C.); Manfred.Rudolph@uni-jena.de (M.R.); han.vos@dcu.ie (J.G.V.); r.tacke@uni-wuerzburg.de (R.T.); wolfgang.weigand@uni-jena.de (W.W.).

Abstract: A series of multifunctional (mercaptomethyl)silanes of the general formula type $R_nSi(CH_2SH)_{4-n}$ ($n = 0–2$; R = organyl) was synthesized, starting from the corresponding (chloromethyl)silanes. They were used as multidentate ligands for the conversion of dodecacarbonyltriiron, $Fe_3(CO)_{12}$, into iron carbonyl complexes in which the deprotonated (mercaptomethyl)silanes act as μ-bridging ligands. These complexes can be regarded as models for the [FeFe] hydrogenase. They were characterized by elemental analyses (C, H, S), NMR spectroscopic studies (^{1}H, ^{13}C, ^{29}Si), and single-crystal X-ray diffraction. Their electrochemical properties were investigated by cyclic voltammetry to disclose a new mechanism for the formation of dihydrogen catalyzed by these compounds, whereby one sulfur atom was protonated in the catalytic cycle. The reaction of the tridentate ligand $MeSi(CH_2SH)_3$ with $Fe_3(CO)_{12}$ yielded a tetranuclear cluster compound. A detailed investigation by X-ray diffraction, electrochemical, Raman, Mössbauer, and susceptibility techniques indicates that for this compound initially $[Fe_2\{\mu\text{-}MeSi(CH_2S)_2CH_2SH\}(CO)_6]$ is formed. This dinuclear complex, however, is slowly transformed into the tetranuclear species $[Fe_4\{\mu\text{-}MeSi(CH_2S)_3\}_2(CO)_8]$.

Keywords: catalysis, hydrogenase, iron, silicon, sulfur

Introduction

Since Peters *et al.*[1] and Fontecilla-Camps *et al.*[2] have determined the structure of the [FeFe]-hydrogenases' active site, much effort was made to mimic the properties of the enzyme.[3] Especially the

protonation features of model complexes - namely the formation of terminal and bridging hydrides as well as a possible shift of protons to the diiron core *via* adjacent bases - were in the focus of many investigations.[4] Whereas the propanedithiolato complex [Fe$_2$(μ-pdt)(CO)$_6$] reveals addition of a proton to the diiron center and formation of a hydride,[5] the azadithiolato complex [Fe$_2$(μ-adt)(CO)$_6$] shows first protonation of the amino group and consecutive shift of this proton to an iron atom, forming a terminal hydride.[6] Recently, alkylation[7] as well as oxidation[8] of the thiolato sulfur atoms in [FeFe] hydrogenase model complexes was reported and confirmed the high reactivity of the thiolato sulfur atoms. However, Darensbourg *et al.* calculated that protonation of the Fe−Fe bond pair should be favored.[7a] Contrary to that report, we investigated the chemical and electrochemical properties of [Fe$_2$(μ-SCH$_2$SCH$_2$S)(CO)$_6$] and observed interaction of pivalic acid with at least one sulfur atom.[9] This might be an alternative pathway for the formation of hydrides via an initial protonation of the thiolato sulfur atoms.

Inspired by these results and investigations of Glass *et al.* on [Fe$_2$\{μ-SCH$_2$Sn(CH$_3$)$_2$CH$_2$S\}(CO)$_6$],[10] which exhibits an increased electron density at the thiolato sulfur atoms by hyperconjugation of the σ(Sn−C) and 3p(S) orbitals, we have prepared a series of model compounds for the [FeFe] hydrogenase with silicon-containing thiolato ligands bridging the diiron moiety. These complexes should offer the possibility to investigate protonation processes at the coordinating thiolato sulfur atoms by spectroscopic (IR, NMR) as well as electrochemical (cyclic voltammetry, difference pulse voltammetry) techniques.

It is well known from silicon-containing drugs that the presence of one or more silicon atoms in these molecules influences their chemical, physical, and biological properties.[11] The pharmacodynamics and pharmacokinetics of drugs can be affected significantly by replacement of a carbon by a silicon atom (sila-substitution). This can be exploited in medicinal chemistry for drug design; and indeed, the carbon/silicon switch strategy has been successfully used for the development of new silicon-based drugs. Likewise, sila-substitution of odorants has also been demonstrated to affect their olfactory properties, and the carbon/silicon switch strategy has been successfully used for the development of new

silicon-based odorants.[12] Recently, we have also shown that the impact and friction sensitivity of explosives can be affected by carbon/silicon exchange.[13]

The main focus of this work was the synthesis of iron complexes containing silicon-based thiolato ligands derived from (mercaptomethyl)silanes of the formula type $R_nSi(CH_2SH)_{4-n}$ (n = 0–2; R = organyl) and the determination of the electrochemical properties of these complexes (in comparison to the corresponding carbon analogues) to investigate the influence of silicon on electrocatalysis and the formation of dihydrogen. These studies were also performed as part of our systematic investigations on functionalized tetraorganylsilanes of the formula type $R_nSi(CH_2X)_{4-n}$ (n = 0–3; R = organyl; X = functional group).[13,14]

Results and Discussion

Synthesis and Characterization of the Silicon-Containing Thiolato Ligands. The di- and trifunctional (mercaptomethyl)silanes **4a–d** were synthesized according to Scheme 1, starting from the respective chlorosilanes **1a–d**. Thus, treatment of **1a–d** with (chloromethyl)lithium, generated *in situ* from bromochloromethane and *n*-butyllithium in tetrahydrofuran,[15] afforded the (chloromethyl)silanes **2a–d** (37–77% yield), which upon treatment with potassium thioacetate in tetrahydrofuran furnished the corresponding (acetylthiomethyl)silanes **3a–d** (77–97% yield). Reaction of **3a–d** with lithium aluminum hydride in diethyl ether, followed by workup with hydrochloric acid, finally afforded the respective (mercaptomethyl)silanes **4a–d** (67–92% yield). Compounds **2a–d**, **3a–d**, and **4a–d** were isolated as liquids. Their identities were established by elemental analyses (C, H, S) and ^1H, ^{13}C, and ^{29}Si NMR spectroscopic studies (solvent, $CDCl_3$).

Scheme 1. Syntheses of the bis(mercaptomethyl)silanes **4a–c** and the tris(mercaptomethyl)silane **4d**

Me, Cl — Si — Me, Cl **1a**
$\xrightarrow[\text{BrCH}_2\text{Cl}]{n\text{-BuLi}}$
Me, CH$_2$Cl — Si — Me, CH$_2$Cl **2a**

$\downarrow$ KSAc

Me, CH$_2$SH — Si — Me, CH$_2$SH **4a**
$\xleftarrow[\text{2) HCl / H}_2\text{O}]{\text{1) LiAlH}_4}$
Me, CH$_2$SAc — Si — Me, CH$_2$SAc **3a**

(H$_2$C)$_n$ Cl — Si — Cl **1b,c**
$\xrightarrow[\text{BrCH}_2\text{Cl}]{n\text{-BuLi}}$
(H$_2$C)$_n$ CH$_2$Cl — Si — CH$_2$Cl **2b,c**

b: n = 1
c: n = 2

$\downarrow$ KSAc

(H$_2$C)$_n$ CH$_2$SH — Si — CH$_2$SH **4b,c**
$\xleftarrow[\text{2) HCl / H}_2\text{O}]{\text{1) LiAlH}_4}$
(H$_2$C)$_n$ CH$_2$SAc — Si — CH$_2$SAc **3b,c**

Me, Cl — Si — Cl, Cl **1d**
$\xrightarrow[\text{BrCH}_2\text{Cl}]{n\text{-BuLi}}$
Me, CH$_2$Cl — Si — ClCH$_2$, CH$_2$Cl **2d**

$\downarrow$ KSAc

Me, CH$_2$SH — Si — HSCH$_2$, CH$_2$SH **4d**
$\xleftarrow[\text{2) HCl / H}_2\text{O}]{\text{1) LiAlH}_4}$
Me, CH$_2$SAc — Si — AcSCH$_2$, CH$_2$SAc **3d**
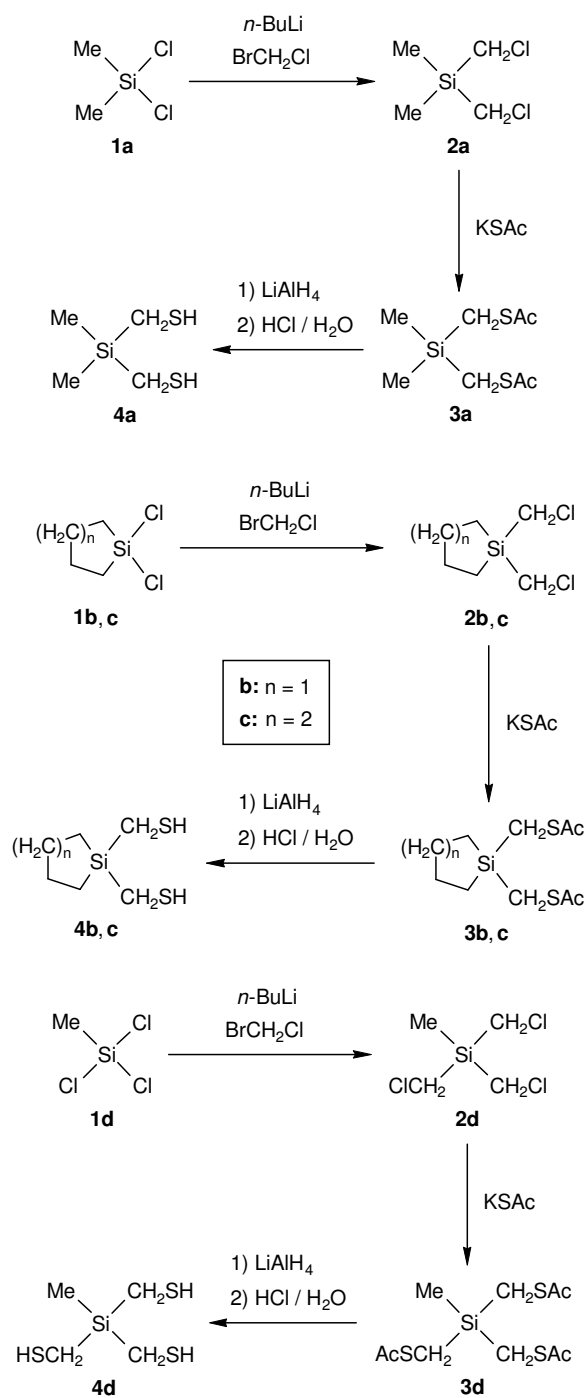
Synthesis and Characterization of the Iron Complexes. Treatment of the bis(mercaptomethyl)silanes **4a–c** with two molar equivalents of dodecacarbonyltriiron, Fe$_3$(CO)$_{12}$, in

toluene afforded the diiron complexes **5a–c** (Scheme 2). Compounds **5a–c** were isolated in 57–89%

yield as red crystalline solids. Their identities were established by elemental analyses (C, H, S), NMR

spectroscopic studies (^{1}H, ^{13}C, ^{29}Si; solvent, CDCl$_3$), mass-spectrometric investigations, IR

spectroscopic studies, and crystal structure analyses (Figure 1; Figures S1 and S2, Table S1, see

Supporting Information).

Scheme 2. Syntheses of the diiron complexes **5a–c**
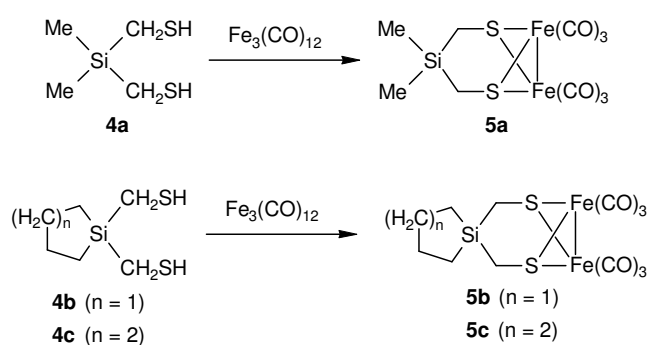
As can be seen from Figure 1 as well as Figures S1 and S2, both iron coordination centers of **5a–c** are

surrounded by two bridging sulfur atoms, one iron atom, and three carbonyl groups. The iron

coordination polyhedra can be best described as strongly distorted octahedra, with the three carbonyl

groups in facial positions. The bicyclic [2Fe2S] skeletons of **5a–c** display a "butterfly" structure. The

silicon atoms of **5a–c** are surrounded in a distorted tetrahedral fashion. It is interesting to note that all

Si–C–S angles (118.22(12)–122.05(13)°) differ significantly from the ideal tetrahedral angle.
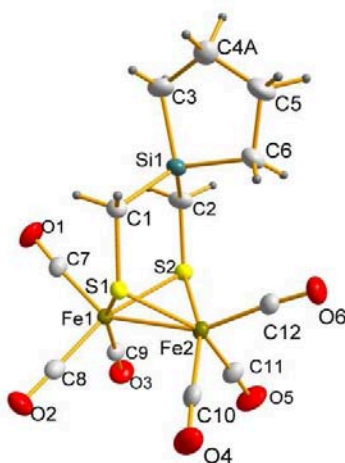
Figure 1. Molecular structure of **5b** in the crystal (probability level of displacement ellipsoids 50%)

To obtain a [4Fe6S] cluster with two tridentate threefold deprotonated $MeSi(CH_2SH)_3$ ligands, the tris(mercaptomethyl)silane **4d** was treated with $Fe_3(CO)_{12}$. Reaction of $Fe_3(CO)_{12}$ with the corresponding carbon-based trithiol, $MeC(CH_2SH)_3$, has already been reported to form the tetrairon complex $[Fe_4\{\mu\text{-}MeC(CH_2S)_3\}_2(CO)_8]$ with an $[Fe^IFe^{II}Fe^{II}Fe^I]$ assembly that catalyzes electrochemical dihydrogen generation at moderate potential.[16] Treatment of the silicon compound **4d** with one molar equivalent of $Fe_3(CO)_{12}$ afforded the diiron complex **6a** (7% yield) and the tetrairon complex **6b** (9% yield) (Scheme 3). The identities of **6a** and **6b** were established by NMR spectroscopic studies (^{1}H, ^{13}C, ^{1}H,^{13}C HSQC, ^{1}H,^{1}H COSY), mass-spectrometric investigations (FAB-MS), IR and Raman studies, as well as powder X-ray diffractometry. In addition, compound **6b** was structurally characterized by single-crystal X-ray diffraction (Figure 2; Table S2, see Supporting Information). Single crystals of **6b** were obtained by slow evaporation of the solvent from a solution of **6a** and **6b** in trichloromethane. It was noticed via powder X-ray diffractometry and thin layer chromatography that **6a** in solution was slowly transformed into **6b**.

Scheme 3. Syntheses of the diiron complex **6a** and the tetrairon complex **6b**
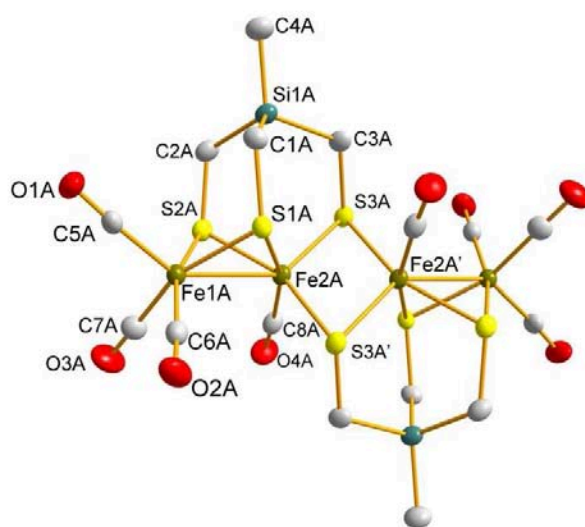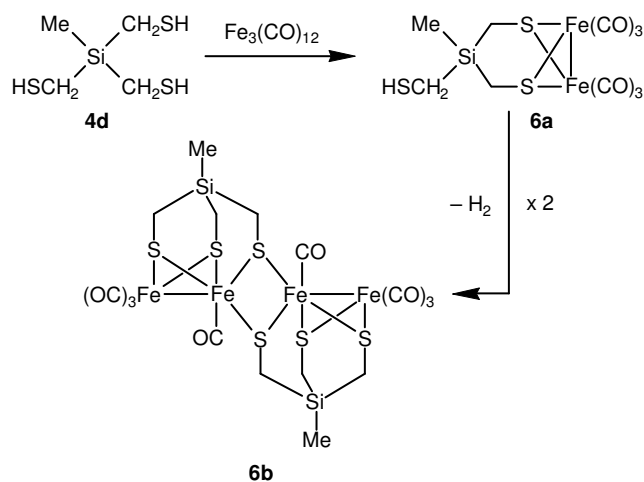
Figure 2. Molecular structure of Molecule A in the crystal of **6b** (probability level of displacement ellipsoids 50%). Hydrogen atoms are omitted for clarity.

To further prove the presence of a free thiol group and the [Fe^{I}Fe^I] assembly in **6a**, Raman spectroscopy, Mössbauer, and susceptibility techniques were used. The Raman spectrum of **6a** (Figure S3, see Supporting Information) is dominated by methyl and methylene group vibrations, e.g., the strong C–H stretching vibration at 2914 cm^{-1}, the C–S and C–Si stretching vibrations at 701 cm^{-1}, different CH$_3$ and CH$_2$ deformation modes at 1606 and 980 cm^{-1}, and the Fe–S stretching vibrations at 513 cm^{-1}. The signal at 2593 cm^{-1} is assigned to an S–H stretching mode. In this spectral region, no

other vibrational frequencies occur, making this signal a very strong indicator for the existence of an SH group in **6a**.

To obtain further information concerning the structure of **6a** and the redox state of the two iron centers, Mössbauer and susceptibility measurements were carried out for both compound **6a** and the reference compound **5a**. The latter was taken as a well-established example of a [2Fe2S] cluster with an [Fe^{I}Fe^I] arrangement.

The Mössbauer spectra were fitted by the standard least-squares minimization procedure. The spectrum for **5a** shows a quadrupole doublet with an isomer shift $\delta = -0.04 \pm 0.02$ mm s^{-1} relative to α_{Fe} and a quadrupole splitting $\Delta = 0.78 \pm 0.02$ mm s^{-1} (Table 1, Figure 3). These values are in agreement with those obtained for the structurally related diiron complex [Fe$_2$(μ-SCH$_2$OCH$_2$S)(CO)$_6$][17] ($\delta = -0.02$ mm s^{-1}, $\Delta = 0.81$ mm s^{-1}). The asymmetry of the spectrum of **5a** indicates the presence of some of the iron atoms (~ 16 %) in a second site giving a doublet with broadened lines and $\delta = 0.19 \pm 0.02$ mm s^{-1} and $\Delta = 0.52 \pm 0.02$ mm s^{-1}. Susceptibility measurements on this compound in the liquid helium temperature range showed that less than 1% of the iron atoms in the sample had an unpaired spin. Hence, any unpaired electrons in the low-spin Fe^I centers of **5a** are paired to form covalent bonds. Since the covalent bond length expected for a Fe^I–Fe^I bond is 233 pm, the experimentally established Fe–Fe distance of **5a** (252 pm) is in agreement with this interpretation.

The Mössbauer spectrum of compound **6a** is similar to that of **5a** (Table 1, Figure 3). The main doublet again has a negative isomer shift $\delta = -0.04 \pm 0.02$ mm s^{-1} and a quadrupole splitting $\Delta = 0.82 \pm 0.02$ mm s^{-1}, and the minority site (~ 7 % of the iron atoms) gives a doublet with broadened lines and $\delta = 0.17 \pm 0.04$ mm s^{-1} and $\Delta = 0.51 \pm 0.04$ mm s^{-1}. The Curie-law susceptibility data in this case is consistent with 8% of the iron atoms possessing a spin of ½, or 1% of the iron atoms being present as high-spin Fe^{II} centers (Figure S4, see Supporting Information). The spins of the iron atoms are coupled antiferromagnetically.
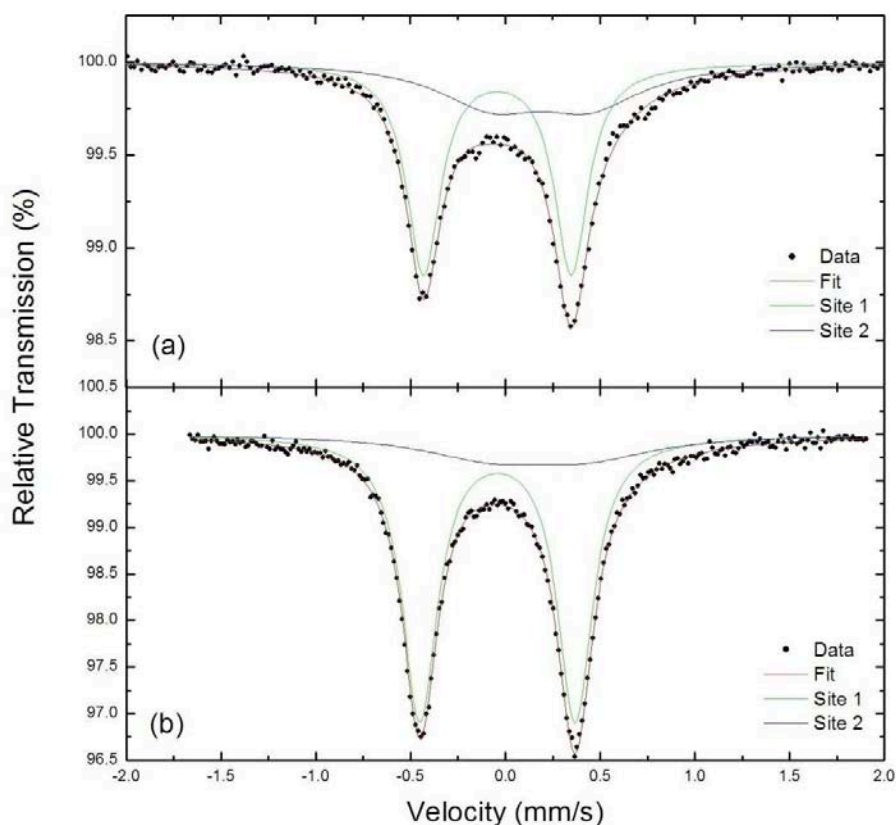
Figure 3. Room-temperature Mössbauer spectra for compounds (a) **5a** and (b) **6a**. The fit parameters for the quadrupole doublets are shown in the Table below.

Table 1. Room-Temperature Mössbauer Data for Compounds **5a** and **6a**

compound	isomer shift [mm s^{-1}]	quadrupole splitting [mm s^{-1}]	linewidth [mm s^{-1}]	relative area [%]
5a	–0.04(2)	0.78(2)	0.11(1)	84
	0.19(2)	0.52(2)	0.34(2)	16
6a	–0.04(2)	0.82(2)	0.11(1)	93
	0.17(4)	0.51(4)	0.42(4)	7

These investigations further confirmed the identity of compound **6a**. Based on the Raman spectrum and the Mössbauer spectra, the presence of a non-coordinated thiol group can be assumed. A coordination of the thiol group to the iron center should lead to both a shift of ν_{SH} to lower

wavenumbers and a significant difference in the quadrupole splitting due to the different coordination sphere of the distal and the proximal iron site.

Compound **6b** crystallizes in the space group $P\bar{1}$, with two molecules (Molecules A and B) in the asymmetric unit, which display very similar centrosymmetric structures. As shown for Molecule A in Figure 2, the tetrairon complex **6b** is a centrosymmetric [4Fe6S] cluster, with two [2Fe3S] cores that are connected via two bridging thiolato groups; i.e., the two tripodal S,S,S ligands derived from **4d** are threefold deprotonated. The terminal iron coordination centers Fe1A and Fe1A' are surrounded each by two bridging sulfur atoms (S1A/S2A, S1A'/S2A'), one of the two internal iron atoms (Fe2A, Fe2A'), and three carbonyl groups. The internal iron coordination centers Fe2A and Fe2A' are each surrounded by four bridging sulfur atoms (S1A/S2A/S3A/S3A', S1A'/S2A'/S3A'/S3A), one of the two terminal iron atoms (Fe1A, Fe1A'), and one carbonyl group. All four iron coordination polyhedra are best described as strongly distorted octahedra. The central Fe2A···Fe2A' distance (262.84(8) pm) is significantly longer than the Fe1A–Fe2A and Fe1A'–Fe2A' distances (252.97(6) pm). As also observed for compounds **5a–c**, the two bicyclic [2Fe2S] skeletons of **6b** display a "butterfly" structure. The silicon atoms of **6b** are surrounded in a distorted tetrahedral fashion; the Si–C–S angles amount to 111.71(16) (Si1A–C1A–S1A, Si1A'–C1A'–S1A'), 116.91(16) (Si1A–C2A–S2A, Si1A'–C2A'–S2A'), and 116.10(16)° (Si1A–C3A–S3A, Si1A'–C3A'–S3A'), respectively. The structure of **6b** is very similar to that reported for the related compound [Fe$_4${μ-MeC(CH$_2$S)$_3$}$_2$(CO)$_8$] with its [Fe^{I}Fe^{II}Fe^{II}Fe^I] arrangement.[16]

To study the coordination mode of tetrakis(mercaptomethyl)silane (**4e**), this compound was also treated with Fe$_3$(CO)$_{12}$. With this tetrafunctional ligand, a large number of different types of iron complexes can be expected. However, in our studies, only one compound, namely the tetrairon complex **7**, could be isolated, and no coordination polymers or charged complexes were found. In contrast to the described synthesis of the carbon analogue of **7**, [Fe$_4${μ-C(CH$_2$S)$_4$}(CO)$_{12}$],[3g] the silicon compound **7** was obtained in the absence of triethylamine by direct conversion of Fe$_3$(CO)$_{12}$ with **4e** (molar ratio, 2:1) in refluxing toluene (40% yield) (Scheme 4). Variation of the molar ratio of Fe$_3$(CO)$_{12}$:**4e** to 1:1

should lead to the diiron complex [Fe$_2$\{μ-SCH$_2$Si(CH$_2$SH)$_2$CH$_2$S\}(CO)$_6$]; however, no such complex could be isolated. In every case, exclusively **7** was obtained in varying yields. The identity of **7** was established by elemental analysis (C, H, S), NMR spectroscopic studies (^{1}H, ^{13}C, ^{29}Si; solvent CDCl$_3$), mass-spectrometric investigations, IR spectroscopic studies, and crystal structure analysis (Figure 4; Table S3, see Supporting Information).

Scheme 4. Synthesis of the tetrairon complex **7**
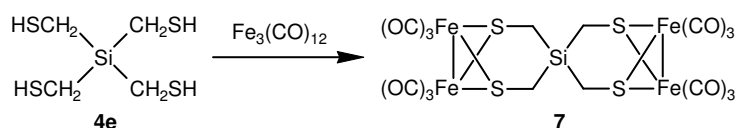
As can be seen from Figure 4, each of the four iron coordination centers of **7** is surrounded by two bridging sulfur atoms, one iron atom, and three carbonyl groups. The four iron coordination polyhedra can be best described as strongly distorted octahedra, with three carbonyl groups in facial positions. All sulfur atoms of the tetradentate fourfold deprotonated Si(CH$_2$SH)$_4$ ligand act as μ_2-bridging atoms, leading to two bicyclic [2Fe2S] skeletons with a "butterfly" structure. The silicon atom is surrounded in a slightly distorted tetrahedral fashion. As already observed for **5a–c** and **6**, the Si–C–S angles (120.03(16)–121.88(16)°) differ significantly from the ideal tetrahedral angle.
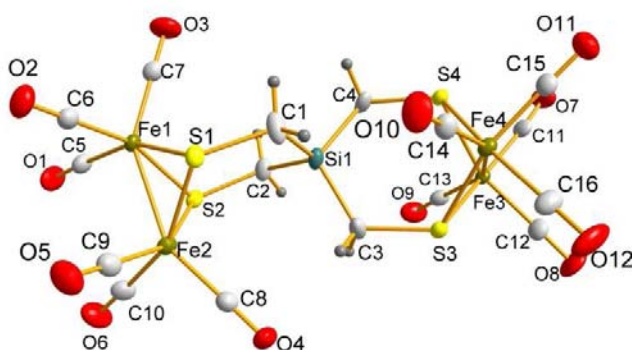
Figure 4. Molecular structure of **7** in the crystal (probability level of displacement ellipsoids 50%).

Electrochemical and Electrocatalytic Properties. *Cyclic voltammetry.* The electrocatalytic dihydrogen formation of [2Fe2S]-based model compounds for the [FeFe] hydrogenases has been well established.[5b,18] Therefore, it was of great interest to study also the electrochemical and related electrocatalytic properties of the model compounds **5a–c**, **6b**, and **7**.

The electrochemical behavior of these compounds in terms of their cyclic voltammograms is considered first. Analysis of **5a–c** shows the presence of an reversible anodic wave at around −1.48 V as expected for reduction of the diiron complexes.[19,20] The values obtained for the redox potentials recorded for **5a–c** are within the experimental error. This suggests that changes in the substituents on the silicon atom of these diiron complexes result in a minimal change of the electron density around the diiron centers and has negligible effect on the redox chemistry (Table 2). Since complexes **5a–c** exhibit similar electrochemical features, we focused our investigation on compound **5b** and a detailed discussion of the electrochemical properties will be given representatively. The cyclic voltammetric reduction of **5b** in acetonitrile on a mercury dropping electrode (using tetraethylammonium perchlorate as the supporting electrolyte) is shown in Figure 5. The experimental cyclovoltammograms (CVs) are in good agreement with theoretical curves simulated on the basis of a two-electron reduction, where the second charge-transfer step is thermodynamically favored ($E°_2 > E°_1$) and kinetically faster ($k°_2 > k°_1$). CVs measured with slow scan rates (< 5 V s^{-1}) exhibit a distinct deviation from the ideal reversible behavior. It can be readily explained in terms of a slow irreversible follow-up reaction that occurs after the first reduction process, forming the decomposition product Q (reaction (4)). The best fit between experimental and simulated CVs was obtained with the following parameter set:

$$Fe–Fe + e^- \rightleftharpoons Fe–Fe^- \qquad (E°_1 = -1.538 \text{ V}, \alpha_1 = 0.22, k°_1 = 0.4 \pm 0.1 \text{ cm s}^{-1}) \qquad (1)$$

$$Fe–Fe^- + e^- \rightleftharpoons {}^-Fe–Fe^- \qquad (E°_2 = -1.475 \text{ V}, \alpha_2 = 0.5, k°_2 \geq 1 \text{ cm s}^{-1}) \qquad (2)$$

$${}^-Fe–Fe^- + Fe–Fe \rightleftharpoons Fe–Fe^- + Fe–Fe^- \qquad (k_{f3} \approx 650 \text{ l mol}^{-1} \text{ s}^{-1}) \qquad (3)$$

$$Fe–Fe^- \rightarrow Q \text{ (decomposition)} \qquad (k_{f4} \approx 50 \text{ s}^{-1}) \qquad (4)$$
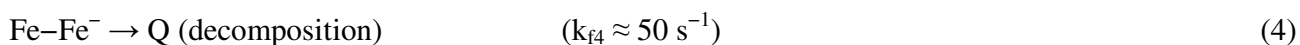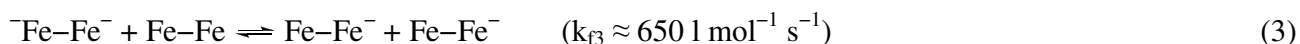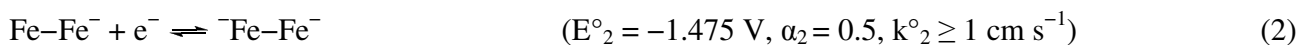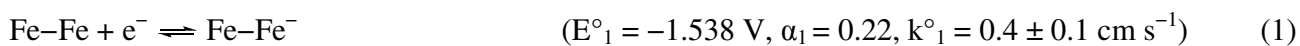
It should be mentioned that the electrochemical reduction of **5b** is strongly dependent on the applied solvent-supporting electrolyte system. For instance, while $k°_2 > k°_1$ was found in acetonitrile/tetraethylammonium perchlorate, the reverse order $k°_1 > k°_2$ was observed when using tetra-*n*-butylammonium perchlorate. A much bigger difference in the electrochemical behavior (affecting even the qualitative appearance of the CVs) is observed when using *N,N*-dimethylformamide (DMF) instead of acetonitrile. The strong effect of the solvent and the supporting electrolyte can be readily explained *via* the stabilization of an *in situ* formed rotated state by the formation of a nitrile complex, which is not possible when using DMF (see also *Reduction of 5b with sodium amalgam and quantum chemical calculations*).
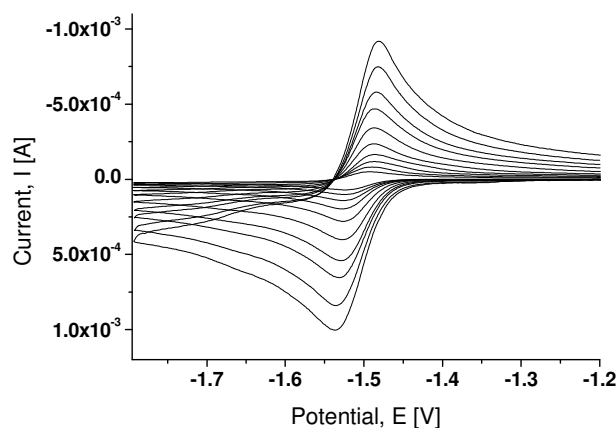
Figure 5. Cyclic voltammetric reduction of compound **5b** in acetonitrile (1.4 mM) on a mercury drop electrode using scan rates of 1, 3, 5, 10, 20, 40, 80, 120, 200, and 300 V s^{-1}.

When compared with $[Fe_2\{\mu\text{-}SCH_2C(CH_3)_2CH_2S\}(CO)_6]$[21] and similar diiron complexes like $[Fe_2\{\mu\text{-}SCH_2XCH_2S\}(CO)_6]$ (X = CR$_2$, NR),[22] the $[Fe^I Fe^I]$ state of the silicon-based analogues is easier to oxidize (E$_{ox,1}$) by about 100 mV; somewhat surprisingly, the reduction waves show that **5a–c** are also easier to reduce to the $[Fe^0 Fe^0]$ level (E$_{red,1}$) by a similar amount, which is difficult to understand. The less positive oxidation potential would suggest that the electron density at the iron center has increased, but if this was the case, the reduction would be more difficult. The fact that this is not observed may suggest that the two redox processes involve different orbitals.

Table 2. Electrochemical Data for Compounds **5a–c** and **7** vs. an Ag/Ag$^+$ Reference Electrode on a Carbon/Glassy Electrode

compound	$E_{ox,1}$ [V]	$E_{red,1}$ [V]	$E_{red,2}$ [V]
5a	+0.79	−1.48 (E_{pc}), −1.40 (E_{pa})	-
5b	+0.81	−1.49 (E_{pc}), −1.40 (E_{pa})	-
5c	+0.81	−1.49 (E_{pc}), −1.39 (E_{pa})	-
7	+0.99	−1.05 (E_{pc}) irr.	−2.15 (E_{pc}), −1.89 (E_{pa})

Where **5a–c** have one active site for the binding and production of dihydrogen, complex **7** has four iron centers bridged by an Si(CH$_2$S-μ)$_4$ moiety and therefore contains two redox active sites. For this compound, one irreversible anodic wave is observed in the cyclic voltammetry representing the oxidation of the Fe^I center to Fe^{II} (see Figure 6). Although there are two diiron active sites in this complex, only one anodic wave is observed suggesting that the oxidation of each active site occurs simultaneously, and therefore this wave represents two one-electron processes.[5b] This result also indicates that there is little or no interaction across the Si(CH$_2$S-μ)$_4$ bridge in the molecule.
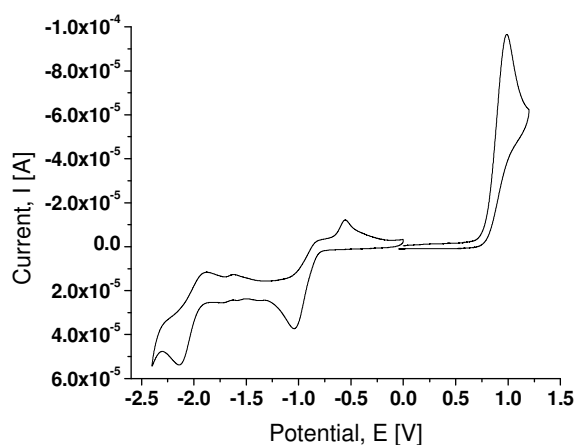
Figure 6. Cyclic voltammogram of compound **7** on a GC macro electrode, vs. Ag/Ag$^+$, using 0.05 M [n-Bu$_4$N][PF$_6$] in CH$_3$CN as the supporting electrolyte.

This is again reflected by the presence of one irreversible reduction representing two one-electron processes corresponding to the $[Fe^IFe^I] + e^- \rightarrow [Fe^0Fe^I]$ process for each diiron center ($E_{red,1} = -1.05$ V). This is a positive shift of approximately 440 mV when compared to compounds **5a–c**.

The electrochemistry of the dinuclear complex **6b** is very different from that observed for the other species. The cyclic voltammogram and the differential pulse data in Figure 7 show reduction potentials at −1.38 and −1.57 V in the potential area for the commonly discussed $[Fe^IFe^I] + e^- \rightarrow [Fe^0Fe^I]$ reduction step in [2Fe2S] complexes.[20,23] A third reversible reduction is noted at more negative potentials ($E_{pc} = -2.16$ V). Compound **6b** shows two irreversible positive processes (see Figure 7), which might indicate an oxidation process as observed for **5a−c**. The presence of two separate anodic peaks may be due to the different coordination environment of the two metal centers and may also indicate electronic coupling across the dithiolato bridges between the two active sites as recently described by Surawatanawong *et al.*.[24]
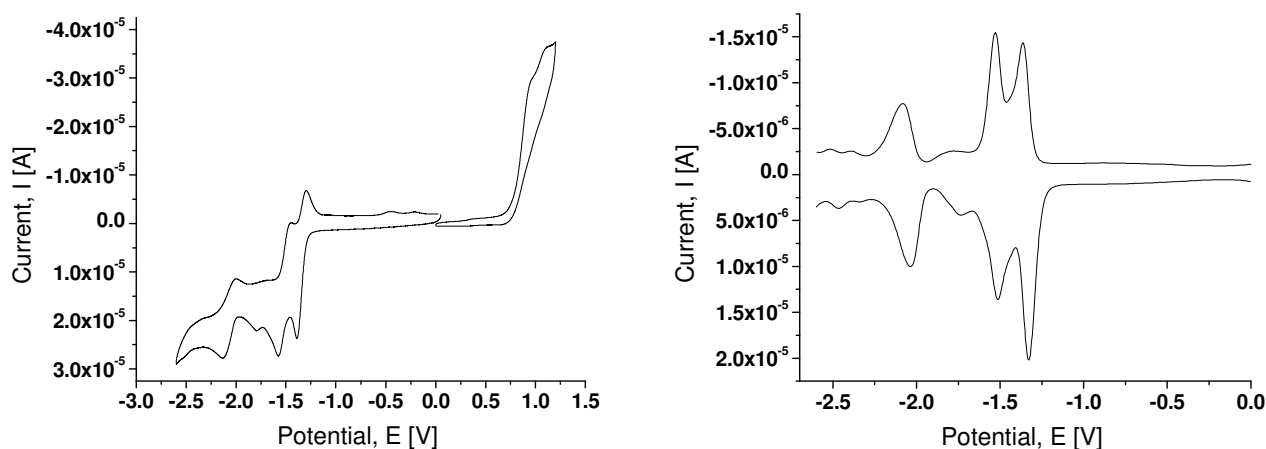
Figure 7. Cyclic voltammogram (left) and differential pulse voltammogram (right) of compound **6b** on a GC macro electrode, vs. Ag/Ag$^+$, using 0.05 M [n-Bu$_4$N][PF$_6$] in CH$_3$CN as the supporting electrolyte.

To allow comparison with the data reported by Pickett *et al.*,[16] the electrochemistry of compound **6b** has been carried out in dichloromethane, and the results obtained are shown in Table 3. The redox processes of these iron hydrogenase models are clearly solvent dependent, with negative shifts of approximately 100 mV observed when changing from dichloromethane to acetonitrile. An ill-defined

oxidation is observed at a more positive potential than the corresponding process in acetonitrile. This wave is not associated with oxidation of the solvent since in blank electrolyte no such process is observed. The third reductive process detected in acetonitrile is not observed in dichloromethane due to solvent cutoff.

Table 3. Electrochemical Data for Compound **6b** and the Related Carbon Compound $[Fe_4\{\mu\text{-}MeC(CH_2S)_3\}_2(CO)_8]$ in Acetonitrile and Dichloromethane. All Values Have Been Corrected against the Ag/Ag$^+$ Reference Electrode Using the Fc/Fc$^+$ Redox Couple as an Internal Standard.

compound (solvent)	E_{pa} [V] $Fe^IFe^{II}/Fe^{II}Fe^{II}$	$E_{\frac{1}{2}}$ [V] $Fe^{II}Fe^I/Fe^IFe^I$	$E_{\frac{1}{2}}$ [V] Fe^IFe^I/Fe^0Fe^I
6b (CH$_3$CN)	+0.91	−1.35	−2.16
	+1.04	−1.52	-
6b (CH$_2$Cl$_2$)	+1.44	−1.25	-
		−1.43	-
$[Fe_4\{\mu\text{-}MeC(CH_2S)_3\}_2(CO)_8]$[16] (CH$_2Cl_2$)	-	−1.11	-
		−1.48	

The first reduction wave of $[Fe_4\{\mu\text{-}MeC(CH_2S)_3\}_2(CO)_8]$ occurs at a potential that is approximately 140 mV more positive than that of the corresponding process in the related silicon compound $[Fe_4\{\mu\text{-}MeSi(CH_2S)_3\}_2(CO)_8]$ (**6b**). A difference of 100 mV is noted for the second reduction potential. However, comparison of the silicon-based hydrogenase analogue with the related carbon-based species would suggest that the presence of silicon does not greatly affect the reduction potentials. Based on the results obtained so far we are not in the position to assess the redox states of the iron centers in the silicon compound **6b** exactly and further studies are underway to clarify this issue. However, compared to the carbon analogue described by Pickett *et al.,* an $[Fe^IFe^{II}Fe^{II}Fe^I]$ system can be assumed.

Electrocatalysis. To investigate the possible catalytic proton reduction of compounds **5a–c**, **6b**, and **7**, the electrochemistry of each complex was analyzed in the presence of a weak acid, acetic acid (AcOH) or pivalic acid (HP) in acetonitrile. In the case of compound **5b**, both acids (AcOH and HP) gave very similar results, and solely the results obtained with pivalic acid will be reported in the following.

The cyclic voltammetric reduction of **5b** in the presence of varying HP concentrations is shown in Figures 8 and S5 (see Supporting Information).
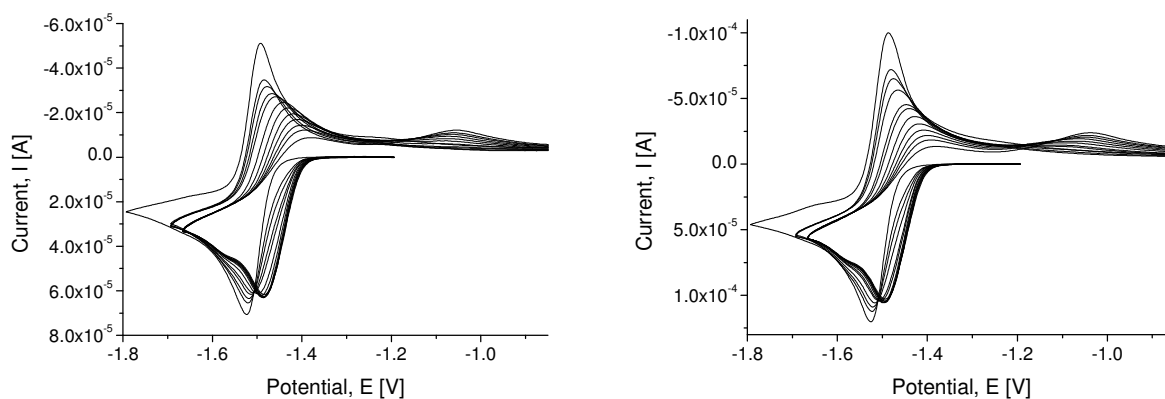
Figure 8. Cyclic voltammetric reduction of a 1.4 mM solution of **5b** in acetonitrile on a mercury drop electrode in the presence of varying concentrations of pivalic acid (right) and simulated CVs (left). The scan rate is 1 V s^{-1}. The HP concentration was varied as follows: [HP]/[**5b**] = 0 (left-most CV), 1/3, 2/3, 1, 4/3, 5/3, 2, 8/3, 10/3, 4, 14/3, 16/3, and 20/3 (right-most CV). Mechanism and simulation parameters are given by reactions (1) to (11).

Independently of the applied scan rate (1, 3, 5, and 10 V s^{-1}), the CVs are shifted on the potential scale in positive direction, while the peak current is slightly decreased upon HP addition. Interestingly, a kind of "isosbestic point" is formed in the course of this. In analogy to UV-VIS spectroscopy, such a behavior can be theoretically expected if there is an equilibrium between compound **5b** and another species formed upon HP addition, provided the CVs refer to the same scan rate and the kinetics of adjusting the equilibrium does not disturb the linear relationship between the current and the concentration within the time scale of the experiment. In view of the weakness of HP in acetonitrile[25,26] and the relatively low HP concentrations used in our experiments, it is unlikely that a direct protonation of **5b** resulting in Fe−Fe−H$^+$ is responsible for the "isosbestic point". It is therefore more likely that an undissociated HP molecule is coordinated to the complex through hydrogen bonds, and the

deprotonation of this HP molecule is initiated by the reduction of **5b** (either in form of a concerted process or as a follow-up reaction). Indeed, a good agreement between experimental and simulated CVs (Figures 8 and S5) was obtained by adding the following reactions to the equations (1)−(4).

$$Fe–Fe + HP \rightleftharpoons Fe–Fe–HP \qquad (K_5 \approx 350 \pm 200, k_{f5} < 10^3 \text{ l mol}^{-1} \text{ s}^{-1})^{27} \qquad (5)$$

$$^-Fe–Fe^- + HP \rightleftharpoons {}^-Fe–Fe–HP^- \qquad (K_6/K_5 \approx 4, k_{f6} \approx 5 \times 10^8 \text{ l mol}^{-1} \text{ s}^{-1}) \qquad (6)$$

$$^-Fe–Fe–HP^- + HP \rightleftharpoons H–Fe–Fe–HP^- + P^- \quad (K_7 \le 1, \text{ diffusion controlled}) \qquad (7)$$

$$P^- + HP \rightleftharpoons HP–P^- \qquad (K_8 \ge 5000, k_{f8} > 2 \times 10^6 \text{ l mol}^{-1} \text{ s}^{-1}) \qquad (8)$$

$$Fe–Fe–HP + e^- \rightleftharpoons Fe–Fe–HP^- \qquad (E^\circ_3 = -1.48 \text{ V}, \alpha_3 = 0.55, k^\circ_3 \approx 0.4 \text{ cm s}^{-1}) \qquad (9)$$

$$Fe–Fe–HP^- + e^- \rightarrow {}^-Fe–Fe–H + P^- \qquad (E^\circ_4 = -1.168 \text{ V}, \alpha_4 = 0.45, k^\circ_4 = 1.75 \times 10^{-5} \text{ cm s}^{-1})^{28} \quad (10)$$

$$Fe–Fe^- + HP + e^- \xleftarrow{\ P^-\ } {}^-Fe–Fe–H \qquad (E^\circ_5 = -1.168 \text{ V}, \alpha_5 = 0.6, k^\circ_5 = 0.1 \text{ cm s}^{-1})^{29} \qquad (11)$$
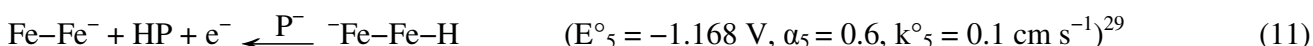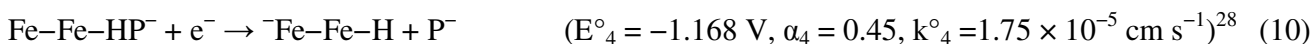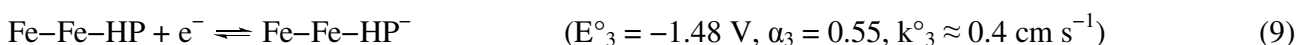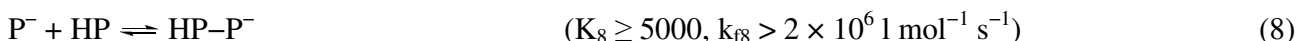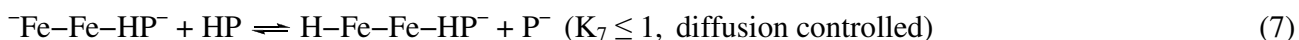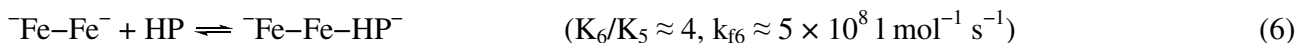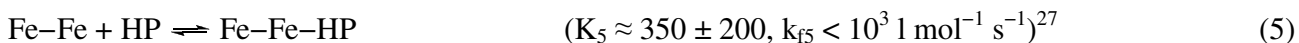
This mechanism also correctly reflects the experimental observation that the shift of the CVs in positive direction upon HP addition converges to a constant value when reaching a ratio [HP]/[**5b**] of about 4:1. Any larger excess affects only the reverse (re-oxidation) scan of the CVs. It has virtually no effect on the forward (reduction) scan.[30]

As expected, no catalytic dihydrogen generation is observed in the presence of weak acids as long as two electrons are consumed by compound **5b**. However, a catalytic current is observed in the presence of pivalic (or acetic) acid if the electrode potential becomes more negative than about −1.8 V. Experimental CVs measured with a scan rate of 1 V s^{-1} are shown in Figure 9. They are in excellent agreement with simulated ones (Figure 9).
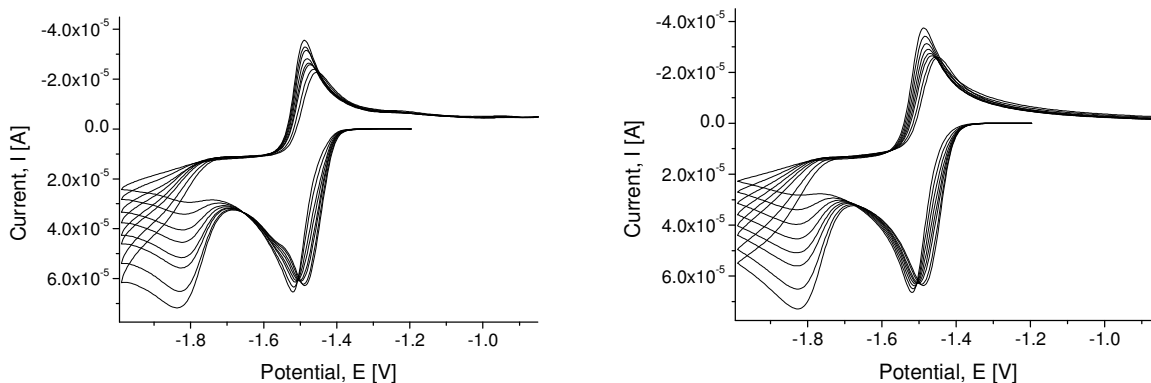
Figure 9. Cyclic voltammetric reduction of a 1.4 mM solution of **5b** in acetonitrile on a mercury drop electrode in the presence of varying concentrations of pivalic acid (left) and simulated CVs (right). The scan rate is 1 V s^{-1}. The HP concentration was varied as follows: [HP]/[**5b**] = 1/3, 2/3, 1, 4/3, 5/3, 2, 8/3, 10/3. The mechanism and simulation parameters are given by reactions (1)–(11).

The latter were obtained by adding the following reactions to the previous equations (1)–(11):

$$H-Fe-Fe-HP^- + e^- \rightleftharpoons {}^-H-Fe-Fe-HP^- \qquad (E^\circ_6 = -1.77 \text{ V}, \alpha_6 = 0.5, k^\circ_6 \approx 0.2 \text{ cm s}^{-1}) \qquad (12)$$

$$^-H-Fe-Fe-HP^- \rightarrow Fe-Fe^- + P^- + H_2 \qquad (k_{f13} = 7 \text{ s}^{-1}) \qquad (13)$$

$$^-H-Fe-Fe-HP^- + HP \rightarrow Fe-Fe-HP^- + P^- + H_2 \qquad (k_{f14} = 2300 \text{ l mol}^{-1} \text{ s}^{-1}) \qquad (14)$$

$$^-H-Fe-Fe-HP^- + HP \rightarrow H-Fe-Fe-HP^- + P^- + H_2 \qquad (k_{f15} = 13500 \text{ l mol}^{-1} \text{ s}^{-1}) \qquad (15)$$
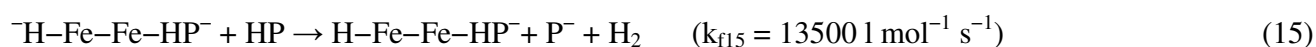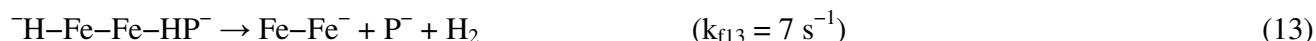
At least three catalytic reactions (reactions (13)–(15)) must be taken into consideration to render the correct height and position of the cathodic current in the potential range at around -1.85 V as well as the correct shape and position of the re-oxidation peak at around -1.5 V as a function of the HP concentration. Figure 10 shows experimental CVs, which were measured on a mercury drop electrode.
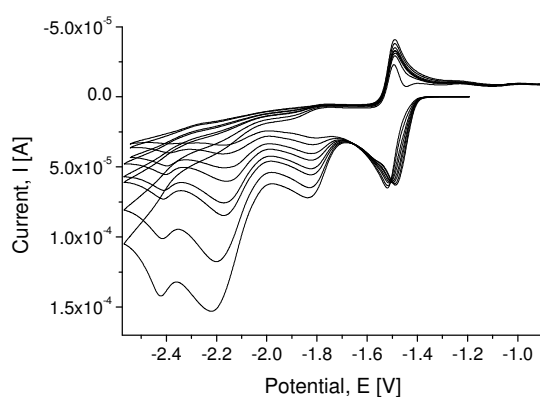
Figure 10. Cyclic voltammetric reduction of a 1.4 mM solution of **5b** in acetonitrile on a mercury drop electrode in the presence of varying concentrations of pivalic acid. The scan rate is 1 V s^{-1}. The HP concentration was varied as follows: [HP]/[**5b**] = 1/3, 2/3, 1, 4/3, 5/3, 2, 8/3, 10/3.

Unlike the direct reduction of HP (which is thermodynamically possible but kinetically inhibited at the mercury drop electrode in the underlying potential range), the indirect reduction by homogeneous electron (reaction (15)) becomes the dominating catalytic process for the three-fold reduced complex. However, because of the second-order character of reaction (15), this statement holds true only for

sufficiently high HP concentrations. At lower HP concentrations ([HP]/[**5b**] < 4 : 3), only the effect of reaction (13) is visible. Reaction (14) leads only to a marginal visible improvement but the standard deviation between simulated and experimental CVs becomes distinctly worse when disregarding this reaction. Finally, it must be mentioned that reactions (12)−(15) do not yet correctly describe some details observed on the short-time scale. Most noteworthy is the fact that the cathodic current in the potential range around −1.85 V is no longer peak shaped when using scan rates of several hundred volts per second. It converges to a plateau current. It is therefore more likely that the species initiating the catalytic cycle according to equation (12) is not the species H−Fe−Fe−HP⁻ itself but rather a species formed in a preceding chemical reaction such as:

$$H-Fe-Fe-HP^- \rightleftharpoons H-Fe-Fe-H + P^- \tag{16}$$

In other words, it might be necessary to formulate reactions (12)–(15) in terms of H−Fe−Fe−H instead of H−Fe−Fe−HP⁻.

Upon addition of acid to a 1 mM solution of complex **7** in acetonitrile, shifts are noted for each of the reduction waves. The first of the cathodic peaks representing $[Fe^IFe^I] + e^- \rightarrow [Fe^0Fe^I]$ exhibits a shift of approximately 160 mV in the negative direction, and the wave appears to split into two waves ($E_{pc} = -1.20$ and -1.36 V) when the concentration of acid in solution is 1 mM. These two waves appear to merge again when the concentration of acid is 4 mM and above. The second reduction waves corresponding to the $[Fe^0Fe^I] + e^- \rightarrow [Fe^0Fe^0]$ process are shifted initially by approximately 200 mV to a more positive potential. This shift is decreasing with each increment of acid added. Both waves experience an increase in current intensity upon addition of 1 mM acid with this rise continuing for the second of these peaks as the concentration of acid increases (Figure 11).
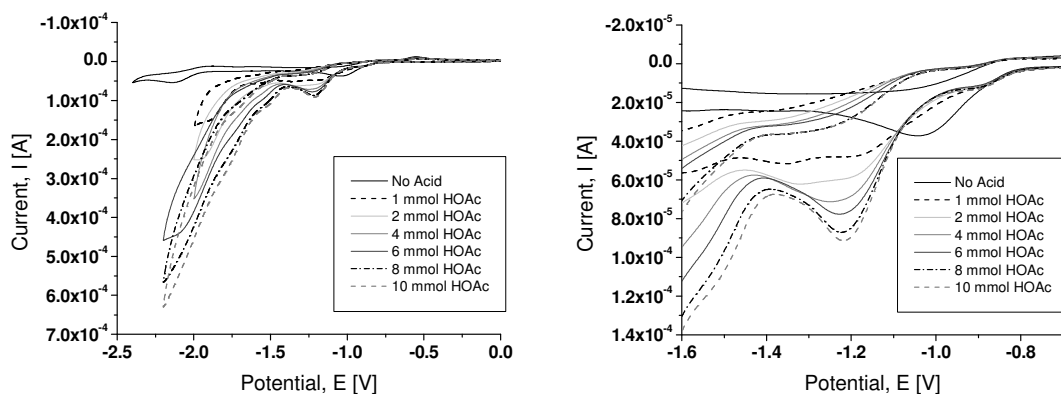
Figure 11. Cyclic voltammograms of compound **7** in acetonitrile (1 mM) in the presence of HOAc (0–10 mM), vs. Ag/Ag$^+$.

The electrocatalytic properties towards dihydrogen formation of compound **6b** were also investigated. Upon addition of acid, the reduction potentials of the first two reduction peaks were shifted to more positive potentials by 15 and 120 mV for the first and second reduction processes, respectively. An increase in current intensity is observed with each sequential increment of acid added, suggesting dihydrogen formation catalyzed by the [Fe^{I}Fe^I] redox couple. As observed for compounds **5a–c**, large currents are found in the region of ~ –1.8 V with increasing intensity for growing acid concentration suggesting an electrochemical catalytic process from the [Fe^{I}Fe^I] state (Figure 12).
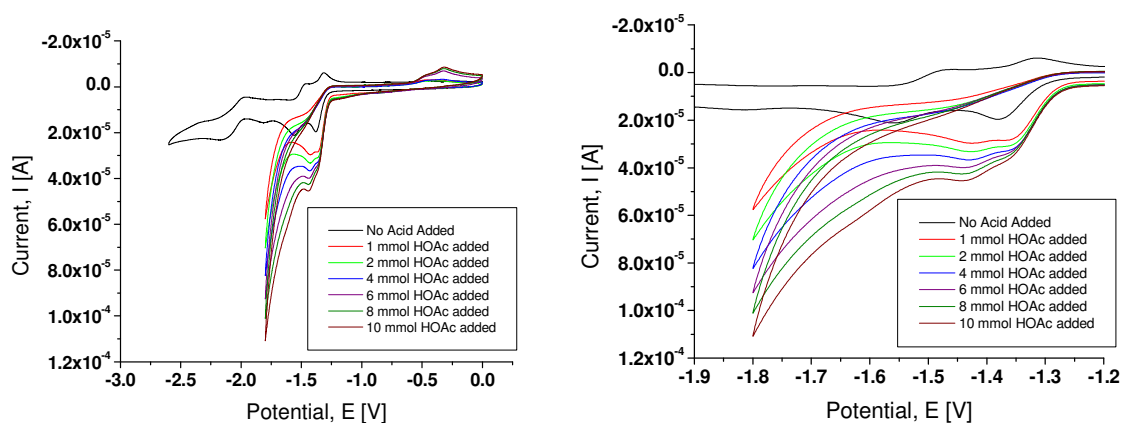

Figure 12. Cyclic voltammograms of compound **6b** in acetonitrile (1 mM) in the presence of HOAc (0–10 mM), vs. Ag/Ag$^+$.

Tentative mechanism. The most striking results obtained in this study are the observation of an "isosbestic point", the formation of dihydrogen at three different potentials, and a shift in positive

23

direction for the reduction potentials of compounds **5a–c** in the presence of acid. Similar anodic shifts have only been observed for functionalized diiron azadithiolates, interpreted in that case by protonation of the amino function. In the absence of a basic group for the compounds under consideration here, no currently proposed mechanism[5b,17,23] can explain the results obtained in this study. A possible alternative mechanism could be a "protonation" of the sulfur atom. However, to the best of our knowledge, no electrochemical and spectroscopic evidence for the protonation of coordinating sulfur in [FeFe] hydrogenase model systems has been reported. On the other hand, Glass *et al.* have shown on the basis of DFT calculations and photoelectron spectroscopy that for related tin containing [2Fe2S] systems the σ(Sn–C) orbital interacts with a 3p(S) orbital.[10] These inductive and hyperconjugative interactions increase the electron density at the sulfur atom. As a direct result, the basicity of the thiolato sulfur atom increases. Taking into account the anodic shift observed for the compounds discussed in this contribution and the investigations of Glass *et al.*,[10] a new possible mechanism is proposed on the basis of equations (1)–(15) (see Scheme 5), whereby ⁻Fe–Fe–H and ⁻Fe–Fe–HP⁻ might be convertible under consideration of equation 16 (see also Supporting Information). Beside the aforementioned kinetic and thermodynamic characterization, four main aspects are visible from Scheme 5:

i)   The two electron reduction step in the absence of acid is accompanied by a structural rearrangement forming a rotated state.

ii)   In the presence of acid, an interaction between protons and the thiolato sulfur atoms is established.

iii)   The catalytically active species is generated by reduction of compound **5b** (Fe–Fe⁻ or ⁻Fe–Fe–HP).

iv)   Dihydrogen can be generated *via* three different pathways depending on the acid concentration.

Scheme 5. Tentative simplified mechanism for the dihydrogen formation of the silicon-containing [FeFe] hydrogenase models **5a–c** according to reaction equations (1)−(15). For simplicity, the influence of equation (16) was neglected in this scheme
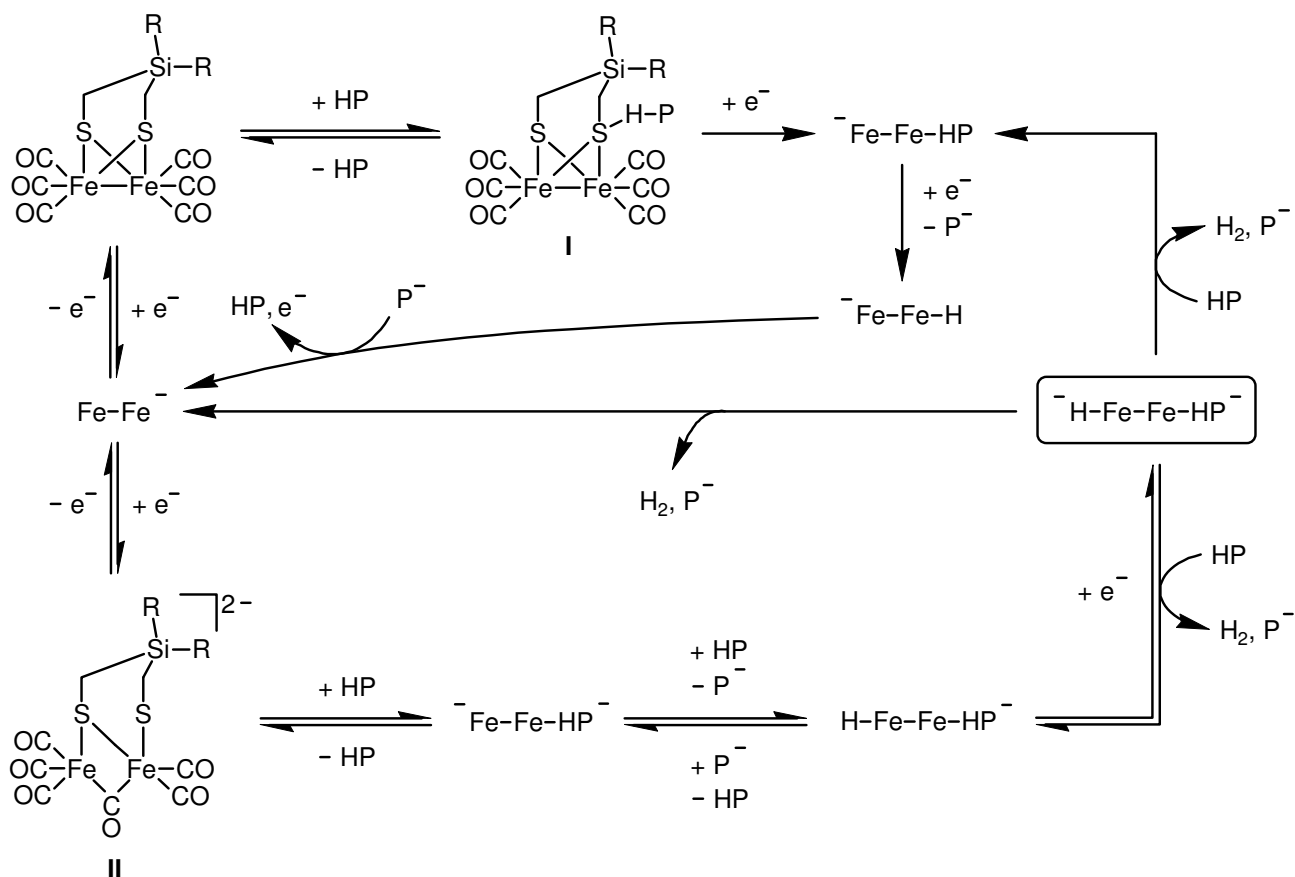
In order to verify this catalytic mechanism, further experiments were performed that confirmed the presence of states **I** and **II** in the catalytic cycle shown in Scheme 5.

*Protonation of **5b** with HBF$_4$·Et$_2$O.* To further prove the catalytic cycle and sulfur "protonation", compound **5b** was treated with tetrafluoroboric acid etherate (HBF$_4$·Et$_2$O); the resulting product was studied by IR spectroscopy. Figure 13 shows the difference between the IR spectra of **5b** before and after addition of HBF$_4$·Et$_2$O. Upon addition of HBF$_4$·Et$_2$O, a new absorption band at 2099 cm^{-1} in the area of the C≡O vibrations is observed. This vibration suggests the existence of ligand protonated **5b**, as similar shifts were observed for [Fe$_2$(μ-SCH$_2$NHCH$_2$S)(CO)$_6$] derivatives upon protonation.[31] ^{1}H NMR spectroscopic studies provided no signal at higher field (> −3 ppm) as reported for analogous μ- or terminal-hydrides[32] and hint at a protonation at the sulfur atoms as depicted in Scheme 5. This, however,

is in contrast to the calculations done by Darensbourg *et al.*, who showed that protonation of the Fe−Fe bond pair should be favored opposed to the thiolato sulfur atoms.[7b]
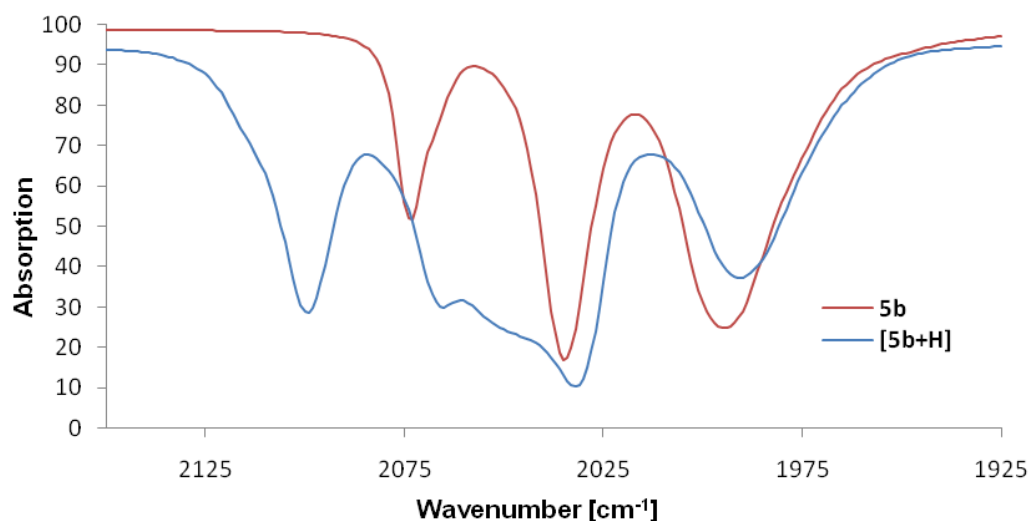
Figure 13. IR spectra of compound **5b** before (red) and after (blue) addition of HBF$_4$·Et$_2$O.

Reduction of 5b with Na/Hg and quantum chemical calculations. In order to elucidate the nature of the product formed in the two-electron reduction, compound **5b** was reacted with the strong reducing agent sodium amalgam in acetonitrile, whereupon the color of the solution changed to dark red. Figure 14 displays the experimental spectral properties of **5b** and the reduced species as well as the calculated IR bands.
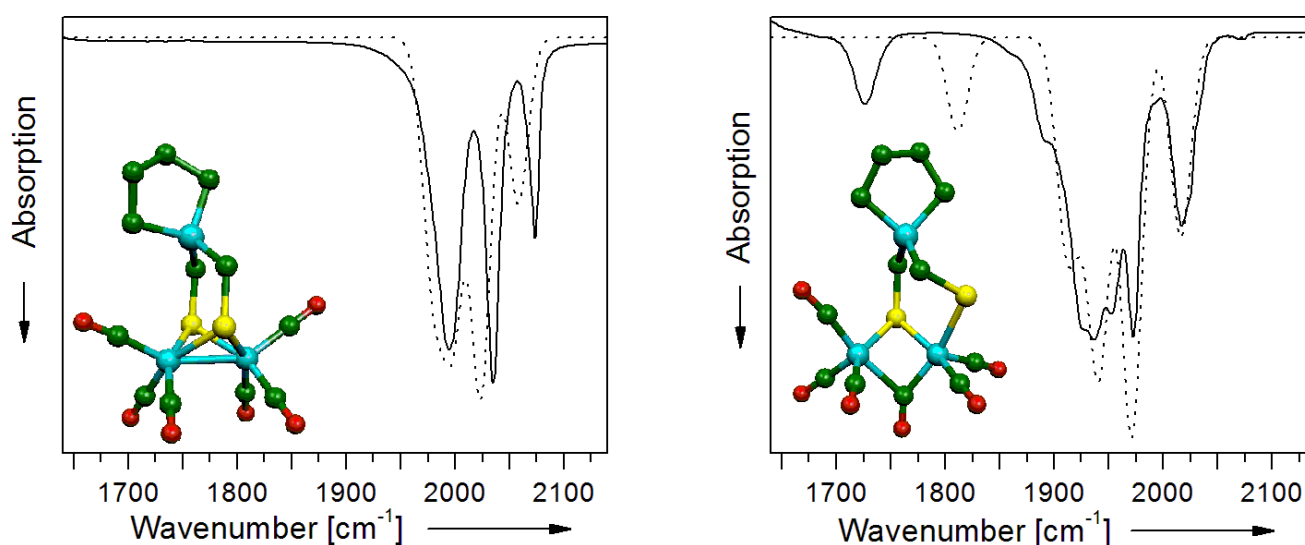
Figure 14. IR spectra (solid) and calculated IR spectra (dashed) of compound **5b** before (left) and after (right) addition of sodium amalgam.

26

In contrast to **5b**, the reduced species reveals an additional band at $1726\,\text{cm}^{-1}$ and hints at the formation of a bridging carbonyl ligand. To prove this assumption, quantum chemical calculations were performed. The experimental and calculated spectra of **5b** match very well (Figure 14). On this basis, the reduced species **5b²⁻** was also calculated. The best fit was obtained for the structure depicted in Figure 14, which is characterized by a broken sulfur–iron bond and a bridging CO ligand. The shift of the IR band (compared to the experimental IR band) of the bridging CO ligand to higher wavenumbers can be explained by the fact that these quantum chemical calculations were performed in the gas phase, and we have noticed that the solvent has a strong influence on the product formation: In contrast to the reduction in acetonitrile, reaction of **5b** with sodium amalgam in dichloromethane did not reveal any bridging CO band. We therefore assume that the resulting reduced complex is stabilized via a weak interaction with acetonitrile. This assumption is further supported by calculations performed with an iron-bound acetonitrile molecule. In this case, a better agreement between theory and experiment was observed (Figure S9, see Supporting Information); however, at higher wavenumbers the shape and the position of the CO bands strongly deviate.

Conclusions

This study aimed at the investigation of the influence of sila-substitution (C/Si exchange) of carbon-based thiolato ligand systems of known [FeFe] hydrogenase models. For this purpose, the bis-, tris-, and tetrakis(mercaptomethyl)silanes **4a–e** were synthesized and used as ligands for the synthesis of the iron complexes **5a–c**, **6a**, **6b**, and **7**. These compounds were characterized by elemental analyses (C, H, S), ^{1}H, ^{13}C, and ^{29}Si NMR spectroscopy, mass spectrometry, and single-crystal X-ray diffraction. The electrochemical behavior of the iron complexes was investigated via cyclic voltammetry, and the electrocatalytic properties for dihydrogen formation were studied. Sila-substitution was found to strongly affect the catalytic pathway. By introducing silicon, the basicity of the sulfur atoms increases, and this allows proton interaction with the thiolato sulfur atoms as observed by cyclic voltammetry and

protonation experiments, coupled with IR studies. This finding is in contrast to the behavior of related complexes with carbon-based thiolato ligands; as shown by computational methods, for these compounds protonation of the Fe–Fe bond pair is favored.[7b] The redox features of **5a–c**, **6b**, and **7** are not straightforward. Introduction of silicon (C/Si exchange) seems to lead to compounds that are both easier to oxidize and to reduce. At this stage, this behavior is not fully understood. Compound **6b** has structural features similar to those reported by Pickett *et al.*[16] for the related carbon compound [Fe$_4$\{μ-MeC(CH$_2$S)$_3$\}$_2$(CO)$_8$]. Addition of protons to compound **5b** does not result in the formation of hydride complexes as observed by NMR spectroscopy but IR studies do suggest protonation of sulfur. This observation is of great importance for the mechanism of the electrocatalytical dihydrogen formation proposed on the basis of electrochemical studies of **5b**. Furthermore, complex **5b** is, to the best of our knowledge, the only example leading to dihydrogen development at three different reduction potentials with high activity towards dihydrogen formation.

Experimental Section

General Procedures. All syntheses were carried out under dry nitrogen or argon. The organic solvents used were dried and purified according to standard procedures and stored under dry nitrogen or argon. Chemicals were used as received from Fluka or Acros without further purification. Thin layer chromatography (TLC): Merck silica gel 60 F$_{254}$ plates; detection under UV light at 254 nm. Flash chromatography (FC): Fluka silica gel 60. A Büchi GKR-51 apparatus was used for the bulb-to-bulb distillations. The ^{1}H, ^{13}C\{^{1}H\}, and ^{29}Si\{^{1}H\} NMR spectra were recorded at 23 °C on a Bruker DRX-300 NMR spectrometer (^{1}H, 300.1 MHz; ^{13}C, 75.5 MHz; ^{29}Si, 59.6 MHz). CDCl$_3$ or CD$_2$Cl$_2$ were used as the solvent. Chemical shifts (ppm) were determined relative to internal CHCl$_3$ (^{1}H, δ 7.24; CDCl$_3$), internal CH$_2$Cl$_2$ (^{1}H, δ 5.32; CD$_2$Cl$_2$), internal CDCl$_3$ (^{13}C, δ 77.0; CDCl$_3$), internal CD$_2$Cl$_2$ (^{13}C, δ 53.8; CD$_2$Cl$_2$), or external TMS (^{29}Si, δ 0; CDCl$_3$, CD$_2$Cl$_2$). Analysis and assignment of the ^{1}H NMR data were supported by ^{1}H,^{1}H COSY, ^{13}C,^{1}H HMQC, and ^{13}C,^{1}H HMBC experiments. Assignment of the

^{13}C NMR data was supported by DEPT 135, ^{13}C,^{1}H HMQC, and ^{13}C,^{1}H HMBC experiments. IR spectra were recorded on a Perkin-Elmer 2000 FT-IR spectrometer. A Jobin Yvon LabRam HR inverse spectrometer with a 632 nm HeNe-laser (Sacher Lasertechnik) was used for recording the Raman spectra. Mass-spectrometric studies (FAB/MS, DEI/MS) were performed on a SSQ710 Finnigan MAT spectrometer. Iron Mössbauer spectra were collected on a conventional constant acceleration spectrometer, with a source of ^{57}Co in Rh. The data were obtained at room temperature. Spectra were fitted to Lorentzian doublets using a standard least-squares minimization routine. The susceptibility measurements were made using a Quantum design SQUID magnetometer, in the range 4–300 K, with samples of mass approximately 10 mg mounted in gel caps in a plastic straw.

Method A: Bis(chloromethyl)dimethylsilane (2a). A 2.5 M solution of n-butyllithium in hexane (124 mL, 310 mmol of n-BuLi) was added dropwise at –70 °C (±3 °C, temperature measurement within the flask) within 5 h to a stirred mixture of dichlorodimethylsilane (**1a**) (20.0 g, 155 mmol), bromochloromethane (60.2 g, 465 mmol), and tetrahydrofuran (190 mL) (the n-butyllithium solution was added via a special horizontally elongated side neck of the three-necked flask, which itself was immersed in the cooling bath to ensure precooling of the n-butyllithium solution before making contact with the reaction mixture). After the addition was complete, the mixture was stirred at –78 °C for 5 h and was then warmed to 20 °C within 17 h. The solvent was removed under reduced pressure (formation of a precipitate), and the residue was extracted with water (800 mL) and diethyl ether (800 mL). The organic extract was dried over anhydrous sodium sulfate, the solvent was removed under reduced pressure, and the residue was purified by bulb-to-bulb distillation (oven temperature 46 °C, 12 mbar) to give **2a** in 77% yield as a colorless liquid (18.8 g, 120 mmol). ^{1}H NMR (CDCl$_3$): δ 0.23 (s, 6 H, SiCH_3), 2.87 (s, 4 H, SiCH_2Cl). ^{13}C NMR (CDCl$_3$): δ –5.9 (SiCH$_3$), 28.1 (SiCH$_2$Cl). ^{29}Si NMR (CDCl$_3$): δ 3.9. Anal. Calcd for C$_4$H$_{10}$Cl$_2$Si: C, 30.58; H, 6.42. Found: C, 30.5; H, 6.5.

Method B: Bis(acetylthiomethyl)dimethylsilane (3a). Compound **2a** (5.00 g, 31.8 mmol) was added in a single portion at 20 °C to a stirred suspension of potassium thioacetate (10.9 g, 95.4 mmol) in

tetrahydrofuran (250 mL), and the resulting mixture was stirred at 20 °C for 21 h. The solvent was removed under reduced pressure, diethyl ether (300 mL) and water (200 mL) were added, the organic phase was separated, and the aqueous phase was extracted with diethyl ether (2 × 200 mL). All organic extracts were combined and dried over anhydrous sodium sulfate, the solvent was removed under reduced pressure, and the residue was purified by bulb-to-bulb distillation (oven temperature 95–100 °C, 0.5 mbar) to give **3a** in 86% yield as a yellowish liquid (6.44 g, 27.2 mmol). ^{1}H NMR (CDCl$_3$): δ 0.08 (s, 6 H, SiCH_3), 2.09 (s, 4 H, SiCH_2S), 2.28 (s, 6 H, C(O)CH_3). ^{13}C NMR (CDCl$_3$): δ –3.8 (SiCH$_3$), 12.3 (SiCH$_2$S), 30.0 (C(O)CH$_3$), 196.0 (C(O)CH$_3$). ^{29}Si NMR (CDCl$_3$): δ 3.4. Anal. Calcd for C$_8$H$_{16}$O$_2$S$_2$Si: C, 40.64; H, 6.82; S, 27.12. Found: C, 40.3; H, 6.6; S, 26.5.

Method C: Bis(mercaptomethyl)dimethylsilane (4a). A solution of **3a** (6.04 g, 25.5 mmol) in diethyl ether (90 mL) was added dropwise at 0 °C within 2 h to a stirred suspension of lithium aluminum hydride (4.91 g, 129 mmol) in diethyl ether (150 mL), and the resulting mixture was stirred at 0 °C for a 90 min and then at 20 °C for a further 19 h. Subsequently, hydrochloric acid (2 M, 50 mL) was added dropwise with stirring at 0 °C within 30 min, and the resulting mixture was then warmed to 20 °C, followed by the addition of water (100 mL). The organic phase was separated, the aqueous phase was extracted with diethyl ether (2 × 200 mL), the combined organic extracts were dried over anhydrous sodium sulfate, the solvent was removed under reduced pressure, and the residue was purified by bulb-to-bulb distillation (oven temperature 40–45 °C, 0.2 mbar) to give **4a** in 80% yield as a colorless liquid (3.13 g, 20.5 mmol). ^{1}H NMR (CDCl$_3$): δ 0.15 (s, 6 H, SiCH_3), 1.16 (t, $^3J_{HH}$ = 7.2 Hz, 2 H, SH), 1.72 (d, $^3J_{HH}$ = 7.2 Hz, 4 H, SiCH_2S). ^{13}C NMR (CDCl$_3$): δ –4.9 (SiCH$_3$), 5.9 (SiCH$_2$S). ^{29}Si NMR (CDCl$_3$): δ 5.1. Anal. Calcd for C$_4$H$_{12}$S$_2$Si: C, 31.53; H, 7.94; S, 42.09. Found: C, 31.4; H, 7.6; S, 41.3.

1,1-Bis(chloromethyl)-1-silacyclopentane (2b). This compound was synthesized according to Method A from 1,1-dichloro-1-silacyclopentane (**1b**) (25.0 g, 161 mmol), bromochloromethane (62.7 g, 485 mmol), a 2.5 M solution of *n*-butyllithium in hexanes (129 mL, 323 mmol of *n*-BuLi), and tetrahydrofuran (170 mL) to give **2b** in 61% yield as a colorless liquid (18.0 g, 98.3 mmol); bp 83–

86 °C/8 mbar. ^{1}H NMR (CDCl$_3$): δ 0.76–0.81 (m, 4 H, SiCH_2C), 1.63–1.68 (m, 4 H, SiCH$_2$CH_2C), 2.97 (s, 4 H, SiCH_2Cl). ^{13}C NMR (CDCl$_3$): δ 8.69 (SiCH$_2$C), 26.6 (SiCH$_2$Cl), 26.9 (SiCH$_2$$CH_2$). ^{29}Si NMR (CDCl$_3$): δ 20.9. Anal. Calcd for C$_6$H$_{12}$Cl$_2$Si: C, 39.35; H, 6.60. Found: C, 39.3; H, 6.7.

1,1-Bis(acetylthiomethyl)-1-silacyclopentane (3b). This compound was synthesized according to Method B from **2b** (4.00 g, 21.8 mmol), potassium thioacetate (7.48 g, 65.5 mmol), and tetrahydrofuran (150 mL) to give **3b** in 77% yield as a yellowish liquid (4.40 g, 16.8 mmol); bp 130 °C/0.2 mbar. ^{1}H NMR (CDCl$_3$): δ 0.60–0.65 (m, 4 H, SiCH_2C), 1.54–1.59 (m, 4 H, SiCH$_2$CH_2C), 2.19 (s, 4 H, SiCH_2S), 2.30 (s, 6 H, C(O)CH_3). ^{13}C NMR (CDCl$_3$): δ 10.4 (SiCH$_2$S), 11.1 (SiCH$_2$C), 27.0 (SiCH$_2$$CH_2$C), 30.0 (C(O)$CH_3$), 196.1 ($C$(O)CH$_3$). ^{29}Si NMR (CDCl$_3$): δ 19.6. Anal. Calcd for C$_{10}$H$_{18}$O$_2$S$_2$Si: C, 45.76; H, 6.91; S, 24.43. Found: C, 46.2; H, 6.8; S, 23.9.

1,1-Bis(mercaptomethyl)-1-silacyclopentane (4b). This compound was synthesized according to Method C from **3b** (4.27 g, 16.3 mmol), lithium aluminum hydride (4.00 g, 105 mmol), and diethyl ether (170 mL) to give **4b** in 67% yield as a colorless liquid (1.95 g, 10.9 mmol); bp 80–90 °C/0.1 mbar. ^{1}H NMR (CDCl$_3$): δ 0.67–0.72 (m, 4 H, SiCH_2C), 1.20 (t, $^{3}J_{HH}$ = 7.2 Hz, 2 H, SH), 1.58–1.63 (m, 4 H, SiCH$_2$CH_2C), 1.81 (d, $^{3}J_{HH}$ = 7.2 Hz, 4 H, SiCH_2S). ^{13}C NMR (CDCl$_3$): δ 4.3 (SiCH$_2$S), 9.4 (SiCH$_2$C), 27.1 (SiCH$_2$$CH_2$C). ^{29}Si NMR (CDCl$_3$): δ 22.7. Anal. Calcd for C$_6$H$_{14}$S$_2$Si: C, 40.40; H, 7.91; S, 35.95. Found: C, 40.5; H, 7.7; S, 35.2.

1,1-Bis(chloromethyl)-1-silacyclohexane (2c). This compound was synthesized according to Method A from 1,1-dichloro-1-silacyclohexane (**1c**) (27.0 g, 160 mmol), bromochloromethane (62.0 g, 479 mmol), a 2.5 M solution of *n*-butyllithium in hexanes (128 mL, 320 mmol of *n*-BuLi), and tetrahydrofuran (185 mL) to give **2c** in 37% yield as a colorless liquid (11.8 g, 59.8 mmol); bp 112–114 °C/15 mbar. ^{1}H NMR (CDCl$_3$): δ 0.82–0.86 (m, 4 H, SiCH_2C), 1.39–1.46 (m, 2 H, Si(CH$_2$)$_2$CH_2C), 1.65–1.73 (m, 4 H, SiCH$_2$CH_2C), 2.95 (s, 4 H, SiCH_2Cl). ^{13}C NMR (CDCl$_3$): δ 8.5 (SiCH$_2$C), 24.0 (SiCH$_2$$CH_2$C), 26.1 (Si$CH_2$Cl), 29.3 (Si(CH$_2$)$_2$$CH_2$C). ^{29}Si NMR (CDCl$_3$): δ –1.3. Anal. Calcd for C$_7$H$_{14}$Cl$_2$Si: C, 42.64; H, 7.16. Found: C, 42.6; H, 7.1.

1,1-Bis(acetylthiomethyl)-1-silacyclohexane (3c). This compound was synthesized according to Method B from **2c** (3.98 g, 20.2 mmol), potassium thioacetate (6.95 g, 60.9 mmol), and tetrahydrofuran (150 mL) to give **3c** in 91% yield as a yellowish liquid (5.09 g, 18.4 mmol); bp 130–140 °C/0.3 mbar. ^{1}H NMR (CDCl$_3$): δ 0.64–0.69 (m, 4 H, SiCH_2C), 1.30–1.38 (m, 2 H, Si(CH$_2$)$_2$CH_2C), 1.58–1.66 (m, 4 H, SiCH$_2$CH_2C), 2.14 (s, 4 H, SiCH_2S), 2.28 (s, 6 H, C(O)CH_3). ^{13}C NMR (CDCl$_3$): δ 10.1 (SiCH$_2$S), 10.6 (SiCH$_2$C), 23.9 (SiCH$_2$$CH_2$C), 29.3 (Si(CH$_2$)$_2$$CH_2$C), 30.0 (C(O)$CH_3$), 196.1 ($C$(O)CH$_3$). ^{29}Si NMR (CDCl$_3$): δ –1.6. Anal. Calcd for C$_{11}$H$_{20}$O$_2$S$_2$Si: C, 47.78; H, 7.29; S, 23.19. Found: C, 47.6; H, 7.1; S, 23.1.

1,1-Bis(mercaptomethyl)-1-silacyclohexane (4c). This compound was synthesized according to Method C from **3c** (2.47 g, 8.93 mmol), lithium aluminum hydride (2.19 g, 57.7 mmol), and diethyl ether (85 mL) to give **4c** in 69% yield as a colorless liquid (1.19 g, 6.18 mmol); bp 95 °C/0.2 mbar. ^{1}H NMR (CDCl$_3$): δ 0.73–0.78 (m, 4 H, SiCH_2C), 1.21 (t, $^3J_{HH}$ = 7.1 Hz, 2 H, SH), 1.35–1.43 (m, 2 H, Si(CH$_2$)$_2$CH_2C), 1.61–1.69 (m, 4 H, SiCH$_2$CH_2C), 1.80 (d, $^3J_{HH}$ = 7.1 Hz, 4 H, SiCH_2S). ^{13}C NMR (CDCl$_3$): δ 3.3 (SiCH$_2$S), 9.6 (SiCH$_2$C), 24.2 (SiCH$_2$$CH_2$C), 29.5 (Si(CH$_2$)$_2$$CH_2$C). ^{29}Si NMR (CDCl$_3$): δ 0.2. Anal. Calcd for C$_7$H$_{16}$S$_2$Si: C, 43.69; H, 8.38; S, 33.33. Found: C, 43.7; H, 8.3; S, 33.0.

Tris(chloromethyl)methylsilane (2d). This compound was synthesized according to Method A from trichloro(methyl)silane (**1d**) (13.5 g, 90.3 mmol), bromochloromethane (52.9 g, 409 mmol), a 2.5 M solution of *n*-butyllithium in hexanes (110 mL, 275 mmol of *n*-BuLi), and tetrahydrofuran (150 mL) to give **2d** in 72% yield as a colorless liquid (12.5 g, 65.3 mmol); bp 65 °C/0.4 mbar. ^{1}H NMR (CDCl$_3$): δ 0.37 (s, 3 H, SiCH_3), 3.01 (s, 6 H, SiCH_2Cl). ^{13}C NMR (CDCl$_3$): δ –8.6 (SiCH$_3$), 25.3 (SiCH$_2$Cl). ^{29}Si NMR (CDCl$_3$): δ 2.5. Anal. Calcd for C$_4$H$_9$Cl$_3$Si: C, 25.08; H, 4.74. Found: C, 25.3; H, 4.8.

Tris(acetylthiomethyl)methylsilane (3d). This compound was synthesized according to Method B from **2d** (5.76 g, 30.1 mmol), potassium thioacetate (15.5 g, 136 mmol), and tetrahydrofuran (400 mL) to give **3d** in 92% yield as a yellowish liquid (8.57 g, 27.6 mmol); bp 140–150 °C/0.1 mbar. ^{1}H NMR (CDCl$_3$): δ 0.16 (s, 3 H, SiCH_3), 2.18 (s, 6 H, SiCH_2S), 2.31 (s, 9 H, C(O)CH_3). ^{13}C NMR (CDCl$_3$): δ

−5.4 (SiCH$_3$), 10.8 (SiCH$_2$S), 30.1 (C(O)CH$_3$), 195.6 (C(O)CH$_3$). ^{29}Si NMR (CDCl$_3$): δ 3.4. Anal. Calcd for C$_{10}$H$_{18}$O$_3$S$_3$Si: C, 38.68; H, 5.84; S, 30.98. Found: C, 38.7; H, 5.8; S, 30.9.

Tris(mercaptomethyl)methylsilane (4d). This compound was synthesized according to Method C from **3d** (8.57 g, 27.6 mmol), lithium aluminum hydride (7.80 g, 206 mmol), and diethyl ether (350 mL) to give **4d** in 92% yield as a colorless liquid (4.69 g, 25.4 mmol); bp 80–90 °C/0.1 mbar. ^{1}H NMR (CDCl$_3$): δ 0.25 (s, 3 H, SiCH$_3$), 1.27 (t, $^3J_{HH}$ = 7.4 Hz, 3 H, SH), 1.84 (d, $^3J_{HH}$ = 7.4 Hz, 6 H, SiCH$_2$S). ^{13}C NMR (CDCl$_3$): δ −7.1 (SiCH$_3$), 3.8 (SiCH$_2$S). ^{29}Si NMR (CDCl$_3$): δ 5.1. Anal. Calcd for C$_4$H$_{12}$S$_3$Si: C, 26.05; H, 6.56; S, 52.16. Found: C, 26.0; H, 6.4; S, 51.5.

Tetrakis(mercaptomethyl)silane (4e). This compound was synthesized according to ref [14a].

Method D: General Procedure for the Synthesis of the Iron Complexes. The respective (mercaptomethyl)silane (50 mg) and 0.5 molar equivalents of Fe$_3$(CO)$_{12}$ per SH group were dissolved in toluene (30 mL). The resulting solution was heated under reflux for 2 h, the solvent was removed under reduced pressure, and the residue was purified via FC (eluent, THF/n-hexane (1:6 (v/v)); detection of the relevant fractions via TLC) to afford the respective iron complexes **5a–c**, **6a**, **6b**, and **7** as red crystalline solids.

Diiron Complex 5a. This compound was prepared according to Method D by treatment of **4a** (50 mg, 328 μmol) with Fe$_3$(CO)$_{12}$ (166 mg, 330 μmol) to afford **5a** (81 mg, 188 μmol) in 57% yield. ^{1}H NMR (CDCl$_3$): δ 0.09 (s, 6 H, SiCH$_3$), 1.44 (s, 4 H, SiCH$_2$S). ^{13}C NMR (CDCl$_3$): δ −0.3 (SiCH$_3$), 5.9 (SiCH$_2$S), 207.5 (CO). ^{29}Si NMR (CDCl$_3$): δ 0.3. MS (DEI): m/z, 430 [M]$^+$, 402 [M − CO]$^+$, 374 [M − 2CO]$^+$, 346 [M − 3CO]$^+$, 318 [M − 4CO]$^+$, 290 [M − 5CO]$^+$, 262 [M − 6CO]$^+$. IR (KBr): 2074 (vs), 2031 (vs), 1987 (vs), 1949 (s), 1935 (s). Anal. Calcd for C$_{10}$H$_{10}$Fe$_2$O$_6$S$_2$Si: C, 27.93; H, 2.34; S, 14.91. Found: C, 28.5; H, 2.6, S; 14.4.

Diiron Complex 5b. This compound was prepared according to Method D by treatment of **4b** (50 mg, 280 μmol) with Fe$_3$(CO)$_{12}$ (142 mg, 282 μmol) to afford **5b** (116 mg, 250 μmol) in 89% yield (related to **5b·0.1THF**). ^{1}H NMR (CDCl$_3$): δ 0.61–0.65 (m, 4 H, SiCH$_2$C), 1.45–1.55 (m, 8 H, SiCH$_2$S

and SiCH$_2$CH_2C). ^{13}C NMR (CDCl$_3$): δ 5.9 (SiCH$_2$S), 13.2 (SiCH$_2$C), 26.5 (SiCH$_2$$CH_2$C), 207.3 ($C$O). ^{29}Si NMR (CDCl$_3$): δ 19.3. MS (DEI): m/z, 456 [M]$^+$, 428 [M – CO]$^+$, 400 [M – 2CO]$^+$, 372 [M – 3CO]$^+$, 344 [M – 4CO]$^+$, 316 [M – 5CO]$^+$, 288 [M – 6CO]$^+$. IR (KBr): 2070 (vs), 2028 (vs), 2004 (vs), 1971 (vs), 1956 (vs). Anal. Calcd for C$_{12}$H$_{12}$Fe$_2$O$_6$S$_2$Si·0.1THF: C, 32.14; H, 2.78; S, 13.84. Found: C, 32.2; H, 3.1; S, 14.2.

Diiron Complex 5c. This compound was synthesized according to Method D by treatment of **4c** (50 mg, 260 μmol) with Fe$_3$(CO)$_{12}$ (131 mg, 260 μmol) to afford **5c** (84 mg, 173 μmol) in 67% yield (related to **5c**·0.2THF). ^{1}H NMR (CDCl$_3$): δ 0.63–0.68 (m, 4 H, SiCH_2C), 1.28–1.60 (m, 10 H, SiCH$_2$S, SiCH$_2$CH_2C, and Si(CH$_2$)$_2$CH_2C). ^{13}C NMR (CDCl$_3$): δ 3.9 (SiCH$_2$S), 13.4 (SiCH$_2$C), 23.8 (SiCH$_2$$CH_2$C), 29.2 (Si(CH$_2$)$_2$$CH_2$C), 207.5 ($C$O). ^{29}Si NMR (CDCl$_3$): δ –4.5. MS (DEI): m/z, 470 [M]$^+$, 442 [M – CO]$^+$, 414 [M – 2CO]$^+$, 386 [M – 3CO]$^+$, 358 [M – 4CO]$^+$, 330 [M – 5CO]$^+$, 302 [M – 6CO]$^+$. IR (KBr): 2914 (s), 2854 (m), 2070 (vs), 2017 (vs, b), 1637 (m), 1445 (m). Anal. Calcd for C$_{13}$H$_{14}$Fe$_2$O$_6$S$_2$Si·0.2THF: C, 34.21; H, 3.24, S; 13.23. Found: C, 34.2; H, 3.2; S, 13.5.

Diiron Complex 6a and Tetrairon Complex 6b. These compounds were synthesized according to Method D (except for the stoichiometric ratio) by treatment of **4d** (300 mg, 1.63 mmol) with Fe$_3$(CO)$_{12}$ (819 mg, 1.63 mmol) to afford two products, the orange-colored compound **6a** (isolated as **6a**·0.2hexane; 58 mg, 121 µmol) in 7% yield and the dark red compound **6b** (isolated as **6b**·1.3hexane; 132 mg, 143 µmol) in 9% yield.

Compound 6a: ^{1}H NMR (CDCl$_3$): δ 0.22 and 0.31 (2 s, 6 H, SiCH_3), 0.98–1.14 (m, 1 H, SH), 1.37–1.79 (m, 6 H, SiCH_2S). ^{13}C NMR (CDCl$_3$): δ –2.54 (SiCH$_3$), 4.1 and 9.0 (SiCH$_2$S), 207.1 (CO). MS (FAB, in nba): m/z, 464 [M + 2H]$^+$, 436 [M + 2H – CO]$^+$, 408 [M + 2H – 2CO]$^+$, 380 [M + 2H – 3CO]$^+$, 352 [M + 2H – 4CO]$^+$. IR (KBr): 2960 (m), 2925 (m), 2853 (m), 2073 (vs), 2032 (vs), 1995 (vs). Raman: 2593 cm^{-1} (ν_{S-H}). Anal. Calcd for C$_{10}$H$_{10}$Fe$_2$O$_6$S$_3$Si·0.2hexane: C, 28.1; H, 2.7, S; 20.1. Found: C, 28.1; H, 2.7; S, 15.2. Although the analytical data for ''S'' are unsatisfactory, the results of the FAB-MS studies and the NMR, IR, and Raman data are consistent with the formula C$_{10}$H$_{10}$Fe$_2$O$_6$S$_3$Si.

Compound 6b: ^{1}H NMR (CD$_2$Cl$_2$): δ 0.05 (s, 6 H, SiCH_3), 0.52 (d, $^2J_{HH}$ = 14.8 Hz, 2 H, SiCH_2S-a), 0.86 (d, $^2J_{HH}$ = 14.8 Hz, 2 H, SiCH_2S-a), 1.55 (d, $^2J_{HH}$ = 14.4 Hz, 2 H, SiCH_2S-b), 1.83 (d, $^2J_{HH}$ = 14.4 Hz, 2 H, SiCH_2S-c), 2.24 (d, $^2J_{HH}$ = 14.4 Hz, 2 H, SiCH_2S-b), 3.20 (d, $^2J_{HH}$ = 14.4 Hz, 2 H, SiCH_2S-c). ^{13}C NMR (CD$_2$Cl$_2$): δ −1.6 (SiCH_3), 5.6 (SiCH_2S-a), 9.9 (SiCH_2S-b), 21.4 (SiCH_2S-c), 208.0 and 208.8 (C*O*). MS (FAB, in nba): m/z, 810 [M]$^+$, 782 [M − CO]$^+$, 754 [M − 2CO]$^+$, 726 [M − 3CO]$^+$, 698 [M − 4CO]$^+$, 670 [M − 5CO]$^+$, 642 [M − 6CO]$^+$, 614 [M − 7CO]$^+$, 586 [M − 8CO]$^+$. IR (KBr): 2922 (m), 2854 (m), 2071 (m), 2038 (vs), 1982 (vs), 1943 (m). Anal. Calcd for C$_{16}$H$_{18}$Fe$_4$O$_8$S$_6$Si$_2$·1.3hexane: C, 31.0; H, 4.0, S; 20.9. Found: C, 30.9; H, 4.1; S, 20.6.

Tetrairon Complex 7. This compound was synthesized according to Method D by treatment of **4e** (50 mg, 231 μmol) with Fe$_3$(CO)$_{12}$ (233 mg, 463 μmol) to afford **7** (72 mg, 93.3 μmol) in 40% yield. ^{1}H NMR (CDCl$_3$): δ 1.51 (s, 8 H, SiCH_2S). ^{13}C NMR (CDCl$_3$): δ 5.3 (SiCH_2S), 206.8 (C*O*). ^{29}Si NMR (CDCl$_3$): δ −6.4. MS (DEI): m/z, 772 [M]$^+$, 744 [M − CO]$^+$, 716 [M − 2CO]$^+$, 688 [M − 3CO]$^+$, 660 [M − 4CO]$^+$, 632 [M − 5CO]$^+$, 604 [M − 6CO]$^+$, 576 [M − 7CO]$^+$, 548 [M − 8CO]$^+$, 520 [M − 9CO]$^+$, 492 [M − 10CO]$^+$, 464 [M − 11CO]$^+$, 436 [M − 12CO]$^+$. IR (KBr): 2925 (s), 2854 (m), 2072 (vs), 2034 (vs), 2012 (vs), 1630 (m). Anal. Calcd for C$_{16}$H$_8$Fe$_4$O$_{12}$S$_4$Si: C, 24.89; H, 1.04; S, 16.62. Found: C, 25.1; H, 1.0; S, 16.5.

Reaction of 5b with HBF$_4$·Et$_2$O. Compound **5b** (86 mg, 189 μmol) was dissolved in dichloromethane (3 mL), and the resulting solution was cooled to 0 °C. Subsequently, HBF$_4$ (51−57% in Et$_2$O) (26 μL, 189 μmol) was added, the mixture was stirred for 45 min at 0 °C, pentane (2 mL) was added, and the resulting solution was stored at −20 °C for 12 h. The formed precipitate was separated by filtration and washed with hexane (50 mL) to afford a red solid. IR (KBr): 2099 (vs), 2065 (vs), 2032 (vs), 1990 (vs).

Reaction of 5b with Na/Hg. In a 10 mL Schlenk vessel, compound **5b** (19 mg, 41.7 µmol) was dissolved in acetonitrile (5 mL), followed by the addition of sodium amalgam (0.2 % Na in Hg), and the

resulting two-phase system was shaken for 30 min. Within this time, the solution colored to dark red. Subsequently, this solution was investigated via IR spectroscopy under an argon atmosphere.

Electrochemistry: Instrumentation and Procedures. Cyclic voltammograms were recorded against a non-aqueous Ag/Ag$^+$ reference electrode (0.1 M [n-Bu$_4$N][PF$_6$] and 0.01 M AgNO$_3$ in acetonitrile) and Ag/AgCl using 0.45 M [n-Bu$_4$N][BF$_4$] in dichloromethane as the supporting electrolyte. A glassy carbon (GC) macroelectrode and a platinum wire were used as the working and auxiliary electrodes, respectively. A solution of 0.05 M [n-Bu$_4$N][PF$_6$] (Fluka, electrochemical grade) in acetonitrile (Aldrich, anhydrous, 99.8%) was used as the supporting electrolyte. Electrochemical experiments were carried out using a CHI750C electrochemical bipotentiostat. Prior to each experiment, the electrochemical cell was degassed for at least 10 minutes using argon, and a blanket of argon was maintained throughout. The GC working electrode was prepared by successive polishing with 1.0 and 0.3 micron alumina pastes and sonicated in Millipore water for 5 minutes. All cyclic voltammograms were recorded at a scan rate of 100 mV s^{-1}. In case of the studies of **5b**, cyclic voltammetric measurements were conducted in 3-electrode technique using a Reference 600 potentiostat (Gamry Instruments, Warminster, USA), which was controlled by DigiElch 5.R.[33] This program provides not only routines for the digital simulation of electrochemical experiments but also those for performing the measurements in a consistent way making use of the Gamry Electrochemical Toolkit^{TM} library. Unless otherwise stated, the experiments were performed in acetonitrile (containing 0.25 M [Et$_4$N][ClO$_4$]) under a blanket of solvent-saturated argon. The ohmic resistance, which had to be compensated for, was determined by measuring the impedance of the system at potentials where the faradic current was negligibly small. Background correction was accomplished by subtracting the current curves of the blank electrolyte (containing the same concentration of supporting electrolyte) from the experimental CVs. The reference electrode was an Ag/AgCl electrode in acetonitrile containing 0.25 M [n-Bu$_4$N]Cl. However, all potentials reported in this paper refer to the ferrocenium/ferrocene couple, which was measured at the end of a series of experiments. The reduction processes were studied on a hanging

mercury drop ($m_{Hg\text{-}drop} \approx 4$ mg) produced by a CGME instrument (Bioanalytical Systems, Inc.,West Lafayette, USA).

Quantum Chemical Calculations. The density functional programs provided by the TURBOMOLE 5.71 suite[34] were used for all calculations. The calculations were arranged with the density functional BP86[35,36] in combination with the resolution-of-the-identity (RI) technique[37] as implemented in TURBOMOLE. The BP86 functional is composed of the Becke exchange functional B88[35] and the Perdew correlation functional P86.[36] The preoptimizations of the geometries were performed with the basis set SVP.[38] The final structures and frequency calculations were calculated by applying the basis set TZVP.[39] The output IR line spectra were convoluted with a Gaussian profile of 15 cm^{-1} width to better match the experimental spectra.

Crystal Structure Determinations. Compounds **5a–c**, **6b**, and **7** were crystallized from solutions in trichloromethane by slow evaporation of the solvent at 4 °C. The intensity data were collected on a Nonius Kappa CCD diffractometer using graphite-monochromated Mo-K$_\alpha$ radiation. Data were corrected for Lorentz and polarization effects but not for absorption.[40,41] Crystallographic data as well as structure solution and refinement details are summarized in Table 4.

The structures were solved by direct methods (SHELXS)[42] and refined by full-matrix least squares techniques against F_o^2 (SHELXL-97).[42] All non-hydrogen atoms were refined anisotropically.[42] The hydrogen atoms were included at calculated positions according to the riding model.

Table 4. Crystal Data and Refinement Details for the Crystal Structure Analyses of Compounds **5a–c**, **6b**, and **7**

	5a	5b	5c	6b	7
empirical formula	$C_{10}H_{10}Fe_2O_6S_2Si$	$C_{12}H_{12}Fe_2O_6S_2Si$	$C_{13}H_{14}Fe_2O_6S_2Si$	$C_{16}H_{18}Fe_4O_8S_6Si_2$	$C_{16}H_8Fe_4O_{12}S_4Si$
formula mass [g·mol^{-1}]	430.09	456.13	470.15	810.24	771.95
collection T [°C]	–90(2)	–90(2)	–90(2)	–90(2)	–90(2)
λ (Mo K$_\alpha$) [Å]	0.71073	0.71073	0.71073	0.71073	0.71073
crystal system	monoclinic	monoclinic	triclinic	triclinic	triclinic
space group (No.)	$P2_1/m$ (11)	$P2_1/c$ (14)	$P\bar{1}$ (2)	$P\bar{1}$ (2)	$P\bar{1}$ (2)
a [Å]	8.9368(5)	9.0756(3)	7.4982(2)	10.2124(5)	9.1887(18)
b [Å]	10.6475(5)	13.2900(4)	11.7114(5)	11.7804(5)	11.601(2)
c [Å]	9.5294(5)	14.5302(4)	12.0123(5)	14.1788(6)	12.549(3)
α [°]	90	90	65.435(2)	67.448(3)	99.58(3)
β [°]	115.403(3)	98.718(2)	84.890(2)	75.255(3)	93.84(3)
γ [°]	90	90	75.842(2)	65.836(3)	94.50(3)
V [Å^3]	819.09(7)	1732.31(9)	930.14(6)	1427.66(11)	1310.6(4)
Z	2	4	2	2	2
ρ_{calcd} [g·cm^{-3}]	1.744	1.749	1.679	1.885	1.956
μ [mm^{-1}]	2.117	2.008	1.872	2.553	2.591
$F(000)$	432	920	476	812	764
crystal dimensions [mm]	$0.04 \times 0.04 \times 0.02$	$0.04 \times 0.04 \times 0.04$	$0.04 \times 0.04 \times 0.04$	$0.04 \times 0.04 \times 0.03$	$0.04 \times 0.04 \times 0.04$
2θ range [deg]	6.08–54.94	4.18–54.96	6.42–54.96	4.80–54.94	4.42–54.92
	$-10 \leq h \leq 11$,	$-11 \leq h \leq 11$,	$-9 \leq h \leq 9$,	$-13 \leq h \leq 12$,	$-11 \leq h \leq 11$,
index ranges	$-13 \leq k \leq 13$,	$-16 \leq k \leq 17$,	$-15 \leq k \leq 12$,	$-15 \leq k \leq 15$,	$-15 \leq k \leq 13$,
	$-12 \leq l \leq 12$	$-18 \leq l \leq 18$	$-15 \leq l \leq 15$	$-15 \leq l \leq 18$	$-16 \leq l \leq 15$
measured reflections	5815	11846	6712	9688	9110
unique reflections/R_{int}	1974/0.0438	3949/0.0355	4219/0.0229	6448/0.0325	5901/0.0324
reflections used	1974	3949	4219	6448	5901
data with $I > 2\sigma(I)$	1540	3348	3512	5280	5231
parameters	111	208	217	327	334
S^a	1.010	1.027	1.012	1.005	1.020
R_1 [$I > 2\sigma(I)$]^b	0.0323	0.0280	0.0293	0.0340	0.0331
wR_2 [all data, on F^2]^c	0.0780	0.0698	0.0698	0.0899	0.0919
max./min. residual electron density [e·Å^{-3}]	0.536/–0.443	0.446/–0.564	0.355/–0.474	0.545/–0.615	0.778/–0.578
CCDC No.	697007	697008	697009	697011	697010

[a] $S = \{\Sigma[w(F_o^2 - F_c^2)^2] / (n - p)\}^{0.5}$; n = no. of reflections; p = no. of parameters; [b] $R_1 = \Sigma||F_o| - |F_c|| / \Sigma|F_o|$; [c] $wR_2 = \{\Sigma[w(F_o^2 - F_c^2)^2] / \Sigma[w(F_o^2)^2]\}^{0.5}$.

Supporting Information Available: Selected crystallographic data for **5a−c**, **6b**, and **7**, Raman spectrum of **6a**, additional discussion of the electrochemical properties of **5a−c**, and quantum chemical calculation of **5b^{2-}**·CH₃CN. This material is available free of charge via the Internet at http://pubs.acs.org.

(1) Peters, J. W.; Lanzilotta, W. N.; Lemon, B. J.; Seefeldt, L. C. *Science* **1998**, *282*, 1853–1858.

(2) Nicolet, Y.; Piras, C.; Legrand, P.; Hatchikian, C. E.; Fontecilla-Camps, J. C. *Structure* **1999**, *7*, 13–23.

(3) (a) Razavet, M.; Davies, S. C.; Hughes, D. L.; Pickett, C. J. *Chem. Commun.* **2001**, 847–848. (b) Razavet, M.; Davies, S. C.; Hughes, D. L.; Barclay, J. E.; Evans, D. J.; Fairhurst, S. A.; Liu, X.; Pickett, C. J. *Dalton Trans.* **2003**, 586–595. (c) Tard, C.; Liu, X.; Ibrahim, S. K.; Bruschi, M.; De Gioia, L.; Davies, S. C.; Yang, X.; Wang, L.-S.; Sawers, G.; Pickett, C. J. *Nature* **2005**, *433*, 610–613. (d) Song, L.-C.; Cheng, J.; Yan, J.; Wang, H.-T.; Liu, X.-F.; Hu, Q.-M. *Organometallics* **2006**, *25*, 1544–1547. (e) Windhager, J.; Görls, H.; Petzold, H.; Mloston, G.; Linti, G.; Weigand, W. *Eur. J. Inorg. Chem.* **2007**, 4462–4471. (f) Apfel, U.-P.; Halpin, Y.; Gottschaldt, M.; Görls, H.; Vos, J. G.; Weigand, W. *Eur. J. Inorg. Chem.* **2008**, 5112–5118. (g) Song, L.-C.; Fang, X.-N.; Li, C.-G.; Yan, J.; Bao, H.-L.; Hu, Q.-M. *Organometallics* **2008**, *27*, 3225–3231. (h) Singleton, M. L.; Bhuvanesh, N.; Reibenspies, J. H.; Darensbourg, M. Y. *Angew. Chem.* **2008**, *120*, 9634–9637; *Angew. Chem. Int. Ed.* **2008**, *47*, 9492–9495. (i) Apfel, U.-P.; Kowol, C. R.; Halpin, Y.; Kloss, F.; Kübel, J.; Görls, H.; Vos, J. G.; Keppler, B. K.; Morera, E.; Lucente, G.; Weigand, W. *J. Inorg. Biochem.* **2009**, *103*, 1236–1244. (j) Harb, M. K.; Apfel, U.-P.; Kübel, J.; Görls, H.; Felton, G. A. N.; Sakamoto, T.; Evans, D. H.; Glass, R. S.; Lichtenberger, D. L.; El-khateeb, M.; Weigand, W. *Organometallics* **2009**, *28*, 6666-6675.

(4) Tard, C.; Pickett, C. J. *Chem. Rev.* **2009**, *109*, 2245–2274, and references cited herein.

(5)   (a) Borg, S. J.; Behrsing, T.; Best, S. P.; Razavet, M.; Liu, X.; Pickett, C. J. *J. Am. Chem. Soc.* **2004**, *126*, 16988–16999. (b) Chong, D. S.; Georgakaki, I. P.; Mejia-Rodriguez, R.; Sanabria-Chinchilla, J.; Soriaga, M. P.; Darensbourg, M. Y. *Dalton Trans.* **2003**, 4158–4163

(6)   (a) Capon, J.-F.; Ezzaher, S.; Gloaguen, F.; Pétillon, F. Y.; Schollhammer, P.; Talarmin, J. *Chem. Eur. J.* **2008**, *14*, 1954–1964. (b) Olsen, M. T.; Barton, B. E.; Rauchfuss, T. B. *Inorg. Chem.* **2009**, *48*, 7507–7509.

(7)   (a) Zhao, X.; Chiang, C.-Y.; Miller, M. L.; Rampersad, M. V.; Darensbourg, M. Y. *J. Am. Chem. Soc.* **2003**, *125*, 518–524. (b) Tye, J. W.; Darensbourg, M. Y.; Hall, M. B. *J. Mol. Struct.*: *THEOCHEM* **2006**, *771*, 123–128.

(8)   (a) Windhager, J.; Seidel, R. A.; Apfel, U.-P.; Görls, H.; Linti, G.; Weigand, W. *Chem. Biodiv.* **2008**, *5*, 2023–2041. (b) Windhager, J.; Apfel, U.-P.; Yoshino, T.; Nakata, N.; Görls, H.; Rudolph, M.; Ishii, A.; Weigand, W. *Chem. Asian J.* **2010**, DOI: 10.1002/asia.200900733. (c) Liu, T.; Li, B.; Singleton, M. L.; Hall, M. B.; Darensbourg, M. Y. *J. Am. Chem. Soc.* **2009**, *131*, 8296–8307. (d) Li, B.; Liu, T.; Singleton, M. L.; Darensbourg, M. Y. *Inorg. Chem.* **2009**, *48*, 8393–8403.

(9)   Windhager, J.; Rudolph, M.; Bräutigam, S.; Görls, H.; Weigand, W. *Eur. J. Inorg. Chem.* **2007**, 2748–2760.

(10)   Glass, R. S.; Gruhn, N. E.; Lorance, E.; Singh, M. S.; Stessman, N. Y. T.; Zakai, U. I. *Inorg. Chem.* **2005**, *44*, 5728–5737.

(11)   Recent publications dealing with sila-substituted drugs: (a) Showell, G. A.; Barnes, M. J.; Daiss, J. O.; Mills, J. S.; Montana, J. G.; Tacke, R.; Warneck, J. B. H. *Bioorg. Med. Chem. Lett.* **2006**, *16*, 2555–2558. (b) Ilg, R.; Burschka, C.; Schepmann, D.; Wünsch, B.; Tacke, R. *Organometallics* **2006**, *25*, 5396–5408. (c) Büttner, M. W.; Burschka, C.; Daiss, J. O.; Ivanova, D.; Rochel, N.; Kammerer, S.; Peluso-Iltis, C.; Bindler, A.; Gaudon, C.; Germain, P.; Moras, D.; Gronemeyer, H.; Tacke, R. *ChemBioChem* **2007**, *8*, 1688–1699. (d) Tacke, R.; Popp, F.; Müller, B.; Theis, B.; Burschka, C.; Hamacher, A.; Kassack, M. U.; Schepmann, D.; Wünsch, B.; Jurva, U.; Wellner, E.

ChemMedChem **2008**, *3*, 152–164. (e) Warneck, J. B.; Cheng, F. H. M.; Barnes, M. J.; Mills, J. S.; Montana, J. G.; Naylor, R. J.; Ngan, M.-P.; Wai, M.-K.; Daiss, J. O.; Tacke, R.; Rudd, J. A. *Toxicol. Appl. Pharmacol.* **2008**, *232*, 369–375. (f) Lippert, W. P.; Burschka, C.; Götz, K.; Kaupp, M.; Ivanova, D.; Gaudon, C.; Sato, Y.; Antony, P.; Rochel, N.; Moras, D.; Gronemeyer, H.; Tacke, R. *ChemMedChem* **2009**, *4*, 1143–1152. (g) Tacke, R.; Müller, V.; Büttner, M. W.; Lippert, W. P.; Bertermann, R.; Daiß, J. O.; Khanwalkar, H.; Furst, A.; Gaudon, C.; Gronemeyer, H. *ChemMedChem* **2009**, *4*, 1797–1802. (h) Johansson, T.; Weidolf, L.; Popp, F.; Tacke, R.; Jurva, U. *Drug Metab. Dispos.* **2010**, *38*, 73–83. (i) Tacke, R.; Nguyen, B.; Burschka, C.; Lippert, W. P.; Hamacher, A.; Urban, C.; Kassack, M. U. *Organometallics* **2010**, *29*, 1652–1660.

(12) Recent publications dealing with sila-substituted odorants: (a) Büttner, M. W.; Penka, M.; Doszczak, L.; Kraft, P. *Organometallics* **2007**, *26*, 1295–1298. (b) Doszczak, L.; Kraft, P.; Weber, H.-P.; Bertermann, R.; Triller, A.; Hatt, H.; Tacke, R. *Angew. Chem.* **2007**, *119*, 3431–3436; *Angew. Chem. Int. Ed.* **2007**, *46*, 3367–3371. (c) Büttner, M. W.; Metz, S.; Kraft, P.; Tacke, R. *Organometallics* **2007**, *26*, 3925–3929. (d) Büttner, M. W.; Burschka, C.; Junold, K.; Kraft, P.; Tacke, R. *ChemBioChem* **2007**, *8*, 1447–1454. (e) Büttner, M. W.; Nätscher, J. B.; Burschka, C.; Tacke, R. *Organometallics* **2007**, *26*, 4835–4838. (f) Tacke, R.; Metz, S. *Chem. Biodiv.* **2008**, *5*, 920–941. (g) Metz, S.; Nätscher, J. B.; Burschka, C.; Götz, K.; Kaupp, M.; Kraft, P.; Tacke, R. *Organometallics* **2009**, *28*, 4700–4712. (h) Nätscher, J. B.; Laskowski, N.; Kraft, P.; Tacke, R. *ChemBioChem* **2010**, *11*, 315–319.

(13) Recent publications dealing with sila-substituted explosives: (a) Klapötke, T. M.; Krumm, B.; Ilg, R.; Troegel, D.; Tacke, R. *J. Am. Chem. Soc.* **2007**, *129*, 6908–6915. (b) Evangelisti, C.; Klapötke, T. M.; Krumm, B.; Nieder, A.; Berger, R. J. F.; Hayes, S. A.; Mitzel, N. W.; Troegel, D.; Tacke, R. *Inorg. Chem.* **2010**, *49*, 4865–4880.

(14) Recent publications dealing with functional tetraorganylsilanes of the formula type $R_n Si(CH_2X)_{4-n}$ (R = organyl; X = functional group; n = 0–3): (a) Daiss, J. O.; Bart, K. A.; Burschka, C.; Hey, P.;

Ilg, R.; Klemm, K.; Richter, I.; Wagner, S. A.; Tacke, R. *Organometallics* **2004**, *23*, 5193–5197. (b) Ilg, R.; Troegel, D.; Burschka, C.; Tacke, R. *Organometallics* **2006**, *25*, 548–551. (c) Troegel, D.; Walter, T.; Burschka, C.; Tacke, R. *Organometallics* **2009**, *28*, 2756–2761. (d) Troegel, D.; Möller, F.; Burschka, C.; Tacke, R. *Organometallics* **2009**, *28*, 5765–5770. (e) Weidner, T.; Ballav, N.; Siemeling, U.; Troegel, D.; Walter, T.; Tacke, R.; Castner, D. G.; Zharnikov, M. *J. Phys. Chem. C* **2009**, *113*, 19609–19617. (f) Troegel, D.; Lippert, W. P.; Möller, F.; Burschka, C.; Tacke, R. *J. Organomet. Chem.* **2010**, *695*, 1700–1707.

(15) (a) Kobayashi, T.; Pannell, K. H. *Organometallics* **1990**, *9*, 2201–2203. (b) Kobayashi, T.; Pannell, K. H. *Organometallics* **1991**, *10*, 1960–1964.

(16) Tard, C.; Liu, X.; Hughes, D. L.; Pickett, C. J. *Chem. Commun.* **2005**, 133–135. (b) Cheah, M. H.; Tard, C.; Borg, S. J.; Liu, X.; Ibrahim, S. K.; Pickett, C. J.; Best, S. P. *J. Am. Chem. Soc.* **2007**, *129*, 11085–11092.

(17) Song, L.-C.; Yang, Z.-Y.; Bian, H.-Z.; Hu, Q.-M. *Organometallics* **2004**, *23*, 3082–3084.

(18) (a) Schwartz, L.; Eriksson, L.; Lomoth, R.; Teixidor, F.; Viñas, C.; Ott, S. *Dalton Trans.* **2008**, 2379–2381. (b) Yu, Z.; Wang, M.; Li, P.; Dong, W.; Wang, F.; Sun, L. *Dalton Trans.* **2008**, 2400–2406. (c) Ezzaher, S.; Orain, P.-Y.; Capon, J.-F.; Gloaguen, F.; Pétillon, F. Y.; Roisnel, T.; Schollhammer, P.; Talarmin, J. *Chem. Commun.* **2008**, 2547–2549. (d) Li, P.; Wang, M.; Pan, J.; Chen, L.; Wang, N.; Sun, L. *J. Inorg. Biochem.* **2008**, *102*, 952–959. (e) Song, L.-C.; Wang, H.-T.; Ge, J.-H.; Mei, S.-Z.; Gao, J.; Wang, L.-X.; Gai, B.; Zhao, L.-Q.; Yan, J.; Wang, Y.-Z. *Organometallics* **2008**, *27*, 1409–1416.

(19) Liu, T.; Wang, M.; Shi, Z.; Cui, H.; Dong, W.; Chen, J.; Åkermark, B.; Sun, L. *Chem. Eur. J.* **2004**, *10*, 4474–4479.

(20) Apfel, U.-P.; Halpin, Y.; Görls, H.; Vos, J. G.; Schweizer, B.; Linti, G.; Weigand, W. *Chem. Biodiv.* **2007**, *4*, 2138–2148.

(21) Singleton, M. L.; Jenkins, R. M.; Klemashevich, C. L.; Darensbourg, M. Y. *C.R. Chimie* **2008**, *11*, 861–874.

(22) Felton, G. A. N.; Mebi, C. A.; Petro, B. J.; Vannucci, A. K.; Evans, D. H.; Glass, R. S.; Lichtenberger, D. L. *J. Organomet. Chem.* **2009**, *694*, 2681–2699, and references cited herein.

(23) (a) Liu, Z.-P.; Hu, P. *J. Chem. Phys.* **2002**, *117*, 8177–8180. (b) Song, L.-C.; Gao, J.; Wang, H.-T.; Hua, Y.-J.; Fan, H.-T.; Zhang, X.-G.; Hu, Q.-M. *Organometallics* **2006**, *25*, 5724–5729. (c) Greco, C.; Zampella, G.; Bertini, L.; Bruschi, M.; Fantucci, P.; De Goia, L. *Inorg. Chem.* **2007**, *46*, 108–116. (d) Gao, W.; Ekström, J.; Liu, J.; Chen, C.; Eriksson, L.; Weng, L.; Åkermark, B.; Sun, L. *Inorg. Chem.* **2007**, *46*, 1981–1991.

(24) Surawatanawong, P.; Hall, M. B. *Inorg. Chem.* **2010**, *49*, 5737–5747.

(25) The pK_a value of acetic acid is 22.6 and that of pivalic acid should not be significantly different.

(26) I. Kosuke, *Acid-Base Dissociation Constants in Dipolar Aprotic Solvents*, Blackwell Scientific Publications: Oxford (**1990**).

(27) The minimum of the standard deviation is only slightly depending on the exact value of K_5. There are several combinations of $K_6/K_5 \approx 4$ yielding virtually the same standard deviation between simulated and experimental CVs.

(28) Reaction (10) is fully irreversible. Consequently, there is an infinite number of $E°/k°$ combinations yielding exactly the same current curve. For this reason, the "right" combination cannot be determined exclusively from electrochemical data.

(29) Reaction (11) should be considered an overall reaction that occurs in several steps. It describes the re-oxidation of the species generated in reaction (10) and is necessary only to render the re-oxidation peak observed in the reverse scan at around -1.05 V.

(30) It should be mentioned that this behavior is strongly dependent on the applied supporting electrolyte. It becomes even more pronounced when using tetra-*n*-butylammonium perchlorate instead of tetraethylammonium perchlorate. In that case, the "isosbestic point" is lost and a

positive shift of less than 10 mV is observed virtually independently of the HP concentration unless the HP concentration becomes distinctly lower than [HP]/[**5b**] = 1.

(31) (a) Stanley, J. L.; Heiden, Z. M.; Rauchfuss, T. B.; Wilson, S. R.; De Gioia, L.; Zampella, G. *Organometallics* **2008,** *27,* 119–125. (b) Jiang, S.; Liu, J.; Shi, Y.; Wang, Z.; Åkermark*,* B.; Sun, L. *Dalton Trans.* **2007**, 896–902. (c) Xu, F.; Tard, C.; Wang, X.; Ibrahim, S. K.; Hughes, D. L.; Zhong, W.; Zeng, X.; Luo, Q.; Liu, X.; Pickett, C. J. *Chem. Commun.* **2008**, 606–608.

(32) (a) Barton, B. E.; Rauchfuss, T. B. *Inorg. Chem.* **2008**, *47*, 2261–2263. (b) Wang, N.; Wang, M.; Zhang, T.; Li, P.; Liu, J.; Sun, L. *Chem. Commun.* **2008**, 5800–5802.

(33) DigiElch 5.R developed by M. Rudolph available from http://www.gamry.com/Products/DigiElch5.htm

(34) Ahlrichs, R.; Bär, M.; Häser, M.; Horn, H.; Kölmel, C. *Chem. Phys. Lett.* **1989**, *162*, 165–169.

(35) Becke, A. D. *Phys. Rev. A* **1988**, *38*, 3098–3100.

(36) Perdew, J. P. *Phys. Rev. B* **1986**, *33*, 8822–8824.

(37) (a) Eichkorn, K.; Treutler, O.; Öhm, H.; Häser, M.; Ahlrichs, R. *Chem. Phys. Lett.* **1995**, *240*, 283–290. (b) Eichkorn, K.; Weigend, F.; Treutler, O.; Ahlrichs, R. *Theor. Chem. Acc.* **1997**, *97*, 119–124.

(38) Schäfer, A.; Horn, H.; Ahlrichs, R. *J. Chem. Phys.* **1992**, *97*, 2571–2577.

(39) Schäfer, A.; Huber, C.; Ahlrichs, R. *J. Chem. Phys.* **1994**, *100*, 5829–5835.

(40) COLLECT, Data Collection Software; Nonius B. V., The Netherlands, **1998**.

(41) Otwinowski, Z.; Minor, W. *Methods Enzymol.* **1997**, *276*, 307–326.

(42) Sheldrick, G. M. *Acta Cryst. Sect. A* **2008**, *64*, 112–122.

SUPPORTING INFORMATION

Models for the Active Site in [FeFe] Hydrogenase with Iron-Bound Ligands Derived from Bis-, Tris-, and Tetrakis(mercaptomethyl)silanes

Ulf-Peter Apfel, Dennis Troegel, Yvonne Halpin, Stefanie Tschierlei, Ute Uhlemann, Michael Schmitt, Jürgen Popp, Helmar Görls, Peter Dunne, Munuswamy Venkatesan, Michael Coey, Manfred Rudolph, Johannes G. Vos, Reinhold Tacke, Wolfgang Weigand
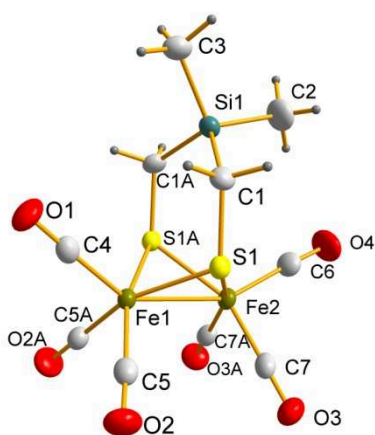
Figure S1. Molecular structure of **5a** in the crystal (probability level of displacement ellipsoids 50%).
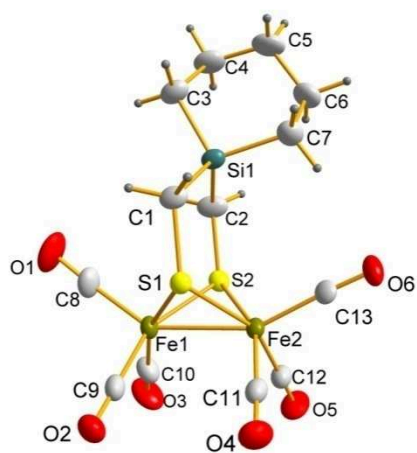
Figure S2. Molecular structure of **5c** in the crystal (probability level of displacement ellipsoids 50%).

Table S1. Selected Bond Distances (pm) and Angles (deg) for Compounds **5a c**

	5a	5b	5c
Fe1–Fe2	252.16 (6)	252.21(4)	251.23(4)
Fe1–S1	225.68(6)	225.12(6)	225.40(6)
Fe1–S2/Fe1–S1A	225.67(6)	225.95(6)	225.41(6)
Fe2–S1	225.97(6)	226.27(6)	225.24(5)
Fe2–S2/Fe2–S1A	225.97(6)	226.04(6)	225.46(6)
S1–C1	182.3(3)	182.7(2)	182.5(2)
S2–C2/S1A–C1A	182.3(3)	182.5(2)	181.5(2)
C1–Si1	187.1(3)	187.1(2)	186.7(2)
C2–Si1/C1A–Si1	187.1(3)	187.1(2)	186.8(2)
Si1–C3	186.1(4)	188.3(2)	187.1(2)
Si1–C2/Si1–C6/Si1–C7	186.7(4)	187.3(2)	186.0(3)
S1–Fe1–S2/S1–Fe1–S1A	87.97(3)	87.94(2)	87.29(2)
S1–Fe2–S2/S1–Fe2–S1A	87.83(3)	87.64(2)	87.31(2)
S1–Fe1–Fe2	56.116(18)	56.247(15)	56.087(15)
S1–Fe2–Fe1	56.006(17)	55.816(15)	56.149(16)
S2–Fe1–Fe2/S1A–Fe1–Fe2	56.117(17)	56.100(16)	56.147(16)
S2–Fe2–Fe1/S1A–Fe2–Fe1	56.004(17)	56.065(16)	56.128(16)
C1–S1–Fe1	112.75(8)	113.40(8)	114.05(8)
C1–S1–Fe2	119.01(8)	118.80(7)	120.12(7)
C2–S2–Fe1/C1A–S1A–Fe1	112.75(8)	112.75(8)	113.37(9)
C2–S2–Fe2/C1A–S1A–Fe2	119.01(8)	117.95(8)	118.81(8)
S1–C1–Si1	121.52(13)	118.22(12)	120.34(11)
S2–C2–Si1/S1A–C1A–Si1	121.52(13)	119.24(12)	122.05(13)
C1–Si1–C2/C1–Si1–C1A	108.95(15)	107.79(10)	109.16(11)
C1–Si1–C3	108.28(10)	113.40(11)	110.51(11)
C3–Si1–C2/C3–Si1–C6/C3–Si1–C7	108.8(2)	96.10(11)	104.00(12)

Table S2. Selected Bond Distances (pm) and Angles (deg) for Compound **6b** (Data for Molecule A; the structure of Molecule B is very similar)

Fe1A–Fe2A	252.97(6)	S1A–C1A	183.0(3)
Fe2A Fe2A'	262.84(8)	S2A–C2A	182.5(3)
Fe1A–S1A	226.32(8)	S3A–C3A	182.6(3)
Fe1A–S2A	224.98(3)	C1A–Si1A	186.6(3)
Fe2A–S1A	229.99(8)	C2A–Si1A	186.0(3)
Fe2A–S2A	224.99(8)	C3A–Si1A	187.6(3)
Fe2A–S3A	223.72(8)	C4A–Si1A	186.4(3)
Fe2A–S3A'	222.13(8)		
S1A–Fe1A–S2A	88.89(3)	C1A–S1A–Fe2A	116.76(11)
S1A–Fe2A–S2A	87.98(3)	C2A–S2A–Fe1A	115.02(11)
S1A–Fe2A–S3A	105.02(3)	C2A–S2A–Fe2A	112.38(10)
S1A–Fe2A–S3A'	83.16(3)	C3A–S3A–Fe2A	110.58(10)
S2A–Fe2A–S3A	95.92(3)	C3A–S3A–Fe2A'	116.12(11)
S2A–Fe2A–S3A'	156.14(3)	Fe1A–S1A–Fe2A	67.33(3)
S3A–Fe2A–S3A'	107.75(3)	Fe1A–S2A–Fe2A	68.42(3)
S1A–Fe1A–Fe2A	57.03(2)	Fe2A–S3A–Fe2A'	72.25(3)
S2A–Fe1A–Fe2A	55.79(2)	S1A–C1A–Si1A	111.71(16)
S1A–Fe2A–Fe1A	55.64(2)	S2A–C2A–Si1A	116.91(16)
S2A–Fe2A–Fe1A	55.79(2)	S3A–C3A–Si1A	116.10(16)
S3A–Fe2A–Fe1A	142.69(3)	C1A–Si1A–C2A	106.40(15)
S3A'–Fe2A–Fe1A	101.43(3)	C1A–Si1A–C3A	109.42(14)
S1A–Fe2A–Fe2A'	96.89(3)	C1A–Si1A–C4A	112.80(15)
S2A–Fe2A–Fe2A'	149.40(3)	C2A–Si1A–C3A	111.32(14)
S3A–Fe2A–Fe2A'	53.60(2)	C2A–Si1A–C4A	108.96(16)
S3A'–Fe2A–Fe2A'	54.16(2)	C3A–Si1A–C4A	107.98(15)
C1A–S1A–Fe1A	113.61(11)		

Table S3. Selected Bond Distances (pm) and Angles (deg) for Compound **7**

Fe1–Fe2	250.67(8)	Fe4–S4	225.39(9)
Fe3–Fe4	252.21(7)	S1–C1	183.5(3)
Fe1–S1	225.98(10)	S2–C2	181.7(3)
Fe1–S2	225.46(8)	S3–C3	182.6(3)
Fe2–S1	260.01(10)	S4–C4	181.2(3)
Fe2–S2	225.79(9)	C1–Si1	187.3(3)
Fe3–S3	224.70(9)	C2–Si1	186.9(3)
Fe3–S4	224.62(9)	C3–Si1	186.9(3)
Fe4–S3	224.67(10)	C4–Si1	187.6(3)
S1–Fe1–S2	87.66(3)	C2–S2–Fe2	119.39(9)
S1–Fe2–S2	87.58(3)	C3–S3–Fe3	116.10(10)
S3–Fe3–S4	88.05(3)	C3–S3–Fe4	117.10(10)
S3–Fe4–S4	87.87(4)	C4–S4–Fe3	111.46(9)
S1–Fe1–Fe2	56.32(3)	C4–S4–Fe4	120.24(9)
S2–Fe1–Fe2	56.32(3)	S1–C1–Si1	120.03(16)
S1–Fe2–Fe1	56.31(3)	S2–C2–Si1	120.82(14)
S2–Fe2–Fe1	56.19(2)	S3–C3–Si1	121.88(16)
S3–Fe3–Fe4	55.85(3)	S4–C4–Si1	121.28(14)
S4–Fe3–Fe4	56.06(3)	C1–Si1–C2	109.02(12)
S3–Fe4–Fe3	55.86(3)	C1–Si1–C3	112.71(16)
S4–Fe4–Fe3	55.77(3)	C1–Si1–C4	109.08(14)
C1–S1–Fe1	115.26(11)	C2–Si1–C3	110.14(13)
C1–S1–Fe2	118.60(10)	C2–Si1–C4	104.40(13)
C2–S2–Fe1	112.41(9)	C3–Si1–C4	111.13(12)
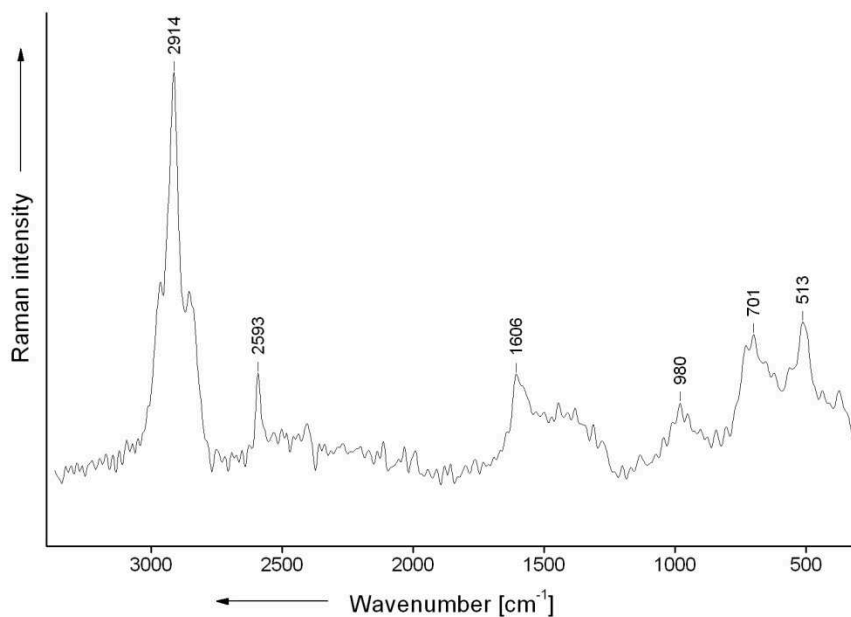
Figure S3. Raman spectrum of **6a** showing the S–H vibration at 2593 cm^{-1}.
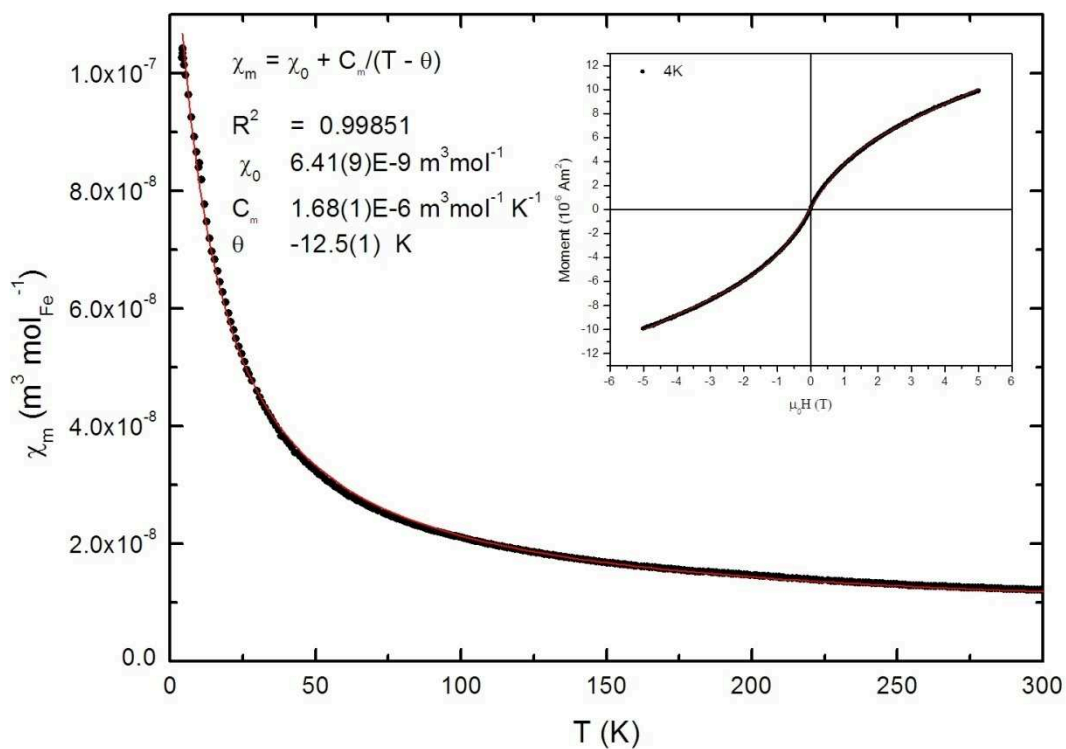

Figure S4. Scan of the magnetization of compound **6a**, measured in an applied field of 800 kA m^{-1}. The data are fitted to a law of the form $\chi = \chi_0 + C/(T - \theta)$, where χ_0 is a small temperature-independent term. The Curie constant C is used to deduce the presence of unpaired spins, using the result $C = 1.57 \; 10^{-6} \; 4S(S+1)$ per mol of iron atoms.

Additional Discussion of the Electrochemical Properties

The estimated value of the diffusion coefficient is $1.18(-0.07) \times 10^{-5}$ cm^2 s^{-1}. The relatively large error for the diffusion coefficient and for $k°_1$ results from the fact that **5b** is slightly adsorbed at the mercury drop electrode, visible by the formation of a broad shoulder. Unfortunately, we were not able to find an adsorption isotherm that worked well enough to completely eliminate the adsorption effect on the charge transfer parameters independently of the applied scan rate. Finally, a Frumkin isotherm with $\Gamma_{max} = 5 \times 10^{-11}$ mol cm^{-2}, $\beta = 5 \times 10^{6}$ cm^3 mol^{-1} and a self-interaction parameter a $= -0.5$ was used in our simulations.

As in the absence of HP, the agreement between simulated and experimental CVs can be slightly improved by taking adsorption reactions into consideration. The simulations shown in Figure S5 were obtained by assuming that not only the starting complex, Fe−Fe, but also Fe−Fe−HP is slightly adsorbed on the mercury drop electrode.
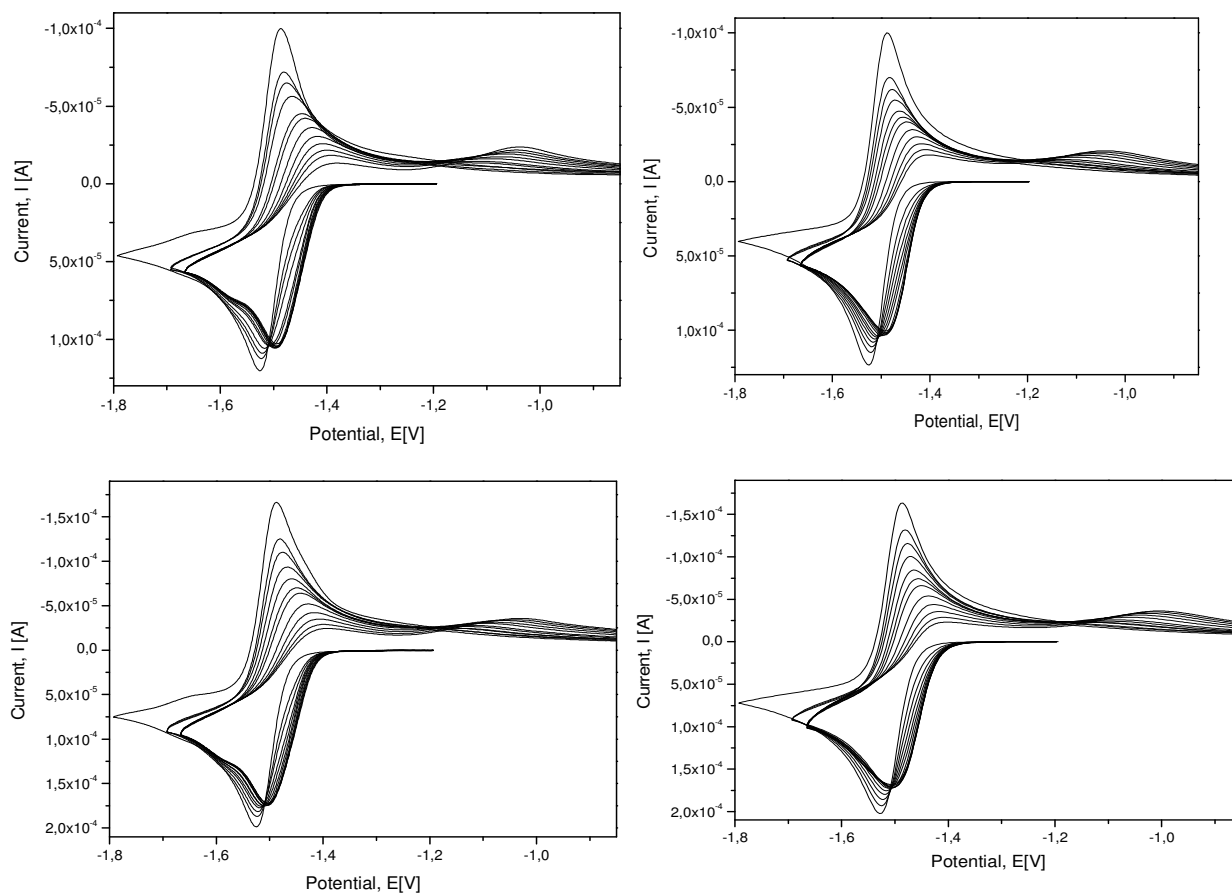

Figure S5. Cyclic voltammetric reduction of a 1.4 mM solution of **5b** in acetonitrile on a mercury drop electrode in the presence of varying concentrations of pivalic acid (right) and simulated CVs (left). The scan rate is

7

3.5 V s^{-1} (top) and 10 V s^{-1} (bottom). The HP concentration was varied as follows: [HP]/[**5b**] = 0 (left-most CV), 1/3, 2/3, 1, 4/3, 5/3, 2, 8/3, 10/3, 4, 14/3, 16/3, and 20/3 (right-most CV). Mechanism and simulation parameters are given by reaction (1) to (11).

The adsorption parameters are similar to those reported in the reaction equations (1)−(4). Unfortunately, the current version of our simulation software[1] does not allow the simulation of reactions which may occur between adsorbed species. The fact that diffusion control was obtained for reaction (7) may therefore result from compensating contributions of surface reactions (comprising adsorbed pivalic acid and adsorbed complex species) neglected in our simulations.

The question which of the two species is the catalytically active one in the potential range at around −1.85 V cannot be answered easily. It requires the inclusion of CVs into the fitting process, which were measured with such high scan rates that the effect of reaction (16) becomes visible. Unfortunately, the adsorption phenomena already described in this and the previous section prevented quantitative studies of the system at sufficiently high scan rates. A few tentative studies concerning the catalytic reactions accompanying the third electron transfer step were also carried out using a glassy carbon working electrode. The changes in the CVs after addition of a weak Brønsted acid are analogous as reported above but the charge transfer processes are distinctly slower (Figure S6).
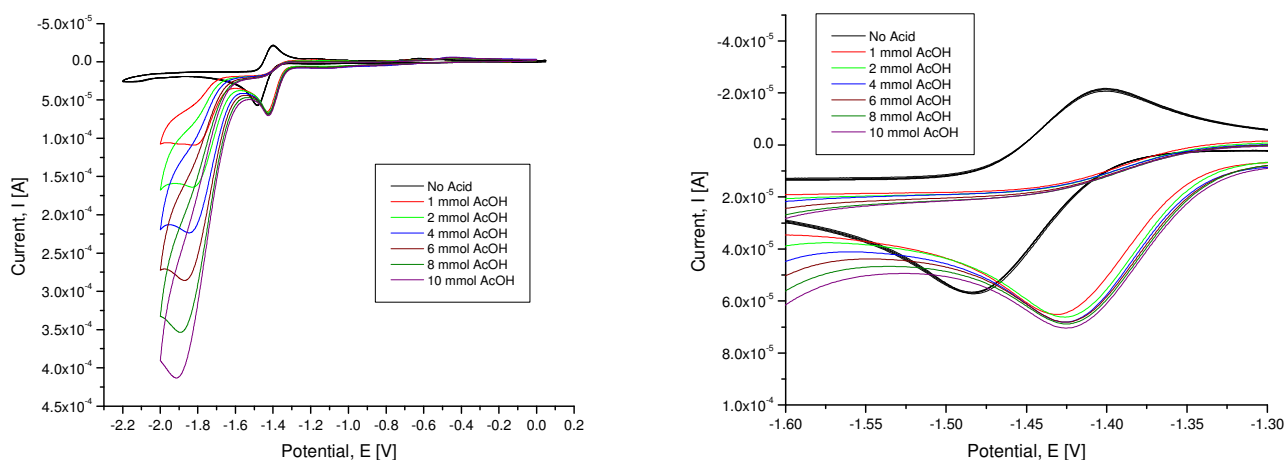

Figure S6. Cyclic voltammograms of compound **5b** in acetonitrile (1 mM) in the presence of HOAc (0–10 mM), vs. Ag/Ag$^+$, as representative for compounds **5a–c** on a glassy carbon electrode.

Unfortunately, the reproducibility of the experiments on glassy carbon was not good enough for a quantitative analysis by data fitting. However, as can be seen from Figure S7, there is at least a qualitative agreement in the development of the catalytic current (in the potential range at around −1.85 V) upon HP addition.
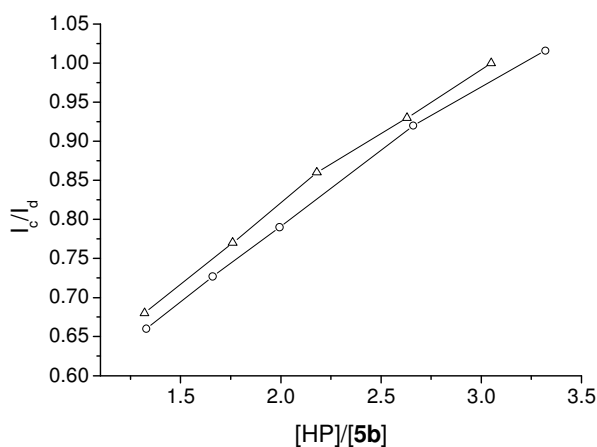
Figure S7. Development of the catalytic current on a glassy carbon (Δ) and mercury drop (○) electrode as function of the HP concentration. I_c is the peak current observed after HP addition in the potential range of about −1.85 V, I_d is the diffusion controlled peak current referring to the two-reduction of **5b** in the absence of pivalic acid. The data refer to a scan rate of 1 V s^{-1}.

This statement holds no longer true for the catalytic reactions accompanying the fourth reduction step. Figure 10 shows experimental CVs, which were measured on a mercury drop electrode. Similar CVs are also obtained on glassy carbon but Figure S8 reveals that the development of the catalytic current (in the potential range at around −2.2 V) is quite different on glassy carbon.
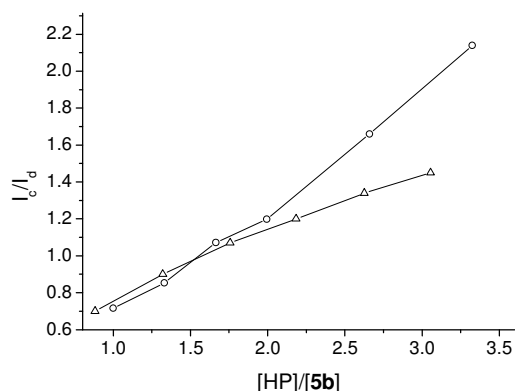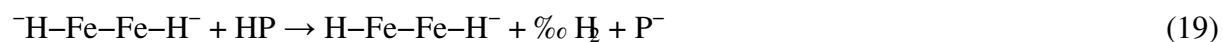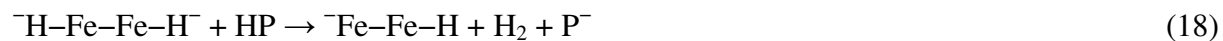
Figure S8. Development of the catalytic current on a glassy carbon (Δ) and mercury drop (○) electrode as function of the HP concentration. I_c is the peak current observed after HP addition in the potential range of about −2.2 V, I_d is the diffusion controlled peak current referring to the two-reduction of **5b** in the absence of pivalic acid. The data refer to a scan rate of 1 V s^{-1}.

It is therefore likely that the catalytic process is governed by homogeneous chemical reactions as long as only the three-fold reduced species is involved in the catalytic cycle (or as long as the electrode potential does not become more negative than about −2 V). On the contrary, surface reactions (involving adsorbed protonated complex species and/or adsorbed HP) seem to play a remarkable role in the catalytic reactions observed on the mercury drop electrode in the potential range at around −2.2 V. Since surface reactions cannot be simulated with the actual version of DigiElch, it is not surprising that we were not able to model the underlying catalytic process exclusively on the basis of homogeneous chemical reactions such as:

$$^-\text{H–Fe–Fe–H}^- \rightarrow {}^-\text{Fe–Fe}^- + \text{H}_2 \tag{17}$$

$$^-\text{H–Fe–Fe–H}^- + \text{HP} \rightarrow {}^-\text{Fe–Fe–H} + \text{H}_2 + \text{P}^- \tag{18}$$

$$^-\text{H–Fe–Fe–H}^- + \text{HP} \rightarrow \text{H–Fe–Fe–H}^- + ‰o\ \text{H}_2 + \text{P}^- \tag{19}$$

where $^-$H–Fe–Fe–H$^-$ comes either from the reduction of H–Fe–Fe–H produced by reaction (16) or from reactions (12) and (15) according to:

$$^-\text{H–Fe–Fe–HP}^- \xrightarrow{\text{e}^-} {}^-\text{H–Fe–Fe–H}^- + \text{P}^- \tag{20}$$

10

H–Fe–Fe–HP⁻ → H–Fe–Fe–H + P⁻ (21)
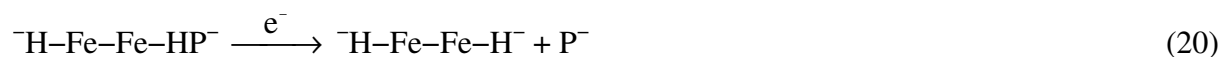
Even when using unrealistically large rate constants for the reactions (17)–(21) and no matter whether the reduction in (20) was modelled as a concerted electron transfer step or as a follow-up reaction, there was no way to simulate the shape and the HP concentration dependence of the catalytic peak current observed in the experimental CVs on the mercury drop electrode. The HP concentration in the surrounding of the electrode is simply too small to establish the relatively high current observed for the second catalytic process in the potential range at around −2.2 V. Looking at the simulated concentration profiles reveals that most of the pivalic acid has already been consumed in the first catalytic process given by reactions (13)–(16). Consequently, the catalytic current simulated for the mercury drop electrode on the basis of reactions (17)–(21) is about 33% smaller than the experimental one when [HP]/[**5b**] is 10/3. Actually, it is in good agreement with that shown in Figure S8 for the glassy carbon electrode.
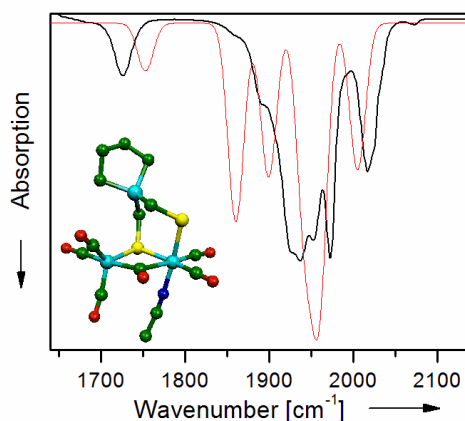
Figure S9. Quantum chemical calculation of the acetonitile coordinated species **5b**$^{2-}$. The output IR line spectra were convoluted with a Gaussian profile of 15 cm^{-1} width to better match the experimental spectra.

(1)   DigiElch 5.R developed by M. Rudolph available from http://www.gamry.com/Products/DigiElch5.htm.

Influence of the introduction of cyanide and phosphine ligands in multifunctionalized (mercapto-methyl)silanes [FeFe] hydrogenase model systems

**Ulf-Peter Apfel,[a] Yvonne Halpin,[b] Helmar Görls, [a] Johannes G. Vos,*[b] and Wolfgang Weigand*[a]**

Cyanide and phosphine substituted [FeFe] hydrogenase models are known to show increased basicity of the [Fe2S] cluster. Following our continued interest in [Fe2S2(Si)] compounds, substitution reactions of such complexes with tetraethylammonium cyanide as well as triphenylphosphine were investigated to yield the respective mono-substituted triphenylphosphine complexes **2a-c** and cyanide complexes **3a-c**. Cyclic voltammetry was used to investigate the electrocatalytic H_2-formation with acetic acid.

Introduction

Since the structure of the active site of the [FeFe] hydrogenase was determined,[1,2] much attention has been payed to the synthesis of structural and functional model complexes, containing different S-to-S linkers.[3-7] Recently, [2Fe2S(Si)] complexes containing functionalized (mercapto-methyl)silanes were reported and the influence of the silicon moiety to the catalytic cycle during electrocatalysis as well as their unique structural features were investigated.[8] Thereby a sulphur-proton interaction was observed, which can be explained by an increased nucleophilicity of the bridgehead atom.[8]

It has been reported that substitution of a carbonyl ligand with either cyanide[9] or phosphine[10] leads to increased basicity of the iron atoms in the [2Fe2S] subsite. This enables a facilitated formation of terminal or bridging hydrides.[11] However since CN⁻ ligands in model systems are not protected by the peptide environment,[1] stable isocyanic acid complexes can be formed which was pictured out in detail for several M-CN complexes (Scheme 1).[12,13]
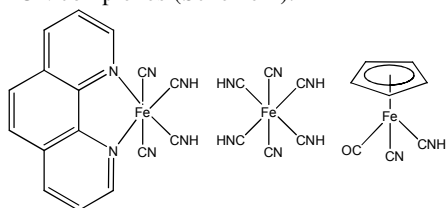
Scheme 1 Isocyanic acid complexes.

In contrast to CN⁻, triphenylphosphine is an abiological ligand and can not be protonated. Nevertheless, trimethylphosphine reveals similar donor character and can serve as an abiological surrogate.[14] Inspired by the properties of [2Fe2S(Si)]
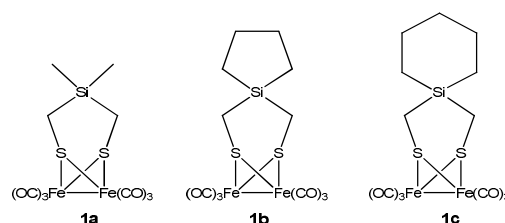
Scheme 2 [Fe2S2(Si)] model complexes (**1a-c**).[8]

complexes and the natural abundance of the strong donor ligand CN⁻,[15] [FeFe] hydrogenase model complexes **1a-c** (Scheme 2) were reacted with triphenylphosphine and tetraethylammonium cyanide to afford mono-substituted, asymmetric [2Fe2S(Si)] cluster compounds. The resulting products were investigated according to their chemical and structural properties by cyclic voltammetry and crystal structure analysis.

Results and Discussion

Synthesis and characterization of the PPh₃ substituted diiron complexes (2a-c)

Initial attempts to obtain the PPh₃ substituted complexes **2a-c** *via* reaction of the hexacarbonyl complexes (**1a-c**) with triphenylphosphine at room temperature[16] or in refluxing toluene[17] require long reaction times and only partial conversions. A fast and selective exchange of CO was established *via* oxidative cleavage of CO using trimethylamine-*N*-oxide, followed by addition of triphenylphosphine.[18] (Scheme 3).
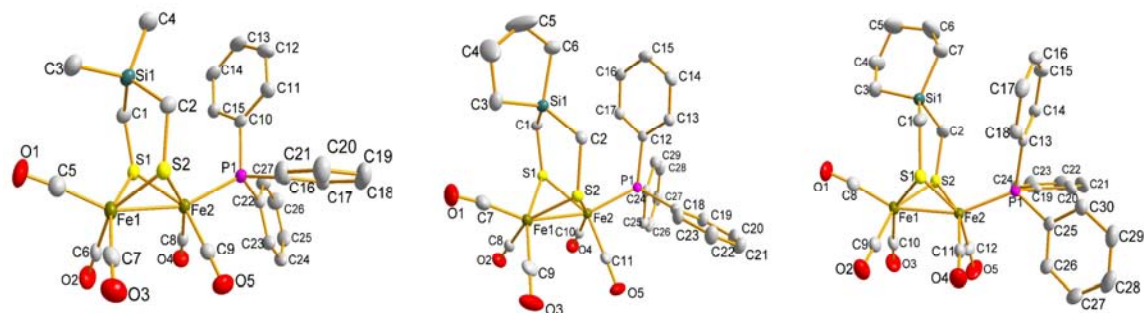
Figure 1 Molecular structures of compounds **2a–c** (left to right) (ellipsoids at the 50% level). The molecular structure of **2c** shows one of two independent molecules.

Initial reaction of trimethylamine-*N*-oxide with complexes **1a-c** in acetonitrile yields the respective acetonitrile complexes *via* oxidative cleavage of a CO ligand.[19] Attempts to isolate the instable nitrile complexes failed and the synthesis was therefore performed as a one-pot reaction. Further treatment of the *in situ* formed acetonitrile complexes with triphenylphosphine resulted in the mono-substituted compounds **2a-c**. The identities of **2a-c** were verified by elemental analysis, NMR, MS and IR studies. Thus mass spectrometry afforded the [M]$^+$ peaks at *m/z* 664 (**2a**), 690 (**2b**) and 704 (**2c**).
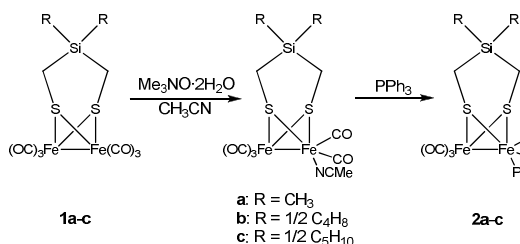
Scheme 3 Reaction pathway towards PPh$_3$ mono-substituted compounds **2a-c**.

IR spectroscopy provides additional confirmation for the structures of **2a-c**: $\tilde{\nu}_{CO}$ bands are visible between 2041 and 1930 cm^{-1}. Single-crystal X-ray analysis revealed the proposed structures as depicted in Figure 1. The iron atoms in **2a-c** are distorted octahedrally coordinated by the S-to-S linker and by CO groups and triphenylphosphine in equatorial position. The Fe(2)-P(1) distances and the bonding angles (Fe(1)-Fe(2)-P(1)) of **2a-c** are the same within the standard deviation and are in good agreement to the recent reported complex [Fe$_2$(CO)$_5$(PPh$_3$){(SCH$_2$)$_2$CHOH}].[20] Short Fe-Fe bonds are detected within all three molecules and reveal bond lengths of 250.81(6) (**2a**), 251.16(5) (**2b**) and 249.68(5) pm (**2c**) (cf. Table 1). The silicon atoms exhibit a tetrahedral geometry. However, the angles S(1)-C(1)-Si(1) and S(2)-C(2)-Si(1) are about 120° and therefore much larger than the expected 109.5° for sp^3-hybridisation (cf. Table 1).

**Table 1** Bond Lengths [pm] and Angles [°] for compounds **2a-c**.

	2a	**2b**	**2c**
Fe(1)-Fe(2)	250.81(6)	251.16(5)	249.68(5)
Fe(2)-P(1)	224.30(9)	225.60(8)	223.71(7)
Fe(1)-S(1)	226.69(9)	227.71(7)	226.91(7)
Fe(2)-S(2)	229.26(9)	226.21(8)	227.44(7)
S(1)-C(1)	183.0(3)	182.1(3)	181.21(3)
S(2)-C(2)	182.3(3)	182.9(3)	183.5(3)
C(1)-Si(1)	188.1(4)	187.5(3)	186.0(3)
C(2)-Si(1)	186.6(4)	186.3(3)	186.1(3)
Si(1)-C(3)	186.3(4)	188.5(3)	186.1(3)
Si(1)-C(4)/C(6)/C(7)	186.2(4)	188.6(3)	186.7(3)
S(1)-Fe(1)-S(2)	86.18(3)	85.80(3)	86.66(2)
S(1)-Fe(2)-S(2)	86.30(3)	86.08(3)	86.45(2)
Fe(1)-Fe(2)-P(1)	156.74(3)	156.66(3)	156.26(3)
S(1)-C(1)-Si(1)	122.05(19)	120.08(15)	121.76(15)
S(2)-C(2)-Si(1)	118.37(18)	117.65(15)	119.30(13)
C(1)-Si(1)-C(2)	108.19(15)	108.29(13)	108.09(12)
C(1)-Si(1)-C(3)	112.85(18)	115.41(14)	113.82(13)
C(3)-Si(1)-C(4)/C(6)/C(7)	108.58(18)	95.22(15)	103.63(13)

Synthesis and characterization of the CN$^-$ substituted diiron complexes (3a-c)

The replacement of a CO ligand *with* CN$^-$ follows similar procedures[21] as described for the tiphenylphosphine complexes **2a-c** and leads to the negatively charged complexes **3a-c**. Again, the labile acetonitrile complex is formed first and is easily substituted by addition of tetraethylammonium cyanide. Following purification affords compounds **3a-c** (Scheme 2) as dark red oily substances.
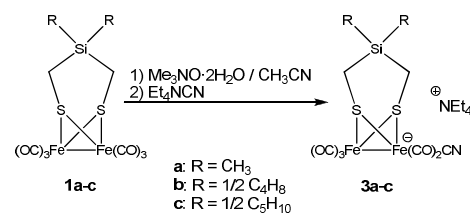
Scheme 2 Synthesis of CN$^-$ mono-substituted complexes **3a-c**.

The identities of **3a-c** were established by NMR, MS and IR studies. Consequently, mass spectrometry reveals the [M]$^-$ peaks at *m/z* 428 (**3a**), 454 (**3b**) and 468 (**3c**). IR spectroscopy shows the $\tilde{\nu}_{CO}$ bands between 2030 and 1930 cm^{-1} and the $\tilde{\nu}_{CN}$ band at around 2088 cm^{-1}. Slow diffusion of hexane into a solution of **3b**, dissolved in THF, at 0°C affords single crystals suitable for structure determination (Figure 3).
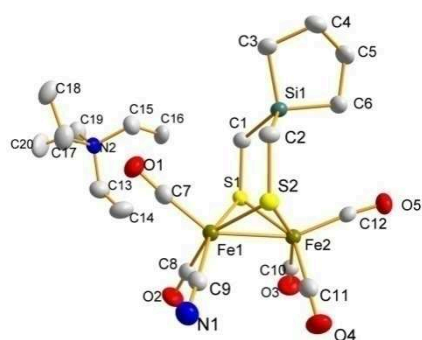
Figure 3 Molecular structure of compound **3b** (ellipsoids at the 50% level). Hydrogen atoms are omitted for clarity.

The molecular structure of **3b** shows the complex anion [2Fe2S(Si)(CN)]⁻, where the counter ion is a tetraethyl-ammonium cation. The iron atom Fe(1) is coordinated by a cyanide group in basal position, two CO groups, the Fe(2) atom, and the dithiolato-bridge. Both iron atoms are coordinated in a distorted octahedral way. In contrast to the phosphine complex **2b** the iron-iron distance is significantly longer (cf. Table 2). The silicon atom is tetrahedral surrounded showing the unusual large bond angles S(1)-C(1)-Si(1) and S(2)-C(2)-Si(1) of 118.4(2)° and 119.8(2)°, respectively (see Table 2). The distances for Fe(1)-C(9) and C(9)-N(1) are in good agreement to literature reported (Et₄N)[Fe₂(S₂C₃H₆)(CN)(CO)₅].[22]

Table 2 Bond Lengths [pm] and Angles [°] for compound **3b**.

Fe(1)-Fe(2)	252.32(8)	C(2)-Si(1)	186.9(4)
Fe(1)-S(1)	224.82(11)	Si(1)-C(3)	187.5(4)
Fe(2)-S(2)	227.36(10)	Si(1)-C(6)	187.5(84)
S(1)-C(1)	182.8(4)	Fe(1)-C(9)	193.5(4)
S(2)-C(2)	183.0(4)	C(9)-N(1)	115.4(5)
C(1)-Si(1)	187.3(4)		
S(1)-Fe(1)-S(2)	88.49(4)	C(1)-Si(1)-C(2)	106.57(18)
S(1)-Fe(2)-S(2)	87.22(4)	C(1)-Si(1)-C(3)	112.32(19)
S(2)-C(2)-Si(1)	119.8(2)	C(3)-Si(1)-C(6)	95.64(19)
S(1)-C(1)-Si(1)	118.4(2)	Fe(2)-Fe(1)-C(9)	107.50(13)

Experiments using two or more equivalents of CN⁻ or PPh₃ exclusively afforded mono-substituted complexes *via* this route. This implies a decreased electrophilic character of the CO ligand due to the CN⁻ or PPh₃ ligands.[23] Further reactions of **1a-c** with 1,10-phenantrolin were carried out. Using the same reaction conditions as for **2a-3c**, the desired [2Fe2S(phenantrolin)] complex was not obtained,[24] instead decomposition to [Fe(phenantrolin)₃]²⁺ was observed, analyzed using mass spectrometry, NMR spectroscopy, as well as X-ray crystallography.

IR spectroscopy

As pointed out, the basicity of the iron centers can be increased using the strong-field ligands CN⁻ and PPh₃, whereby CN⁻ is more relevant in the hydrogenase system.[1,2] The basicity (electron density) of the iron atoms depends mainly on two different aspects: *i*) the oxidation state[17,25] and *ii*) the σ/π-bonding properties of the ligands.[9,10] A characteristic value to determine the basicity of the iron centers is given by $\tilde{v}_{CO}$. The smaller $\tilde{v}_{CO}$ the larger the basicity of the iron centers.[26] The infrared spectroscopic data for complexes **1a**, **2a** and **3a** are listed in Table 3 and are representative for **1b-c**, **2b-c** as well as **3b-c**. Evaluating the IR data, a decrease of $\tilde{v}_{CO}$ can be observed from **1a** to **2a** and **3a**, showing an enhancement of the electron density on the iron atoms. Thus CN⁻ is the strongest donor ligand in this series. Similar electronic effects have been previously reported for cyanide and phosphine derivatives of [Fe₂(CO)₆(SR)₂] type complexes.[22,27]

Table 3 $\tilde{v}_{CO}$ shifts of complexes **1a-3a** (KBr pellets).

Compound	CO shift	CN⁻ shift
1a[8]	2074 (vs), 2031 (vs), 1989 (vs)	-
2a	2041 (vs), 1981 (vs, b)	-
3a	2027 (vs), 1973 (vs)	2088

Electrochemistry

Cyclic and differential pulse voltammetry was carried out to reveal the electrocatalytic properties of the triphenylphosphine complexes **2a-c** and cyanide complex **3c** towards H₂ development. The reduction and oxidation potentials of the complexes are listed in Table 4. We were not able to investigate the electrochemical properties of compound **3a** and **3b**, since they were not soluble in any solvent.

Table 4 Electrochemical data of the hexa- and pentacarbonyl diiron hydrogenase analogues **1a-c**, **2a-c** and **3c**. All potentials are corrected for the Ag/Ag⁺ reference electrode.

Compound	$Fe^I Fe^I / Fe^{II} Fe^{II}$ [V]	$Fe^I Fe^I / Fe^0 Fe^0$ [V]
1a (Acetonitrile)[8]	+0.79 (E_{pa})	-1.40 (E_{pa})
		-1.48 (E_{pc})
1b (Acetonitrile)[8]	+0.81 (E_{pa})	-1.40 (E_{pa})
		-1.48 (E_{pc})
1c (Acetonitrile)[8]	+0.81 (E_{pa})	-1.39 (E_{pa})
		-1.49 (E_{pc})
2a (Dichloromethane)	+0.57 (*E_{pa}*)	-1.83 (E_{pc})
	+0.44 (*E_{pc}*)	
2b (Dichloromethane)	+0.62 (*E_{pa}*)	-1.80 (E_{pc})
	+0.49 (*E_{pc}*)	
2c (Dichloromethane)	+0.61 (*E_{pa}*)	-1.85 (E_{pc})
	+0.46 (*E_{pc}*)	
3c (Acetonitrile)	+0.86 (E_{pa})	-2.04 (E_{pc})

The addition of a triphenylphosphine ligand to the diiron centres of complexes **2a-c** leads to an increase in electron density around the diiron centre. This is clearly indicated in the oxidation and reduction potentials of the three hydrogenase models (cf. Table 4). Comparing these complexes with their hexacarbonyl analogues **1a-c**, allowing for effects of the different solvent (dichloromethane results in positive shifts compared to the corresponding process in acetonitrile) it is evident that the former are both easier to oxidise and harder to reduce. Upon inspection of the cathodic

waves in each of the CVs a second reduction process is observed occurring at potentials very close to the first (least negative) reduction process although not at all clear in the differential pulse. This type of two-electron reduction has been observed for a similar mono-substituted complex, [Fe$_2$(bdt)(CO)$_5$(P(OMe)$_3$)] (bdt = 1,2-benzenedithiolate)[28] and may be related to the coordination asymmetry of the two Fe centres in the molecules. The two-electron reduction step is in good coincidence with the hexacarbonyl complexes **1a-c**, where the first reduction signal has been assigned to an ECE mechanism.[8] From the cyclic voltammogram in Figure 4 it is noted that the reversibility of the oxidative process is greatly improved with the substituted PPh$_3$ complexes. This is because the σ-donor character of this ligand stabilises the Fe^{II}Fe^{II} redox state whereas the reduced state is destabilised by this ligand as indicated by the irreversibility of the cathodic waves in each cyclic voltammogram.[29] The PPh$_3$ functionalised complexes are oxidised at potentials approximately 200 – 250 mV less positive than the hexacarbonyl analogues. However, it must be noted that this is not a direct comparison as the electrochemical solvent used for the PPh$_3$ complexes is dichloromethane (these complexes were insoluble in acetonitrile) whereas acetonitrile was the solvent for the hexacarbonyl derivatives.
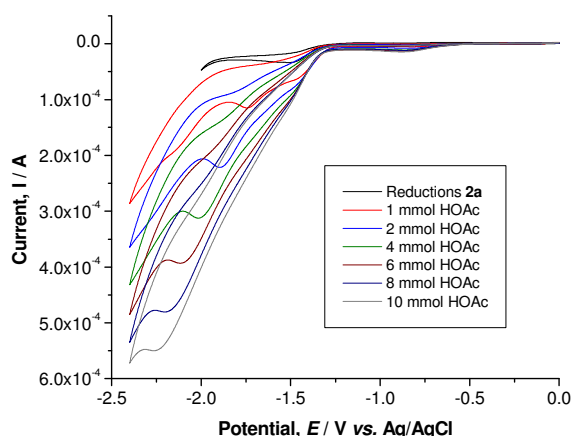
Figure 4 Cyclic voltammetry and differential pulse voltammetry of compound **2a** (representative also for **2b** and **2c**) on a glassy carbon working electrode, in dichloromethane, using 0.05 M TBA PF$_6$ as the supporting electrolyte.

Upon addition of 1 mmol HOAc, the separation of this first cathodic wave into two peaks is observed with a minor positive shift in potential as for the first wave. The second, now more prominent peak experiences a shift of approximately 200 mV towards more negative potentials. An increase in the current of this second cathodic wave is observed and the process shifts to more negative potentials with these shifts continuing with each increment of acid added thereafter. It is tentatively proposed that any hydrogen evolved occurs from the Fe^{0}Fe^0 redox state. This type of behaviour is observed for all three of the PPh$_3$ mono-substituted complexes, Figure 5.
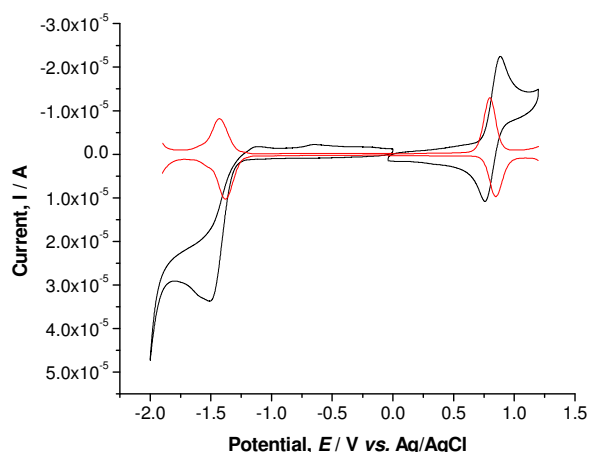
Figure 5 Cyclic voltammetry of 2a with HOAc (0-10 mmol) in dichloromethane, representative also for compound **2b** and **2c**.

The pentacarbonyl diiron complex **3c** was electrochemically investigated using acetonitrile as solvent. The oxidation wave observed for this complex occurs at a potential (+0.86 V, *vs.* Ag/Ag$^+$) that is approximately 50 mV more positive than the corresponding process in the hexacarbonyl analogue **1c** that is oxidised at +0.81 V, *vs.* Ag/Ag$^+$. This is counterintuitive considering the presence of the CN$^-$ ligand which should increase the electron density around the diiron active site. The complex appears to pacify the electrode with each successive cycle as indicated by the gradual decrease in current.

The increased electron density on the metal is reflected in the reduction potential recorded for **3c** (Figure 6). The (Fe^{I}Fe^I + 2e$^-$ → Fe^{0}Fe^0) is observed at a potential (-2.04 V, *vs.* Ag/Ag$^+$) that is approximately 500 mV more negative than that of the hexacarbonyl analogue **1c**. A similar negative shift of the reduction potential was already observed for the negatively charged mono-cyanide {Fe$_2$[μ-S$_2$(CH$_2$)$_3$](CN)(CO)$_5$}$^-$.[22] However, the reduction potential obtained for compound **3c** is about 300 mV more negative than for the respective propanedithiolato species.
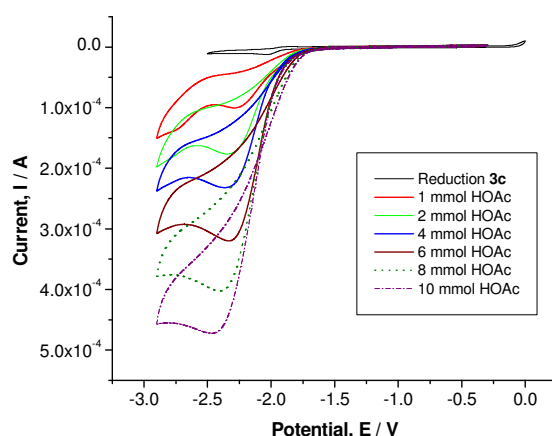
Figure 6 Cyclic voltammetry of compound **3c** [1 mM] with HOAc (0-10 mmol) in acetonitrile.

The expected basicity around the diiron metal bond or the nitrile ligand itself in **3c** is not reflected in its electrocatalytic

behaviour in the presence of acetic acid. The presence of these basic sites lead to an increased susceptibility to protonation prior to reduction of the complex which is indicated by a positive shift in the reduction potential of the least negative cathodic process.[30] Upon addition of 1 mmol HOAc the reduction potential of this process is shifted by approximately 200 mV in the negative direction and an increase in the height of the peak is observed. The intensity of the current continues to increase with each increment of acid added thereafter - indicative of an electrocatalytic current. These results suggest that the evolution of hydrogen is mediated from the Fe^0Fe^0 redox state. However, the observed catalytic wave is within the region of that observed when acetic acid itself is reduced in the absence of a catalyst (~-2.4 V, *vs.* Ag/Ag$^+$). Also observed by Darensbourg et al.[29] and as such it is not possible at this moment to clearly assign this process as hydrogen evolution catalysed by the FeFe complex. In contrast to literature known complex {Fe$_2$[μ-S$_2$(CH$_2$)$_3$](CN)(CO)$_5$}$^-$ a protonation at the N atom of the cyanide was not observed.[23,31]

Conclusions

In the course of this study a suitable synthesis to mono-substituted asymmetric [Fe2S2(Si)] model complexes, containing triphenylphosphine (**2a-c**) and cyanide (**3a-c**) was established. Single crystal X-ray determination revealed a basal configuration mode of the introduced cyanides and and an apical for the triphenylphosphines in solid state. As already shown for **1a-c**, the substitution pattern on the silicon atom reveal no or negligible influence on the electrcocatalytic cycle.[7] During the investigation of the electrochemical properties, unexpected trends arose in the evaluation of the redox potentials in certain complexes of this series. Addition of the σ-donor ligands such as CN$^-$ or PPh$_3$ lead to an increase in electron density around the metal centres which should result in an increase in basicity of the active site. This theory is not completely consistent with all oxidation potential values obtained. In contrast to results of Poilblanc *et al.*,[32] who showed that complexes of the Fe$_2$(SR)$_2$(CO)$_4$L (L = donor ligand) are both easier to oxidise and harder to reduce, the mono-substituted cyano complex **3c** experiences an oxidation potential that is more positive than that of the corresponding hexacarbonyl analogues. Therefore the effect of these ligands on the nature of the HOMO and LUMO must be considered. The addition of a negatively charged ligand may change the location of these orbitals resulting in a complicated interpretation of results. Both the oxidation and reduction potentials of complexes **2a-c** experience shifts in the negative direction. Two closely spaced reduction steps are observed for these compounds. Catalytic behaviour is observed for all complexes. However, direct comparison of all six complexes is not possible as a result of solubility issues in different solvents.

Experimental Section

General Procedures

All syntheses were carried out under dry nitrogen or argon. The organic solvents used were dried and purified according to standard procedures and stored under dry argon. Chemicals were used as received from Fluka and Acros without further purification. Compounds **1a-c** were prepared according to literature procedures.[7] Thin layer chromatography (TLC): *Merck* silica gel 60 F$_{254}$ plates; detection under UV light at 254 nm. Flash chromatography (FC): *Fluka* silica gel 60. ^{1}H NMR, ^{13}C{^{1}H} and ^{31}P{^{1}H} NMR spectra were recorded on a Bruker AVANCE 200 MHz or 400 MHz spectrometer, whereby the splitting of proton resonances are defined with s (singlet), d (doublet) and m (multiplet). CDCl$_3$ was used as the solvent. Chemical shifts (ppm) were determined relative to internal CHCl$_3$ (^{1}H, δ 7.24; CDCl$_3$), CDCl$_3$ (^{13}C, δ 77.0; CDCl$_3$), or external TMS (^{1}H, δ 0; CDCl$_3$). Analysis and assignment of the ^{1}H NMR data were supported by ^{1}H,^{1}H COSY, ^{13}C,^{1}H HMQC, and ^{13}C,^{1}H HMBC experiments. Assignment of the ^{13}C NMR data was supported by DEPT 135, ^{13}C,^{1}H HSQC, and ^{13}C,^{1}H HMBC experiments. IR-spectra were recorded on a *Perkin-Elmer 2000 FT-IR*. Electron impact and atom bombardment mass spectrometry was carried out at 70 eV with a Finnigan SSQ710 using desorption electron ionisation (DEI) or fast atom bombardment (FAB) mode.

Synthetic Methods

Method A

Substitution of CO with PPh$_3$ was performed as followed: The hexacarbonyl complex (**1a-c**) was dissolved in 20 cm^3 acetonitrile. 1eq. Me$_3$NO•2H$_2$O was added to give the respective nitrile complex withihin 30 min, visible by darkening of the red solution. Subsequently 1eq. PPh$_3$ was added and the reaction mixture stirred for 7 hours at room temperature. Evaporation to dryness affords the crude product, which was purified *via* FC (THF : hexane 1:3).

Method B

A solution of the complex (**1a-c**), dissolved in 20 cm^3 acetonitrile, was reacted with 1eq. Me$_3$NO•2H$_2$O and stirred for 30 min at room temperature. Following, 1.eq tetraethyl ammonium cyanide was added and the solution stirred for 20 hours. Removal of the solvent under reduced pressure afforded the crude product. The residue was dissolved in THF and the remaining solid filtered off. Reiterated evaporation and washing with hexane affords the respective cyanide complexes.

Pentacarbonyl triphenylphosphine diiron complex 2a

Method A, 148 mg (0.344 mmol) **1a** was treated with 39 mg (0.348 mmol) trimethylammonium-*N*-oxid dihydrate and 93 mg (0.48 mmol) triphenylphosphine to yield 66 mg (29%) of **2a**. ^{1}H NMR (CDCl$_3$, 200MHz): δ 7.67 (m, 9H, H-c/d), 7.43 (m, 6H, H-b), 0.09 (s, 6H, SiCH_3), -0.31 (s, 4H, SCH_2Si). ^{13}C NMR (CDCl$_3$, 50MHz): δ 213.8/209.4 (CO), 135.8 (C-a), 133.5 (C-b), 130.1 (C-d), 128.5 (C-c), 4.9 (SCH_2Si), 0.5 / -0.2 (SiCH_3). ^{31}P NMR(CDCl$_3$, 81MHz): δ 68.5. MS(DEI): 664 [M]$^+$, 608 [M-2CO]$^+$, 580 [M-3CO]$^+$, 524 [M-5CO]$^+$, 262 [PPh$_3$]$^+$. IR (KBr): 3060 (w), 2041 (vs), 1981 (vs, b), 1628 (m), 1435 (m). Anal. calcd. for C$_{27}$H$_{25}$Fe$_2$O$_5$S$_2$SiP: C, 48.81%;

H, 3.79%, S, 9.65%. Found: C, 48.65%; H, 3.83%, S, 9.49%.

Pentacarbonyl triphenylphosphine diiron complex 2b

Method A, 147 mg (0.322 mmol) **1b** was treated with 36 mg (0.322 mmol) trimethylamine-*N*-oxide dihydrate and 84 mg (0.322 mmol) triphenylphosphine to yield 48 mg (21.6%) of the desired product as a brownish powder. ^{1}H NMR (CDCl$_3$, 200MHz): δ 7.69 (m, 9H, H-c/d), 7.41 (m, 6H, H-b), 1.55-1.24 (m, 8H, SiCH$_2$C*H*$_2$C and SC*H*$_2$Si), 0.65 (t, ^{3}J = 7 Hz, 4H, SiC*H*$_2$C). ^{13}C NMR (CDCl$_3$, 50MHz): δ 213.2/209.2 (CO), 136.1 (C-a), 133.4 (C-b), 130.1 (C-d), 128.6 (C-c), 26.9/26.2 (SiCH$_2$C*H*$_2$C), 13.8 (SiC*H*$_2$C), 3.8 (SC*H*$_2$Si). ^{31}P NMR (CDCl$_3$, 81MHz): δ 68.7. MS(DEI): 690 [M]$^+$, 634 [M-2CO]$^+$, 606 [M-3CO]$^+$, 550 [M-5CO]$^+$, 262 [PPh$_3$]$^+$. IR (KBr): 3056 (w), 2925 (s), 2854 (m), 2041 (vs), 1982 (vs, b), 1630 (m), 1436 (m). Anal. calcd. for C$_{29}$H$_{27}$Fe$_2$O$_5$S$_2$SiP: C, 50.45%; H, 3.94%, S, 9.29%. Found: C, 50.56%; H, 3.69%, S, 8.99%.

Pentacarbonyl triphenylphosphine diiron complex 2c

50 mg (0.106 mmol) **1c** was reacted with 12 mg (0.106 mmol) trimethylammonium-*N*-oxide dihydrate and 28 mg (0.106 mmol) triphenylphosphine according to *Method A*. After purification 19 mg (25%) **2c** were obtained. ^{1}H NMR (CDCl$_3$, 200MHz): δ 7.63 (m, 9H, H-c/d), 7.38 (m, 6H, H-b), 1.53-1.26 (m, 10H, C*H*$_2$SiCH$_2$C*H*$_2$C*H*$_2$), 0.70 (m, 2H, SiC*H*$_2$). ^{13}C NMR (CDCl$_3$, 50MHz): δ 213.8/209.4 (CO), 135.8 (C-a), 133.5 (C-b), 130.1 (C-d), 128.4 (C-c), 29.3 (SiCH$_2$C*H*$_2$C*H*$_2$C), 23. 8 (SiCH$_2$C*H*$_2$C), 13.5 (SiC*H*$_2$C), 2.9 (SC*H*$_2$Si). ^{31}P NMR (CDCl$_3$, 81MHz): δ 68.6. MS(DEI): 704 [M]$^+$, 648 [M-2CO]$^+$, 620 [M-3CO]$^+$, 564 [M-5CO]$^+$, 262 [PPh$_3$]$^+$. IR (KBr): 3054 (w), 2919 (m), 2852 (m), 2041 (vs), 1981 (vs), 1930 (s), 1637 (m), 1435 (m). Anal. calcd. for C$_{30}$H$_{29}$Fe$_2$O$_5$S$_2$SiP: C, 51.15%; H, 4.15%, S, 9.10%. Found: C, 51.49%; H, 4.10%, S, 9.11%.

Pentacarbonyl diiron cyanide complex 3a

Pentacarbonyl diiron cyanide complex **3a** was prepared according to *Method B*. Thereby, 55 mg (0.128 mmol) **1a** were reacted with 14 mg (0.128 mmol) trimethylammonium-*N*-oxid and 20 mg (0.128 mmol) tetraethylammonium cyanide to yield 41 mg (57%) of compound **3a**. ^{1}H NMR (CD$_3$CN, 200MHz): δ 3.19 (m, 8H, NC*H*$_2$C), 1.39 (s, 2H, SC*H*$_2$Si), 1.21 (m, 14H, SC*H*$_2$Si and C*H*$_3$), 0.10/-0.05 (2s, 6H, SiC*H*$_3$). ^{13}C NMR (CD$_3$CN, 50MHz): δ 216.9/213.3 (CO), 53.6 (NCH$_2$C), 8.3 (*C*H$_3$), 7.3 (SC*H*$_2$Si), -1.0 (SiC*H*$_3$). MS(FAB-neg.): 428 [M-Et$_4$N]$^-$. IR (KBr): 2924 (m), 2088 (w), 2027 (vs), 1973 (vs), 1630 (m), 1484 (m). Elemental analysis was not obtained.

Pentacarbonyl diiron cyanide complex 3b

Method B, 53 mg (0.116 mmol) **1b** were reacted with 13 mg (0.116mmol) trimethylammonium-*N*-oxid dihydrate and 18 mg (0.116 mmol) tetraethylammonium cyanide to afford 37 mg (54%) **3b** as a red oily substance. ^{1}H NMR (CD$_3$CN, 400MHz): δ 3.14 (m, 8H, NC*H*$_2$C), 1.45-1.19 (m, 18H, SC*H*$_2$Si, SiCH$_2$C*H*$_2$C and C*H*$_3$), 0.65/0.49 (2m, 4H, SiC*H*$_2$C). ^{13}C NMR (CD$_3$CN, 50MHz): δ 216.8/212.9 (CO), 53.2 (NCH$_2$C), 27.3 (SiCH$_2$C*H*$_2$C), 13.9 (SiC*H*$_2$C), 7.8 (*C*H$_3$), 6.9 (SC*H*$_2$Si). MS(FAB-neg.): 454 [M-Et$_4$N]$^-$. IR (KBr): 2982 (s), 2925 (s), 2853 (m), 2087 (w), 2027 (vs), 1974 (vs), 1630 (s), 1484 (m). Elemental analysis was not obtained.

Pentacarbonyl cyanide diiron complex 3c

Method B, 57 mg (0.12 mmol) **1c** were reacted with 13 mg (0.12 mmol) trimethyalammonium-*N*-oxid dihydrate and 19 mg (0.12 mmol) tetraethylammonium cyanide. Yield: 32 mg (44%). ^{1}H NMR (CD$_3$CN, 400MHz): δ 3.14 (m, 8H, NC*H*$_2$C), 1.57 (m, 4H, SC*H*$_2$Si), 1.19 (m, 16H, SiCH$_2$C*H*$_2$C, SiCH$_2$CH$_2$C*H*$_2$C and C*H*$_3$), 0.88 (m, 2H, SiCH$_2$C*H*$_2$C), 0.74/0.54 (2m, 4H, SiC*H*$_2$C). ^{13}C NMR (CD$_3$CN, 50MHz): δ 212.4 (CO), 54.1 (NCH$_2$C), 30.3 (SiCH$_2$CH$_2$C*H*$_2$C), 26.2 (SiCH$_2$C*H*$_2$C), 24.6 (SiC*H*$_2$C), 8.7 (*C*H$_3$), 5.0 (SC*H*$_2$Si). MS(FAB-neg.): 468 [M-Et$_4$N]$^-$. IR (KBr): 2922 (s), 2089 (w), 2027 (vs), 1973 (vs), 1637 (m). Elemental analysis was not obtained.

Structure Determinations.

The intensity data for the compounds were collected on a Nonius KappaCCD diffractometer using graphite-monochromated Mo-K$_\alpha$ radiation. Data were corrected for Lorentz and polarization effects but not for absorption effects.[33, 34]. Crystallographic data as well as structure solution and refinement details are summarized in Table 2. The structures were solved by direct methods (SHELXS[35]) and refined by full-matrix least squares techniques against Fo^2 (SHELXL-97[36]). All hydrogen atom positions were included at calculated positions with fixed thermal parameters. All non-hydrogen atoms were refined anisotropically.[36] XP (SIEMENS Analytical X-ray Instruments, Inc.) was used for structure representations.

Table 4 Crystal data and refinement details for the X-ray structure determinations of the compounds **2a**, **2b**, **2c**, and **3b**.

Compound	2a	2b	2c	3b
formula	C$_{27}$H$_{25}$Fe$_2$O$_5$PS$_2$Si 0.5 (C$_2$H$_8$O$_2$)	C$_{29}$H$_{27}$Fe$_2$O$_5$PS$_2$Si	C$_{30}$H$_{29}$Fe$_2$O$_5$PS$_2$Si	C$_{12}$H$_{12}$Fe$_2$NO$_5$S$_2$Si C$_8$H$_{20}$N
fw (g·mol^{-1})	696.39	690.39	704.41	584.39
T/°C	-90(2)	-90(2)	-90(2)	-90(2)
crystal system	triclinic	triclinic	monoclinic	monoclinic
space group	P ī	P ī	P 2$_1$/n	P 2$_1$/c
a/¯	10.0550(4)	10.4099(5)	16.6325(3)	17.1886(9)
b/¯	12.8059(4)	12.6449(5)	20.7724(3)	12.5652(6)
c/¯	13.8444(6)	12.8477(3)	18.3780(5)	12.2768(3)
α/°	75.360(3)	105.563(2)	90	90
β/°	77.349(3)	94.001(3)	99.982(1)	100.704(3)
γ/°	68.226(3)	110.728(2)	90	90
V/¯^{3}	1586.08(11)	1498.03(10)	6253.4(2)	2605.4(2)
Z	2	2	8	4
ρ (g·cm^{-3})	1.458	1.531	1.496	1.490
μ (cm^{-1})	11.73	12.39	11.88	13.52
measured data	11013	10386	43489	18053
data with I >2σ(I)	5500	5132	8918	3858
unique data / R$_{int}$	7136/0.0293	6813/0.0327	14280/0.0627	5955/0.0752
wR$_2$(all data, on F^2)$^{a)}$	0.1312	0.0829	0.0832	0.1324
R$_1$ (I > 2σ(I))$^{a)}$	0.0465	0.0384	0.0382	0.0500
s$^{b)}$	1.022	1.025	0.962	1.019
Res. dens./e·$^{-3}$	1.844/-0.576	0.403/-0.459	0.673/-0.362	1.170/ -0.506
absorpt method	NONE	NONE	NONE	NONE
CCDC No.	753495	753496	753497	753498

$^{a)}$ Definition of the *R* indices: R$_1$ = (Σ ‖ F$_o$ ‖ $-$ ‖ F$_c$ ‖ ‖)/Σ‖ F$_o$ ‖
wR$_2$ = {Σ[w(F$_o^2$-F$_c^2$)^2]/Σ[w(F$_o^2$)^2]}$^{1/2}$ with w^{-1} = σ^2(F$_o^2$) + (aP)^2.
$^{b)}$ s = {Σ[w(F$_o^2$-F$_c^2$)^2]/(N$_o$-N$_p$)}$^{1/2}$.

Electrochemical procedures

Cyclic voltammograms were recorded against a non-aqueous Ag/Ag$^+$ or Ag/AgCl reference electrode (0.1 M nBu$_4$NPF$_6$ and 0.01 M AgNO$_3$ in CH$_3$CN). The Ag/Ag$^+$ reference electrode was used with acetonitrile and the Ag/AgCl reference was used when the electrochemical solvent was dichloromethane. Both reference electrodes were measured against the Fc/Fc$^+$ redox couple and the potential values in Table 4 were all corrected against the Ag/Ag$^+$ reference. A glassy carbon (GC) macro electrode and a platinum wire were used as the working and auxiliary electrodes, respectively. A solution of 0.05 M nBu$_4$NPF$_6$ (Fluka, electrochemical grade) in either acetonitrile (Aldrich, anhydrous, 99.8%) or dichloromethane (depending on the solubility of the compound) was used as the supporting electrolyte. Electrochemical experiments were carried out using a CHI750C electrochemical bipotentiostat. Prior to each experiment, the electrochemical cell was degassed for at least 10 minutes using argon and a blanket of argon was maintained throughout. The GC working electrode was prepared by successive polishing with 1.0 and 0.3 micron alumina pastes and sonicated in Millipore water for 5 minutes. All cyclic voltammograms were recorded at a scan rate of 100 mVs^{-1}.

Acknowledgments

Notes and references

[a] Institut für Anorganische und Analytische Chemie, Friedrich-Schiller Universität Jena, August-Bebel-Straße 2, 07743 Jena , Germany;Fax: (+49) 3641 948102; E-mail: wolfgang.weigand@uni-jena.de

[b] Yvonne Halpin, Prof. Johannes G. Vos, Solar Energy Conversion SRC, School of Chemical Sciences, Dublin City University, Dublin 9, Ireland, E-mail: han.vos@dcu.ie

† Electronic Supplementary Information (ESI) available: Crystallographic data (excluding structure factors) has been deposited with the Cambridge Crystallographic Data Centre as supplementary publication CCDC-753495 for **2a**, CCDC-753496 for **2b**, CCDC-753497 for **2c** and CCDC-753498 for **3b**. Copies of the data can be obtained free of charge on application to CCDC, 12 Union Road, Cambridge CB2 1EZ, UK [E- mail: deposit@ccdc.cam.ac.uk].. See DOI: 10.1039/b000000x/

[1] Y. Nicolet, C- Piras, P. Legrand, C. E. Hatchikian, J. C. Fontecilla-Camps, Structure 1999, 7, 13.

[2] W. Peters, W. N. Lanzilotta, B. J. Lemon, L. C. Seefeldt, Science 1998, 282, 1853.

[3] F. Gloaguen, J. D. Lawrence, M. Schmidt, S. R. Wilson, T. B. Rauchfuss, J. Am. Chem. Soc. 2001, 123, 12518.

[4] M. Razavet, S. C. Davies, D. L. Hughes, J. E. Barclay, D. J. Evans, S. A. Fairhurst, X. Liu, C. J. Pickett, Dalton Trans. 2003, 586.

[5] J. D. Lawrence, H. Li, T. B. Rauchfuss, M. Bernard, Angew. Chem. Int. Ed. 2001, 40, 1768; H. Li, T. B. Rauchfuss, J. Am. Chem. Soc., 2002, 124, 726.

[6] L.-C. Song, Z. Y. Yang, H.-Z. Bian, Y. Liu, H.-T. Wang, X.-F. Liu, Q.-M. Hu, Organometallics 2005, 24, 6126.

[7] J. Windhager, M. Rudolph, S. Bräutigam, H. Görls, W. Weigand, Eur. J. Inorg. Chem. 2007, 2748; L.-C. Song, Z.-Y. Yang, Y.-J. Huan, H.-T. Wang, Y. Liu, Q.-M. Hu, Organometallics 2007, 26, 2106.

[8] U.-P. Apfel, D. Troegel, Y. Halpin, M. Rudolph, U. Uhlemann, M. Schmitt, J. Popp, H. Görls, P. Dunne, M. Venkatesan, M. Coey, J. G. Vos, R. Tacke, W. Weigand, *Manuscript in preparation.*

[9] Zhao, X.; Georgakaki, I. P.; Miller, M. L.; Yarbrough, J. C.; Darensbourg, M. Y. J. Am. Chem. Soc. 2001, 123, 9710.

[10] M. S. Arabi, R. Mathieu, R. Poilblanc, *J. Organomet. Chem.* **1979**, *177*, 199; K. Fauvel, R. Mathieu, R. Poilblanc, *Inorg. Chem.* **1976**, *15*, 976; M. S. Arabi, R. Mathieu, R. Poilblanc, *J. Organomet. Chem.* **1979**, *177*, 199; J.-M. Savariault, J.-J. Bonnet, R. Mathieu, J. Galy, *C. R. Acad. Sci. Paris* **1977**, *284*, C663.

[11] S. Ezzaher, J. F. Capon, F. Gloaguen, F. Y. Petillon, P. Schollhammer, J Talarmin, *Inorg. Chem.* **2007**, *46*, 3426; B. E. Barton, T. B. Rauchfuss, *Inorg. Chem.* **2008**, *47*, 2261.

[12] W. Beck, W. Weigand, U. Nagel, M. Schaal, *Angew. Chem., Int. Ed.* 1984, **23**, 377; W. Weigand, U. Nagel, W. Beck, *Z. Naturforsch. Sect. B-A, J. Chem. Sci.* 1988, **43**, 328; W. Weigand, W. Beck, *Z. Anorg. Allg. Chem.* 1991, **600**, 227; E. Bär, W. P. Fehlhammer, W. Weigand, W. Beck, *J. Org. Chem.* 1988, **347**, 101; C. Bianchini, F. Laschi, M. F. Ottaviani, M. Peruzzini, P. Zanello, F. Zanobini, *Organometallics* 1989, **8**, 893; C. Nataro, J. Chen, R. Angelici, J. *Inorg. Chem.* **1998**, *37*, 1868.

[13] F. Gloaguen, J. D. Lawrence, T. B. Rauchfuss, M. Bénard, M.-M. Rohmer, *Inorg. Chem.* 2002, *41*, 6573; F. Gloaguen, J. D. Lawrence, T. B. Rauchfuss, *J. Am. Chem. Soc.* 2001, *123*, 9476.

[14] P. Li, M. Wang, C. He, G. Li, X. Liu, C. Chen, B. ⁻kermark, L. C. Sun, *Eur. J. Inorg. Chem.* 2005, 2506.

[15] M. Nakamura, *Angew. Chem., Int. Ed.* 2009, *48*, 2638.

[16] P. I. Volkers, T. B. Rauchfuss, *J. Inorg. Biochem.* 2007, *101*, 1748.

[17] M. L. Singleton, N. Bhuvanesh, J. H. Reibenspies, M. Y. Darensbourg, *Angew. Chem. Int. Ed.* 2008, *47*, 9492.

[18] L.-C. Song, H.-T. Wang, J.-H. Ge, S.-Z. Mei, J. Gao, L.-X. Wang, B. Gai, L.-Q. Zhao, J. Yan, Y.-Z. Wang, *Organometallics*, 2008, **27**, 1409.

[19] L. Schwartz, J. Ekström, R. Lomoth, S. Ott, *Chem. Commun.* 2006, **40**, 4206; S. P. Best, S. J. Borg, J. M. White, M. Razavet, C. J. Pickett, *Chem. Commun.* 2007, **42**, 4348. J. Windhager, U.-P. Apfel, T. Yoshino, N. Nakata, H. Görls, M. Rudolph, A. Ishii, W. Weigand, *Chem. Asian J.* 2010, accepted; P. C. Ellgen, J. N. Gerlach, *Inorg. Chem.* **1973**, *12*, 2526.

[20] L.-C. Song, X.-F. Liu, J.-B- Ming, J.-H. Ge, Z.-J. Xie, Q.-M. Hu, *Organometallics* **2010**, *29*, 610.

[21] A. I. Cloirec, S. C. Davies, D. J. Evans, D. L. Hughes, C. J. Pickett, S. P. Best, S. J. Borg, *Chem. Commun.* **1999**, 2285; E. J. Lyon, I.P. Georgakaki, J. H. Reibenspies, M. Y. Darensbourg, *Angewandte Chem. Int. Ed.* **1999**, *38*, 3178; M. Schmidt, S. M. Contakes, T. B. Rauchfuss, *J. Am. Chem. Soc.* **1999**, *121*, 9736; C. A. Boyke, J. I. van der Vlugt, T. B. Rauchfuss, S. R. Wilson, G. Zampella, L. De Gioia, *J. Am. Chem. Soc.* **2005**, *127*, 11010; J. D. Lawrence, H. Li, T. B. Rauchfuss, M. Beanard, M.-M. Rohmer, *Angew. Chem. Int. Ed.* **2001**, *40*, 1768.

[22] F. Gloaguen, J. D. Lawrence, M. Schmidt, S. R. Wilson, T. B. Rauchfuss, *J. Am. Chem. Soc.* 2001, *123*, 12518.

[23] E. Lyon, I. P. Georgakaki, J. H. Reibenspies, M. Y. Darensbourg, *J. Am. Chem. Soc.* **2001**, *123*, 3268.

[24] S. Ezzaher, P.-Y. Orain, J.-F. Capon, F. Gloaguen, F. Y. Petillon, T. Roisnel, P. Schollhammer, J. Talarmin, *Chem. Commun.* **2008**, 2547.

[25] C. M. Thomas, T. B. Liu, M. B. Hall, M. Y. Darensbourg, *Inorg. Chem.* 2008, *47*, 7009; A. J. Justice, M. J. Nilges, T. B. Rauchfuss, S. R. Wilson, L. De Gioia, G. Zampella, *J. Am. Chem. Soc.* 2008, **130**, 5293; A. K. Justice, T. B. Rauchfuss, S. R. Wilson, *Angew. Chem., Int. Ed.* 2007, *46*, 6152; C. Tard, X. Liu, D. L. Hughes, C. J. Pickett, *Chem. Commun.* 2005, 133; M. H. Cheah, C. Tard, S. J. Borg, X. Liu, S. K. Ibrahim, C. J. Pickett, S. P. Best, *J. Am. Chem. Soc.* 2007, *129*, 11085.

[26] Nakamoto, K. *Infrared and Raman Spectra of Inorganic and Coordination Compounds*; John Wiley: New York, 1986.

[27] J. A. de Beer, R. J. Haines, R- Greatrex, N. N. Greenwood, *J. Chem. Soc. A* **1971**, *21*, 3271; J. A. de Beer, R. J. Haines, *J. Organomet. Chem.* **1972**, *37*, 173.

[28] Gloaguen, F.; Morvan, D.; Capon, J.F.; Schollhammer, P.; Talarmin, J.: *J. Electroanal. Chem.*, 2007, **603**, 15.

[29] D. Chong, I. P. Georgakaki, R. Mejia-Rodriguez, J. Sanabria-Chinchilla, M. P. Soriaga, M. Y. Darensbourg, *Dalton Trans.*, 2003, 4158.

[30] T. Liu, M. Wang, Z. Shi, H. Cui, W. Dong, J. Chen, B. Akermark, L. Sun, *Chem. Eur. J.*, 2004, **10**, 4474.

[31] A. Le Cloirec, S. C. Davies, D. J. Evans, D. L. Hughes, C. J. Pickett, S. P. Best, S. Borg, *J.Chem.Commun.* **1999**, 2285.

[32] R. Mathieu, R. Poilblanc, P. Lemoine, M. Gross, *J. Organomet. Chem.* **1979**, *165*, 243; M. S. Arabi, R. Mathieu, R. Poilblanc, *J. Organomet. Chem.* **1979**, *177*, 199.

[33] COLLECT, Data Collection Software; Nonius B.V., Netherlands, **1998**.

[34] Processing of X-Ray Diffraction Data Collecte d in Oscillation Mode":Otwinowski, Z.; Minor, W. in Carter, C. W.; Sweet, R. M. (eds.): *Methods in Enzymology, Vol. 276, Macromolecular Crystallography, Part A*, pp. 307-326, Academic Press **1997**.

[35] Sheldrick, G. M. *Acta Crystallogr. Sect. A* 1990, **46**, 467.

[36] Sheldrick, G. M. *SHELXL-97* (Release 97-2), University of Göttingen, Germany, 199.

Hydroxyl functionalized (Mercapto-methyl)silanes as ligands for [FeFe] hydrogenase models

*Ulf-Peter Apfel,[a] Dennis Troegel,[b] Yvonne Halpin,[c] Helmar Görls,[a] Johannes G. Vos,[*c] Reinhold Tacke,[*b] Wolfgang Weigand[*a]*

Institut für Anorganische und Analytische Chemie, Friedrich-Schiller Universität Jena, August-Bebel-Straße 2, D-07743 Jena

Universität Würzburg, Institut für Anorganische Chemie, Am Hubland, D-97074 Würzburg, Germany

School of Chemical Sciences, Dublin City University, Dublin 9, Ireland

E-mail: wolfgang.weigand@uni-jena.de, r.tacke@uni-wuerzburg.de, han.vos@dcu.ie

Abstract: The substitution of a carbon by a silicon atom leads to a serious change of properties of [2Fe2S] cluster compounds. As an extension of this initial work the hydroxyl functionalized (mercaptomethyl)silanes $(HSCH_2)_3Si(CH_2OH)$ (**8**) and $(HSCH_2)_2Si(CH_2OH)_2$ (**9**) as well as $(HSCH_2)_2Si(CH_2OH)CH_3$ (**11**) will be synthesized and reacted with $Fe_3(CO)_{12}$ to the respective [2Fe2S(Si)] complexes **12**-**14**. The [2Fe2S(Si)]

---

[a] Universität Jena – IAAC

[b] Universität Würzburg.

[c] Dublin City University.

complexes were investigated according to their spectroscopic, electrochemical and structural properties.

Keywords: silicon, iron, sulfur, hydrogenase, electrochemistry.

Introduction

Recently the first silicon containing hydrogenase model compounds, [2Fe2S(Si)], were established[1,2] and the influence of the silicon atom to the electrocatalytic pathway was investigated.[1] As extension of these first studies, now we present hydroxyl functionalized (mercapto-methyl)silanes as building blocks for the synthesis of [2Fe2S(Si)] clusters.

It is already known that the basicity of the sulfur atoms increases as a result of the silicon atom and enables the possibility of sulfur-proton-interaction.[1,3] Besides these properties the introduction of hydoxyl functions to silicon enables the possibility of further derivatizations and linking to surfaces.[4] The attachment of silicon containing thiols on silica *via* a Si-O-Si linkage has recently been described (Scheme 2) and the metal uptake to the $Si(CH_2SH)_x$ (x = 1,2) containing silica was shown.[5]
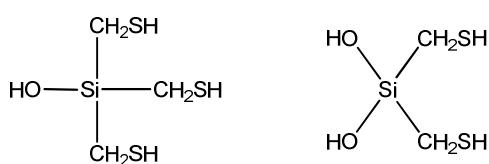
Scheme 1. Silicon containing thiols suitable for immobilization of the Si(CHSH) (x = 1,2) group on silica *via* a Si-O-Si linkage.

Herein we report the synthesis of (hydroxyl-methyl)(mercapto-methyl)silanes as well as their respective [Fe2S2(Si)] complexes. The spectroscopic (^{1}H NMR, ^{13}C NMR, IR), structural (single-crystal X-ray analysis) and electrochemical (cyclic voltammetry) properties will be presented.

Results and Discussion

Syntheses of the silicon-containing ligands. The hydroxyl functionalized thiols **8-10** were prepared according to Scheme 2. Starting from *tetra*-chlorosilane **1**,[6] treatment with sodium acetate afforded compounds **2**-**4** within 24 hours as colourless liquid substances in the presence of 18-crown-6. The reactions of sodium thioacetate with the halogenides **2**-**4** in tetrahydrofurane resulted in the corresponding thioacetates **5**-**7**. These were converted to the respective thiols **8**-**10** *via* treatment with lithium aluminium hydride at 0°C and subsequent workup with hydrogen chloride. Compounds **2**-**10** were characterized using ^{1}H, ^{13}C{^{1}H} NMR spectroscopic techniques, as well as elemental analysis.
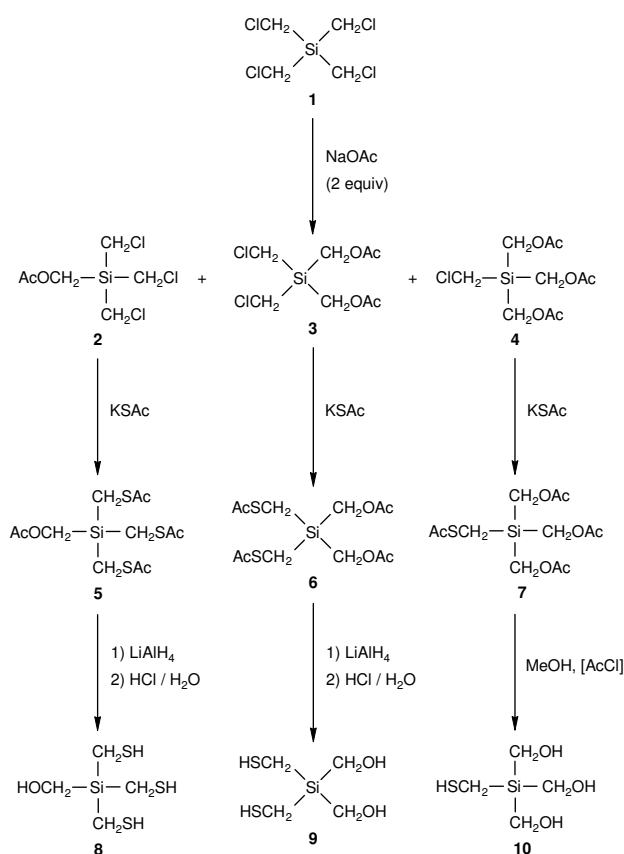
Scheme 1. Synthesis of the thiol compounds **8**-**10**.

Crystallization of compound **10** from acetonitrile afforded crystals suitable for the single crystal X-ray analysis. A tetrahedral geometry at the silicon atom, surrounded by three hydroxymethyl groups and on mercaptomethyl group is visible as depicted in Figure 1.
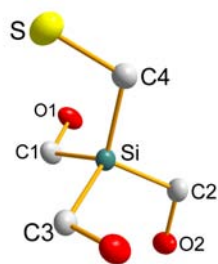
Figure 1. Molecular structure of compound **10** (thermal ellipsoids at the 50% probability level). Hydrogen atoms are omitted for clarity.

Furthermore, the dithiol **11** was synthesized following the procedures described by Troegel *et al.* (Scheme 3).[7]
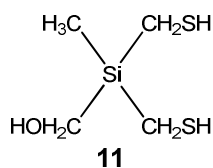
Scheme 2. Dithiol **11**.

Syntheses of the hexacarbonyl diiron complexes. According to procedures supported by literature,[8] complexes **12-14** were synthesized *via* reaction of $Fe_3(CO)_{12}$ with the corresponding thiols **8**, **9** and **11** in refluxing toluene (Scheme 3).
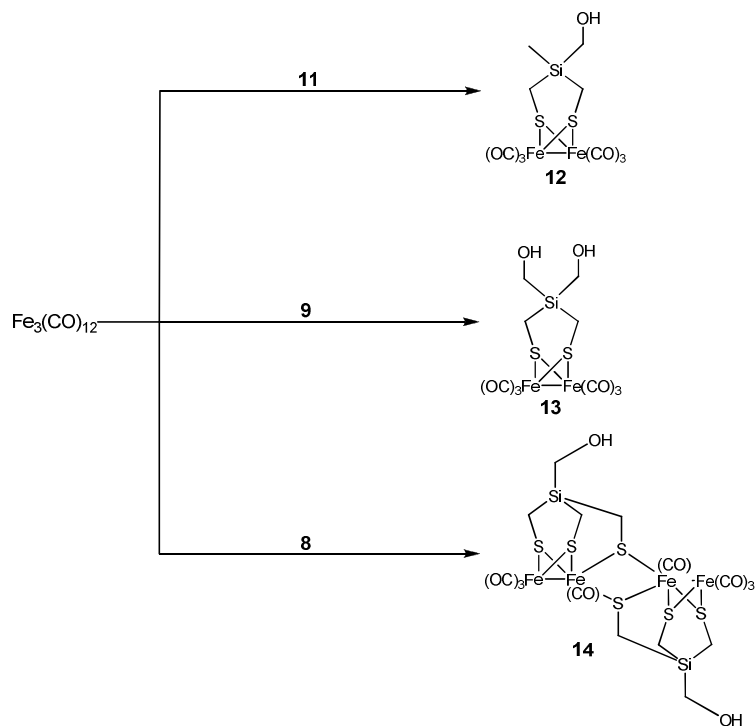
Scheme 2. Syntheses of hexacarbonyl diiron complexes **12**-**14**.

Reaction of (hydroxymethyl)bis(mercaptomethyl)methylsilane (**11**) and $Fe_3(CO)_{12}$ in refluxing toluene afforded a red crystalline product in 74 % yield, which was confirmed as compound **12** *via* ^{1}H, ^{13}C NMR spectroscopy, mass spectrometry and elemental analysis. Slow diffusion of pentane into a solution of compound **12**, dissolved in chloroform afforded red crystals suitable for structure determination (Figure 2). The ordinary [2Fe2S] butterfly arrangement[9] and a short Fe-Fe distance of about 250.46(14) pm (Table 1) were observed. As reported for other [2Fe2S(Si)] complexes, large bonding angles S(2)-C(2)-Si(1) and S(1)-C(1)-Si(1) with 122.3(5) and 118.9(4)°, respectively are visible.[1,2] In accordance to DFT calculations[3] and electrochemical investigations on recently published complexes,[1] this widening of the bonding angles lead to an increase of the electron density at the bridgehead sulfur atoms and enables a possible S•••H interaction. Four molecules form intermolecular hydrogen bonds so that each four molecules are arranged together to form a ring shaped system (Figure 2). The intermolecular interactions are of the type O(1A)–H(1OA)•••O(1B) with two different distances between O(1A)•••O(1B)of 273.5 and 272.2 pm.
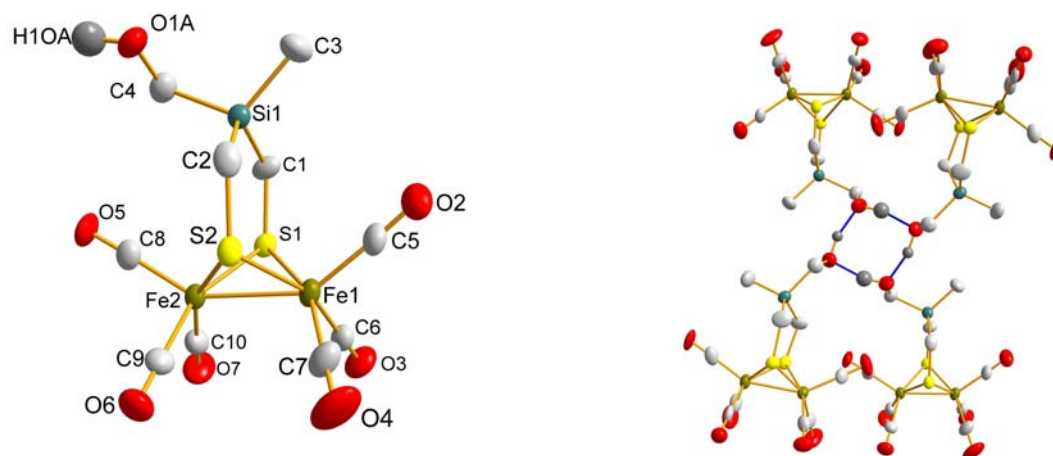
Figure 2. (Left) Molecular structure of compound **12** showing one of two independent molecules (thermal ellipsoids at 50% probability level). (Right) Arrangement of complex **12** in the crystal structure showing the hydrogen bonds.

Table 1. Selected distances and bonding angles of compound **12**.

Bond lengths [pm]			
Fe(1)-Fe(2)	250.46(14)	C(2)-Si(1)	185.6(9)
Fe(1)-S(1)	225.0(2)	Si(1)-C(3)	185.3(8)

Fe(1)-S(2)	227.0(2)	Si(1)-C(4)	189.6(9)
S(1)-C(1)	181.3(9)	C(4)-O(1)	142.1(10)
S(2)-C(2)	183.7(9)	O(1)-H(1)	109(10)
C(1)-Si(1)	186.9(8)		
Bond angles [°]			
Fe(1)-S(1)-Fe(2)	67.43(7)	S(2)-C(2)-Si(1)	118.9(4)
Fe(1)-S(1)-C(1)	117.0(3)	C(1)-Si(1)-C(2)	109.3(4)
Fe(2)-S(2)-C(2)	110.6(3)	C(1)-Si(1)-C(3)	114.9(4)
S(1)-C(1)-Si(1)	122.3(5)	C(1)-Si(1)-C(4)	106.1(4)

Increasing the number of hydroxyl functions, bis(hydroxymethyl)bis(mercaptomethyl)silane (**9**) was reacted with one molar equivalent of $Fe_3(CO)_{12}$ in refluxing toluene. Isolation *via* flash chromatography (FC) and crystallization by diffusion of pentane into a solution of compound **13**, dissolved in chloroform afforded red crystals. The molecular structure of compound **13** is depicted in Figure 3 and reveals similar properties as described for compound **12**. Due to the increased number of hydroxyl functions, compound **13** forms layers, where the molecules are connected *via* hydrogen bonds with an average length of 278.5 pm (Figure 3).
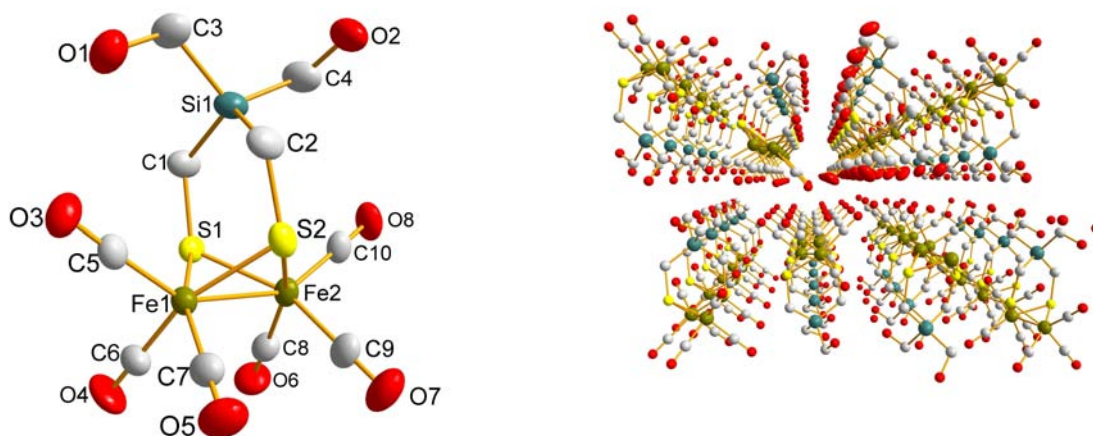
Figure 3. (Left) Molecular structure of compound **13** with thermal ellipsoids at the 50% probability level. Hydrogen atoms are omitted for clarity. (Right) Solid structure arrangement of compound **13**.

Table 2. Selected bond distances and angles of compound **13**.

Bond lengths [pm]			
Fe(1)-Fe(2)	251.62(9)	C(2)-Si(1)	186.0(5)
Fe(1)-S(1)	225.02(13)	Si(1)-C(3)	188.4(6)
Fe(1)-S(2)	224.15(13)	Si(1)-C(4)	189.5(6)
S(1)-C(1)	181.8(5)	C(3)-O(1)	145.1(7)

S(2)-C(2)	182.0(5)	C(4)-O(2)	143.5(8)
C(1)-Si(1)	186.2(5)		
Bond angles [°]			
Fe(1)-S(1)-Fe(2)	68.11(4)	S(2)-C(2)-Si(1)	121.3(3)
Fe(1)-S(1)-C(1)	116.12(17)	C(1)-Si(1)-C(2)	112.6(2)
Fe(2)-S(2)-C(2)	111.63(18)	C(1)-Si(1)-C(3)	106.3(3)
S(1)-C(1)-Si(1)	121.4(3)	C(1)-Si(1)-C(4)	111.3(3)

Inspired by mixed valent [4Fe6S] clusters[10] and especially of [4Fe6S(Si)] clusters,[1] a similar cluster was synthesized containing an additional hydroxyl function. By reaction of (hydroxymethyl)tris(mercaptomethyl)silane (**8**) and $Fe_3(CO)_{12}$ in boiling toluene a black suspension occurs within 45 minutes, which afforded a small amount of compound **14** as a red brown solid after following workup. It has to be noted that this compound is rather instable in solution and decomposes very fast even at moderate temperatures (~ 30°C). ^1H NMR spectra afforded a doublet at 3.46 ppm, representing the CH_2OH groups, and the remaining methylene protons as a multiplet in the area of 2.54 - 1.67 ppm. In comparison, the $^{13}C\{^1H\}$ NMR spectrum showed only one signal for the methylene protons at 22.3 ppm and two additional signals at 31.9 ppm for the methylene carbons, next to the hydroxyl function. Furthermore the typical signal for the CO ligands at 207.2 ppm was observed. Mass spectrometry (Micro-ESI) afforded the mole peak at *m/z* 841.6 and therefore giving addition proof for compound **14**. Slow evaporation of a solution of compound **13**, dissolved in chloroform at 4°C afforded suitable crystals for structure analysis (Figure 4). This structure is very similar to that reported by Picket and co-workers for the carbon analogue[8] and our recently published silicon containing [4Fe6S(2Si)] cluster.[1] The X-ray determination reveals that compound **14** is a centro-symmetric [4Fe6S] cluster, where two identical [2Fe3S] clusters are connected *via* two bridging thiolato groups. The iron center Fe(2) wears three CO groups and is surrounded by two sulfur atoms S(1) and S(2) and one iron atom Fe(1A). The "inner" iron atoms Fe(1A) and Fe(1B), respectively are connected each to one CO ligand. The iron-iron distance Fe(1A)–Fe(2) was determined as 250.66(10) pm, whereas the distance Fe(1A)–Fe(1B)

(261.21(14) pm) is significantly longer. To the best of our knowledge this is the first compound, possessing an $Fe^{I}Fe^{II}$•••$Fe^{II}Fe^{I}$ assembly with a functionalized backbone. The present hydroxyl function enables the establishment of hydrogen bridges with an average length of d(O-H•••O) = 376 pm. Derivatizations of these hydroxyl groups are currently under investigation.
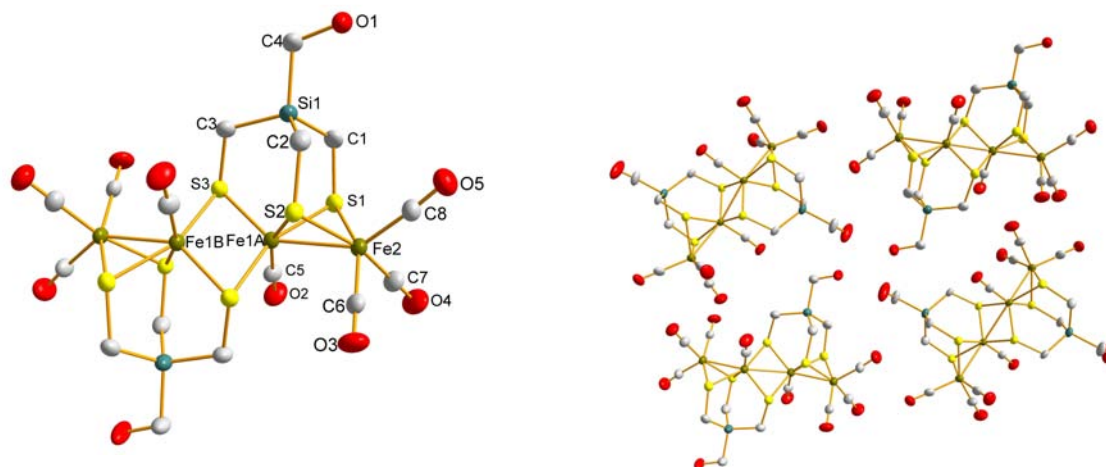
Figure 4. (Left) Molecular structure of compound **14** (Hydrogen atoms are omitted for clarity; Thermal ellipsoids at 50% probability level). (Right) Spatial arrangement of four molecules of compound **14**, picturing out the hydrogen bonds.

Table 3. Selected bond lengths and angles of compound **14**.

Bond lengths [pm]			
Fe1A-Fe2	250.66(10)	S3-C3	183.1(5)
Fe1A-Fe1B	261.21(14)	C1-Si1	185.2(5)
Fe1A-S3	223.70(14)	C2-Si1	186.7(6)
Fe1A-S2	224.97(15)	C3-Si1	186.8(6)
Fe1A-S1	230.50(15)	Si1-C4	189.0(6)
S1-C1	182.9(5)	C4-O1	141.6(9)
S2-C2	181.9(6)		
Bond angles [°]			
S(1)–Fe(1A)–S(2)	88.14(5)	S(1)–C(1)–Si(1)	112.3(3)
S(1)–Fe(2)–S(2)	89.23(5)	S(3)–C(3)–Si(1)	116.1(3)
S(1)–Fe(1A)–S(3)	105.68(5)	C(1)–Si(1)–C(2)	107.7(3)
S(2)–Fe(1A)–S(3)	95.38(6)	C(1)–Si(1)–C(3)	110.3(2)
S(2)–C(2)–Si(1)	115.5(3)	C(2)–Si(1)–C(4)	108.8(3)

Electrochemistry. The cyclic and differential pulse voltammetry was carried out under an argon atmosphere on a glassy carbon working electrode. Both reference electrodes were measured against the Fc/Fc$^+$ redox couple and the potential values in Table 4 were all corrected against the Ag/Ag$^+$ reference using this method.

Table 4. Electrochemical data of the hexacarbonyl diiron hydrogenase analogues. The potentials are corrected for the Ag/Ag$^+$ reference electrode and are measured in [a] dichloromethane or [b] acetonitrile.

Compound	$Fe^IFe^I/Fe^{II}Fe^{II}$ [V]	Fe^IFe^I/Fe^0Fe^0 [V]
12[a]	+1.02 (E_{pa})	-1.57 (E_{pc})
		-1.39 (E_{pa})
13[b]	+0.82 (E_{pa})	-1.43 (E_{pc}),
		-1.36 (E_{pa})

An irreversible anodic wave is observed in the cyclic voltammogram of **12** and **13**, representing the Fe^{I}Fe^I → Fe^{II}Fe^{II} + 2e$^-$ process (see also ref. [1]). The oxidation of the diiron centre of compound **12** results in the formation of an intermediate that pacifies the electrode surface. This can be seen by decrease in current intensity with each successive cycle (Figure 5). Direct comparison between the oxidation potentials of these two hydroxyl functionalized models is not straightforward because of the different solvents used in the electrochemistry.
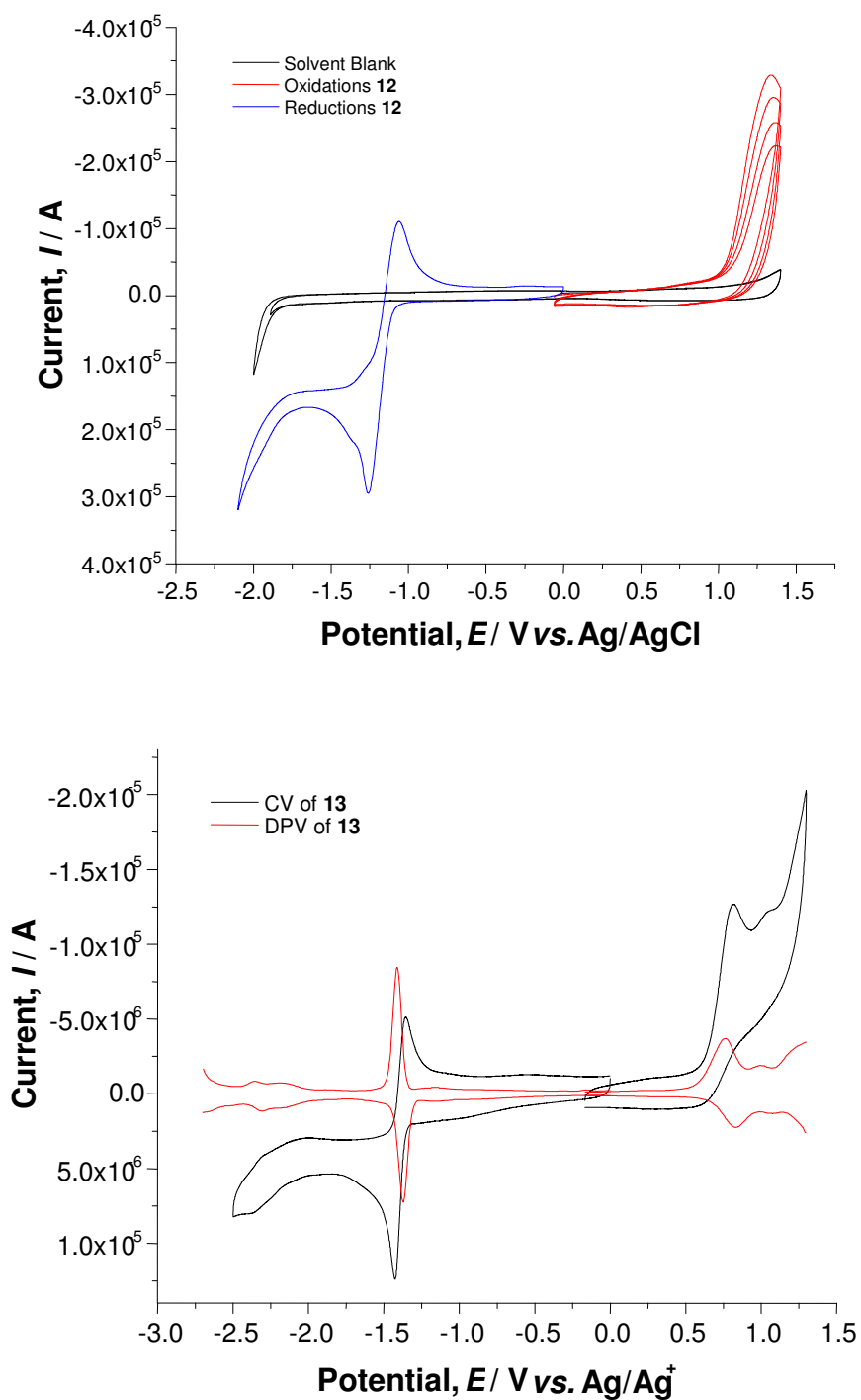
Figure 5. Cyclic voltammetry (CV) and differential pulse voltammetry (DPV) of compound **12** (top, dichloromethane) and **13** (bottom, acetonitrile) on a glassy carbon working electrode using 0.05 M TBA PF$_6$ as the supporting electrolyte.

The catalytic properties of both hydroxyl functionalized compounds were investigated using the weak acid, acetic acid as proton source. The first (least negative) reduction process of compound **12** experiences a 30 mV shift in the positive direction upon addition of acid.

However, the potential of this wave gradually shifts back in the negative direction with further addition of acid. The appearance of a new wave (at approximately -2.1 V, *vs.* Ag/Ag$^+$) suggests that the Fe^{0}Fe^0 intermediate undergoes protonation followed by a second reduction. From this state, evolution of hydrogen is observed as indicated by the increase in the current of this second peak with each increment of acid added (Figure 6).
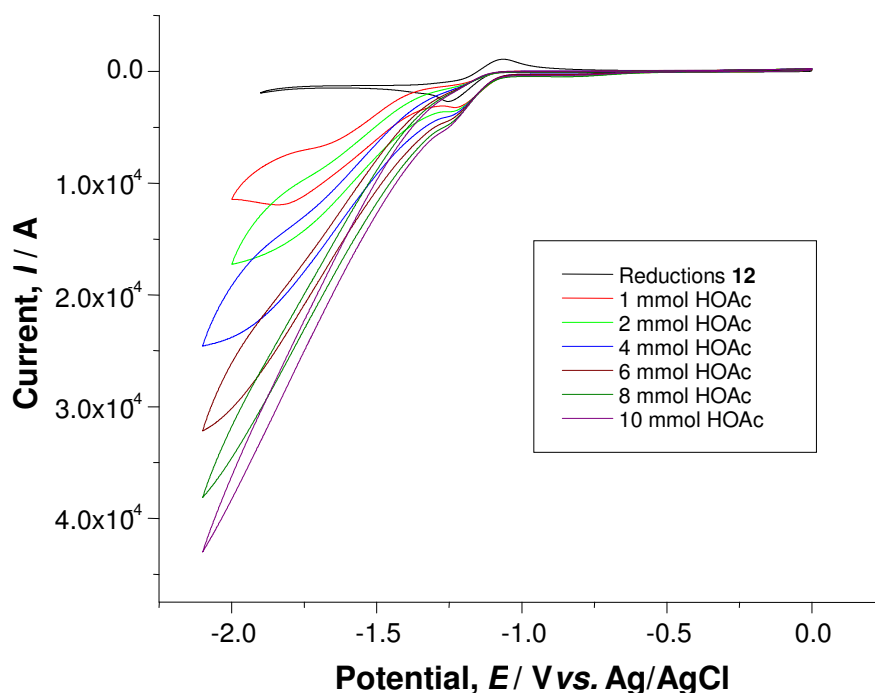
Figure 6. Cyclic voltammetry of compound **12** [1 mM] with HOAc (0-10 mmol) in dichloromethane.

The catalytic activity of compound **13** is revealed in Figure 7. The redox potential of the first cathodic wave (Fe^{I}Fe^I + 2e$^-$ → Fe^{0}Fe^0) is not altered in either direction upon addition of acid. This suggests that the first step in the mechanism of proton reduction is electrochemical with the complex being reduced followed by the addition of a proton as indicated by the positive shift in the reduction potential of the second cathodic wave. It is from this state that the electrocatalytic current is observed. It is notable that the catalytic increase of current already starts after the first reduction, suggesting that H$_2$ development starts at moderate potential.
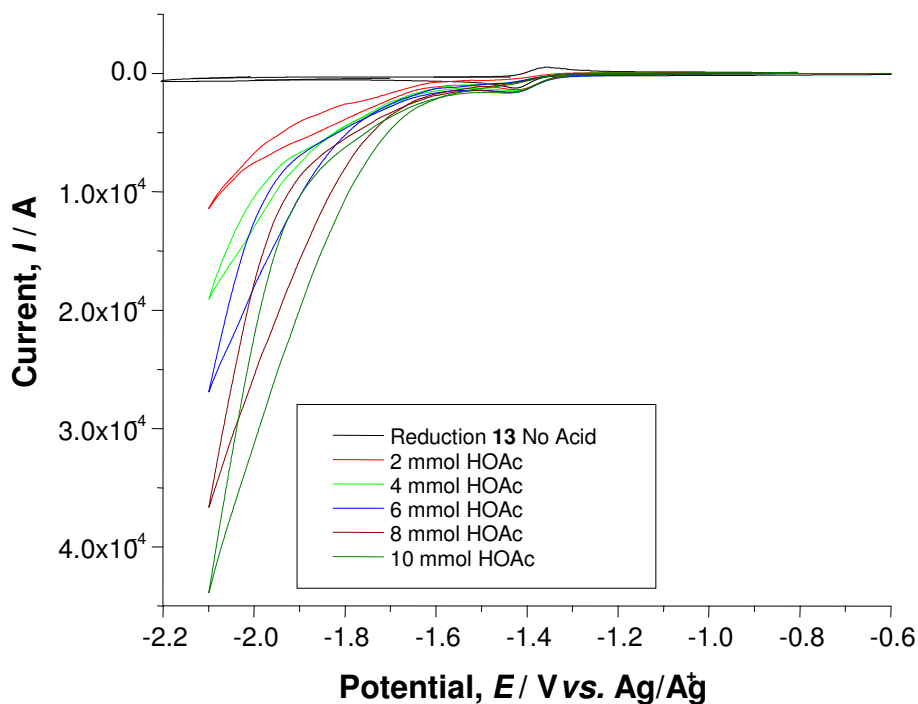
Figure 7. Cyclic voltammetry of compound **13** [1 mM] with HOAc (0-10 mmol) in acetonitrile.

Due to the instability of compound **14** we were not able to determine the electrochemical properties of this compound.

Conlcusion

This investigation was aimed on hydroxyl functionalized [2Fe2S(Si)] complexes as models for the [FeFe] hydrogenase, enabling further derivatizations of these complexes. For this purpose the hydroxyl functionalized compounds **8**-**11** were synthesized and reacted to the [2Fe2S(Si)] complexes **12**-**14**. These compounds were characterized by elemental analyses (C, H, S), ^{1}H, ^{13}C NMR spectroscopy, mass spectrometry, and single-crystal X-ray diffraction. The electrochemical behavior was investigated *via* cyclic voltammetry and the electrocatalytic properties for dihydrogen development were studied using acetic acid, revealing similar properties than reported for earlier described [2Fe2S(Si)] complexes.[1] Therefore, these complexes are ideal precursors for new [2Fe2S(Si)] complexes, as the hydroxy function offers the ability of further derivatization (*e.g.* immobilization on surfaces).

Experimental Section

General Procedures. All syntheses were carried out under dry nitrogen or argon. The organic solvents used were dried and purified according to standard procedures and stored under dry nitrogen or argon. Chemicals were used as received from Fluka or Acros without further purification. Tetrakis(chloromethyl)silane (**1**) was prepared according to ref [11]. (Hydroxymethyl)bis(mercaptomethyl)methylsilane (**11**) was synthesized according to ref [7]. Thin layer chromatography (TLC): Merck silica gel 60 F_{254} plates; detection under UV light at 254 nm. Flash chromatography (FC): Fluka silica gel 60. A Büchi GKR-51 apparatus was used for the bulb-to-bulb distillations. The ^{1}H, ^{13}C{^{1}H}, and ^{29}Si{^{1}H} NMR spectra were recorded at 23 °C on a Bruker DRX-300 NMR spectrometer (^{1}H, 300.1 MHz; ^{13}C, 75.5 MHz; ^{29}Si, 59.6 MHz). CDCl$_3$ was used as the solvent. Chemical shifts (ppm) were determined relative to internal CHCl$_3$ (^{1}H, δ 7.24; CDCl$_3$), internal CDCl$_3$ (^{13}C, δ 77.0; CDCl$_3$), or external TMS (^{29}Si, δ 0; CDCl$_3$). Analysis and assignment of the ^{1}H NMR data were supported by ^{1}H,^{1}H COSY, ^{13}C,^{1}H HMQC, and ^{13}C,^{1}H HMBC experiments. Assignment of the ^{13}C NMR data was supported by DEPT 135, ^{13}C,^{1}H HMQC, and ^{13}C,^{1}H HMBC experiments. IR spectra were recorded on a Perkin-Elmer 2000 FT-IR spectrometer. Mass-spectrometric studies (FAB/MS, DEI/MS) were performed on a SSQ710 Finnigan MAT spectrometer.

(Acetoxymethyl)tris(chloromethyl)silane (2), Bis(acetoxymethyl)bis(chloromethyl)-silane (3), and Tris(acetoxymethyl)(chloromethyl)silane (4). Silane **1** (10.4 g, 46.0 mmol) was added in one single portion to a stirred suspension of sodium acetate (7.55 g, 92.0 mmol) and 18-crown-6 (274 mg, 1.04 mmol) in dimethylformamide (140 mL), and the resulting mixture was stirred at 20 °C for 24 h. The solvent was removed by distillation (45 °C/10 mbar), diethyl ether (250 mL) and water (250 mL) were added, the organic phase was separated, and the aqueous phase was extracted with diethyl ether (2 ×250 mL) and

discarded. The organic phases were combined, dried over anhydrous sodium sulfate, the solvent was removed under reduced pressure, and the residue was purified by column chromatography on silica gel (column dimensions, 340 ×45 mm; silica gel (32–63 μm, ICN 02826); eluent, n-hexane/ethyl acetate (9:1 (v/v))). The relevant first fractions (GC control) were combined, and the solvent was removed under reduced pressure to give **2** in 18% yield as a colorless liquid (2.09 g, 8.37 mmol). ^{1}H NMR (300.1 MHz, CDCl$_3$): δ 2.05 (s, 3 H, CH_3), 3.09 (s, 6 H, SiCH_2Cl), 4.04 (s, 2 H, SiCH_2O). ^{13}C NMR (75.5 MHz, CDCl$_3$): δ 20.4 (CH$_3$), 23.9 (SiCH$_2$Cl), 51.5 (SiCH$_2$O), 172.0 (C=O). ^{29}Si NMR (59.6 MHz, CDCl$_3$): δ –4.0. Anal. calcd for C$_6$H$_{11}$Cl$_3$O$_2$Si: C, 28.87; H, 4.44. Elemental analysis was not obtained due to the high content of halogen (> 40%).

After further eluation with n-hexane/ethyl acetate (9:1 (v/v)), compound **3** was obtained. The relevant fractions (GC control) were combined, and the solvent was removed under reduced pressure to give **3** in 44% yield as a colorless liquid (5.54 g, 20.3 mmol). ^{1}H NMR (300.1 MHz, CDCl$_3$): δ 2.03 (s, 6 H, CH_3), 3.04 (s, 4 H, SiCH_2Cl), 3.98 (s, 4 H, SiCH_2O). ^{13}C NMR (75.5 MHz, CDCl$_3$): δ 20.3 (CH$_3$), 25.0 (SiCH$_2$Cl), 52.3 (SiCH$_2$O), 172.0 (C=O). ^{29}Si NMR (59.6 MHz, CDCl$_3$): δ –7.0. Anal. calcd for C$_8$H$_{14}$Cl$_2$O$_4$Si: C, 35.17; H, 5.17. Found: C, 35.3; H, 5.1.

After further eluation with n-hexane/ethyl acetate (9:1 (v/v)), compound **4** was obtained. The relevant fractions (GC control) were combined, and the solvent was removed under reduced pressure to give **4** in 19% yield as a colorless liquid (2.65 g, 8.93 mmol). ^{1}H NMR (300.1 MHz, CDCl$_3$): δ 2.00 (s, 9 H, CH_3), 2.96 (s, 2 H, SiCH_2Cl), 3.93 (s, 6 H, SiCH_2O). ^{13}C NMR (75.5 MHz, CDCl$_3$): δ 20.3 (CH$_3$), 25.9 (SiCH$_2$Cl), 53.0 (SiCH$_2$O), 172.0 (C=O). ^{29}Si NMR (59.6 MHz, CDCl$_3$): δ –9.6. Anal. calcd for C$_{10}$H$_{17}$ClO$_6$Si: C, 40.47; H, 5.77. Found: C, 40.5; H, 5.8.

Method A:

(Acetoxymethyl)tris(acetylthiomethyl)silane (5). Compound **2** (1.03 g, 4.13 mmol) was added in one single portion at 20 °C to a stirred suspension of potassium thioacetate (2.07 g, 18.1 mmol) in tetrahydrofuran (50 mL), and the resulting mixture was stirred at 20 °C for 40 h. The solvent was removed under reduced pressure, diethyl ether (50 mL) and water (50 mL) were added, and the aqueous phase was extracted with diethyl ether (2 × 50 mL). The organic extracts were combined, dried over anhydrous sodium sulfate, and the solvent was removed under reduced pressure. The residue was purified by bulb-to-bulb distillation (oven temperature 210 °C, 0.23 mbar) to give **5** in 91% yield as a yellowish liquid (1.39 g, 3.77 mmol). ^{1}H-NMR (500.1 MHz, CDCl$_3$): δ 2.01 (s, 3 H, OC(O)CH_3), 2.24 (s, 6 H, SiCH_2S), 2.30 (s, 9 H, SC(O)CH_3), 3.84 (s, 2 H, SiCH_2O). ^{13}C-NMR (125.8 MHz, CDCl$_3$): δ 8.7 (SiCH$_2$S), 20.6 (OC(O)CH$_3$), 30.0 (SC(O)CH$_3$), 53.0 (SiCH$_2$O), 171.4 (OC(O)C), 195.3 (SC(O)C). ^{29}Si-NMR (99.4 MHz, CDCl$_3$): δ –0.5. Anal. Calc for C$_{12}$H$_{20}$O$_5$S$_3$Si: C, 39.11; H, 5.47; S, 26.10. Found: C, 39.1; H, 5.3; S, 26.2.

Bis(acetoxymethyl)bis(acetylthiomethyl)silane (6). This compound was synthesized according to Method A from compound **3** (2.70 g, 9.88 mmol), potassium thioacetate (3.39 g, 29.7 mmol), and tetrahydrofuran (60 mL) to give **6** in 90% yield as a yellowish liquid (3.12 g, 8.86 mmol); bp 140–160 °C/0.03 mbar. 1H-NMR (500.1 MHz, CDCl3): δ 2.00 (s, 6 H, OC(O)CH3), 2.25 (s, 4 H, SiCH2S), 2.29 (s, 6 H, SC(O)CH3), 3.87 (s, 4 H, SiCH2O). 13C-NMR (125.8 MHz, CDCl3): δ 8.3 (SiCH2S), 20.5 (OC(O)CH3), 29.9 (SC(O)CH3), 52.9 (SiCH2O), 171.5 (OC(O)C), 195.5 (SC(O)C). 29Si-NMR (99.4 MHz, CDCl3): δ –3.5. Anal. Calc for C12H20O6S2Si: C, 40.89; H, 5.72; S, 18.19. Found: C, 40.5; H, 5.7; S, 18.2.

Tris(acetoxymethyl)(acetylthiomethyl)silane (7). This compound was synthesized according to Method A from compound **4** (2.00 g, 6.74 mmol), potassium thioacetate (1.15 g, 10.1 mmol), and tetrahydrofuran (30 mL) to give **7** in 93% yield as a yellowish liquid (2.11 g, 6.27 mmol); bp 145–155 °C/0.05 mbar. ^{1}H-NMR (500.1 MHz, CDCl$_3$): δ 1.97 (s, 9 H, OC(O)CH_3), 2.22 (s, 2 H, SiCH_2S), 2.26 (s, 3 H, SC(O)CH_3), 3.86 (s, 6 H, SiCH_2O). ^{13}C-NMR (125.8 MHz, CDCl$_3$): δ 8.0 (SiCH$_2$S), 20.4 (OC(O)CH$_3$), 29.8 (SC(O)CH$_3$), 53.1 (SiCH$_2$O), 171.6 (OC(O)C), 195.7 (SC(O)C). ^{29}Si-NMR (99.4 MHz, CDCl$_3$): δ –7.3. Anal. Calc for C$_{12}$H$_{20}$O$_7$SSi: C, 42.84; H, 5.99; S, 9.53. Found: C, 42.5; H, 6.0; S, 9.8.

Method B:

(Hydroxymethyl)tris(mercaptomethyl)silane (8). A solution of **5** (1.30 g, 3.53 mmol) in diethyl ether (15 mL) was added dropwise at 0 °C within 30 min to a stirred suspension of lithium aluminium hydride (803 mg, 21.2 mmol) in diethyl ether (25 mL), and the resulting mixture was stirred at 0 °C for 90 min and then at 20 °C for 21 h. Hydrochloric acid (2 M, 20 mL) was added dropwise at 0 °C within 30 min, and the resulting mixture was then warmed to 20 °C. Water (60 mL) and diethyl ether (60 mL) were added, the organic phase was separated, and the aqueous phase was extracted with diethyl ether (2 × 60 mL). The organic extracts were combined, dried over anhydrous sodium sulfate, and the solvent was removed under reduced pressure. The residue was purified by bulb-to-bulb distillation (oven temperature 160–175 °C, 0.04 mbar) to give **8** in 79% yield as a colorless liquid (559 mg, 2.79 mmol). ^{1}H-NMR (500.1 MHz, CDCl$_3$): δ 1.46 (t, $^3J_{HH}$ = 7.5 Hz, 3 H, SH), 1.90 (d, $^3J_{HH}$ = 7.5 Hz, 6 H, SiCH_2S), 1.93 (s, 1 H, OH), 3.67 (s, 2 H, SiCH_2O). ^{13}C-NMR (125.8 MHz, CDCl$_3$): δ 1.4 (SiCH$_2$S), 50.5 (SiCH$_2$O). ^{29}Si-NMR (99.4 MHz, CDCl$_3$): δ –0.4. Anal. Calcd for C$_4$H$_{12}$OS$_3$Si: C, 23.97; H, 6.03; S, 48.00. Found: C, 24.2; H, 5.7; S, 48.0.

Bis(hydroxymethyl)bis(mercaptomethyl)silane (9). This compound was synthesized according to Method B from compound **6** (3.00 g, 8.51 mmol), lithium aluminium hydride (1.94 g, 51.1 mmol), and diethyl ether (95 mL) to give 9 in 58% yield as a colorless liquid (905 mg, 4.91 mmol); bp 160–175 °C/0.03 mbar. ^{1}H-NMR (500.1 MHz, CDCl$_3$): δ 1.47 (t, $^3J_{HH}$ = 7.4 Hz, 2 H, SH), 1.88 (d, $^3J_{HH}$ = 7.4 Hz, 4 H, SiCH$_2$S), 2.84 (s, 2 H, OH), 3.70 (s, 4 H, SiCH$_2$O). ^{13}C-NMR (125.8 MHz, CDCl$_3$): δ 1.0 (SiCH$_2$S), 50.9 (SiCH$_2$O). ^{29}Si-NMR (99.4 MHz, CDCl$_3$): δ –4.7. Anal. Calcd for C$_4$H$_{12}$O$_2$S$_2$Si: C, 26.06; H, 6.56; S, 34.79. Found: C, 26.2; H, 6.7; S, 34.7.

Tris(hydroxymethyl)(mercaptomethyl)silane (10). Acetyl chloride (63 mg, 803 μmol) was added dropwise at 20 °C within 1 min to a stirred solution of **7** (2.00 g, 5.94 mmol) in methanol (90 mL), and the resulting solution was heated under reflux for 23 h. The solvent was removed under reduced pressure, and the resulting oily residue was crystallized from boiling acetonitrile (10 mL; crystallization at –20 °C over a period of 24 h). The product was isolated by removal of the solvent via a syringe and then dried in vacuum (0.08 mbar, 20 °C, 2 h) to give **10** in 76% yield as a colorless crystalline solid (758 mg, 4.50 mmol). ^{1}H NMR (300.1 MHz, [D$_6$]DMSO): δ 1.72 (d, $^3J_{HH}$ = 7.3 Hz, 2 H, SiCH$_2$S), 2.07 (t, $^3J_{HH}$ = 7.3 Hz, 1 H, SH), 3.37 (s, 6 H, SiCH$_2$O), 3.99 (br. s, 3 H, OH). ^{13}C NMR (75.5 MHz, [D$_6$]DMSO): δ –0.1 (SiCH$_2$S), 47.8 (SiCH$_2$O). ^{29}Si NMR (59.6 MHz, [D$_6$]DMSO): δ –6.0. Anal. calcd for C$_4$H$_{12}$O$_3$SSi: C, 28.55; H, 7.19; S, 19.05. Found: C, 28.2; H, 7.4; S, 18.5.

Hexacarbonyl diiron complex 12. (Hydroxymethyl)-bis(mercaptomethyl)methylsilan (**11**) (50 mg, 0.297 mmol) and Fe$_3$(CO)$_{12}$ (150 mg, 0.297 mmol) were dissolved in 20 mL toluene and refluxed for 2 hours. Filtration, evaporation to dryness and purification *via* FC (THF/hexane 1:3) gave 98 mg (74%) of compound **12**. ^{1}H-NMR (200 MHz, CDCl$_3$): δ

3.32/3.30 (2H, d, ^3J = 4Hz, CH_2O), 1.54 (4H, s, CH_2), 0.04 (3H, s, CH_3). ^{13}C-NMR (50 MHz, CDCl$_3$): δ 207.3 (CO), 53.3 (CHO), 2.7 (CH$_2$), -7.8 (CH$_3$). MS(DEI): 390 [M-2CO]$^+$, 362 [M-3CO]$^+$, 334 [M-4CO]$^+$, 306 [M-5CO]$^+$, 278 [M-6CO]. IR (KBr): 3422 (s), 2925 (m), 2072 (vs), 2022 (vs, b), 1636 (m). Anal. calcd for C$_{10}$H$_{18}$Fe$_2$O$_7$S$_2$Si*THF: C, 32.45; H, 3.50; S, 12.38. Found: C, 33.05; H, 3.56; S, 12.43.

Hexacarbonyl diiron complex 13. Bis(hydroxymethyl)-bis(mercaptomethyl)silan (**9**) (50 mg, 0.27 mmol) and Fe$_3$(CO)$_{12}$ (137 mg, 0.27 mmol) were dissolved in 30 mL toluene. After 1 hour reflux, the solution was evaporated to dryness and purified *via* FC (THF/hexane 1:3). 76 mg (61%) of the hexacarbonyl diiron complex **13** were obtained as red solid. ^{1}H NMR (200 MHz, CDCl$_3$): δ 3.57 (4H, s, CH_2O), 1.61 (4H, s, CH_2). ^{13}C NMR (50 MHz, CDCl$_3$): δ 207.1 (CO), 53.1 (CHO), 0.3 (CH$_2$). MS(DEI): 406 [M-2CO]$^+$, 378 [M-3CO]$^+$, 350 [M-4CO]$^+$, 322 [M-5CO]$^+$, 294 [M-6CO]. IR (KBr): 3419 (s), 2953 (m), 2932 (m), 2860 (m), 2072 (vs), 2031 (vs), 1994 (vs), 1628 (m). Anal. Calcd for C$_{10}$H$_{10}$Fe$_2$O$_8$S$_2$Si*2THF: C, 35.66; H, 4.32; S, 10.58. Found: C, 35.79; H, 4.14; S, 10.97.

Octacarbonyl tetrairon complex 14. (Hydroxymethyl)-tris(mercaptomethyl)silan (**8**) (50 mg, 0.249 mmol) and Fe$_3$(CO)$_{12}$ (126 mg, 0.249 mmol) were refluxed for 45 minutes in toluene. Evaporation and FC (diethylether) yield 13 mg (12%) of a red brown solid, identified as compound **14**. ^{1}H NMR (200 MHz, CDCl$_3$): δ 3.47/3.45 (4H, d, ^3J = 8 Hz, CH_2O), 2.54-1.67 (12H, m, CH_2). ^{13}C NMR (50 MHz, CDCl$_3$): δ 207.2 (CO), 31.9 (CH$_2$OH), 22.3 (CH$_2$). MS(Micro-ESI): 841.6 [M]$^+$. IR (KBr): 3435 (s), 2959 (m), 2924 (m), 2855 (m), 2073 (vs), 2033 (vs), 1992 (vs, b), 1630 (m). Anal. Calcd for C$_{16}$H$_{18}$Fe$_4$O$_{10}$S$_6$Si$_2$: no elemental analysis was obtained.

Electrochemistry: Instrumentation and Procedures. Cyclic voltammograms were recorded against a non-aqueous Ag/Ag$^+$ or Ag/AgCl reference electrode (0.1 M nBu$_4$NPF$_6$ and 0.01 M AgNO$_3$ in CH$_3$CN). The Ag/Ag$^+$ reference electrode was used with acetonitrile and the Ag/AgCl reference was used when the electrochemical solvent was dichloromethane. Both reference electrodes were measured against the Fc/Fc$^+$ redox couple and the potential values in Table 44 were all corrected against the Ag/Ag$^+$ reference. A glassy carbon (GC) macro electrode and a platinum wire were used as the working and auxiliary electrodes, respectively. A solution of 0.05 M nBu$_4$NPF$_6$ (Fluka, electrochemical grade) in either acetonitrile (Aldrich, anhydrous, 99.8%) or dichloromethane (depending on the solubility of the compound) was used as the supporting electrolyte. Electrochemical experiments were carried out using a CHI750C electrochemical bipotentiostat. Prior to each experiment, the electrochemical cell was degassed for at least 10 minutes using argon and a blanket of argon was maintained throughout. The GC working electrode was prepared by successive polishing with 1.0 and 0.3 micron alumina pastes and sonicated in Millipore water for 5 minutes. All cyclic voltammograms were recorded at a scan rate of 100 mVs^{-1}.

Crystal Structure Determination. Compounds **12**, **13**, and **14** were crystallized from solutions in trichloromethane by either slow evaporation of the solvent at 4 °C or by diffusion of pentane into the solution under the same conditions. The intensity data were collected on a Nonius Kappa CCD diffractometer using graphite-monochromated Mo-K$_\alpha$ radiation. Data were corrected for Lorentz and polarization effects but not for absorption.[12,13] Crystallographic data as well as structure solution and refinement details are summarized in Table 5.

The structures were solved by direct methods (SHELXS)[16,14] and refined by full-matrix least squares techniques against F$_0$^{2} (SHELXL-97).[14] All non-hydrogen atoms were refined anisotropically.[14] The hydrogen atoms were included at calculated positions according to the riding model.

Table 5. Crystal Data and Refinement Details for the Crystal Structure Analyses of Compounds **12, 13** and **14.**

	12	**13**	**14**
empirical formula	$C_{10}H_{10}Fe_2O_7S_2Si$	$C_{10}H_{10}Fe_2O_8S_2Si$	$C_{16}H_{18}Fe_4O_{10}S_6Si_2$
formula mass [$g \cdot mol^{-1}$]	446.09	462.59	842.24
collection T [°C]	-90(2)	-90(2)	-90(2)
λ (Mo K_α) [$\bar{}$]	0.71073	0.71073	0.71073
crystal system	orthorhombic	triclinic	triclinic
space group (No.)	Fdd2 (43)	P$\bar{1}$ (2)	P$\bar{1}$ (2)
a [$\bar{}$]	27.0613(11)	7.4855(4)	7.6222(5)
b [$\bar{}$]	37.3589(17)	13.4935(6)	13.1482(9)
c [$\bar{}$]	13.4933(5)	17.5876(6)	15.3004(11)
α [°]	90	78.071(2)	94.879(5)
β [°]	90	84.115(3)	101.311(4)
γ [°]	90	85.530(2)	102.030(4)
V [$\bar{}^3$]	13641.5(10)	1725.98(13)	1457.84(17)
Z	32	4	2
ρ_{calcd} [$g \cdot cm^{-3}$]	1.738	1.780	1.919
μ [mm^{-1}]	2.041	2.024	2.509
$F(000)$	7168	930	844
crystal dimensions [mm]	0.05 x 0.05 x 0.03	0.05 x 0.05 x 0.02	0.05 x 0.05 x 0.05
2θrange [deg]	2.65-27.47	3.08-27.49	2.74-27.46
index ranges	$-10 \leq h \leq 11,$ $-13 \leq k \leq 13,$ $-12 \leq l \leq 12$	$-9 \leq h \leq 9,$ $-15 \leq k \leq 17,$ $-22 \leq l \leq 22$	$-9 \leq h \leq 9,$ $-16 \leq k \leq 17,$ $-18 \leq l \leq 19$
measured reflections	22851	12278	9312
unique reflections/R_{int}	7777	7855	6392
reflections used	22851	12278	9312
data with $I > 2\sigma(I)$	4781	5620	4609
parameters	405	419	345
S^a	0.998	1.015	1.022
$R1$ [$I > 2\sigma(I)$][b]	0.0604	0.0569	0.0523
$wR2$ [all data, on F^2][c]	0.0999	0.1392	0.1207
max./min. residual electron density [$e \cdot \bar{}^{-3}$]	0.450/-0.510	1.175/-0.711	1.292/-0.977

[a] $S = \{\Sigma[w(F_o^2 - F_c^2)^2] / (n - p)\}^{0.5}$; n = no. of reflections; p = no. of parameters; [b] $R1 = \Sigma\|F_o| - |F_c\| / \Sigma|F_o|$; [c] $wR2 = \{\Sigma[w(F_o^2 - F_c^2)^2] / \Sigma[w(F_o^2)^2]\}^{0.5}$.

Acknowledgment

1 U.–P. Apfel, D. Troegel, Y. Halpin, S. Tschierlei, U. Uhlemann, M. Schmitt, J. Popp, H. Görls, P. Dunne, M. Venkatesan, M. Coey, M. Rudolph, J. G. Vos, R. Tacke, W. Weigand, **2010**, submitted.

2 U.–P. Apfel, Y. Halpin, H. Görls, J. G. Vos, W. Weigand, unpublished results.

3 R. S. Glass, N. E. Gruhn, E. Lorance, M. S. Singh, N. Y. T. Stessman, U. I. Zakai, *Inorg. Chem.* **2005**, *44*, 5728–5737.

4 Selected publications dealing with the silylation of silica surfaces and their applications: (a) P. Van Der Voort, E. F. Vansant, *J. Liq. Chromatogr. Relat. Technol.* **1996**, *19*, 2723–2752. (b) A. R. Cestari, C. Airoldi, *J. Colloid Interface Sci.* **1997**, *195*, 338–342. (c) C. Giacomini, A. Villarino, L. Franco–Fraguas, F. Batista–Viera, *J. Mol. Catal. B:Enzym.* **1998**, *4*, 313–327. (d) M. E. Mahmoud, M. S. M Al Saadi,. *Anal. Chim. Acta* **2001**, *450*, 239–246. (e) A. G. S. Prado, C. Airoldi, *J. Colloid Interface Sci.* **2001**, *236*, 161–165. (f) P. Facci, D. Alliata, L. Andolfi, B. Schnyder, R. Kötz, *Surf. Sci.* **2002**, *504*, 282–292. (g) S. W. Park, Y. I. Kim, K. H. Chung, S. I. Hong, S. W. Kim, *React. Funct. Polym.* **2002**, *51*, 79–92. (h) N. Rochat, A. Troussier, A. Hoang, F. Vinet, *Mater. Sci. Eng., C* **2003**, *23*, 99–103. (i) S. W. Park, J. Lee, S. I. Hong, S. W. Kim, *Process Biochem.* **2003**, *39*, 359–366. (j) E. F. Murphy, D. Ferri, A. Baiker, *Inorg. Chem.* **2003**, *42*, 2559–2571. (k) R. J. P. Corriu, E. Lancelle–Beltran, A. Mehdi, C. Reye, S. Brandes, R. Guilard, *Chem. Mater.* **2003**, *15*, 3152–3160. (l) F. Zhang, M. P. Srinivasan, *Langmuir* **2004**, *20*, 2309–2314. (m) J. Horniakova, T. Raja, Y. Kubota, Y. Sugi, *J. Mol. Catal. A:Chem.* **2004**, *217*, 73–80. (n) Luderer, F.; Walschus, U. *Top. Curr. Chem.* **2005**, *260*, 37–56. (o) Tacke, R.; Schmid, T.;

Merget, M. *Organometallics* **2005**, *24*, 1780–1783. (p) Yamaguchi, K.; Imago, T.; Y. Ogasawara, J. Kasai, M. Kotani, N. Mizuno, *Adv. Synth. Catal.* **2006**, *348*, 1516–1520. (q) I. H. Gübbük, R. Güp, M. Ersöz, *J. Colloid Interface Sci.* **2008**, *320*, 376–382. (r) K. Ishii, Y. Kikukawa, M. Shiine, N. Kobayashi, T. Tsuru, Y. Sakai, A. Sakoda, *Eur. J. Inorg. Chem.* **2008**, 2975–2981.

5   D. Troegel, T. Walter, C. Burschka, R. Tacke, *Organometallics,* DOI: 10.1021/om8010118.

6   J. O. Daiss, K. A. Barth, C. Burschka, P. Hey, R. Ilg, K. Klemm, I. Richter, S. A. Wagner, R. Tacke, *Organometallics* **2004**, *23,* 5193–5197.

7   D. Troegel, F. Moeller, C. Burschka, R. Tacke, *Organometallics* **2009**, *28*, 5765–5770.

8   For examples see: M. H. Goodrow, W. K. Musker, *Synthesis* **1981**, 457–460; L. Song, F. Gong, T. Meng, J. Ge, L. Cui, Q. Hu, *Organometallics* **2004**, *23*, 823–831 ; U.–P. Apfel, Y. Halpin, H. Görls, J. G. Vos, B. Schweizer, G. Linti, W. Weigand, *ChemBiodiv* **2007**, *4*, 2138–2148.

9   L. F. Dahl, C. H. Wie, *Inorg. Chem.* **1963**, *2*, 328 – 333.

10 C. Tard, X. M. Liu, D. L. Hughes, C. J. Pickett, *Chem. Commun.* **2005**, 133 – 135; M. H. Cheah, C. Tard, S. J. Borg, X. M. Liu, S. K. Ibrahim, C. J. Pickett, S. P. Best, *J. Am. Chem. Soc.* **2007**, *129*, 11085 – 11092; S. J. Borg, T. Behrsing, S. P. Best, M. Razavet, X. M. Liu, C. J. Pickett, *J. Am. Chem. Soc.* **2004**, *126*, 16988 – 16999.

11 J. O. Daiss, K. A. Barth, C. Burschka, P. Hey, R. Ilg, K. Klemm, I. Richter, S. A. Wagner, R. Tacke, *Organometallics* **2004**, *23*, 5193–5197.

12 COLLECT, Data Collection Software; Nonius B. V., The Netherlands, **1998**.

13 Otwinowski, Z.; Minor, W. *Methods Enzymol.* **1997**, *276*, 307–326.

14 Sheldrick, G. M. *Acta Cryst. Sect. A* **2008**, *64*, 112–122.

Sterically Demanding Silicon containing Ligands in [FeFe] Hydrogenase Models

Ulf-Peter Apfel,[a] **Manfred Rudolph,**[a] **Joachim Kübel,**[a] **Helmar Görls,**[a] **and Wolfgang Weigand*[a]**
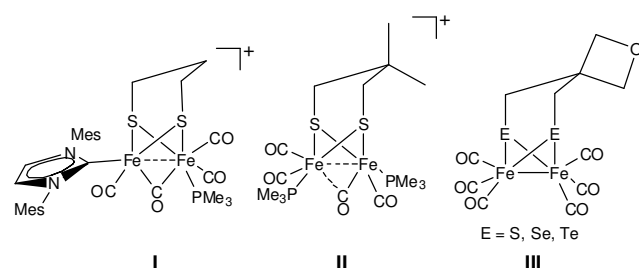
In order to increase the sterical demand to the [Fe2S2] unit, which should favour a "rotated" state in the Fe^IFe^{II} or the Fe^IFe^0 level, bis(mercaptomethyl)diphenylsilane (**1**), bis(benzylthio)dimethylsilane (**2**) and bis(benzylthio)diphenylsilane (**6**) was reacted with 10 $Fe_3(CO)_{12}$. The obtained complexes $[(C_{14}H_{14}SiS_2)Fe_2(CO)_6]$ (**7**), $[(C_{16}H_{18}SiS_2)Fe_2(CO)_6]$ (**8**) and $[(C_{26}H_{22}SiS_2)Fe_2(CO)_6]$ (**9**) were investigated according to their spectroscopic, structural and catalytical properties. Furthermore substitution reactions of CO with PPh_3 (**10-12**) and PMe_3 (**13-17**), were carried out with these complexes to increase the sterical demand of the [Fe2S2] subsite further. The properties of these complexes will be displayed and compared to the unsubsited 15 $Fe_2(CO)_6$ complex fragments. Cyclic voltammetry of **7-17** exhibit electrocatalytic activity towards development of dihydrogen.
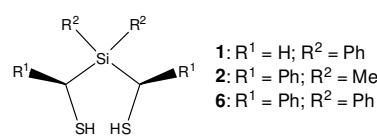
Introduction

Since the discovery of the structure of the [FeFe] hydrogenase active site,[1] tremendous effort can be seen towards mimicking 20 the properties of the enzyme and the so called "rotated state" is an important feature of the enzyme.[2] This state provides a vacant coordination site, a bridging or semibridging CO ligand and is stabilized by the enzymatic environment.[1] It is suggested that the enzym forms terminal hydrides, which 25 seems to play a crucial role during the catalytic development of dihydrogen.[3] Rauchfuss *et al.* pictured out the importance of a terminal hybrid, since these complexes exhibit reduction at more positive potentials compared to related μ-H species.[4] Recently, Darensbourg *et al.* described the synthesis of model 30 complexes **I** and **II** (Scheme 1), replicating the mixed-valence H_{ox} state with a rotated iron site.[5,6] In contrast to the Fe^IFe^I state,**Fehler! Textmarke nicht definiert.** the Fe^IFe^{II} system reveals a

Scheme 1. Recent model complexes **I** - **III** revealing a rotated state in the oxidized form.

vacant coordination site and a semi-bridging CO ligand. It is assumed that especially in case of **II** the sterical demand of 35 the S-to-S linker and the establishement of assymetrical bisphosphine complexes stabilizes the oxidized form.[7] However, a recent study on [Fe2E2] complexes **III** (E = S, Se, Te) (Scheme 1) revealed that reduction and/or oxidation also lead to the "rotated state" in the absence of phosphines and a

40 marginally larger S-to-S linker than compared to **II**.[8] Likewise, the necessity of sulphur as bridgehead atom was emphasized, as DFT calculations revealed a mindered ability for selenium and tellurium complexes to form structures with rotated $Fe(CO)_3$ fragments.

45 Furthermore investigations on silicon containing [Fe2S2(Si)] complexes exhibit different structural and electrochemical behaviour[9] compared to $Fe_2(CO)_3(pdt)$ [pdt = $S(CH_2)_3S$].[10] Following our continued interest on [Fe2S2(Si)] cluster compounds, sterically high demanding ligands 50 bis(mercaptomethyl)-diphenylsilane (**1**), bis(benzylthio)-dimethylsilane (**2**) and bis(benzylthio)diphenylsilane (**6**) were synthesized (Scheme 2). These compounds were reacted with $Fe_3(CO)_{12}$ to afford the hexacarbonyl complexes **7-10**. Additionally, the synthesis of the triphenylphosphine 55 complexes **10-12** and trimethylphosphine complexes **13-17** will be described. Furthermore, the electrocatalytic properties of **7-17** will be studied and displayed.

Scheme 2. Dithiol compounds **1,2** and **6**.

Results and discussion

60 ### Synthesis and Characterization of the ligands

In order to force a distorted geometry and to avoid "flipping" of the S-to-S linker in the [Fe2S2] clusters the sterical bulky compounds, bis(mercaptomethyl)-diphenylsilane (**1**),[11] *meso*-bis(benzylthio)-dimethylsilane (**2**)[12] and *meso*-65 bis(benzylthio)diphenylsilane (**6**) were synthesized. Compounds **1** is well described in literature.[11] The first is easily accessible from dichlorodiphenylsilan *via* standard procedures.[11] To obtain compounds **2** and **6**, a comparable
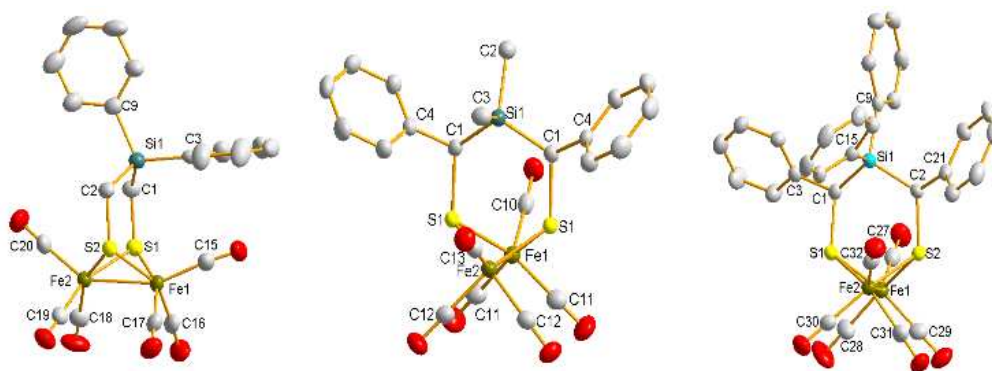
Figure 1. Molecular structures of **7** (left), **8** (middle) and **9** (right) (50% probability). Hydrogen atoms are omitted for clarity.
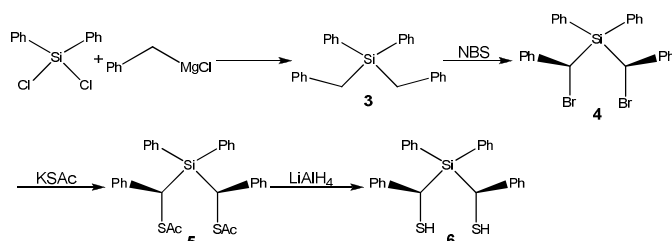
Scheme 3. Synthesis of *meso*-bis(benzylthio)diphenylsilane (**6**).
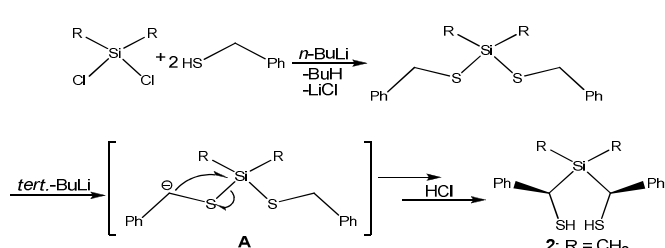
Scheme 4. Synthesis of **2** and **6** via double Wittig-rearrangement.

route was choosen (cf. Scheme 3). However, attempts to prepare compound **2** according to Scheme 3 failed as the two stereo centers entails problems of purifying the resulting stereoisomers. In comparison, compound **6** was accesible *via* this route. Reaction of dichlordiphenylsilan and benzyl-magnesiumchlorid afforded the coresponding dibenzyldiphenylsilane **3** in 82% yield.[13] Amazingly, the following conversion of **3** to **4** with *N*-bromsuccinimid (NBS) afforded exclusively the *meso*-form in 25% yield.[14] The conversion of compound **4** to **5** was the crucial point and only a small amount (18% yield) of **5** was obtained. Finally, compound **5** was reacted with lithium aluminium hydride to afford compound **6**. The overall-yield for this four steps was very low (~1%). Therefore compound **2** and **6** were synthesized according to the procedure described by Zubieta *et al.* (Scheme 4).[12] Thereby, the dichlorsilane component was reacted with benzylmercaptane in the presence of *n*-butyllithium, whereas compound **A** was generated. *In situ* treatment of **A** with *tert.*-butyllithium afforded **2** and **6** as mixtures of the *d,l*- and *meso*-forms. Crystalization from hexane exclusively yield the *meso*-forms. Since compound **6** is not discribed in literature, the absolut configuration was established by single crystal X-ray analyisis, as depicted in Figure 2, and further confirms *meso*-**6**. All three compounds were entirely analysed by NMR techniques, mass spectrometry and elemental analysis.

Synthesis and characterization of the hexacarbonyl-diiron complexes (7-9)

Reaction of Fe$_3$(CO)$_{12}$ and bis(mercaptomethyl)-diphenylsilane (**1**), *meso*-bis(benzylthio)-dimethylsilane (**2**) and *meso*-bis(benzylthio)diphenylsilane (**6**) in refluxing

Figure 2. Molecular structure of compound **6** (50% probability). Aromatic and methine hydrogen atoms are omitted for clarity.
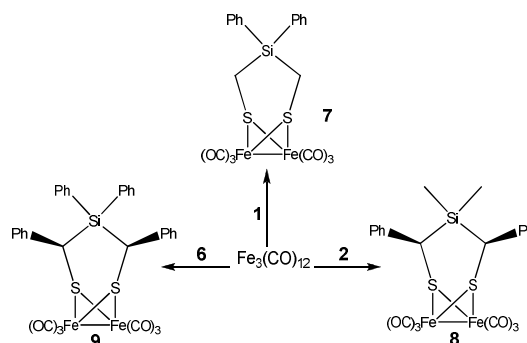
Scheme 5. Synthesis of complexes **7-9**.

toluene afforded the corresponding [Fe2S2] cluster complexes **7-9** within 2 hours in moderate yield (44-64%) (Scheme 5). Compounds **7-9** were characterized *via* ^{1}H, ^{13}C, HSQC, ^{1}H,^{1}H-COSY spectra, as well as elemental analysis and mass spectrometry. Crystals, suitable for the single crystal X-ray analysis were obtained by slow evaporation of a solution of **7** and **8**, dissolved in pentane, or by cooling of **9** dissolved in
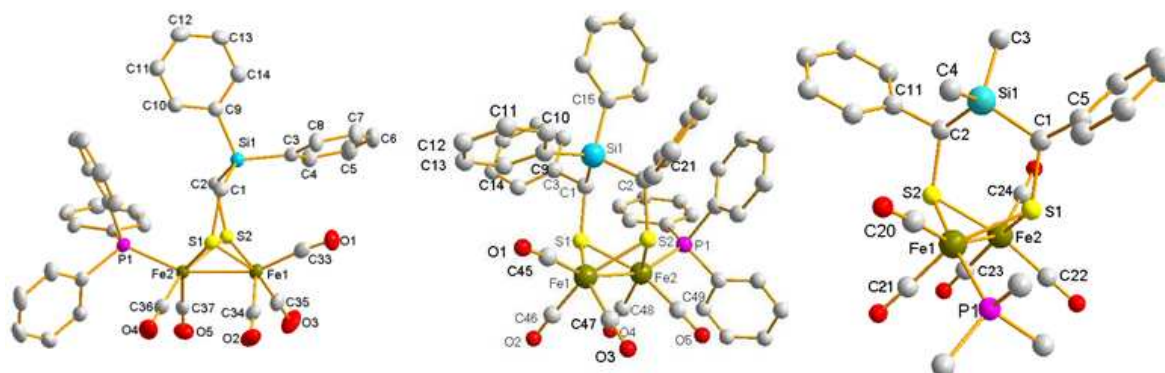
Figure 3. Molecular structures of **10** (left), **12** (middle) and **14** (right) (50% probability). Hydrogen atoms are omitted for clarity.

acetonitrile to -20°C. All three complexes exhibit the basic [Fe2S2] core with a "butterfly arrangement", whereas the iron atoms suggest octahedral geometry and are coordinated by six carbonyl groups and the silicon containing S-to-S linker (Figure 1). Since the distance of the equatorial phenyl-ring to the atom O(1) is only 339.9 pm in average, a π-interaction between the carbonyl group and the phenyl-ring can be assumed. However, IR studies exhibit no significant shift. Similiar behaviour is found for compound **9**. As reported for similar [Fe2S2(Si)] complexes the bonding angles S-C-Si of all three complexes differ rigorously from the expected angle of 109.45° (Table **1**).[9] Nevertheless compound **9** reveals different geometry features as **7** and **8**. In compound **7** and **8**, both S-C-Si bonds offer bonding angles which are the same within the standard deviation. Compound **9** exhibits two totaly different bonding angles (Table 1). As S(2)-C(2)-Si(1) reveals the expected bonding angle of 120°, S(1)-C(1)-Si(1) is strikingly decreased to 113°.

sterical bulky S-to-S linker and two phosphhines to the [Fe2S2] subsite should favour a "rotated state" of the distal iron centre.[6] Therefore it is intimating to implement phosphines (PMe₃ and PPh₃) into the rigid and bulky complexes **7-9**. The introduction of the phosphines followed the standard procedures, described in literature.[15] Thereby the complex is treated with trimethylamine-*N*-oxide and the particular phosphine to form the phosphine complexes. However, even the treatment with 2, 3, 4 or more eqivalents of trimethylamine-*N*-oxide and phosphine only lead to the

7: R¹ = H; R² = Ph
8: R¹ = Ph; R² = Me
9: R¹ = Ph; R² = Ph

10: R¹ = H; R² = Ph; R' = Ph
11: R¹ = Ph; R² = Me; R' = Ph
12: R¹ = Ph; R² = Ph; R' = Ph
13: R¹ = H; R² = Ph; R' = Me
14: R¹ = Ph; R² = Me; R' = Me
15: R¹ = Ph; R² = Ph; R' = Me
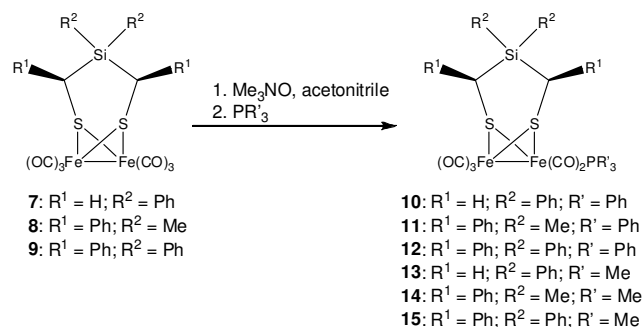
Scheme 6. Synthesis of the PR₃ substituted complexes **10-15**.

formation of the monosubstituted phosphine complexes **10-15** in moderate yields (42 - 53 %) (Scheme 6). The complexes were confirmed by ¹H, ¹³C, ³¹P NMR, IR as well as mass spectrometry and elemental analysis. Crystals of compounds **10**, **12**, **13** (see Figure S1) and **14**, suitable for the single crystal X-ray analysis were obtained by diffusion of pentane into a solution of the respective complex dissolved in chloroform (Figure 3). Whereas complexes **10** and **12** exhibit an apical coordiantion mode of the triphenylphosphine ligand, complex **13** and **14** picture out a basal conifguration of the trimethylphosphine ligand in the solid state. However, in solution (chloroform) both, basal and apical configuration can be observed, visible by two signal sets in the ³¹P NMR spectra. In contrast to **7-9**, the Fe-Fe distances for all compounds are slightly decreased and the Fe-S distances of **10**, **12** and **13** diverge vigorously. Yet, the bonding angles (S-C-Si) differ eminently, which was already observed for compound **9** (Table 2). A similiar π-interaction as discussed for complexes **7** and **9** can be assumed for complexes **10** and **12**. The distance between the oxygen atom of the neighboured

Bond length [pm]			
	7	**8**	**9**
Fe(1)-Fe(2)	249.99(6)	253.27(8)	251.23(6)
Fe(1)-S(1)	225.77(9)	225.27(8)	225.76(9)
Fe(1)-S(2)	226.10(8)	-	226.14(8)
S(1)-C(1)	182.3(3)	184.0(3)	186.0(3)
S(2)-C(2)	181.8(3)	-	184.3(3)
C(1)-Si(1)	187.3(3)	189.1(3)	188.2(3)
C(2)-Si(1)	186.5(3)	186.7(4)	190.9(3)
C(1)-C(4)	-	151.1(4)	-
C(1)-C(3)	-	-	152.0(4)
C(2)-C(21)	-	-	152.7(4)
Bond angle [°]			
S(1)-Fe(1)-S(2)/S(1)	88.02(3)	87.51(4)	87.10(3)
Fe(1)-Fe(2)-S(1)	56.56(2)	55.93(2)	56.94(2)
S(1)-C(1)-Si(1)	119.62(16)	118.48(15)	113.06(15)
S(2)-C(2)-Si(1)	119.13(15)	-	120.21(14)
C(3)-C(1)-Si(1)	-	-	121.5(2)

Table 1. Selected bond lengths and angles of compound **7**, **8** and **9**.

Synthesis and characterization of the PR'₃ mono substituted diiron complexes (10-15)

As Darensbourg *et al.* pictured out, the introduction of a

C≡O and the adjacent phenylring is only 373.6 pm for **10** and 334.8 pm for **12**, respectively.

	Bond length [pm]			
	10	**12**	**13**	**14**
Fe(1)-Fe(2)	252.0	250.47(8)	254.29(8)	255.18(8)
Fe(1)-S(1)	225.7	229.13(12)	227.20(12)	225.64(11)
Fe(1)-S(2)	228.9	225.87(11)	223.50(12)	224.82(11)
S(1)-C(1)	182.8	184.3(4)	182.7(4)	185.1(4)
S(2)-C(2)	182.7	184.4(4)	182.0(4)	1850(4)
C(1)-Si(1)	187.1	184.3(4)	185.3(4)	189.2(4)
C(2)-Si(1)	185.9	190.4(4)	187.5(4)	188.3(4)
Fe(1)/Fe(2)-P(1)	225.1	224.76(12)	222.60(13)	223.55(11)
	Bond angle [°]			
S(1)-Fe(1)-S(2)	86.26(3)	85.54(4)	88.15(4)	87.96(5)
S(1)-Fe(2)-S(2)	85.89(3)	85.63(4)	87.54(4)	87.13(4)
Fe(1)-Fe(2)-S(1)	55.64(2)	57.07(3)	55.81(3)	55.78(3)
P(1)-Fe(2)/Fe(1)-S(1)	112.41(3)	110.03(4)	86.25(4)	86.65(4)
S(1)-C(1)-Si(1)	121.31(14)	114.8(2)	115.6(2)	116.0(2)
S(2)-C(2)-Si(1)	115.37(14)	118.0(2)	121.4(2)	117.77(18)

Table 2. Selected bond lengths and angles of compounds **10**, **12**, **13** and **14**.

Synthesis and characterization of the disubstituted diiron complex (16-17)

Since reactions with trimethyl-*N*-oxide afforded mono-substituted products, compounds **8** and **9** were treated with a distinct (7 - 28 molar equivalents) excess of trimethylposphine under refluxing conditions for 48 hours (Scheme 7).[6] Complexes **16** and **17** were obtained in 49 % and 34 %, respecitvely as dark red substances and were confirmed by ^{1}H, ^{13}C, ^{31}P NMR, IR as well as mass spectrometry. It is notable,
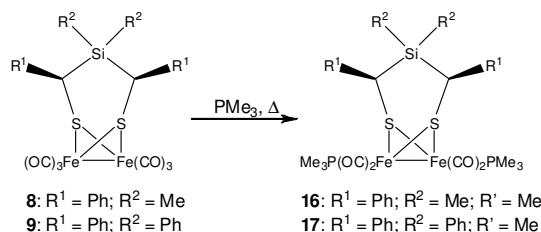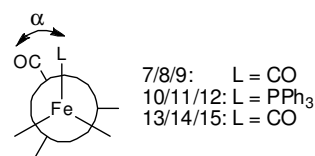
Scheme 7. Synthesis of the disubstituted complexes **16** and **17**.

8: R¹ = Ph; R² = Me
9: R¹ = Ph; R² = Ph

16: R¹ = Ph; R² = Me; R' = Me
17: R¹ = Ph; R² = Ph; R' = Me

that in both cases the CO vibrations appeared below 2000 cm⁻¹. Furthermore, "flipping" of the S-to-S linker is prevented, visible by two well seperated methyl-proton sets in compound **16**. For compound **16** and **17** ^{31}P{^{1}H} NMR exhibits two doublets for an apical and a basal position of the trimethylphosphine groups.

Sterical demand and rotated state

Since the S-to-S linker is partly flexible, the sterical demand is characterizable by the torsion angle α between C-Fe-Fe-L (Scheme 8). The different torsion angles of **7-10**, **12**, **13** and **14** are listed in Table 3. The torsion angle α increases from **8** to **7** and even more to compound **9**. It is somehow fascinating

that even in absence of a phsophine ligand the tilt of the iron center is already 18.03°.

Scheme 8. Torsion angle α in dependence on L (view along the Fe-Fe bond).

7/8/9: L = CO
10/11/12: L = PPh₃
13/14/15: L = CO

	Torsion angle α [°]
7	4.13
8	0
9	18.03
10	29.96
12	7.21
13	26.20
14	11.61
(μ-pdt){Fe(CO)₂PMe₃}₂[6]	29

Table 3. Torsion angles α(OC-Fe-Fe-L) of complexes **7-10**, **12** and **14**.

Yet, substitution of one C≡O ligand with trimethylphosphane shows two different effects. In case of complex **10** the introduction of one PPh₃ forces an unsymetrical distortion of the S-to-S linker and leads to a 16° increased torsion angle α of ~30°, which is comparable to (μ-dpdt){Fe(CO)₂PMe₃}₂.[6] In contrast complex **12** exhibit an ~11° reduced torsion angle α. When introducing PMe₃ an increase of α is observed. In case of complex **13** α was increased to ~26°. However, a smaller tilt of the Fe-Fe bond in **14** was observed. Unlike the system described by Darensbourg *et al*,[16] crystal structure analysis of compound **10** reveals a significant distortion of the S-to-S linker.

Trials to oxidize complexes **7-17** with ferrocenoyl hexafluorophosphate under argon atmosphere at -78°C reveal no change of the IR spectra, which means that the rotated state is not stabilized for such complexes. In contrast, reduciton with Na/Hg according to literature procedure[9] afforded new IR bands at 1790 cm⁻¹, which can be assigned to a bridging C≡O ligand .

Electrochemistry

Conclusions

Experimental

General procedures

Solvents for the syntheses were first dried over KOH and distilled from sodium/benzophenone. Chemicals were used as received from Fluka and Acros without further purification. Thin Liquid Chromatoraphie (TLC): *Merck* silica gel 60 F₂₅₄ plates; detection under UV light at 254 nm. FC (flash

chromatographie): *Fluka* silica gel 60. ^{1}H-, ^{13}C-NMR spectra were recorded on a *Bruker 200 MHz* or *400 MHz*. IR spectra were recorded on a *Perkin-Elmer 2000 FT-IR*. All reactions were carried out under argon atmosphere. Bis(mercaptomethyl)diphenylsilane (**1**) was prepared according literature procedures.[11]

Synthesis of Bis(benzylthio)dimethylsilane (2)

10 g (0.08 mol) Benzylmercaptane were dissolved in 100 mL THF and cooled to 0°C. Subsequently, 32.2 ml (0.08 mol) *n*-butyllithium (2.5 mol/L in hexane) were added dropwise, whereby the solution recolors orange. To this solution 5.2 g (0.04 mol) dimethyldichlorsilan were added slowly and the solution was stirred for additional 23 hours at room temperature, whereupon a white precipitate was formed. Afterwards the solution was cooled to -78°C and 50 mL (0.08 mol) *tert*-butyllithium (1.6 mol/L in pentane) were added. After 24 hours the orange suspension was cooled to 0°C and acidified with 2N HCl to pH = 4. The organic solvents were removed under reduced pressure and the residue extracted 3x 100 mL dichloromethane. The combined organic fractions were extracted with water, dried with sodium sulfate and evaporated to dryness. Crystallization from hexane afforded 2.6 g (21%) bis(benzylthio)dimethylsilane (**2**) as white solid. Found: C, 63.2; H, 6.6; S, 21.2. $C_{16}H_{20}S_2Si$ requires C, 63.1; H, 6.6; S, 21.1%; δH(200 MHz; CDCl$_3$) 7.29-7.10 (10H, m, CH$_{aromatic}$), 3.35 (2 H, d, *J* 7.8, CH), 1.87 (2H, d, *J* 7.8, SH), 0.30 (3H, s, CH$_3$-a), -0.15 (3H, s, CH$_3$-b). δC(50 MHz; CDCl$_3$) 142.6, 128.3, 127.6, 125.9 (CH$_{aromatic}$), 28.6 (CH), -6.5 (CH$_3$-b), -7.1 (CH$_3$-a). *m/z* (DEI) 304 (M$^+$), 271 (M-SH), 237 (M-2SH).

Synthesis of Dibenzyldiphenylsilane (3)

In 50 mL dry diethylether, 3.84 g (0.16 mmol) fine grounded magnesium were suspended and under rigorous stirring 20g (0.16 mmol) benzylchlorid were added. The suspension was refluxed until no magnesium remained (usually 1.5 hours). This solution was added to a solution of 20 g (0.08 mol) diphenyldichlorsilane dissolved in 100 mL toluene, whereupon a white precipitate was formed. The diethylether was distilled off and the remaining suspension stirred under refluxing toluene for additional 20 hours. Afterwards the precipitate was filtered off and the solution was evaporated to dryness and washed several times with ethanol, which affords 23.9 g (82%) of a colourless oil (crystallizes at -20°C). (Found: C, 85.2; H, 6.8;. $C_{26}H_{24}Si$ requires C, 85.6; H, 6.6; Br, 30.6%); δH(200 MHz; CDCl$_3$) 7.56-6.81 (20H, m, CH$_{aromatic}$), 2.63 (4 H, s, CH$_2$). δC(50 MHz; CDCl$_3$) 138.3, 135.4, 134.9, 134.4, 129.5, 129.0, 127.9, 127.6, 124.4 (CH$_{aromatic}$), 22.3 (CH$_2$). *m/z* (DEI) 364 (M$^+$), 273 (M-toluene).

Synthesis of Bis(α-brombenzyl)diphenylsilane (4)

To a solution of 23.85 g (0.065 mmol) dibenzyldiphenylsilane (**3**) in 150 mL tetrachlorocarbon, 23.3 g (0.13 mmol) *N*-bromsuccinimid and 100 mg (0.4 mmol) dibenzoylperoxide were added. Within 5 hours stirring under reflux conditions, the colour changed to pale yellow and a precipitate was observed. Filtration and removing of the solvent under reduced pressure revealed the crude product. Crystallization from ethanol afforded 8.3 g (25%) of *meso*-bis(α-brombenzyl)diphenylsilane (**4**) (Found: C, 59.7; H, 4.1; Br, 30.3. $C_{26}H_{22}Br_2Si$ requires C, 59.8; H, 4.2; Br, 30.6%); δH(200 MHz; CDCl$_3$) 7.75-7.04 (20H, m, CH$_{aromatic}$), 4.95 (2 H, s, CH). δC(50 MHz; CDCl$_3$) 138.2, 137.6, 130.7, 129.5, 128.1, 127.5, 127.4, 127.3 (CH$_{aromatic}$), 39.9 (CH). *m/z* (DEI) 441 (M-Br), 361 (M-2Br).

Synthesis of Bis(α-acetylthiobenzyl)diphenylsilane (5)

Bis(α-brombenzyl)diphenylsilane (**4**) (4.5 g, 8.65 mmol) and 8.9 g (26 mmol) potassium thioacetate were suspended in 150 mL THF and refluxed for 6 hours, followed by filtration and removal of the solvent under reduced pressure. The remaining oil was dissolved in 100 mL dichloromethane and extracted 2 times with 100 mL water. The aqueous fraction was extracted with dichloromethane until the organic phase appears colourless. After combining the organic phases and drying with sodium sulfate, the solvent was removed under reduced pressure. Purification *via* column chromatography (dichloromethane: hexane = 2:1; R$_f$ = 0.32) afforded 810 mg (18%) of the desired product and was used without further purification. δH(200 MHz; CDCl$_3$) 7.54-6.87 (20H, m, CH$_{aromatic}$), 4.65 (2 H, s, CH), 2.23 (6H, s, CH$_3$). δC(50 MHz; CDCl$_3$) 193.8 (C(O)S), 139.6, 136.8, 136.4, 130.6, 129.2, 127.9, 127.6, 126.3 (CH$_{aromatic}$), 31.6 (CH$_3$), 30.2 (CH).

Synthesis of Bis(benzylthio)diphenylsilane (6)

Method A: To a solution of 810 mg (1.58 mmol) bis(α-acetylthiobenzyl)diphenylsilane (**5**) dissolved in 40 mL diethylether, 304 mg (8 mmol) LiAlH$_4$ was added in once at 0°C. The suspension was stirred for additional 1.5 hours at 0°C and 23 hours at room temperature. The mixture was cooled to 0°C again and 20 mL of a 2 N solution HCl$_{aq}$ were added dropwise, followed by addition of 50 mL water. Extraction with 3x150 mL dichloromethane, drying with sodium sulfate and removing of the solvent under reduced pressure afforded the crude product. After crystallization from hexane, 225 mg (33%) bis(benzylthio)diphenylsilane (**6**) were obtained as white solid.

Method B: 10 g (0.08 mol) Benzylmercaptane were dissolved in 100 mL THF and cooled to 0°C. Subsequently, 32.2 ml (0.08 mol) *n*-butyllithium (2.5 mol/L in hexane) were added dropwise, whereby the solution recolors orange. To this solution 10.1 g (0.04 mol) diphenyldichlorsilan were added slowly and the solution was stirred for additional 23 hours at room temperature, whereupon a white precipitate was formed. Afterwards the solution was cooled to -78°C and 50 mL (0.08 mol) *tert*-butyllithium (1.6 mol/L in pentane) was added. After 24 hours the orange suspension was cooled to 0°C and acidified with 2N HCl to pH = 4. The organic solvents were removed under reduced pressure and the residue extracted

3x 100 mL dichloromethane. The combined organic fractions were extracted with water, dried with sodium sulfate and evaporated to dryness. Crystallization from hexane afforded 10.5 g (61%) of **6** as white solid.Found: C, 72.4; H, 5.7; S, 14.6. $C_{26}H_{24}S_2Si$ requires C, 72.9; H, 5.6; S, 14.9%; δH(400 MHz; CDCl$_3$) 7.58-6.98 (20H, m, CH$_{aromatic}$), 3.89 (2 H, d, J 9.6, CH), 1.87 (2H, d, J 9.6, SH). δC(100 MHz; CDCl$_3$) 141.7, 137.6, 130.6, 130.3, 128.7, 127.9, 127.7, 127.2, 126.1 (CH$_{aromatic}$), 26.4 (CH). m/z (DEI) 428 (M$^+$).

Synthesis of [(C$_{14}$H$_{14}$SiS$_2$)Fe$_2$(CO)$_6$] (7)

In 30 mL toluene, 100 mg (0.36 mmol) bis(mercaptomethyl)diphenylsilane (**1**) and 183 mg (0.36 mmol) Fe$_3$(CO)$_{12}$ were dissolved and stirred under reflux for 2 hours. After evaporation to dryness the crude product was purified *via* flash chromatography (THF:hexane = 1:3) to afford 125 mg (63%) of a red solid (Found: C, 43.5; H, 2.7; S, 11.2. $C_{20}H_{14}S_2SiFe_2O_6$ requires C, 43.3; H, 2.6; S, 11.6%; δH(200 MHz; CDCl$_3$) 7.36 (10H, m, CH$_{aromatic}$), 2.28 (4 H, s, CH$_2$). δC(50 MHz; CDCl$_3$) 206.9 (CO), 134.7, 132.7, 130.6, 128.6 (CH$_{aromatic}$), 3.9 (CH). m/z (DEI) 554 (M$^+$), 526 (M-CO), 498 (M-2CO), 470 (M-3CO), 442 (M-4CO), 414 (M-5CO), 386 (M-6CO); ν_{max}(KBr)/cm^{-1} 3069w, 3027w, 3001w, 2891w, 2073vs, 2033vs, 1996vs, 1979vs, 1486w, 1428m).

Synthesis of [(C$_{16}$H$_{18}$SiS$_2$)Fe$_2$(CO)$_6$] (8)

100mg (0.33 mmol) Bis(benzylthio)dimethylsilane (**2**) and 166 mg (0.33 mmol) Fe$_3$(CO)$_{12}$ were dissolved in 80 mL toluene and refluxed for 2 hours. After evaporation to dryness and purification *via* flash chromatography (THF:hexane = 1:6) 85 mg (44%) of a red solid were obtained (Found: C, 45.9; H, 3.6; S, 11.5. $C_{22}H_{18}S_2SiFe_2O_6$ requires C, 45.4; H, 3.1; S, 11.0%; δH(200 MHz; CDCl$_3$) 7.26 (10H, m, CH$_{aromatic}$), 2.77 (2 H, s, CH), -0.10 (3H, s, CH$_3$-a), -0.14 (3H, s, CH$_3$-b). δC(50 MHz; CDCl$_3$) 207.3 (CO), 140.8, 128.6, 128.1, 126.6 (CH$_{aromatic}$), 32.9 (CH), -2.2 (CH$_3$), -7.3 (CH$_3$). m/z (DEI) 582 (M$^+$), 526 (M-2CO), 498 (M-3CO), 470 (M-4CO), 442 (M-5CO), 414 (M-6CO). ν_{max}(KBr)/cm^{-1} 3082w, 3061w, 3022w, 2963w, 2930w, 2072vs, 2030vs, 2002vs/br, 1493w, 1449m).

Synthesis of [(C$_{26}$H$_{22}$SiS$_2$)Fe$_2$(CO)$_6$] (9)

Bis(benzylthio)diphenylsilane (**6**) (200mg, 0.47 mmol) and 239 mg (0.47 mmol) Fe$_3$(CO)$_{12}$ were dissolved in 50 mL toluene and stirred under reflux for 2 hours. Evaporation, purification via column chromatography (THF:hexane = 1:6) afforded 97 mg (64%) of a red powder (Found: C, 57.7; H, 4.0; S, 8.3. $C_{32}H_{22}S_2SiFe_2O_6$ 0.9 hexane requires C, 57.3; H, 4.4; S, 8.2%; δH(200 MHz; CDCl$_3$) 7.35 (20H, m, CH$_{aromatic}$), 3.59 (2 H, s, CH). δC(50 MHz; CDCl$_3$) 207.5, 206.7 (CO), 139.7, 139.0, 135.3, 133.7, 130.6, 130.2, 128.4, 128.1, 127.4, 126.4, 125.6 (CH$_{aromatic}$), 34.4 (CH). m/z (DEI) 706 (M$^+$), 650 (M-2CO), 622 (M-3CO), 594 (M-4CO), 566 (M-5CO), 538 (M-6CO). ν_{max}(KBr)/cm^{-1} 3069w, 3027w, 2927w, 2856w, 2073vs, 2033vs, 1999vs/br, 1596, 1491, 1428).

Synthesis of [(C$_{14}$H$_{14}$SiS$_2$)Fe$_2$(CO)$_5$PPh$_3$] (10)

To a solution of [(C$_{14}$H$_{14}$SiS$_2$)Fe$_2$(CO)$_6$] (**9**) (50 mg, 0.09 mmol) in 20 mL acteonitrile, 2 eq. trimethylamine-*N*-oxide dihydrate (20 mg, 0.18 mmol) were added and stirred 10 minutes at room temperature, whereupon the solution coulors dark red. Subsequently, 2 eq. triphenylphosphine (48 mg, 0.18 mmol) were added and stirred for 5 hours at room temperature. Removal of the solvent under reduced pressure and flash chromatography (THF:hexane = 1:3) yield in 37 mg (52%) of compound **12** (Found: C, 55.7; H, 3.9; S, 8.3. $C_{37}H_{29}S_2SiFe_2O_5$ requires C, 56.4; H, 3.9; S, 8.1%; δH(200 MHz; CDCl$_3$) .64-7.03 (25H, m, CH$_{aromatic}$), 2.04 (2 H, s, CH$_2$-a) , 1.98 (2 H, s, CH$_2$-b). δC(50 MHz; CDCl$_3$) 213.3, 208.6 (CO), 135.6, 134.9, 134.8, 134.3, 133.7, 133.5, 130.1, 129.7, 128.5, 128.4, 128.3, 127.9 (CH$_{aromatic}$), 30.3 (CH). δP(81 MHz, CDCl$_3$) 67.6 (P$_{apical}$), 47.1 (P$_{basal}$); m/z (FAB) 788 (M$^+$), 760 (M-CO), 732 (M-2CO), 704 (M-3CO), 676 (M-4CO), 648 (M-5CO). ν_{max}(KBr)/cm^{-1} 3069w, 3027w, 2931w, 2893w, 2044vs, 1986vs/br, 1924s/br, 1482, 1434).

Synthesis of [(C$_{16}$H$_{18}$SiS$_2$)Fe$_2$(CO)$_5$PPh$_3$] (11)

To a solution of 102 mg (0.18 mmol) [(C$_{16}$H$_{18}$SiS$_2$)Fe$_2$(CO)$_6$] (**8**), dissolved in 10 mL acetonitrile, 39 mg (0.35 mmol) trimethylamine-*N*-oxide were added and after 15 minutes stirring at room temperature 92 mg (0.35 mmol) triphenylphosphine were added in once. The solution was stirred for additional 6 days at room temperature, followed by evaporation to dryness and purification via FC (THF : hexane = 1:3) to yield 69 mg (47%) of compound **11** as a red solid. (Found: C, 60.9; H, 5.0; S, 7.4. $C_{22}H_{18}S_2SiFe_2O_6$ hexane requires C, 59.9; H, 5.3; S, 7.1%; δH(400 MHz; CDCl$_3$) 7.87-7.12 (25H, m, CH$_{aromatic}$), 3.94 (2 H, s, CH-basal), 2.78 (2 H, s, CH-apikal), 0.39 (3H, s, CH$_3$-basal), -0.17 (3 H, s, CH$_3$-apikal), -0.21 (3 H, s, CH$_3$-a), -0.44 (3 H, s, CH$_3$-b). δC(100 MHz; CDCl$_3$) 141.2, 134.0, 133.9, 132.3, 132.2, 131.5, 130.1, 128.5, 128.4, 128.2, 128.1, 128.0, 125.8 (CH$_{aromatic}$), 34.2 (CH), -1.7 (CH$_3$-b), -6.4 (CH$_3$-a). δP(81 MHz, CDCl$_3$) 66.3 (P$_{apical}$), 47.1 (P$_{basal}$); m/z (DEI) 816 (M$^+$), 760 (M-2CO), 676 (M-5CO), 414 (M-5CO-PPh$_3$). ν_{max}(KBr)/cm^{-1} 3061w, 3028w, 2962w, 2926w, 2850w, 2037vs, 1982vs, 1956vs, 1924s, 1482, 1436).

Synthesis of [(C$_{26}$H$_{22}$SiS$_2$)Fe$_2$(CO)$_5$PPh$_3$] (12)

[(C$_{26}$H$_{22}$SiS$_2$)Fe$_2$(CO)$_6$] (**9**) (100 mg, 0.14 mmol) and 32 mg (0.19 mmol) trimethylamine-*N*-oxide were dissolved in 20 mL acetonitrile, wherupon the colour changed to dark red. After 5 minutes stirring at room temperature, 75 mg (0.29 mmol) triphenylphosphine were added and the solution stirred for additional 6 days. Removal of the solvent and purification *via* FC (THF : hexane = 1:3) afforded 57 mg (42%) of compound **12**. (Found: C, 63.9; H, 4.8; S, 6.6. $C_{49}H_{37}S_2SiPFe_2O_5$ requires C, 64.0; H, 4.9; S, 6.3%; δH(400 MHz; CDCl$_3$) 7.67-6.37 (35H, m, CH$_{aromatic}$), 1.40 (2 H, s, CH). δC(100 MHz; CDCl$_3$) 208.7 (CO), 140.5, 138.9, 135.4, 133.6, 133.5, 132.3, 132.2, 131.5, 130.3, 128.9, 128.8, 128.5, 128.4, 127.5, 127.3, 127.1, 125.6 (CH$_{aromatic}$), 29.4 (CH). δP(81 MHz, CDCl$_3$) 67.4

(P_{apikal}), 47.1 (P_{basal}); m/z (micro-ESI) 963.2 (M$^+$). ν_{max}(KBr)/cm^{-1} 3056m, 3024m, 2958m, 2925m, 2855w, 2043vs, 1987vs, 1933vs, 1598, 1482, 1435).

Synthesis of [(C$_{14}$H$_{14}$SiS$_2$)Fe$_2$(CO)$_5$PMe$_3$] (13)

In 10 mL acetonitrile 90 mg (0.16 mmol) [(C$_{14}$H$_{14}$SiS$_2$)Fe$_2$(CO)$_6$] (7) were dissolved and 36 mg (0.32 mmol) trimethylamin-N-oxide added, whereupon the solution became dark red. After 15 minutes stirring at room temperature 4 eq. trimethylphosphine (67 µL, 0.64 mmol) were added to the solution and stirred for 4 days. Removal of the solvent, purification via FC (THF : hexane = 1 : 4) and wahsing with a small amount of pentane yield 48 mg (50%) red solid. (Found: C, 46.0; H, 4.7; S, 10.2. C$_{22}$H$_{25}$S$_2$PSiFe$_2$O$_6$ 0.5 pentane requires C, 45.9; H, 4.9; S, 10.0%; δH(400 MHz; CDCl$_3$) 7.58-7.28 (10H, m, CH$_{aromatic}$), 2.68 (2 H, s,), 2.15(2 H, m, CH$_2$-a), 1.92 (2 H, m, CH$_2$-b), 1.42 (9 H, s, P(CH$_3$)$_3$); δC(100 MHz; CDCl$_3$) 210.2 (CO), 135.1, 134.6, 132.9, 130.3, 130.0, 129.9, 128.3, 128.2, 128.1 (CH$_{aromatic}$), 22.5 (CH$_2$-b) 19.3 ($^2J_{C-P}$ = 30 Hz, P(CH$_3$)$_3$), 5.3 (CH$_2$-a); δP(81 MHz, CDCl$_3$) 30.1 (P(CH$_3$)$_3$); m/z (DEI) 602 (M$^+$), 574 (M-CO), 546 (M-2CO), 518 (M-3CO), 490 (M-4CO), 462 (M-5CO), 386 (M-5CO-P(CH$_3$)$_3$). ν_{max}(KBr)/cm^{-1} 3070w, 3050w, 2963w, 2926w, 2864w, 2036vs, 1980vs, 1964vs, 1921s, 1428).

Synthesis of [(C$_{16}$H$_{18}$SiS$_2$)Fe$_2$(CO) $_5$PMe$_3$] (14)

To a solution of [(C$_{16}$H$_{18}$SiS$_2$)Fe$_2$(CO)$_6$] (8) (50 mg, 0.09 mmol) in 20 mL acetonitrile, 2 eq. trimethylamine-N-oxide dihydrate (19.1 mg, 0.18 mmol) were added and the accruing dark solution was stirred for 45 min, followed by the addition of 2 eq. trimethylphosphine (35.4 µL, 0.36 mmol). The resulting solution was stirred at room temperature until TLC (THF:hexane = 1:3) reveal no remaining starting material (usually 1h). The solvent was removed under reduced pressure and the residue was purified via FC (THF:hexane = 1:3) to yield 26 mg (46%) red solid. (Found: C, 45.4; H, 4.3; S, 10.0. C$_{24}$H$_{27}$S$_2$SiPFe$_2$O$_5$ requires C, 45.7; H, 4.3; S, 10.2%; δH(400 MHz; CDCl$_3$) 7.26 (10H, m, CH$_{aromatic}$), 2.78 (2 H, s, CH), 1.54 (9H, $^2J_{C-P}$ = 8 Hz, d, P(CH$_3$)$_3$), -0.09 (3H, s, CH$_3$-a), -0.21 (3H, s, CH$_3$-b). δC(100 MHz; CDCl$_3$) 213.3, 211.1, 210.2 (CO), 142.4, 128.3, 124.2 (CH$_{aromatic}$), 33.8 (CH), 19.5 ($^2J_{C-P}$ = 80 Hz, P(CH$_3$)$_3$), -1.9 (CH$_3$-b), -7.1 (CH$_3$-a); δP(81 MHz, CDCl$_3$) 29.8 (P$_{apikal}$), 25.8 (P$_{basal}$); m/z (DEI) 630 (M$^+$), 602 (M-CO), 574 (M-2CO), 546 (M-3CO), 518 (M-4CO), 490 (M-5CO), 414 (M-5CO-P(CH$_3$)$_3$). ν_{max}(KBr)/cm^{-1} 3059w, 3030w, 2968w, 2926w, 2857w, 2036vs, 1977vs/br, 1918vs, 1597, 1492, 1449).

Synthesis of [(C$_{26}$H$_{22}$SiS$_2$)Fe$_2$(CO)$_5$PMe$_3$] (15)

To a solution of [(C$_{26}$H$_{22}$SiS$_2$)Fe$_2$(CO)$_6$] (9) (100 mg, 0.14 mmol) in 20 mL acetonitrile, 2 eq. trimethylamine-N-oxide dihydrate (32 mg, 0.28 mmol) were added and the accruing dark solution was stirred for 15 min, followed by the addition of 2 eq. trimethylphosphine (59 µL, 0.57 mmol). The resulting solution was stirred at room temperature until TLC (THF:hexane = 1:3) reveal no remaining starting material (usually 4 days). The solvent was removed under reduced pressure and the residue was purified via FC (THF:hexane = 1:3) to yield 56 mg (53%) red solid. (Found: C, 55.1; H, 4.9; S, 7.4. C$_{34}$H$_{31}$S$_2$SiPFe$_2$O$_5$ 0.3hexane requires C, 55.2; H, 4.6; S, 8.2%; δH(400 MHz; CDCl$_3$) 7.23-7.05 (20H, m, CH$_{aromatic}$), 3.63 (2 H, s, CH), 1.47 (9H, s, P(CH$_3$)$_3$). δC(100 MHz; CDCl$_3$) 210.5, (CO), 140.9, 139.2, 135.3, 130.0, 129.6, 128.8, 128.2, 127.9, 127.7, 127.6, 126.9 (CH$_{aromatic}$), 33.9 (CH), 19.7 ($^2J_{C-P}$ = 30 Hz, P(CH$_3$)$_3$). δP(81 MHz, CDCl$_3$) 25.8. m/z (micro-ESI in CHCl$_3$/methanol) 776.8 (M+Na$^+$). m/z (FAB in nba) 754 (M$^+$), 670 (M-3CO), 642 (M-4CO), 614 (M-5CO), 538 (M-5CO-PMe$_3$); ν_{max}(KBr)/cm^{-1} 3066w, 2962w, 2923w, 2854w, 2036vs, 1982vs/br, 1921vs, 1599, 1491, 1428).

Synthesis of [(C$_{16}$H$_{18}$SiS$_2$)Fe$_2$(CO)$_4$(PMe$_3$)$_2$] (16)

To 98 mg (0.17 mmol) [(C$_{16}$H$_{18}$SiS$_2$)Fe$_2$(CO)$_6$] (8), dissolved in 100 mL toluene, 0.5 mL (4.85 mmol) trimethylphospine were added and resulting solution stirred for 48 hours under refluxing conditions. The solution was evaporated to dryness and the crude product was purified by FC (CH$_2$Cl$_2$:hexane = 1:2) to afford 56 mg (49%) of a dark red solid. (Found: C, 47.8; H, 5.8; S, 8.4. C$_{26}$H$_{36}$S$_2$SiP$_2$Fe$_2$O$_4$ 0.4hexane requires C, 47.9; H, 5.9; S, 9.0%; δH(200 MHz; CD$_2$Cl$_2$) 7.28-7.15 (10H, m, CH$_{aromatic}$), 2.82 (2 H, s, CH), 1.53 (9H, d, $^2J_{H-P}$ = 9 Hz, P(CH$_3$)$_3$-a), 1.49 (9H, d, $^2J_{H-P}$ = 8.6 Hz, P(CH$_3$)$_3$-b), -0.12 (3H, s, CH$_3$-a), -0.24 (3H, s, CH$_3$-b). δC(100 MHz; CD$_2$Cl$_2$) 216.6, 216.2 (CO), 128.8, 128.4, 125.8 (CH$_{aromatic}$), 33.1 (CH), 20.3 ($^2J_{C-P}$ = 33 Hz, P(CH$_3$)$_3$), 19.7 ($^2J_{C-P}$ = 34.9 Hz, P(CH$_3$)$_3$), -1.8 (CH$_3$-b), -6.4 (CH$_3$-a). δP(81 MHz, CD$_2$Cl$_2$) 30.9 (d, $^3J_{P-P}$ = 11.9 Hz, P$_{apical}$), 24.9 (d, $^3J_{P-P}$ = 11.9 Hz, P$_{basal}$). m/z (DEI) 678 (M $^+$), 650 (M-CO), 622 (M-2CO), 566 (M-4CO), 490 (M-4CO-PMe$_3$), 414 (M-4CO-2PMe$_3$); ν_{max}(KBr)/cm^{-1} 3060w, 3023w, 2954w, 2923m, 2852w, 1970m, 1940vs, 1899vs, 1597, 1492, 1421).

Synthesis of [(C$_{26}$H$_{22}$SiS$_2$)Fe$_2$(CO)$_4$(PMe$_3$)$_2$] (17)

To 101 mg (0.13 mmol) [(C$_{26}$H$_{22}$SiS$_2$)Fe$_2$(CO)$_6$] (9), dissolved in 40 mL toluene, 0.1 mL (0.97 mmol) trimethylphospane were added and resulting solution stirred for 48 hours under refluxing conditions. The solution was filtrated and evaporated to dryness. Washing with pentane and a small amount of dichloromethane yield 37 mg (34%) of a dark red oily residue after drying under high vacuum. No elemental analysis was obtained. NMR exhibit remaining solvent, which could not been fully removed. δH(400 MHz; CD$_2$Cl$_2$) 7.80-6.53 (20H, m, CH$_{aromatic}$), 3.68 (2 H, s, CH), 1.61 (9H, d, $^2J_{H-P}$ = 9.2 Hz, P(CH$_3$)$_3$-a), 1.55 (9H, d, $^2J_{H-P}$ = 8.8 Hz, P(CH$_3$)$_3$-b). δC(100 MHz; CD$_2$Cl$_2$) 215.9 (CO), 142.4, 139.3, 135.8, 135.2, 134.2, 128.9, 127.5, 127.3, 126.5, 125.2 (CH$_{aromatic}$), 35.6 (CH), 19.6 ($^2J_{C-P}$ = 26 Hz, P(CH$_3$)$_3$), 19.3 ($^2J_{C-P}$ = 27.5 Hz, P(CH$_3$)$_3$). δP(81 MHz, CD$_2$Cl$_2$) 34.1 (d, $^3J_{P-P}$ = 11.6 Hz, P$_{apical}$), 26.9 (d, $^3J_{P-P}$ = 11.6 Hz, P$_{basal}$). m/z (DEI) 802 (M $^+$), 746 (M-2CO), 718 (M-3CO), 690 (M-4CO), 614 (M-4CO-PMe$_3$), 538 (M-4CO-2PMe$_3$); ν_{max}(KBr)/cm^{-1} 3068w, 3025w, 2963w, 2924m, 2854m, 1980vs, 1942vs, 1912vs, 1891m).

Reaction of complexes with Na/Hg. In a 10 mL Schlenk vessel, 5 mg of the respective compound (7-17) were dissolved in acetonitrile (5 mL), followed by the addition of sodium amalgam (0.2 % Na in Hg), and the resulting two-phase system was shaken for 30 min. Within this time, the solution colored to dark red. Subsequently, this solution was investigated via IR spectroscopy under an argon atmosphere.

Crystal Structure Determinations. Compounds **6-10**, and **12-14** were crystallized from solutions in trichloromethane by slow evaporation of the solvent at 4 °C or from acetonitrile. The intensity data were collected on a Nonius Kappa CCD diffractometer using graphite-monochromated Mo-K$_\alpha$ radiation. Data were corrected for Lorentz and polarization effects but not for absorption.[17,18] Crystallographic data as well as structure solution and refinement details are summarized in supporting information. The structures were solved by direct methods (SHELXS)[19] and refined by full-matrix least squares techniques against F_o^2 (SHELXL-97).[19] All non-hydrogen atoms were refined anisotropically.[19] The hydrogen atoms were included at calculated positions according to the riding model.

Notes and references

[a] Institut für anorganische und analytische Chemie, Friedrich-Schiller Universität, August-Bebel-Straße 2, 07751 Jena, Germany. Fax: +49 3641 948102; Tel: +49 3641 948160; E-mail: wolfgang.weigand@uni-jena.de

† Electronic Supplementary Information (ESI) available: Crystal structure data of compound **6** and the crystal structure of **13**. See DOI: 10.1039/b000000x/

1   Y. Nicolet, C. Piras, P. Legrand, C. E. Hatchikian, J. C. Fontecilla-Camps, *Structure* 1999, **7**, 13–23; J. W. Peters, W. N. Lanzilotta, B. J. Lemon, L. C. Seefeldt, *Science* 1998, **282**, 1853–1858.

2   J. W. Tye, J. Lee, H. W. Wang, R. Mejia-Rodriguez, J. H. Reibenspies, M. B. Hall, M. Y. Darensbourg, *Inorg. Chem.* 2005, **44**, 5550–5552; J. F. Capon, S. El Hassnaoui, F. Gloaguen, P. Schollhammer, J. Talarmin, *Organometallics* 2005, **24**, 2020–2022; L. L. Duan, M. Wang, P. Li, Y. Na, N. Wang, L. C. Sun, *Dalton Trans.* 2007, 1277–1283; U.-P. Apfel, Y. Halpin, H. Görls, J. G. Vos, B. Schweizer, G. Linti, W. Weigand; *Chem. Biodiv.* 2007, **4**, 2138–2147; U.-P. Apfel, Y. Halpin, M. Gottschaldt, H. Görls, J. G. Vos, W. Weigand, *Eur. J. Inorg. Chem.* 2008, **33**, 5112–5118; J. Windhager, R. A. Seidel, U.-P. Apfel, H. Görls, G. Linti, W. Weigand, *Chem. Biodiv.* 2008, **5**, 2023–2041; U.-P. Apfel, C. R. Kowol, Y. Halpin, F. Kloss, J. Kübel, H. Görls, J. G. Vos, B. K. Keppler, E. Morera, G. Lucente, W. Weigand, *J. Inorg. Biochem.* 2009, **103**, 1236–1244; S. Jiang, J. H. Liu, Y. Shi, Z. Wang, B. Akermark, L. H. Sun, *Polyhedron* 2007, **26**, 1499–1504; T. B. Liu, M. Y. Darensbourg, *J. Am. Chem. Soc.* 2007, **129**, 7008–7009; D. Morvan, J. F. Capon, F. Gloaguen, A. Le Goff, M. Marchivie, F. Michaud, P. Schollhammer, J. Talarmin, J. J. Yaouanc, R. Pichon, N. Kervarec, *Organometallics* 2007, **26**, 2042–2052; C. M. Thomas, M. Y. Darensbourg, M. B. Hall, *J. Inorg. Biochem.* 2007, **101**, 1752–1757; C. M. Thomas, T. B. Liu, M. B. Hall, M. Y. Darensbourg, *Inorg. Chem.* 2008, **47**, 7009–7024; C. M. Thomas, T. B. Liu, M. B. Hall, M. Y. Darensbourg, *Chem. Commun.* 2008, 1563–1565; D. Morvan, J.-F. Capon, F. Gloaguen, F. Y. Pétillon, P. Schollhammer, J. Talarmin, J.-J. Yaouanc, F. Michaud, N. Kervarec, *J. Organomet. Chem.* 2009, **694**, 2801–2807; A. Le Cloirec, S. P. Best, S. Borg, S. C. Davies, D. J. Evans, D. L. Hughes, C. J. Pickett, *Chem. Commun.* 1999, 2285–2286; E. J. Lyon, I. P. Georgakaki, J. H. Reibenspies, M. Y. Darensbourg, *Angew. Chem., Int. Ed.* 1999, **38**, 3178–3180; M. Schmidt, S. M. Contakes, T. B. Rauchfuss, T. B. *J. Am. Chem. Soc.* 1999, **121**, 9736–9737; J. Windhager, M. Rudolph, S. Bräutigam, H. Görls, W. Weigand, *Eur. J. Inorg. Chem.* 2007, 2748–2760; J. Windhager, H. Görls, H. Petzold, G. Mloston, G. Linti, W. Weigand, *Eur. J. Inorg. Chem.* 2007, 4462–4471; L. C. Song, Z. Y. Yang, Y. J. Hua, H. T.Wang, Y. Liu, Q.-M. Hu, *Organometallics* 2007, **26**, 2106–2110; H. X. Li, T. B. Rauchfuss, *J. Am. Chem. Soc.* 2002, **124**, 726–727; L.-C. Song, Z. Y. Yang, H. Z. Bian, Y. Liu, H. T. Wang, X. F. Liu, Q. M. Hu, *Organometallics* 2005, **24**, 6126–6135; L.-C. Song, Z. Y. Yang, H. Z. Bian, Q. M. Hu, *Organometallics* 2004, **23**, 3082–3084; G. A. N. Felton, A. K. Vannucci, J. Z. Chen, L. T. Lockett, N. Okumura, B. J. Petro, U. I. Zakai, D. H. Evans, R. S. Glass, D. L. Lichtenberger, *J. Am. Chem. Soc.* 2007, **129**, 12521–12530; S. Loscher, L. Schwartz, M. Stein, S. Ott, M. Haumann, *Inorg. Chem.* 2007, **46**, 11094–11105; L. Schwartz, P. S. Singh, L. Eriksson, R. Lomoth, S. Ott, *C. R. Chimie* 2008, **11**, 875–889; L.-C. Song, C. G. Li, J. Gao, B. S. Yin, X. Luo, X. G. Zhang, H. L. Bao, Q. M. Hu, *Inorg. Chem.* 2008, **47**, 4545–4553; Z. Wang, W. F. Jiang, J. H. Liu, W. Jiang, Y. Wang, B. Akermark, L. C. Sun, *J. Organomet. Chem.* 2008, **693**, 2828–2834; N. Wang, M. Wang, T. B. Liu, P.; Li, T. T. Zhang, M. Y. Darensbourg, L. C. Sun, *Inorg. Chem.* 2008, **47**, 6948–6955.

3   J.-F. Capon, S. Ezzaher, F. Gloaguen, F. Y. Petillon, P. Schollhammer, J. Talarmin, *Chem. Eur. J.* 2008, **14**, 1954–1964.

4   B. E. Barton, T. B. Rauchfuss, *Inorg. Chem.* 2008, **47**, 2261–2263.

5   C. M. Thomas, T. B. Liu, M. B. Hall, M. Y. Darensbourg, *Inorg. Chem.* 2008, **47**, 7009–7024.

6   M. L. Singleton, N. Bhuvanesh, J. H. Reibenspies, M. Y. Darensbourg, *Angew. Chem., Int. Ed.* 2008, **47**, 9492–9495.

7   J. W. Tye, M. B. Hall, M. Y. Darensbourg, *Inorg. Chem.* 2006, **45**, 1552–1559.

8   M. K. Harb, U.-P. Apfel, J. Kübel, H. Görls,a G. A. N. Felton, T. Sakamoto, D. H. Evans, R. S. Glass, D. L. Lichtenberger, M. El-khateeb, W. Weigand, *Organometallics*, **2009**, accepted.

9   Ulf-Peter Apfel, Dennis Troegel, Yvonne Halpin, Stefanie Tschierlei, Ute Uhlemann, Michael Schmitt, Jürgen Popp, Helmar Görls, Peter Dunne, Munuswamy Venkatesan, Michael Coey, Manfred Rudolph, Johannes G. Vos, Reinhold Tacke, Wolfgang Weigand, **2010**, submitted.

10 S. J. Borg, T. Behrsing, S. P. Best, M. Razavet, X. M. Liu, C. J. Pickett, *J. Am. Chem. Soc.* 2004, **126**, 16988–16999.

11 D. Troegel, T. Walter, C. Burschka, R. Tacke, *Organometallics* 2009, **28**, 2756–2761.

12 J. Zubieta, E. Block, G. Ofori-Okai, K Tang, *Inorg. Chem.* 1990, **29**, 4595–4597.

13 A. G. Brook, G. J. D. Peddle, *Can. J. Chem.* 1963, **41**, 2351–2356.

14 P. Voss, C. Meinicke, E. Popowski, H. Kelling, *J. prakt. Chem.* 1978, **320**, 34–42.

15 L.-C. Song, H.-T. Wang, J.-H. Ge, S.-Z. Mei, J. Gao, L.-X. Wang, B. Gai, L.-Q.Zhao, J. Yan, Y.-Z. Wang, *Organometallics*, **2008**, **27**, 1409–1416; F. Gloaguen, J. D. Lawrence, M. Schmidt, S. R. Wilson, T. B. Rauchfuss, *J. Am. Chem. Soc.* 2001, **123**, 12518–12527.

16 M. L. Singleton, R. M. Jenkins, C. L. Klemashevich, M. Y. Darensbourg, *C. R. Chimie*, 2008, **11**, 861–874.

17 COLLECT, Data Collection Software; Nonius B. V., The Netherlands, **1998**.

18 Otwinowski, Z.; Minor, W. *Methods Enzymol.* **1997**, *276*, 307–326.

19 Sheldrick, G. M. *Acta Cryst. Sect. A* **2008**, *64*, 112–122.

Supporting Information

Sterically Demanding Silicon containing Ligands in [FeFe] Hydrogenase Models

Ulf-Peter Apfel, Manfred Rudolph, Joachim Kübel, Helmar Görls, and Wolfgang Weigand

Table S1. Selected Bond Distances (pm) and Angles (°) for Compound **6**

Bond length [pm]			
C(1)-Si(1)	189.9(2)	C(1)-S(1)	184.0(2)
C(2)-Si(1)	191.0(2)	C(1)-C(3)	151.4(3)
C(9)-Si(1)	186.7(2)	C(2)-S(2)	183.7(2)
C(21)-Si(1)	187.0(2)	C(2)-C(15)	151.0(3)
Bond angle [°]			
C(1)-Si(1)-C(2)	105.85(9)	S(1)-C(1)-Si(1)	108.55(11)
C(9)-Si(1)-C(21)	110.19(10)	S(2)-C(2)-Si(1)	107.40(10)

Table S2. Selected Bond Distances (pm) and Angles (°) for Compound **13**

Bond length [pm]			
Fe(1)-Fe(2)	254.29(8)	S(1)-C(1)	183.7(4)
Fe(1)-P(1)	222.60(13)	S(2)-C(2)	182.0(4)
Fe(1)-S(1)	227.20(12)	C(1)-Si(1)	185.3(4)
Fe(1)-S(2)	224.50(12)	C(2)-Si(1)	187.5(4)
Bond angle [°]			
Fe(1)-Fe(2)-S(1)	55.81(3)	S(2)-C(2)-Si(1)	121.4(2)
S(1)-Fe(1)-S(2)	88.15(4)	C(1)-Si(1)-C(2)	108.30(19)
S(1)-C(1)-Si(1)	115.6(2)	C(3)-Si(1)-C(9)	109.61(19)

Table S3. Crystal Data and Refinement Details for the Crystal Structure Analyses of Compounds **6-14**.

	6	7	8	9	10	12	13	14
empirical formula	$C_{26}H_{24}S_2Si$	$C_{20}H_{14}Fe_2O_6S_2Si$	$C_{22}H_{18}Fe_2O_6S_2Si$	$C_{32}H_{22}Fe_2O_6S_2Si$	$C_{37}H_{29}Fe_2O_5PS_2Si$	$C_{52.5}H_{44}Cl_3Fe_2O_5PS_2Si$	$C_{22}H_{23}Fe_2O_5PS_2Si$	$C_{24}H_{27}Fe_2O_5PS_2Si$
formula mass [g·mol^{-1}]	428.66	554.22	582.27	706.41	788.48	1096.11	602.28	630.34
collection T [°C]	-90(2)	-90(2)	-90(2)	-90(2)	-90(2)	-90(2)	-90(2)	-90(2)
λ (Mo K$_\alpha$) [Å]	0.71073	0.71073	0.71073	0.71073	0.71073	0.71073	0.71073	0.71073
crystal system	monoclinic	monoclinic	orthorhombic	monoclinic	triclinic	triclinic	monoclinic	monoclinic
space group (No.)	P2(1)/n (14)	P2(1)/c (14)	Pbcm (57)	P2(1) (4)	P$\bar{1}$ (2)	P$\bar{1}$ (2)	P2(1)/c (14)	P2(1)/n (14)
a [Å]	12.5725(7)	14.5006(7)	9.5019(4)	8.9705(2)	11.4625(6)	10.0697(4)	10.8815(7)	8.9842(2)
b [Å]	10.0053(3)	20.9505(9)	16.5154(9)	13.1314(5)	11.8508(4)	16.2898(7)	10.3618(7)	12.0158(7)
c [Å]	18.5969(9)	7.5734(3)	15.5956(8)	12.9610(5)	12.9583(8)	17.6155(7)	22.8942(10)	25.5785(12)
α [°]	90	90	90	90	88.219(3)	73.258(2)	90	90
β [°]	105.747(2)	92.626(3)	90	92.088(2)	88.582(2)	77.679(2)	98.062(4)	92.112(3)
γ [°]	90	90	90	90	84.306(3)	76.829(2)	90	90
V [Å^3]	2251.54(18)	2298.34(17)	2447.4(2)	1525.73	1750.31(15)	2660.22(19)	2555.9(3)	2759.4(3)
Z	4	4	4	2	2	2	4	4
ρ_{calcd} [g·cm^{-3}]	1.265	1.602	1.580	1.538	1.496	1.368	1.565	1.517
μ [mm^{-1}]	0.3	1.529	1.44	1.171	1.071	0.871	1.439	1.336
$F(000)$	904	1120	1184	720	808	1126	1232	1296
crystal dimensions [mm]	0.06 x 0.06 x 0.05	0.05 x 0.05 x 0.04	0.05 x 0.05 x 0.05	0.05 x 0.05 x 0.04	0.06 x 0.06 x 0.02	0.05 x 0.05 x 0.04	0.04 x 0.04 x 0.04	0.05 x 0.05 x 0.04
2θ range [deg]	3.05-27.48	2.98-27.43	2.89-27.46	2.27-27.46	2.35-27.49	2.68-27.52	2.79-27.48	2.83-27.47
index ranges	$13 \leq h \leq 16$, $11 \leq k \leq 12$, $24 \leq l \leq 19$	$17 \leq h \leq 18$, $23 \leq k \leq 27$, $9 \leq l \leq 9$	$12 \leq h \leq 11$, $21 \leq k \leq 18$, $20 \leq l \leq 19$	$11 \leq h \leq 11$, $16 \leq k \leq 17$, $16 \leq l \leq 15$	$12 \leq h \leq 14$, $15 \leq k \leq 14$, $16 \leq l \leq 14$	$13 \leq h \leq 12$, $21 \leq k \leq 21$, $21 \leq l \leq 22$	$14 \leq h \leq 12$, $11 \leq k \leq 13$, $29 \leq l \leq 26$	$11 \leq h \leq 7$, $12 \leq k \leq 15$, $32 \leq l \leq 32$
measured reflections	14761	14977	14643	10977	12182	18282	15128	10006
unique reflections/R_{int}	5130	5202	2888	6369	7972	11995	5713	5410
reflections used	14761	14977	14643	10977	12182	18282	15128	10006
data with $I > 2\sigma(I)$	3153	3153	1899	5518	5596	7053	2653	3611
parameters	270	280	163	388	433	597	301	321
S^a	0.973	0.959	0.966	1.017	1.009	1.012	0.889	1.003
R_1 [$I > 2\sigma(I)$]^b	0.0455	0.0414	0.0416	0.0328	0.0417	0.0602	0.0485	0.0491
wR_2 [all data, on F^2]^c	0.0917	0.0737	0.0789	0.0669	0.0834	0.1432	0.0760	0.0907
max./min. residual electron density [e·Å^{-3}]	0.540/-0.252	0.336/-0.401	0.572/-0.464	0.296/-0.248	0.305/-0.453	1.196/-0.470	0.541/-0.475	0.476/-0.422

^{a} $S = \{\Sigma[w(F_o^2 - F_c^2)^2] / (n - p)\}^{0.5}$; n = no. of reflections; p = no. of parameters; ^{b} $R_1 = \Sigma||F_o| - |F_c|| / \Sigma|F_o|$; ^{c} $wR_2 = \{\Sigma[w(F_o^2 - F_c^2)^2] / \Sigma[w(F_o^2)^2]\}^{0.5}$.

2-Dimethylsilapropanedichalogenolato [2Fe2E(Si)] (E = S, Se, Te) Complexes – [FeFe] Hydrogenase Models

Ulf-Peter Apfel, Helmar Görls, Greg A. N. Felton, Dennis H. Evans[b], Richard S. Glass[b*], Dennis L. Lichtenberger[b*],Wolfgang Weigand[*]*

[a]*Institut für Anorganische und Analytische Chemie, Friedrich-Schiller-Universität Jena, August-Bebel-Straße 2, 07743 Jena, GERMANY*

[b]*Department of Chemistry, The University of Arizona, Tucson, AZ, 85721, U.S.A.*

E-mail: wolfgang.weigand@uni-jena.de

RECEIVED DATE (to be automatically inserted after your manuscript is accepted if required according to the journal that you are submitting your paper to)

ABSTRACT. Diselenolato and ditellurolato complexes [2Fe2E(Si)] have been prepared and compared with the known diiron dithiolato complex **A**. Treatment of $Fe_3(CO)_{12}$ with 4,4-dimethyl-1,2,4-diselenasilolane (**1**) in boiling toluene affords hexacarbonyl [μ-(2,2-dimethyl-2-sila-1,3-propanselenolato(2–)-*S,S*)]diiron (**2**). The analog ditellurolato complex hexacarbonyl [μ-(2,2-dimethyl-2-sila-1,3-propantelurolato(2–)-*S,S*)]diiron (**3**) was obtained by treatment of $Fe_3(CO)_{12}$ and bis(tellurocyano)dimethylsilane, which was prepared *in situ*. All compounds were characterized by NMR, IR spectroscopy, mass spectrometry, elemental analysis and single crystal X-ray analysis. The electrochemical properties for the [2Fe2S(Si)] model compounds towards dihydrogen formation will be presented.

KEYWORDS: hydrogenase, iron, selenium, tellurium, electrocatalysis.

Introduction

Since the structure of the active site of the [FeFe] hydrogenase has been reported,[1] finding a suitable model with commensurable properties is still a challenge. Recent progress in this topic was done by Darensbourg *et al* concerning the investigations of the "rotated" geometry on [2Fe2S] model complexes[2] and Rauchfuss *et al* figuring out the role of phosphane ligands towards the direction of protons to a bridging or terminal site.[3] Beside the direct protonation of the Fe centers, experiments and calculations pointed out a possible addition of a proton to the bridgehead sulfur atoms.[4] An experimental proof of these calculations was displayed by silicon containing [Fe2S2] models **A**-**D** (Scheme 1).[5]
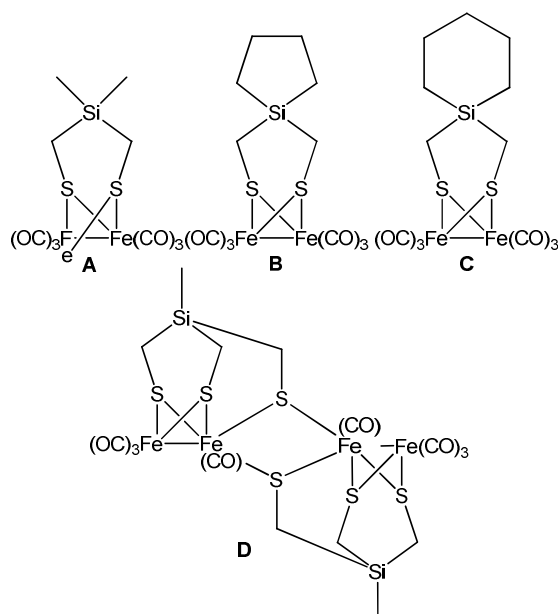
Scheme 1. [2Fe2S(Si)] model complexes showing the ability to protonate the sulfur atoms.

Investigations of us showed that in contrast to DFT calculations on the pdt complexes,[6] an increase of the electron density on the sulfur atoms by hyperconjugation of σ*(Si-C) into the 3p(S) orbital should be assumed, as calculated for similar tin complexes.[7] During electrochemical investigations, protonation occurs on the bridgehead sulfur atom and a proton relay towards the metal atoms could be established. Lately investigations showed that by exchange of the sulfur bridgehead atoms by selenium the activity towards hydrogen production was diminished and the reduction window was shifted to more negative potentials.[8]

To gain a deeper insight into silicon containing [FeFe] hydrogenase model complexes bis(chloromethyl)dimethylsilane was conversed to the respective selenium and tellurium complexes **2** and **3**. The spectroscopic and structural features as well as the elctrocatalytic properties will be presented and compared to the related sulfur containing complex **A**.

Results and Discussions

Since the access to the silicon containing bis(mercaptomethyl)dimethylsilane and its respective [Fe2S2] complex is known,[5,9] an analog way to the corresponding selenium and tellurium complexes has to be

found. Block *et al* established syntheses towards ditelluroloane and diselenolane compounds.[9] In contrast to this work, we used bis(chloromethyl)dimethylsilane instead of bis(iodomethyl)dimethylsilane as starting material. Using bis(mercaptomethyl)dimethylsilane, 4,4-dimethyl-1,2,4-diselenasilolane (**1**) was obtained by treatment with sodium diselenide, which was prepared *in situ* from selenium and sodium borohydride in abs. ethanol to afford **1** in 28% yield (Scheme 2).
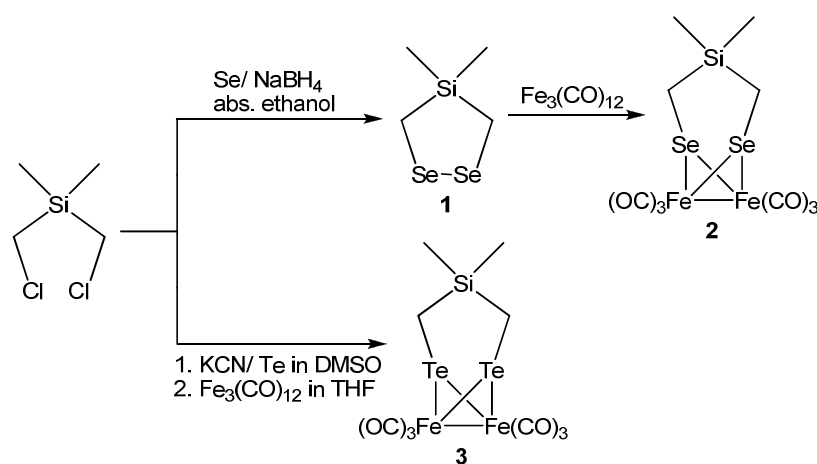
Scheme 2. Synthesis of model complexes **2** and **3**.
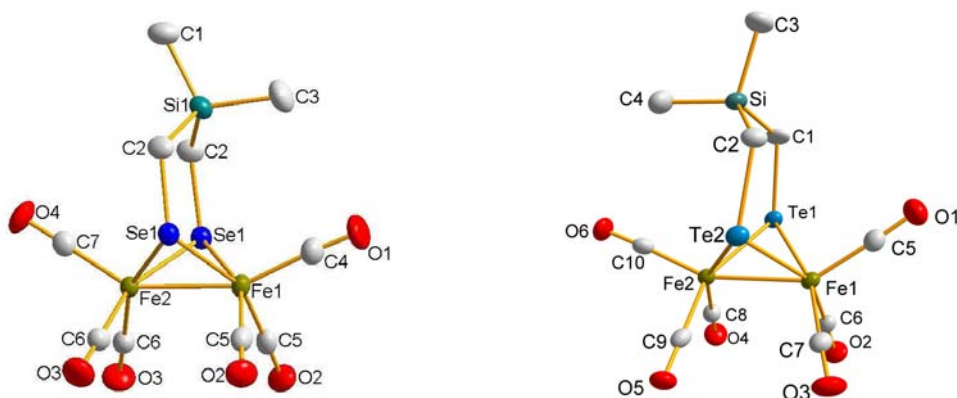
Figure 1. Molecular structure of **2** (left) and **3** (right) in the crystal (probability level of displacement ellipsoids 50%).

The reaction of compound **1** with $Fe_3(CO)_{12}$ provided hexacarbonyl [μ-(2,2-dimethyl-2-sila-1,3-propanselenolato(2–)-*S*,*S*)]diiron (**2**) in moderate yield (66%). ^1H, $^{13}C\{^1H\}$, $^{77}Se\{^1H\}$ NMR and the [M^+] peak at $m/z = 526$, followed by stepwise lose of six CO, revealed the proposed structure. Evaporation of a solution of **2** dissolved in pentane, afforded crystals suitable for single crystal X-ray

structure determination, as depicted in Figure 1. In contrast to the selenium compound, the synthesis of hexacarbonyl [μ-(2,2-dimethyl-2-sila-1,3-propantelurolato(2–)-*S,S*)]diiron (**3**) followed a different route, as the ditellurolato compound turns out to be elusive. Therefore bis(chloromethyl)dimethylsilane was treated with a twofold access of potassium telluro cyanate, freshly prepared by heating tellurium and potassium cyanide in refluxing dimethylsulfoxide.[10] The *in situ* prepared bis(tellurocyano)dimethylsilane was not isolated and therefore instantly added to a solution of $Fe_3(CO)_{12}$ dissolved in THF. Heating of this solution under reflux conditions, followed by extraction with hexane and chromatographic purification afforded a small amount of compound **3** (9%) as orange powder. NMR investigations (^{1}H, ^{13}C{^{1}H}) alludes to compound **3**, additionally confirmed by the [M$^+$] peak at $m/z = 624$. Single crystals suitable for the structure determination were obtained by slow evaporation of a solution of compound **3** in pentane (Figure 1).

Since the CO group is very sensitive towards mutations of the electron density on the iron centers, the ^{13}C{^{1}H} NMR signals and the CO vibrations give important evidence for the influence of the heavy atoms.[11] Comparing compounds **A**, **2** and **3**, the CO vibration shift from 2074 cm^{-1} for the sulfur compound **A** to 2065 cm^{-1} (**2**) for the selenium compound and to 2054 cm^{-1} (**3**) when implementing tellurium. This shift to lower frequencies can be explained by the higher electron density, directed to the iron centers and introduced by the heavier homologous selenium and tellurium.[8e] This tendency is also apparent in the ^{13}C{^{1}H} NMR. A continuous de-shielding of the CO groups and hence a shift to lower field of this signal is observable within the homologous row S (207.5 ppm), Se (208.4 ppm) and Te (210.5 ppm).[11] Another dramatic influence of the exchange of sulfur by selenium or tellurium is detectable for the E-CH$_2$-Si (E = S, Se, Te) carbon shift. Whereas compound **A** exhibit a signal at 5.9 ppm, the selenium derivative **2** reveals this carbon signal at -5.1 ppm. However, the related tellurium compound **3** shows up this signal at -26.6 ppm. This serious high field shift is only explainable by the heavy atom effect.[12]

As the spectroscopic differences strongly deviates, one may assume that the structural properties should differ. However, this could only be confirmed for the Fe-Fe bond distance. As compound **A** reveals a

distance of 252.16(6) pm, compound **2** shows a 254.99(6) pm long Fe-Fe bond. The Fe-Fe bond of compound **3** reveals an increased value of 261.53(8) pm and exhibit the value found in the natural systems.[1,2] At all means, this phenomenon was expected as the atom radii of the higher homologues are enlarged.[11] No other appreciable differences of the structures were observed. Collectively, all three compounds exhibit the typical [Fe2S2] butterfly arrangement and bear six CO groups as seen in many familiar [Fe2S2] complexes.[13] As already recorded for compound **A**, the wide bonding angles E-C-Si are also observed for **2** and **3**. This suggests that also for compounds **2** and **3**, an increased basicity of the bridgehead atom should be expected as a result of an effective overlap $\sigma(C\text{-}Si) \rightarrow n_p(E)$.

Table 1. Selected Bond Distances [pm] and Angles [°] for Compounds **2 3** .

Bond lengths [pm]		
	2	**3**
Fe(1)-Fe(2)	254.99(6)	261.53(8)
Fe(1)-Se(1)/Te(1)	238.03(4)	255.70(6)
Fe(2)-Se(1)/Te(2)	237.73(4)	254.14(5)
Te(1)-C(1)	-	216.0(4)
Se(1)/Te(2)-C(2)	195.8(3)	216.9(4)
Si(1)-C(1)	186.9(4)	186.7(4)
Si(1)-C(2)	187.1(3)	185.8(4)
Si(1)-C(3)	185.8(5)	187.5(5)
Bond angles [°]		
Fe(1)-Se(1)/Te(1)-Fe(2)	64.817(15)	61.777(18)
Te(1)-C(1)-Si	-	121.7(2)
Se(1)/Te(2)-C(2)-Si	121.55(15)	119.4(2)
C(1)-Si-C(2)	107.58(12)	106.70(19)
C(1)-Si-C(3)	109.8(2)	107.8(2)
C(1)-Si-C(4)	-	113.8(2)

Electrochemistry

Conclusion

Experimental Section

General Procedures. All syntheses were carried out under dry nitrogen or argon. The organic solvents used were dried and purified according to standard procedures and stored under dry nitrogen or argon. Chemicals were used as received from Fluka and Acros without further purification. TLC: *Merck silica gel 60 F$_{254}$ plates*; detection under UV light at 254 nm. FC: *Fluka* silica gel 60. A Büchi GKR-51 apparatus was used for the bulb-to-bulb distillations. The ^{1}H, ^{13}C{^{1}H} and ^{34}Se{^{1}H} NMR spectra were recorded at 23 °C on a Bruker 200 MHz spectrometer (^{1}H, 200 MHz; ^{13}C, 50 MHz; ^{77}Se, 76 MHz). CDCl$_3$ was used as the solvent. Chemical shifts (ppm) were determined relative to internal CHCl$_3$ (^{1}H, δ 7.24; CDCl$_3$), CDCl$_3$ (^{13}C, δ 77.0; CDCl$_3$) or SeO$_2$ in D$_2$O. The ^{77}Se chemical shifts are reported relative to neat Me$_2$Se [δ(Me$_2$Se) = δ(SeO$_2$) +1302.6 ppm].[14] IR-spectra were recorded on a *Perkin-Elmer 2000 FT-IR*.

4,4-Dimethyl-1,2,4-diselenasilolane (1): 4,4-Dimethyl-1,2,4-diselenasilolane was prepared referring to reference [9]. Instead of bis(iodomethyl)dimethylsilane, bis(chloromethyl)dimethylsilane was used for the conversion. To 353 mg (4.47 mmol) selenium in 20 mL ethanol, 118mg (3.2 mmol) sodium borohydride was added at 0°C. After 1hour stirring under reflux bis(chloromethyl)dimethylsilane (500 mg, 3.2 mmol) was added and stirred one more hour at roomtemperature. Addition of 20 mL water, extraction with dichloromethane and drying with sodium sulfate afforded a crude red oily product. The crude product was purified via column chromatographie (dichloromethane/ hexane 1:5) to yield 220 mg (28%) of a red oil. ^{1}H NMR (CDCl$_3$): δ 0.21 (s, 6 H, CH_3), 2.32 (s, 4 H, CH_2). ^{13}C NMR (CDCl$_3$): δ –1.6 (CH_3), 14.3 (CH_2). ^{77}Se{^{1}H} NMR (CDCl$_3$): δ 319.8. MS(DEI): *m/z*, 246 [M]$^{+}$.

Hexacarbonyl [μ-(2,2-Dimethyl-2-sila-1,3-propanthiolato(2)- *S,S'*)]diiron (A): was prepared according to reference [5].

Hexacarbonyl [μ-(2,2-dimethyl-2-sila-1,3-propanselenolato(2)- *S,S'*)]diiron (2): In 40 mL toluene, 92 mg (0.37 mmol) 4,4-Dimethyl-1,2,4-diselenasilolane and 190 mg (0.37 mmol) $Fe_3(CO)_{12}$ was dissolved and stirred under reflux for 1.5 hours. Evaporation to dryness and filtration through a silica pad with dichloromethane/ hexane (1:5) afforded 128 mg (66 %) of the desired compound as red crystalline product. ^{1}H NMR (CDCl$_3$): δ 0.09 (s, 6 H, CH_3), 1.35 (s, 4 H, CH_2). ^{13}C NMR (CDCl$_3$): δ – 5.6 (CH_2), -1.0 (CH_3), 208.4 (CO). ^{77}Se{^{1}H} NMR (CDCl$_3$): δ 170.1. MS(DEI): *m/z*, 526 [M]$^+$, 498 [M-CO]$^+$, 470 [M-2CO]$^+$, 442 [M-3CO]$^+$, 414 [M-4CO]$^+$, 386 [M-5CO]$^+$, 358 [M-6CO]$^+$. IR (KBr): 2959 (m), 2922 (m), 2897 (m), 2065 (vs), 2021 (vs), 1986 (vs), 1405 (m), 1367 (m), 1253 (s), 1096 (s). Anal. Calcd for $C_{16}H_8Fe_4O_{12}S_4Si$•0.1 hexane: C, 23.91; H, 2.16. Found: C, 23.7; H, 2.4.

Hexacarbonyl [μ-(2,2-dimethyl-2-sila-1,3-propantelurolato(2)- *S,S'*)]diiron (3): 246 mg (1.92mmol) tellurium and 125 mg (1.92 mmol) KCN were dissolved in 20 mL dimethylsulfoxid and refluxed for 1 hour. After cooling to room temperature 150mg (0.96 mmol) bis(chloromethyl)dimethylsilane was added and the solution was stirred over night and added to a solution of 484 mg (0.96mmol) $Fe_3(CO)_{12}$, dissolved in 20 mL THF. The solution was stirred under reflux for 1 hour and extracted with hexane (until the hexane fraction remains colorless). Evaporation to dryness, followed by column chromatography with hexane yield 51mg (9%) of an orange solid. ^{1}H NMR (CDCl$_3$): δ 0.08 (s, 6 H, CH_3), 1.34 (s, 4 H, CH_2). ^{13}C NMR (CDCl$_3$): δ –26.6 (CH_2), –2.1 (CH_3), 210.5 (CO). MS(DEI): *m/z*, 624 [M]$^+$, 596 [M-CO]$^+$, 568 [M-2CO]$^+$, 484 [M-5CO]$^+$, 454 [M-6CO]$^+$. IR (KBr): 2953 (m), 2922 (m), 2851 (m), 2051 (vs), 2012 (vs), 1987 (vs), 1958 (vs), 1949 (vs), 1463 (m), 1377 (m), 1260 (m). Anal. Calcd for $C_{10}H_{10}Fe_2O_6Te_2Si$•hexane: C, 27.17; H, 3.42. Found: C, 27.53; H, 2.93.

Supporting Information available:

Acknowledgements

References

[1] J. W. Peters, W. N. Lanzilotta, B. J. Lemon, L. C. Seefeldt, *Science* **1998**, *282*, 1853-1858; Y. Nicolet, C- Piras, P. Legrand, C. E. Hatchikian, J. C. Fontecilla-Camps, *Structure* **1999**, *7*, 13-23.

[2] M. L. Singleton, N. Bhuvanesh, J. H. Reibenspies, M. Y. Darensbourg, *Angew. Chem. Int. Ed.* **2008**, *47*, 9492-9495.

[3] B. E. Barton, T. B. Rauchfuss, *Inorganic Chemistry* **2008**, *47*, 2261-2263

[4] J.-F. Capon, S. Ezzaher, F. Gloaguen, F. Y. Pétillon, P. Schollhammer, and Jean Talarmin, *Chem. Eur. J.* **2008**, *14*, 1954-1964; C. Greco, G. Zampella, L. Bertini, M. Bruschi, P. Fantucci, L. De Gioia, *Inorg. Chem.* **2007**, *46*, 108-116.

[5] U.-P. Apfel, D. Troegel, Y. Halpin, S. Tschierlei, U. Uhlemann, M. Schmitt, J. Popp, H. Görls, P. Dunne, M. Venkatesan, M. Coey, M. Rudolph, J. G. Vos, R. Tacke, W. Weigand, **2010**, submitted

[6] J. W. Tye, M. Y. Darensbourg, M. B. Hall, *Journal of Molecular Structure: THEOCHEM* **2006**, *771*, 123–128;

[7] Glass, R. S.; Gruhn, N. E.; Lorance, E.; Singh, M. S.; Stessman, N. Y. T.; Zakai, U. I. *Inorg. Chem.* **2005**, *44*, 5728–5737.

[8] a) Harb, M. K.; Niksch, T.; Windhager, J.; Görls, H.; Holze, R.; Lockett, L. T.; Okumura, N.; Evans, D. H.; Glass, R. S,; Lichtenberger, D. L.; El-khateeb, M.; Weigand, W. *Organometallics* **2009**, *28*, 1039; c) U.-P. Apfel, Y. Halpin, M. Gottschaldt, H. Görls, J. G. Vos, W. Weigand, *Eur.*

J. Inorg. Chem. **2008**, *33*, 5112; d) Song, L.-C.; Gai, B.; Wang, H.-T.; Hu, Q.-M. *J. Inorg. Biochem.* **2009**, *103*, 805; e) M. K. Harb, U.-P. Apfel, J. Kübel, H. Görls, G. A. N. Felton, T. Sakamoto, D. H. Evans, R. S. Glass, D. L. Lichtenberger, M. El-khateeb, W. Weigand, *Organometallics* **2009**, *28*, 6666.

[9]   E. Block, E. V. Dikarev, R. S. Glass, J. Jin, B. Li, X. Li, S.-Z. Zhang, *J. Am. Chem. Soc.* **2006**, *128*, 14949.

[10]   H. K. Spencer, M. V. Lakshmikantham, M. P. Cava, *J. Am. Chem. Soc.* **1977**, *99*, 1470.

[11]   A.F. Hollemann, E. Wiberg, *Lehrbuch der Anorganischen Chemie* **1995**, *101*[th] edtition, Berlin, New York.

[12]   G. A. Kalabin, V. M. Bzehezovskii, D. F. Kushnarev, A. G. Proidakov, *J. Org. Chem. USSR* **1981**, *17*, 1009.

[13]   X. Zhao, I. P. Georgakaki, M. L. Miller, J. C. Yarbrough, M. Y. Darensbourg, *J. Am. Chem. Soc.* **2001**, *123*, 9710; X. Zhao, C. Y. Chiang, M. L. Miller, M. V. Rampersad, M. Y.Darensbourg, *J. Am. Chem. Soc.* **2003**, *125*, 518; F. Gloaguen, J. D. Lawrence, M. Schmidt, S. R. Wilson, T. B. Rauchfuss, *J. Am. Chem. Soc.* **2001**, *123*, 12518; E. J. Lyon, I. P. Georgakaki, J. H. Reibenspies, M. Y. Darensbourg, *J. Am. Chem. Soc.* **2001**, *123*, 3268; J. D. Lawrence, H. Li, T. B. Rauchfuss, M. Benard, M. M. Rohmer, *Angew. Chem. Int. Ed.* **2001**, *40*, 1768; M. Razavet, S. C. Davies, D. L. Hughes, J. E. Barclay, D. J. Evans, S. A. Fairhurst, X. Liu, C. J. Pickett, *Dalton Trans.* **2003**, 586; R. C. Linck, T. B. Rauchfuss, *Bioorganometallics* **2006**, 403; H. Li, T. B. Rauchfuss, *J. Am. Chem. Soc.* **2002**, *124*, 726; S. Ott, M. Kritikos, B. ̄kermark, L. Sun, *Angew. Chem. Int. Ed.* **2003**, *42*, 3285; C. Tard, X. Liu, S. K. Ibrahim, M. Bruschi, L. De Gioia, S. C. Davies, X. Yang, L.-S. Wang, G. Sawers, C. J. Pickett, *Nature* **2005**, *433*, 610; L.-C. Song, Z.-Y. Yang, H.-Z. Bian, Q.-M. Hu, *Organometallics* **2004**, *23*, 3082; D. Seyferth, R. S. Henderson, L.-C. Song, *Organometallics* **1982**, *1*, 125; D. Seyferth, R. S. Henderson, L.-C. Song, *J. Organomet. Chem.*

1980, *192*, C1; U. P. Apfel, Y. Halpin, H. Görls, J. G. Vos, B. Schweizer, G. Linti, W. Weigand, *Chem. Biodivers.* **2007**, *4*, 2138; J. Windhager, R. A. Seidel, U. P. Apfel, H. Görls, G. Linti, W. Weigand, *Eur. J. Inorg. Chem.* **2008**, *10*, 2023; J. Windhager, M. Rudolph, S. Bräutigam, H. Görls, W. Weigand, *Eur. J. Inorg. Chem.* **2007**, *18*, 2748; J. Windhager, H. Görls, H. Petzold, G. Mloston, G. Linti, W. Weigand, *Eur. J. Inorg. Chem.* **2007**, *28*, 4462; L.-C. Song, Z. Y. Yang, H. Z. Bian, Y. Liu, H. T. Wang, X. F. Liu, Q. M. Hu, *Organometallics* **2005**, *24*, 6126.

[14] R. C. Burns, M. J. Collins, R. J. Gillespie, G. J. Schrobilgen, *Inorg. Chem.* **1986**, *25*, 4465.